THE DESIGN AND PERFORMANCE OF AN INTEGRATED HEAT PUMP – LATENT HEAT STORE WATER HEATING SYSTEM

by

Brian H. Cooke

B.Sc. (Edinburgh)

Thesis presented for the Degree of Doctor of Philosophy

Faculty of Science

University of Edinburgh

July, 1987

To my parents

for their encouragement through the years.

"Is that it?"

Bob Geldof

The work described in this thesis is the original work of the author except where specific reference is made to other sources. It has not been submitted, in whole or in part, for any degree at any other University.

CONTENTS

LIST OF FIGURES

LIST OF TABLES

ACKNOWLEDGEMENT

The author would like to express his gratitude to the following people and organisations who have contributed to the successful completion of this research project:

1. Dr C. L. Pritchard for his supervision and encouragement throughout the project
2. Myson Copperand Limited for kindly donating the prototype heat pump used in the experimental work
3. Calor Limited for kindly donating the Calortherm tubes and the prototype storage device used in the experimental work
4. Mr D. Ketchin and all the workshop staff of the Department of Chemical Engineering, University of Edinburgh, for construction and modification of the experimental apparatus
5. Fellow research students for helpful discussion

ABSTRACT

Thermal energy storage devices may be combined advantageously with heat pumps as heating systems for domestic and commercial premises. A condenser-side heat store, which offers substantial energy cost savings and reduced on/off switching of the heat pump, was developed and its performance investigated experimentally and theoretically in this study.

Calortherm 58, a phase change material (melting point 56°C) based on sodium acetate trihydrate was selected as the storage medium. The store consists of 1000 polypropylene tubes containing the PCM, each 25 mm in diameter and 1 m long, giving a nominal storage capacity of 0.159 GJ (44.4 kWh) over a temperature range of 20 degC. An air-to-water heat pump, capable of delivering 7.5 kW at a circulating water temperature of 55°C for an ambient temperature of 7°C, and a microcomputer to perform the control and datalogging functions complete the test facility.

Testing of the store according to a modified form of the ASHRAE standard procedure 94-77 showed the effect of flow direction, inlet temperature and flow rate on store performance. A finite difference model was developed to determine the movement of the phase change front radially and longitudinally through the tubes. The store charge/discharge rates predicted from the temperature profiles were in good agreement with those found experimentally.

Performance of the heat pump was confirmed experimentally to be dependent on the ambient air and desired hot water temperatures. Parameters describing the deviation of the experimental performance from the ideal Rankine cycle were successfully employed by a diagram model to simulate the heat pump performance.

Experimental results are presented which show the performance of the integrated system for typical climatic and load conditions. An elementary model of the integrated system was developed and results presented which show the potential savings, in comparison to a heat pump alone, over a range of economic and operating parameters. A detailed model, which combined the heat store finite difference model with correlations expressing heat pump performance, was successfully employed to simulate operation of the experimental system.

CHAPTER 1

INTRODUCTION

1.1. Heat Pumps for Domestic Heating

With the rising cost of fossil fuels, alternative energy sources for space and process heating are being investigated. The heat pump has been developed as a potential alternative to conventional heating systems for certain domestic applications. Annual sales of heat pumps in the U.K. during 1982 reached 4300 units and was forecast to increase at more than 20% per annum (see Webster 1983).

A heat pump operates on the same vapour compression thermodynamic cycle as the common household refrigerator. The difference (see figure 1.1) is that the latter is designed to maximise the amount of heat extracted from the source while the former maximises the heat output to the sink. In a refrigerator the source is the cold air inside the refrigerator while the sink is the air surrounding the unit in the dwelling. In contrast, a heat pump extracts low grade thermal energy from the building enviroment (source) and supplies the domestic heating load (sink).

From the first law of thermodynamics it is known that

$$q_c + W = q_h. \qquad (1.1)$$

The efficiency, or Coefficient of Performance (COP) of the cycle may then be calculated from the ratio of q_h to W, typically found to be in the range two to three. Since this implies that for every one kWh electrical input to the compressor we can expect two to three kWh thermal output to the sink, further research into heat pump development is certainly justified. The principles governing heat pump operation are thoroughly explained in chapter two.

Despite this attractive COP, heat pumps at present compete unfavourably with conventional gas fired boilers for use as domestic heating systems (see table 1.1). High capital cost, noise and poor reliability have prevented their gaining universal acceptance and sales are targeted at specific areas, for example dwellings not connected to the gas mains.

Another major drawback in employing a heat pump domestic heating system is that at a low source temperature, corresponding to a high heat

demand, the thermal output is low as shown in figure 1.2. Hence if a heat pump system is monovalent, i.e. designed to meet the full heating load at the coldest source temperature, then it is grossly over sized for meeting the normal requirements. Figure 1.3 shows the annual temperature distribution, as reported by Heap (1977), for Edinburgh over the period 1952-1960. Examination of this curve reveals that the temperature is less than 0°C for only 8% of the year and hence a heat pump designed to meet full demand at -5°C will be operating at less than 80% capacity for 92% of the time.

During periods when heat pump output exceeds heat demand the heat pump will be subjected to on/off switching. This not only results in a 5% decrease in seasonal COP (Tassou et al. 1984), but reduces the life of many components and therefore reduces overall system reliability. Researchers are investigating various potential methods of modulating the capacity, the most promising of which appears to be compressor speed control (Hillier and Glicksman 1976). The maximum turn-down ratio is 2.0 however, since lower refrigerant flow rates result in inadequate lubricant distribution.

An alternative solution is to select a smaller heat pump (figure 1.2) designed to meet heating requirements down to a temperature known as the balance point, normally -1°C for British climate (HVCA 1983). There are two major reasons why this arrangement is considered unsatisfactory:

1. There is a high capital cost associated with installing two independent heating systems
2. The resulting step increase in demand for electricity during periods at which it is already stretched (note that it is assumed that electricity would be selected as it provides the cheapest form of auxiliary heating)

1.2. Integrated Heat Pump/Heat Store Systems for Domestic Heating

An integrated heat pump/condenser heat store would appear to offer three potential advantages over a conventional heat pump system:

1. Utilisation of off-peak electricity, easing load on generating capacity and reducing running cost for the consumer

2. Operation of heat pump during periods of high source temperature to obtain benefit of improved COP
3. Reduced on/off switching of heat pump, resulting in improved reliability and performance

Armor (1981) designed and developed a sensible heat store, but examination of figure 3.1 highlights the poor energy density of water in comparison to a phase change material (PCM) such as sodium acetate trihydrate. The comparison is even less favourable when considering a real heating application where the store outlet temperature should be kept as high as possible and certainly limited to a drop of 20 degC.

The Edison Electric Company (see Altman 1971) were the first to develop a commercial integrated system based on a PCM, disodium phosphate dodecahydrate, encapsulated in fruit juice type cans, back in the 1950's. The cans were dumped irregularly into a galvanised fuel oil storage device which resulted in short-circuiting of the transfer fluid and rapid corrosion of the cans. Kopecky (1984) and others at Cranfield developed a peak-lopping store designed to allow the smallest possible heat pump to cope with the peak demand as shown in figure 2.12. Other workers have concentrated on developing evaporator-side heat stores which allow the heat pump to operate with a pseudo-constant source temperature.

We selected sodium acetate trihydrate, as the most suitable PCM for a condenser-side heat store, primarily due to its melting point temperature of 58°C, considered the best compromise between heat pump performance and radiator temperature. Plastic film tubing was employed as an encapsulation technique in the hope that crystals forming on the film surface would be dislodged as a consequence of flow vibration thus reducing the known tendency of the PCM to supercool. However development of a small scale store was severely impeded by leaking tubes and segregation.

These problems had recently been overcome by Calor and the PCM was being marketed under the tradename of Calortherm 58. Their solution was to encapsulate the PCM, stabilised with a nucleating agent to prevent supercooling and a cross linking polymer to prevent segregation, in polypropylene tubes. These tubes were 1 m in length and available in two

diameters: 25 mm and 38 mm. Experimental work with a pilot store of 45 litre capacity with both tube diameters resulted in a design for a prototype 800 litre store with one thousand 25 mm diameter tubes.

1.3. Scope of Thesis

The work presented in this thesis contains:

1. A review of literature and theory (chapter 2)
2. An account of the development of the experimental facility (chapter 3)
3. The results of experimental work (chapters 4, 5 and 6)
4. Development and results of computer simulation (chapter 7)

Since both heat pumping and thermal energy storage are topics of research interest in their own right, chapters 2 and 7 have been subdivided into three sections covering heat pumps, heat storage devices and integrated heat pump/heat storage systems.

Layout of Thesis

The first section in chapter 2 presents a brief introduction to the principles governing heat pump operation, some design considerations and notes on the control devices necessary to guarantee optimal performance. The remainder of the section discusses heating system economics (including determination of space heating and DHW load), evaluation of heat pump performance and a brief review of current heat pump research activities. The second section of chapter two firstly discusses the three main thermal energy storage technologies, and then the characteristics of phase change heat storage in particular. This section concludes by reviewing the development of latent heat storage devices in general and the performance of selected prototype latent heat stores. In the third section, various potential configurations of integrated heat pump/heat storage systems, and several actual systems, are discussed. The final part of chapter two considers the development of thermal storage models including a review of analytical methods for simulating storage devices and the development of a finite difference technique suitable for modelling the performance of the Edinburgh store. A discussion of the heat transfer characteristics for laminar flow in ducts completes the chapter.

The development of the experimental facility is considered in chapter 3, which is concerned with the development of the pilot and prototype storage devices. In addition it discusses the selection of the PCM, the encapsulation technique and the design requirements of an integrated system. The development of the test facility including load, microcomputer system, instrumentation, control and operating software are discussed.

Experimental performance of the two heat stores is presented in chapter 4, starting with a review of the test procedures available and those used in the experimental work. The results obtained from the pilot and prototype stores are then presented. Finally in this chapter there is a separate discussion of the performance of each of the stores.

In chapter 5 the performance of the heat pump is presented, beginning with a consideration of the experimental procedures to be employed both in preparation for and during experimental runs. Heat pump performance is then analysed both for the overall system and for each individual component. Finally, the implications of these performance characteristics are discussed.

Performance of the integrated system is considered in chapter 6. Selected experimental performance data recorded during the development of the experimental system is presented to illustrate operation at typical climatic and load conditions. A discussion of the operating characteristics, experimental problems and recommendations for future work completes the chapter.

Models for simulating the integrated system are developed in chapter 7. This includes development of an enthalpy-pressure diagram model for simulating a heat pump system. Exact analytical solutions for freezing/melting of a superheated/subcooled PCM in a cylindrical geometry are not possible, but an approximate analytical method is derived. Since there is no exact analytical method of modelling the storage device, a finite difference technique was then developed. In the next section, the development of an elementary model of the integrated heat pump/latent heat store is discussed and the economics of such a system considered using the model results. Finally, a detailed model which simulates the integrated system using a combination of the finite difference heat store model and correlations for heat pump performance is developed and evaluated.

Chapter 8 summarises conclusions derived from this work and recommendations for future work.

Chapter 9 is an appendix which contains calibration data for the instrumentation and essential thermophysical property data. A list of the programs employed during the research work are included, and a copy of these is held with the departmental copy of the thesis. An error analysis and the extensive tabulated data which accompany figures 6.6 to 6.9 and figure 7.19 complete the appendix.

Summary of Major Conclusions

(a) Test Facility

Significant effort during this research project was devoted to developing an experimental facility which could control and monitor the operation of a heat store and heat pump. The accuracy and reliability of the test data obtained was limited by the financial constraints imposed on research carried out by a university department. Temperature measurement error (approximately ±0.25% for the extremely small temperature drop across a heat storage device) was considered satisfactory, but the accuracy of the flowmeter (±1.75%) and wattmeter (±2%) could have been significantly improved by the purchase of purpose built equipment. Data analysis could have been speeded up and improved by the use of a microcomputer compatable with the mainframe employed for data processing.

In its final configuration the test facility provided a reasonable method of charging and discharging a prototype latent heat storage device with a heat pump supplying the thermal input and a plate heat exchanger acting as the heating load.

(b) Experimental work with heat store

1. The standard ASHRAE test procedure for evaluating the performance of thermal storage devices requires modification for use with latent heat storage devices of the type developed at Edinburgh.

2. The Calortherm 58 phase change material (PCM) melted at 56°C, approximately 2 degC less than the pure sodium acetate trihydrate, and exhibited subcooling characteristics.

3. It was found impossible to fully utilise the prototype storage device with a

charge temperature less than 62°C and a discharge temperature greater than 46°C.

4. Maximum charge and discharge rates were obtained employing large temperature driving forces, high flow rates and flow assisted by natural convection (i.e. top-down for charge and bottom-up for discharge).

5. Experimental storage capacities were found to be lower (by approximately 8%) than theoretically determined values.

6. It is important to be able to characterise a partly charged heat store especially with respect to its heat transfer characteristics. The use of an overall heat transfer coefficient for this purpose proved unsuccessful.

(c) Experimental work with heat pump

1. Refrigerant leakage from the prototype heat pump resulted in sub-optimal performance during experimental runs.

2. COP was found to improve for lower transfer fluid temperature and higher ambient temperature.

(d) Experimental work with integrated system

1. A significant decrease (approximately 25%) in the performance of the heat pump was observed during the off-peak charge period due to the increasing transfer fluid temperature.

2. It proved impossible to demonstrate operation of the integrated system over prolonged periods due to difficulties experienced in tracking the store condition (UF) accurately.

3. Heat losses (approximately 500 W) from the pipework and storage device, were found to significantly reduce the COP achieved during integrated system operation.

(e) Development of computer models

1. A thermodynamics property package was successfully developed and employed to predict Rankine cycle COPs.

2. Exact analytical models cannot be developed to model latent heat storage in a cylindrical geometry. An approximate method was therefore developed

which satisfactorily simulated (±30%) the pilot storage device but was found unsatisfactory for modelling (±100%) the prototype storage device.

3. For latent heat storage in a semi-infinite slab the Crank Nicolson solution method for solving finite difference equations (FDEs) was found to be less accurate than an explicit technique employing similar computer effort.

4. The constant rate regions expected from a latent heat storage device are much less pronounced in the experimental results than in the simulated data from the finite difference model, however agreement for the standard run is reasonably good. Inclusion of mixed convection heat transfer effects in the finite difference model failed to predict the experimentally determined difference between top-down and bottom-up flow.

5. A reduction of 5% in the annual heating bill was predicted by an elementary integrated system model for a typical domestic application (specified in section 7.4.2).

6. A detailed integrated system model based on the finite difference model of the heat storage device and performance correlations for the heat pump was developed and found to give reasonable agreement with the experimental facility. However excessive computer time limited the potential application of the model.

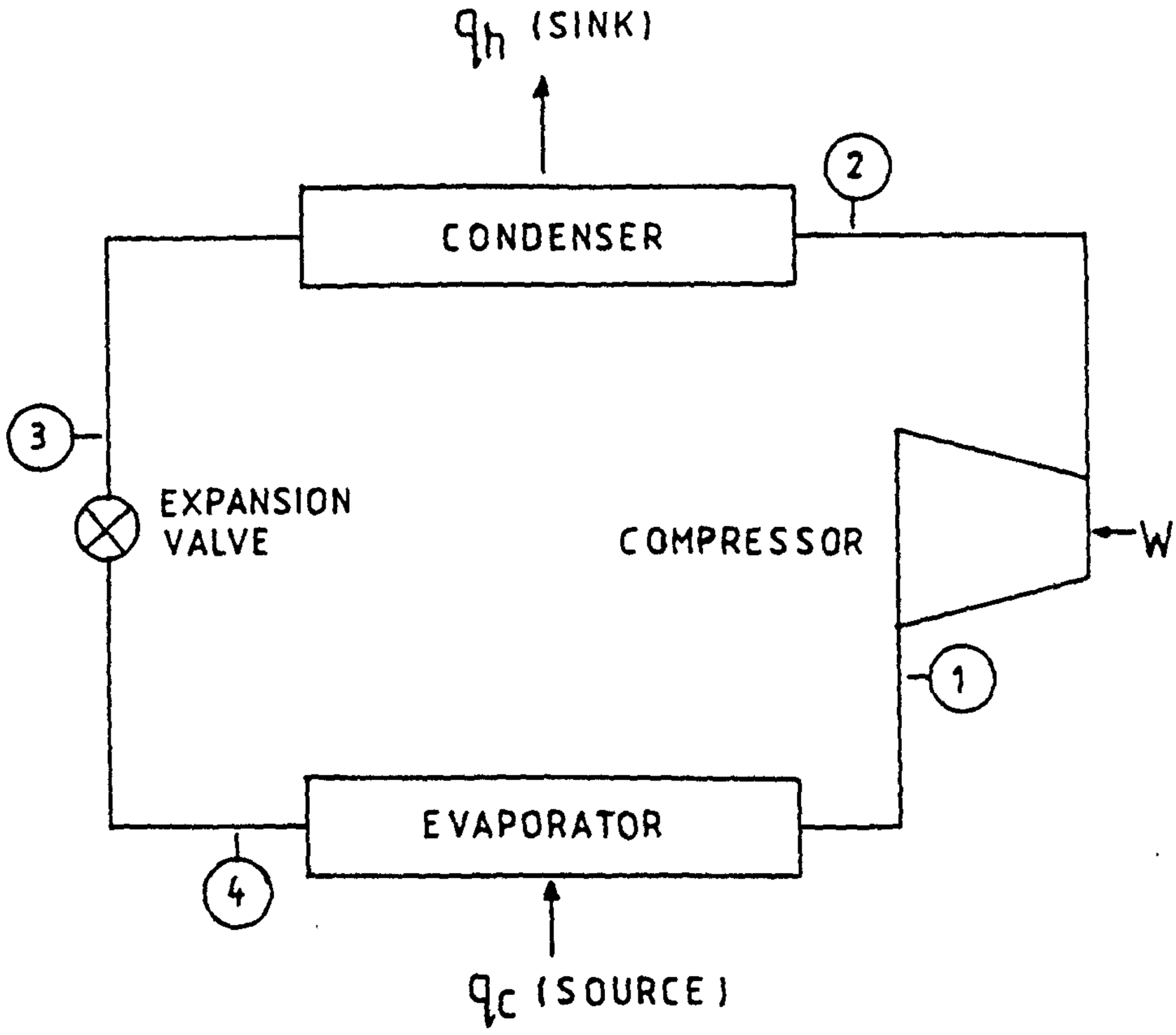

Figure 1.1 Schematic diagram of vapour compression heat heat pump cycle

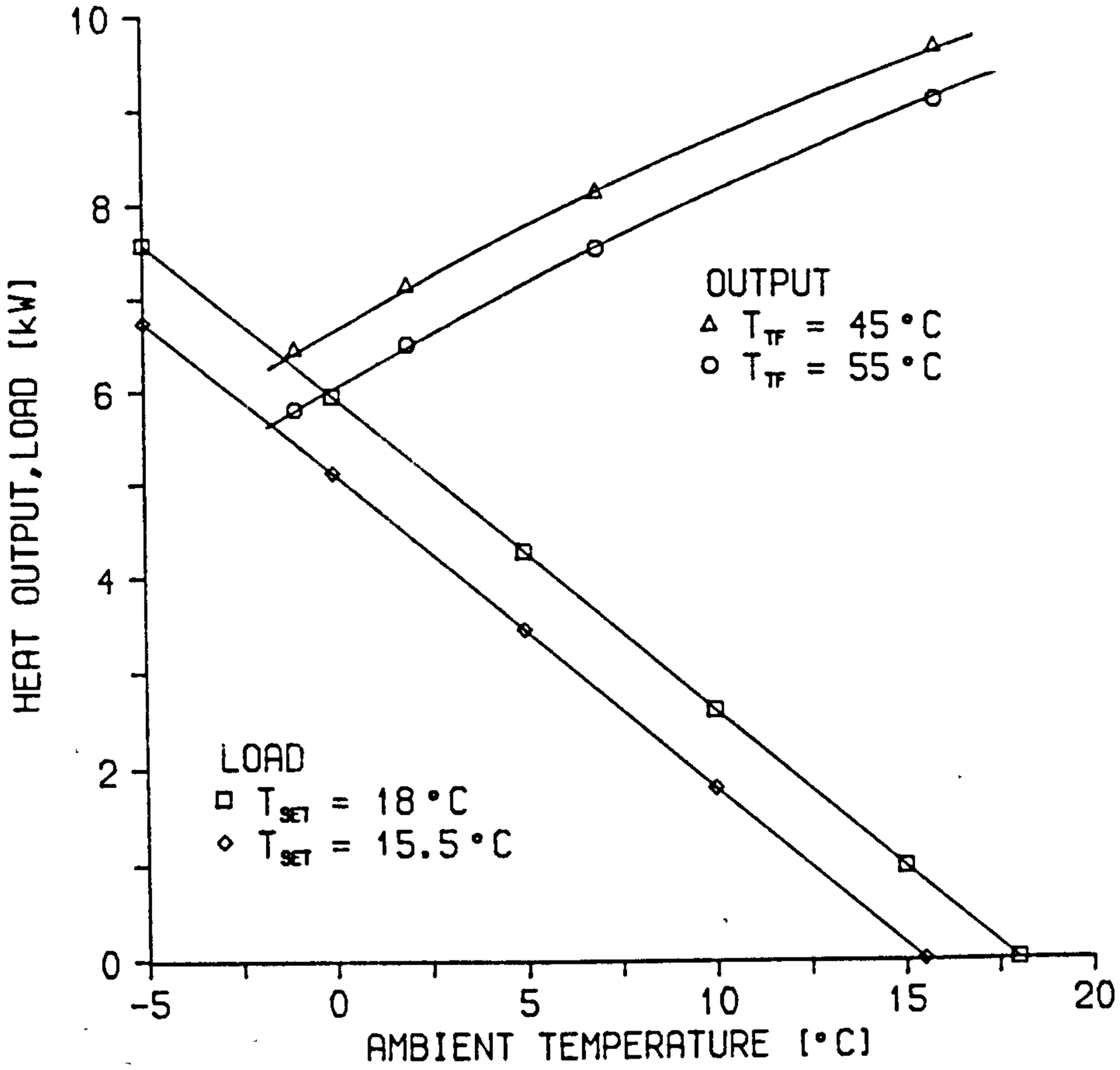

Figure 1.2 Heat pump performance

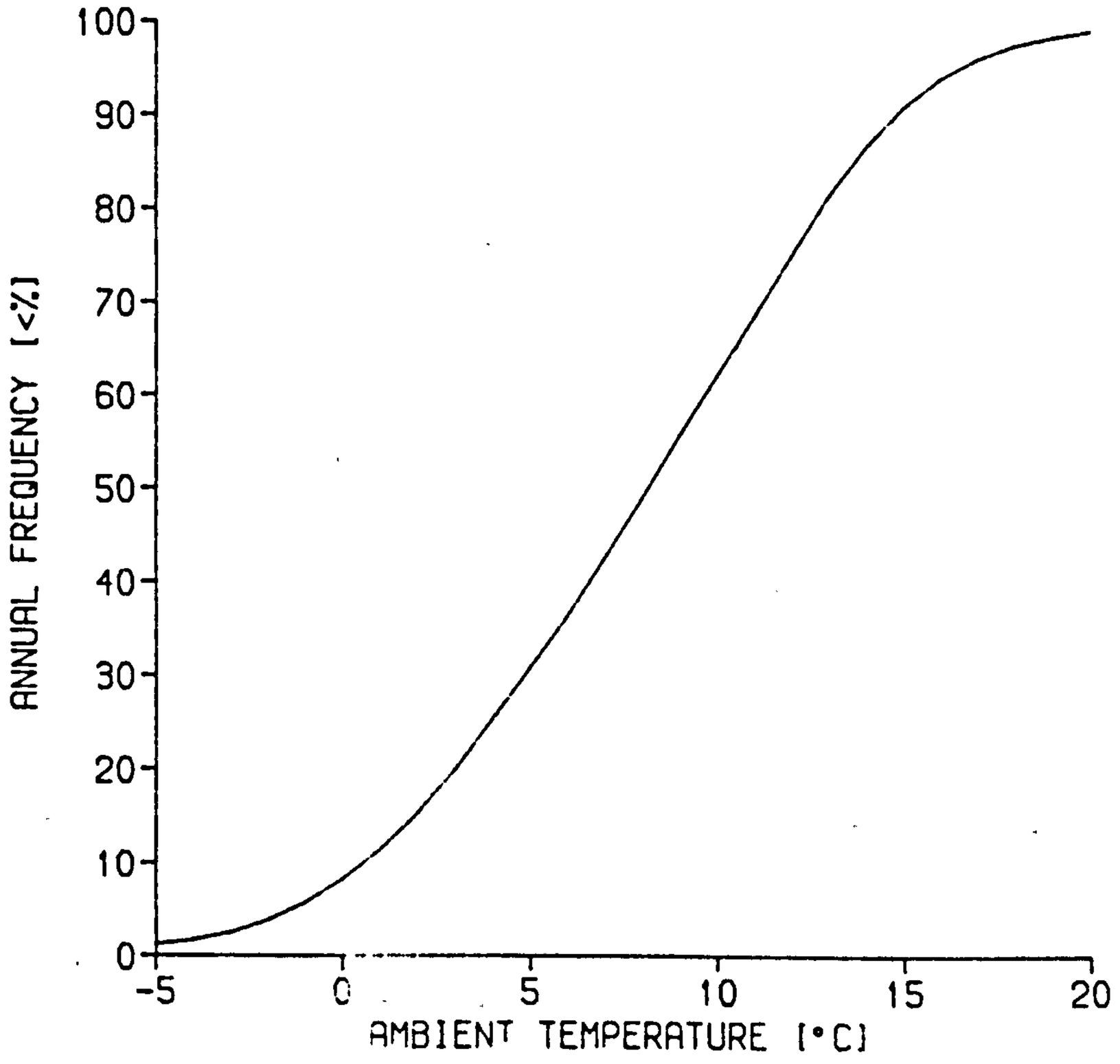

Figure 1.3 Annual temperature distribution for Edinburgh during period 1952-1960 (Data taken from Heap 1977)

Table 1.1 Comparative Heating Costs in Scotland (Winter 1986-87)

		[p/kWh]
Electricity	Standard domestic tariff	5.24
Electricity	Economy 7 rate 2300 - 0730	2.03
	0730 - 2300	5.34
Electric heat pump[1]	Standard domestic tariff	2.14
Electric heat pump[1]	Economy 7 rate 2300 - 0730	0.83
	0730 - 2300	2.18
Oil[2]	13 p/litre, 10.18 kWh/litre	1.82
Coal[2]	15.2 p/kg, 9.05 kWh/kg	2.40
Gas[2]	38 p/therm, 29.3 kWh/therm	1.85

Notes:

1. Manufacturer's specified COP of 2.45 at mean winter temperature (7°C)
2. Data taken from table presented on page 12 of *Solid Fuel*, January 1982, assuming central heating system efficiency of 70%

CHAPTER 2

REVIEW OF LITERATURE AND THEORY

2.1. HEAT PUMPS

2.1.1. Introduction

In order to appreciate the factors affecting the performance of an integrated system it is essential to understand the principles governing heat pump operation. These are explained with reference to theoretically ideal cycles and the differences with real systems then noted. The following may be found in most texts covering heat pump operation; however that presented by McMullan and Morgan (1981) was found particularly comprehensive. The concept of heat pumping is not new, in fact the first design was accredited to Lord Kelvin in 1852. Haldane (1930) however, was the first person to actually build and operate a practical machine which he used to heat his home in Scotland.

2.1.1.1. Reversed Carnot cycle

The heat pump and heat engine may be represented schematically on the same diagram as shown in figure 2.1. In a heat engine, heat is supplied at high temperature to produce work and is then rejected at low temperature. By contrast in a heat pump, heat is supplied at low temperature and work is input before heat is rejected at high temperature. For the heat engine the efficiency is the ratio of the amount of work produced to the input of heat i.e. W/q_h. Now for the heat pump the efficiency or coefficient of performance (COP) is the ratio of heat rejected to amount of work input i.e. q_h/W. Note that it is normal to refer to this ratio as the COP since it is meaningless to discuss an efficiency greater than unity.

The ideal standard cycle for a heat pump is similar to that for the Carnot heat engine and is referred to as the reverse Carnot cycle. This is best illustrated on a temperature-entropy diagram (shown in figure 2.2). The working fluid, a refrigerant, is compressed adiabatically to point 2 before being compressed isothermally (losing heat q_h) to point 3. It is then allowed to expand adiabatically to point 4 before expanding isothermally (gaining heat q_c) back to point 1 and therefore completing the cycle. The COP of the heat pump cycle can then be determined:

$$COP = q_h/W = q_h/(q_h-q_c) = T_h/(T_h-T_c). \qquad (2.1)$$

The expression above is immediately recognisable as the inverse of the efficiency of a Carnot engine. This COP represents the highest possible theoretical performance of a heat pump. Since the Carnot cycle is thermodynamically reversible it means that this performance will be impossible to achieve in practice, e.g. isothermal expansion and compression are impossible, as any real heat exchanger requires a finite temperature difference between working fluid and heat source if it is to work effectively. Even allowing a 5 K difference between the heat source and sink, the COP of a heat pump designed to heat the inside of a dwelling to 20°C (293 K) with an outside temperature of 0°C (273 K) = 298/30 = 9.93. For an electrically driven compressor this implies that only 1 kWh of electrical energy is required to produce 9.93 kWh of thermal energy.

2.1.1.2. Ideal vapour compression cycle

The most common heat pump cycle is the vapour compression cycle (see figure 1.1) which is shown on pressure-enthalpy and temperature-entropy diagrams in figure 2.3. In this cycle the dry, saturated, low temperature, low pressure refrigerant vapour (1) is compressed adiabatically to a high temperature, high pressure superheated vapour (2). In the condenser the refrigerant loses its superheat and then condenses and emerges as a high temperature, high pressure saturated liquid (3). It is then expanded through an orifice where some refrigerant flashes off and finally enters the evaporator as a low temperature, low pressure, low quality vapour (4).

Two irreversiblity losses are apparent in this ideal vapour compression cycle shown in figure 2.3 due to:

1. Isenthalpic throttling process
2. Temperature difference through superheating

The performance of the cycle is easily determined from a pressure-enthalpy diagram since the enthalpies may be read directly from the axis.

$$COP = (h_2-h_3)/(h_2-h_1) \qquad (2.2)$$

2.1.1.3. Real vapour compression heat pump cycle

The cycle shown in figure 2.3 represents an ideal case as the refrigerant must normally be slightly superheated (approx. 5 K) on inlet to compressor. This is because the reciprocating compressors commonly used in heat pumps have a low tolerance for liquid refrigerant. The degree of superheat is controlled by a thermostatic expansion valve which regulates the flow of refrigerant into the evaporator (see section 2.1.2.5). The heat rejected in the condenser can be increased by subcooling the refrigerant; this also improves heat pump performance as more heat is pumped for the same compressor power. However if the condenser is too small then in order to achieve subcooling the condenser temperature has to be increased which cancels out the potential improvement in performance. A better method is to use an intermediate heat exchanger between the liquid line out of the condenser and the compressor suction line. This is often achieved simply by running the two lines side by side and insulating them. In addition to providing subcooling without increased condenser temperature it also superheats the refrigerant entering the compressor, hence increasing the efficiency of the evaporator.

Figure 5.3 shows the operating cycle of the prototype heat pump on a pressure-enthalpy diagram for an ambient temperature of 8.5°C and a circulating water temperature of 63.3°C. The effect of superheating at the compressor inlet, subcooling at the condenser outlet, temperature difference across the heat exchangers and pressure drop through the exchangers (especially the evaporator) can be observed by comparison with the ideal cycle (figure 2.3).

2.1.1.4. Advanced heat pump cycles

In an advanced heat pump cycle the electrically driven compressor is replaced either by an engine-driven compressor or an absorber/generator and circulator pump system. The former requires only minimal modification to the cycle and permits recovery of waste heat from the heat engine.

A schematic diagram of an absorption heat pump cycle is shown in figure 2.4. Low grade heat vapourises the refrigerant in the evaporator causing the transfer of cool refrigerant vapour to the absorber. This vapour dissolves in the absorbent liberating heat of condensation and solution, and the resulting

liquid mixture can then be pumped to the generator. Here, heat is supplied from a high grade source to boil off the refrigerant. The hot vapour refrigerant is passed to the condenser to complete the normal cycle (see 2.1.1.2) while the absorbent is returned via a throttling device to the absorber. Two commonly used absorbent-refrigerant pairs are lithium bromide-water and water-ammonia. The former (where water is used as a refrigerant) is unsuitable for space heating applications using air as the heat source due to freezing of water in the evaporator for low ambient temperatures, while the latter presents difficulties in separation as the absorbent is volatile.

Smith and Carey (see Foster 1981) did some development work on absorption heat pumps for space heating using lithium bromide / zinc bromide (in 2:1 molar ratio) as the absorbent and methanol as the working fluid. This combination was found to decompose (see Aram 1984) and effort was then diverted into finding a suitable fluid pair for the high temperature lift (70 degC) required in wet central heating systems.

2.1.2. Design Considerations

A heat pump is the collective name given to the device used to cycle a working fluid through the processes outlined in the previous section. Selection of the refrigerant, heat exchangers, compressor and expansion device allows a heat pump to be designed for a particular application. In this section some of the criteria which should be considered when selecting heat pump components are summarised. The general design considerations were again taken from McMullan and Morgan (1981) while the specific design details for the prototype heat pump employed were taken from Bartlett and Chabra (1983).

The following considerations should be borne in mind when designing a heat pump.

1. Critical temperature of refrigerant must be above the highest possible condensing temperature
2. Minimum saturation pressure in cycle should be greater than atmospheric to ensure that any leakage is outward
3. Compression ratios between vapour pressure at the evaporator and condenser temperature should be as low as possible

4. Condenser pressure should be as low as possible
5. Specific volume of vapour phase at the compressor inlet should be low and the latent heat of evaporation large to ensure that the volume to be handled by the compressor is as low as possible
6. Saturated liquid line of refrigerant should be steep as this reduces the quality of the vapour at the inlet to the evaporator
7. Condensing temperature should be significantly lower than critical temperature so that latent heat of condensation remains reasonably high
8. Use of single phase electricity to drive an electric motor limits the potential size of the compressor for domestic applications

2.1.2.1. Selection of refrigerant

The choice of refrigerant is governed by its thermodynamic properties although many other considerations such as toxicity, flammability, cost etc. have to be taken into consideration. Of the available refrigerant materials the halogenated hydrocarbons are the most widely used because of their comparative safety and chemical stability. It is impossible to select a refrigerant which exhibits all of the desirable characteristics noted above and a compromise must be sought. In table 2.1 the relevant properties of three commonly used refrigerants R12, R22 and R502 are presented. Note that the refrigerant number represents a systematic code comprised of a three digit number:

1. First digit is number of carbon atoms minus one, if this is zero (i.e. methane derivatives) it is often omitted
2. Second digit is number of unsubstituted hydrogen atoms plus one
3. Third digit is number of flourine atoms
4. "C" is placed in front of number for cyclic hydrocarbons
5. Azeotropic mixtures are represented by numbers beginning with "5", for example R502 is an azeotropic mixture of 48.8% R22 and 51.2% R115

From table 2.1 we can see that higher condensing temperatures can be achieved for R12 at the expense of employing compressors with larger swept

volumes due to the higher specific volume. R12 hermetically sealed compressors are not readily available for a 2-3 kW power input. For comparable condensing temperatures much higher discharge temperatures are experienced with R22 and since oil and refrigerant breakdown occurs at high temperatures, R502 is often selected. Downing and Gray (1972) tested 100 identical heat pumps (except for expansion valves and filters) charging half with R22 and the other half with R502. The maintenance cost and number of failures occuring in the latter were much lower while the capacity was not noticeably affected.

2.1.2.2. Design of evaporator

For air-refrigerant heat transfer, a finned tube heat exchanger with a fan to draw air over the evaporator surface is commonly used. The air-side heat transfer coefficient may be improved by increasing the air velocity. However this would result in a higher pressure drop and therefore require a larger motor which would consequently increase the noise emission from the heat pump. Hence the geometry of the tubes and fins should be arranged to maximise the heat transfer coefficient and minimise air side pressure drop. Blundell (1977) reported that staggered, circular refrigerant tubes with wavy fins on a pitch of 2 mm gave the smallest temperature difference for a given fan power, compared on an equal heat transfer area basis.

The effect of frosting on the surface should also be considered at the design stage. Barrow (1985) showed that while frosting on a plane surface significantly lowers the overall heat transfer coefficient it has almost no effect on a finned surface. The heat transfer coefficient is proportional to the square root of the air velocity, and it can be shown that a 50% decrease in the velocity results in a reduction of approximately 20% in U.

The refrigerant side heat transfer coefficient may also be improved by increasing refrigerant velocity which will inevitably result in higher pressure drops. The refrigerant velocity must also be above the minimum required for oil entrainment. Hence the tube diameter and circuitry must be carefully designed for the particular application. In addition, allowance for adequate drainage of liquid refrigerant must be included if reverse cycle is to be employed for defrost.

Bartlett and Chabra (1983) report that doubling the size of the protoype evaporator and fan/motor combination would increase the heat output and COP by approximately 14% and 7% respectively, while halving it would result in a decrease of similar proportions. They also note that an additional benefit of doubling the size would be that the temperature at which defrost would be necessary would become much lower, thus further improving performance.

2.1.2.3. Design of condenser

In an air-to-water heat pump a liquid-refrigerant heat exchanger is employed as the condenser. Since the condenser removes superheat from the refrigerant vapour exiting from the compressor, counter current flow in a tube-in-tube design is normally selected. This type of exchanger requires inclusion of a separate liquid receiver, an essential feature in the design of any heat pump due to mass flow rate variation with operating conditions. As in design of the evaporator a balance between improved heat transfer coefficient and increased pressure drop has to be achieved. Note that since refrigerant side coefficients are generally much lower than the water side coefficients, the refrigerant side surface area is usually proportionally larger.

2.1.2.4. Design of compressor

A reciprocating compressor is normally used for small scale heat pumps. It is normally contained with its motor in a hermetically sealed outer case which helps reduce noise during operation. Cooling of the electric motor is either by radiation or convection from the case, or by drawing cold refrigerant from the evaporator over the motor on its way to the compressor. In operation these compressors achieve 70% adiabatic efficiency. The volumetric efficiency of a reciprocating compressor is lowered by the necessary top dead centre clearance volume.

Since the compressor is a constant volumetric flow rate process the mass flow rate varies with the density of the refrigerant entering the compressor. If it is assumed that the temperature approach in the evaporator is 8 degC and the degree of superheat 6 degC, the density of refrigerant R502 entering the evaporator for an ambient temperature of -13°C would be 20.2 kg/m^3 (see table 2.1). Increasing the ambient temperature to 2°C raises this to 32.5 kg/m^3 resulting in an increase of 60% in the refrigerant mass flow rate. If the latent

heat remains approximately constant then the heat input to the evaporator must increase. The compressor work input also increases (although there is a net decrease in work per unit mass) resulting in a much greater amount of heat to be rejected in the condenser. The refrigerant side heat transfer coefficient will increase with the mass flow rate to the power of 0.8 while the overall coefficient will be somewhat less dependent. Hence the temperature difference between the condenser saturation temperature and the inlet transfer fluid temperature must increase, thus reducing the COP. Therefore compressor capacity modulation (i.e. controlling refrigerant mass flow rate) would result in lower loading on heat exchangers and compressor thus improving performance and reliability.

Several methods of compressor capacity modulation have been considered including:

1. Hot gas by-pass
2. Clearance volume control
3. Speed control
4. Valve control

The first method returns a fraction of the hot discharge gas straight back to suction which results in the compressor performing unnecessary work. The idea of a variable capacity cylinder is attractive but presents all sorts of practical problems. Tassou et al. (1983) considered compressor speed control to be the most promising method of employing capacity modulation in residential and small commercial heat pumps. They found that a capacity modulated system limited to a speed reduction of 50% due to lubrication requirements could offer more than 10% improvement in energy utilisation efficiency over a conventional fixed speed unit. The single phase a.c. motor normally employed in domestic heat pumps would be incapable of speed reduction without expensive electronic circuitry to vary the frequency of the supply. Hillier and Glicksman (1976) developed an ingenious device to limit the flow rate of refrigerant through the compressor by early closing of the suction valve. The refrigerant drawn into the compressor was thus first expanded and then compressed, which is much more efficient than late discharge valve closing which throttles the refrigerant. This device was tested on a medium size compressor (10 kW) and found to have an unacceptable

power requirement of about 15% of total reduced power, hence it is most likely to find application in large compressors (>10 kW).

2.1.2.5. Design of expansion device

A thermostatic expansion valve (TEV) is normally used as an expansion device in heat pump applications as the variation in control requirements is likely to be too large for the ordinary capillary tube commonly used in refrigerators. The TEV not only reduces the refrigerant temperature and pressure but also controls the flow rate of refrigerant to the evaporator by sensing the vapour pressure in the bulb B (see figures 2.5 and 3.10). If the pressure in bulb B is higher (lower) than that in the system then the diaphragm opens (closes), thereby increasing (decreasing) the refrigerant flow. This expansion device is normally employed to maintain a certain degree of superheat at the inlet to the compressor and this is achieved by adjusting the tension in the spring so that the vapour pressure in the bulb has to be greater than that in the system by the degree of superheat. When designing a TEV it is important to size the orifice correctly. If it is too small, then the refrigerant flow will be too low to fully utilise the evaporator, while if the orifice is too large "hunting" will occur: e.g. if excessive superheat is detected the valve opens up and allows more refrigerant to enter than can be boiled in the evaporator, thereby allowing a slug of liquid to arrive at bulb B which causes the valve to close abruptly.

2.1.3. Controls

A heat pump is a comparatively complicated domestic heating system and its variation of output over the range of operating conditions requires that it be equipped with numerous control devices. The designer of an integrated system must be familiar with these controls and a brief description (see McMullan and Morgan 1981) is given of those commonly found on domestic heat pumps to:

1. Operate system safely
2. Start heat pump without excessive current surge
3. Activate defrost after build-up of ice on evaporator
4. Supply correct load

2.1.3.1. Safety controls

Refrigerator systems are normally fitted with high and low pressure cut outs. The high pressure sensor is located on the compressor discharge so that in the event of no water flow (e.g. circulator failure) the resulting rapid rise of discharge pressure can be used to cut out the compressor. A low pressure sensor is employed to detect a drop in pressure in the compressor suction line e.g. due to loss of refrigerant. Both of these controls can either be manually or automatically reset. From the manufacturers' viewpoint neither sensor should cause a cut out unless a fault has occurred, in which case frequent cycling on these controls could occur if fitted with automatic reset. However, either too high or too low a pressure could be temporary or the result of extreme operating conditions, thereby justifying an automatic reset. An excessive compressor discharge temperature can cause oil and refrigerant breakdown, hence a thermostat is normally clamped to the compressor discharge pipe.

2.1.3.2. Motor Starting Controls

The squirrel cage induction motor is favoured for hermetic compressors because it is brushless, which avoids the problems of brush maintenance or decomposition of the oil or refrigerant by sparks. An induction motor is effectively a transformer in which current is induced in the windings of the rotor by induction from the static coils or stator. The resulting current interacts with the magnetic field of the stator to produce a torque. For a single stator winding connected to a single phase supply, two torques are generated which rotate in opposite directions and in fact cancel each other out at zero rotor speed. Hence it is necessary to give the rotor an initial starting speed before a net torque arises. One commmon method of generating an initial starting torque is to feed an auxiliary winding (wound 90° out of phase with the main winding) via a capacitor with current which is also out of phase with the main winding current. The two phases will only be at right angles for one particular load and there will be a significant unbalance during starting, when the non-ideal phase relationship gives a poor starting torque. This may be corrected by connecting another much larger capacitor in parallel for a period of a second or two during starting. Since this capacitor is only for intermittent duty a large AC electrolytic capacitor is suitable.

Now during the start up period the motor is less efficient as electrical energy is consumed in speeding up the rotor against its mechanical inertia. This and the need to energise the auxiliary winding, results in a starting current which is much greater than the normal running current and quite unacceptable to the electricity generating authorities. One method of reducing the starting current is to place a resistor in series (see figure 2.6) with both windings. However this requires to be shorted out rapidly as it otherwise causes excessive power dissipation. The introduction of a resistive component in the phase diagram causes both current vectors to rotate back towards the voltage vector thereby adversely affecting the phase relationship. Although this leads to a serious reduction in torque it is very cheap to implement and is therefore often used.

Various relays and timing devices are therefore necessary to take the starting resistor out of circuit after start up. The decreased starting torque necessitates a method of equalising the pressure across the compressor at start. This is normally achieved by the use of a solenoid valve. Note that both the starting capacitor and resistor are prone to overheat if used too often so the number of starts per hour is normally restricted.

An alternative method of avoiding this starting surge is tc utilise a 3-phase motor. However while a 3-phase electricity supply may be buried underneath most main roads it can be expensive (see Armor 1981) to have it installed inside a house. This problem has recently been overcome by Chieftain Industries (based in Livingston) who have developed a wave generator control system which converts single phase supplies to 3-phase. The controller, which is a solid state electronic device, gradually steps up the power in the first few seconds after start up, preventing a surge of power.

2.1.3.3. Defrost controls

A method of removing the build-up of ice which occurs whenever the evaporator temperature is below freezing point is essential for satisfactory operation of the heat pump. The reverse cycle technique is generally favoured since it defrosts very rapidly and thoroughly. The reversing valve however is an expensive piece of equipment and direct electric heating is often considered as an alternative. During reverse cycle the fan is switched off and the condenser becomes the evaporator and a second expansion device is

required to control flow into the condenser which now behaves as the evaporator (see figure 3.10). The primary disadvantage is the cost and poor reliability of the reversing valve. Bartlett and Chabra (1983) report that a COP of 2.5 can be achieved during a defrost period and even allowing for replacement of heat taken from the circulating water system is still over 1.4, which is a significant improvement on direct electric heating whose COP can only be 1.0. It is important to minimise defrost time to prevent freezing of water in the condenser and to keep overall COP high, so a timer is often used as an alternative method of terminating defrost.

Three methods of initiating and terminating defrost are presented by Dicker (1978):

1. Time initiation and termination
2. Temperature initiation and termination
3. Air pressure initiation, time/temperature termination

The first method simply initiates defrost at a set frequency for a specified period if the ambient temperature falls below a certain value. This is inefficient as defrost requirements will change with external climatic conditions. The second method utilises the fact that as ice builds up on the coil the temperature difference between the air and coil increases. Once reverse cycle has been initiated the coil temperature rises and the defrost is terminated. In section 2.1.2.2 it was noted that it is actually reduced air flow across the evaporator which lowers the performance during frosting conditions; hence using the air pressure drop across the evaporator appears to be an attractive technique. A timer must be included in this circuit to ensure that wind gusts don't cause premature defrosts. Problems can also occur due to blockage by leaves etc.

2.1.3.4. Optimum operation controls

The heat pump water flow temperature, and consequently the condensing pressure, can increase so that the heat pump is performing very inefficiently but is still well within the limits of the safety controls. Hence a thermostat sensing water temperature is normally fitted on the water flow leaving the condenser. However, this temperature will drop rapidly as soon as the heat

pump is switched off and therefore the differential must exceed the highest expected drop, to prevent rapid switching. Selecting a value for this differential is difficult as increased heat output (due to favourable operating conditions) and decreased flow rate would both allow the temperature drop to become very large. A time delay relay is often included to prevent rapid switching caused by the above problems. It is obvious here again that a relatively high volume of water in a buffer tank is advantageous as it would reduce the frequency of cycling in the cases above.

2.1.3.5. Demand controls

An air-sensing thermostat suitably placed within the building is normally used to switch the heat pump on and off as required. Similarly, if being used to supply domestic hot water, a thermostat is placed in the hot water tank.

It is quite likely that the heat pump will not be designed to supply the demand for all ambient conditions. Instead there will be an ambient temperature (referred to as the balance point) where the heat pump output exactly matches the load, usually between -2 and 2°C in the UK. When the ambient temperature falls below this setpoint, supplementary heating will be required. Since the mean temperature only falls below zero on nine days per year, electrical resistance heating can be utilised without significantly increasing the running costs. An ambient temperature sensor could be employed to switch on auxiliary heating as required.

In common with any domestic heating system, a programmable timer would normally be included with a heat pump control system. There is however an important difference between a gas-fired boiler and a heat pump. The conventional gas-fired boiler may well be capable of supplying in excess of 15 kW since there is little additional capital cost in doubling the size of the boiler. This excess capacity over normal maximum load of 7.5 kW permits a rapid warm up from cold, and hence the heating system can happily be switched off during the night. With a heat pump, where it will be at best costly if not impossible to double its thermal output, the warm-up from cold will be slow and improved comfort may be achieved by employing night set-back controls. This would mean lowering the set point by 5°C for the overnight period, which would result in an overnight heat loss from the dwelling but give a rapid warm up the following morning.

2.1.3.6. Application of microcomputer

A heat pump in any form is more complex and expensive than a boiler or storage heater. Its control is therefore more important to ensure safe, reliable and economic operation, and therefore lends itself to a microcomputer-based control system. All the functions previously described could be improved using such a system connected to relays and electronic transducers. For example, a controller with programmable logic could be usefully employed to determine optimal initiation and termination of the defrost cycle for a wide variety of climatic conditions. Fischer (1980) suggests that a controller equipped with a non-volatile memory for storage of recent historical performance data could be an enormous benefit to service technicians for post-failure analysis.

2.1.4. Heating System Economics

A thorough investigation of the economics of a heat pump-based central heating system is beyond the scope of this thesis. However, an evaluation of the benefit which may be achieved by the integration of a heat storage device into such a system necessitates an explanation of how the design load of a dwelling is calculated and an appropriately sized heat pump selected. Since the selection of any heating system is inevitably based on economic considerations standard methods of determining the cost effectiveness are reviewed.

2.1.4.1. Calculation of space heating design load

It is extremly difficult to define a typical heat load for a dwelling, as it is a function of several independent parameters:

1. Size of dwelling
2. Individual definition of comfortable room temperature
3. Heat loss coefficient
4. Ventilation rate
5. Casual heat gains from occupancy and solar radiation
6. Thermal capacity of fabric

Rosell et al. (1982) in their simulation study considered a bungalow with a

floor area of 100 m^2, while the three bedroomed end-terrace house simulated by Henderson (1982) had a total floor area of 85 m^2. Case examples of buildings utilising heat pumps presented by Armor (1981) have floor areas ranging from 120 m^2 to farmhouses (with three stories and five bedrooms) of 242 m^2.

The rate of heat loss from the dwelling is extremly sensitive to the internal temperature setpoint, typically specified (see Armor 1981) to be 21°C in the living room and 15.5°C in the bedrooms. In experimental testing (Mountford and Freund 1982) and in simulation studies (see section 2.1.5.3) the internal temperature setpoint is assumed constant throughout the dwelling at 18-20°C.

Henderson (1982) presents the thickness of each building fabric utilised in the construction of the roof, ground floor, party walls, ceiling and external walls (of a highly insulated dwelling) and derives the overall heat transfer coefficient for each. Heat transfer coefficient values reported by Rosell et al. (1982) were generally found to be higher (i.e. 'typical' insulation) and the effect of windspeed on the coefficient was considered. The latter values were employed in table 2.2, to determine the heat demand of a dwelling with a floor area of 10 m x 10 m, height 2.5 m and assuming that windows accounted for 20% of the total wall area.

Mountford and Freund (1982) assessed the air leakage of the house under investigation by the pressurisation method and found that 21% was through the windows (not draught stripped); 8% through doors and hence attributed approximately 70% to general leaks in the fabric. They calculated that the infiltration rate was equivalent to 1.3 air changes per hour (at the mean windspeed of 3 m/s). Henderson (1982) in his simulation utilises ventilation rates between 0.5 and 2 air changes per hour, and notes that the actual value will be dependent on occupant behaviour in opening windows. Rosell et al. (1982) employed a ventilation rate of one air change per hour and this value was used in the derivation of a typical demand shown in table 2.2.

Henderson (1982) specified the casual gains in terms of energy inputs to each zone (bedrooms, kitchen, living and dining room) for a 4-person hypothetical occupancy pattern which resulted in a total daily input of 15 kWh. A microprocessor was programmed by Mountford and Freund (1982) to

activate lights and heaters in order to simulate heat gains from people and appliances. This microprocessor was even used to open and close curtains (lowering heat loss through windows) at apppropriate times! Two typical casual gain profiles were used: "heavy" for a family with children at home (16 kwh/day) and "light" for a family with children at school and both parents working (14.5 kWh/day). Rosell et al. (1982) describe a method for including gains by solar radiation transmitted through the windows. A simpler method (described by Neal 1983) is to assume that for an external temperature greater than 15.5°C the casual and solar gains will keep the dwelling at the specified comfort temperature of 18°C. The effect of this on the calculated heat load (table 2.2) is shown in figure 1.2.

There is no easy method of accounting for the thermal inertia of the fabric and Rosell et al. (1983a) reported that this accounted for the poor correlation between simulated and actual performance during the night set-back period. The daily performance however is not affected by this omission and excellent agreement (0.8% error) was achieved between the actual and simulated electricity consumption over a three month period.

2.1.4.2. Domestic hot water load considerations

Heap (1983) specifies that a typical domestic hot water (DHW) load for a British dwelling is 10 kWh per day, while Anderson et al. (1985) in their study in NZ considered 5000 kWh per year (13.7 kWh/day) to represent a high category user. The typical demand profile of such a user, reported by Anderson et al. (1985) is shown in figure 2.7.

Carrington (1982) notes that the required hot water flow temperature in Europe (50-55°C) is lower than in the US (60°C) but is still comparatively high for favourable heat pump operation. During winter the average ambient temperature is 7°C which means that a DHW requirement of 10 kWh will be equivalent to a daily run-off of 182 litres. Mountford and Freund (1982) simulated occupancy in their test house with a daily draw-off of 54-70 litres from a cylinder with a capacity of 120 litres. Anderson et al. (1985) assessed heat pump water heaters in New Zealand and utilised 110 litre tanks in their test houses. A larger tank would permit full utilisation of off-peak electricity tariffs but reduce efficiency due to heat loss.

Hirst et al. (1979) in their study of alternative technologies for US residential water heating conclude that the commercialisation of heat pump water heaters might save 5% of the expected water heating energy use in the year 2000. Air-to-air heat pumps are already well established in the US (due to reversible action which permits both heating and air conditioning functions) as space heating systems, hence the heat pump considered in the above study is a small air-to-water DHW only unit. Carrington (1982) who also considered a DHW only heat pump compared two different flow configurations for the condenser: (1) passive immersion and (2) active circulation. In the former the condenser coil is actually located in the DHW cylinder where natural convection currents cause the tank to become well mixed. Consequently the saturation temperature will vary with the average water temperature; thus increasing the COP for low water temperatures and limiting the maximum water temperature to less than 5°C below the saturation temperature. In the active circulation configuration, cold water is drawn off from the bottom of the tank and heated in a counter current tube-in-tube heat exchanger. Hence for a condenser of sufficient capacity the water temperature can be increased beyond the saturation temperature by removal of superheat from the refrigerant. In normal process heat transfer, it is not generally good practise to design a condenser so that the coolant temperature crosses the dew point of the condensing fluid as the desuperheating region is then dry, which dramatically reduces the film coefficient; however the physical limitations imposed on the heat pump make it worth considering. The inlet water to the condenser will be typically 5-20°C, which means that the refrigerant may be subcooled, hence improving the cycle efficiency.

2.1.4.3. Sizing considerations

The seasonal performance of a heat pump based central heating system is crucially dependent on the size of the unit selected. A heat pump which can meet the severest demand placed on it will be grossly oversized (and hence inefficient) at lower loading. This is true, to some extent, for other heating systems (e.g. gas boilers) but the problem is exacerbated with heat pumps due to the associated additional capital cost.

A guide to good practise (see HVCA 1983) regarding heat pumps for domestic applications published by the Heating and Ventilating Contractors

Association (HVCA) recommends that a heat pump should be able to cope with heat losses from the building at an ambient temperature of -1°C. In figure 1.3, it is shown that the temperature in Edinburgh falls below -1°C for a total of 500 hours (5.71%) of any one year. Two methods are available for maintaining comfort conditions below this temperature:

1. The householder accepts that the heat pump is unable to cope with heat losses from the whole dwelling and hence isolates radiators in unoccupied rooms
2. The designer provides an auxiliary heating source to cope with the extra demand

If the former is selected then the heat pump compares very unfavourably (from the consumers point of view) with conventional gas fired systems which are normally sized to cope with heat losses for the coldest expected ambient temperature (-5 to -10°C) with little additional capital cost penalty.

Bivalent heat pump systems (those where auxiliary heating is required below the balance point) may be subdivided into: (1) supplementary parallel and (2) supplementary alternative systems. In the former, an auxiliary heater is placed in the water flow circuit and is activated if the flow temperature falls below a critical value. An electric resistance heater is likely to be used to keep additional capital cost low, but care must be taken to ensure that high temperature water cannot enter the heat pump condenser and trip out the heat pump. For the latter, control valves are positioned in the circuit to divert flow through an auxiliary heater as soon as the heat pump is incapable of supplying the full demand. Often an existing fossil-fuelled boiler can be used for this purpose, which minimises additional capital cost. Utilisation of direct electric heating results in a low load factor consumer of electricity during peak demand periods and hence neither scheme would be attractive to the generating authorities.

The overall seasonal performance of a heat pump is often determined by the "temperature bin" method. Meteorological data for a particular location is used to find the number of hours that the ambient temperature is within ±0.5°C of a temperature in the range -5 to 20°C. Hence if the loss coefficient for a particular dwelling is known the yearly heat load corresponding to each

ambient temperature can be calculated and used to find the yearly heat demand. Since the performance of the heat pump is known as a function of the ambient temperature the yearly power input can also be determined. Seasonal COP is then simply the ratio of annual heat demand to annual power input. Heap (1977) presents annual temperature distributions for Croydon, Pembroke Dock and Edinburgh.

2.1.4.4. Cost effectiveness

Butler (1985) assessed the cost effectiveness of heat pumps in highly insulated dwellings as part of the research program into heat pumps being carried out at the Building Research Establishment. He concluded that the present savings in running costs of heat pumps compared with most conventional heating systems did not justify their extra capital cost. However if a 40% reduction in capital cost, a 43% increase in performance or smaller improvements in both were achieved then the heat pump would become a cost effective replacement for fossil fuelled heating systems. This study was particularly concerned with highly insulated dwellings where a larger proportion of operation will be at low ambient temperature which lowers performance. It also only considered monovalent heat pump systems which are known to have substantially greater capital cost (see section 2.1.4.3). A discounted cash flow method was utilised to account for the capital cost of the heating system with an interest rate of 5% which is the standard value used for public sector investment in energy supply capacity. It was assumed that the heat pump was connected to an economy 7 meter and operated on 63% peak / 37% off-peak electricity.

A prototype heat pump with a small thermal output (2 kW) similar in size to a conventional storage heater is claimed by its inventor, Dr Keith Cornell from Heriot Watt University, to be 62% cheaper to run than electricity and 10% cheaper than gas. A production line was opened in North Berwick to produce the first commercial units which has subsequently been taken over by a Dundee company.

Several case examples of heat pump installations which have given simple payback periods of ten years or less were cited by Armor (1981). The complexity of heat pump based central heating systems is reflected in the fact that half of the sample cases presented were in the homes of retired

engineers. In one case the evaporator was positioned in the loft to extract heat lost through the ceiling, an option not advertised by most manufacturers due to the difficulty of installation. One case example reports on a bivalent supplementary air-to-air system installed in a large house. A faulty controller (designed for US climate) initiated defrost unnecessarily (1400 times in one year!) and also switched on auxiliary heating during periods when heat pump was in part load operation resulting in an astronomical heating bill.

Another major cost in operating a heat pump system is maintenance. Heap (1983) records that an early survey of a heat pump service contract scheme showed that the average heat pump could be expected to experience in a fifteen year lifetime five refrigeration circuit failures, four control failures, four fan and motor failures plus one compressor failure. This resulted in an average yearly maintenance cost of 10% of purchase price.

2.1.4.5. Energy effectiveness

When electricity is generated from a primary fuel such as coal, oil or gas the conversion efficiency is known to be approximately 33% (see Neal 1983) and transmission accounts for a further 5% loss. Hence if a primary energy ratio (PER) is defined as

$$\text{PER} = \text{useful total heat output} / \text{primary energy input}, \qquad (2.3)$$

then a direct electric resistance heater has a PER of 0.28. This compares extremly unfavourably with using a fossil fuel boiler, where an efficiency of 0.7 is normal and designs with efficiencies of 0.9 are available but expensive (see Kernan and Brady 1977). Utilisation of a heat pump (with a seasonal COP of 2.5) permits extraction of low grade heat from the enviroment to attain a PER of 0.7. If half of the 67% of heat wasted during the generation of electricity could be utilised in district heating or combined heat and power (CHP) schemes then the overall use of primary energy would be very high at 103%. Chapman (1981) in his study of energy options for Britain suggests that heating systems should be assessed using energy rather than money as a basis for analysis. Hence zero or even negative interest rates could be assumed on the grounds that energy is being produced from finite resources. The energy cost of manufacture of various alternatives should also be

considered in the analysis.

Berghams (1983) in his review of domestic heat pump applications in Belgium notes that where a high proportion of electricity is produced from nuclear power, the relative cost of electricity to oil and natural gas will be extremely significant. It is expected that the finite nature of fossil fuels will cause the price to increase and stimulate growth in the heat pump market, assuming that a payback period of eight years for the additional capital cost in comparison to a direct electric heating system is acceptable. Jacobsen (1983) reports that the government in Denmark has periodically organised schemes with 20-30% support of investment in renewable energy systems, including heat pumps. In Austria, investments in energy conserving schemes such as heat pumps are eligible for tax deduction and electricity tariffs are reduced for heat pump customers (see Reichl 1983). Government aid in the UK is limited to 25% financial assistance for projects registered with the Energy Conservation Demonstration Scheme where the aim is primarily to spark off private investment (see Jonas 1983).

2.1.5. Performance Evaluation

2.1.5.1. Test facilities

The Energy Study Group at the New University of Ulster has been extensively involved in the construction and design of domestic heat pumps. Optimal design requires that the heat pump be tested for a range of climatic conditions and Buick et al. (1977) describe a controlled environment laboratory equipped for this purpose. A pre-fabricated building of area 6 m x 9 m with minimum height 2.5 m was partitioned to provide a 6.1 m square laboratory (with no windows) whose environmental condition was stable to within 1°C and 5% relative humidity. Sample results show an approximately linear relationship (slope 0.04 $^{\circ}C^{-1}$) between COP and increasing ambient temperature. A later paper by Rosell et al. (1983b) describes in detail actual control algorithms utilised to control the environment (for steady state conditions) to within 0.1°C and 1% relative humidity of the desired conditions. This facility was utilised to examine the effect of transients such as on/off switching of the heat pump.

2.1.5.2. Experimental performance

El Meniawy et al. (1981) studied the operating characteristics of a water-to-water heat pump with R22 as the refrigerant. The following correlation expresses the relationship between experimentally measured COP and the temperature lift between evaporator and condenser

$$1-COP^{-1} = 0.9386 - 0.003917(T_{co}-T_{ev}). \quad (2.4)$$

The maximum error was estimated to be 6% for a condensing temperature of 44.6°C.

The prototype air-to-water heat pumps designed by the Energy Study Group were installed in test houses and their performance evaluated as part of the development program. McMullan et al. (1981) reported that the seasonal performance of the units placed in the test houses was found to be substantially better than that achieved under laboratory test conditions. This discrepancy may be explained by considering the effect of the large volume of water in the heat distribution system. During part-load operation the heat pump will be switched off, and when it is switched back on again the radiator panels will slowly heat up towards the design temperature. It is possible that the radiator will not reach its design temperature because it can meet the heat demand at a lower temperature, hence the condensing temperature remains below the design temperature thus increasing the COP. In addition, at a lower condensing temperature the heat pump can deliver more heat than the system is designed for, thus reducing the load factor still further.

Mountford and Freund (1982) monitored the performance of a well insulated house with a heat pump supplying hot water to an underfloor heating system. They found that the COP could be expressed as a linear function of the ambient temperature

$$COP = 2.11 + 0.042T_a, \quad (2.5)$$

for a circulating water temperature of 45°C. The seasonal COP was determined to be 2.3 but estimated to actually be 2.5 if the manufacturer's recommended flow rate (15 lit/min rather than 11.5 lit/min) had been used and the circulation pump electricity consumption not included. In primary energy

terms the heat pump performance was equivalent to a natural gas boiler running at 70% efficiency.

Tassou et al. (1983) investigated the performance characteristics of a variable speed heat pump, sized to meet the heat demand at 2°C at full speed (740 rpm) and the heat losses at 6°C while running at half speed (400 rpm). They found that for ambient temperatures greater than 6°C the heat pump running at half speed showed a 11.4% improvement in COP over the same heat pump running at maximum speed (see 2.1.2.3). When the steady state output of the heat pump exceeds the heating requirements, the unit is cycled on and off to match the load. At the instant that the compressor is switched on, the heating capacity of the heat pump is zero even though it uses electrical energy. A transient period follows where the temperature difference across the condenser was found to approach its steady state value according to the following equation (note that this was independent of air temperature and compressor speed)

$$\Delta T = \Delta T_{SS}(1-e^{t/\tau}). \qquad (2.6)$$

A constant power input to the compressor was assumed and a part load factor (PLF) defined as the ratio of COP during cycling to that for steady state was determined as shown below

$$PLF = 1-\tau/t_{on}(1-e^{t}{}_{on}{}^{/\tau}). \qquad (2.7)$$

The compressor on time (t_{on}) depends on the cycling rate which is a function of thermostat characteristics (typically 3 cycles per hour for 50% load) and the ratio of heat demand to maximum possible output. Hence the actual COP for any temperature may be attained by multiplying the steady state COP by this part load factor.

Tassou et al. (1983) employed the temperature bin method (see 2.1.4.3) to compare the seasonal COP of a capacity controlled and conventional on/off controlled heat pump. They found that the cycling losses could be reduced by 1% (from 6.1%) and the steady state efficiency improved by 9.4% using capacity control. Tassou et al. (1984) further developed this approach to allow selection of the optimal balance point corresponding to highest system

efficiency as a trade-off between cycling losses and losses due to use of auxiliary heating. For the case considered the optimal balance point was determined to be 0°C.

Foxley and Weaver (1981) investigated the discrepancy between laboratory and field performance of selected heat pumps. Several factors important in explaining an observed reduction in performance during field trials were identified:

1. On/off cycling
2. Reduction of water flow rate below manufacturers recommended minimum
3. Reduction of air flow through evaporator
4. Low inertia heating systems e.g. low water content radiators or no buffer tank causing increased on/off cycling
5. Low radiator surface area which forces up the required water flow temperature for a given heat output
6. Poorly set controls e.g. narrow dead bands in thermostats causing frequent on/off cycling
7. Incorrect refrigerant charge

Greater care at the design and installation stage could eliminate factors 2-7, but on/off cycling during part load operation cannot be avoided. Normally laboratory performance data and that quoted by manufacturers is determined with heat pump operating under full load at steady conditions which represents optimal operation. When tested under partially loaded conditions, it was found that a heat pump cycling 4 times an hour had an overall COP which was only 80% of that achieved under continuous operation. They then plotted a curve of heating load factor against the ratio of COP (cycling) to COP (steady state). The seasonal COP was then found using these modified COPs (now accurate for part load operation) by the conventional temperature bin method. A case example was presented for a bivalent parallel heat pump (balance point -1°C) which had a seasonal COP of 2.36 using the steady state values but only 1.80 using the part load approach. The significance of part load operation obviously increases with lower balance points.

2.1.5.3. Computer simulation

In an attempt to verify the discrepancy between actual and test performance, McMullan et al. (1981) developed a simple diagram model based on the refrigerant state point properties. In the model the adiabatic efficiency was taken as 0.65, the volumetric efficiency as 1 and the electric motor efficiency as 0.85. Superheat at the compressor inlet was taken as 5 degC and subcooling at the condenser exit as 0 degC. Temperature approaches at the condenser and evaporator were taken to be 5 degC and 7 degC respectively. The water circulation pump power was not considered and the evaporator fan power taken as 200 W. With the above assumptions the heat pump model predicted similar performance characteristics to the experimental units.

A detailed computer simulation of an air-to-refrigerant heat exchanger was developed by Fleming (1978) and then incorporated in an engine-driven air-to-air heat pump model. Heat exchanger specifications, ambient and internal setpoint temperatures, compression index and clearance volume were required as input to the model. From the heat exchanger area and fan power, the air flow rate and hence the air side film coefficient could be calculated. The condenser saturation temperature was initially assumed to be 12°C higher than the set point temperature and the evaporator saturation temperature 10°C less than the ambient temperature. Refrigerant is assumed to leave the condenser as a saturated liquid (i.e. no subcooling) and expansion is assumed to be an isenthalpic process. The above assumptions specify h_3 and h_4, and h_1 is found by taking the superheat at the compressor inlet to be 4 degC. The mass flow rate of refrigerant and compressor outlet temperature are then determined from the volumetric efficiency (calculated from pressure ratio, clearance volume and compression index) for the compressor. Heat input to the refrigerant and the refrigerant film heat transfer can then be calculated for both heat exchangers and used to calculate the overall heat transfer coefficient between the air and refrigerant. The air outlet temperatures can then be found and the heat transferred to/from the air determined. If the heat flows are not equal then an iterative procedure adjusts the values assumed above (i.e. superheat, evaporator and condenser saturation temperature) until a heat balance is achieved for the complete system.

The model indicated that variable speed resulted in better utilisation of

individual components and hence an improved seasonal COP. However it was concluded that a more detailed model of the compression process would be required as the predicted output power of the heat pump was greater than expected.

Henderson (1982) presents a simulation of the complete heating system where the heat demand of the building is determined from a multiple zone finite difference model which calculates energy flows resulting from meteorological stimuli, ventilation and occupancy. The steady state performance of the heat pump was modelled utilising a detailed model of the 4 basic components. Predicted thermal output and compressor power input were plotted as functions of ambient and water temperature and multiple regression expressions then fitted to the data. Evaporator fan power was asssumed constant at 150 W and equation (2.6) used to predict the dynamic performance of the heat pump. Time constants (τ) of 55 secs and 133 secs were used to model heating systems with rapid and slow response characteristics. A heating season of 7 months is considered using meteorological data running from October 1964 to April 1965. Seven 8-day weather samples distributed over the heating season were employed in the simulation and it was found that the seasonal COP employing the steady state performance characteristic was 2.41. The dynamic model with the fast response had a seasonal COP of 2.33 while the slower response was 2.24, a decrease of 7% in the steady state value normally assumed in this type of simulation.

Rosell et al. (1982) of the Energy Study Group developed a model of their heat pump as part of a complete heating system. The heat pump thermal output and power input were plotted as functions of ambient and water temperatures and regression expressions calculated. The radiators were modelled using simple expressions for radiant and convective heat transfer. Solar gains and heat losses were determined from hourly data observed by the meteorological office. In the simulation, additional heat required to meet the heat demand below the balance point was available in the flow circuit at a COP of unity. It was assumed for simplicity that the boost heater could be controlled to meet the deficit exactly rather than in steps of 3 kW, and that the boosted outlet temperature reached the required radiator temperature which was used to calculate the heat pump performance.

The model was employed to examine the effect of varying heat pump type, radiator area and various insulation alternatives on the seasonal COP and annual energy requirement. Increasing the radiator area by 50% was shown to increase seasonal COP by 10% and therefore reduce annual energy requirement by 10%. Three typical dwellings were considered:

1. Air cavity walls, single glazing
2. Insulated cavity walls, single glazing
3. Insulated cavity walls, double glazing

Insulation of the cavity walls was shown to represent an energy saving of approximately 25% while installation of double glazing gave a further 20% increase in energy savings.

2.1.6. Other Research

2.1.6.1. Reviews of meetings, symposia and collected papers

An open meeting on heat pumps, organised by the Energy Research Support Unit of the Science Research Council and the Energy Technology Support Unit of the Department of Energy, was held at the Rutherford Appleton Laboratories in November 1979. The meeting was well attended with representatives from industry, university and government bodies. Three papers were presented on:

1. Requirements and applications
2. Technical problems and improvements to established technology
3. Direct fired heat pumps

The following discussion resulted in the identification of 30 possible areas of research (see Foster 1980).

Two years later the heat pump panel of the Energy Committee organised a meeting of all those academic groups who were in receipt of a Science and Engineering Research Council (SERC) grant award for research into some aspect of heat pumps. Twelve papers (see Foster 1981) were presented on selected topics from those identified at the open meeting in 1979 including

research into:

1. Stability of working fluids
2. Dynamic performance of heat pumps
3. Development of heat pump with lower operating pressures
4. Development of advanced heat pumps (i.e. absorption and heat engine driven systems)
5. Development of absorption heat pumps with storage capability
6. Free piston expander/compressor for direct fired heat pump

Another meeting of heat pump research grant holders was organised by the heat pump panel at The Cosener's House, Abingdon in June 1983 (see Aram 1984). Nineteen papers were presented on a wide range of subjects including:

1. Ground source heat pumps
2. Control systems and microprocessor controls

in addition to those specified for the 1981 meeting.

Energy World, a monthly publication by the Institute of Energy included a heat pump supplement in the October 1981 issue. Eight papers were presented including an introduction to the theory, prospects in the UK, Western Europe and USA, a summary of current research on electrically and gas engine-driven heat pumps, in addition to a list of current academic research programmes.

The Institute of Energy held a one-day symposium on "Prospects for Domestic Heat Pumps" at the University of Warwick, in September 1983. Papers were presented by manufacturers on a variety of practical topics covering standards in testing, installation and approval, field experience, engineering development, controls and market prospects. A paper on heat pump futures discussing gas engine drives and thermal storage by Buick and Smith of Cranfield was the only contribution from an academic establishment.

A recently introduced publication called *Energy Management Focus*

considered heat pumps in its first issue of April 1985. Two interesting items on absorption and engine driven heat pump systems were included in its research section. The first reported on a prototype fossil-fuelled absorption heat pump developed by Calor, with a targetted COP of 1.25. In the second a prototype engine driven heat pump, designed and built by Task Power and Control Ltd., is reported to be capable of delivering 12 kW of heat (for an ambient of 1°C) to a space heating circuit at 70°C.

2.1.6.2. Industrial applications

This study was primarily concerned with domestic heat pump applications since domestic space and water heating consume some 19% of the national energy used per annum (see Neal 1983). Industrial process heating also consumes a significant proportion (8%) of the national primary energy. This may be broken down according to the temperature at end use; 0.125 is below 80°C, 0.375 between 80 and 200°C and the remainder greater than 200°C. At present the upper operating temperature of most heat pumps is below 100°C although the refrigerant R114 can be used at temperatures up to 130°C. A significant amount of research effort is presently engaged in investigating the stability of high temperature working fluids.

Two processes in particular have been identified as being particularly suitable for heat pump operation: (1) drying and (2) distillation. Significant research effort has also been directed to the development of heat pump systems suitable for the heating and dehumidification duties of municipal swimming pools.

2.2. THERMAL ENERGY STORAGE DEVICES

The design of the Edinburgh integrated system was based on a latent heat store containing a salt hydrate. Alternative heat storage systems are considered in this literature review to demonstrate the strengths and weaknesses of the system selected. An excellent historical review of thermal energy storage is given by Lane (1983).

2.2.1. Introduction

Increased awareness of the limited availability of conventional fuels has created interest in alternative energy sources. These alternatives, unlike the conventional energy sources, are not available to be converted into thermal energy on demand. For example, solar energy is normally available exactly out of phase with demand. Hence in order for these alternatives to become acceptable, methods of storing thermal energy must be developed.

2.2.1.1. Sensible heat storage

In sensible heat storage, thermal energy is stored by changing the temperature of the storage medium.

$$Q = MCp\Delta Tp \qquad (2.8)$$

Due to its extremly high specific heat (4.186 kJ/kgK), water is often selected as an energy storage medium. If water is also employed as the heat transfer medium, a high system efficiency is achieved since heat transfer occurs at only one interface. However if the store is to be interfaced: for example to a solar collector, then an antifreeze mixture heat transfer medium has to be employed (to avoid freezing), in which case a heat exchanger in the storage tank will be required.

Bell et al. (1983), working at Cranfield, are among many researchers developing stratified water stores for integration with solar heating systems. During discharge the water returning from the heating system will be colder than the bulk store temperature and can therefore be piped directly into the bottom of the store. In the charging process the water will leave the solar collector at a variable temperature and must therefore be encouraged to find its own temperature level to maintain stratification within the store. Various

methods of achieving this are presently being investigated. A perfectly stratified or a well mixed water store is often employed as a basis of comparison for other thermal energy storage devices.

Pebble beds have also been selected as an energy storage medium despite their low specific heat (0.88 kJ/kgK). Their energy storage density is further decreased since they must be designed with adequate void volume to prevent excessive pressure drop. This is offset slightly by a relatively high specific gravity. A 7 m^3 store (95 kWh) was developed and tested by the National Bureau of Standards in Washington (see Jones and Hill 1979).

The most commonly used form of sensible heat storage is the familiar night storage heater. These have been commercially available for over 30 years and sales in the UK were reported by Eeles (1981) to have steadied at 100,000-150,000 units per annum, down from a peak of 500,000 in 1972. Room radiator storage heaters have a core of feolite (iron oxide brick) which is charged, using a resistive heating element, up to 800°C overnight to take advantage of off-peak electricity. Storage densities of 167-222 kWh/m^3 are claimed for a feolite core with microporous silica insulation. A major problem with storage heaters is the uncontrolled heat loss by natural convection through the case. New designs have better insulation and the bricks are arranged so as to form vertical channels with a hinged flap (activated by an external temperature sensor) to control the heat output. Some development work has been carried out on central stores; but there is little demand since the main attraction of storage heaters is simple installation and suitability for individual room heating.

Since sensible heat storage requires a significant temperature interval to minimise volume, controlling the heat output is a common design problem.

2.2.1.2. Latent heat storage

The reversible solid-liquid phase transformation is the most commonly used form of latent heat storage.

$$Q = M[\lambda + Cp_s(T_{mp}-T_o) + Cp_l(T_o+\Delta Tp-T_{mp})] \qquad (2.9)$$

Liquid-vapour phase transformations are not suitable for heat storage

applications because of the associated large volume change. The differences between latent heat storage and the much better understood sensible heat storage is best illustrated by an example. Consider two 1 litre containers; the first is filled with water at 80°C, and the second with molten sodium acetate trihydrate at 60°C. The former is too hot to touch and the latter is just too hot to hold comfortably. On being cooled to 50°C the former releases 0.125 MJ while the latter releases almost three times that amount, 0.36 MJ. Hence it may be concluded that latent heat storage offers the following advantages:

1. Improved energy density which permits design of lighter, more compact thermal storage units
2. Lower storage temperature and consequently less heat loss for similar levels of insulation
3. Almost isothermal operation, permitting simpler controls and design applications

A comprehensive list of candidate latent heat storage materials is presented by Lane (1983) in chapter two of his book covering the background and scientific principles of solar heat storage. The characteristics and performance of latent heat storage devices are considered in subsections 2.2.2 - 2.2.4.

2.2.1.3. Thermochemical heat storage

The potentially most favourable method of storing heat is that based on thermochemical heat storage,

$$Q = M\Delta h_r \tag{2.10}$$

where Δh_r is the heat of reaction per unit mass [kJ/kg]. Perhaps the greatest advantage of this system is that the charged device may be kept at ambient temperature without insulation and still suffer no heat loss. There are significant problems in developing a thermochemical heat storage device. The chemical reactions selected must have a high selectivity with no by-products and must be completely reversible.

Some of the reactions under investigation include metal hydride decomposition, oxide or peroxide decomposition, metal hydroxide dehydration,

sulphuric acid dilution, ammonium salt decomposition, synthesis gas equilibria and salt complexes. It is not within the scope of this review to discuss this area further but rather to highlight the attraction of a storage device with such a high energy density and low insulation requirement. Wettermark et al. (1979) devote chapter six of their excellent document on heat storage to thermochemical reactions.

2.2.2. Characteristics of Phase Change Heat Storage

There are many good reasons for using phase change materials (PCMs) in heat storage devices. However there are also significant difficulties in actually operating a PCM storage device due to problems associated with the phase change:

1. Reversibility and segregation
2. Supercooling
3. Heat transfer

2.2.2.1. Reversibility and segregation

Congruent melting occurs when only one solid phase is involved and the composition of the liquid and solid is identical at the phase change. In incongruent melting the solubility of the anhydrous salt in water is not great enough to dissolve all the anhydrous salt in the water of crystallisation and consequently there are more than two phases in equilibrium with each other. Considerable research (see Marks 1980) has been performed on the incongruent melting behaviour of sodium sulphate dodecahydrate, better known as Glauber's salt. During melting the solid phase [$Na_2SO_4.10H_2O$] melts to a liquid with a different composition [saturated Na_2SO_4(l)] while a new solid phase of anhydrous salt [Na_2SO_4(s)] is formed. These phases are stratified according to their densities (see figure 2.8). Hence during solidification instead of a homogenous solution which solidifies completely, the Na_2SO_4(s) plus saturated Na_2SO_4 combine to form another solid phase with the original composition $Na_2SO_4.10H_2O$ (see figure 2.8). Unfortunately this is formed at the boundary of the other two phases thus hindering further combination.

Since only part of the PCM is undergoing phase change, its storage capacity is significantly reduced and some method of preventing this

segregation has to be developed. Various methods of preventing segregation have been utilised:

1. Micro-encapsulation, which prevents the layers ever becoming physically separated
2. Addition of a thickening agent, which stops the dense phase from sinking.
3. Extra water principle, which ensures that all the anhydrous salt can be dissolved in the water of crystallisation at the melting point

Micro-encapsulation of PCM in capsules with diameters ranging from 50-500 µm can be achieved using techniques of colloidal chemistry. Mancini (1980) tested various paraffin samples using an accelerated thermal cycling technique and found that capsules with gelatin walls leaked after only 60 cycles. This size of particle is not suitable for operation in the form of a packed bed and is usually employed in the form of a slurry with an effective specific heat two or three times that of water. While this technique reduces the thermal segregation it actually increases the likelihood of supercooling (see section 2.2.2.2)!

Marks (1980) recommends the use of attapulgite clay as a thickening agent for Glauber's salt. It does not eliminate thermal segregation as a consequence of thermal cycling but significantly reduces its effect. Calor's research effort, described by Page and Swayne (1981), concentrated on a range of water-soluble synthetic polymers which could be further reacted in solution with cross-linking agents to form a stabilised gel network. Wada et al. (1984) describe a method of thickening sodium acetate trihydrate using polyvinyl alcohol which resulted in a mixture whose performance remained approximately constant after 500 cycles.

The extra water principle is reported by Furbo (1980) to result in a stabilised PCM storage device. A salt-water mixture (saturated salt solution) with 58% of the anhydrous salt [CH_3COONa] was shown to have a storage capacity of approximately 360 MJ/m^3 between 48 and 68°C.

2.2.2.2. Supercooling

Supercocling, the inability of a melt to solidify at its melting point, is most common when the PCM is very pure but also occurs in bulk quantity grade PCM. Since one of the main advantages of latent heat storage is its isothermal operation, considerable effort has been put into eliminating supercooling characteristics in candidate PCMs.

Increasing the viscosity of a melt makes it more difficult for the different species to diffuse, combine and form an embryo of the solid phase; and hence supercooling is more likely. To encourage solidification, a nucleating agent or an embryo former is required. Nucleation can be induced by unevenness in vessel walls, dust particles etc. which produce an embryo of the new phase. The following techniques are often employed to induce nucleation:

1. Incomplete melting, ensuring that some of the solid phase remains frozen at the end of the charge period
2. Cold finger, as above but does not involve any control difficulties
3. Nucleating agent, introducing a crystal which is structurally similar to the PCM (size ± 10%) with a melting point approx. 10°C higher than the PCM melting point
4. Agitation, enhancing nucleation by breaking up growing crystals and redistributing in melt
5. Crystal forming surface, for example utilising imperfections on interior tube walls, or artificially induced scratches

Van Galen (1980) solved the problem of supercooling in a storage device employing sodium acetate trihydrate as the PCM, utilising a cold finger technique. A metal needle at the end of the encapsulating tube stabs an insulating surface and rests on a cold suface, which keeps its temperature below the crystallisation temperature. It was intended that this surface should be cooled in a useful way utilising either cold tap water or mechanical ventilation air.

Stunic (1978) reported that the cooling curve of a pure melt of sodium acetate trihydrate showed no distinct liquid-solid phase transition temperature. Addition of 0.2% activated charcoal was found to result in the salt crystallising

at 55°C with no supercooling at all. Wada and Yamamoto (1982) found that tetrasodium pyrophosphate decahydrate [$Na_4P_2O_7.10H_2O$] acted as a nucleation catalyst for sodium acetate trihydrate. Supercooling was limited to 5 degC with 0.1 g of $Na_4P_2O_7.10H_2O$ in a 10 g melt, and the latent heat hardly affected, even when subjected to 1000 thermal cycles. The nucleating agent is often denser than the PCM and hence requires a thickening agent (see section 2.2.2.1) to prevent it from collecting at the bottom of the storage device.

In a heat storage device utilising the extra water principle it is practical to prevent supercooling by agitation of the storage medium. When oil (immiscible in the storage medium) is utilised as a direct contact heat transfer medium (see Furbo 1980) then the oil bubbing through the PCM will cause a soft stirring thus preventing supercooling.

Altec, a company based in Dorset, have recently developed (1985) a mixture based on sodium acetate trihydrate with gum and other unstated materials added, which may be effectively supercooled to ambient, without losing its latent heat. The gel is activated by a mechanical process (believed to be a shearing action) when it is required to release its latent heat.

2.2.2.3. Heat transfer

The characteristic heat transfer is quite different for a PCM being charged and discharged. In the former the heat exchanger is in contact with the melt so heat transfer is by conduction and convection, while in the latter it is in contact with the solid so heat transfer is by conduction alone. Consequently, higher charge than discharge rates are generally possible for similar temperature driving driving forces and heat exchange areas. If the discharge rate is inadequate it may be improved by either making the heat transfer area very large or keeping it free of crystals. One method of achieving both these aims is by direct contact of the heat transfer medium with the PCM. Furbo (1980) designed a heat exchanger which employed oil as the heat transfer medium for a heat storage device utilising the extra water principle (see 2.2.2.1). It should be noted that addition of a thickening agent will suppress natural convection effects during the charge process.

Large heat exchange areas can be achieved by encapsulation of the PCM in small units. Various modes of encapsulation have been employed:

1. Polypropylene tubes
2. Tin cans
3. Polypropylene spheres (diameter 10-30 mm)
4. Trays
5. Finned annulus
6. Steel pipes
7. Plastic "sausages"
8. Particles (micro-encapsulation diameter 20-200 µm)

and the relative merits of each are discussed in section 3.1.2.

2.2.2.4. Control of melting point

Ulman and Valentin (1983) reported that addition of acetate salts or acetamide to sodium acetate trihydrate lowers its melting point. They found that 7% w/w of acetamide [CH_3CONH_2] lowered the melting point to 54°C while addition of the same amount of lithium acetate dihydrate [$CH_3COOLi.2H_2O$] depressed the melting point to 50°C. It was claimed that the positive thermal storage properties of sodium acetate trihydrate were retained but no data for latent heat was presented.

2.2.3. Development of Latent Heat Storage Devices.

2.2.3.1. Hist .rical background

Ice is probably the best known PCM and has long been used as a method of keeping an area or object cool. Several other PCMs based on low-melting salt mixtures have been used in the transport of dairy products and perishables.

At the turn of this century, salt hydrate filled containers were employed by railway operators as a method of breaking the winter chill. PCMs have long been utilised in "hot bottles" for direct application of warmth to the human body. Hydrated sodium acetate was often selected; and despite its erratic performance many designs were patented. Crooker and Sterling in 1928 patented a mixture with a carefully controlled water content with calcium chloride added to soften the crystalline solid. In 1929, Jost and Byleveld patented a device where the encapsulated PCM was mixed with finely divided

sand and contained chunks of metal or pebbles. Heat release was achieved by shaking the container and thus crystallising the supercooled salt solution. A variation on this theme was patented by Othmer where a flexible diaphragm allowed an internal device to scrape the interior wall and hence initiate crystallisation.

During the 1960's, NASA sponsored research programs into PCM thermal control devices, such as heat sinks for inertial navigation systems to operate over the limited temperature range 49 - 57°C. The Apollo 15 Lunar Rover Vehicle employed three PCM systems on the signal processing unit, drive control electronics and lunar communications relay unit; the heat generated during sorties was stored in the paraffin PCM. Between sorties, movable insulation devices allowed the heat to dissipate by radiation.

In 1979, Truelock patented a storage device where the supercooled solution was held in one compartment with the nucleating materials in another. The device was designed so that the wall of the nucleating compartment could be ruptured and the heat released as the contents mixed and crystallised. These hot and cold pack devices are often used in health care and sports medicine. Other developments include diving and aviation suits with the PCM in back packs, and survival sleeping bags made from sponge rubber filled with PCM and laminated between two rubber sheets.

The above are useful and interesting examples of the various uses in which PCM thermal storage devices have been utilised. The remainder of this section considers the application of PCMs for heating and cooling buildings. Again a Scotsman, A.A.H. Douglas in 1932 is credited with inventing the first heat storage apparatus containing sealed tubes of PCM in a liquid heat transfer medium. The store was designed to be charged with off-peak electricity and provide domestic heating and hot water supplies.

2.2.3.2. The Dover House - solar heating

Although Douglas pioneered the concept of latent heat storage for domestic heating it was Dr Maria Telkes who attempted the first practical application. She concluded that solar heating was not economically attractive if it required an auxiliary heating system and hence decided on PCM storage since the volume required for a water, rock or other sensible heat storage was

prohibitive.

Miss Amelia Peabody, a wealthy sculptress, who was interested in solar energy, funded the building of a demonstration house on the grounds of her estate in Dover, Massachusetts. The solar collectors (67 m^2) were arranged as a vertical south wall for the attic. Three heat storage "bins" each containing 19-litre insecticide cans filled with Glauber's salt were located between the rooms. In all there were 19000 kg (13.3 m^3) of PCM with a theoretical storage capacity (TSC) of 1378 kWh, enough to provide 12 days' heating load at 114.8 kWh per day. Heat was transferred by circulating air through ducts behind the absorber plates to the bins. Radiation from the bins kept the room warm normally, and blowers were available when extra heating was required.

The house was first occupied by Dr A. Nemethy, a second cousin of Telkes, with his wife and young child on Christmas Eve 1948. In their first 11 days, the solar system was put to a serious test with some cold and bleak weather, exhausting the stored solar heat. Fortunately this passed and they remained comfortable in a winter which was abnormally mild. During the second winter, apart from some chilliness following week-long periods of overcast weather the system was reported to have performed satisfactorily "without a fuel bill".

In the middle of the third winter however the storage system failed. The Glauber's salt had separated into anhydrous and supernatent layers with the consequential loss of most of its storage capacity. In addition many of the cans had corroded and begun to leak.

2.2.3.3. Calmac heat bank

Calmac Manufacturing Corporation of Englewood, New Jersey developed a range of heat bank systems. They utilised bulk containment of the PCM in 0.9 m (or 1.2 m) diameter, 1.2 m high, plastic cylinders with internal spirals of close-spaced plastic tubing for heat exchange. A small pump operated intermittently when the salt was in a liquid state to prevent stratification. The heat bank-115 which was being marketed in 1980 (see Michaels 1980) contained sodium thiosulphate pentahydrate. Other heat banks based on ice, magnesium chloride hexahydrate and a modified Glauber's salt (m.p. 7°C) were also available. The heat bank-115 had a storage capacity of 111.4 kWh for a ΔT of 19 degC, and a price of $3000 was quoted (see Michaels 1980) for a

single unit equivalent to almost $29 per kWh in 1980!

MacCracken (1981) notes that 1.27 cm diameter plastic tubing was selected to ensure a very high area for heat transfer. It was found that the plastic tubing separated by 2.5 cm of salt provided far better performance than copper tubing separated by 5 cm. In fact, equal performance was achieved using only 10% more plastic tubing than copper. Table 3.2 shows that an extremly high proportion (0.87) of the containment volume is filled with PCM in comparison to other storage devices. Nucleation and segregation problems are avoided using the stirring pump which keeps the salt around it warm and melted, thus preventing internal solidification. The salt shrinks by 8% during solidification but good thermal contact is always maintained since the liquid PCM on top settles into any cracks or openings in the shrinking solid salt. The flow of water in adjoining tubes is arranged to be in opposite directions so that temperature averaging takes place, thus ensuring uniform freezing and melting. The containers are distributed empty for easier handling and to prevent damage en route; they are then tested and filled on site.

Little data is available on performance although the typical heating-cooling curves presented by MacCracken (1981) for a 24 hour cycle are almost flat, indicating almost ideal latent heat storage characteristics. One thousand thermal cycles were reported to have had no effect on storage capacity.

2.2.3.4. Other commercially available latent heat storage devices

Michaels (1980) presents a review of commercially available latent heat storage devices including a unit produced by TES Inc. of San Diego, California which is very similar to the Calmac heat bank-115 discussed above. It uses the same PCM (with propriety additives) but utilises aluminium double-finned strips as the internal heat exchanger. The storage capacity was lower (73.3 kWh) and the total cost even higher at $3500.

A direct-contact heat exchange unit marketed by OEM Products of Plant City, Florida with a storage capacity of 71.9 kWh had a quoted cost of $3500. This "heat battery" unit used Glauber's salt and pumped an immiscible mineral oil out of nozzles located in the salt-oil mixture. The oil stirs the salt and enhances the heat exchange between the salt and the two copper coils used for heat input and output. No performance data was reported but no

significant loss in storage capacity was found for thermal cycling.

Dow Chemical Company produced a chemically modified form of calcium chloride hexahydrate called Thermol 81 which melted congruently and exhibited minimal supercooling. PSI Inc. of Fenton, Missouri produce energy storage rods (8.9 cm diameter, 1 m long), which are carbon black-coated HDPE cylinders filled with Thermol 81, of capacity 0.65 kWh, for $29.80 per rod. Swisher and Frier (1981) present a possible design based on these cylinders for a 140 kWh system with air as the heat transfer fluid.

2.2.4. Performance of Prototype Latent Heat Stores

2.2.4.1. Delft-tubes [69 kWh]

At the International TNO Symposium held in Amsterdam in November 1980, van Galen (1980) reported on the development of a latent heat storage system based on sodium acetate trihydrate. It was constructed at the Institute of Applied Physics at Delft in Holland and intended for short term storage of solar energy for house heating. A stabilising colloidal polymer matrix was added to the PCM to prevent segregation but found to be only partly effective, allowing a 20% decrease in thermal capacity over 400 cycles. The nucleating agent was also found unreliable and a zone of permanent cooling (see section 2.2.2.2) was established to prevent supercooling. The PCM was encapsulated in 200 cylindrical containers (material not specified but appears to be metallic) of length 1.5 m and diameter 44 mm. A TSC of 69 kWh over the temperature range 20-80°C was reported by van Galen (1980) but specified as 50 kWh over the same temperature interval a year later (see van Galen 1981). In the latter it is reported that a stabilising colloidal matrix, which solved the aging problem of segregation had been discovered resulting in a lower heat of fusion (235 kJ/kg) for the storage medium, which may help explain the discrepancy. The tubes were contained in a tank of height 1.63 m and diameter 0.707 m. Antifreeze solution was employed as the heat transfer fluid.

Testing of the storage device was achieved by simulating the heat input from a solar collector (using an electrical heater) and the heat demand of a dwelling (using a heat exchanger) and investigating the store performance. A microcomputer uses weather data to calculate the heat input from the collector and heat demand of the dwelling. The performance of the storage

device is compared with that of an unstratified water store whose performance is easy to predict with a computer model. Heat loss tests were performed on the device and a loss coefficient of 3.5 W/m^2K determined. Van Galen (1980) tested the store for a solar collector input which couldn't melt the PCM - and unsurprisingly found the water store to have a superior heat capacity. Dimensionless plots of discharge temperature drop across the store against time, presented by van Galen (1981), of experimental and computer model predicted values show extremely good agreement.

2.2.4.2. Foster Wheeler-metal tubes [38.7 kWh]

Development work on a PCM based heat storage module performed by Foster Wheeler Development Corporation was reported by Dietz (1984). Thermol 81 manufactured by Dow Chemical Company (see 2.2.3.4) was selected as the PCM. Encapsulation was in 7.62 cm (dia.) ordinary galvanised stove pipe, with each tube containing about 5.62 kg of PCM. The total weight of PCM was 729 kg giving a total latent heat capacity of 38.7 kWh. Air was employed as the heat transfer medium.

Charge and discharge rates were plotted against time for different flow rates (0.252-0.832 kg/s) and temperature step changes (8-24 degC). Eight runs were performed and the storage device cooled (heated) so that it was just completely frozen (melted) for the charge (discharge) test. Thermocouples were positioned within the tubes and prior to the charge (discharge) test, these all indicated 2.8°C below (above) the melting point (27.2°C). For all the lower flow rate tests the rate-time profiles were quite linear with max rates of 2-5 kW (at t=0) and a minimum of 1.5 - 2.5 kW (t=10 hr).

These results were employed to verify a model of the phase change process which predicted the heat transfer rate as a function of the fraction charged/discharged.

2.2.4.3. NBS-plastic trays [73.3 kWh]

Jones and Hill (1979) at the National Bureau of Standards, Washington tested a phase change thermal energy storage device, utilising sodium sulphate dodecahydrate as the PCM, according to the procedure specified in the ASHRAE Standard 94-77. The PCM was encapsulated in 726 one litre, high

density polythene trays giving a TSC of 73.3 kWh. Air was employed as the heat transfer fluid and heat loss from the huge 3 m x 1.6 m x 1 m plywood cabinet was limited by 15 cm of foam insulation.

The theoretical heat loss from the storage device was calculated to be 4.7 W/degC but the actual heat loss was found to be five times greater. This was thought to be due to air leakage from the device. Two test flow rates were employed (0.21 and 0.42 m^3/s) and the charge and discharge capacities defined in the ASHRAE Standard 94-77 (see section 4.1) were found to be significantly lower than the TSC. An alternative method of presenting the storage capacity at the end of the test period, referred to as the "Peformance Factor" was suggested. This was defined simply as the ratio of the storage capacity to the TSC and thought to offer the following advantages over the conventional method:

1. Dimensionless number, hence value independent of size of unit
2. Less subject to variations in inlet temperature and flow rate
3. More meaningful since related to a theoretical limit

The performance factors for charge and discharge were respectively 0.58 and 0.33. Very low temperature driving forces during discharge operation were thought to account for the discrepancy between charge and discharge, while the generally low values are probably due to thermal degradation of the salt during previous runs. Internal temperature profiles of the heat transfer fluid show a high degree of stratification in the flow direction and a significant amount of bypassing.

Jones and Hill (1979) recommended that plots of charge/discharge rate against time would be extremly useful to designers of thermal energy storage systems and should therefore be included as part of the test procedure.

2.2.4.4. Bremen-hybrid store [29.5 kWh]

Schlif (1981) describes the performance of a vacuum insulated hybrid heat storage system developed by ERNO at Bremen. Several storage materials have been investigated and two prototype hybrid heat storage systems [HWS-80 and HWS-52] containing PCMs with melting points of 80 and 52°C respectively have been manufactured and tested. Limited details of the

system were available but it appeared to be comprised of a reservoir filled with a number of discrete containers, containing the PCM. The containers can be spheres, tins or bottles and the space between them was filled with a fluid which can be heated or cooled by means of a primary heat exchanger in the form of several U-tubes. Vacuum insulation is utilised to minimise heat losses and maximise heat transfer effectiveness. The evacuated space was filled with a powdery substance acting as the supporting structure so that the vacuum envelope can be manufactured from relatively thin walled inexpensive sheets. A loss coefficient of only 0.11 W/m^2K was achieved with an insulation thickness of 5 cm. The tank utilised had a volumetric capacity of approximately 450 litres which, with a filling factor of 0.7, gave a storage capacity of 29.5 kWh for a temperature interval of 14 degC.

A single graph of outlet temperature against time was presented for a constant discharge rate of 8 kW which indicated that the temperature would not fall below 60°C for 3.5 hours (equivalent to 28 kWh). The sytem is intended for operation as part of a conventional heating system where significant energy savings (15%) could be achieved by eliminating the inefficient energy consumption associated with intermittent operation.

2.2.4.5. Stuttgart-finned heat pipe [3.7 kWh]

Abhat (1984) presented a detailed report on the thermal performance of a finned heat-pipe latent heat store developed at the Energy Conversion Division, IKE, University of Stuttgart. The aluminium heat pipe (3.07 m long with an outer diameter of 40 mm) was filled with ammonia as the working fluid. Approximately two metres in the middle of the tube was finned with aluminium plate fins having a square cross section, 200 mm x 200 mm in size, which is boxed-in to form the storage chamber. At either end, annular (jacket) heat exchangers, 500 mm long and having an annular gap of 1.5 mm for water flow, provide the heat-source and heat-sink regions. The storage chamber was filled with 70 kg of myristic acid which gave a latent heat capacity of 3.7 kWh plus a sensible heat effect of 0.046 kWh/K.

Measurement of flow rate in the test facility was inaccurate (± 10%) which, combined with errors in temperature measurement, resulted in heat transfer rates which could only be considered accurate within ± 15%. The heat pipe was tested independently; and for selected operating conditions an axial heat

transport rate as high as 3.5 kW could be attained for a maximum axial wall temperature difference along the heat pipe of less than 10K. Heat loss tests were performed on the device by heating it up to 68°C and letting it cool down to ambient. The temperature profile recorded by a thermocouple placed centrally on the longitudinal axis of the heat pipe showed a rapid decrease from 68°C to the melting point temperature 53°C in 0.8 days. A much less rapid decrease then followed (corresponding to loss of latent heat) as the temperature dropped to 50°C over a period of 4.5 days. Once the latent heat had been released the profile again steepened as the temperature decreased to 42°C in 0.8 days. At the phase transition temperature the heat loss was found to be fairly low at 30 W (equivalent to 0.12 kWh for a four hour run) compared to normal charge discharge rates (error of ± 3%) and was therefore neglected.

The test facility used a thermostatically controlled water bath to provide a step input in the inlet temperature during charge. However, a 300 litre tank was used to achieve the step input during discharge which meant that initially the inlet temperature was equal to the initial temperature of the tank (normally 10°C) but increased as the store was discharged. Since the discharge data is of limited applicability, the charge performance characteristics are considered in greater detail. Steady state conditions prior to a test were achieved by ensuring that the temperature difference between the inlet and outlet temperatures at the charging/ discharging calorimeters remained below 0.5 K for an hour. Temperature profiles and charging rate against time plots were presented for a flow rate of 350 l/h and $T_{in}-T_{mp}$ of 25 K which indicated a latent heat regime at the melting point with a charge rate of 1.5 kW. This regime accounted for approximately 70% of the storage capacity of the device. Thermocouples located on the heat pipe at the inlet and middle of the storage chamber exhibited no significant stratification. Abhat (1984) suggests the use of a parameter ϕ defined as

$$\phi = \text{charge or discharge rate / storage capacity of unit,} \qquad (2.11)$$

to evaluate the performance of a store. Hence, in the latent heat regime a charge rate of 1.5 kW for a unit storage capacity (latent) of 3.7 kWh gives ϕ = 0.41. The significance of this value is best explained by considering what ϕ values would be specified in a store design. A store which had to be fully

charged with off-peak electricity available for only seven hours at a maximum thermal input power of qmax, would have ϕ = qmax/(qmax*7) = 0.143. Hence the finned heat pipe would be more than capable of satisfying this design criterion.

The performance of the store was investigated for three mass flow rates and three different driving temperature potentials ($\Delta T = T_{in}-T_{mp}$). For a constant mass flow rate the rate of heat penetration into the storage medium depends essentially on the internal heat transfer resistance offered by the store design. Abhat (1984) hence defined the effective store conductance, G

$$G = q(t)/(T_{in}-T_{mp}), \qquad (2.12)$$

as a characteristic of the latent heat store. At a constant flow rate of 350 l/h the curves of G against time for the three temperature potentials overlapped in the latent heat regime at 60 W/K. Similar curves were found when the flow rate was increased to 600 l/h implying that no significant improvement in the heat transfer coefficient on the flow side is attained for higher flow rates. However when the flow rate was lowered to 100 l/h the conductance decreased to 30 W/K and it was discovered that the flow regime in the annulus had changed from turbulent to laminar.

2.2.4.6. Cranfield-tin cans [3 kWh]

Manley (1983) reported on the performance of a small experimental store of 3 kWh capacity with the PCM encapsulated in tin cans which was developed at Cranfield. Sodium thiosulphate pentahydrate was employed as the PCM and extensive research went into the selection of the nucleating and thickening agents. Two mixtures were actually tested, one utilising 0.1-0.3% w/w activated charcoal and a second using 1% w/w sodium sulphate as a nucleator with 1.5% w/w versicol WN33 (a synthetic hydrophilic polymer) as a phase stabiliser. Not surprisingly, the thermal capacity of the activated charcoal mixture with no thickening agent rapidly decreased and was considered unsatisfactory. A total of 133 tin cans (diameter 73 mm, height 61 mm) were employed to encapsulate the heat storage mixture. The storage container had a diameter of 0.394 m which permitted 19 cans in a hexagonal close packed arrangement to be placed in each of seven layers. Each layer had an identical

packing arrangement but was rotated a few degrees to maximise surface area for heat transfer. Water was employed as the heat transfer medium and distributed by a weir located above the top layer of cans for top-down flow, and by a manifold located underneath the support plate for bottom-up flow.

A heat loss coefficient was determined by maintaining the store at 40°C for 5 hours and then recording the internal temperature of the store (at 3 locations) and the ambient temperature every hour for 18 hours. The total heat loss was then evaluated and the heat loss coefficient determined from the averaged temperature differnce to be 0.5 W/K.

Three cans in the second, fourth and sixth layers were each instrumented with two thermocouples located on the can surface and in the centre of the PCM. A thermocouple was also placed in the space adjacent to each of these instrumented cans to measure the water flow temperature. An energy balance between the rate of heat lost from the transfer fluid between layers 2 and 4 and the rate of heat transfer to the PCM in layers 2 and 4 was employed to determine the outer film coefficient. The inner film heat transfer coefficient and hence the overall h.t.c. were then determined from a heat balance on each can. For Reynolds number in the range 85-15, a plot of U against time yielded an approximately straight line constant at 40 W/m^2K for charge and 20 W/m^2K for discharge. Preliminary design calculations indicated that, for satisfactory performance, NTU had to be greater than 2. A plot of NTU against Reynolds number shows that this would be achieved for $Re<45$ during charge and $Re<15$ during discharge.

Manley (1983) assumes that the latent heat effect can be neglected for modelling purposes if the melting zone length is less than the total length of the bed. In this case a model of a sensible heat regenerator may be utilized with the latent heat included as an effective heat capacity. A responsive model, which optimises the heat transfer coefficient between the heat transfer fluid and storage material in order to produce a best fit with experimental data, was used to predict the temperature response of the store. Good agreement was achieved with the exception that the model could not predict the minimum found in the experimental result as a consequence of slight supercooling (3 degC).

2.2.4.7. Other

Abhat et al. (1980) describe the development of the finned annulus storage device being investigated at the University of Stuttgart. This store consists of a number of finned annulus heat exchanger elements bundled together in a conventional shell-and-tube arrangement. Each element is comprised of an inner tube and outer tube maintained in thermal contact with each other through longitudinal fins. The region in the annulus and between the fins is filled with PCM. Heat is input by hot fluid flowing through the inner tube of an element while fluid pumped through the shell side of the exchanger is delivered to the heating system. No exact dimensions were presented but the volume of PCM per unit storage volume must be relatively low. However Abhat notes that such a system combining both latent and sensible heat storage would be attractive for domestic hot water production. A test model 0.1 m long filled with paraffin showed that natural convection is still the dominant heat transfer regime although the fins initially suppress the effect. A prototype heat exchanger element, 1 m long (0.5 kWh) was tested with myristic acid and an extremly high heat transfer rate of 350 W/m was achieved resulting in ϕ=0.7 for both charge and discharge.

Bell (1981) describes the development at Cranfield of a small scale store employing sodium acetate solution as the heat storage medium. Various direct contact heat exchanger prototypes were developed, but problems associated with heat extraction from the store have not permitted a thorough evaluation of the experimental performance of such a store.

A pseudo-sensible heat store using small diameter (20 mm) capsules of PCM has also been developed at Cranfield and is described by Wood et al. (1981). Conventional storage systems normally require some form of container spacing system, to prevent complete flow passage blockage. The additional complexity and cost can be eliminated using a self supporting packed bed. Extremly high charge power densities of between 150 and 450 kW/m^3 for a temperature interval of 10 degC were reported. This opens up the potential for industrial applications where a short charge period and associated large number of cycles per year results in industrially attractive payback periods of less than two years.

2.3. INTEGRATED HEAT PUMP/HEAT STORAGE SYSTEMS

2.3.1. Introduction

2.3.1.1. Background

In July 1979 the Science Research Council published a review of heat pump research in UK universities, polytechnics and institutes of technology (see Foster 1979). They identified twelve possible research topics for domestic heat pumps and included storage as a medium priority area, since it was thought that combination with a thermal store having a diurinal capacity would greatly facilitate the adoption of heat pumps. Approximately three years later the Science and Engineering Research Council (SERC) organised a workshop (see Russel 1982) to consider the case for, and technological aspects of, combined heat stores and heat pumps. As a starting point for the workshop it was assumed that some of the reasons for attempting to combine heat stores and heat pumps were to:

1. Gain access to "off-peak" electricity, leading to lower energy costs
2. Improve efficiency of heat pumps by increasing the evaporator temperature, leading to lower energy use
3. Reduce peak power rating required of heat pump, leading to lower capital costs

A total of 40 interested researchers from both fields working in industry, universities and government agencies attended. Short talks were presented on heat storage and heat pumps to give the necessary background information. From the ensuing discussion topics for future research interest were identified. These included recommendations that:

1. The charge/discharge characteristics of heat stores should be defined more clearly so that realistic data could be used in studying models of coupled heat stores and pumps
2. A standardised set of reference data should be made available and used in model work so that comparisons between different studies could be made easily
3. Instrumentation and control of coupled systems would be of great

importance and determination of the energy content of a store was likely to present difficulties in practice

4. Investigation into indigenous storage in buildings, such as in concrete floors, should be pursued since such systems were able to offset their cost against other functions and were therefore economically attractive
5. A test system consisting of a heat store, a heat pump, specified controls including instrumentation and valves should be studied in detail, to enable design-guides to be developed so that potential application areas could be rapidly assessed and costed

Heat storage may be combined with a heat pump in several different configurations and the design of an integrated system will depend on the intended application. The integrated system is normally classified according to the location of the store viz. condenser-side, evaporator-side or central; and the merits of each type are discussed in the following paragraphs.

2.3.1.2. Condenser-side heat store

The main attraction of including a condenser-side store is to allow the heat pump to be operated with off-peak tariff electricity. Since this is normally available during the night when the ambient temperature is lowest with associated lower COP, this mode of operation does not function as an energy saver but simply lowers running costs. In figure 1.2 it can be seen that, if the heat pump is sized to meet the demand at an ambient temperature of -1°C, then at temperatures greater than this the heat pump is capable of delivering heat increasingly far in excess of that required. As has already been discussed in section 2.1.4, variable capacity control is expensive and is normally achieved by on/off switching only. Frequent on/off switching can lower the seasonal performance of the heat pump (see section 2.1) and limit its useful life; hence continuous charging into a condenser-side store should improve performance and reliability of the system.

Three possible arrangements of an integrated system with a condenser-side heat store are shown in figures 2.9, 2.10 and 2.11. In figure 2.9 the configuration chosen for further research is presented. During the

off-peak period the heat pump charges the store; and during the following day the store supplies the heating load until it is completely discharged, whereafter the heat pump supplies the load in the normal fashion. Kopecky (1984) at Cranfield proposed a slightly different operating philosophy where the store performed a peak-lopping role. To achieve this, the heat pump was designed to supply the base load and the store was sized to perform rather like an auxiliary heater to cope with the peaks in demand (see figure 2.12). Where possible this system would utilise off-peak electricity to charge the store and hence reduce running costs. Since the heat pump no longer has to be sized for peak loads the total cost of the integrated system with a smaller sized heat pump and low cost heat store may have similar capital costs to the original heating system. Further details of this system are presented in section 2.3.2.3.

The finned annulus storage device developed at the University of Stuttgart (see section 2.2.4.7) based on a PCM with a melting point of 48°C is presently being developed as a condenser-side heat store. The heat pump has a thermal output of 12 kW at an external air temperature of 2°C with a circulating hot water temperature of 55°C. Hence the store with a storage capacity of 25 kWh is likely to be employed in a peak-lopping role.

A feasibility study into the use of a condenser-side heat store in a greenhouse heated by a heat pump utilising the warm, humid greenhouse air as a heat source was completed by Wilson et al. at the Polytechnic of Central London. No details of the heat pump or storage device were presented (see Aram 1984).

Figure 2.10 shows the system considered by Frysinger (1979) at the Institute of Energy Conversion, University of Delaware. An air-to-air heat pump was assumed for this theoretical study which concentrated primarily on heat pump assisted cooling rather than heating. The store was positioned in the warm air ducting downstream of the heat pump condenser. Again it was suggested that off-peak electricity could be employed to charge the store in preparation for discharge the following day. In the diagram given it would appear that the store would have to be sized to meet the total heat demand since there appears to be no facility for supplying the heat load directly from the heat pump. However this could easily be rectified by arranging for a

bypass around the store.

Henderson (1984) at the School of Architecture, University of Newcastle, simulated a condenser-side store which is part of the distribution system (see figure 2.11). In this model the dwelling was fitted with underfloor heating consisting of a long length of plastic pipe embedded in the floors. It was found that the thermal capacity of the storage system is a critical design constraint. If the thermal capacity is high so that the heat pump may utilise off-peak electricity then to ensure full utilisation of the stored energy it is really essential to have a knowledge of the likely energy demand for the following day. With a lower thermal capacity this problem is less significant but advantage from off-peak electricity and reduction of short cycling frequency are minimised.

It should be noted that underfloor heating allows water circulation at lower temperatures (due to increased heat transfer area) and hence operation of heat pump with higher COP. Since it was considered uneconomic to retrofit a heating system with underfloor coils, the main emphasis in this work has been on systems which could be connected directly to an existing central heating system, though the results are readily applicable to an underfloor heating system.

2.3.1.3. Evaporator-side heat store

Perhaps the simplest method of introducing storage into the evaporator side of the heat pump is to have a pipe network (see figure 2.13) buried underneath the ground. At a depth of 1-2 m the ground temperature is almost constant and behaves as a kind of natural store for solar energy. The heat pump can then be sized to meet the maximum demand for an evaporator temperature which is significantly greater than the lowest ambient temperature. Hence a smaller heat pump with the resulting improved COP offers lower capital and running costs. However the cost of the pipework and difficulty in installing it will limit these cost benefits.

The actual extraction temperature will depend on the heat transfer properties of the soil. Moist soil has a much higher thermal conductivity than dry soil, hence ground which is not too well drained performs as the most useful energy store. Heat extraction from the ground may be: (i) indirect - as

shown in figure 2.13 where an intermediate heat transfer fluid is pumped through pipes buried in the soil, or (ii) direct - where the refrigerant itself is pumped through coils in the ground. The former is normally favoured despite the introduction of an additional heat transfer interface and pumping requirement, since pumping the refrigerant directly through the coil would result in a significant pressure drop and cause problems in oil circulation. A system of this type has been operated in the UK by Sumner (1976) since 1951. A 144 m length of 19 mm i.d. copper pipe immersed at 1 m depth and covering an area of 130 m^2 was used to achieve an extraction rate of 40-50 W/m. Since the large area required by horizontal systems is not always available, vertical coils (8-10 m deep) in the form of concentric tubes or U-tubes are being considered as an alternative.

Jardine (1976) in Colorado has also performed research into solar assisted heat pumps. Since solar energy is exactly out of phase with demand any solar system must have storage and the necessary integrated system configuration is shown in figure 2.14. In the solar assisted case the auxiliary source would be a solar collector which in good weather would be capable of charging the store to temperatures in excess of 30°C. However in extreme bad weather it may have a delivery temperature not much greater than zero. Hence for the substantial additional cost of the solar collector the performance of the system would still be poor at very low ambient temperatures. It would be possible to size the store so that it was large enough to cope with a cold spell but this would further add to the cost, complexity and size of the system. Alternatively the system could be primarily charged by solar heat and supplemented by an electric heater. Such a system may prove to be economically attractive with operation of heat pump at high evaporator temperature and the low capital cost for supplementary heating. This configuration is not limited solely to solar assisted applications; the store could be charged with waste heat from the dwelling.

2.3.1.4. Central Heat Store

A theoretical study of an integrated system with a central store was performed by Sigmon et al. (1980) of the Research Triangle Institute. Their integrated system configuration is shown in figure 2.15. This mode of operation was selected as a method of utilising off-peak electricity to improve

heat pump efficiency dramatically. Overnight the refrigerant is diverted through the store which performs as a condenser and becomes charged. The following day refrigerant flows through the condenser as normal but after passing through the expansion valve is diverted through the store which now behaves as an evaporator. If the store operates at a temperature midway between the condenser and evaporator temperatures it is possible to imagine this system as a 2-stage heat pumping process with a time shift. The efficiency is maximised by utilising a very small temperature lift and the first stage is performed with an extremely low running cost. However the design of a storage device which performs efficiently as both a condenser and evaporator would be extremly complex and must inevitably be a compromise. During the off-peak period the heat pump would be run continuously but during the day it would be subject to even more frequent cycling than a conventional heat pump.

Von Cube (1981) discussed a slightly different configuration (see figure 2.16) which is primarily intended to improve the efficiency of the heat pump rather than to gain access to off-peak electricity tariffs. For external temperatures above the balance point the refrigerant leaves the condenser and flows through the store where any remaining condensation enthalpy not required by the circulating water is transferred to the storage material. In addition some subcooling of the refrigerant may also occur which, as discussed in section 2.1, further improves performance. When the external temperature is below the balance point, refrigerant flows from the condenser through an expansion valve and into the store which performs as an evaporator.

The frequency of on/off cycling is significantly reduced for the period that the store is being charged. Note that unless the store is very large it will only be employed infrequently for those periods when the external temperature is very low. Hence the only real attraction for this system is that the heat pump would require no supplementary heating despite being sized for a balance point temperature of say 5°C. The cost of the supplementary heating and storage are likely to be similar, so the real beneficiary would be the generating authority who would have a reduced peak demand.

2.3.1.5. Storage in absorption heat pump systems

Wilson and Knight (see Aram 1984 and Foster 1981) of Oxford University developed a heat pump which used ammonia as a refrigerant and incorporated an absorbent to provide thermochemical energy storage (see figure 2.17). In the discharged state, ammonia is chemically combined with the absorbent. When off-peak electricity becomes available refrigerant vapour is withdrawn from the generator/absorber and compressed before losing its latent heat in the condenser to vapourise more refrigerant. The liquid exiting from the condenser passes through a throttle and is then stored in the liquid accumulator. During the heat pumping phase, ambient heat boils the ammonia and allows refrigerant vapour to return to the generator/absorber where it is re-absorbed. Heat of absorption is emitted at a higher useful temperature and removed by the load coil. Since the demand for heat occurs during the day while the outside air temperature is highest, the performance of the heat pump is not lowered as a consequence of utilising off-peak electricity unlike the conventional condenser-side system.

The first prototype heat pump used barium chloride absorbent which gave a temperature boost of 35 degC between evaporator and absorber/generator. The absorbent, comprising 9.73 kg of $BaCl_2$ and 0.41 kg of NaSCN liquid binder (to prevent migration of absorbent) was spread on 6 trays equipped with heat exchange coils. A refrigerant charge (6.51 kg of ammonia) was introduced to the liquid accumulator at 8°C and during the first discharge water was warmed from 16 to 32°C as it passed through the load coil. The first attempt at regeneration with the compressor speed set at 460 rpm yielded no liquid refrigerant. Thermal insulation and doubling the compressor speed increased the regeneration rate to 50% of that predicted theoretically, a discrepancy which was still thought to be due primarily to thermal losses.

The second prototype system used calcium chloride which is a sparingly soluble absorbent. To achieve good heat transfer and rapid absorption and desorption of ammonia, a stirred slurry of $CaCl_2$ granules (5 µm) in kerosene (an inert liquid with low vapour pressure) was utilised. Calcium chloride absorbent gave a temperature boost of 58 degC which necessitated a two stage compression process. Two open compressors were directly coupled to motors whose shaft torque could be measured to calculate the power input. The generator/absorber was a vertical 40 litre capacity mild steel pressure

vessel, filled with 5.8 kg of $CaCl_2$ granules and 19.3 litres of kerosene and fitted with a stirrer and internal heat exchange coils. The liquid accumulator, a 25 litre capacity mild steel pressure vessel mounted on a weighing machine, was charged with 7.1 kg of refrigerant. The complete system was fitted with thermocouples and flowmeters to determine the thermal inputs and outputs of the various components. The rate of regeneration of liquid ammonia was again below expectation and a detailed heat balance is now being determined to discover whether thermal losses account for the low generation rate of liquid ammonia. Once problems have been eliminated in the second prototype, a domestic sized unit capable of storing 60 kWh of energy will be developed.

2.3.2. Development and Performance of Prototype Systems

2.3.2.1. Condenser-side water store

In his guide to heat pumps and houses, Armor (1981) discussed the potential for integrated systems, and presented a case history showing how a water store was successfully combined with a heat pump. The system was designed to utilise off-peak electricity to charge the store, with the heat pump sized to meet the maximum load and the store sized to be capable of receiving a full charge at the balance point temperature during the off-peak period. A maximum heat pump output temperature of 60°C and minimum acceptable flow temperature set the maximum amount of sensible heat that could be stored per litre of water. At the balance point temperature of 0°C the heat pump could deliver 8 kW so a heat store of 2000 litres was required and a second hand 500 gallon stainless steel glass-lined brewery tank acquired for the system.

The control philosophy was quite straightforward with valves positioned to direct the flow either from heat pump to store, heat pump to load or store to load. Hence at midnight, the beginning of the off-peak period, the heat pump was switched on and the valves to the store opened. If the heat pump was required for domestic heating or hot water then the valves were closed and flow directed to the load. Towards the end of the off-peak period the heat store is isolated and the heat pump utilised to supply the heating load of the dwelling. At the end of the off-peak period the heating load is supplied from

the store until the store outlet temperature falls below 43°C at which point the heat pump is switched back in to satisfy demand. For this particular system the store will be unable to supply the domestic hot water towards the end of the discharge period (except in the case of perfect stratification) and the heat pump is switched on in this eventuality.

The payback period can be determined from the additional capital cost for the tank, pipework, control, valves and insulation against the reduced running cost resulting from up to 45 kWh per day being supplied with off-peak electricity. The lower ambient air temperature for heat pump operation during the off-peak period will be somewhat compensated for by the improvement in performance with continuous operation. In addition the control philosophy described will fully charge the store irrespective of expected demand which will lead to unnecessary heat losses. A 500 gallon tank occupies a lot of space and even if positioned outside is not aesthetically pleasing. Hence any economic comparisons with conventional heating systems would have to include some form of cost penalty to include the effect of the store size.

In the first issue (1985) of *Energy Management Focus* it was reported that in a test house in Clacton, Essex, a condenser-side water store permitted over 60% of central heating energy to be produced at off-peak electricity rates. The project was carried out by John Laing Construction Limited with two heat pumps, one utilising ground water as its source and the other ambient air, which achieved seasonal COPs of 2.1 and 1.9 respectively. The heat pumps were also utilised for the generation of domestic hot water and 90% of the hot water requirement was produced at off-peak rates. The cost of useful energy for the house - which was fully occupied throughout the project - was between 1.3 and 1.6 p/kWh which showed a running cost advantage over conventional gas or oil fired boilers. Evaluation of the system as part of a new dwelling package is continuing.

2.3.2.2. First integrated heat pump/latent heat store system

A joint committee of the Association of Edison Illuminating Companies (AEIC) and Edison Electric Institute (EEI) was set up to consider heat pump applications in 1947. This committee was originally interested in the possible use of a solar system as a supplementary heat source for a heat pump. During the 1950's the committee became interested in integrated systems and

disodium hydrogen phosphate dodecahydrate ($Na_2HPO_4.12H_2O$) known as DSP was investigated as a potentially suitable PCM (see table 3.1). This had a rather low melting point of 36°C but a high latent heat (278 kJ/kg). Lime-rich foamed glass floating on top of the PCM had been patented by Telkes as a nucleating agent. Tinned steel cans (0.05 m x 0.07 m (dia.)) were employed to encapsulate the DSP. Five sample containers were constructed and subjected to 100 thermal cycling tests. The results (see AEIC-EEI Heat Pump Committee 1952) appeared favourable and 50000 of the cans were prepared for testing in eight different field locations.

The cans (see Altman 1971) were dumped irregularly into a 1.4 m^3 galvanised fuel oil storage tank. Water circulation was inadequate and poor heat transfer was obtained. Unfortunately despite the favourable test results the PCM was not completely effective. Consequently the system was only capable of 22-40% of the expected capacity. In addition the cans corroded, as they were not well enough protected from the water heat transfer medium and the project was abandoned.

2.3.2.3. Cranfield's peak-lopping store

A prototype integrated system with a small condenser-side latent heat storage capability is being developed at Cranfield, where Kopecky (1984) identified a two-peak characteristic in the demand curve (see figure 2.12). This implied that a heat pump designed to supply these peak demands (5 kW) was grossly oversized for normal demand (3 kW). Hence a system was designed which utilised a heat pump with a 3 kW thermal output (for a hot water temperature of 55°C at a balance point temperature of 0°C) with a heat store of 10 kWh thermal capacity.

A latent heat store was selected due to its higher energy density and ability to store heat over a small temperature interval. Paraffin wax (melting point 48-52°C) was employed as the PCM with wire mesh added to improve the effective thermal conductivity. It was encapsulated in tin cans designed for a power output of 5 kW which were placed in a large mild steel vessel. A standard heat pump available from Mysons was located inside a controlled environment facility where the temperature and humidity of the inlet air to the evaporator could be monitored and controlled. The complete system was monitored and controlled by a test facility which was based on a

microcomputer.

Results of store performance for heat loss, charge and discharge tests with specified temperatures and/or flow rates and heat pump performance for various source air and circulating water temperatures were presented. Difficulty was found in obtaining reproducible results due to refrigerant leakage from the heat pump.

2.4. DEVELOPMENT OF THERMAL STORAGE MODELS

2.4.1. Analytical Models of Thermal Storage Devices

Although exact solutions by analytical techniques are not available for the problem of phase change in a convectively heated or cooled cylinder, solutions for special cases can be used as a useful check on the finite difference techniques developed in the next subsection. In addition the approximations described here require significantly less computer time and hence may be employed to pre-select design variables for final optimisation with the more complex finite difference models.

2.4.1.1. Sensible heat for various geometries

The fundamental differential equation for one dimensional heat transfer by conduction (Fourier's law)

$$dQ/dt = -kAdT/dx, \tag{2.13}$$

and a heat balance are used to obtain the general differential equation for transient conduction (see McAdams 1954). Consider an elemental volume of area dydz, thickness dx and constant isotropic thermal conductivity k. The heat entering along the x-axis is found from

$$Q_x = -k(dydz)(\partial T/\partial x)dt,$$

and that leaving from

$$Q_{x+dx} = k(dydz)[\partial T/\partial x + \partial/\partial x(\partial T/\partial x)dx]dt.$$

The difference between the heat entering and leaving along all three axes is equated to that stored in the element

$$Q_{stored} = (dxdydz)\rho Cp\,\partial T,$$

to yield the general unsteady state heat conduction equation in cartesian coordinates

$$\alpha(\partial^2T/\partial x^2 + \partial^2T/\partial y^2 + \partial^2T/\partial z^2) = \partial T/\partial t. \quad (2.14)$$

The desired temperature-time-position relations for the heating or cooling of various shapes are obtained by integration of equation (2.14), substituting in the boundary conditions for the case in question. In the case of an infinite slab (i.e. one having a very large ratio of surface to thickness) the heat flow is unidirectional and (2.14) reduces to

$$\alpha(\partial^2T/\partial x^2) = \partial T/\partial t. \quad (2.15)$$

For the special case of a slab having a thickness $2x_n$ and a negligible surface resistance, corresponding to an infinite value of the surface heat transfer coefficient, the surface temperature changes to the temperature of the surroundings immediately at zero time. The boundary conditions are then $T=T_a$ at $x=0$ and at $x=2x_n$; $T=T_o$ at $t=0$, and $T=T_a$ at $t=\infty$. A solution is given by the rapidly converging infinite series

$$T^* = 4/\pi[e^{-aaFo}\sin(\pi x/2x_n) + 1/3e^{-9aaFo}\sin(3\pi x/2x_n) \quad (2.16)$$
$$+ 1/5e^{-25aaFo}\sin(5\pi x/2x_n) + \ldots],$$

where T^* is the dimensionless temperature ratio $(T_a-T)/(T_a-T_o)$ and aa equals $(\pi/2)^2$.

For the same slab having a finite surface resistance corresponding to constant film heat transfer coefficient h, the boundary conditions become

$$k(\partial T/\partial x)_{x=0} = h(T_w-T_a), \quad (2.17)$$

$$k(\partial T/\partial x)_{x=2xn} = -h(T_w-T_a), \quad (2.18)$$

$T=T_o$ at $t=0$; $T=T_a$ at $t=\infty$. Integration of equation (2.15) for these conditions leads to a dimensionless relation among T,t,x and h. Solutions for solids of various shapes are available in the literature (e.g. see Carslaw and Jaeger 1959) but computations from the equations are very tedious because of the large number of terms and the relationships are normally presented in chart form.

2.4.1.2. Latent heat storage

The first published discussion on melting and solidification is thought to be that by Stefan, in 1891, in his study of the thickness of polar ice, hence problems of this type are frequently referred to as "Stefan problems". In fact the more general result known as Neumann's solution was presented by Franz Neumann in his lectures in the 1860's (see Carslaw and Jaeger 1959). His exact solution for a semi-infinite region is presented here since the only simple exact solution in cylindrical coordinates corresponds to the supply or removal of heat by a continuous line source. For the region bounded internally or externally by a circular cylinder with constant surface temperature, only an approximate solution is available.

In the solution it was assumed that there was no volume change on solidification, so that the density of the solid and liquid phases would be identical. For linear heat flow the temperatures in the liquid and solid regions have to satisfy the general equation for unsteady state heat conduction

$$\partial^2 T_s/\partial x^2 - (1/\alpha_s)(\partial T_s/\partial t) = 0, \qquad (2.19)$$

$$\partial^2 T_l/\partial x^2 - (1/\alpha_l)(\partial T_l/\partial t) = 0. \qquad (2.20)$$

The first boundary condition specifies that at the interface, the temperature of both solid and liquid phases must be equal to the melting point

$$T_l = T_s = T_{mp} \text{ when } x=X(t). \qquad (2.21)$$

The second boundary condition concerns the absorption or liberation of latent heat at the interface. If the region $x>X(t)$ contains liquid at temperature $T_l(x,t)$ and $x<X(t)$ contains solid at temperature $T_s(x,t)$, then as the surface of separation moves a distance dX, a quantity of heat, $\lambda\rho dX$ per unit area is liberated and must be removed by conduction

$$k_s(\partial T_s/\partial x) - k_l(\partial T_l/\partial x) = \lambda\rho(dX/dt). \qquad (2.22)$$

In addition to the two boundary conditions specified above there will be additional conditions at the fixed boundaries of the region under consideration. In Neumann's solution the region $x>0$ is initially liquid at a constant

temperature T_o with the surface x=0 maintained at zero temperature for t>0 (see figure 2.18)

$$T_s = 0 \text{ , } x=0, \tag{2.23}$$

$$T_l \text{ -> } T_o \text{ , as } x \text{ -> } \infty. \tag{2.24}$$

From Carslaw and Jaeger (1959)

$$T_s = A\text{erf}\{x/(2[\alpha_s t]^{0.5})\}, \tag{2.25}$$

is a solution (where A is a constant) of the linear heat flow equation (2.19) with boundary conditions (2.23). Also if B is a constant

$$T_l = T_o - B\text{erfc}\{x/(2[\alpha_l t]^{0.5})\}, \tag{2.26}$$

satisfies (2.20) and (2.24). Then the first boundary condition (2.21) requires that

$$A\text{erf}\{X/(2[\alpha_s t]^{0.5}\} = T_o - B\text{erfc}\{X/(2[\alpha_l t]^{0.5}\} = T_{mp}. \tag{2.27}$$

Since (2.27) has to be specified for all values of time, X must be proportional to $t^{0.5}$, that is, say

$$X = 2\Lambda[\alpha_s t]^{0.5}, \tag{2.28}$$

where Λ is a numerical constant to be determined from the remaining condition (2.22). Using (2.27) and (2.28) in this, gives

$$\Lambda\lambda\pi^{0.5}/(Cp_s T_{mp}) = e^{-\Lambda^2}/\text{erf}\Lambda \tag{2.29}$$

$$- [k_l \alpha_s^{0.5}(T_o - T_{mp})e^{-\alpha s \Lambda^2/\omega}]/[k_s \alpha_l^{0.5} T_{mp} \text{erfc}\Lambda(\alpha_l/\alpha_s)^{0.5}]$$

When Λ has been found from (2.29), T_s and T_l can be derived from (2.25), (2.26), (2.27) and (2.28), as noted below

$$T_s = (T_{mp}/\text{erf}\Lambda)\text{erf}\{x/(2[\alpha_s t]^{0.5})\}, \tag{2.30}$$

$$T_l = T_o - [(T_o - T_{mp})/(\text{erfc}\Lambda[\alpha_s/\alpha_l]^{0.5})]\text{erfc}\{x/(2[\alpha_l t]^{0.5})\}. \quad (2.31)$$

For the important special case in which the liquid is initially at its melting point so that $T_o = T_{mp}$, equation (2.29) reduces to

$$\Lambda e^{\Lambda^2}\text{erf}\Lambda = Cp_s T_{mp}/(\lambda \pi^{0.5}). \quad (2.32)$$

2.4.1.3. Approximation for latent heat storage in various geometries

London and Seban (1943) developed a general approximate method for the solution of the freezing problem at spherical, cylindrical and plane boundaries. Figure 2.19(a) describes the temperature conditions in a solid layer on the surface of a liquid which is uniformly at its freezing temperature. Solid formation occurs at the interface as a result of heat transfer by conduction through the solid and by convection to the surroundings at temperature T_a. The solid layer is thus subcooled except for the growing surface which is in contact with the liquid at freezing temperature. In this analysis it was assumed that the solid had negligible thermal capacity (i.e. the heat abstracted in subcooling the solid was very small in comparison to the latent heat), resulting in a temperature distribution through the solid as shown in figure 2.19(b). The error introduced by neglecting the solid thermal capacity was investigated, and London and Seban (1943) concluded that the assumption yielded results of sufficient accuracy for most engineering applications.

Fourier's law, see equation (2.13), for steady state radial heat transfer in a cylindrical geometry may be expressed as

$$\hat{q} = -2\pi r k(dT/dr), \quad (2.33)$$

where $\hat{q}$ is the heat transfer rate per unit length of cylinder [W/m]. Integrating (2.33) between the phase change interface and the cylinder boundary (see figure 2.20)

$$\int_X^{rw} (dr/r) = -(2\pi k/\hat{q})\int_{Tmp}^{Tw} T dT, \quad (2.34)$$

gives the heat transfer rate by conduction through the solid annulus

$$\hat{q} = -[2\pi k(T_w - T_{mp})]/\ln(r_w/X). \tag{2.35}$$

The heat transfer rate by convection to the surroundings is found from

$$\hat{q} = 2\pi r_w h(T_w - T_a). \tag{2.36}$$

The total temperature drop between the interface and surroundings can be found by adding (2.35) and (2.36)

$$T_{mp} - T_a = \hat{q}[\ln(r_w/X)/(2\pi k) + 1/(2\pi r_w h)]. \tag{2.37}$$

The rate of heat absorbed as the surface moves per unit length of cylinder is given by

$$\hat{q} = -2\pi X \rho \lambda (dX/dt). \tag{2.38}$$

Combination of equation (2.38) with rearranged (2.37) provides the differential equation expressing the interface position as a function of time

$$-2\pi\rho\lambda X(dX/dt) = (T_{mp} - T_a)/[(\ln(r_w/X)/2\pi k) + 1/(2\pi r_w h)] \tag{2.39}$$

The desired dimensionless parameters are formed according to the following

$$X^* = X/r_w, \tag{2.40}$$

$$t^* = [(T_{mp} - T_a)k/(\rho\lambda r_w^2)]t, \tag{2.41}$$

$$Bi = hr_w/k. \tag{2.42}$$

Hence

$$dX/dt = d/dt(X^* r_w) = r_w(dX^*/dt),$$

$$dX^*/dt = (dX^*/dt^*)(dt^*/dt) = (dX^*/dt^*)[(T_{mp} - T_a)k/(\rho\lambda r_w^2)],$$

$$dX/dt = r_w[(T_{mp} - T_a)k/(\rho\lambda r_w^2)](dX^*/dt^*) = \tag{2.43}$$

$$[(T_{mp} - T_a)k/(\rho\lambda r_w)](dX^*/dt^*).$$

Substituting (2.43) in (2.39)

$$-2\pi\rho\lambda X[(T_{mp}-T_a)k/(\rho\lambda r_w)](dX^*/dt^*) =$$

$$(T_{mp}-T_a)/[(\ln(r_w/X)/2\pi k) + 1/(2\pi r_w h)],$$

which may be rearranged to the following dimensionless form

$$(-\ln X^* + 1/Bi)X^*dX^* = -dt^*. \tag{2.44}$$

The relevant boundary conditions in both dimensional and dimensionless form are

$$X = r_w \text{ at } t=0 \quad \text{or} \quad X^* = 1 \text{ at } t^*=0, \tag{2.45}$$

$$X = X \text{ at } t=t \quad \text{or} \quad X^* = X^* \text{ at } t^*=t^*. \tag{2.46}$$

Integration of (2.44) between these limits yields

$$\int_0^{t^*} -1dt^* = -\int_1^{X^*} X^*\ln X^*dX^* + \int_1^{X^*}(X^*/Bi)dX^*.$$

The first part of the right hand side was integrated by parts

$$\int_1^{X^*} X^*\ln X^*dX^* = [(X^{*2}/2)\ln X^*]_1^{X^*} - \int_1^{X^*}(X^*/2)dX^*.$$

Hence

$$[-t^*]_0^{t^*} = [-\{(X^{*2}/2)\ln X^*\} + (X^{*2}/4) + (X^{*2}/2Bi)]_1^{X^*},$$

which may be arranged to give

$$t^* = (X^{*2}/2)\ln X^* + [0.25+(0.5/Bi)](1-X^{*2}). \tag{2.47}$$

The time required for complete freezing can be found for $X^*=0$

$$t^*_{X^*=0} = [0.25+(0.5/Bi)]. \tag{2.48}$$

To test the validity of the approximate method, particularly in regard to the assumption of uniform inward freezing and negligible solid thermal capacity,

Seban and London (1945) performed experiments on the freezing of water contained in right circular cylinders. Test cylinders were suspended in a refrigerated wind tunnel with a variable air velocity in the range 4.4-11 m/s. Film coefficients for heat transfer between the air stream and solid copper cylinders (of the same diameter as the test cylinders) were determined experimentally by the transient method (see McAdams 1959). Tests to validate the analysis were made for the incomplete freezing of water in 25.4 mm (o.d.) and 15.9 mm (o.d.) copper cylinders. Determination of X*, the ratio of the radius of the water-ice interface to the radius of the container, was made gravimetrically. The density change (8%) between ice and water was shown to cause a maximum error of 4% in the calculation of X* using this technique.

The cylinder to be tested was pre-cooled, then filled with ice water, weighed and immediately placed in the tunnel, and timing begun. At the end of the desired cooling period the cylinder was removed, drained of unfrozen water, and again weighed. The resulting data was presented in the form of X* against t* with Bi equal to 0.385, 0.495 and 0.655 for the large cylinder. The majority of the experimental points are within 5% of the predicted magnitude and few exhibit deviations of greater than 10%, which was regarded as an adequate check on the analysis. Consideration of the experimental errors in measurement of air temperature (0.8%), film heat transfer coefficient (2%) and X* (approx. 3%) gave an expected error of 5-7% which is the same order of accuracy as the computed results.

Menon et al. (1983) compared experimental heat transfer fluxes in cylindrical storage containers with those predicted by a quasi-steady model. This model was identical to the one derived by London and Seban (1943) except that subcooling and superheating of the PCM were included in an effective latent heat λ' used to calculate the dimensionless time, see (2.41). For example during freezing it was assumed that any initial superheat was removed as freezing occured, and that the PCM just frozen was subcooled to a temperature midway between the surroundings and melting point

$$\lambda' = \lambda + Cp_l(T_o - T_{mp}) + Cp_s[T_{mp} - (T_{mp} + T_a)/2]. \qquad (2.49)$$

The storage unit was a vertical, double pipe heat exchanger with water

flowing in the annulus and the PCM held inside the concentric inner tube. The outer tube of 57.2 mm i.d. and 760 mm length was insulated with 18 mm of glasswool. The copper PCM-containing inner tube, which was insulated at the bottom and open at the top to allow free expansion of the PCM, was suspended by a collar from the top of the outer tube. An inverted cone diffuser located just above the water inlet distributed flow over the annulus. In order to increase the film heat transfer coefficient from the water to the PCM tube, perforated ring diffusers were located along the length of the inner tube at 100 mm intervals. Inner tubes of 19.1, 25.4 and 31.8 mm diameter filled to a height of 305, 457 or 610 mm with PCM, were employed in the tests.

The heat transfer rate was obtained by a heat balance from the enthalpy change of the water. A flow rate of 400 ml/min gave the optimal combination of high film heat transfer coefficient and measurable temperature difference in the water flow. The water which was circulated to the heat exchanger from a constant temperature bath had an inlet temperature of 60 or 70°C for charge and 20 or 30°C for discharge with the PCM initially at 21 and 70°C respectively. The water-side heat transfer coefficient was calculated for a 25.4 mm tube, by measuring the temperature response at the centre of a steel bar, to be 272 W/m^2K. A figure of dimensionless heat flux against dimensionless time showed that the quasi-steady conduction model predicted the freezing fluxes very well.

Menon et al. (1983) also performed visual studies of melting by taking photographs of a cylindrical glass tube of PCM at 21°C when placed in a water bath at 70°C. Tracer particles (crayon chips) were imbedded in the solid PCM and clearly demonstrated density-driven fluid motions in the molten PCM. The flow adjacent to the solid-liquid interface was downward while that adjacent to the tube wall was upward. Hence the top of the solid PCM contacted the warmest liquid, causing it to melt most rapidly and yielding a conical shape in the interface profile. An effective thermal conductivity which accounted for this natural convection effect was determined, and when included in the quasi-steady model successfully predicted the melting heat fluxes.

2.4.1.4. Review of other approaches

Shih and Isay (1971) used an analytical iteration technique to determine the frozen layer thickness and temperature profile of a saturated liquid freezing inside a cylindrical container immersed in a coolant with constant heat transfer coefficient. The dynamics of the solidification assuming that the liquid temperature was initially at the freezing point were described by equation (2.15) expressed in cylindrical coordinates

$$\partial T_s/\partial t = \alpha_s\{(\partial^2 T_s/\partial r^2) + (1/r)(\partial T_s/\partial r) \quad \text{for } X(t)<=r<=r_w, \tag{2.50}$$

with the boundary conditions

$$X=r_w \text{ at } t=0, \tag{2.51}$$

$$dX/dt = \alpha(\partial T)/\partial r)\, I_X \text{ at } r=X(t) \tag{2.52}$$

$$T = T_{mp} \text{ at } r=X(t), \tag{2.53}$$

$$(q/A) = -k_s \partial T/\partial r = h(T_w-T_a) \quad \text{at } r=r_w, \tag{2.54}$$

where (q/A) is the heat flux [W/m^2] and h is the sum of the heat conductances of the cylinder wall and the coolant film. By defining suitable dimensionless variables the heat conduction equation in cylindrical coordinates was transformed into a rectangular configuration. The transformed version of equation (2.50) was then integrated and solved by an iterative procedure for the specified boundary conditions. A third order approximation solution was compared with the experimental data of Seban and London (1945) and showed good agreement.

Shamsundar and Sparrow (1974), solved the same equations for the boundary conditions specified above for both the case of constant heat transfer coefficient (2.54) and that of constant heat flux. Again dimensionless variables were introduced and the solution was then found by applying a method according to Mergerlin (referenced in a German journal!). The expected Stefan number of the solar thermal power system being developed was 0.05 and it was found that the results were hardly distinguishable (maximum error 2-3%) from those for Ste=0 (i.e. equivalent to negliglible solid thermal capacity). A parameter referred to as "excess liquid", which is the

square of the ratio of the interface radius to the cylinder radius was introduced and its effect on the temperature drop across the solid layer investigated. Not surprisingly at high Bi (100) for all but large amounts of excess liquid (>0.9) the major proportion of the temperature drop (90%) was across the solid layer. For lower Bi and a half discharged store (excess liquid = 0.5), 70% of the temperature drop was across the coolant. Another curve was presented which showed that a constant heat flux during the extraction period is favoured by a design with a low Bi (1) rather than high (100).

2.4.2. Finite Difference Models of Energy Storage Devices

An excellent introduction to finite difference techniques for solving partial differential equations is given by Smith (1978). Numerous examples are presented to demonstrate explicit and semi-implicit approaches, derivative type boundary conditions and cases involving cylindrical coordinates. Examples of finite difference solutions, particularly in heat transfer calculations, are given by Croft and Lilley (1977) who also include listings of programs (in FORTRAN) used for selected problems.

2.4.2.1. Finite difference approximations to derivatives

When a function f and its derivative are single valued, finite and continuous functions of x, then by Taylor's theorem

$$f(x+\delta x) = f(x) + \delta x f'(x) + (1/2)\delta x^2 f''(x) + (1/6)\delta x^3 f'''(x) + \dots , \qquad (2.55)$$

$$f(x-\delta x) = f(x) - \delta x f'(x) + (1/2)\delta x^2 f''(x) - (1/6)\delta x^3 f'''(x) + \dots . \qquad (2.56)$$

Addition of the two equations given above yields

$$f(x+\delta x) + f(x-\delta x) = 2f(x) + \delta x^2 f''(x) + O(\delta x^4),$$

where $O(\delta x^4)$ denotes terms containing fourth and higher order powers of δx. Assuming that these are negligible in comparison with other terms it follows that

$$f''(x) = (d^2f/dx^2)_{x=x} \simeq (1/\delta x^2)\{f(x+\delta x) - 2f(x) + f(x-\delta x)\}, \qquad (2.57)$$

with an error of order δx^2. Subtraction of (2.56) from (2.55) and neglecting terms of order δx^3 leads to

$$f'(x) = (df/dx)_{x=x} \simeq (1/2\delta x)\{f(x+\delta x) - f(x-\delta x)\}, \tag{2.58}$$

with an error of order δx^2. Figure 2.21 shows that (2.58) clearly approximates the slope of the tangent at P by the slope of chord AB and is referred to as a central difference approximation. The slopes of chords PB and AP give the forward difference and backward difference approximations respectively

$$f'(x) = 1/\delta x\{f(x+\delta x) - f(x)\}, \tag{2.59}$$

$$f'(x) = 1/\delta x\{f(x) - f(x-\delta x)\}. \tag{2.60}$$

Both of the above could have been written down immediately from (2.55) and (2.56) by assuming that second and higher order terms in δx were negligible. Hence the error in both these formula is of order δx.

2.4.2.2. Solution of FDEs for sensible heat problem

Consider the case of an infinite slab having a thickness $2x_n$ and a negligible surface resistance as specified in section 2.4.1.1. The general heat conduction equation for 1-D unsteady state heat flow, see equation (2.15), can be converted into non-dimensional form using the following dimensionless variables,

$$x^* = x/x_n, \tag{2.61}$$

$$T^* = (T-T_a)/(T_o-T_a) = (T-T_a)/\Delta Tp, \tag{2.62}$$

$$t^* = \alpha t/x_n^2, \tag{2.63}$$

where the half thickness x_n is employed as the characteristic length due to symmetry. Then

$$\partial T/\partial x = \partial\{T^*(\Delta Tp) + T_a\}/\partial x = \Delta Tp\,\partial T^*/\partial x,$$

$$\partial T^*/\partial x = (\partial T^*//\partial x^*)(\partial x^*/\partial x) = \partial T^*/\partial x^*(1/x_n).$$

Hence

$$\partial T/\partial x = (\Delta Tp/x_n)(\partial T^*/\partial x^*),$$

and

$$\partial^2 T/\partial x^2 = \partial/\partial x(\partial T/\partial x) = \partial/\partial x^*(\partial T/\partial x)\partial x^*/\partial x \qquad (2.64)$$

$$= \partial/\partial x^*(\Delta Tp/x_n)(\partial T^*/\partial x^*)(1/x_n) = (\Delta Tp/x_n^2)(\partial^2 T^*/\partial x^{*2}).$$

Then

$$\partial T/\partial t = \partial\{T^*\Delta Tp + T_a\}/\partial t = \Delta Tp\,\partial T^*/\partial t,$$

$$\partial T^*/\partial t = \partial T^*/\partial t^*(\partial t^*/\partial t) = \partial T^*/\partial t^*(\alpha/x_n^2).$$

Hence

$$\partial T/\partial t = \Delta Tp\alpha/x_n^2(\partial T^*/\partial t^*). \qquad (2.65)$$

Substituting (2.64) and (2.65) into equation (2.15) yields the parabolic non-dimensional partial differential equation (PDE)

$$\partial T^*/\partial t^* = \partial^2 T^*/\partial x^{*2}. \qquad (2.66)$$

The slab is divided into N slices of thickness δx^*, see figure 2.22, hence there are N+1 nodes with the first node (i=0) representing the slab surface and the last node (i=N) representing the axis of symmetry at $x^*=1$. If $x^*=i\delta x^*$ and similarly $t^* = j\delta t^*$ then $T^*_{i,j}$ represents the temperature at position x^* and time t^*. Hence one finite difference approximation to (2.66) for $0<i<N$ would be

$$(T^*_{i,j+1}-T^*_{i,j})/\delta t^* = (T^*_{i+1,j}-2T^*_{i,j}+T^*_{i-1,j})/\delta x^{*2}$$

which can be rearranged to

$$T^*_{i,j+1} = Fo\{T^*_{i-1,j}+[(1/Fo)-2]T^*_{i,j}+T^*_{i+1,j})\} \qquad (2.67)$$

where $Fo=\delta t^*/\delta x^{*2}=\alpha\delta t/\delta x^2$. It is often easier to think in engineering terms rather than mathematical terms and the same FDE is readily derived by the heat balance technique. Consider a slab (see figure 2.22) sliced into elements

δx thick with a cross sectional area A, then for node i

$$[kA(T_{i-1,j}-T_{i,j})]/\delta x - [kA(T_{i,j}-T_{i+1,j})]/\delta x = [\rho CpA\delta x(T_{i,j+1}-T_{i,j})]/\delta t,$$

which can readily be rearranged to

$$T_{i,j+1} = Fo\{T_{i-1,j} + [(1/Fo)-2]T_{i,j} + T_{i+1,j}\}.$$

If the temperatures are made non-dimensional then the above is equivalent to equation (2.67). At the axis of symmetry (i=N) there is no heat flow, hence since $T^*_{N-1,j}$ must equal $T^*_{N+1,j}$ then

$$T^*_{N,j+1} = Fo\{2T^*_{N-1,j}+[(1/Fo)-2]T^*_{N,j}\} \qquad (2.68)$$

The above is known as an explicit method of solution since the unknown temperature at the (j+1)th time step is calculated from known values at the jth time step. The initial conditions specify the temperature ($T^*_{i,0}$) at all points for time=0. Hence the solution simply begins at the node next to the boundary (i=1) and calculates all the new temperatures for i<N using (2.67). The new temperature at i=N is then calculated using (2.68) and the procedure repeated at the next time step.

Finite difference methods are approximate in the sense that derivatives at a point are approximated by difference quotients over a small interval i.e. $\partial f/\partial x$ is replaced by $\delta f/\delta x$, where δx is small. The accuracy of a finite difference solution can therefore be improved by decreasing the size of δx in succeeding solutions until no further improvement is noted. However if a time step δt^* is specified (to minimise computational effort), then decreasing δx^* so that Fo becomes greater than 0.5 results in a negative coefficient of $T^*_{i,j}$ in (2.67) which causes the solution to oscillate about the correct value.

For example, consider a semi-infinite slab of hot metal, initially at 100°C, which is then quenched in a well stirred, large capacity oil bath. After a very short period of time the surface of the slab attains the constant temperature of the bath (30°C) while its central temperature will remain almost unchanged (say 95°C). If the temperature at the slab surfaces are represented by $T^*_{i-1,j}$

and $T^*_{i+1,j}$ [=0], and the centre by $T^*_{i,j}$ [=0.93], then a negative coefficient of $T^*_{i,j}$ would result in the new centre temperature being lower than that in the water bath which is thermodynamically impossible. An example of this instability is included in the results presented in section 7.3.1. Hence although the explicit method is computationally simple, the time step $\delta t^*=0.5\delta x^{*2}$ is necessarily small since δx^* must be kept small to attain reasonable accuracy.

An alternative solution called the Crank-Nicolson method replaces the r.h.s. of (2.66) by the mean of its finite difference approximations for the (j+1)th and jth time steps. Hence for i=1,2,...N

$$(T^*_{i,j+1}-T^*_{i,j})/\delta t^* = 0.5\{(T^*_{i+1,j+1} - 2T^*_{i,j+1} + T^*_{i-1,j+1})/\delta x^{*2} + (T^*_{i+1,j} - 2T^*_{i,j} + T^*_{i-1,j})/\delta x^{*2}\},$$

which may be rearranged to

$$Fo\{-T^*_{i-1,j+1} + [(2/Fo)+2]T^*_{i,j+1} - T^*_{i+1,j+1}\} = Fo\{T^*_{i-1,j} + [(2/Fo)-2]T^*_{i,j} + T^*_{i+1,j}\}, \quad (2.69)$$

where $T^*_{0,j}$ is known and by symmetry $T^*_{N-1,j}=T^*_{N+1,j}$ for $t>0$. This method results in N simultaneous equations to be solved for N unknown values at the (j+1)th time step in terms of the known values at the jth time step, and is therefore known as a semi-implicit method.

The set of equations corresponding to (2.69) can be represented by

$$\begin{aligned} &d_1T^*_1 - a_1T^*_2 = c_1 \text{ , at node 1} \quad (2.70)\\ &-b_2T^*_1 + d_2T^*_2 - a_2T^*_3 = c_2 \text{ , at node 2}\\ &-b_iT^*_{i-1} + d_iT^*_i - a_iT^*_{i+1} = c_i \text{ , at node i}\\ &-b_NT^*_{N-1} + d_NT^*_N = c_N \text{ , at node N} \end{aligned}$$

where c represents the evaluated r.h.s. of the expression and a,b,d are the coefficients: above diagonal, below diagonal and on the diagonal respectively. The solution technique involves eliminating T^*_1 from the second equation by addition of a suitable multiple of the first equation (i.e. b_2/d_1). This process is

repeated for the third and subsequent equations employing where possible the updated form of the previous equation which results in the last equation having only one unknown. This value is then determined and the remaining unknowns found by back substitution. An example demonstrating the use of this technique known as the tri-diagonal matrix algorithm (TDMA) is presented in section 7.3.1.

2.4.2.3. Methods of dealing with phase change

The simplest method of dealing with phase change is to determine the temperature fall that would occur if the latent heat were abstracted from a unit mass of the PCM

$$PCT = \lambda/Cp. \tag{2.71}$$

Hence, whenever a node temperature is greater (lower) than the melting point during charge (discharge) the temperature of that node is maintained at the melting point and the difference between T_{mp} and the predicted temperature recorded. In the following time steps this procedure is repeated until the cumulative total is greater than PCT. At that point the node temperature is permitted to increase (decrease) in the normal manner. This method is demonstrated in section 7.3.2.

Murray and Landis (1959) refer to the above approach as the "conventional" method and proposed two new methods to yield considerably greater accuracy especially near the fusion point. The first approach utilized a travelling space network, where the fusion point travel could be accurately determined, but local temperature-time histories within the medium had to be interpolated. The second method used a fixed space network and involved tracing the fusion front as it travelled through each node which gave an accurate prediction of the transient temperature in the fusion front region. Both these techniques however are of limited applicability since much greater improvements in accuracy can be achieved by increasing the number of nodes, an approach only recently possible due to the enormous increase in available computer power for analysing such problems. Two sample problems were considered.

1. Stefan: semi-infinite slab initially at fusion temperature and subjected to a step decrease in surface temperature. An analytical solution to this problem was derived in section 2.4.1.2 and results are presented in section 7.2.2. The predicted response by the conventional FDE method (described above) is compared with the analytical solution in section 7.3.2.
2. General: symmetrical finite slab initially at a uniform temperture above the fusion temperature subjected to a step decrease in surface temperature below the melting point. There is no analytical solution to this problem and the results predicted by conventional FDE method were compared with the two new methods.

In both cases the proposed new methods were found to give superior accuracy when compared to the conventional method utilising only 8 nodes.

In the finite difference method proposed by Shamsundar and Sparrow (1975) the enthalpy is used as a dependent variable along with the temperature. This method, sometimes called the "weak solution" technique, does not explicitly determine the phase boundary, although its position can be approximately determined from a knowledge of the enthalpy distribution. In this method the problem .is made equivalent to one of heat conduction without phase change, which is solved by a fully implicit finite difference scheme.

Shamsundar (1978) considered a simple 1-D test case of solidification of pure saturated liquid by convective cooling at a plane wall. The dimensionless heat flux

$$(q/A)^* = [h(T_w-T_a]/[h(T_{mp}-T_a], \qquad (2.72)$$

and non-dimensional interface position were calculated for three spatial step sizes (0.1, 0.05 and 0.01). For each spatial step size the timewise step was successively reduced until it had no observable (to three significant figures) effect. For all three spatial step sizes the prediction of the interface position was found to be in excellent agreement with a correct solution by other (unspecified!) numerical methods. The predicted heat flux, on the other hand, was wavy in nature, and the waviness was directly influenced by the spatial

step size. This behaviour was caused by the quasi-steady nature of the temperature profiles for low Ste. As a node solidified its temperature was held constant at T_{mp} allowing (q/A)* to become nearly constant. Then when the node was completely solidified its temperature was allowed to change and the heat flux dropped rapidly to its new quasi-steady value. This waviness diminished and the predicted values converged to the correct solution as the spatial step-size was reduced.

2.4.2.4. FDEs for Edinburgh Storage Device

The Edinburgh store utilises plastic tubes 1 m in length and either 25 or 38 mm in diameter to contain the PCM. Since the diameter to length ratio is very small, axial conduction was considered to be negligible while it was hoped that the regular tube arrangement would give a constant circumferential wall temperature. Hence radial heat transfer was assumed to be dominant and a 1-D FDE in cylindrical coordinates derived for modelling purposes.

Consider figure 2.23(a) which shows the heat flows of a typical internal node in a cylinder. The heat balance per unit length of cylinder at node i may be written as

$$[kP_{i-1/2}(T_{i-1,j}-T_{i,j})]/\delta r - [kP_{i+1/2}(T_{i,j}-T_{i+1,j})]/\delta r = [\rho CpA_i(T_{i,j+1}-T_{i,j})]/\delta t, \quad (2.73)$$

where A_i is the cross sectional area of elemental cylinder (shaded) at node i = $\pi[r^2_{i+1/2}-r^2_{i-1/2}] = 2\pi r_i\delta r$. The area for heat transfer into and out of the elemental cylinder is respectively $P_{i-1/2}=2\pi(r_i-\delta r/2)$ and $P_{i+1/2}=2\pi(r_i+\delta r/2)$. Substitution of the above into (2.73) and dividing by 2π yields

$$[k(r_i-\delta r/2)(T_{i-1,j}-T_{i,j})]/\delta r - [k(r_i+\delta r/2)(T_{i,j}-T_{i+1,j})]/\delta r = [\rho Cpr_i\delta r(T_{i,j+1}-T_{i,j})]/\delta t.$$

Multiplying throughout by $\delta r/kr_i$

$$[1-(\delta r/2r_i)](T_{i-1,j}-T_{i,j}) - [1+(\delta r/2r_i)](T_{i,j}-T_{i+1,j}) = [(\rho Cp\delta r^2)/(k\delta t)](T_{i,j+1}-T_{i,j}),$$

which may be rearranged to

$$Fo\{[1-(\delta r/2r_i)]T_{i-1,j} - 2T_{i,j} + [1+(\delta r/2r_i)]T_{i+1,j}\} = T_{i,j+1}-T_{i,j}.$$

Hence the explicit FDE for an internal node may be written as

$$T_{i,j+1} = Fo\{[1-\delta/2r_i)]T_{i-1,j} + [(1/Fo)-2]T_{i,j} + [1+(\delta r/r_i)]T_{i+1,j}\}. \quad (2.74)$$

At the surface of the tube the rate of heat transferred to the PCM is determined from a heat transfer coefficient representing both the thermal resistance of the fluid film and the tube wall. Hence the heat flows per unit length of cylinder shown in figure 2.23(b) for the boundary node may be written as

$$[kP_{N-1/2}(T(N-1,j)-T_{N,j})]/\delta r - hP_N(T_{N,j}-T_a) = [\rho CpA_N(T_{N,j+1}-T_{N,j})]/\delta t \quad (2.75)$$

where A_N is the cross sectional area of the boundary node (shown shaded) = $\pi[r_N\delta r-(\delta r^2/4)]$, which is approximated to $\pi r_N\delta r$ with an error in the range 2.5-0.25% for a total of 10-100 nodes. The area for heat transfer into and out of this elemental cylinder is respectively $P_{N-1/2}=2\pi[r_N-(\delta r/2)]$ and $P_N=2\pi r_N$. Substituting these values into equation (2.75) and dividing throughout by π yields

$$[2k(r_N-\delta/2)(T_{N-1,j}-T_{N,j})]/\delta r - 2hr_N(T_{N,j}-T_a) = [\rho Cpr_N\delta r(T_{N,j+1}-T_{N,j})]/\delta t.$$

Multiplying throughout by $\delta r/kr_N$ gives

$$(2-\delta r/r_N)(T_{N-1,j}-T_{N,j}) - [(2h\delta r)/k](T_{N,j}-T_a) = [(\rho Cp\delta r^2)/(k\delta t)](T_{N,j+1}-T_{N,j}),$$

which may be rearranged to

$$Fo\{[2-(\delta r/r_N)]T_{N-1,j} + 2BiT_a + [(\delta r/r_N)+2-2Bi]T_{N,j}\} = T_{N,j+1}-T_{N,j}.$$

Hence the explicit FDE for a boundary node may be written as

$$T_{N,j+1} = Fo\{[2-(\delta r/r_N)]T_{N-1,j} + 2BiT_a + [(1/Fo-(\delta r/r_N)-2-2Bi]T_{N,j}\}. \quad (2.76)$$

The FDE for the central node is determined using the PDE replacement

method. In cylindrical coordinates the 1-D PDE for radial heat transfer, equation (2.50) is given in section 2.4.1.4. The term $(1/r)(\partial T/\partial r)$ becomes indeterminate at the central axis of the tube and can be replaced by $\partial^2 T/\partial r^2$ as $r \rightarrow 0$. Hence the PDE becomes

$$\partial T/\partial t = 2\alpha(\partial^2 T/\partial r^2), \tag{2.77}$$

which can be approximated by

$$(T_{0,j+1}-T_{0,j})/\delta t = [2\alpha(T_{-1,j}-2T_{0,j}+T_{1,j})]/\delta r^2.$$

Since there is no heat transfer across the central axis (i.e. $\partial T/\partial r = 0$ at $r=0$) then by symmetry $T_{1,j}=T_{-1,j}$ and

$$T_{0,j+1}-T_{0,j} = 2Fo\{2T_{1,j}-2T_{0,j}\}.$$

Hence the explicit FDE for the central node becomes

$$T_{0,j+1} = Fo\{4T_{1,j} + [(1/Fo)-4]T_{0,j}\} \tag{2.78}$$

The stability conditions, viz. keeping coefficients of $T_{i,j}$, $T_{N,j}$ and $T_{0,j}$ positive for ordinary, boundary and central node respectively are

$$Fo <= 0.5, \tag{2.79}$$

$$Fo <= \{1/[2-(\delta r/r_N)+2Bi]\}, \tag{2.80}$$

$$Fo <= 0.25. \tag{2.81}$$

In the pilot scale store the residence time of the transfer fluid within the store and the thermal capacity of the PCM were both small, which made it permissible to assume that there was negligible longitudinal variation of the transfer fluid temperature. Hence the entire store could be modelled quite straightforwardly using the above equations. However the residence time in the prototype storage device is quite large (approximately 30 minutes for 0.192 kg/s) as is the thermal capacity, so there is a significant longitudinal variation

in the transfer fluid temperature as it passes through the store. Dusinberre (1961) included the formulation of FDEs for regions in which flow occurs and the following derivation is based on his discussion.

Consider a discretized region of flow in a channel as shown in figure 2.24. A heat balance on the shaded area yields

$$\dot{m}\,Cp(T_{i-1,j}-T_{i,j}) - hP\delta z[(T_{i-1,j}+T_{i,j})/2-T_{PCM}] = [\rho CpA_f\delta z(T_{i,j+1}-T_{i,j})], \qquad (2.82)$$

where A_f is the cross sectional flow area and P is the heat transfer area per unit length of flow channel. To simplify the analysis the following variables are introduced

$$\text{capacity rate} \quad V = \dot{m}\,Cp, \qquad (2.83)$$

$$\text{conductance} \quad H = hP\delta z, \qquad (2.84)$$

$$\text{heat capacity} \quad C = \rho CpA_f\delta z, \qquad (2.85)$$

and substituted in to equation (2.82), which when divided throughout by C yields

$$T_{i,j+1}-T_{i,j} = [V\delta t/C](T_{i-1,j}-T_{i,j}) - [H\delta t/2C][T_{i-1,j}+T_{i,j}-2T_{PCM}],$$

and can be rearranged to

$$T_{i,j+1}-T_{i,j} = [(2V-H)/2C]\delta tT_{i-1,j} + [H\delta t/C]T_{PCM} + [1-(2V+H)/2C]\delta tT_{i,j}.$$

Hence the explicit FDE for the transfer fluid in a flow channel can be written as

$$T_{i,j+1} = [H\delta t/C]T_{PCM} + [(2V-H)/2C]\delta tT_{i-1,j} + \{1-[(2V+H)/2C]\delta t\}T_{i,j}. \qquad (2.86)$$

For the solution to remain stable the coefficient of $T_{i,j}$ must remain positive, hence

$$\delta t <= 2C/(2V+H), \qquad (2.87)$$

and to keep $T_{i-1,j}$ positive in (2.86)

$$H <= 2V, \tag{2.88}$$

which puts a limit on the incremental length δz.

2.4.2.5. Review of other literature

Talwar and Dilpare (1977) investigated the freezing of an ice plug in a 50 mm diameter mild steel pipe. The water was initially at the fusion temperature and a step decrease in surface temperature was achieved by injection of liquid nitrogen into a cooling jacket. A 2-D finite difference solution in cylindrical coordinates was utilised to predict the time required for complete freezing of the plug. An explicit solution technique was employed, which determined its own optimum integration time to ensure stability and convergence. The latent heat effect was included by defining an equivalent specific heat over a small temperature interval, however it should be noted that it was found that if this interval was larger than 3 degC, the predicted time to freeze was affected. The choice of twelve radial nodes was reported to combine good accuracy with reasonable computer time (776 seconds) for the solution. The nitrogen temperature was maintained at either -45 or -100 °C, resulting in experimental freezing times of 515 and 262 seconds respectively. The model over-predicted the freezing times by 13.6 and 23%, although it was not certain that the correct heat transfer coefficient had been determined for the boiling nitrogen. In addition, the method of experimentally determining when the ice plug had formed, using a thread, was thought to perhaps have interfered with the nucleation process. It was concluded that the effect of axial conduction was negligible.

A number of workers have developed methods for dealing with moving boundary problems utilising an immobilisation transformation technique. This consists of transforming the governing PDEs into a coordinate system where the phase boundaries correspond to fixed coordinate surfaces. An example problem involving the solidification of a finite cylinder (with an aspect ratio of 1) was considered by Duda et al. (1975), where the upper surface was initially maintained at a temperature above the melting point and the lower below the melting point. The circumference of the cylinder was thermally insulated until

t=0 when it was exposed to a fluid maintained at a third temperature. Results for a range of conditions were presented; and for one case the final steady state position of the interface was determined from an analytical solution and found to be in excellent agreement (error <1%) with the predicted results.

The above technique was limited to cylindrical geometries, but the transformation method developed by Saitoh (1978) was utilised for multidimensional freezing problems in arbitrary domains. A sample solution is presented for the cylindrical freezing problem with the origin of the computation eccentrically located to test the method for an irregular geometry. The predicted solution agreed well with the quasi-steady solution, with the exception of the final stage of freezing.

Katayama et al. (1981) presented heat flux against time curves for charge and discharge of a horizontal cylinder (diameter 40 mm) containing naphthalene. Heat fluxes calculated from an explicit finite difference method were reported to agree well with experimental results for solidification, but showed different trends during melting due to the effects of natural convection. No exact details of the solution scheme or the method of dealing with phase change were reported.

2.4.3. Nusselt Number for Laminar Flow in Ducts

The channels formed between the tubes used in the store may be approximated to pipes with an equivalent diameter defined as

$$De = 4 \times \text{flow cross sectional area} / \text{wetted perimeter.} \qquad (2.89)$$

In an infinite triangular array of tubes the flow area and wetted perimeter are easily obtained, and Shah and London (1978) presented the following generalised equation for different tube diameter and spacing

$$De/D_t = \{[(2\sqrt{3})/\pi](s/D_t)^2\} - 1. \qquad (2.90)$$

In the following subsection methods of calculating the Nusselt number, both by approximation of the duct formed between the tubes to a pipe, and where available for in-line flow over rod bundles, are reviewed.

2.4.3.1. Fully developed laminar flow in long tube

An excellent analysis of laminar forced convection under fully developed conditions in a long tube is presented by Kreith and Bohn (1986). For laminar flow in a duct the hydraulic entry length (x_{FDV}) at which the velocity profile approaches its fully developed shape is defined as

$$(x_{FDV}/De) = 0.05\ Re_{De}, \tag{2.91}$$

while the distance (x_{FDT}) from the inlet at which the temperature profile approaches its fully developed shape is given by the relation

$$(x_{FDT}/De) = 0.05\ Re_{De}Pr. \tag{2.92}$$

A force balance on a cylindrical element inside the tube is employed to derive the radial distribution of axial velocity. For the boundary conditions u=0 at $r=r_w$ (tube wall) and $u=u_{max}$ at r=0 (centre) the velocity distribution in fully developed flow can be decribed by the following dimensionless expression

$$u/u_{max} = 1 - (r/r_w)^2. \tag{2.93}$$

(a) Uniform heat flux

For uniform heat flux, the fluid temperature will vary linearly with the axial distance x, while the temperature difference between the surface of the tube and the bulk will be constant, except for the entrance region where the heat transfer coefficient decreases due to the developing boundary layer. An energy balance, where heat is transferred by conduction into and out of the element in a radial direction, and by convection in the axial direction yields

$$(1/ur)(\partial/\partial r)(r\partial T/\partial r) = (\rho Cp/k)(\partial T/\partial x). \tag{2.94}$$

For the velocity distribution given by (2.93) and the boundary conditions $\partial T/\partial r=0$ at r=0 and $k\partial T/\partial r=q''_w$=constant at $r=r_w$, the temperature distribution is defined by

$$T-T_c = (1/\alpha)(\partial T/\partial x)[(u_{max}r_w^2)/4][(r/r_w)^2-0.25(r/r_w)^4] \quad (2.95)$$

The average bulk temperature T_b can then be determined and the average heat transfer coefficient found from

$$h_{av} = q/[A_w(T_w-T_b)] = k(\partial T/\partial r)_{r=rw}/(T_w-T_b), \quad (2.96)$$

and hence the Nusselt number found to be

$$Nu_D = h_{av}D/k = 4.364. \quad (2.97)$$

(b) Uniform surface temperature

When it is the tube surface temperature that is uniform rather than the heat flux, the analysis is more complicated because the temperature difference between the wall and the bulk varies along the tube. Equation (2.94) can be solved using $T(x,r_w)$=constant as the second boundary condition, but an iterative procedure is required. The result is not a simple algebraic expression, but the Nusselt number is again found to be a constant:

$$Nu_D = h_{av}D/k = 3.66. \quad (2.98)$$

Due to the constant temperature boundary condition the log-mean temperature difference (shown in square brackets below) must be used to evaluate the rate of heat transfer

$$q = h_{av}A_w[(\Delta T_{out}-\Delta T_{in})/\ln(\Delta T_{out}/\Delta T_{in})]. \quad (2.99)$$

2.4.3.2. Fully developed laminar flow in rod bundles

A theoretical study of heat transfer for laminar in-line flow through unbaffled rod bundles was performed by Dwyer and Berry (1970). The rods were considered to be arranged in a regular equilateral triangular array with the pitch to diameter ratio (s/D_t) varied from 1.001 to 2.0. It was assumed that the tube bundle was open (i.e. one in which there were no perturbations due to spacing devices) and that fully developed flow and heat transfer conditions prevailed. Two sets of boundary conditions were considered:

1. Type A – uniform circumferential wall temperature and uniform wall heat flux
2. Type B – uniform wall heat flux in all directions

The electrical heating rods generally used in experimental studies have ceramic cores encased in metallic claddings. For the limiting condition of uniform wall heat flux on the inner wall of the cladding, boundary conditions of type A were considered to occur for thick and high conductivity claddings, while those of type B were approached for thin and low conductivity claddings. For the energy storage case it was thought that the low thermal conductivity of the polypropylene tube would prevent a uniform wall temperature and that a uniform heat flux in all directions (type B) would more closely approximate the experimental conditions.

Figure 2.25 presents a representative portion of a bundle, where the area between rod (c) and the surrounding hexagon is the cross sectional flow area for that portion of the transfer fluid exchanging heat with that particular rod. In other words, there is no heat transferred across the hexagonal boundary. This boundary also represents the locus of maximum velocity points in the flow area between rod (c) and its six neighbours. The governing differential energy balance equation for heat transfer in the elemental coolant area (shown shaded) in figure 2.25 is

$$(1/r)k\{[\partial(r\partial T/\partial r)]/\partial r\} + (1/r^2)k(\partial^2 T/\partial\theta^2) = C_p u \rho(dT/dz). \qquad (2.100)$$

For thermal boundary condition B, equation (2.100) is solved with the following boundary conditions

$$\partial T/\partial\theta = 0 \quad \text{at } \theta = 0 \text{ and } 30 \text{ deg}, \qquad (2.101)$$

$$-k(\partial T/\partial r)_{rw} = \text{a constant , at all } \theta, \qquad (2.102)$$

$$\cos\theta(\partial T/\partial r) = (\sin\theta/r)(\partial T/\partial\theta) \text{ , at } r = s/2\cos\theta. \qquad (2.103)$$

For thermal boundary condition A, condition (2.102) is replaced by

$$T_{rw} = T_w = \text{a constant , at all } \theta. \qquad (2.104)$$

The above equations were converted into non-dimensional form and the local velocity in the elemental coolant flow area (evaluated by means of an expression presented by Sparrow and Loeffler (1961)) substituted in. Equation (2.100) was solved numerically, using a system of finite difference equations and the resulting rod-average Nusselt numbers are presented in table 2.3. Also shown in the table is the resulting rod-average heat transfer coefficient when water at 56°C is employed as the transfer fluid. It can be seen that the heat transfer coefficient goes through a maximum as the s/D_t ratio is varied, with the maximum occuring at $s/D_t \approx 1.1$ and 1.2 for type A and B boundary conditions respectively.

2.4.3.3. Laminar flow in tubes and ducts of intermediate length with uniform wall temperature

The Sieder and Tate expression given below is the most commonly used correlation for laminar flow in tubes and ducts with uniform wall temperature.

$$Nu = 1.86[Re_{De}Pr(De/L)]^{0.333}(\mu_w/\mu_b)^{0.14} \qquad (2.105)$$

Whitaker (1972) recommends use of (2.105) only when $[Re_{De}Pr(De/L)]^{0.333}$ is larger than 2. At this lower bound the solution (Nu=3.66, L/De->∞) for fully developed laminar flow in a long tube should be utilised.

2.4.3.4. Mixed convection in vertical tubes

The determination of the heat transfer coefficient in laminar flow becomes more complicated when the buoyancy forces are of the same order of magnitude as the external forces due to forced circulation. When the buoyancy forces are in the same direction as the external forces, such as a fluid being heated in upward flow, heat transfer is enhanced. When the external and buoyancy forces act in opposite directions, the heat transfer is reduced. Metais and Eckert (1964) studied heat transfer in mixed flow and figure 2.26 shows the regions of free, forced and mixed convection for flow through vertical tubes. In the darkly shaded area the contribution of free convection to the total heat transfer is less than 10%, wheras in the lightly shaded area, forced convection effects are less than 10% and free convection predominates. In the unshaded area, natural and forced convection are of the same order of magnitude. The transition region between laminar and turbulent

flow is shown with solid grey shading.

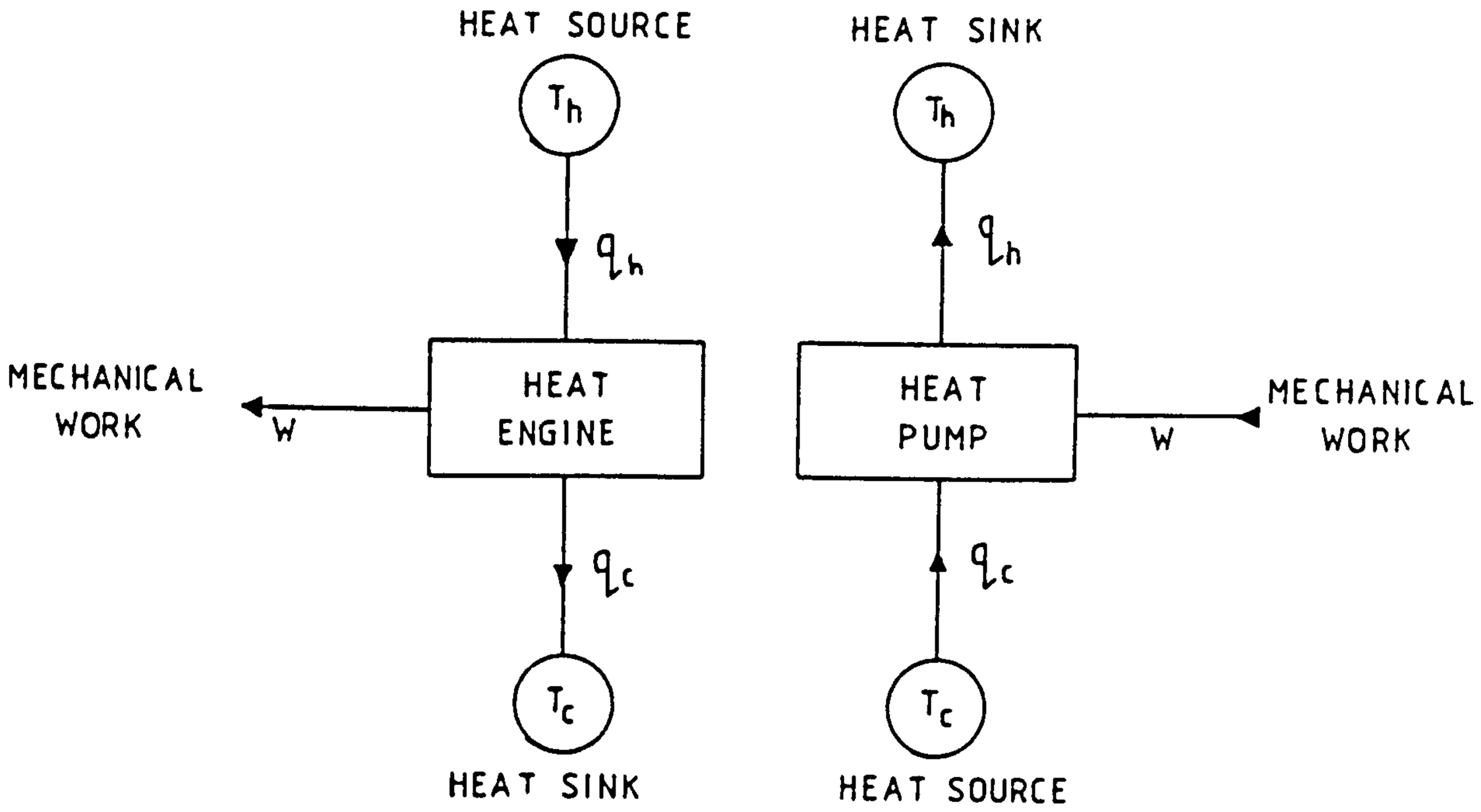

Figure 2.1 Schematic diagram of heat engine and heat pump operation (after McMullan and Morgan 1981)

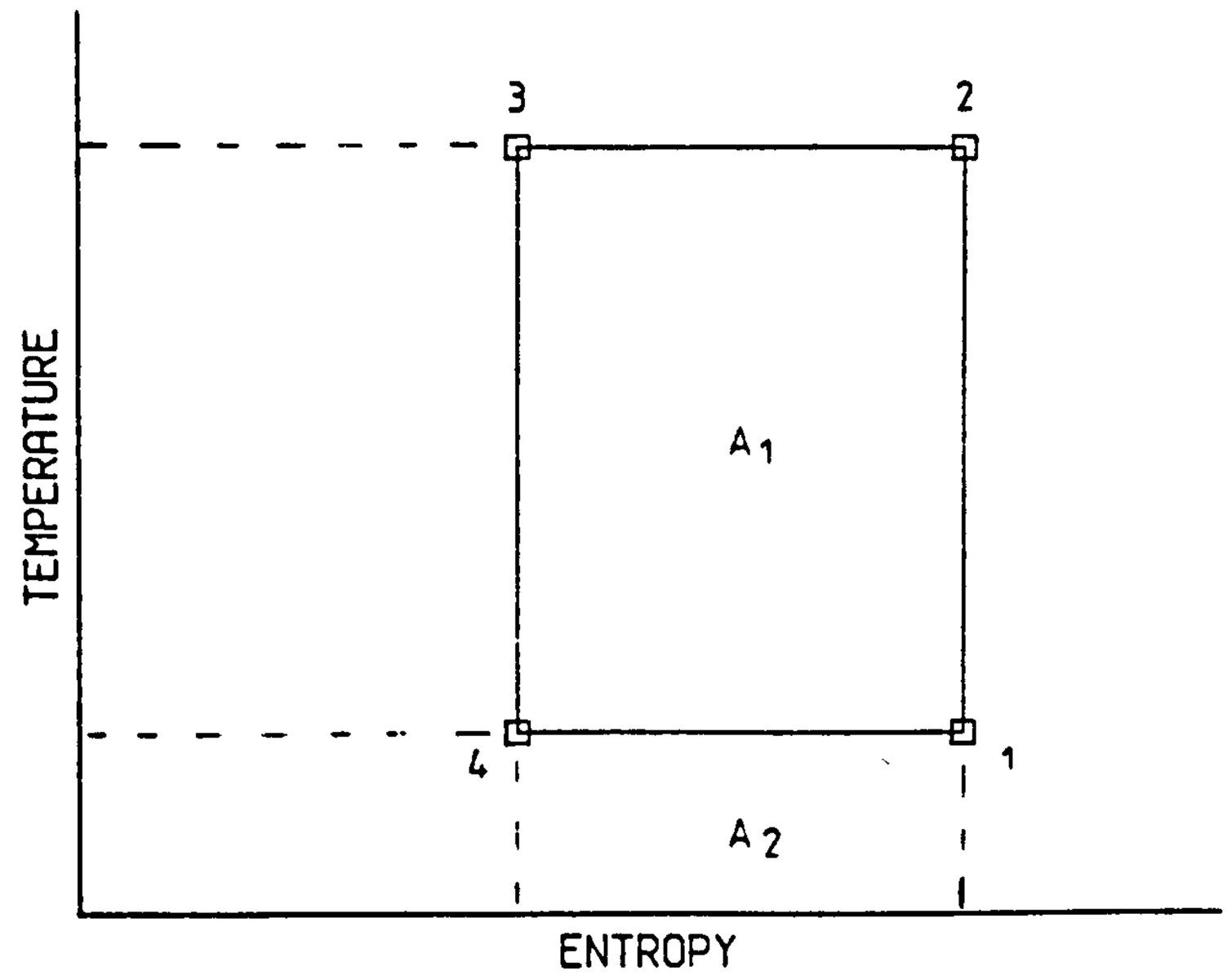

Figure 2.2 Temperature-entropy diagram for a reversed Carnot cycle heat pump (after McMullan and Morgan 1981)

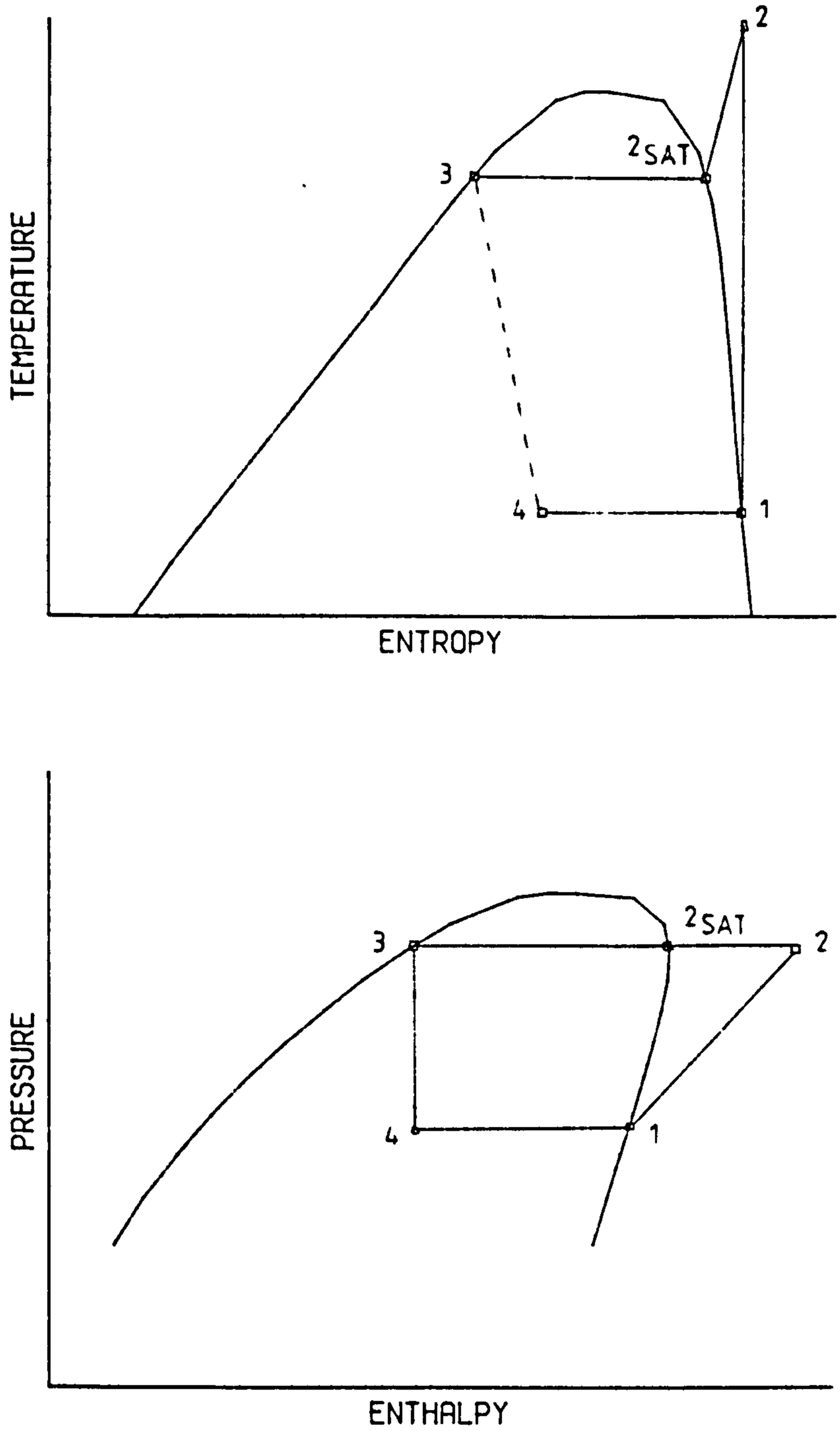

Figure 2.3 Pressure-enthalpy and temperature-entropy diagrams for a vapour compression cycle heat pump

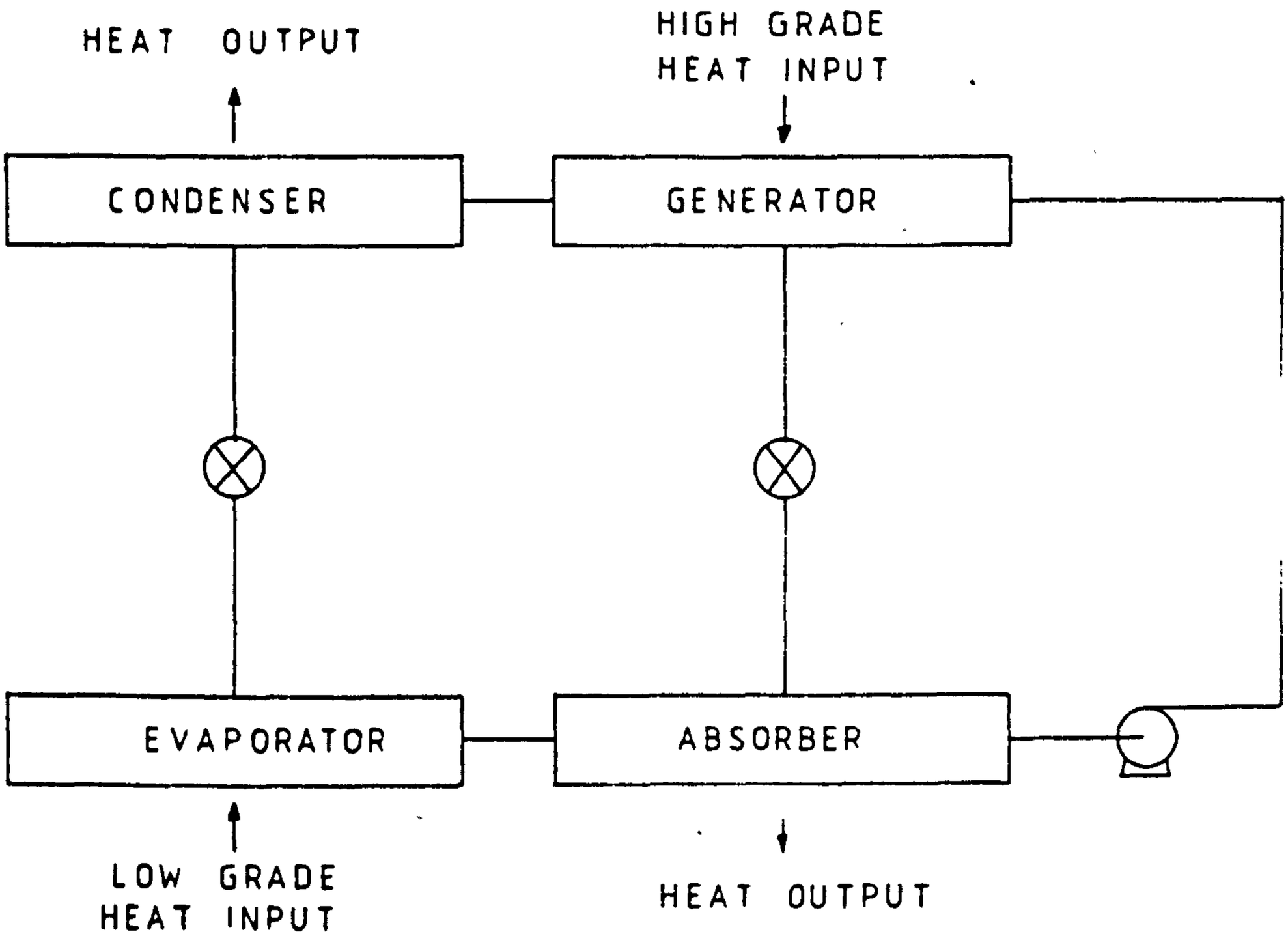

Figure 2.4 Schematic diagram of absorption heat pump cycle

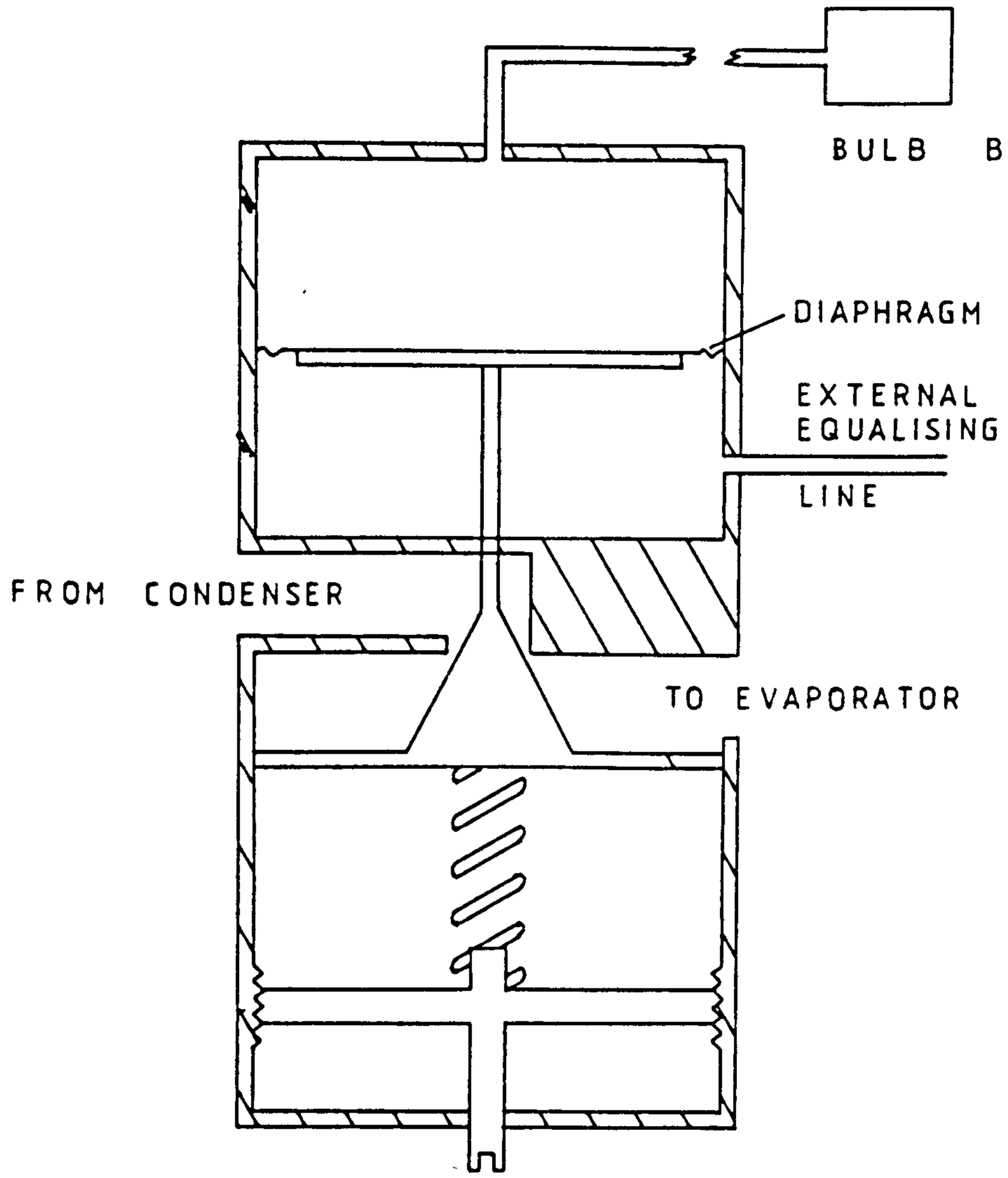

Figure 2.5 Diagram showing thermostatic expansion valve operation (after McMullan and Morgan 1981)

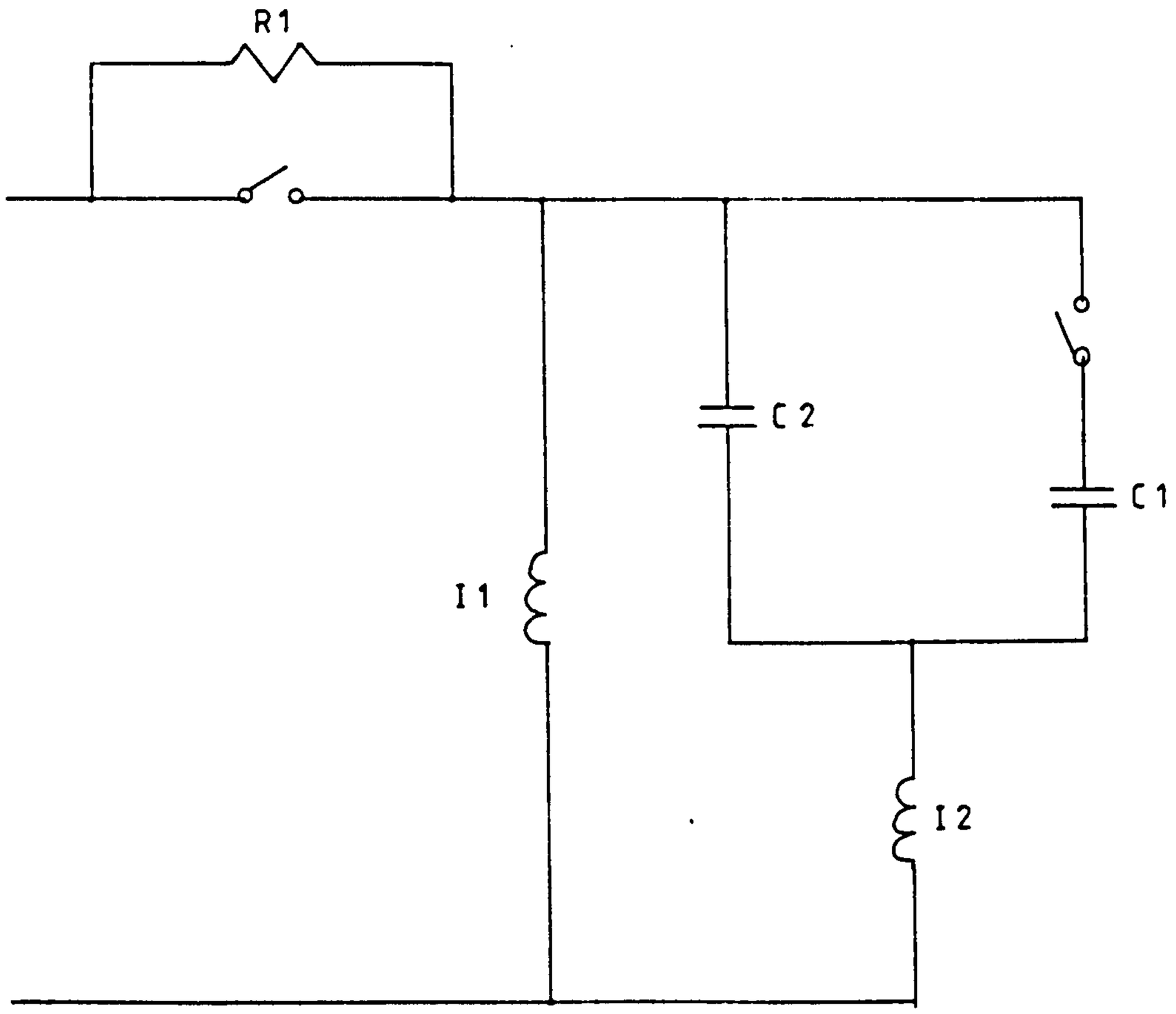

R1	START CAPACITOR
C2	RUN CAPACITOR
R1	START RESISTOR
I1	MAIN WINDING
I2	AUXILIARY WINDING

Figure 2.6 Circuit diagram for "soft start"

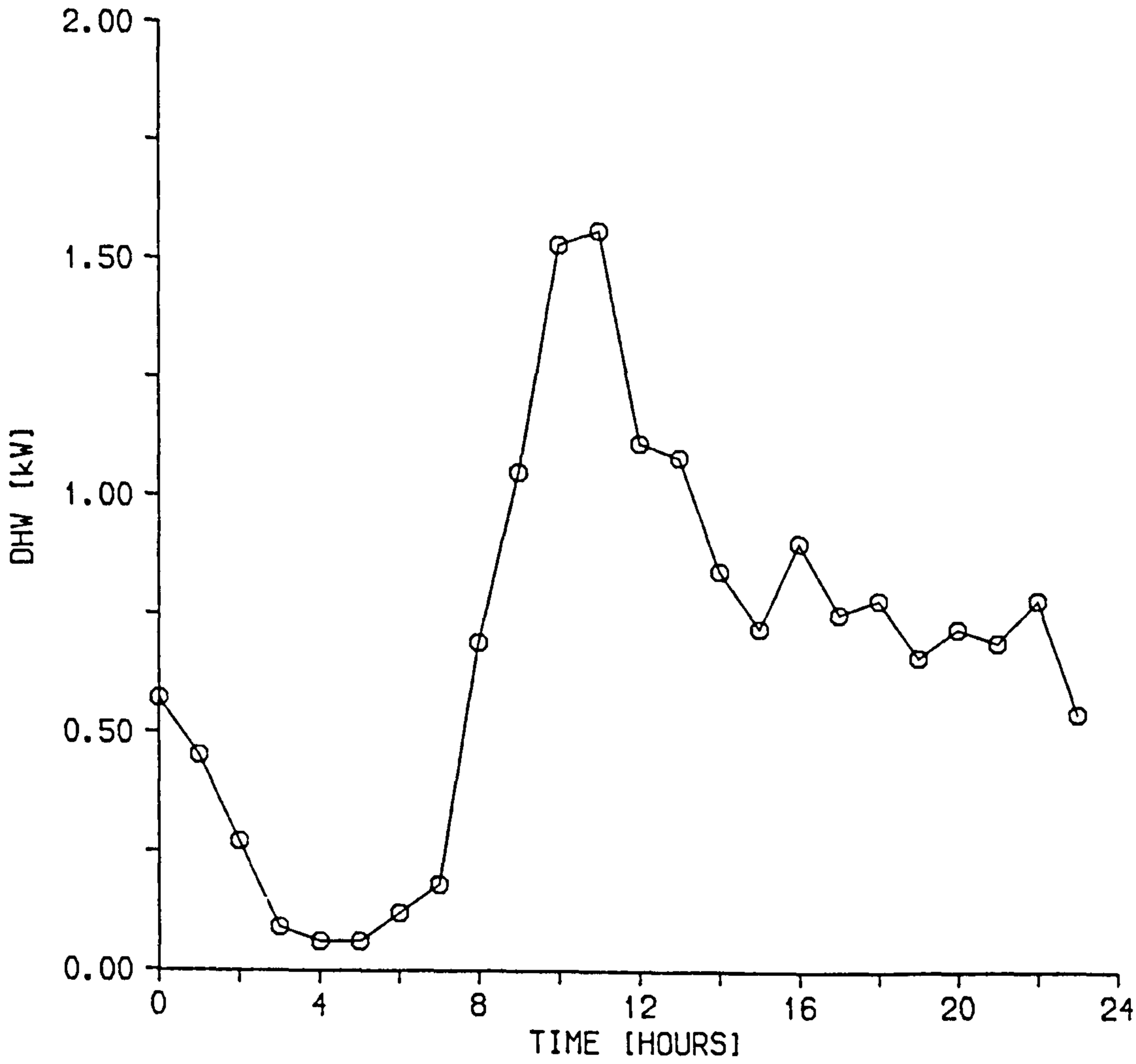

Figure 2.7 Typical hot water demand profile (after Anderson et al. 1985)

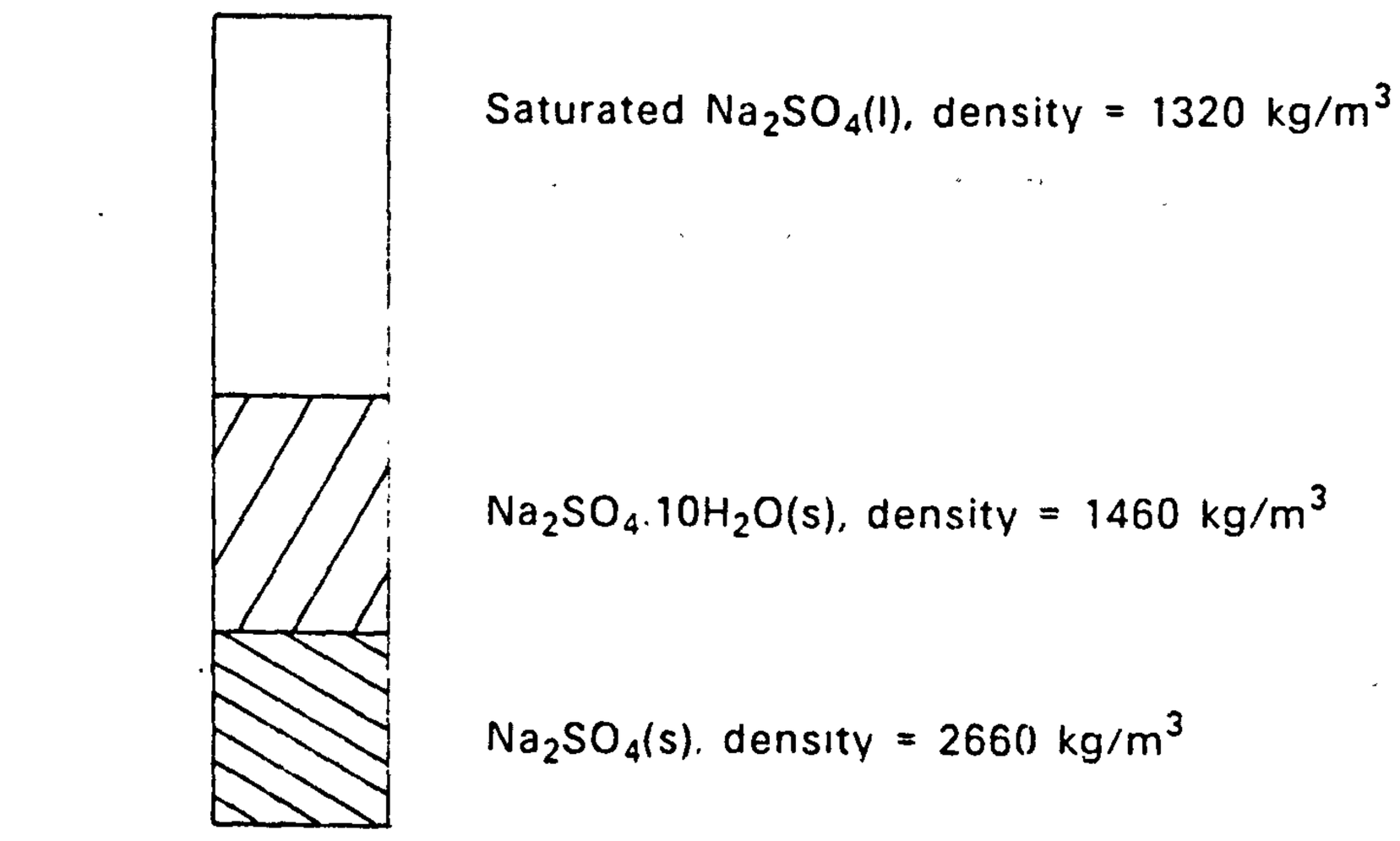

Figure 2.8 Thermal segregation of Glauber's salt (after Wettermark et al. 1979)

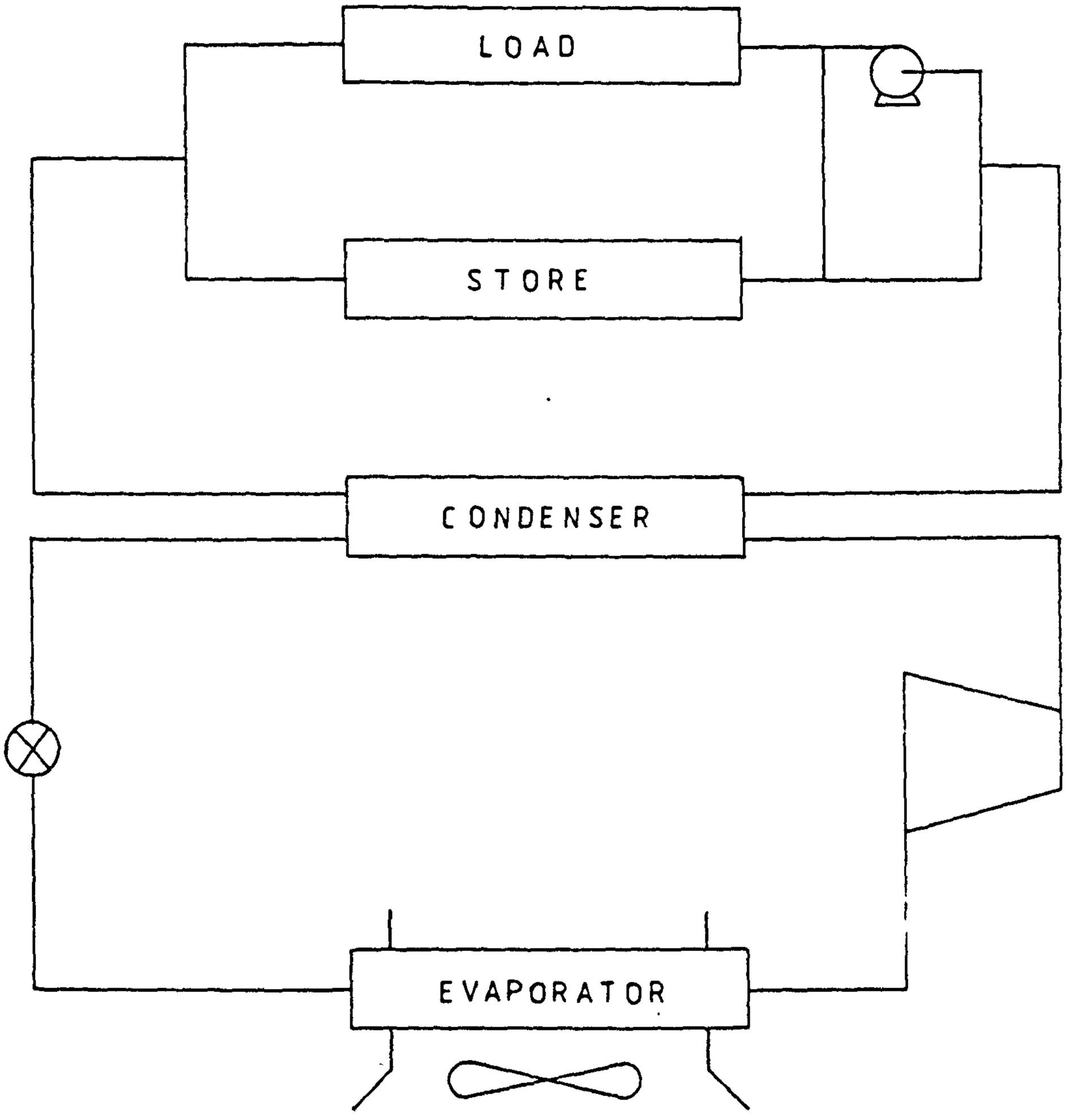

Figure 2.9 Integrated system with water condenser-side external store

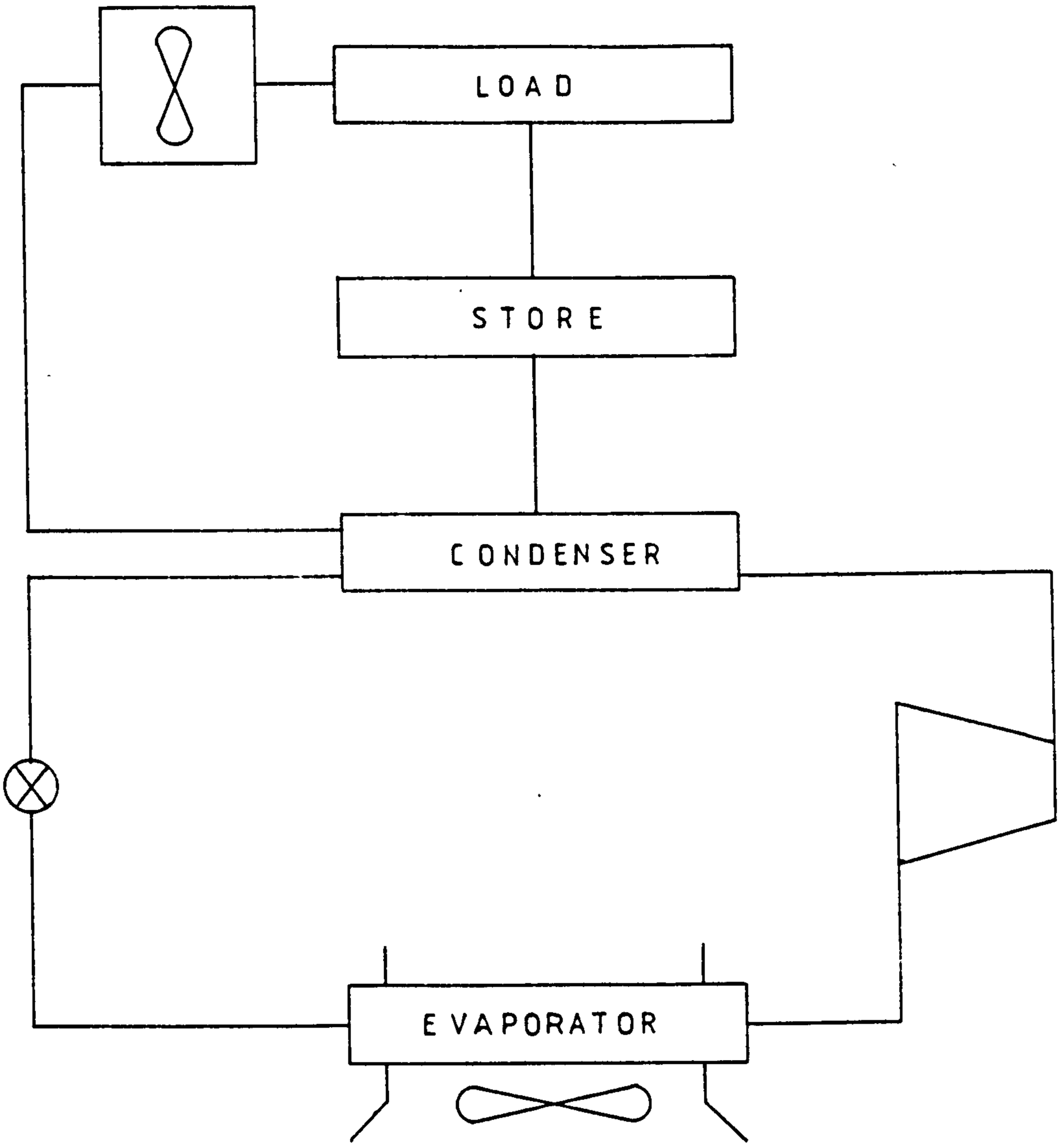

Figure 2.10 Integrated system with air condenser-side external store

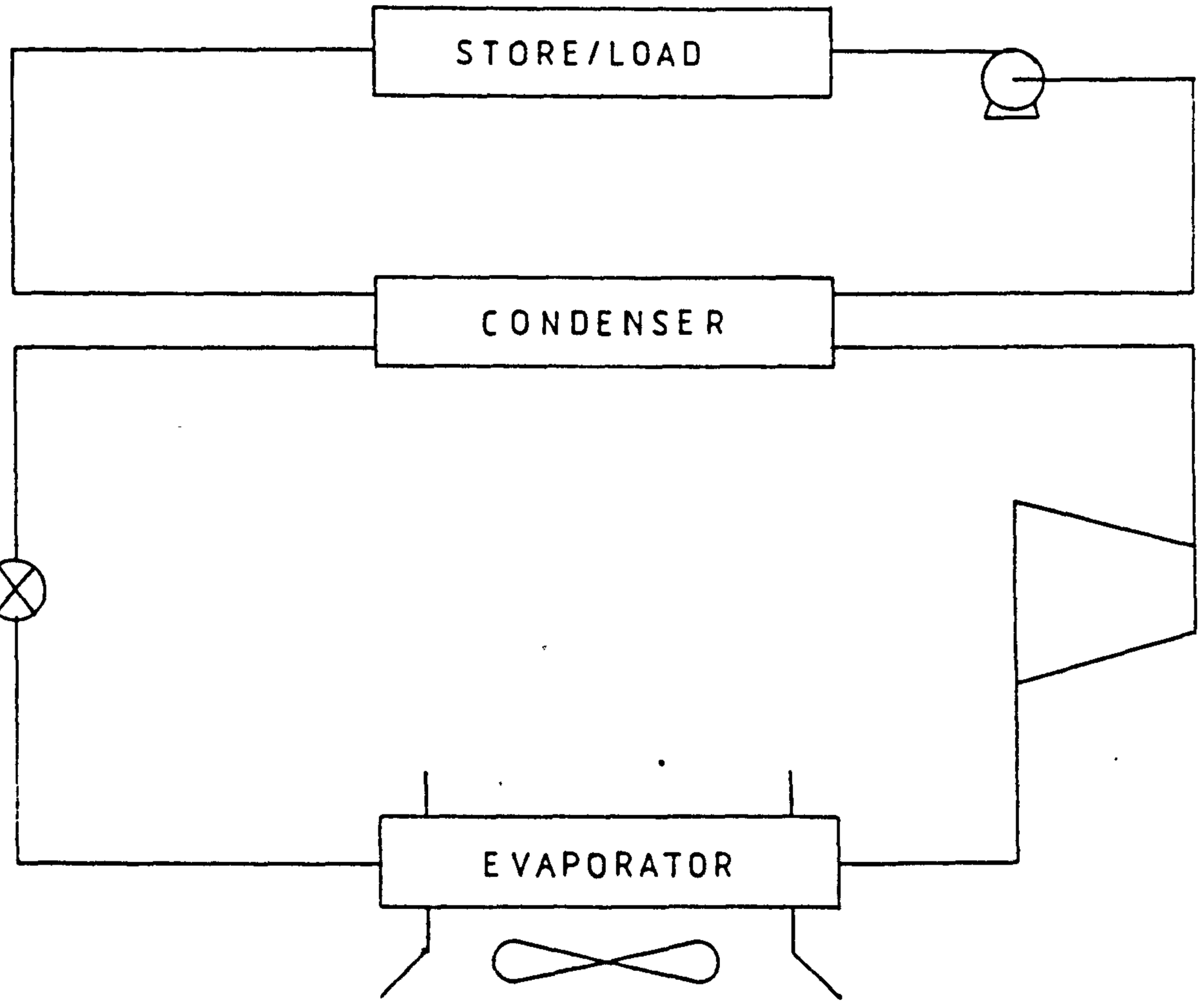

Figure 2.11 Integrated system with water condenser-side external store/load

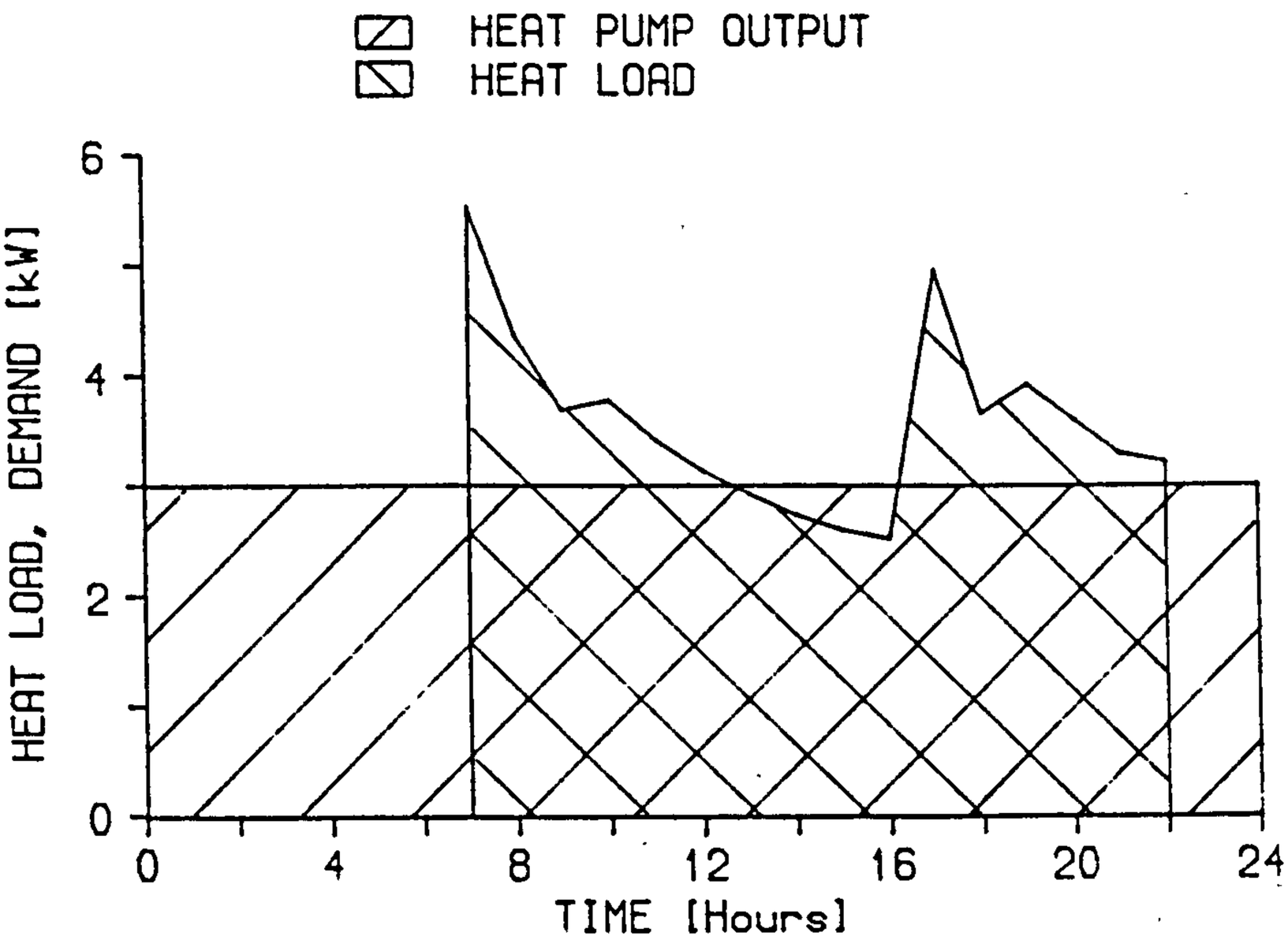

Figure 2.12 Utilisation of Cranfield's peak-lopping store (after Kopecky 1984)

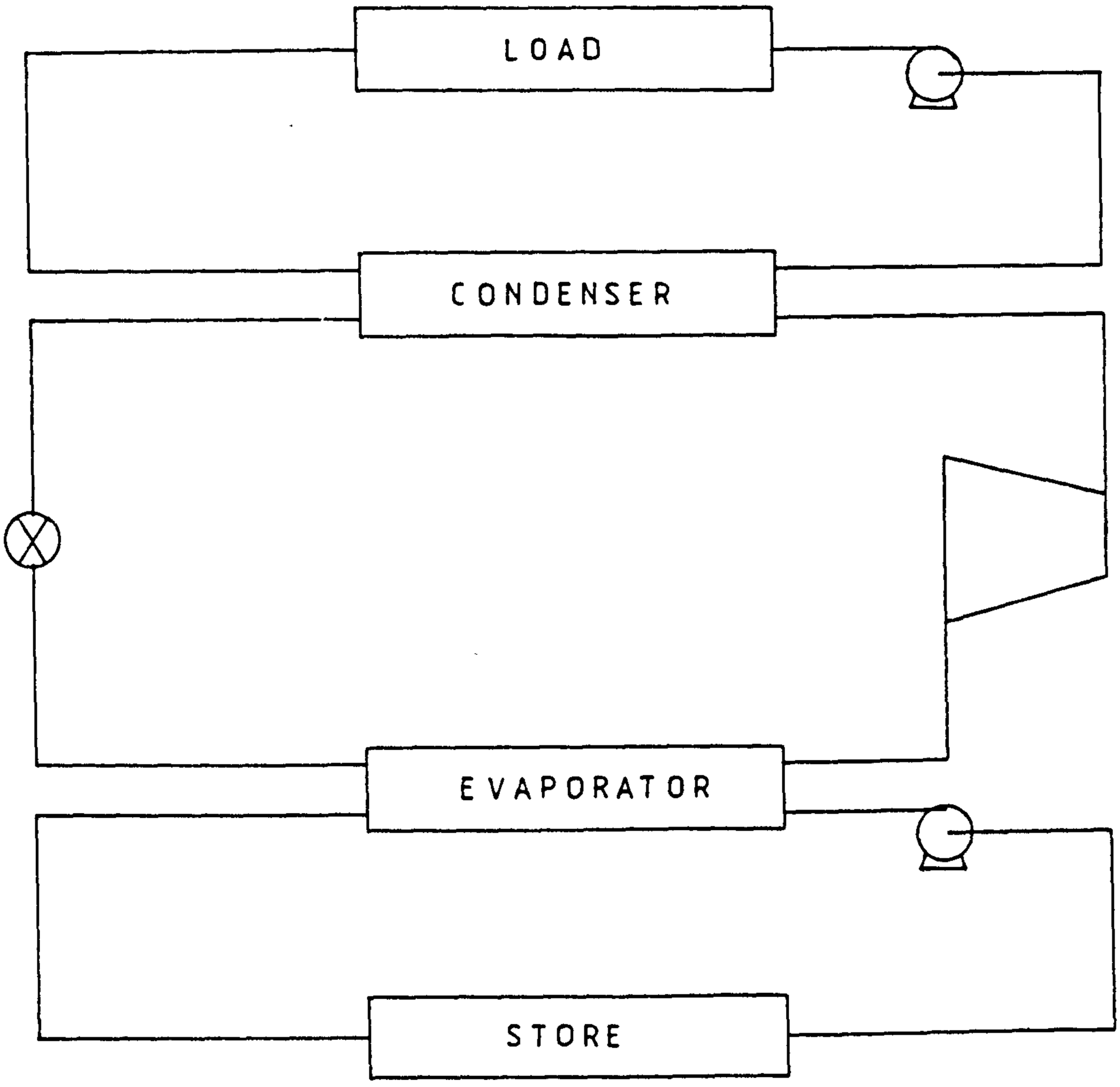

Figure 2.13 Integrated system with water evaporator-side external ground store

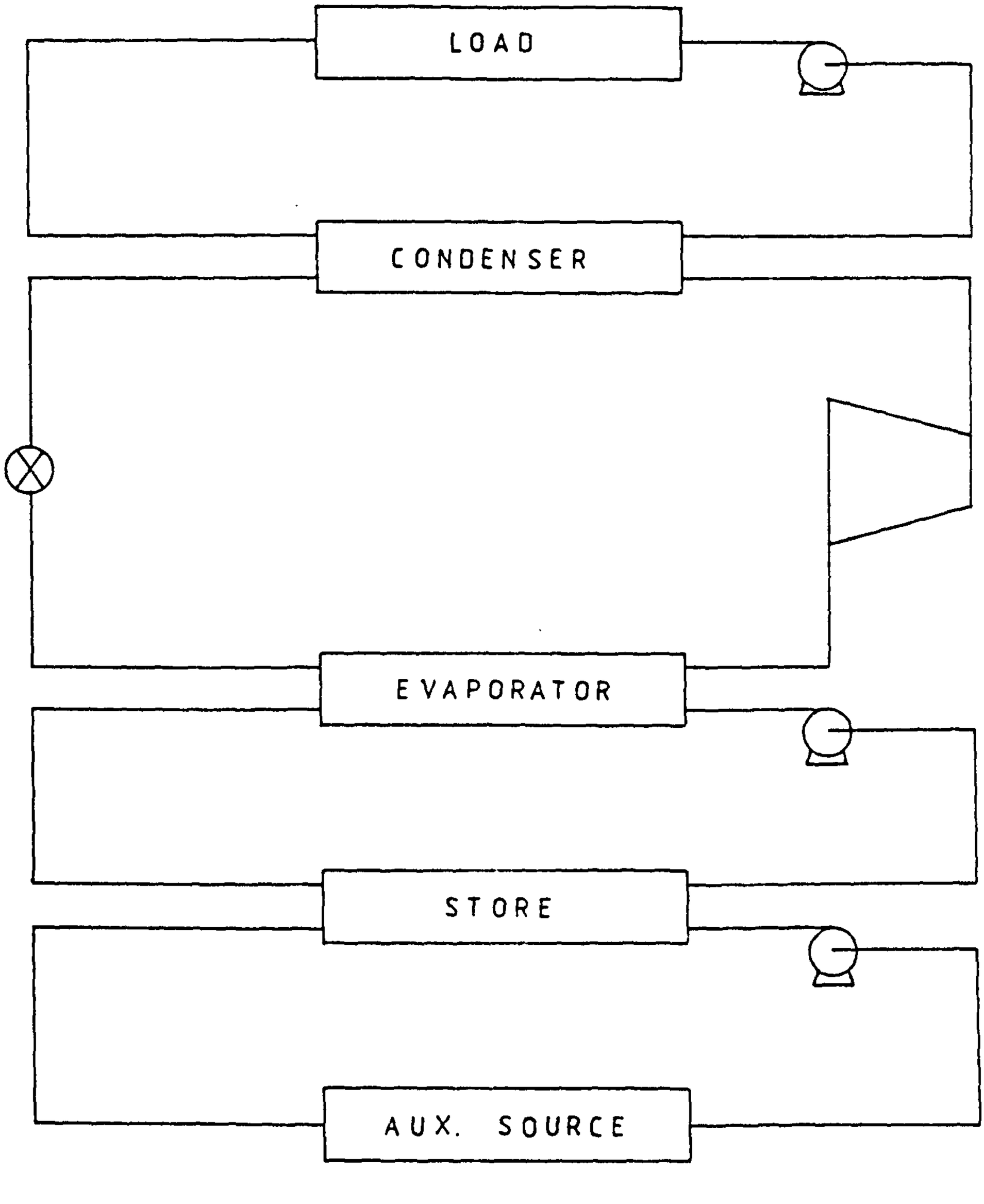

Figure 2.14 Integrated system with water evaporator-side external store with auxiliary source

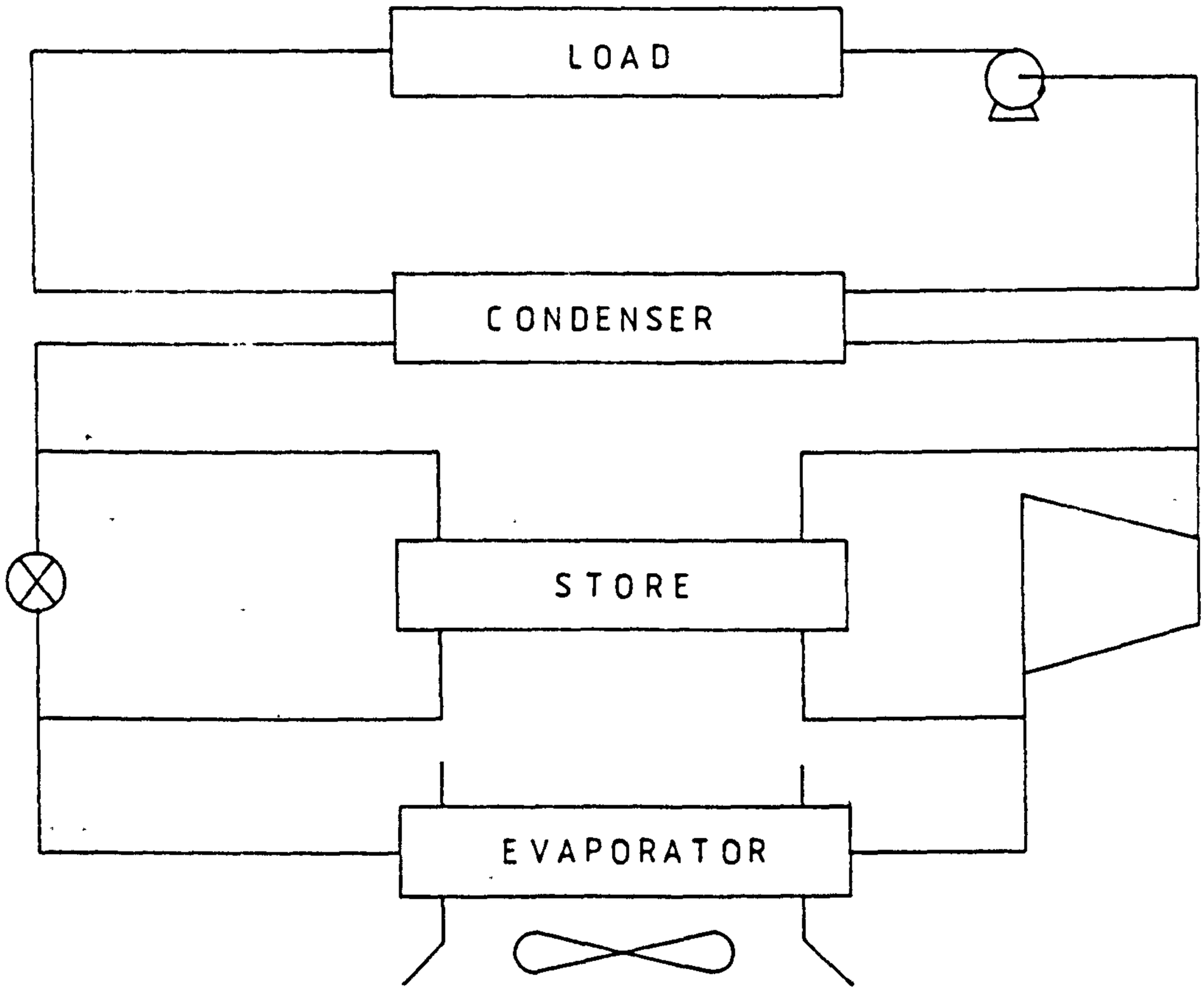

Figure 2.15 Integrated system with central internal store

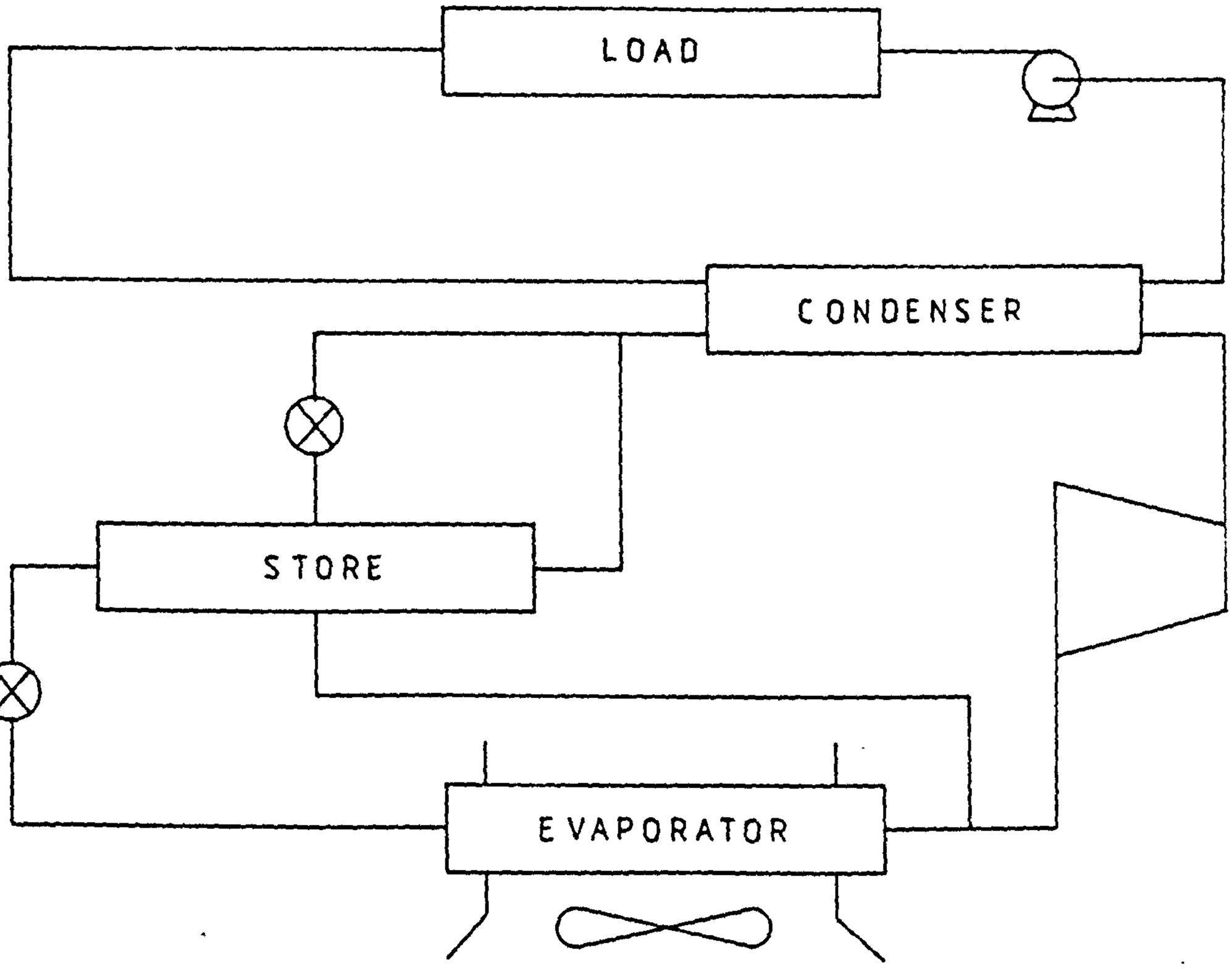

Figure 2.16 Integrated system with central/evaporator-side store

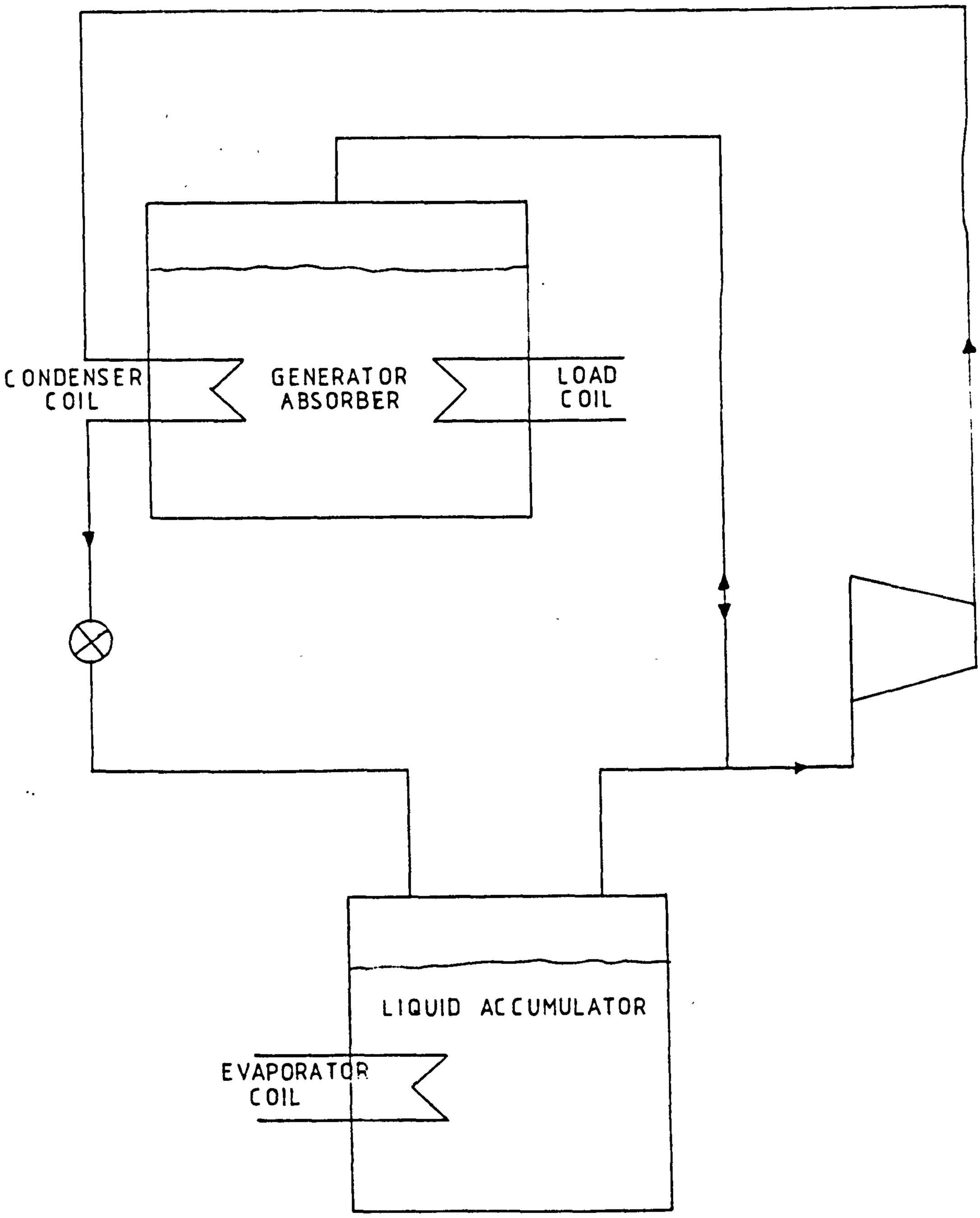

Figure 2.17 Schematic refrigerant circuit of storage heat pump (for single stage compression)

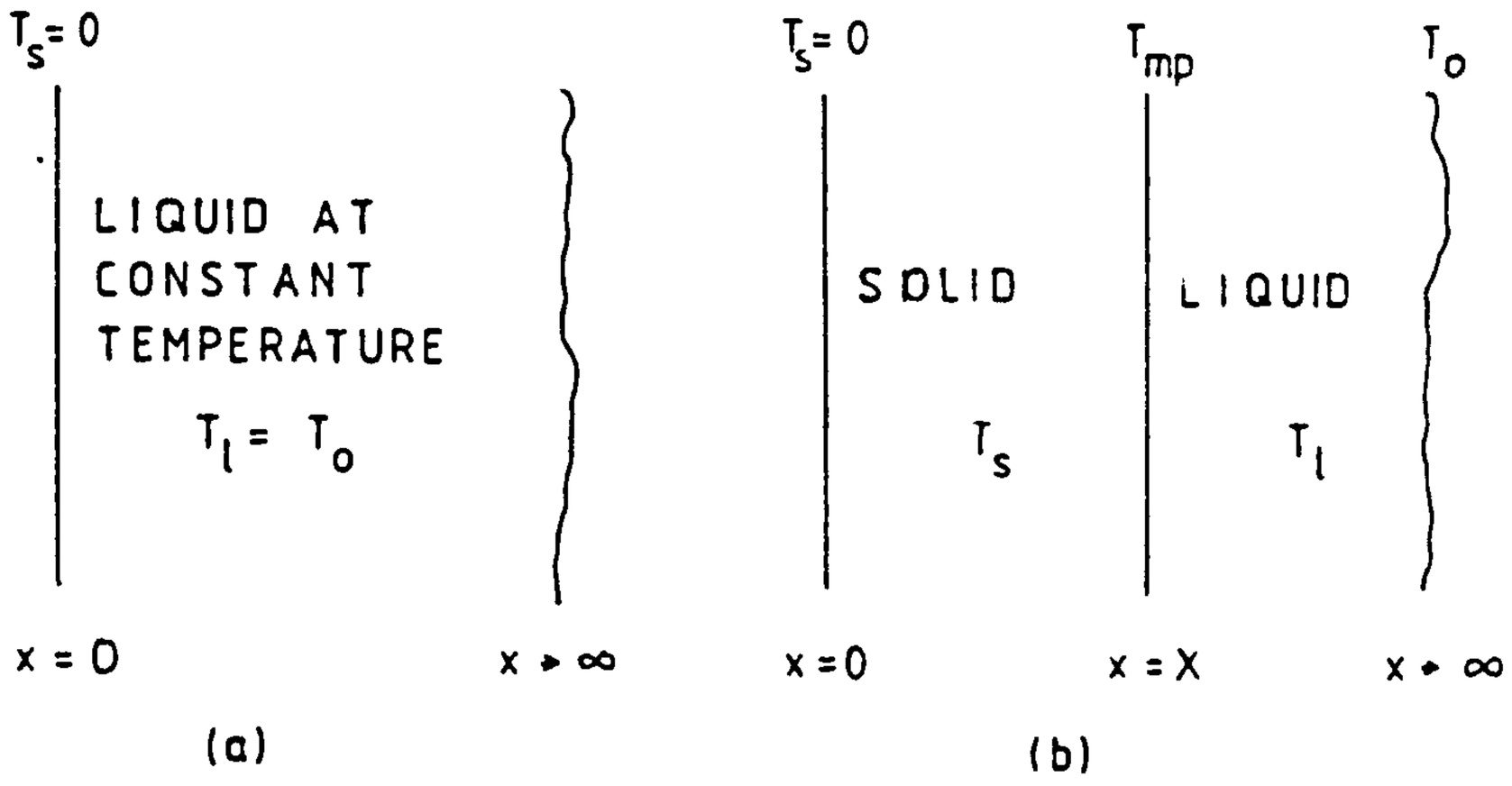

Figure 2.18 Schematic diagram showing semi-infinite region considered in Neumann's solution (a) at t=0, (b) at t>0

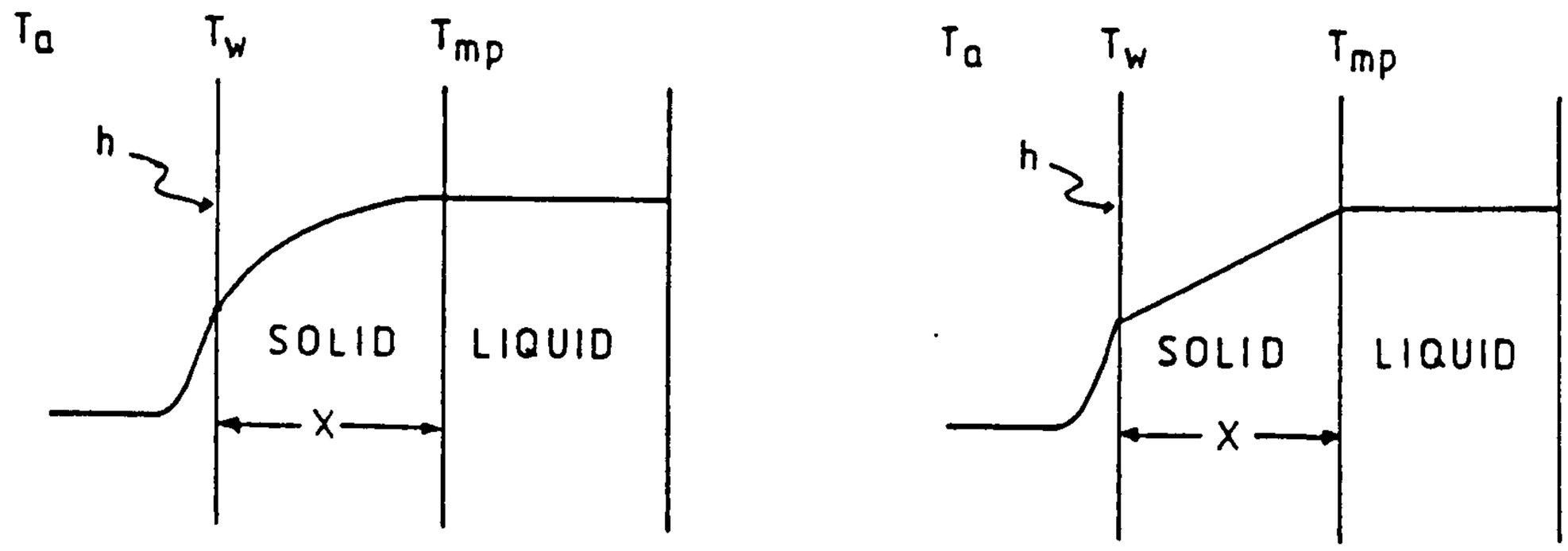

Figure 2.19 Temperature profiles during freezing in slab (a) actual, (b) assuming negligible thermal capacity

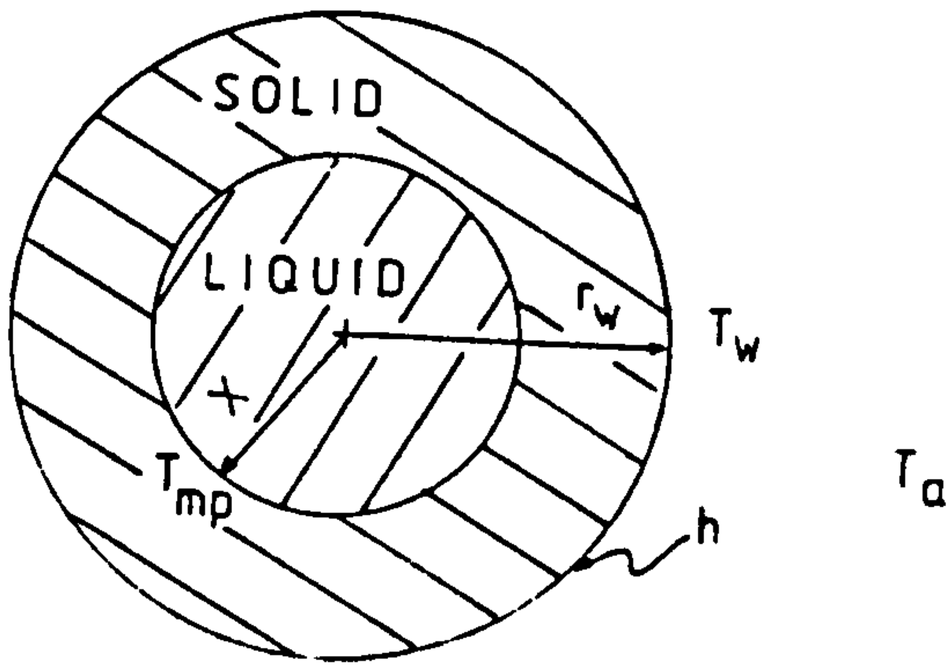

Figure 2.20 Schematic diagram of freezing in cylindrical geometry

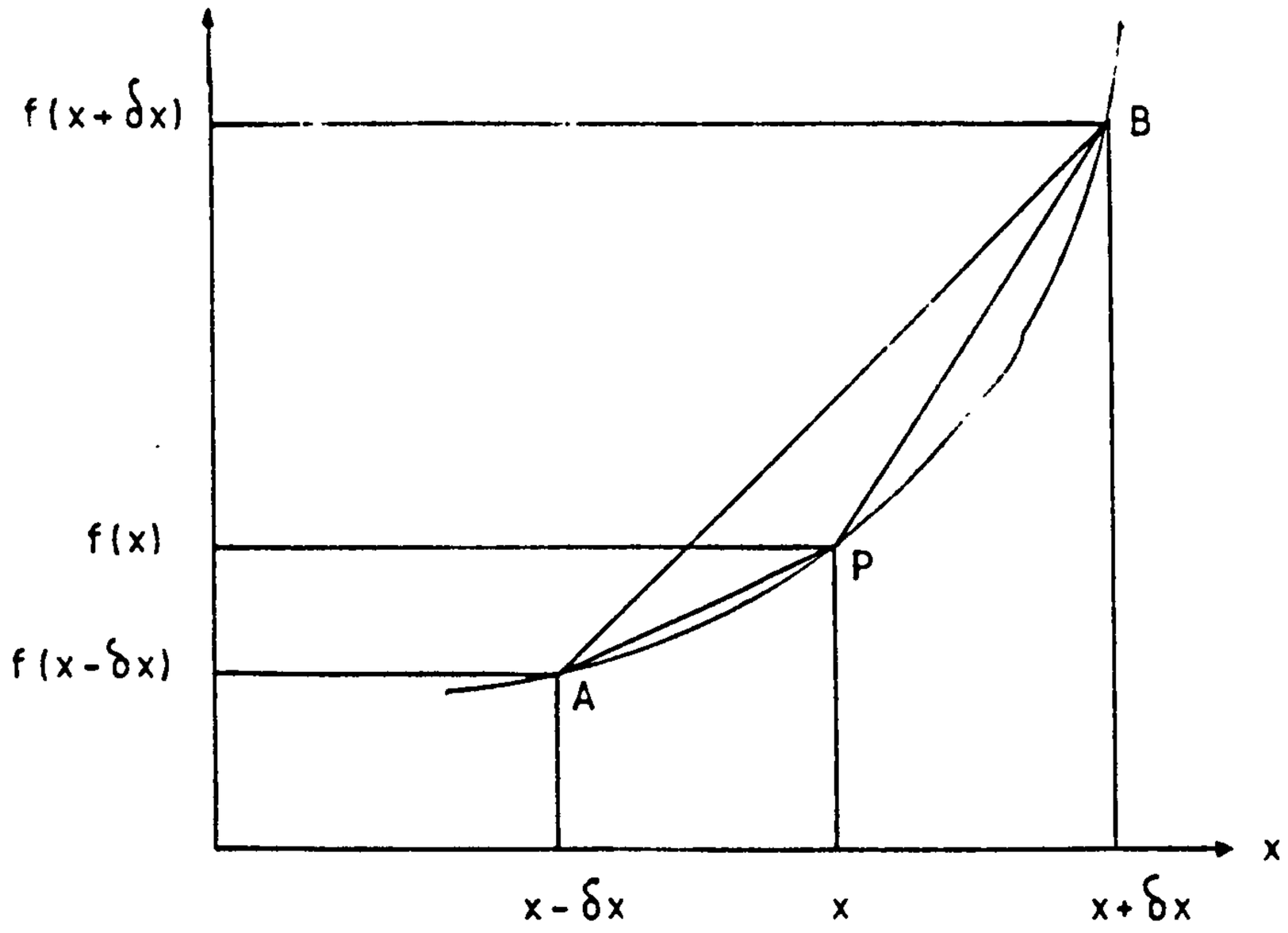

Figure 2.21 Finite difference approximations to derivatives

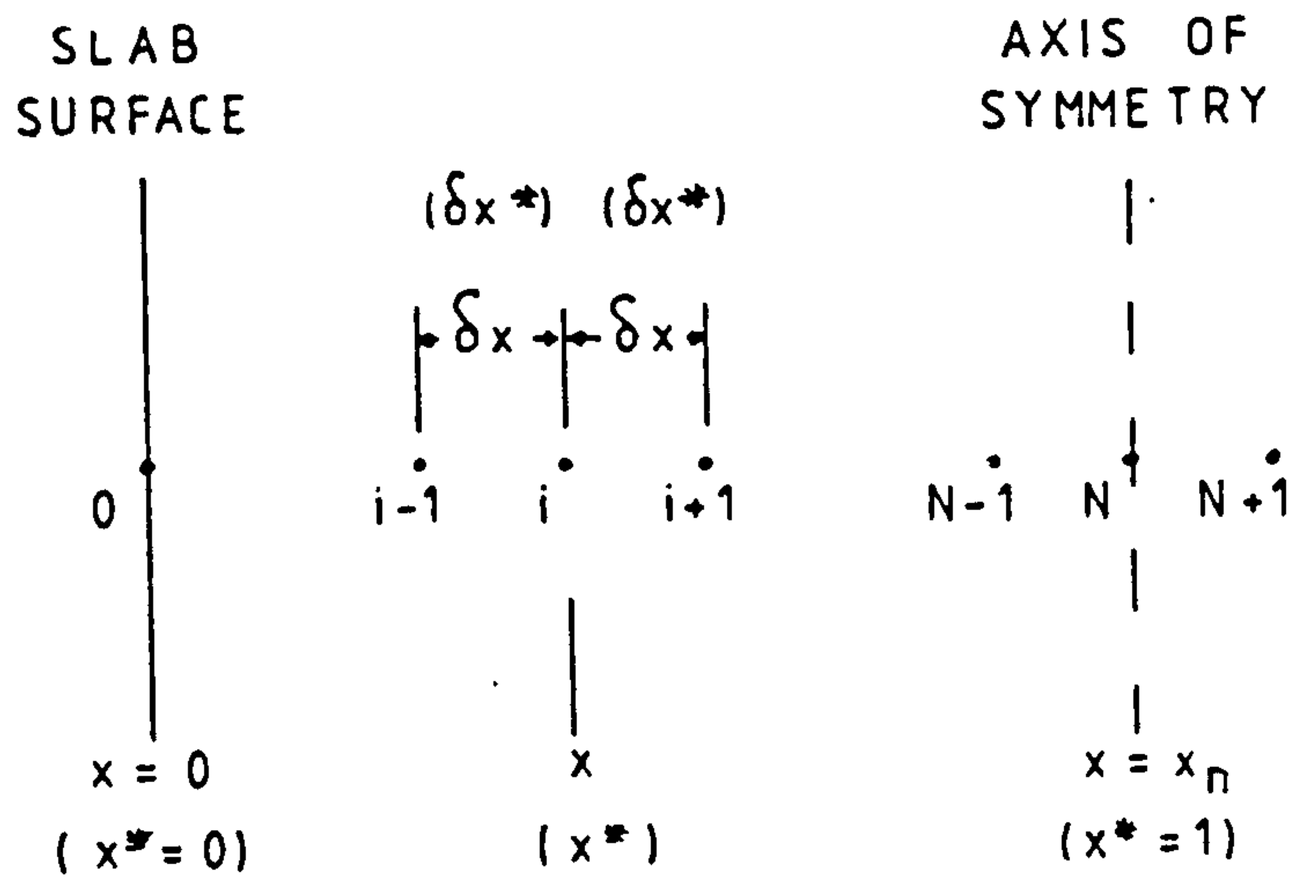

Figure 2.22 Subdivision of slab for finite difference approximation

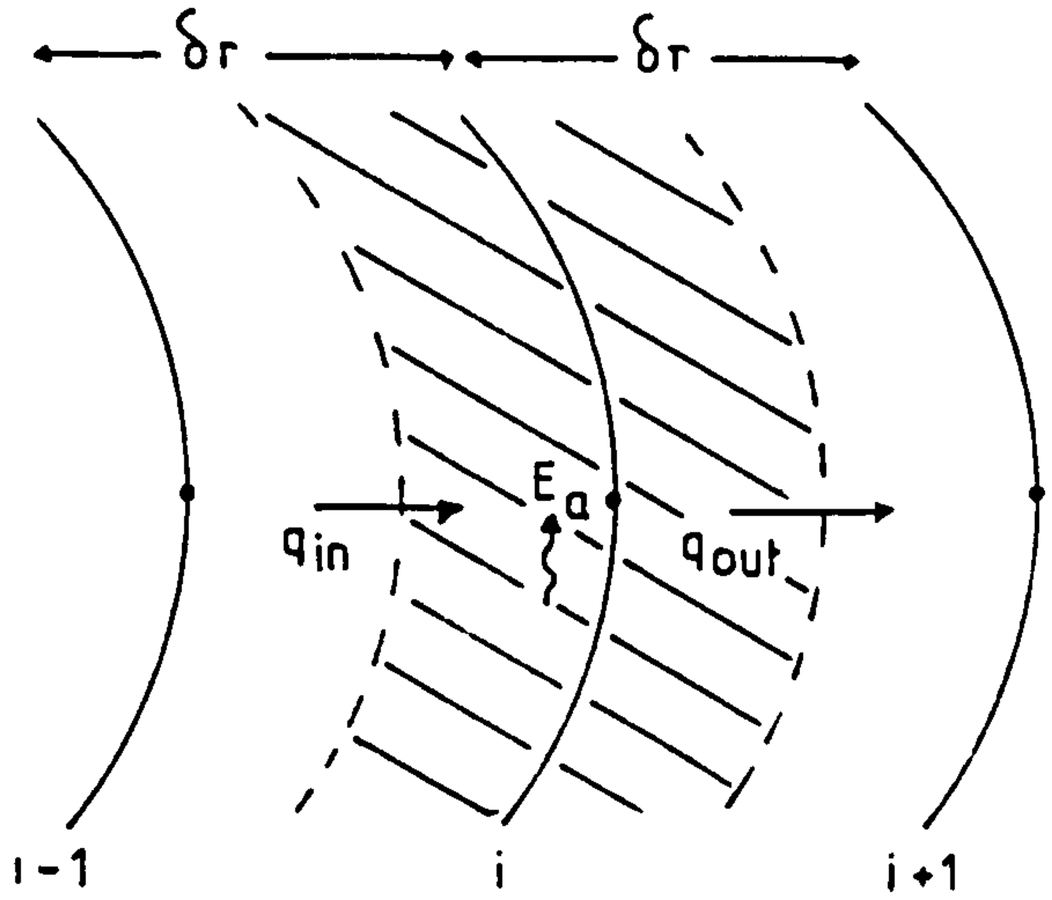

(a)

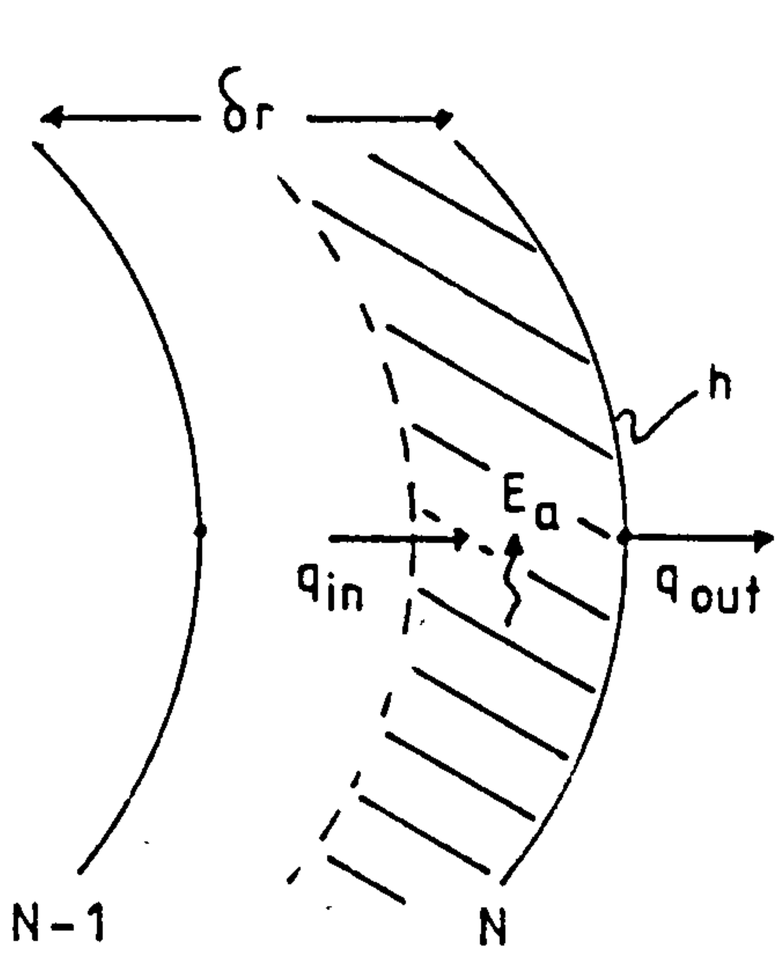

(b)

Figure 2.23 Subdivision of cylinder for finite difference approximation (a) heat flows at a typical internal node (b) heat flows at a boundary node

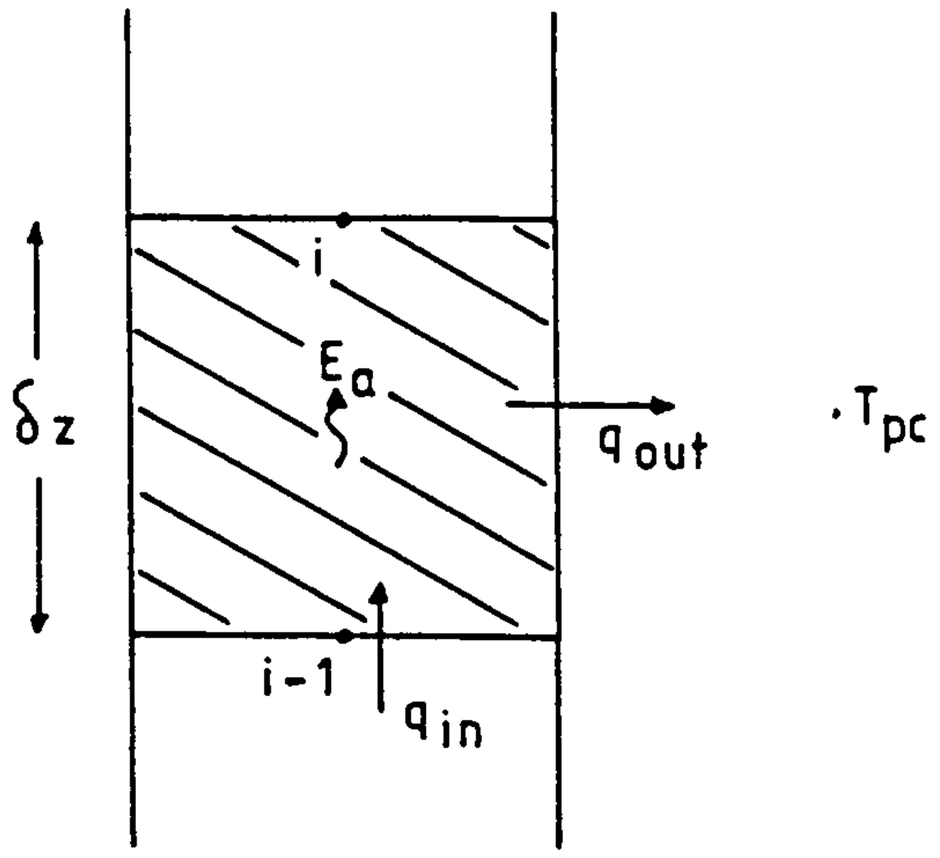

Figure 2.24 Subdivision of flow channel for finite difference approximation

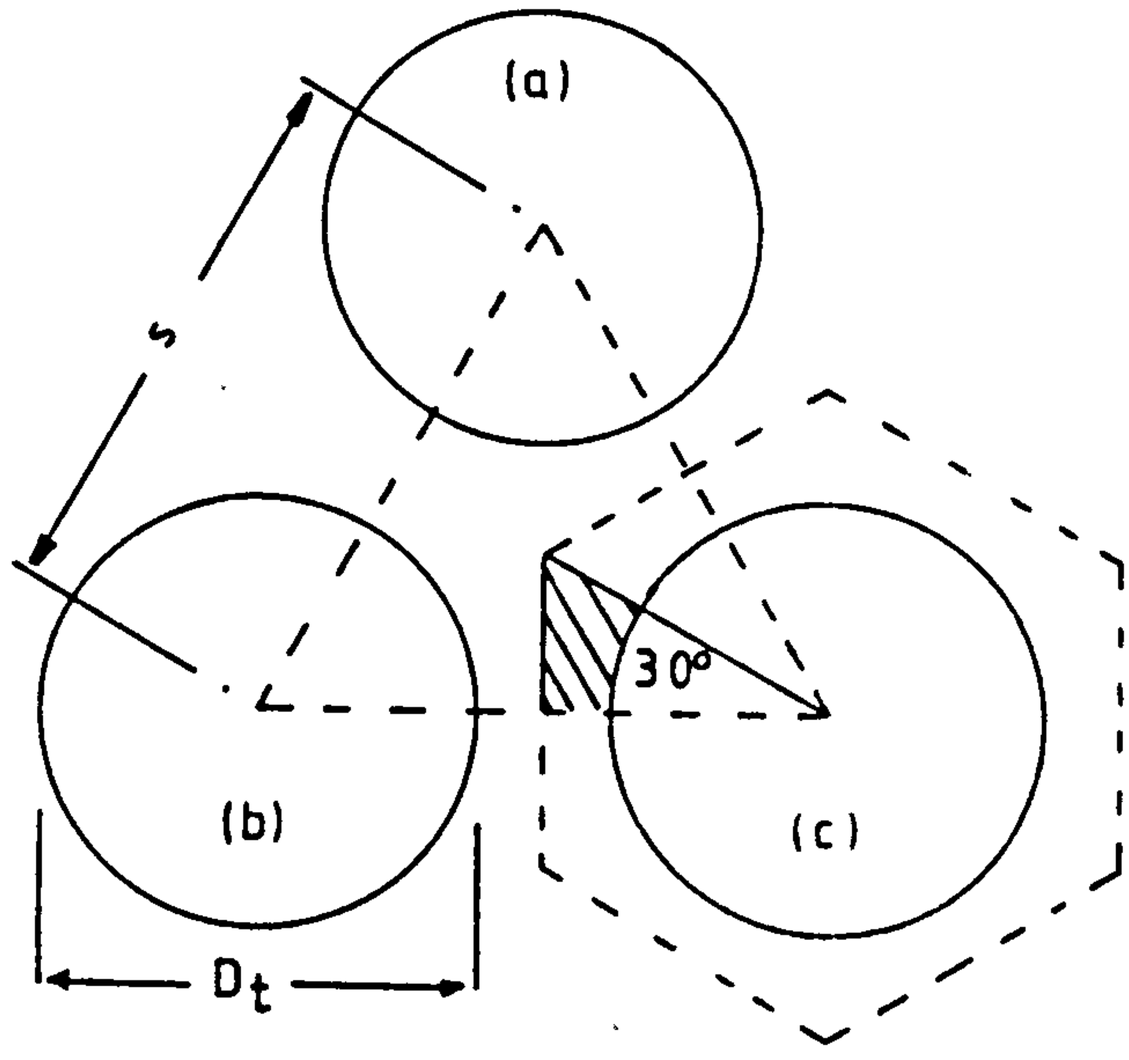

Figure 2.25 Cross section of a three-rod portion of rod bundle having an equilateral triangular arrangement (after Dwyer and Berry 1970)

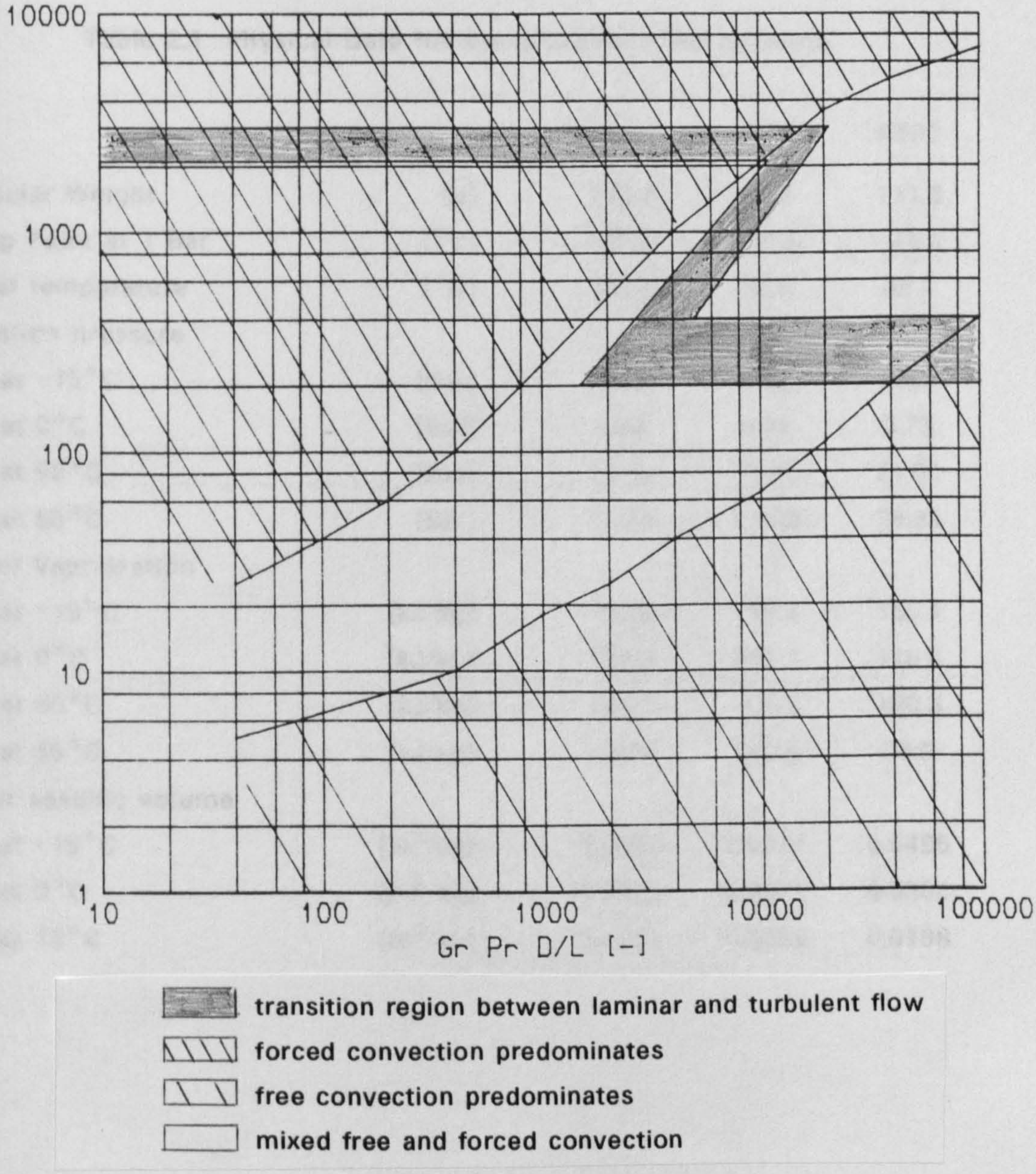

Figure 2.26 Regimes of free, forced and mixed convection for flow through vertical tubes, $0.01 < Pr\ D/L < 1$ (after Metais and Eckert 1964)

Table 2.1 Physical Data for some Common Refrigerants

		R12	R22	R502
Molecular Weight	[g]	120.9	86.5	111.6
Boiling Point at 1 Bar	[°C]	-29.8	-40.8	-45.4
Critical temperature	[°C]	111.5	96.0	82.2
Saturation pressure				
at -15°C	[Bar]	1.83	2.96	3.49
at 0°C	[Bar]	3.09	4.98	5.73
at 50°C	[Bar]	12.19	19.42	21.01
at 65°C	[Bar]	16.99	27.00	28.84
Heat of Vaporisation				
at -15°C	[kJ/kg]	157.8	215.4	155.1
at 0°C	[kJ/kg]	151.4	205.3	146.6
at 50°C	[kJ/kg]	121.0	154.5	100.8
at 65°C	[kJ/kg]	108.8	132.5	78.9
Vapour specific volume				
at -15°C	[m^3/kg]	0.0905	0.0771	0.0495
at 0°C	[m^3/kg]	0.0553	0.0471	0.0308
at 15°C	[m^3/kg]	0.0353	0.0299	0.0198

Table 2.2 Derivation of a Typical Heat Loss Coefficient

	U [W/m^{2}K]	Area [m^2]	Loss [W/K]
External walls	0.5	80	40
Windows	4.1	20	82
Fllor	0.69	100	69
Roof (actually ceiling)	0.5	100	50
Total			241

Specific heat of air (at 6°C)	[J/kgK]	1010
Density of air (at 6°C)	[kg/m^3]	1.26
Volume of dwelling	[m^3]	250
Air change rate	[s^{-1}]	2.78x10^{-4}
Ventilation loss	[W/K]	88
TOTAL LOSS	[W/K]	329

Table 2.3 Rod-Average Nusselt Numbers for In-Line Laminar Flow Through Unbaffled Rod Bundles (after Dwyer and Berry 1970)

	Type A		Type B	
s/D_t [-]	Nu_{De} [-]	$h(D_t=25mm)$ $[W/m^2K]$	Nu_{De} [-]	$(D_t=25mm)$ $[W/m^2K]$
1.04	2.48	335	0.795	107
1.05	2.82	340	1.06	128
1.053[1]	2.93	-	1.18	-
1.06	3.18	346	1.36	148
1.07	3.54	351	1.70	168
1.08[1]	3.90	354	2.11	192
1.10	4.62	359	2.94	229
1.20	7.48	331	6.90	305
1.30	9.19	277	9.03	272

Notes

1. These s/D_t ratios correspond to 38 and 25 mm tubes with pitches of 40 and 27 mm respectively; the Nusselt numbers were interpolated from the original tabulated data

CHAPTER 3

DEVELOPMENT OF EXPERIMENTAL FACILITY

3.1. Development of Storage Device

3.1.1. Selection of PCM

The proposed use of the storage device on the condenser side of a domestic heat pump heating system, placed considerable restriction on the selection of the storage material. Latent heat was preferred to sensible heat due to the greater energy density which allowed design of a more compact store. Other materials which were seriously considered included sodium sulphate pentahydrate and paraffin wax, and data is presented on these and other PCMs in table 3.1. Paraffin wax was eliminated, despite low cost, because of its low energy density (see figure 3.1) and poor thermal conductivity.

Sodium acetate trihydrate was finally selected; primarily because of its melting point which was thought to represent the best compromise between radiator temperature and heat pump performance. Higher radiator temperatures improve heat transfer to the dwelling and allow use of less bulky circulation systems. Lower distribution temperatures are associated with an improved heat pump performance as shown in figure 1.2. In addition if the system was to be fully utilised then the store should also be capable of meeting the domestic hot water load. This implies a minimum phase change temperature of 55°C.

3.1.2. Encapsulation of PCM

Initially experiments were performed employing layflat plastic tubing but polypropylene tubes developed by Calor were employed for all the results presented in this thesis.

3.1.2.1. Layflat tubing

In section 2.2.2.2 the supercooling problem associated with latent heat storage was discussed. Pure sodium acetate trihydrate was known to have a tendency to supercool, and in the laboratory it was relatively easy to supercool a 200 g sample down to room temperature. It was thought that encapsulation in layflat plastic tubing would reduce the degree of subcooling since:

1. Plastic film was reported by Bochenek and Drury (1975) to have a high resistance to crystal adherence of Glauber's salt, which implied that during freezing, crystals that were formed on the wall would be free to move and initiate nucleation in adjacent molten PCM
2. Non-rigid walls would allow natural flexure as a consequence of flow which would again reduce tendency for crystals to form on film wall and increase the movement of crystals in molten PCM

In addition, layflat plastic tubing offers a cheap method of encapsulation and attractive heat transfer characteristics since no solid, low thermal conductivity layer of PCM builds up around the tube walls. However encapsulation of the PCM in polythene layflat plastic tubing caused many problems. The tubing was sealed with a heat sealer, which produced sharp corners, and consequently after only a very few cycles the bags would burst. Attempts to eliminate this tendency to burst using rounded edges formed by making several angled seals also proved unsuccessful. Altman (1971) reported similar experience and noted that the heat sealing technique is still unsuitable even with thicker films. He further added that the plastic film will transmit water in vapour form which alters the PCM composition detrimentally.

The pure PCM which was being used was extremely prone to thermal segregation (see section 2.2.2.1) and even after only a few cycles a significant proportion of the PCM could be observed to be no longer taking part in the phase change process.

It was difficult to decide on an appropriate packing arrangement for these polythene tubes. The tubes were loaded into the storage device at ambient temperature with the PCM in its solid phase, and hence a tube bundle inside a shell heat exchanger type arrangement was achieved. However when the PCM melted this regular bundle arrangement collapsed, almost certainly resulting in the formation of cusps and hence channeling of the flow.

3.1.2.2. Polypropylene tubes

Investigation of the various alternative encapsulation geometries and materials indicated that thin polypropylene tubes, despite their poor thermal conductivity, would provide a good compromise of cost, voidage, surface area density, reliability and thermal performance. Two important parameters in the

design of a storage device are the interface density S and the voidage ξ which are defined as

$$S = \text{ratio of heat exchanger surface area to the volume enclosed by that surface,} \quad (3.1)$$

$$\xi = \text{ratio of volume occupied by PCM to total non-insulated volume occupied by storage device.} \quad (3.2)$$

Table 3.2 presents details on the heat exchanger and store dimensions for the Edinburgh storage devices and several others reported in the literature. The two parameters described above were calculated for each store and it was found that the 25 mm tubes gave the highest interface density and a reasonably low voidage. The Calmac commercially available storage device gave the lowest interface density and an extremely low voidage.

3.1.3. Design Requirements of Integrated Storage Device

Myson donated a standard domestic heat pump to be employed in the development of the integrated heat pump/latent heat store system This was a model 7.5, capable of delivering 7.5 kW at a circulating water temperature of 55°C for an ambient temperature of 7°C. At an ambient temperature of -1°C for a circulating water temperature of 62°C however, the maximum delivery rate decreases to 5 kW.

The store was designed to be capable of receiving an almost complete charge during the off-peak period at a very low ambient temperature. Since the off-peak tariff is available for only 7.5 hours and some of that period (approximately 1.5 hours) may be required for house pre-heat, it was assumed that the heat pump could charge the store for approximately 6 hours with off-peak electricity. Hence, since the storage device required an inlet temperature of 62°C for satisfactory thermal performance, it had to be capable of storing a minimum of 30 kWh. A standard Calor store comprising 38 mm tubes was calculated to have a TSC of 59.5 kWh while the 25 mm tubes had a TSC of 44.4 kWh (see section 3.1.5).

The results of a simple model, presented in section 7.2, predicted that the charge/discharge rate from the 38 mm tubes would be less than 3 kW for a

UF of 0.9. This was expected to produce difficulties during charge by requiring high condensing temperatures, unless the integrated system was operated in part load mode. It was also desired to keep the discharge rate as high as possible so that the storage device could be usefully employed to meet the domestic heating load until it was fully discharged. Consequently the design based on 25 mm tubes was selected.

3.1.4. Development of Pilot Storage Device

3.1.4.1. Design details

The pilot storage device (see figure 3.2) was constructed from two glass cylindrical sections each 0.217 m diameter and 0.615 m in length. A brass flange sealed the storage device at either end and uniform distribution was ensured by dural plates drilled with 2.37 mm holes and mounted on 90 mm pillars to give a mixing area at both ends. Since the store was mounted vertically, the tubes were placed on a stainless steel mesh support plate positioned 20 mm above the bottom distribution plate.

The tubes were placed in bundles (to prevent formation of cusps) held together by wire wrapped around them, see figure 3.3. Since the diameter of the storage device was fixed, the optimum arrangement of tube bundles was determined by trial and error on a scale diagram. However in figure 3.2 it can be seen that this resulted in a packing arrangement which formed irregularly shaped channels and large voids around the circumference of the store.

A summary of the important dimensions is presented in table 3.3(a). The theoretical storage capacity (TSC) of the pilot store was found from the sum of the latent and sensible heats of the PCM, encapsulation and tank fabric, see table 3.3(b). This resulted in the following expressions for the store based on 25 and 38 mm diameter tubes respectively

$$TSC = 6824 + 187.8\Delta Tp \quad (104.1), \tag{3.3}$$

$$TSC = 7332 + 190.9\Delta Tp \quad (106.1), \tag{3.4}$$

where the sensible heat term in brackets is that calculated without accounting for the sensible heat contribution of the transfer fluid. A breakdown of the

TSC for a step change of 20 degC in a store comprised of 25 mm tubes is presented in table 3.3(c).

3.1.4.2. Calculation of design heat loss

Heat loss from the store was minimised by insulating the store with 4 cm thick fibreglass insulation. Since the glass walls have a much higher thermal conductivity it was assumed that they provided negligible resistance to heat transfer. The total area for heat loss (0.982 m^2) was found by averaging the insulated and non-insulated surface area of the store presented in table 3.3(a). The heat loss may be calculated from the steady state one dimensional formulation of Fourier's Law

$$q = kA(T_m - T_a)/\Delta x. \qquad (3.5)$$

The heat loss factor was found from the rearranged form of (3.5)

$$L = q/(T_m - T_a) = kA/\Delta x, \qquad (3.6)$$

to be 0.859 W/degC. This gave a heat loss coefficient based on the uninsulated store surface area of 0.963 W/m^2K.

3.1.4.3. Calculation of flow parameters

The mean hydraulic radius of a duct is equal to the cross-sectional flow area divided by the wetted perimeter. For a circular duct this implies that the hydraulic radius is one quarter of the diameter. Hence the equivalent diameter employed in the determination of Reynolds number is equal to four times the hydraulic radius. In figure 3.2 it is apparent that the ducts formed are bounded by 3,4 or even 5 tubes. This makes it difficult to determine a meaningful mean velocity for flow over the tubes and an equivalent diameter with which to calculate the Reynolds number.

A mean velocity was determined by dividing the volumetric flow rate by the free flow area. The hydraulic radius was calculated by dividing the free flow area by the total wetted surface of the tubes plus the wetted surface of the storage device. The equivalent diameter, calculated as four times the hydraulic radius, presented in table 3.3(a) is large compared with that

calculated assuming a regular triangular arrangement of tubes (see section 3.1.5.3). This is because the latter does not consider the large voids at the boundary with the storage device. The Reynolds number is defined as

$$Re = (\rho u_m De)/\mu, \tag{3.7}$$

and was found to be 254.7 and 364.7 at a flow rate of 0.192 kg/s for a store comprised of 25 and 38 mm tubes respectively.

3.1.5. Development of Full Scale Storage Device

3.1.5.1. Design details

The storage device was constructed from mild steel in the form of a rectangular cabinet (see figure 3.4) with a removable door held in place by bolts and sealed with a neoprene gasket. Mild steel permitted easy fabrication of the specially designed support plates but suffered severely from corrosion (note that it is difficult to weld stainless steel). The 25 mm tubes (see figure 3.5) were supported on discs welded onto the perforated plates while the 38 mm tubes (see figure 3.6) were located on dimples pressed into the plate. This ensured a regular triangular array of tubes and an optimal flow regime. Flow enters and exits through the flow distribution manifolds which have semicircular notches (7 mm dia.) at 25 mm centres on the y-direction sections. The tubes are divided into 6 identical sections by two sets of fixed ties in the y-direction and a single set of removable ties in the x-direction (see figure 3.4). Four connections to the tank are shown: two manifold inlet/outlets, drain cock and vent line.

A summary of the important dimensions is presented in table 3.4(a). The theoretical storage capacity may be expressed as the sum of the latent and sensible heats of the PCM, encapsulation and store fabric determined in table 3.4(b). This results in the following expressions for a store comprising 25 and 38 mm tubes respectively

$$TSC = 110 + 2.571\Delta Tp, \tag{3.8}$$

$$TSC = 162 + 2.616\Delta Tp. \tag{3.9}$$

A breakdown of the TSC (step change 20 degC) for a store based on 25 mm tubes is presented in table 3.4(c). The energy density was found to be 211 MJ/m^3 while utilisation of 38 mm tubes would increase the TSC by 33% to yield an extremely high energy density of 280 MJ/m^3.

3.1.5.2. Calculation of design heat loss

The prototype storage device was insulated by 10 cm of polystyrene in an attempt to minimise heat losses. A design heat loss factor of 1.762 W/degC was found from equation (3.6) with the area for heat loss taken as the mean of the insuated and non-insulated surface areas of the store, see table 3.4(a). Hence the design heat loss coefficient, based on the uninsulated surface area of the store was determined as 0.290 W/m^2K which is a significant improvement on the pilot store.

Heat Loss During a 24 Hour Period

When the store has been charged and subsequently not fully discharged, it can be assumed that the mean temperaure will remain constant at the phase change temperature of 56°C. If the store surroundings are at 20°C then the heat loss in a 24 hour period would be 5.481 MJ, which is equivalent to approximately 3.4% of the TSC.

3.1.5.3. Calculation of flow parameters

The equivalent diameter employed to determine the Re of flow in a duct is defined in 3.1.4.3. In an infinite triangular array of tubes the flow area and wetted perimeter are easily obtained and Shah and London (1978) presented a generalised equation for different tube diameter and spacing

$$De/D_t = \{[(2\sqrt{3})/\pi](s/D_t)^2\} - 1. \qquad (3.10)$$

The mean velocity was determined by dividing the volumetric flow rate by the free flow area. Since the system was expected to operate over a range of flow rates, flow parameters were calculated for a low flow rate of 8 lit/min and a high flow rate of 15 lit/min. Hence the Reynolds number for a store comprised of 25 mm tubes was found from equation (3.7) to be 16.2 and 8.64 for high and low flow rates respectively.

3.2. Development of Test Facility

3.2.1. Requirements for Integrated System

The overall requirement from the test facility was to control and monitor the performance of an integrated heat pump/latent heat store system operating in real time with user-specified demand. In addition it was desired to assess the performance of the storage device and heat pump according to well established test procedures. Consequently a microcomputer complete with a special input/output device, printer and disk drive formed the heart of the system. Considerable effort was put into developing cheap, reliable and accurate methods of monitoring and controlling the necessary inputs/outputs for this system.

3.2.1.1. Thermal Storage Device

In order to evaluate the performance of the storage device under various operating conditions, it was essential to be able to determine the heat transfer rate with the transfer fluid accurately. This required the monitoring of the temperature drop across the store and the mass flow rate of the transfer fluid through the store. An accurate determination of the heat transfer rate and a real time clock was required to carefully track the total amount of heat transferred and hence determine the store condition. To obtain useful comparative data the test facility had to be capable of controlling the mass flow rate, the store inlet temperature and the direction of flow.

3.2.1.2. Heat Pump

Determination of the COP of the heat pump required monitoring of the mass flow rate and temperature drop of the transfer fluid through the condenser, in addition to the power input to the compressor. Additional data such as the humidity of the source air and the saturation pressure of the condenser and evaporator were determined to improve our understanding of heat pump performance. A load simulating the requirements of a domestic dwelling was required initially for testing the performance of the heat pump and later for the integrated system.

3.2.2. Design and development of load

3.2.2.1. Design requirements

The expected performance of the heat pump employed in the experimental work is shown in figure 1.2 for two circulating water temperatures. At an ambient temperature of 2°C the heat pump is capable of delivering 6.47 kW at a circulating temperature of 55°C. This was assumed to be the maximum load requirement of the heat exchanger since designing for a higher load would assume a higher balance point temperature requiring utilisation of a supplementary heating system for more than 10% of the heating season (see figure 1.3).

The heat exchanger was designed to simulate both a domestic hot water heater and a complete heating system. The former required that the cold water outlet temperature be as high as possible and a plate heat exchanger was selected primarily because it was capable of a temperature approach of 1 degC. The high heat transfer coefficients, resulting in compact design, and the limited heat loss with no insulation, also favoured a plate heat exchanger design. A second-hand Alfa-Laval heat exchanger with an area of 0.56 m^2 was available and the following section confirms that it was capable of meeting the duty.

3.2.2.2. Design procedure to determine required h/e area

Since the largest area will be required for the lowest log mean temperature difference (ΔT_{LM}), the lowest heat pump output temperature (50°C) and highest cold water inlet temperature (20°C) were employed in the design calculations. The cold water outlet temperature for an approach of 1 degC will be 49°C and hence the cold water flow rate by rearrangement of

$$q = \dot{m} Cp \Delta T, \qquad (3.11)$$

was found to be 0.053 kg/s (3.2 lit/min) for a maximum load of 6.5 kW. The hot water flow rate was in the range 8-15 lit/min and the lowest value was selected to keep ΔT_{LM} small. The hot water outlet temperature determined from a rearrangemet of equation (3.11) was calculated to be 38.3°C

The ΔT_{LM} was calculated from the expression below to be 5.95.

$$\Delta T_{LM} = (\Delta T_{in} - \Delta T_{out}) / \ln[\Delta T_{in}/\Delta T_{out}] \quad (3.12)$$

Number of Transfer Units (NTU) was calculated from the equation given below to be 4.87.

$$NTU = U_{av} A / \dot{m} Cp = \Delta T_c / \Delta T_{LM} \quad (3.13)$$

The log mean temperature difference correction factor F was determined from a chart presented by Raju and Chand (1980) to be 0.9.

Reynolds number was calculated from equation (3.7) and Prandtl number from

$$Pr = Cp\mu/k \quad (3.14)$$

with the physical properties evaluated at 44 and 35.5°C, the average temperature of the hot and cold streams respectively (see section 9.2.3). A diagram showing the geometrical arrangement of the heat exchanger is presented in figure 3.7. There are fourteen plates in total, 11 of which are thermal, 2 with only cold or hot fluid and one blank plate to seal the heat exchanger at the left hand end. This flow configuration is known as a looped flow - U arrangement with 6 channels in a single pass for each fluid. The equivalent diameter which is defined in section 3.1.4.3 was found to be 4.09 mm from

$$De = 4Wb/(2W+2b), \quad (3.15)$$

where W and b are as specified in figure 3.7. Mean velocity in each channel may be determined from the following

$$u = \dot{m}/6Wb\rho. \quad (3.16)$$

Hence the velocity and Re were determined for the hot and cold flows.

Velocity	[cm/s]	21.04	3.555
Reynolds Number	[-]	1389	469

Heat transfer coefficients for turbulent flow (Re>400) were calculated from

$$h = 0.2536\ (k/De)\ (Re_{av})^{0.65}\ (Pr_{av})^{0.4}, \qquad (3.17)$$

to be 7595 and 3961 W/m^2K for the hot and cold streams respectively.

The overall heat transfer coefficient (2411 W/m^2K) was determined from the two film coefficients above plus a term for the thermal resistance of the 0.5 mm thick stainless steel plate itself. No fouling was included since it was easy to clean the plates.

$$1/U_{av} = (1/h_h + x_w/k_w + 1/h_c) \qquad (3.18)$$

The required area of heat exchanger was then calculated by re-arranging

$$q = U_{av}\ A\ \Delta T\ F, \qquad (3.19)$$

to yield 0.503 m^2

Hence the Alfa-Laval heat exchanger of 0.56 m^2 was capable of meeting the design duty.

3.2.3. Microcomputer System and Interface

A Commodore PET microcomputer with 32K of memory was selected primarily due to existing operating expertise within the department and its proven ability in control/datalogging capacities. Input/output transfers were achieved through a CIL user port interface (Pupi) and the IEEE bus. The former provided for two analog inputs, four analog outputs and four digital inputs in addition to the operation of four relays. A CIL Microsystems PCI 1002 thermocouple amplifier could be connected to the IEEE bus which reads twelve thermocouple signals in addition to two low voltage inputs.

A printer was incorporated into the test facility to provide a hard copy of all the monitored inputs and derived quantities. Plotting and further analysis of the results required that a disk drive was connected to the PET to permit the storage of data on disk before transfer to the mainframe. A diagram showing how the microcomputer was interfaced to the test facility is presented in

figure 3.8.

3.2.4. Instrumentation

A schematic diagram showing the layout of the complete test facility and its instrumentation is presented in figure 3.9. A more detailed diagram of the refrigerant flow circuit and its instrumentation is shown in figure 3.10.

3.2.4.1. Temperature measurement

Type K thermocouples (NiCr-NiAl) made from a single roll of wire were employed as temperature sensors in the test-cell. One of the most important measurements in evaluation of the performance of a TES device is that of the temperature drop of the transfer fluid across the store. For practicable flow rates this difference may be less than 1 degC. This implies that the use of two thermocouples with a quoted accuracy of ± 0.1 degC would result in an error of approximately 20% in the measured temperature difference across the store.

This problem was overcome by building a thermopile (see figure 3.11) which consists simply of a number (2n) of thermocouple junctions arranged in series. If the junctions are placed alternately in a hot and cold location then the emf generated will be n times greater than that produced by a single pair of thermocouples.

A CIL Microsystems PCI 1002 thermocouple amplifier was used to convert the thermocouple voltage into a twelve bit signal which was input to the PET via the IEEE bus. The twelve thermocouple inputs were internally connected to a cold junction to generate an emf which was then amplified before conversion to a digital signal. One input was rewired to allow the emf produced by the thermopile to be connected directly to the differential amplifier.

A subroutine supplied by CIL Microsystems was used to read the signal in bits from the IEEE bus and convert it to a voltage in microvolts. This value had to be corrected for the internal cold junction (whose value was determined by a platinum resistance thermometer) for all inputs save the thermopile. A fourth order polynomial (see section 9.1.1) was utilised to calculate temperature from the voltage while the standard constant of 41

μV/degC was employed for the thermopile.

3.2.4.2. Flow measurement

A Rhodes turbine-type flowmeter which produced a frequency output was chosen to measure hot water flow rate. Every half revolution of the rotor in the flowmeter caused a reed switch to open and close. For a maximum flow rate of 50 lit/min, the rotor will rotate at 2000 rpm corresponding to a frequency of 67 Hz. As the relationship between frequency and flow rate is linear, determination of the frequency output will yield the flow rate.

Two methods of determining this frequency output were investigated. The first approach was to build a circuit (see figure 3.12) incorporating a C-MOS 4040B twelve bit binary counter which divided or slowed down the frequency output. This allowed the output to be connected to the Pupi and the time between pulses to be determined. Although this method worked satisfactorily it had the disadvantage that the microcomputer could perform no other useful function while timing the pulse length. This was a serious problem as in order to achieve the required sensitivity of ± 0.2 lit/min, the time required was several minutes.

In the second approach a tachometer which converted frequency to voltage was utilised. Since the voltage output from this circuit (see figure 3.13) was quite low it was put through an amplifier with a gain of ten to improve the sensitivity. Flow rate in lit/min was then determined from the square mean root of the voltage input from the Pupi using a linear calibration (see section 9.1.1), achieved with a bucket and stopwatch. The flow rate predicted by the rotameter with corrections for the properties of antifreeze was found to be significantly different from that obtained experimentally and hence was not employed for calibration purposes. Common to both circuits is an RC network which is included to eliminate the inevitable "bounce" produced as the reed switch opens and closes.

Cold water flow rates in the range 0.8 to 3.5 lit/min were measured by positioning an RS flow sensor in a loop which bypassed an orifice disk (see figure 3.9). This arrangement was necessary as the maximum flow rate through the sensor was limited to 1.67 lit/min. The desired total flow rate (3.5 lit/min) specified an orifice diameter which would divert approximately half the flow

through the flowmeter. The standard orifice equation

$$F = CA\{(2\Delta P)/(\rho[(A^2/a^2)-1])\}^{0.5}, \quad (3.20)$$

where C is the coefficient of discharge, A the cross sectional flow area of the pipe and a the area of the orifice, was re-arranged to calculate the required orifice diameter for a given pressure drop and flow rate. Radio Spares report the pressure drop across the flowmeter to be 0.1 bar at 0.5 lit/min and this gave the orifice diameter to be approx. 2 mm for a total flow of 1 lit/min. A flow of greater than a 0.85 lit/min through the flowmeter resulted in too large a pressure drop for the cold water feed. Hence a 2.7 mm dia. orifice was utilised which diverted only 1/4 of the flow through the flowmeter with a maximum total flo v of 3.5 lit/min.

A standard circuit for converting the RS flow sensor output to a voltage was employed (see figure 3.14). The output from this circuit was input to the microcomputer via the Pupi interface and an averaged value employed to determine the flow rate by a quadratic equation (see section 9.1.1).

3.2.4.3. Pressure measuremet

The saturation pressures in the condenser and evaporator were measured by Druck PDCR510 integrated silicon strain gauge bridge pressure transducers. Output from these transducers was linear with a maximum output of 198.50 mV and 198.02 mV at 15 barg and 35 barg respectively. Amplifiers (see figure 3.15) with a gain of 4.75 were constructed to produce a maximum output of approx. 1 V which was compatable with the input range of the Pupi. An equation presented by Downing (1974) was used to calculate the saturation temperatures from the recorded pressures in the evaporator and condenser.

3.2.4.4. Power measurement

A standard (dial type) kWh meter was employed to measure the input power to the heat pump. The disk rotated at 180 revolutions per kWh; equivalent to 9 rpm for a 3 kW power input to the compressor. Since there was no readily available frequency to voltage conversion device for such a low frequency (0.15 Hz), a timed pulse input system was developed. Half the disk was painted matt black and an optical sensor was mounted above the disk to

produce a pulse input proportional to the rotating speed of the disk. The circuit employed to produce a clean pulsed signal for input to the Pupi is shown in figure 3.16. Included in the design of this circuit is a Schmidt trigger to eliminate the spikey change from high to low or vice versa which can cause erroneous values. In the program the pulse length was determined by firstly identifying whether the signal is high or low and then timing the next pulse of high to high or low to low.

3.2.4.5. Humidity measurement

The humidity of the inlet air to the evaporator was calculated using a pair of wet and dry bulb thermocouples. The saturation humidity was calculated from the saturated vapour pressure of water at the wet bulb temperature. Using this value and the wet and dry bulb temperatures the humidity at the dry bulb temperature was determined from the slope of the adiabatic saturation line. A percentage relative humidity was then determined from the the ratio of the partial pressure of water vapour in the moist air to the saturated vapour pressure at the dry bulb temperature. The equations used are presented in section 9.1.1. and the property data for air and water vapour in section 9.1.2.

3.2.5. Control

3.2.5.1. Temperature – heat input

A water tank with a capacity of fifty litres was fitted with three 3 kW heating elements. The power supply to these heating elements was controlled by solid state relays which were in turn energised by the relays in the Pupi, see figure 3.17. The required heating load was determined from the proportional control equation

$$q = Kp(T_{set}-T), \tag{3.21}$$

where Kp is the gain constant and was determined empirically to be 6-9 kW/degC, giving a bandwidth of 1.5-1.0°C. Too low a value for Kp made it difficult to simulate a step change in inlet temperature and too high a value caused instability. The actual operation of the temperature control subroutine is summarised in section 9.1.1. Proportional heating for loads less than 3 kW

was attained by switching the heater on for an appropriate fraction of the time constant.

Note that the maximum heat input which could be supplied was 9 kW. Unfortunately this makes it impossible to increase the inlet temperature from T_0 to $T_0 + 0.9\Delta Tp$ within 2% of the test duration, as specified in ASHRAE 94-77. However this problem caused little concern, since the primary aim of these tests was to obtain performance data for a store designed to be interfaced to a heat pump with a maximum thermal output of 7.5 kW.

3.2.5.2. Temperature – heat removal

An Alfa-Laval plate heat exchanger was used to perform the cooling duty (see section 3.2.2 for design details). This heat exchanger was designed to simulate either the space heating load or the domestic hot water load. The resulting low cold water flow rate made it possible to assume that T18 was approximately equal to T9 (see figure 3.9) since T18 was not normally connected to the thermocouple amplifier. The cooling duty was determined from

$$q_h = (\dot{m}\, Cp)_h\, (T_9 - T_{set}), \tag{3.22}$$

and hence the required cold water flow rate from

$$\dot{m}_c = q_h/[Cp_c(T_9 - T_{17})]. \tag{3.23}$$

This method of controlling the discharge temperature performed satisfactorily until the required cold water flow rate fell below 0.8 lit/min (1.2 kW for cold water inlet temperature of approx. 20°C). Flow rate measurement below this was, at best, unreliable.

3.2.5.3. Hot water flow rate control

Hot water flow control was achieved by a Platon pneumatic control valve operating from a 4-20 mA current to pressure converter. This current is greater than the maximum 5 mA available from the Pupi so the voltage output was connected to a unity gain amplifier (see figure 3.18) in which the resistance across the output was chosen to give the desired current range.

The output voltage required to position the control valve for a specific flow rate was determined from a third order polynomial (see section 9.1.1). Since the control valve exhibited hysteresis, the flow control subroutine fully opened the valve for half a second before re-positioning which eliminated the hysteresis effect. This coarse flow control subroutine was employed to set the flow rate initially. A fine flow measurement and control subroutine measured the flow rate and took appropriate corrective action on the control valve according to the following equation

$$VP = VP + Kp\ (F_{set} - F). \qquad (3.24)$$

Note VP represents the valve position in bits and Kp the gain constant was found empirically to be 40 bits/[lit/min].

3.2.5.4. Cold water flow rate

Two methods were employed in the course of the experimental work to control the cold water flow rate. The first controlled the speed of a pump while the second utilised a control valve on the mains water supply.

Initially the cold water flow rate was controlled by varying the input voltage to a dc motor via a Parvalux motor speed controller. This controller was designed for manual operation by a potentiometer and the circuit shown in figure 3.19 was employed to vary the output in proportion to the Pupi output. A Stuart Turner number 10 pump head was mounted on the shaft of the motor. The flow control subroutine initially sets the pump at maximum flow rate. Subsequently it then measures the flow rate and adjusts the output to the motor in a stepwise fashion until the flow rate is correct to ± 0.1 lit/min.

For the final part of the experimental work, an accurate control of the load was required which necessitated fine flow control of cold water. It was found that after continuous operation at low flow rate, air accumulated in sections of the cold water syphon circuit, which meant that the input voltage to the dc pump had to be increased to achieve the same flow rate. Hence a point was reached when the flow rate could not be increased further to maintain constant load as the inlet hot water temperature to the load dropped. No obvious leaks were found when pressure tested by temporarily blocking the

outlet. It was therefore concluded that dissolved air was forming bubbles in the low pressure sections of the circuit, and accumulating in the high sections of the pipework which caused the syphon to break. Without a syphon the pump was incapable of delivering the head necessary to overcome the pressure drop in the system (a major proportion of which is through the turbine flowmeter bypass arrangement).

Hence an alternative arrangement where a control valve regulated the flow of water from the mains was employed instead. Hardware similar to that described above for the hot water flow rate controlled the valve position but a slightly different control philosophy was required. It was necessary to control the flow rate to ± 0.1 lit/min and employing the same fine flow control, see equation (3.24), resulted in the flow rate oscillating on either side of the set point. This was thought to be due to mechanical friction causing the valve stem to stick and only move by a minimum amount, which unless exactly equal to the required movement would result in an oscillating flow rate. Subsequent experimentation with various gain constants and reset times yielded values which minimised this problem.

An alternative technique employed in earlier runs reset the flow if the error was greater than ± 0.1 lit/min by fully opening the valve for 4 secs and gradually approaching the correct valve position (using equation (3.24)) smoothly from a fully open condition. A total reset took 20 seconds with only 10 seconds at a significantly different flow rate. This was considered to be satisfactory as once set the flow rate remained constant and the flow rate variation with real-time load was limited to once in half an hour.

3.2.5.5. Flow direction control

Four possible operating modes were anticipated for the integrated system. It was desired to be able to switch between these modes automatically in addition to switching the heat pump and circulating pump on and off independently. A simplified diagram of the integrated system which makes it easier to consider flow direction control is presented in figure 3.20. It had been discovered in the development work with the pilot store that it was advantageous to charge the store top-down and discharge bottom-up, and achieving this caused the greatest problems in devising the flow direction control strategy. The method which required the minimum number of relays

employed two three-way and two solenoid valves. The status of these valves for each operating mode is presented in table 3.5. Note that the solenoid valves are normally closed (i.e. non-actuated when signal is zero) so by inverting the signal to SV2, both SV1 and SV2 can be controlled by the same Pupi relay. The heat pump is only switched on in the first three modes and therefore it can controlled by the same Pupi relay employed for TV2. The relay circuits shown in figure 3.17 were designed so that the LEDs gave visual indication of when the relays were actuated and provided a facility for controlling the flow direction manually (e.g. during charge/discharge testing of store).

3.2.6. Operating Program

A complete listing of the final version of the program used to control the integrated system is presented in section 9.2.1, along with a list of variables and their definition.

3.2.6.1. Control of store operation

A start-up check mode is included in the test program and prompts the user to carry out a set of instructions contained on a "page" before continuing with the test. The first page ensures that mains supplies are switched on, air supply line valve is open and that a data disk has been inserted. As the test facility is designed for several different modes of operation the next page checks for the correct status of each valve. There is a facility to vent the storage device and a detailed procedure is included on the third page. The final page confirms the thermocouple selection for the amplifier, status of flow direction control switches and relay connections.

After completion of the start-up check the program proceeds to the second page of the control and display mode. This permits the user to specify the operating parameters selected for a particular run:

1. Dwelling loss coefficient (320 W/degC)
2. Initial UF (0)
3. Hot water flow rate (11.5 lit/min)
4. Domestic hot water load (3 kW)
5. Time step (60 seconds)

6. Printer output (10 minutes)
7. Run number (1.1)
8. Date (00-00-00)
9. Start time (00-00-00)
10. Heat loss coefficient from store (7 W/degC)
11. Records per file (10)
12. Disk reset (No)
13. Charge or maximum temperature (64°C)
14. Discharge or minimum temperature (44°C)
15. Internal set-point temperature (18°C)

Default values are shown above in brackets. Pages 4-6 of the control and display mode specify the location of each thermocouple and page 7 permits selection of eleven thermocouples to be monitored during the test (note that user must manually check that thermocouples connected to amplifier correspond to those selected). Page 8 defines the five operating modes employed by the test facility. The final page permits the user to select one of six load types. The first three determine the load from the dwelling loss coefficient, internal set point temperature and outside ambient temperature while the last three set the load to the DHW load specified on page two. The parameters may then be output to the printer before the program selects the appropriate test procedure mode.

3.2.6.2. Shut down

A test or run can be terminated by typing 'S'. This causes program operation to branch to a subroutine where all relays and outputs are set to zero apart from the cold water control valve which is closed. A page advising the user to switch off power supplies, isolate heat pump and close air supply valve is printed to the screen.

3.2.6.3. Input/output and datalogging

The measurement and control functions described in previous subsections each form a separate subroutine. This means that each test procedure will call selected subroutines as required. During normal operation the program displays the third page of the control and display mode with an update of variable values at the end of every time period. Included on this page are:

- 11 thermocouple inputs
- thermopile input
- control setpoint temperature
- saturation pressure of condenser (PH) and evaporator (PL)
- saturation temperature of condenser (CT) and evaporator (ET)
- power input to heat pump
- relative humidity of air entering the evaporator
- flow rates of primary (HOT) and secondary (COLD) transfer fluids
- thermal output of heat pump and its COP
- flow direction operating mode
- store condition presented as utilisation factor
- store charge/discharge rate and domestic hot water (DHW) load

A default selection of thermocouples is specified for each test procedure but those not used for control or derivation of humidity may be changed by branching to page 7 where the thermocouple selection may be re-specified. The values determined for each time step are averaged over a specified time interval before being output to the printer as a permanent record. Five or six of these mean values are held in the computer memory before being written to a data disk once the allocated memory is full. At the end of a run the data files on the disk are transferred to a single file on the mainframe for plotting and subsequent analysis via a BBC microcomputer (see section 9.2.1 for detailed procedure of this data transfer).

3.2.6.4. Performance Evaluation

Known specific heats and densities of the transfer fluid are employed along with the experimentally determined flow rates and temperature drops to calculate the heat transfer rates at the store, condenser and load. The total heat transferred to the store, determined from the rate and the time period (typically 60 seconds) corrected for heat loss, is presented as a fraction of the total theoretical storage capacity, known as the UF.

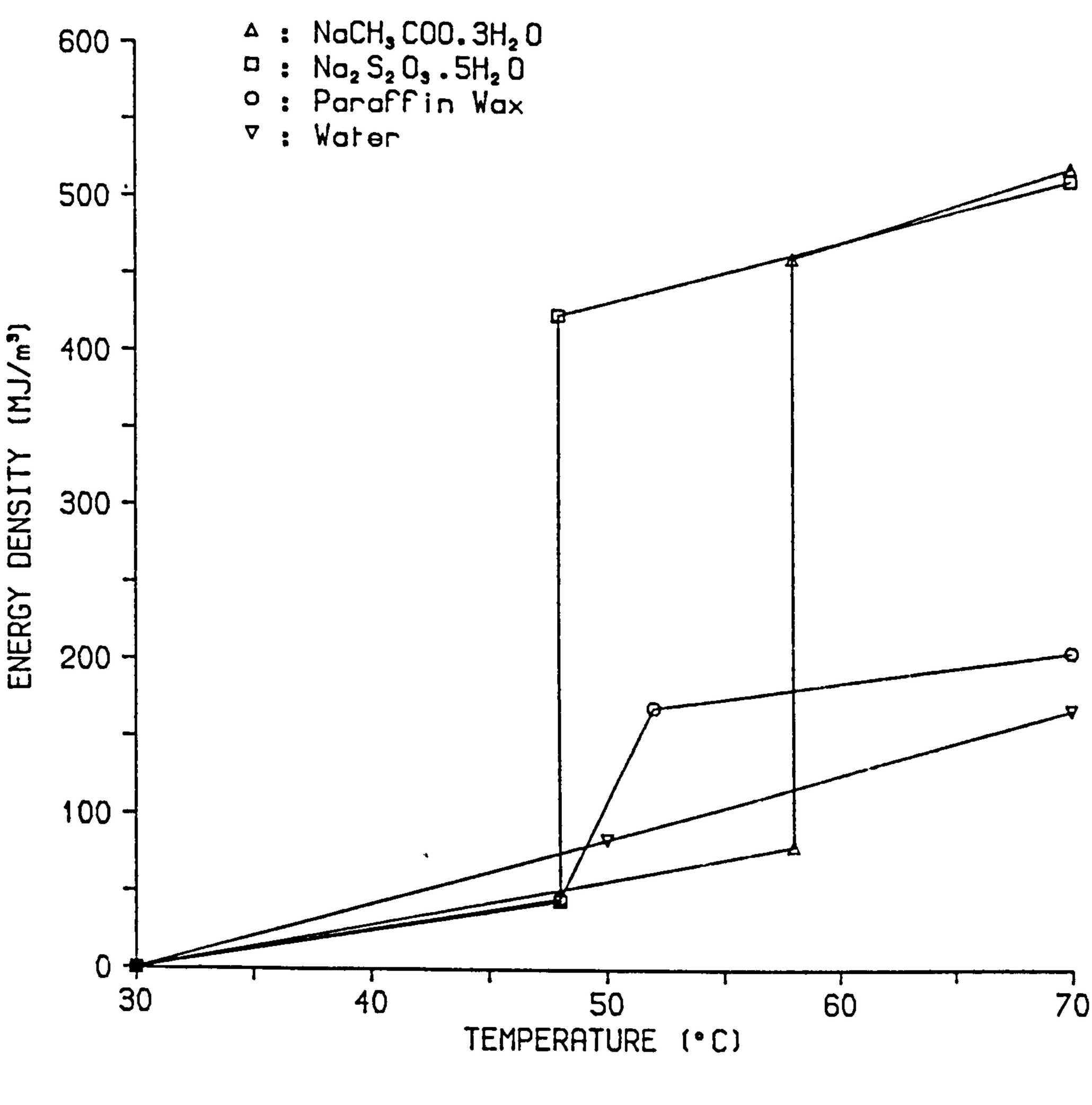

Figure 3.1 Energy densities of candidate PCMs

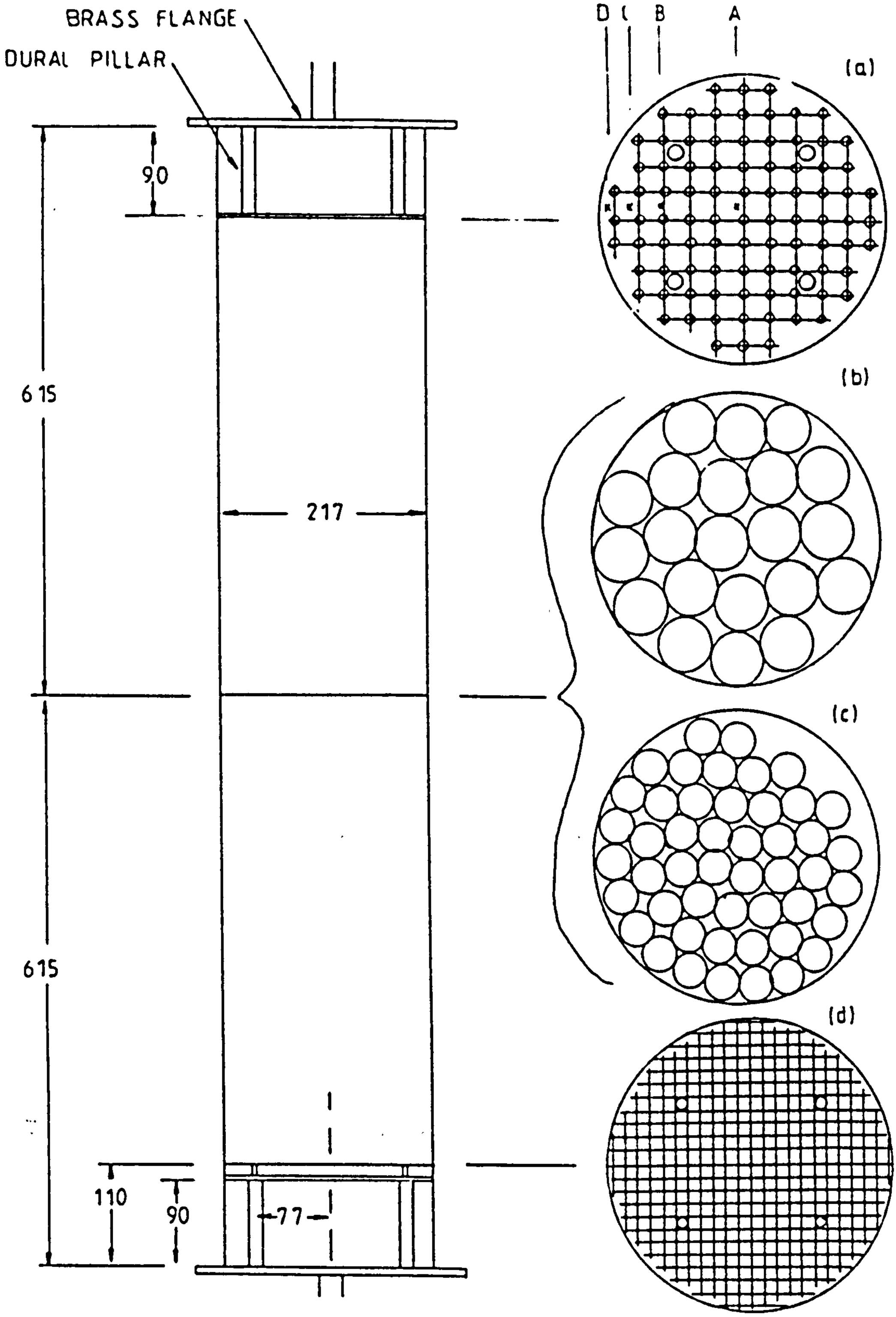

Figure 3.2 Schematic diagram of pilot storage device, sections through (a) distribution plate (b) 38 mm tube bundles (c) 25 mm tube bundles (d) mesh support plate

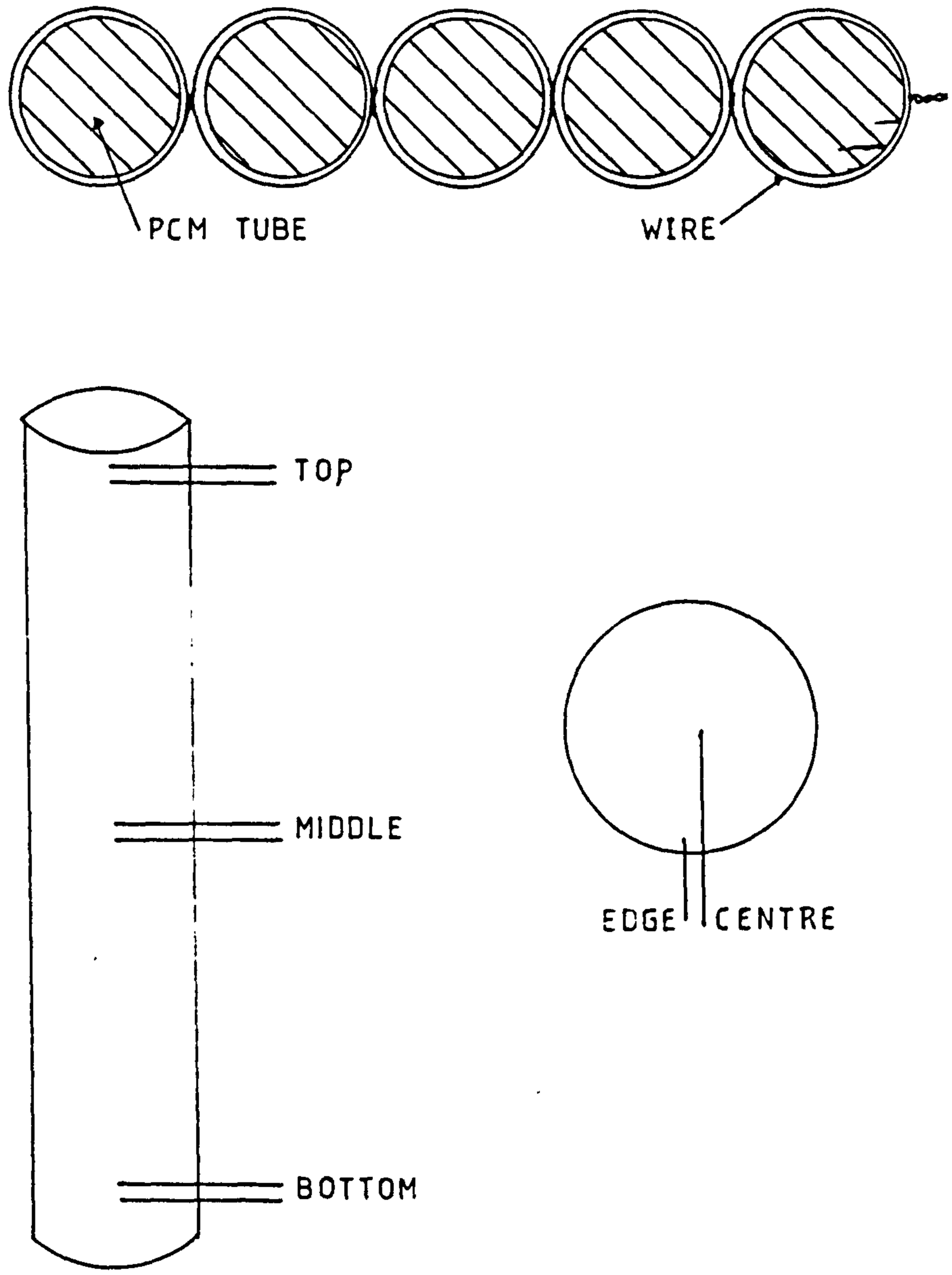

Figure 3.3 Photograph of typical tube bundle

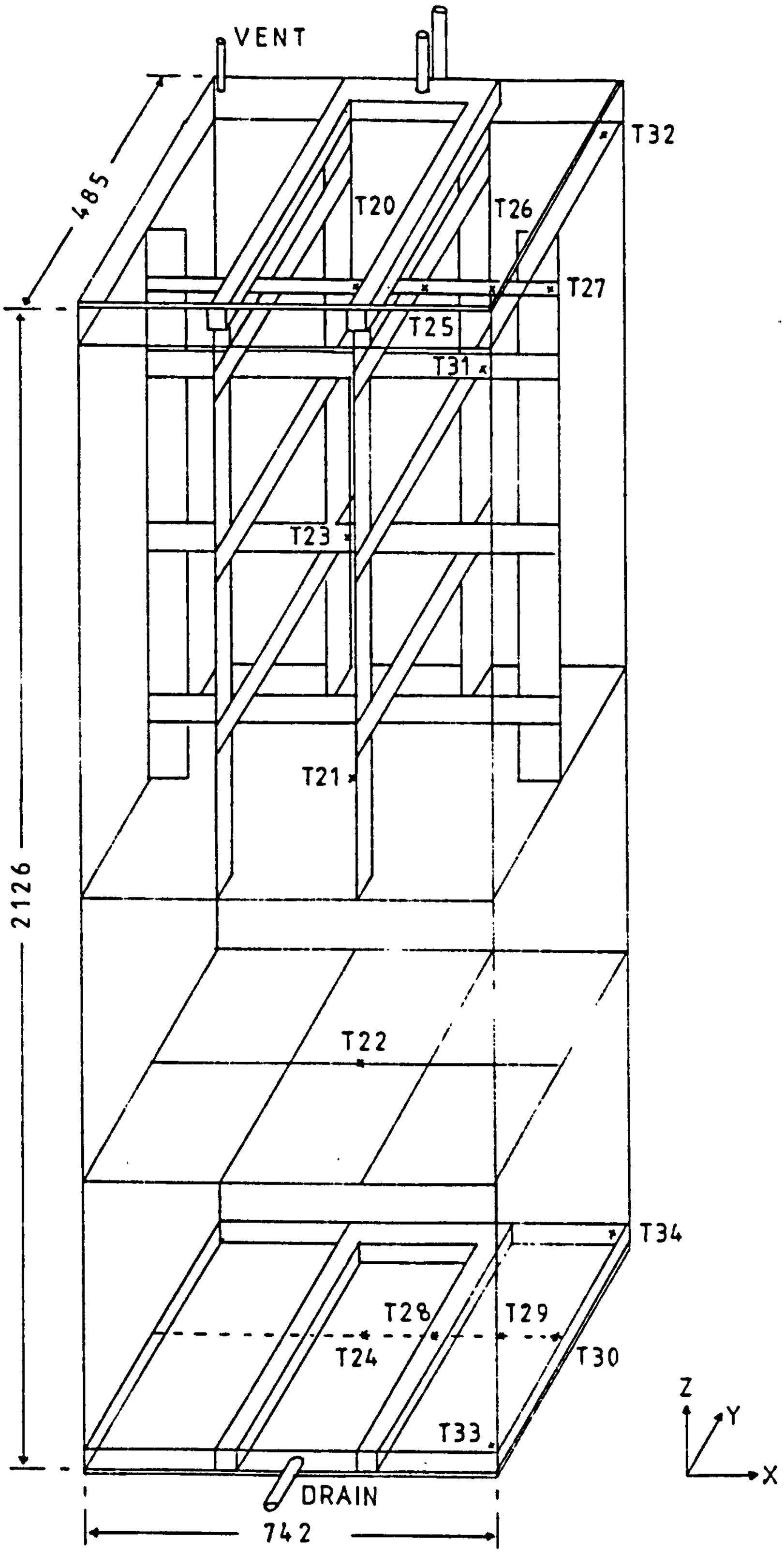

Figure 3.4 Diagram showing internal layout of prototype storage device

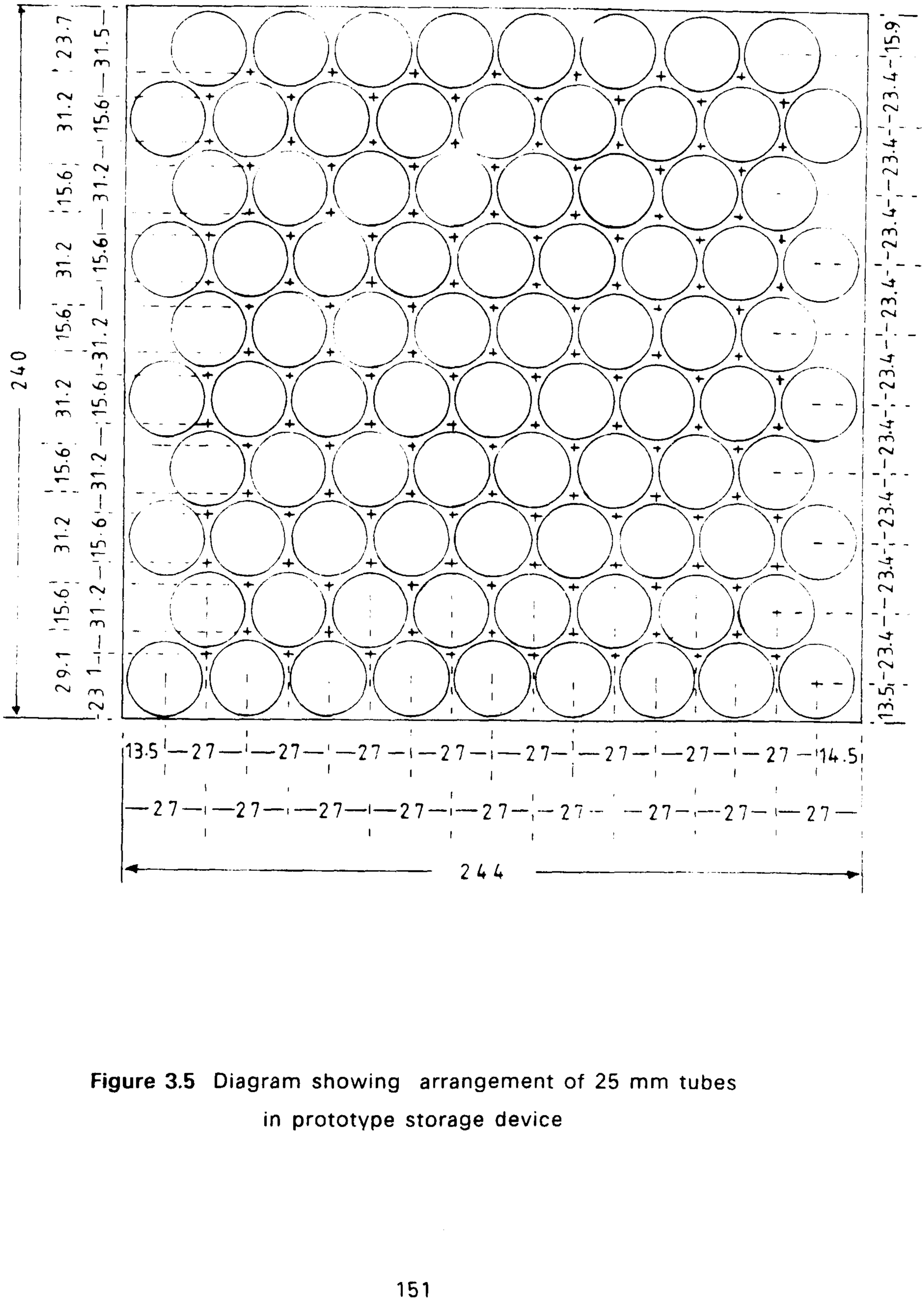

Figure 3.5 Diagram showing arrangement of 25 mm tubes in prototype storage device

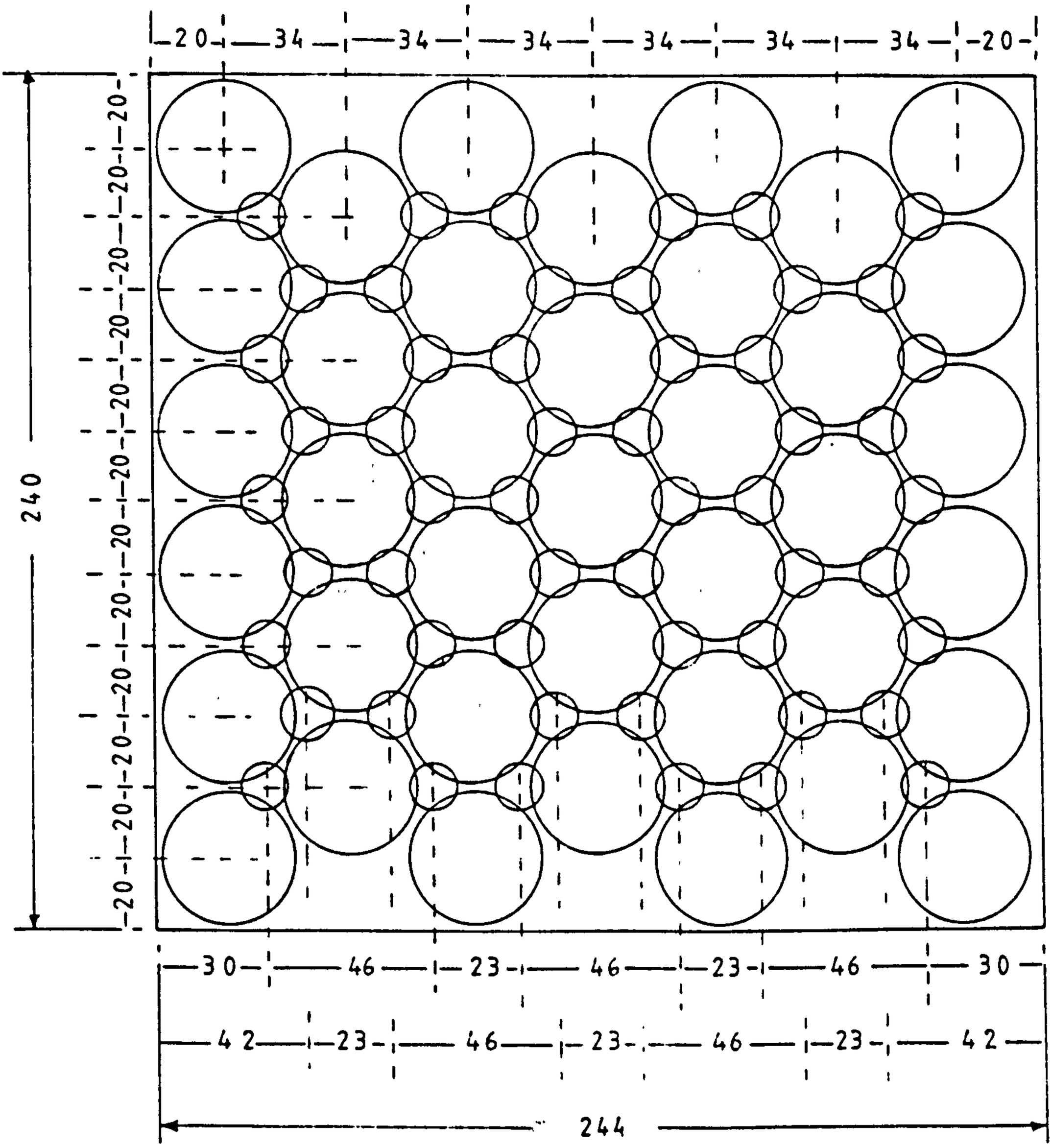

Figure 3.6 Diagram showing arrangement of 38 mm tubes in prototype storage device

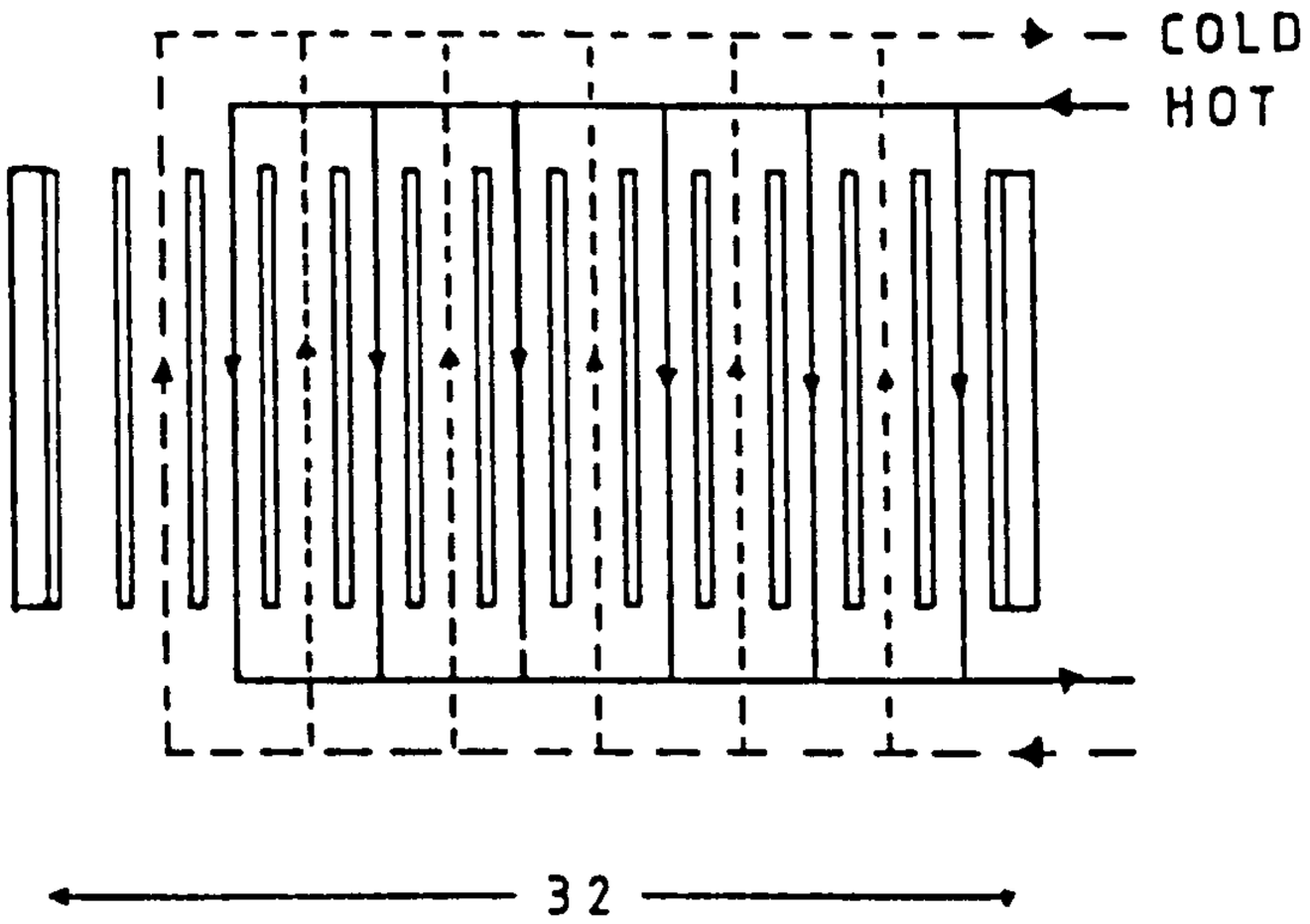

b = DISTANCE BETWEEN PLATES = 32/15 = 2·13 mm
W = WIDTH OF PLATE = 50 mm

Figure 3.7 Geometrical arrangement of plate heat exchanger

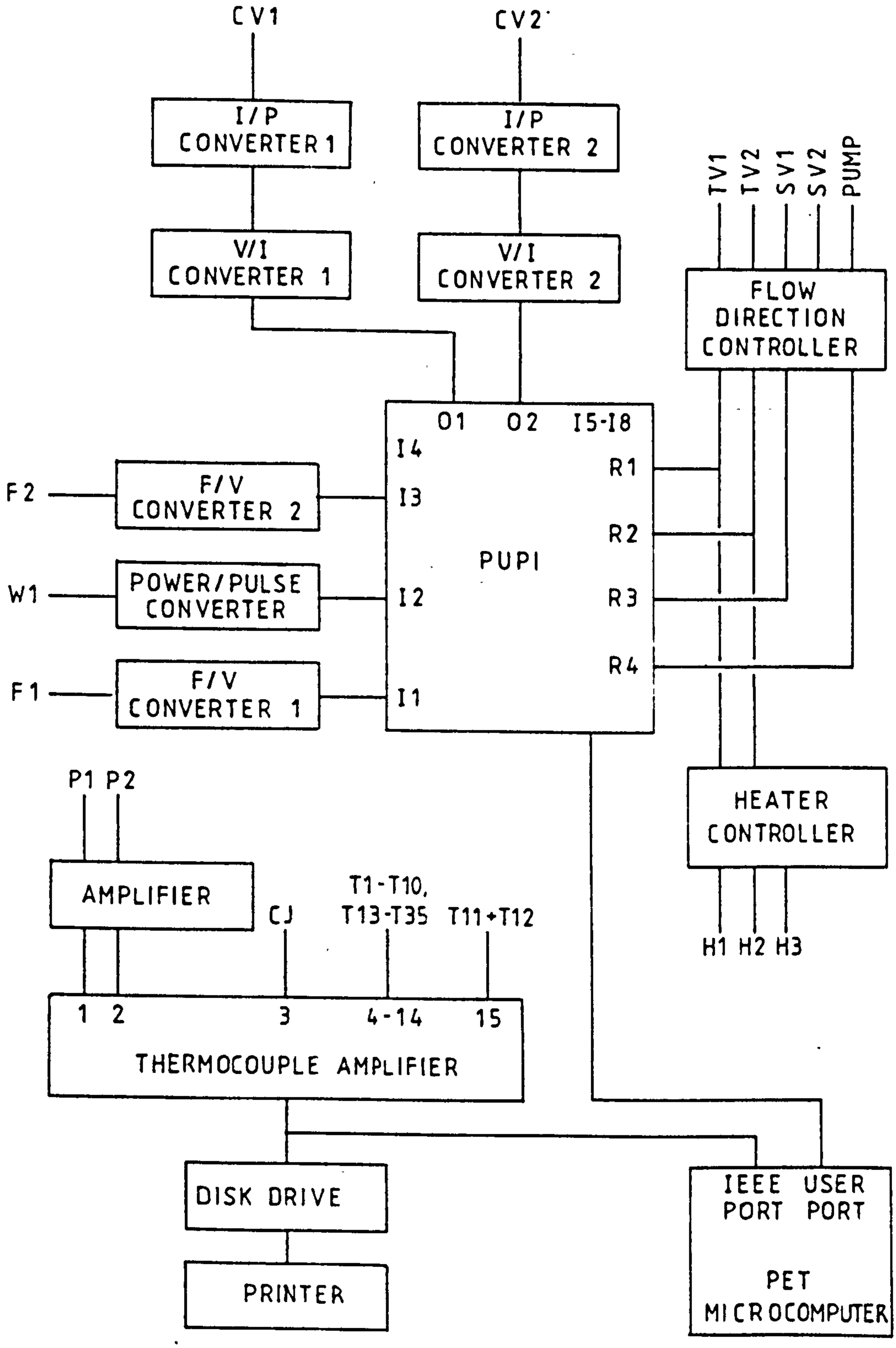

Figure 3.8 Schematic diagram showing microcomputer system interfaced to test facility

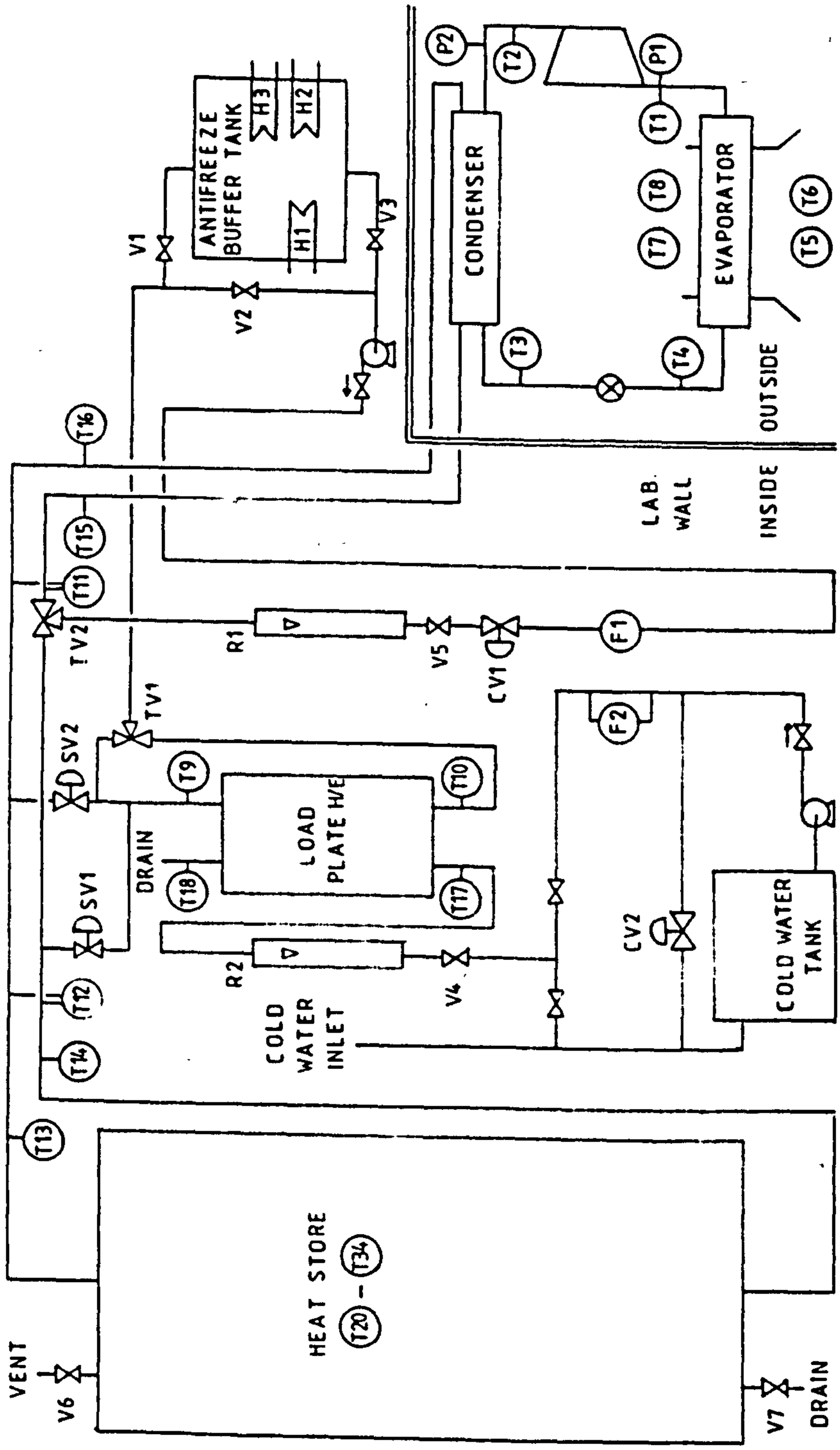

Figure 3.9 Schematic diagram showing layout of test facility

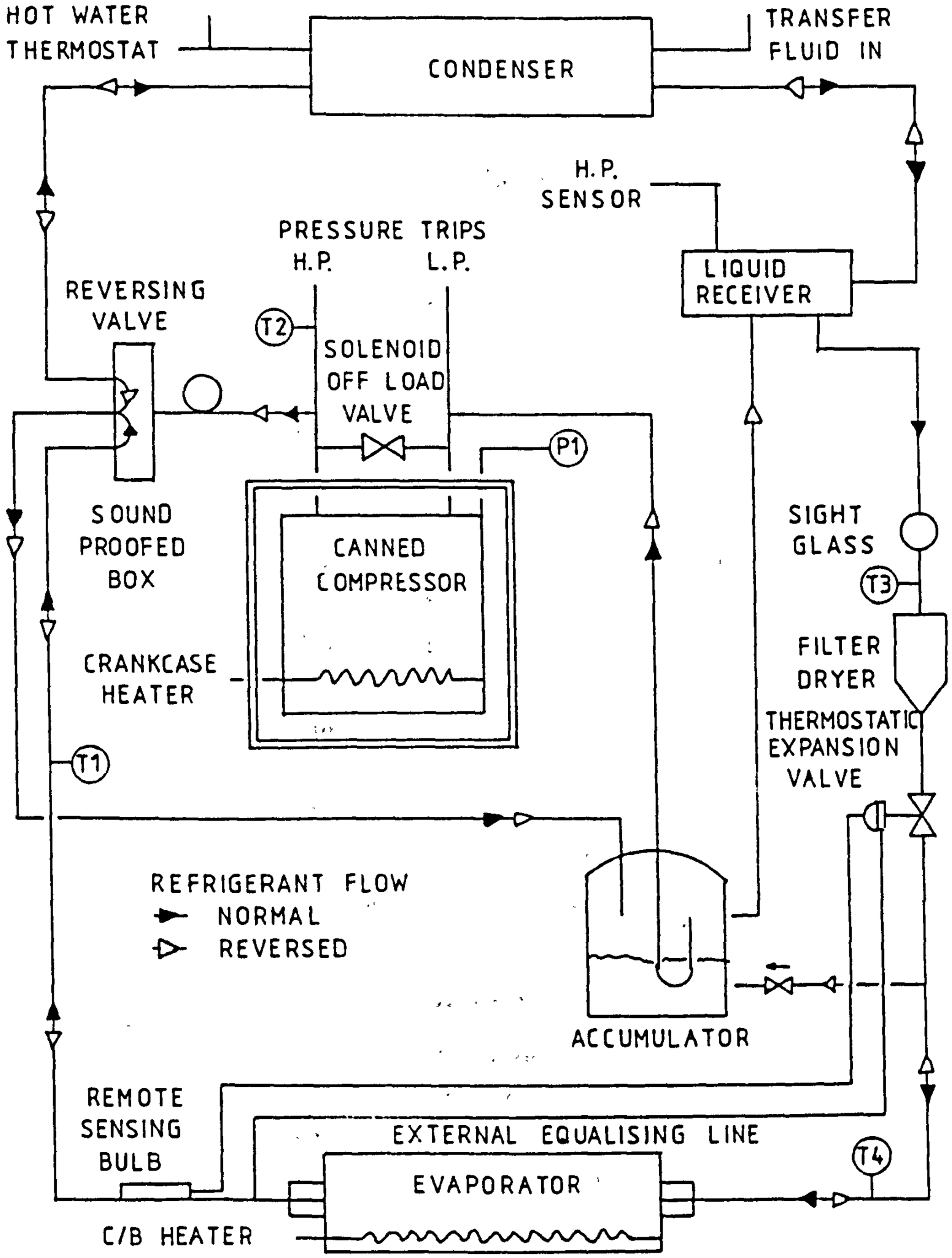

Figure 3.10 Schematic diagram showing layout of heat pump

Key to figures 3.8 - 3.10

(a) Temperature sensors	T1	Refrigerant compressor inlet
	T2	Refrigerant compressor outlet
	T3	Refrigerant condenser outlet
	T4	Refrigerant evaporator inlet
	T5	Air inlet (dry bulb)
	T6	Air inlet (wet bulb)
	T7	Air outlet (dry bulb)
	T8	Air outlet (wet bulb)
	T9	Hot water load inlet
	T10	Hot water load outlet
	T11	Condenser hot water temperature drop
	T12	Store hot water temperature drop
	T13	Store hot water top
	T14	Store hot water bottom
	T15	Hot water condenser inlet
	T16	Hot water condenser outlet
	T17	Cold water inlet
	T18	Cold water outlet
	T19	Ambient air in laboratory
	T20-T34	Store internals (see figure 3.4)
(b) Pressure sensors	P1	Evaporator side
	P2	Condenser side
(c) Flowmeters	F1	Hot water turbine type
	F2	Cold water RS flow sensor
	R1	Hot water rotameter
	R2	Cold water rotameter
(d) Other	CV1-CV2	Control valves
	SV1-SV2	Solenoid valves
	TV1-TV2	Three-way valves
	V1-V8	Gate valves

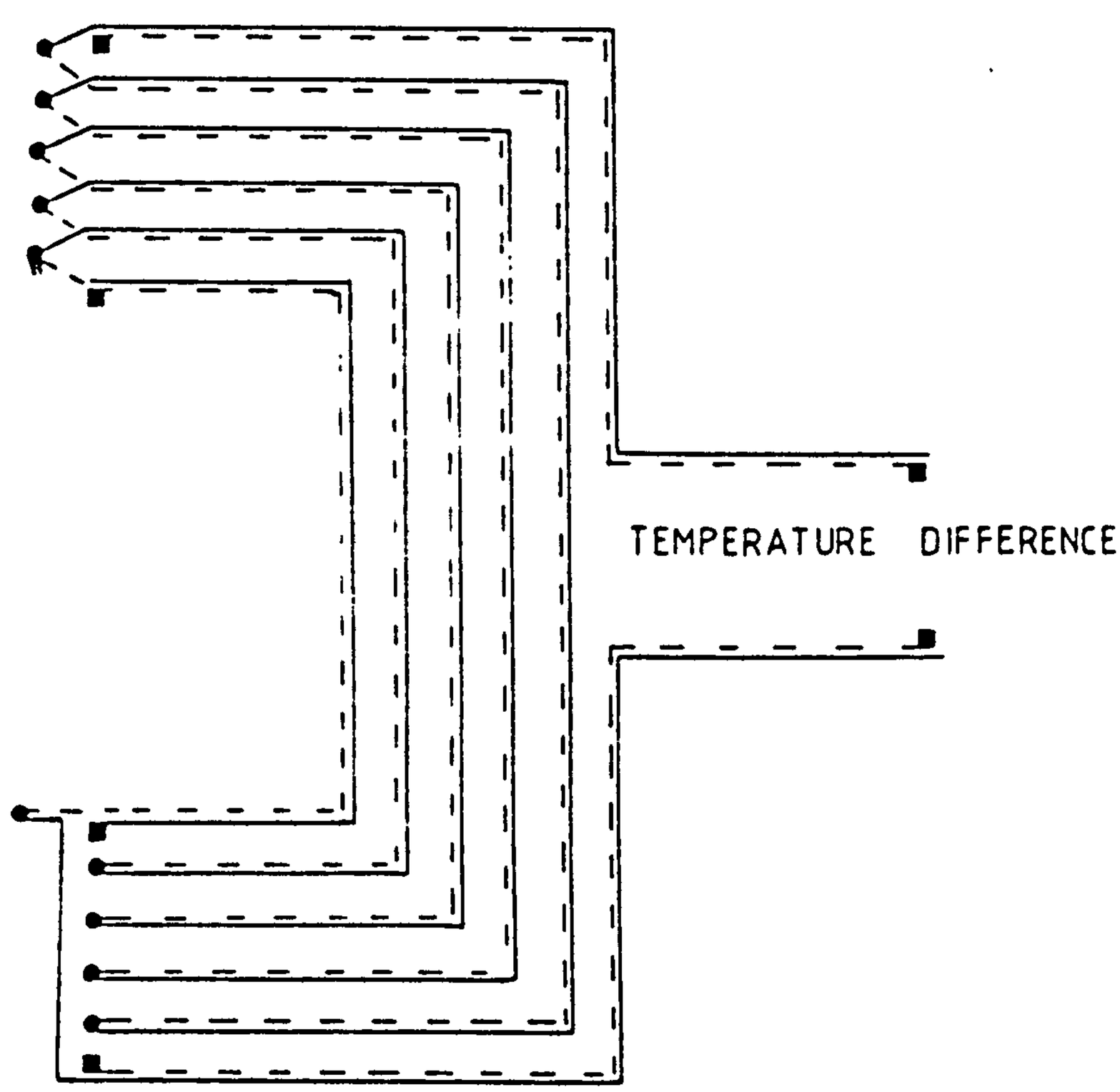

Figure 3.11 Diagram of thermopile

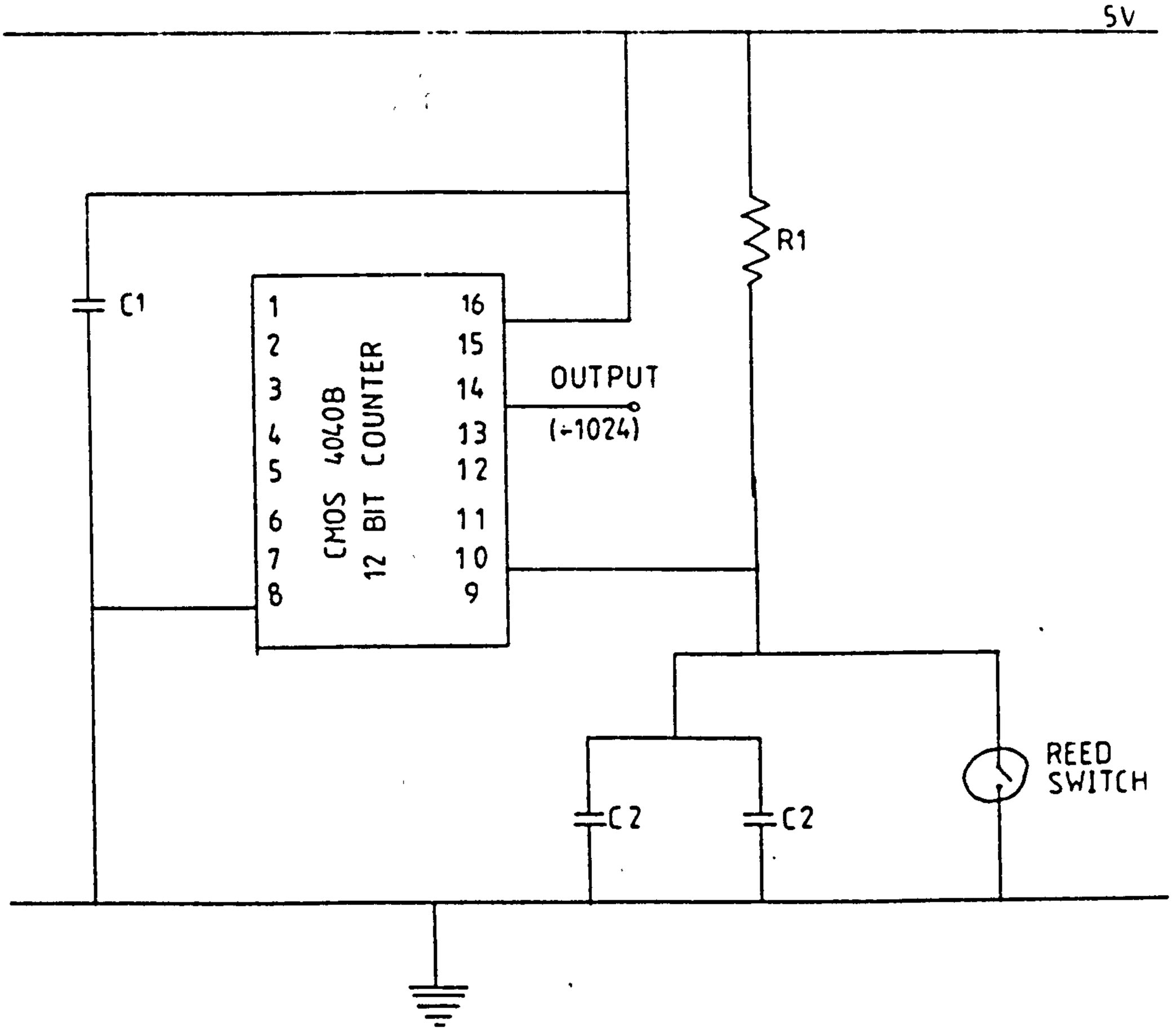

C1 = 0·1 μF R1 = 10 kΩ
C2 = 15 nF

Figure 3.12 Circuit diagram for pulse counting flow measurement

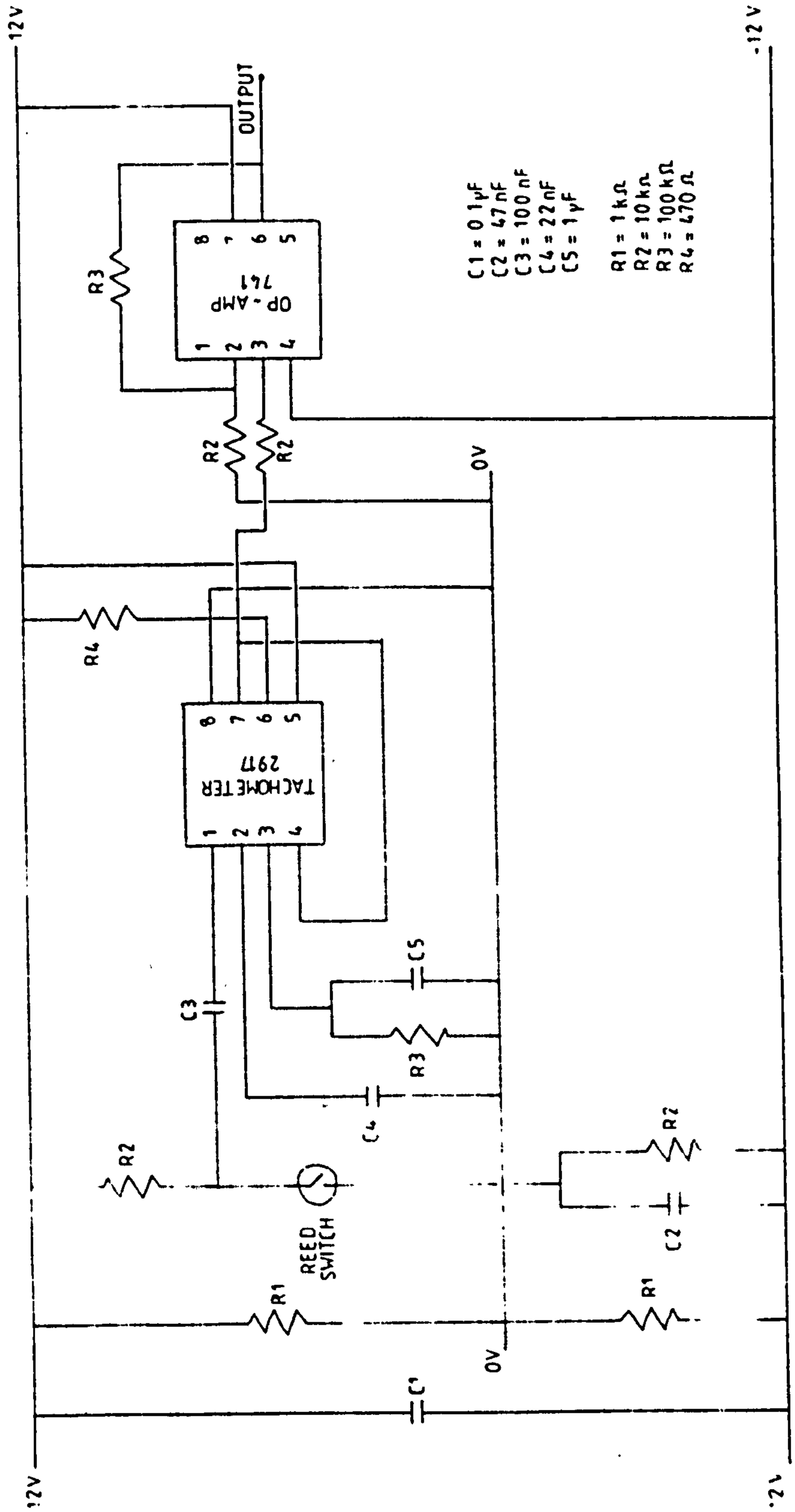

Figure 3.13 Circuit diagram for frequency to voltage converter

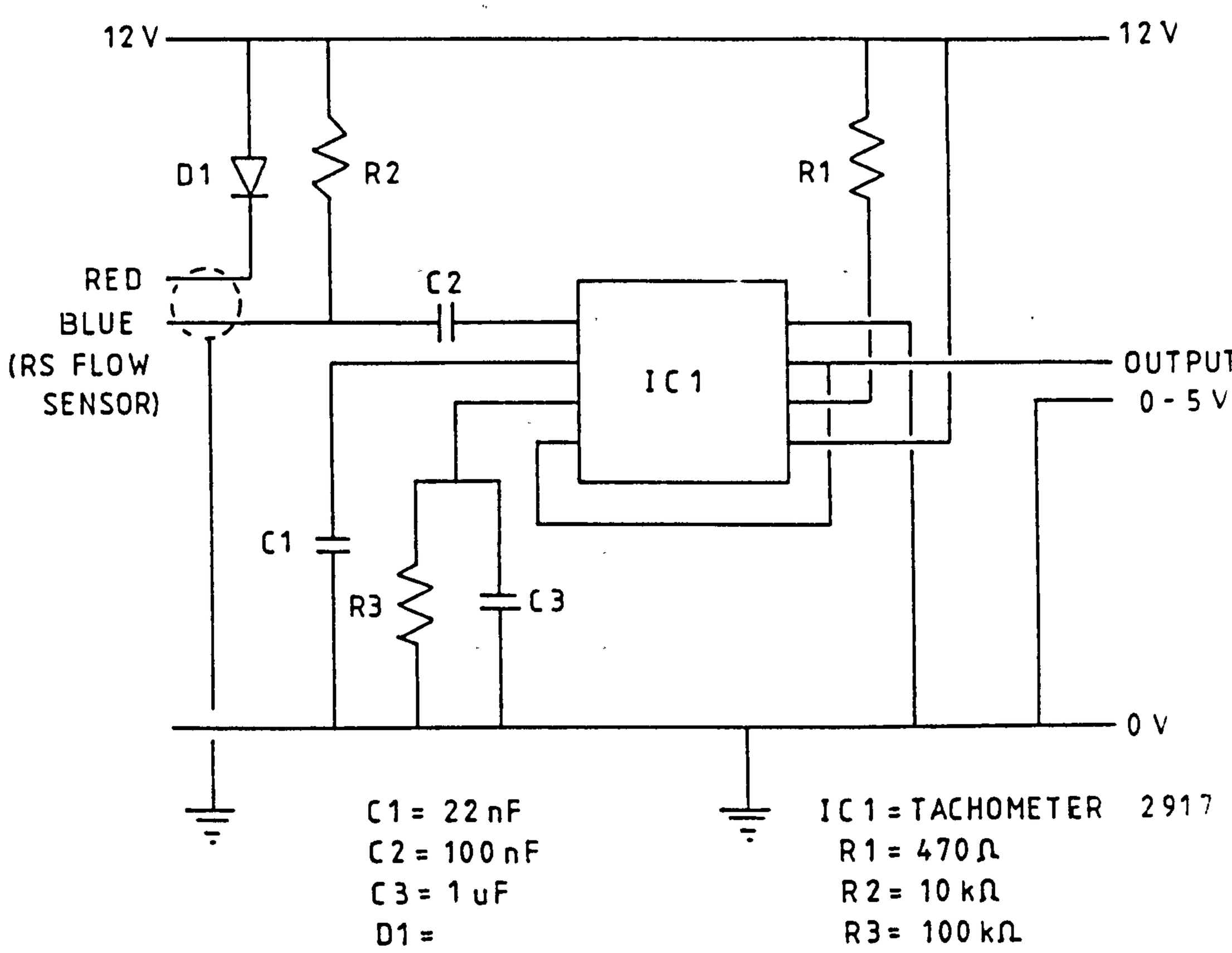

Figure 3.14 : Circuit diagram for RS flow sensor output to voltage converter

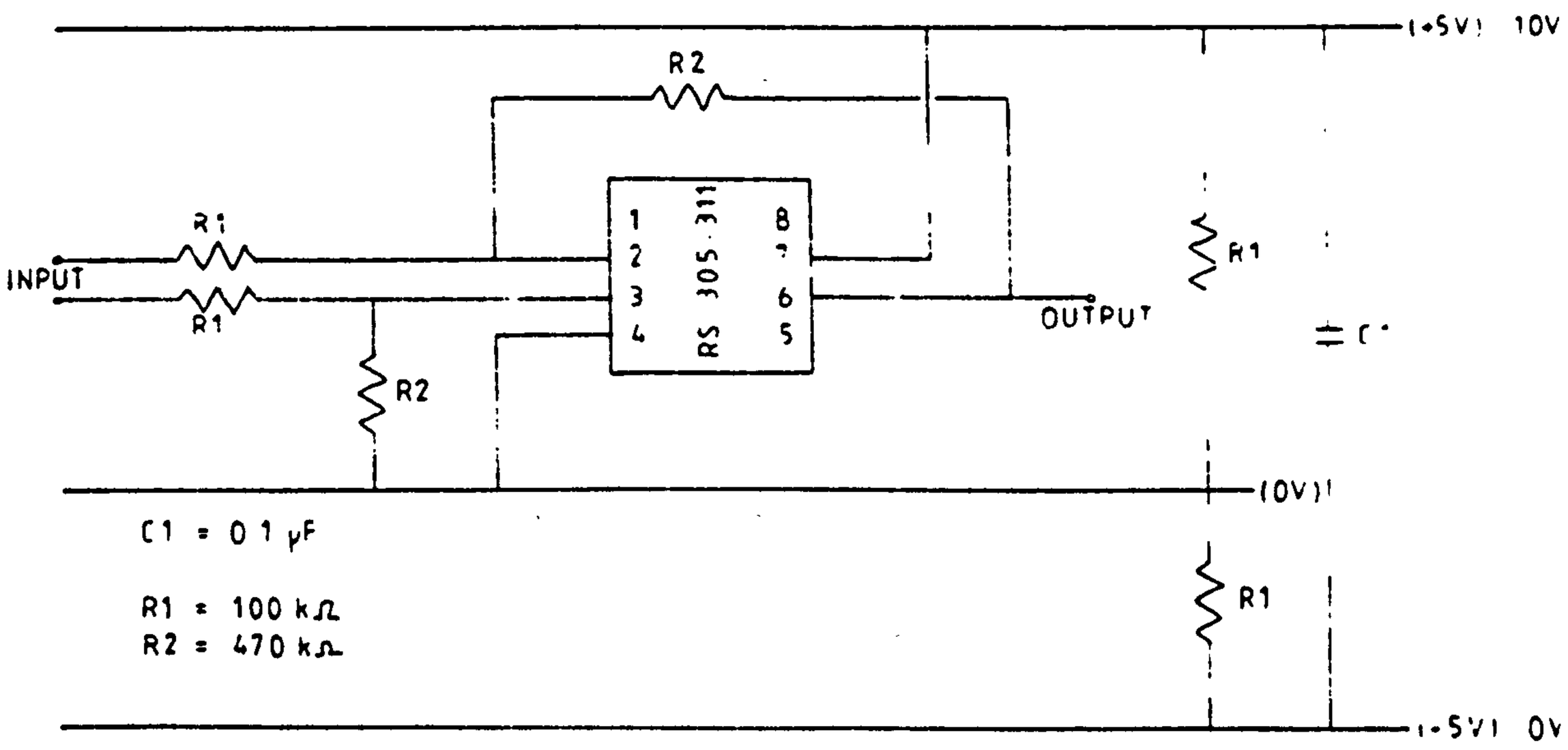

Figure 3.15 Circuit diagram for pressure transducer amplifier

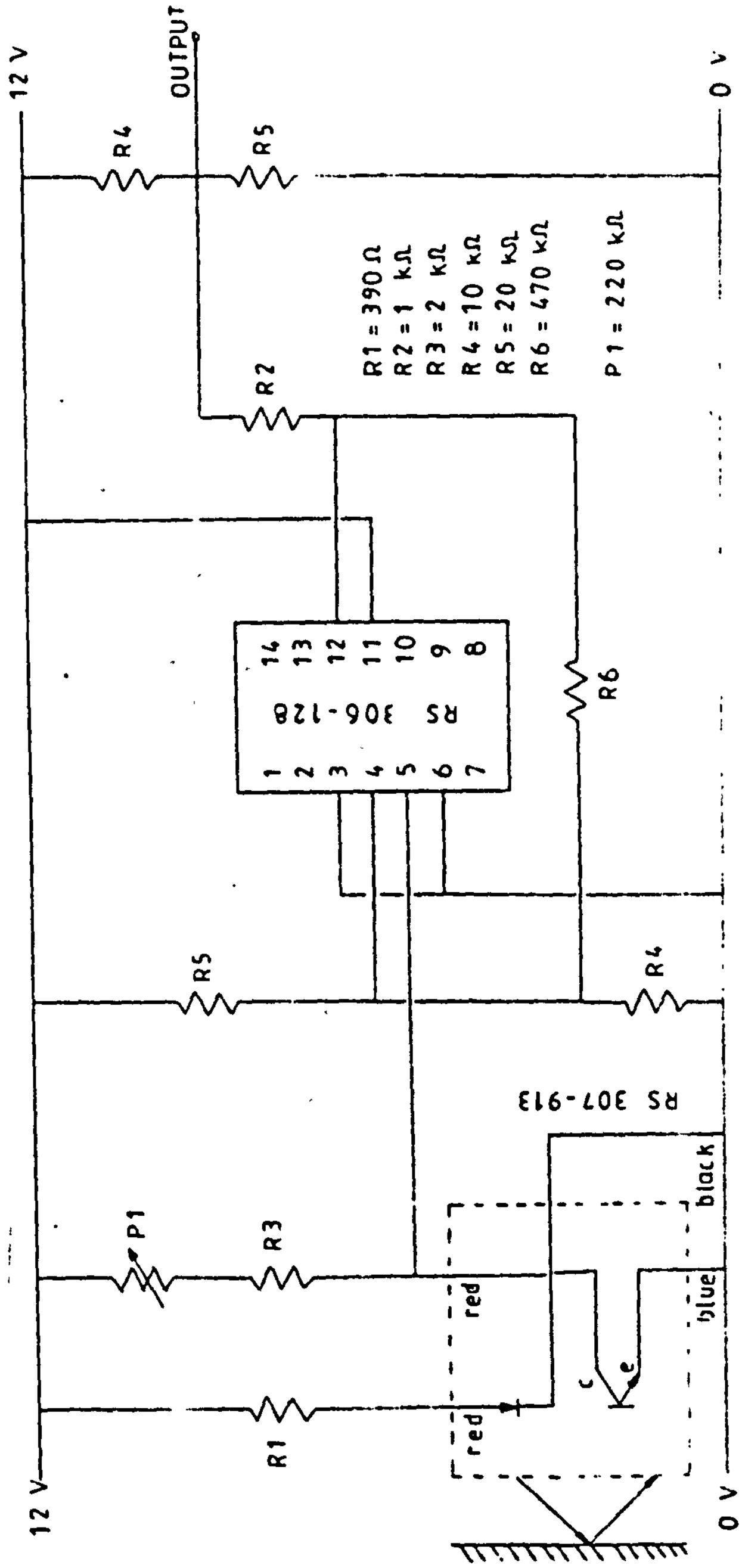

Figure 3.16 Circuit diagram for power meter

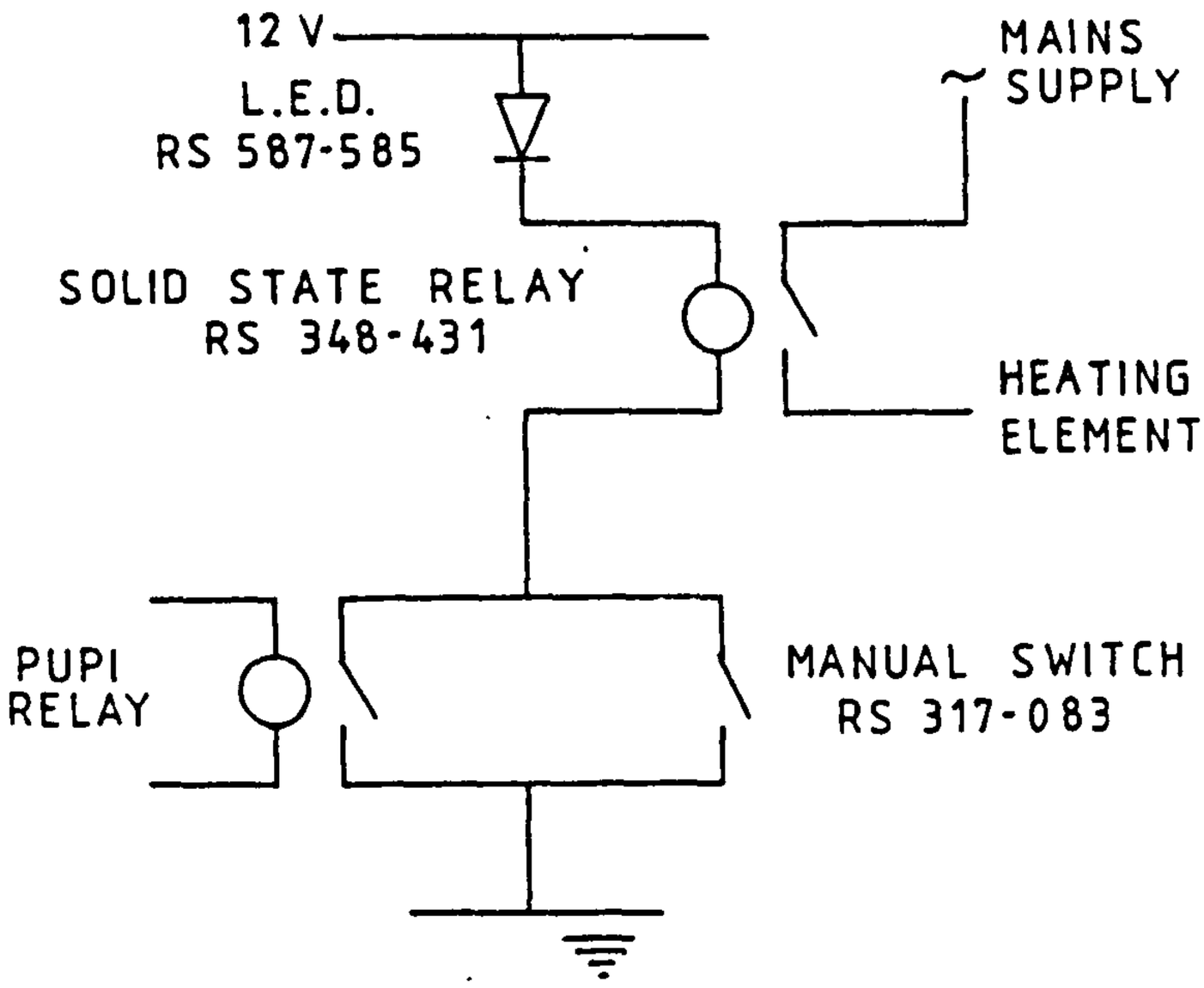

Figure 3.17 Diagram showing operation of relays

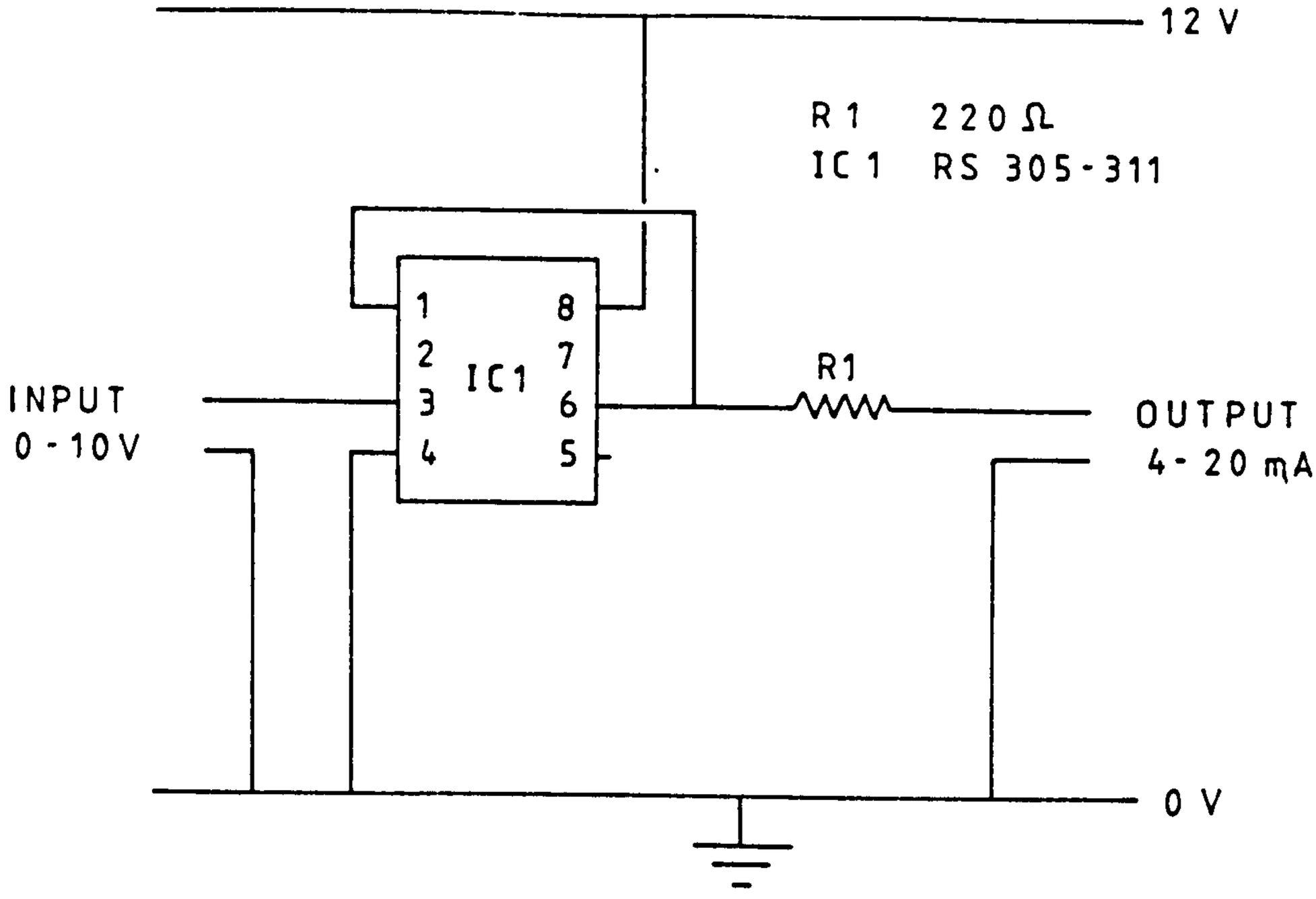

Figure 3.18 Circuit diagram for unity gain amplifier (V/I converter)

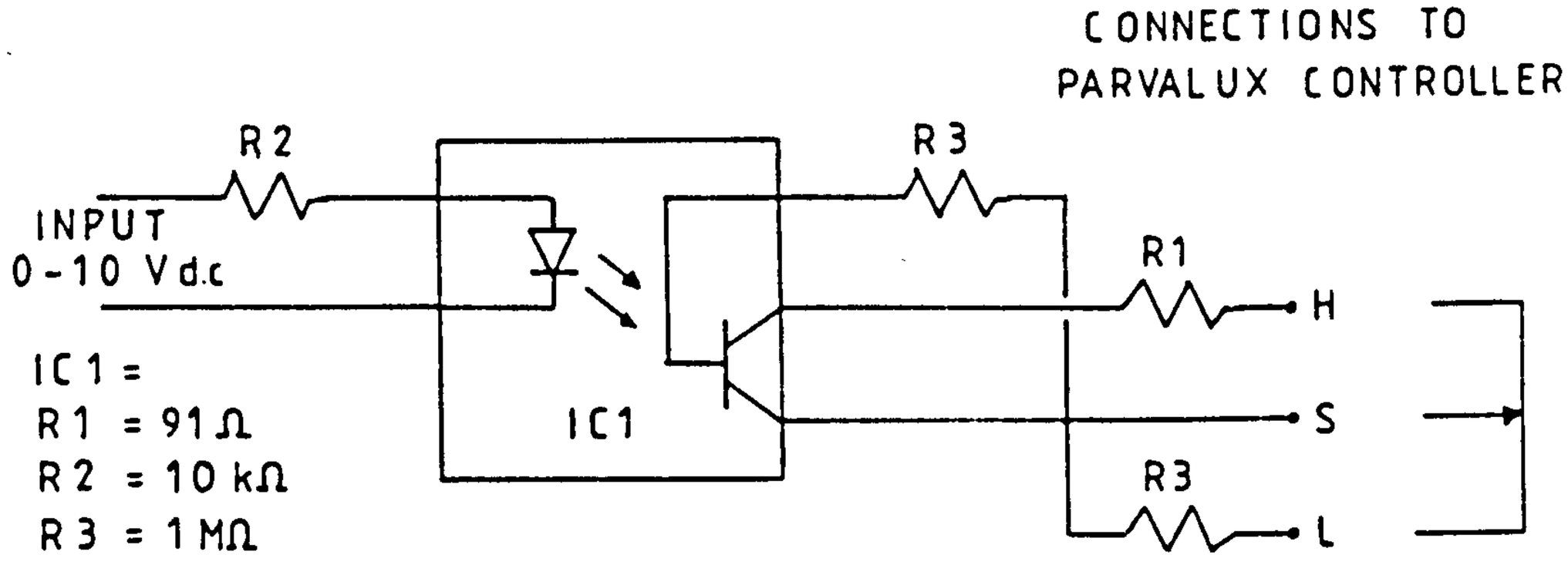

Figure 3.19 Circuit diagram of dc motor controller

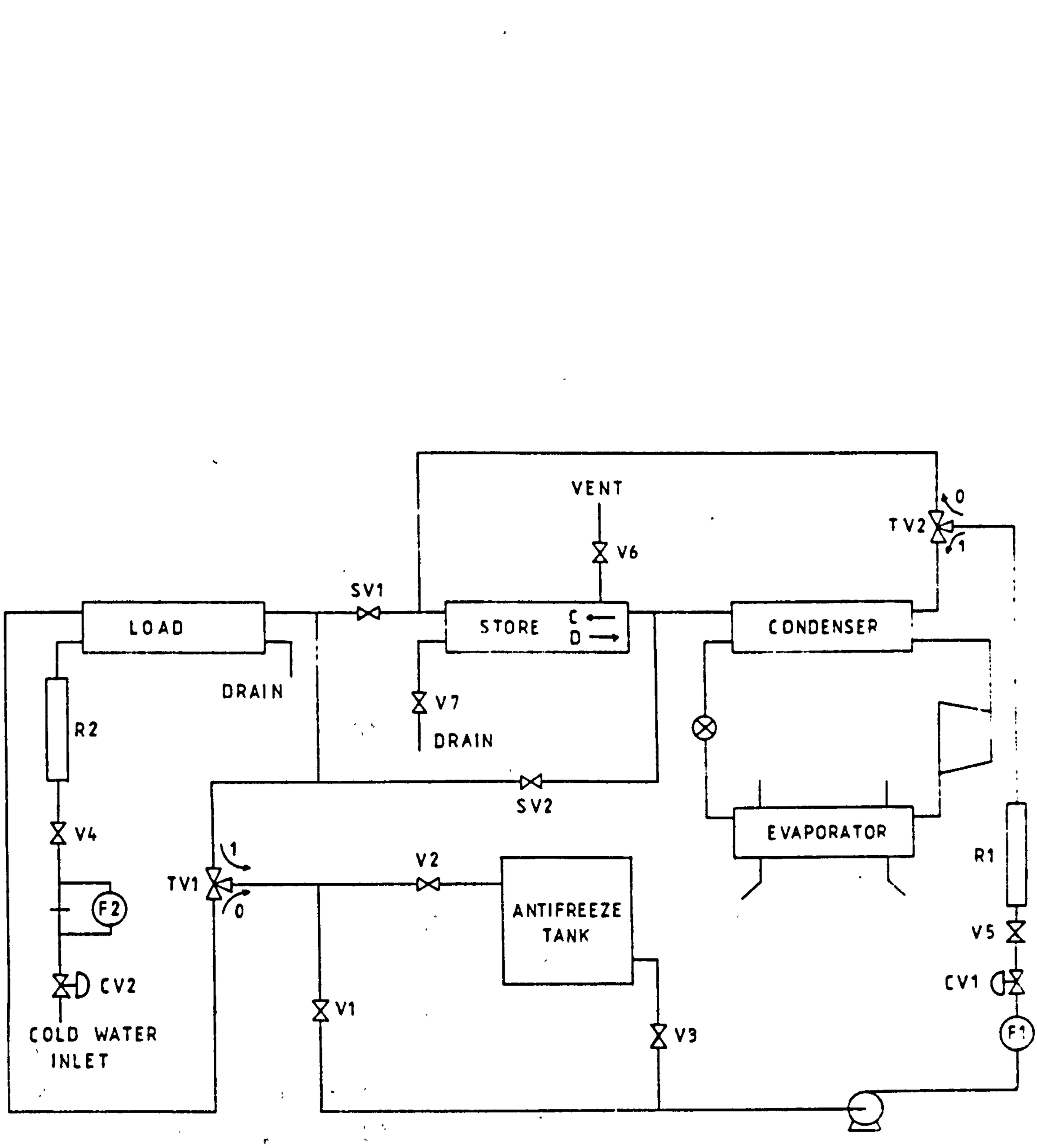

Figure 3.20 Simplified diagram of transfer fluid flow through test facility

Table 3.1 Properties of Candidate PCMs

PCM	T_{mp} [°C]	λ [kJ/kg]	Cp [kJ/kgK]	ρ [kg/m^3]	k [W/mK]
1	58.3	263	1.97-3.35	1450	-
2	56-58	270	1.90-2.50	1150	0.5
3	56	242	2.46	1460	0.65
4	54	187	1.6-2.7	840	-
5	48-52	140	2.9-2.1	880-870	0.21
6	49	200	1.46-2.39	1690-1660	-
7	36	278	1.55-3.18	1520-1442	-
8	32	251	1.76-3.31	1460	2.16-0.59
9	29.7	170	1.44-2.32	1712-1520	1.11-0.52

Key to PCMs:

1. Sodium acetate trihydrate, $CH_3COONa.3H_2O$, Telkes (1980).
2. Sodium acetate trihydrate, $CH_3COONa.3H_2O$, van Galen (1980).
3. Calortherm 58, based on sodium acetate trihydrate with stabilising additives, Calor
4. Myristic acid, Abhat (1981).
5. Parraffin wax, Kopecky (1985).
6. Sodium thiosulphate pentahydrate, $Na_2S_2O_3.5H_2O$, Telkes (1980).
7. Disodium hydrogen phosphate dodecahydrate, $Na_2HPO_4.12H_2O$, You Jae Burn (1982).
8. Sodium sulphate decahydrate, $Na_2SO_4.10H_2O$, Kopecky (1985).
9. Calcium chloride hexahydrate, $CaCl_2.6H_2O$, Carlsson and Wettermark (1980).

Table 3.2 Comparison of Various Encapsulation Geometries

Note	Heat Exchanger [mm]	Storage Device [m]	S $[m^{-1}]$	ξ [-]
1	966 tubes,L=1000,D=25,Δr=1.3	0.742x0.495x2.126	160.1	0.488
2	452 tubes,L=1000,D=38,Δr=1.3	0.742x0.495x2.126	105.4	0.570
3	49 tubes,L=1000,D=25,Δr=1.3	0.217(dia)x1.2	160.1	0.435
4	21 tubes,L=1000,D=38,Δr=1.3	0.217(dia)x1.2	105.4	0.465
5	130 tubes,L=910,D=76.2,Δr=3.2	0.67x0.91x1.52	54.7	0.488
6	133 cans,L=61,D=73,Δr=1.5	0.394(dia)x0.794	87.6	0.342
7	2398 cans,L=69.5,D=52.8,Δr=1	0.64x0.64x1.42	112.9	0.573
8	530 capsules,D=20	volume 3.9 lit	170	0.569
9	726 trays,320x320x10	1.3x0.7x2.7	112.5	0.301
10	Tubing,L=2031m,D=12.7	volume 1.98m^3	40.9	0.87

Key to Storage Devices:

1,2 Edinburgh prototype

3,4 Edinburgh pilot

5 Foster Wheeler prototype, Dietz (1984)

6 Cranfield pilot, Manley (1983)

7 Cranfield prototype, Kopecky (1984)

8 Cranfield pilot, Wood et al. (1981)

9 NBS prototype, Jones and Hill (1979)

10 Calmac commercial, MacCracken (1981)

Table 3.3 Design Details of Pilot Storage Device

(a) Encapsulation and storage device dimensions

		25mm	38mm
Tube pitch	[mm]	27	40
Length of tube	[m]	1.0	1.0
Thickness of tube wall	[mm]	1.3	1.3
Number of tubes in tank	[-]	49	21
Cross sectional area of tube	[cm^2]	4.909	11.34
Cross sectional area of tubes	[cm^2]	240.5	238.4
Diameter of store	[cm]	21.7	21.7
Height of store	[cm]	120	120
Cross sectional area of store	[cm^2]	369.8	369.8
Insulated surface area	[m^2]	1.072	1.072
Non-insulated surface area	[m^2]	0.892	0.892
Free flow area	[cm^2]	129.3	131.4
Mean velocity (0.192 kg/s)	[cm/s]	1.49	1.46
Total wetted surface	[m^2]	4.530	3.189
Equivalent diameter of channel	[cm]	1.14	1.65
Volume occupied by tubes	[lit]	24.05	23.8
Enclosed volume of store	[lit]	44.38	44.38
Volume of transfer fluid	[lit]	20.33	20.58
Voidage of storage device	[%]	45.8	46.4
Heat transfer area of tube	[cm^2]	785.4	1194
Heat transfer area of tubes	[m^2]	3.848	2.507
Surface area density of tube	[m^{-1}]	160.1	105.4
Diameter of hole in plates	[mm]	2.37	2.37
Number of holes	[-]	86	86
Total hole area	[cm^2]	3.79	3.79

(b) Determination of TSC

		25mm	38mm
Average full weight of tube	[kg]	0.667	1.585

Average empty weight of tube	[kg]	0.0915	0.140
Weight of PCM in each tube	[kg]	0.5755	1.445
Total number of tubes	[-]	49	21
Weight of PCM	[kg]	28.2	30.3
Latent heat of PCM	[kJ]	6824	7332
Sensible heat of PCM	[kJ/K]	69.7	74.8
Weight of encapsulation	[kg]	4.48	5.66
Sensible heat of encapsulation	[kJ/K]	8.63	5.66
Weight of glass walls	[kg]	19.6	19.6
Sensible heat of glass walls	[kJ/K]	16.4	16.4
Weight of brass flanges	[kg]	20.2	20.2
Sensible heat of brass flanges	[kJ/K]	7.6	7.6
Weight of dural plates	[kg]	1.8	1.8
Sensible heat of dural plates	[kJ/K]	1.7	1.7
Sensible heat of transfer fluid	[kJ/K]	83.72	84.77

(c) Breakdown of TSC for $\Delta Tp=20$ degC [25 mm tubes]

	[kJ]	[%]
Latent heat of PCM	6824	64.5
Sensible heat of PCM	1394	13.2
Sensible heat of transfer fluid	1674	15.8
Sensible heat of encapsulation	173	1.6
Sensible heat of tank fabric	514	4.9
TOTAL	10579	100

Note: See 9.1.1 for property data

Table 3.4 Design Details of Prototype Storage Device

(a) Encapsulation and storage device dimensions

		25mm	38mm
Tube pitch	[mm]	27	40
Equivalent diameter of channel	[mm]	7.154	8.428
Length of tube	[m]	1.0	1.0
Thickness of tube wall	[mm]	1.3	1 3
Number of tubes in section	[-]	85	39
Number of tubes in tank (1)	[-]	966	452
Cross sectional area of tube	[cm^2]	4.909	11.34
Cross sectional area of tubes (2)	[m^2]	0.237	0.256
Breadth of tank	[m]	0.742	0.742
Depth of tank	[m]	0.485	0.485
Height of tank	[m]	2.126	2.126
Cross sectional area of store	[m^2]	0.360	0.360
Insulated surface area	[m^2]	7.845	7.845
Non-insulated surface area	[m^2]	6.072	6.072
Free flow area	[m^2]	0.123	0.104
Mean velocity (0.192 kg/s)	[cm/s]	0.155	0.185
Volume occupied by tubes	[m^3]	0.474	0.512
Enclosed volume of store	[m^3]	0.765	0.765
Volume of transfer fluid	[m^3]	0.291	0.253
Voidage of storage device	[%]	38.0	33.1
Heat transfer area of tube	[cm^2]	7.854	11.94
Heat transfer area of tubes	[m^2]	75.87	53.96
Surface area density of tube	[m^{-1}]	160.1	105.4
Diameter of hole in plates	[mm]	3.18	14.0
Number of holes	[-]	1083	324
Total hole area	[cm^2]	86.0	498.8

Notes

1. Not equivalent to number of tubes per section times twelve since some sections have slightly different dimensions due to door. This results in the omission of sixteen 38 mm tubes and fifty-four 25 mm tubes.

2. Cross sectional area of tubes in flow direction calculated from half the total number of tubes times the cross sectional area of a single tube.

(b) Determination of TSC

		25mm	38mm
Average full weight of tube	[kg]	0.540	1.600
Average empty weight of tube	[kg]	0.069	0.120
Weight of PCM in each tube	[kg]	0.471	1.48
Total number of tubes	[-]	966	452
Weight of PCM	[kg]	455	669
Latent heat of PCM	[MJ]	110	162
Sensible heat of PCM	[MJ/K]	1.119	1.646
Weight of encapsulation	[kg]	66.7	54.2
Sensible heat of encapsulation	[MJ/K]	0.128	0.104
Weight of storage tank	[kg]	234	234
Sensible heat of storage tank	[MJ/K]	0.108	0.108
Volume of transfer fluid	[lit]	290.9	252.5
Sensible heat of transfer fluid	[MJ/K]	1.140	0.990

(c) Breakdown of TSC for ΔTp=20 degC [25 mm tubes]

	[MJ]	[%]
Latent heat of PCM	110	68.8
Sensible heat of PCM	22.38	14.0
Sensible heat of transfer fluid	22.8	14.3
Sensible heat of encapsulation	2.56	1.6
Sensible heat of tank fabric	2.15	1.3
TOTAL	159.9	100

Note: See 9.1.1 for property data

Table 3.5 – Flow Direction Control Operating Philosophy

Mode	Flow direction	TV1	TV2	SV1	SV2	P1
1	Condenser – load	0	1	0	1	1
2	Condenser – store(TD)	1	1	1	0	1
3	Condenser – store(TD) – load	0	1	1	0	1
4	Store(BU) – load	0	0	0	1	1
5	Off	0	0	0	0	0

CHAPTER 4

THERMAL ENERGY STORAGE DEVICES

4.1. Test Procedures

Thermal performance data for storage devices is normally obtained by following selected test procedures. The ASHRAE Standard 94-77 was found to be the most commonly used test procedure and hence was adopted into the experimental program to permit comparison with data available in the literature. However, as it was felt that it was not specifically intended for PCM TES, it was employed only as a guide and modified where it was felt necessary.

A second test procedure published by the same body, the ASHRAE Standard 94.2-81, was intended to supplement the original, but was issued as a separate document due to the difference between the procedures. This again has limited application to the storage devices which were being tested but for the sake of completeness a brief mention has been made in section 4.1.2.

The ASHRAE test procedures investigate the store performance when subjected to a step change in temperature. The Edinburgh store was designed to be an integral part of a domestic heat pump heating system and was therefore expected to be charged at an approximately constant rate. The experimental test procedure was essentially a temperature step change test, similar to ASHRAE with a limiting maximum rate, and is described in section 4.1.3.

4.1.1. ASHRAE Standard 94-77

The tests outlined in the ASHRAE Standard 94-77 consist of the following:

1. One test to determine a heat loss factor for the thermal energy storage device
2. Two tests to determine the response characteristics (charge capacity) of the device to a step increase (above the initial temperature) in the entering fluid temperature
3. Two tests to determine the response characteristics (discharge capacity) of the device to a step decrease (below the initial temperature) in the entering transfer fluid temperature

4.1.1.1. Heat loss test

The heat loss test consists of passing the transfer fluid through the storage device with an inlet temperature 25 degC above the ambient air temperature. After steady state conditions are reached, measurements are made of the average temperature difference between the inlet and outlet transfer fluid and the ambient air temperature over a one hour period. Steady state conditions are achieved by circulating the transfer fluid through the storage device until the inlet and outlet fluid temperatures vary by less than ± 0.5°C during a one hour period. The heat loss factor (L) is defined in the standard by

$$L = \{(\dot{m}\,Cp)_{tf}/[(3600s)(25degC)]\} \int_{t=0}^{t=3600}(T_{in}-T_{out})dt. \quad (4.1)$$

The mass flow rate of the transfer fluid to be used for the heat loss test is determined by

$$\dot{m} = (TSC)_L/[Cp_{tf}(14400s)(25degC)]. \quad (4.2)$$

The theoretical storage capacity for the heat loss test, TSC_L, is the amount of energy that could be stored in the device if all the device components underwent an increase in temperature of 25 degC, starting with an initial temperature equal to T_a, the ambient air temperature. It is further specified that it be calculated as the summation of the product of mass and specific heat of the various components comprising the device (storage medium, container, insulation, etc.) multiplied by the temperature increase of 25 degC.

4.1.1.2. Charge and discharge tests

The concept of test fill time (t_f) is introduced and defined in the standard as

$$t_f = TSC/[(\dot{m}\,Cp)_{tf}\Delta Tp]. \quad (4.3)$$

A sensible heat storage device with no heat loss to the ambient and with perfect stratification of the storage medium would be completely charged or discharged in the time defined by equation (4.3). Since such an ideal storage

device does not exist, the fill time defined above is found to be less than the time required to completely charge or discharge actual storage devices. In the standard it is suggested that thermal energy storage devices of widely different design could be equitably compared if each were tested for the same period of time defined by equation (4.3). In other words, the flow rates for the different devices are adjusted so that the amount of energy entering or leaving the device (denominator of (4.3)) per unit thermal energy storage capacity (numerator of (4.3)) is the same for each device.

The standard specifies that the charge and discharge tests be conducted for specific test fill times and step changes in the inlet temperature of the transfer fluid. The recommended temperature step change values for devices which use either air or liquid were based on consideration of the way in which they are currently used in typical (solar) heating and cooling systems.

The recommended values specified in the standard for devices using water as the transfer fluid are:

$t_{C,D}$ = 2 hr or 4 hr , ΔTp = 15 degC.

With the test fill times designated, the mass flow rates are determined by the use of equation (4.3). Therefore the mass flow rates for the transient tests are determined by

$$\dot{m}_{C,D} = TSC/[t_{C,D}Cp_{tf}\Delta Tp]. \qquad (4.4)$$

In cases where the storage device was designed for a particular flow rate, the Standard allows use of this design flow rate.

Figure 4.1 represents the charge and discharge cycles of a theoretical energy storage device undergoing the transient response tests in accordance with the Standard. The initial temperature of the storage medium is chosen based on the intended operating range of the device. The flow is adjusted to the value, $\dot{m}$, defined by equation (4.4) and the device is brought to a uniform initial temperature. The temperature of the entering transfer fluid is then raised in a step like manner from the initial temperature T_o, to a final temperature T_o + ΔTp, and measurements necessary for computing the charge capacity are made over the charge test fill time, t_C . The storage medium is then allowed

to reach steady state conditions at the temperature T_o + ΔTp. Once steady state has been established a discharge test is performed by decreasing the entering transfer fluid temperature in a step like manner from T_o + ΔTp to a value of T_o. Measurements necessary in computing the discharge capacity are then recorded over the discharge test fill time, t_D. The measurements required for the charge and discharge test computations are the temperature difference between the entering and leaving transfer fluid over the test fill time, the transfer fluid flow rate, and the ambient air temperature.

The charge and discharge capacities are computed as

$$C_C = (\dot{m}_C Cp)_{tf} \int_{t=0}^{t=tC} (T_{in} - T_{out}) dt - Lt_C (T_o + (T_{in} - T_{out})/2 - T_a), \quad (4.5)$$

and

$$C_D = (\dot{m}_D Cp)_{tf} \int_{t=0}^{t=tD} (T_{out} - T_{in}) dt. \quad (4.6)$$

It should be noted that the charge and discharge capacities are a function of the specific heat of the transfer fluid and hence a function of the transfer fluid used.

4.1.2. ASHRAE Standard 94.2-81

This standard is intended to apply to both sensible and latent heat thermal storage devices which are charged electrically and discharged thermally. The procedure requires that four tests be carried out:

1. Pre-conditioning
2. Initial charge
3. Maximum standby emission
4. Discharge

Pre-conditioning test

This test provides verification of the control system performance of any storage device. Maximum charge is selected and then maintained for 24 hours before the whole system is brought back to ambient conditions. No measurements are required.

Initial charge test

The storage device is initially at the test room ambient temperature. Maximum charge is selected and the total electrical input energy E_1, required to reach the first controller cut off is recorded.

Maximum standby emission

In this test it is intended to measure the standby emission (heat loss) from the storage device under maximum charge conditions. It is specified that this test be performed immediately after the initial charge test and that the steady state period should be maintained for not less than three cycles of the charge controller, and for a minimum of eight hours. The electrical input energy E_2 required to maintain steady state conditions for the total test period (t_2) is noted. Hence the maximum standby emission rate is calculated from

$$q_{L,max} = E_2 / t_2. \qquad (4.7)$$

This procedure appears confusing since most storage devices are designed with multiple small heaters rather than a single large one and therefore the time required to reach the first controller cut off would only be the first step towards a charge condition. Certainly in an integrated heat pump /heat store system, the heat pump maximum charge rate may be appoximately constant, but a proportion of this may be used for house preheat e.g. at end of off-peak charge period.

Discharge test

The purpose of this test is to determine the amount of useful heat that can be extracted from the thermal storage device without recharging. Immediately after the conclusion of the maximum standby emission test the store is discharged for a period of time (t_3) until the outlet temperature drops below its set point by more than a quarter of the difference between the outlet set point and inlet temperatures. The device is then charged for a period (t_4), until the controller shuts off. The electrical input energy E_4, for this recharge is noted. This procedure is repeated for a period of time (t_5) and the electrical energy E_5 used in this period by the pump is recorded. A final recharge is performed and the required electrical input energy defined as E_6. The following equations may then be employed to determine the device

performance:

Discharge capacity

$$Q_D = Cp\int_0^{t5} \dot{m}\,\Delta Tp\,dt. \qquad (4.8)$$

Residual capacity

$$Q_r = E_1-[(E_4 +E_6)/2]. \qquad (4.9)$$

Effectiveness

$$\eta = 100\ Q_D /[(E_4 +E_6)/2+E_5]. \qquad (4.10)$$

4.1.3. Experimental Test Procedure

Since the ASHRAE test procedure was not strictly adhered to at Edinburgh a section describing the actual test procedure has been included.

4.1.3.1. Experimental heat loss test

Heat loss was found by performing a normal charge/discharge cycle (see section 4.1.3.2) and monitoring the temperature drop across the store once steady state had been achieved. The mass flow rate determined by equation (4.2) does not include the latent heat storage capability of the store being investigated and is therefore of limited value. Hence a flow rate typical of normal operation (11.5 lit/min) was selected instead.

4.1.3.2. Experimental charge/discharge cycle test

For a test fill time of six hours and a step change in temperature of 20 degC, the recommended mass flow rate as determined by equation (4.4) was calculated to be 0.09 kg/s (5.4 lit/min). The recommended flow rate range for the heat pump was 7-12 lit/min, hence tests were performed at 8 and 11.5 lit/min. One test was also performed at 15 lit/min as employing higher flow rates is one method of minimising the condenser temperature in the heat pump.

Since the PCM melting temperature was 56°C, the initial temperature was

44°C and the final temperature 64°C for the charge test and vice versa for the discharge test. In section 4.1.2 it was noted that the recommended temperature step changes were based on the way in which the store will be used. As it was intended to use this store in combination with a heat pump the effect of smaller temperature step changes were also investigated. It is possible to operate the store in two modes viz. with the flow top-down or bottom-up, and tests were performed using both modes.

While the store is being charged or discharged the rate of heat transfer to or from the store is calculated for each time period. This value is then corrected for heat loss and used to determine the total amount of heat actually transferred to or from the store. In section 4.1.2, equation (4.5) correctly indicates how to allow for heat loss in the charge test, but equation (4.6) incorrectly assumes that all heat transferred out of the store during discharge is assimilated by the transfer fluid. This assumption would lead to a very low discharge capacity as there will inevitably be heat transferred from the store to both the transfer fluid and the surroundings. Hence the modified expression given below should be used to evaluate the discharge capacity

$$C_D = (\dot{m}_D\, Cp)_{tf} \int_{t=0}^{t=t_D} (T_{out}-T_{in})dt + Lt_D[T_o-(T_{out}-T_{in})/2 - T_a]. \qquad (4.11)$$

The ratio of the amount of heat transferred to the theoretical storage capacity gives an indication of the store condition i.e. how "charged" or "discharged", and is referred to as the utilisation factor, UF. Hence a completely discharged store has a UF of 0 while a fully charged store has a UF of 1.0.

4.1.3.3. Static heat loss test

A static heat loss test was performed which determined the heat loss from the store while the pump was not running, to confirm the operating heat loss calculated in section 4.1.3.1. There will be many periods when the storage device is neither being charged nor discharged and it was considered important to obtain information on the heat loss while in this static mode. The store was simply brought to steady state at a selected temperature and then left with the pump switched off for a period of up to a few days while

the computer monitored the temperature throughout the store. From these values the average temperature was calculated and its variation with time used to determine a static heat loss coefficient.

4.2. Results from Pilot Store

The construction of the pilot storage device permitted it to be filled with either 25 or 38 mm dia. tubes. It was also possible to place an instrumented tube which had 6 thermocouples (centre-line and edge at top, middle and bottom) mounted in the PCM (see figure 3.3(b)) into the device. The results from the tests performed were employed to finalise the design of the prototype store.

Since section 4.3 presents detailed results obtained during testing of the prototype store, this section will only include results which could not be reproduced in that store:

1. Internal temperature profiles of the PCM
2. Comparison of the thermal performance of 25 and 38 mm diameter tubes

The operating parameter values and results for the runs considered are presented in table 4.1.

4.2.1. Temperature Profiles within PCM

It can be seen that the two cases considered for examination of internal profiles, runs 8.8 and 8.19 represent the limits of operating conditions in the pilot store. Run 8.8 is performed at high flow with small diameter tubes and run 8.19 at low flow rate with large diameter tubes.

In figure 4.2 the PCM temperature along the centre line of the tube is presented for both runs. The profile described by the top sensor in the 25 mm tube appears to follow the inlet temperature very closely and exhibits no evidence of a phase change. All the other sensors exhibit some evidence of phase change although it would be extremely difficult to deduce the melting point to better than 56 ± 2°C. Note that the curious effect of the middle temperature lagging that at the bottom for UF < 0.75 is evident in both tubes

and is therefore unlikely to be a characteristic of the thermocouple.

The discharge profiles presented in figure 4.3 provide clear evidence of subcooling, particularly in the case of the 25 mm tube. Again in this plot the top thermocouple profile in the 25 mm tube is the only one which does not describe a phase change trajectory. Once phase change has been initiated it was expected that the temperature would rapidly rise to the melting point and remain constant at that value. This is clearly demonstrated in the temperature profile described by each sensor in the 38 mm diameter tube and indicates a phase change temperature of 56°C. However if this is assumed to be true it is difficult to explain the rise in the bottom sensor temperature in the 25 mm diameter tube up to 58°C and the middle sensor to only 54°C.

4.2.2. Comparison of Thermal Performance of 25 and 38 mm Tubes

Figure 4.4 presents a comparison of 25 mm and 38 mm diameter tubes. Very substantial improvements in both charge and discharge rates are apparent especially at higher UF. In both cases the discharge rate against UF curve describes a minimum and its location was dependent on the degree of subcooling experienced in the tube.

An approximate overall heat transfer coefficient was defined to allow comparison of performance of the storage device when composed of 25 and 38 mm tubes

$$U_{ap} = q/[A(T_{in}-T_{mp}] \tag{4.12}$$

where A is the outside surface area of the tubes. During charge at a UF of 0.75 the 25 mm tubes have an approximate heat transfer coefficient (39.6 W/m^2K), marginally higher than that determined for the 38 mm tubes (35.9 W/m^2K). During discharge at the same UF both values were lower, with the 38 mm tubes having a slightly greater coefficient (32.9 to 30.9 W/m^2K).

4.3. Results from Prototype Store

4.3.1. Determination of Heat Loss

4.3.1.1. Operating heat loss

The storage device was initially brought to a steady state temperature of 48°C and maintained at that temperature for approximately eight hours. Then over an additional period of two hours the average heat transfer rate from the transfer fluid to the store and surroundings was recorded. Since the storage medium was assumed to be at steady state then this value must represent the heat loss solely to the surroundings. Table 4.2 presents the mean heat loss from the store (five readings in approximately six minutes) taken over the two hour period. Flow through the store was top-down for the first test. To check that the calculated heat loss was constant for both flow directions the test was repeated with the flow reversed for an identical test period but a shorter approach (one hour) to steady state.

A discrepancy was observed between the top-down mode (190.5 W) and bottom-up mode (162.4 W) of approximately 30 W. While this is significant it represents an error of only ± 0.04 degC in the reading from the thermopile. These two values were then averaged and the heat loss factor, for an average ambient temperature of 23°C, was calculated to be 7 W/degC. Specifying this value in a later run produced very satisfactory results at both ends of the temperature range. This heat loss factor is equivalent to a heat loss coefficient of 1.153 W/m^2K based on the non-insulated surface area of the store.

4.3.1.2. Static heat loss

The storage device was brought to and maintained at a steady state temperature of 50°C for a period of four hours. The pump was then switched off and temperatures at 10 locations were monitored and averaged. Heat loss from the store was then calculated from

$$q_L = (MCp)_{store}\Delta T_{ave}/\Delta t \qquad (4.13)$$

where $(MCp)_{store}$ was 2.571 MJ/degC (see section 3.1.5.1). Results are presented in table 4.3 and figure 4.5 for 6 hour intervals over a period of 5 days. The results indicate that initially the rate is close to 7 W/degC (operating

value) but afterwards decreases to approx. 5 W/degC. This was thought to be caused by inaccurate calculation of the mean store temperature due to thermal stratification in the store.

4.3.2. Charge/Discharge Cycle Performance

4.3.2.1. Storage capacity

A summary of the charge and discharge runs performed and the relevant operating parameters is presented in table 4.4. Note that the value of UF_D given was the store condition as the discharge rate fell below 1.5 kW. The important points from these results are noted below:

1. Results appear to be reproducible, standard run (*) has UF_C = 0.930 ± 0.01 and UF_D = 0.095 ± 0.01
2. Changing flow rate has negligible effect on the storage capacity
3. Decreasing charge temperature below 62°C significantly decreases the charge capacity
4. Increasing discharge temperature above 46°C reduces the discharge capacity

4.3.2.2. Thermal effectiveness

The concept of using a nondimensional plot to show the thermal performance of storage devices relative to ideal devices was proposed by Kelly and Hill (1977). Figure 4.6 shows this non-dimensional plot for various ideal storage units. The ordinate is referred to as the dimensionless temperature difference

$$\Delta T^* = (T_{in}-T_{out})/\Delta Tp, \qquad (4.14)$$

while the abscissa represents a non-dimensional time

$$t^* = [(\dot{m}\, Cp)_{tf}\Delta Tpt)]/TSC. \qquad (4.15)$$

The charge/discharge rate of any storage device is proportional to $T_{in}-T_{out}$ and will be a maximum when $T_{in}-T_{out} = \Delta Tp$ (i.e. $\Delta T^* = 1$). This performance

can only be achieved by a perfectly insulated, completely stratified sensible heat storage unit. Equation (4.3) shows that the dimensionless time required to charge/discharge a completely stratified store will be equal to 1.0.

If a perfectly insulated, completely mixed sensible heat storage device was possible then the resulting curve would be exponential as is shown in figure 4.6. The total area under this curve if integrated to $t^* = \infty$ would again be found to equal 1.0. The area under this curve for $t^* = 0$ to 1.0 is 0.632 which corresponds to the ratio of the energy stored by the completely mixed device compared to the ideal stratified device, for the test fill time $t_{C,D}$.

Latent heat storage devices have very different performance characteristics. An ideal, perfectly insulated, completely stratified latent heat storage device with a phase change temperature $T_{mp} = 56°C$ operating in the temperature range 44 to 64°C would have charge and discharge curves as shown in figure 4.6. These can be derived by assuming that all the TSC could be stored as latent heat and released to the transfer fluid via a heat exchanger with negligible thermal resistance. Hence during charge the inlet and outlet temperatures would be 64 and 56°C respectively which gives a ΔT^* of 0.4. The maximum charge/discharge rate will be proportional to $T_{in}-T_{mp}$ and the corresponding test fill time can be determined by substitution of $T_{in}-T_{mp}$ for ΔTp in equation (4.3). Clearly the store would not be fully charged/discharged at $t^*=1$ but rather at $t^* = \Delta Tp/(T_{in}-T_{mp})$. In this analysis it was assumed that the ideal latent heat storage device has no sensible heat contribution while table 3.4(c) indicates that for a real device it may be as large as 30% of the TSC

In table 4.4, thermal effectiveness data relative to an ideal completely stratified sensible heat storage device (η_s) and that relative to the ideal latent charge/discharge case (η_l) is presented. Operating the store bottom-up for charge and top-down for discharge results in relatively low thermal effectiveness. Decreasing the charge temperature improves performance but is less significant for temperatures lower than 64°C, while varying the discharge temperature does not show a consistent trend. Decreasing the flow rate in both cases is shown to significantly improve thermal effectiveness.

Figure 4.7 presents the curves of ΔT^* against t^* for the two operating modes and three selected flow rates. For both charge and discharge,

selection of the correct operating mode results in the outlet temperature and hence ΔT^* approaching that for the ideal charge/discharge case. Increasing the flow rate is shown to have the opposite effect, while operation at the lowest flow rate initially results in a performance better than the ideal charge/discharge case.

4.3.2.3. Temperature-time variation of transfer fluid

Figure 4.8 shows the variation of the transfer fluid inlet and outlet temperature during the standard test cycle. Comparison with figure 4.1 which shows the expected profiles (ASHRAE Standard 94-77) highlights the limitations of the test facility.

1. Instantaneous step change of the transfer fluid inlet temperature cannot be achieved. For charge it takes approximately 2 hours before the inlet temperature achieves the specified setpoint, while discharge is slightly better and requires only an hour.
2. During the discharge test period the inlet temperature is shown to vary significantly (± 1°C) even after the initial period has elapsed. However during charge the inlet temperature is controlled to ± 0.5°C once the setpoint has been achieved.

4.3.2.4. Transverse temperature profiles of the transfer fluid within the storage device

Tables 4.5 and 4.6 present temperature profiles recorded during standard charge/discharge runs on the top and bottom plates. The exact locations of the sensors T25-T34 are shown in figure 3.4. The values recorded for UF=0 and 1 should be identical but due to unavoidable variations in thermocouple output, a discrepancy of 0.6 degC was observed.

(i) Charge (TD)

Only limited temperature variation (less than 0.6 degC) is observed in the top plate, hence the inlet distribution manifold can be assumed to be performing satisfactorily. On the bottom plate (x-axis) T29 describes a minimum at UF=0.156 and again at 0.884, while in the y-axis the largest variations of 1.1 and 1.6 degC occur at UF=0.156 and 0.884.

(ii) Discharge (BU)

An extremely large variation (2 degC) in the x-direction on the bottom plate is observed at UF=0.757 with T30 remaining significantly higher than the other sensors. In the y-direction the only significant variation was also at UF=0.757. No significant variation was observed in the temperatures of the top plate.

4.3.2.5. Longitudinal temperature profiles of the transfer fluid within the storage device

Temperature-time profiles for sensors located on the centre line of the storage device are presented in figures 4.9 and 4.10. The exact locations of the sensors T20-T24 are shown in figure 3.4

(i) Charge (TD)

From figure 4.9 it may be deduced that there is an approximately constant temperature gradient throughout the store, with the largest deviations existing in the top at the beginning and the bottom at the end of the discharge period.

(ii) Discharge (BU)

During discharge there is an initially steep temperature gradient in the bottom of the store. The sensors below the middle of the store do not exhibit the characteristic minimum of the outlet temperature profile with time.

4.3.2.6. Variation of charge/discharge rate with UF

(i) Charge

In figure 4.11 it is obvious that a greater charge rate may be attained by operation with the flow top-down rather than bottom-up. Increasing the charge temperature or flow rate was also shown to significantly improve the performance.

(ii) Discharge

Higher discharge rates (see figure 4.12) are achieved by operating the store with the flow entering the bottom of the store. Top-down operation, in addition to decreasing the discharge rate, is incapable of completely discharging the store. Decreasing the discharge temperature or increasing the flow rate is shown to improve the discharge rate. However since the maximum rate of heat removal for the operating temperature range .was achieved at a flow rate of 11.5 lit/min, no observable improvement was

attained by increasing the flow rate to 15 lit/min. Operation with a discharge temperature of 50°C resulted in a totally unsatisfactory performance due to limitations of the test facility.

4.3.2.7. Variation of charge/discharge rate with time

(i) Charge

For a complete charge of the storage device during the off peak period a minimum charge period is desired. Figure 4.14 clearly demonstrates the advantages of a high charge temperature, high flow rates and operation in the top-down mode.

(ii) Discharge

A maximum discharge rate over the entire discharge period represents the optimum operating characteristics of a storage device. Figure 4.15 shows that this can best be achieved by operation at low discharge temperatures, high flow rates and in bottom-up mode. Note that little benefit is observed for increasing flow rate above 11.5 lit/min due to the limited heat removal capability of the test facility.

4.3.2.8. Approximate heat transfer coefficient

The experimental error (± 2%) in determining the rate of heat transfer to/from the prototype store (see section 9.3.1.2) suggested that considerable difficulty in tracking the store condition would be experienced after only a few charge/discharge cycles. Consequently an attempt was made to establish a relationship between an approximate heat transfer coefficient

$$U_{ap} = q/A\Delta T_{LM}, \tag{4.16}$$

and the store condition. The log mean temperature difference, defined in equation (3.12), cannot be calculated from the experimental data as the temperature of the PCM is not known. However if ideal latent heat store performance is assumed then the centre-line temperature of the PCM would remain at its melting point for the duration of the test. Employing this assumption and using only experimental data with an outlet temperature greater (less) than 56 °C for charge (discharge), allowed calculation of the log mean temperature difference. Figures 4.17 and 4.18 show the relationship

between the approximate heat transfer coefficient and store condition for a range of operating conditions. The spread of points in each figure suggests that the assumption above is of limited validity while the difference in shape between the two curves indicates a fundamental difference between the charge and discharge heat transfer characteristics.

4.4. Discussion of Results from Pilot Store

4.4.1. Temperature Profiles Within PCM

When the instrumented 25 mm tube was removed from the storage device the top of the tube felt hollow and it was suspected that the tube had been leaking through the holes drilled for the thermocouple sensors. If this top section had then filled with water the top thermocouple would have responded in a manner very similar to that shown in figures 4.2 and 4.3.

The melting point temperature of the PCM was determined to be 56°C since the sensors in the 38 mm tube appeared to be more consistent. This is 2°C less than the quoted melting point of pure sodium acetate trihydrate but thickening agents are reported in the literature to work towards a lowering of the melting point. The apparent phase change temperature of 58°C exhibited during discharge by the bottom sensor in the 25 mm tube cannot be easily explained, except by faulty sensors in the 25 mm and/or 38 mm tube.

During charge (TD) the middle temperature lags behind that at the bottom of the tube. This was thought to be due to flow being channeled around the edges of the tube bundles (see figure 3.2) resulting in a minimum transfer fluid temperature at the midpoint of the axial flow path.

4.4.2. Thermal Performance of 25 and 38 mm Diameter Tubes in the Pilot Store

In the pilot store data the TSC employed in the calculation of the UF incorrectly omitted the sensible heat capacity of the transfer fluid. This explains why the final UF for a significant number of the runs presented in table 4.1 was greater than one.

If the storage device was completely subcooled then the minimum discharge rate would occur at a UF equivalent to the total removal of sensible heat. This was calculated to be 0.353 and 0.338 using equations (3.3) and (3.4)

for the 25 and 38 mm tubes respectively. Note that the TSC was determined using the sensible heat term in the brackets while the total sensible heat was found from the value which included the sensible heat of the transfer fluid. In section 4.2.1 it was noted that the 25 mm tubes experienced complete subcooling which was confirmed by the position of the discharge rate-UF curve minimum at a UF of 0.351, see figure 4.4(b). The 38 mm tubes showed a minimum in discharge rate at a UF of 0.277, see figure 4.4(b), indicating that only partial subcooling had occured.

A store capable of a charge rate of 5 kW for an inlet temperature of 60°C was specified for the prototype design. The approximate heat transfer coefficient, defined by equation (4.12), required for such a charge performance was 23.2 and 16.5 W/m^2K for a store based on 38 and 25 mm tubes respectively. Hence the equivalent minimum charge rate in the pilot store was 0.46 and 0.51 kW respectively. In figure 4.4(a) it can be observed that the store comprising 38 mm tubes would be unable to meet such a duty for a UF greater than 0.925 whilst the performance of the 25 mm tubes would remain satisfactory until the UF became greater than one. Hence a significant proportion of the extra capacity gained through lower voidage with 38 mm tubes would be effectively lost as it would prove impossible to utilise. Further comparison of 25 and 38 mm tubes is performed on a theoretical basis in section 7.2.

4.5. Discussion of Results from Prototype Store

4.5.1. Heat Loss

4.5.1.1. Operating heat loss

The discrepancy between the heat loss found for top-down and bottom-up operation is difficult to explain. A faulty reading from the thermopile was suspected but when tested in a constant temperature stirred water bath it produced almost exactly zero, 0.00 ± 0.01°C. It is possible that there is a natural convection effect even with the very small temperature drop across the store recorded here.

Comparison of the loss coefficients with that predicted for the store in section 3.1.5.2 indicates a significant discrepancy. This was primarily due to

the assembly of the insulating jacket. It was initially intended to be a four sided cover, similar to a fireguard, with a single section designed to be a tight fit at the front. Difficulties with the adhesive made assembly of such a jacket impractical. Instead the individual sections of the jacket were held in place by wrapping carpet tape around the whole device. Consequently small air gaps were present in the jacket which proved impossible to seal completely.

The heat loss coefficient is almost four times the theoretically predicted value of 0.29 W/m^2K (see section 3.1.5.2), but is significantly less than that found by van Galen (see section 2.2.4.1).

4.5.1.2. Static heat loss

The ten temperatures averaged to determine the mean store temperature included those along the centre-line and at the edges of the store. The recorded profiles showed:

1. A high degree of thermal stratification increasing to a maximum of 16 degC between T32 and T34 (see figure 3.4)
2. Little horizontal variation with T20, T27 and T32 at the top approx. equal within 1 degC and T24, T30 and T34 at the bottom equal within 2 degC

Calculation of a heat loss factor requires that an average temperature for the entire non-insulated surface area be assumed. After steady state has been achieved with the pump running it was reasonable to assume that the average store temperature was simply equal to the arithmetic mean of the inlet and outlet temperatures. Once the pump has been switched off the thermal stratification noted above develops and it is difficult to determine an appropriate mean store temperature. The actual temperatures employed may result in an incorrect value for the mean temperature resulting in a low value for the heat loss factor.

4.5.2. Charge/Discharge Cycle Performance

4.5.2.1. Storage capacities

The discrepancy between the UF_C and UF_D and the expected values of 1 and 0 was probably caused by one or more of the following:

1. Measurement error of temperature or flow rate
2. Incorrect thermophysical properties for transfer fluid and/or the PCM
3. Incorrect calculation of the TSC

While measurement errors were significant (see section 9.3), the storage capacities could not be as consistently low for the standard charge run if this was the primary source of error. Properties for the antifreeze (see section 9.1.2) were taken from data available in the literature for ethylene glycol/water mixtures and hence may not be strictly accurate for the ethylene glycol, water and methanol mixture actually used. The theoretical viscosity and density however, were verified experimentally.

The calculation of the theoretical storage capacity, see table 3.4(b), was thought to be the most likely source of error. In this calculation the determination of the latent heat, which represents 70% of the total, was most suspect. There was a significant discrepancy between the latent heat of pure sodium acetate trihydrate (263 kJ/kg) and that quoted for the stabilised Calortherm 58 (242 kJ/kg) which was employed in the calculations. In addition a constant value of specific heat (2.46 kJ/kgK) was specified by Calor for both the solid and liquid phases while Telkes (1980) reported a lower value for the pure solid (1.97 kJ/kgK) and a higher value for the pure liquid (3.35 kJ/kgK). This data should be confirmed by calorimetric testing of a 200 g sample in the phase change calorimeter.

It was initially thought (during experimental work with the pilot store) that the sensible heat of the transfer fluid contained in the store should not be included in the determination of the TSC. However the method used to calculate the heat transfer from the fluid to the PCM by definition includes the sensible heat of the water. Consider the case if there were no tubes in a storage device of 300 litres capacity and the rate of heat transfer was calculated from

$$q = \dot{m}\, Cp(T_{in}-T_{out}). \qquad (4.17)$$

Then, if plug flow was maintained a quantity of heat equal to the sensible heat of the water would appear to have been transferred to/from the storage device. The rate at which this heat was transferred would be extremely high, with a maximum determined by how rapidly the inlet temperature can increase to its new setpoint.

Charge capacities shown in table 4.4 were found to be approximately 3% larger than discharge capacities. This discrepancy was almost certainly due to the method of controlling the inlet temperature during discharge. If the discharge rate was less than 1.5 kW the pump had to be switched off and the run completed since an accurate low flow rate could not be maintained. It was noted that for the standard charge run (e.g. 9.2) the UF_C corresponding to a charge rate of 1.5 kW was approximately 0.905 which was exactly equivalent to the UF_D for the standard discharge run of 0.095. This inspired a reasonable degree of confidence in the ability of the test facility to measure the store performance.

It was considered possible that the difference between the experimental and expected values could have been due to a small proportion (7%) of the PCM remaining permanently subcooled within the 64-44°C temperature range employed during the tests. Hence some additional tests were performed which yielded values of 0.962 for UF_C during a standard charge cycle and a UF_D of 0.051 for discharge down to 32°C. These results show that decreasing the inlet temperature lowers the storage capacity but cannot be considered significant as the difference is less than the difference recorded (± 0.03) between the original and extra set of data.

4.5.2.2. Thermal effectiveness

Decreasing the flow rate increases the residence time of the transfer fluid in the store and hence allows the transfer fluid outlet temperature to tend towards the PCM temperature near the flow exit. Since the sensible heat contribution above or below the phase change is small (approx. 15%) then this temperature will tend toward the phase change temperature. For extremely low flow rates with their characteristic long residence times and a plug flow effect, it is possible that the store behaviour may approach that of a fully

stratified, sensible heat store.

The improvement in thermal performance gained by decreasing the charge temperature from 66 to 64°C is not further improved by decreasing from 64 to 60°C. The net benefit will be a balance between greater temperature driving force to improve heat transfer and the reduced test period allowed for extracting heat from the store. No significant effect is observed by varying the discharge temperature and this is due to poor control of the discharge temperature during the run. (This resulted from an uncontrollable decrease in the max. cold water flow rate during the discharge period.)

Perhaps the most striking result is the improvement in thermal performance achieved by selection of the best operating mode.

The significance of the assumed phase change temperature cannot be omitted from consideration in these results. If the phase change temperature was exactly in the middle of the operating range (54°C) then the ideal ΔT^* for both charge and discharge would become 0.5. This would lower η_1 for charge and increase it for discharge which makes it extremely difficult to compare charge and discharge performance with any confidence.

4.5.2.3. Temperature time variation of transfer fluid

An instantaneous step change could be achieved by increasing the heat input and removal rate by the test facility, or alternatively employing two buffer tanks, one at the initial steady state temperature and the other at the selected charge/discharge temperature. Since the test facility was designed for developing an integrated system with a max. supply or demand of 7.5 kW and the ASHRAE tests were considered to be of limited importance, neither of the above alternatives were implemented. It should be noted that lower flow rates, lower charge and higher discharge temperatures all result in more rapid step changes and this may affect the analysis of results.

Subcooling was thought to be responsible for the discharge inlet temperature profile hump (minimum followed by a maximum) in comparison to the asymtotic approach to the setpoint exhibited during charge. During the subcooling stage the control system reaches the desired set point temperature employing the maximum permissable cold water flow rate. As the stored latent

heat is released, the discharge rate increases and the maximum cooling water flow rate limits the heat removal rate of the test facility so the inlet temperature rises. This maximum in the discharge inlet temperature profile is further increased if the cold water flow rate cannot reach its normal maximum.

4.5.2.4. Temperature time profiles of the transfer fluid temperature within the storage device

The limited accuracy of the thermocouples could possibly have been improved by individual calibration and addition of the appropriate constant in the software. This was considered, but it would have limited the flexibility of selecting any thermocouple for any input channel on the thermocouple amplifier.

The minimum described by T29 occurs whilst the average bottom plate temperature is itself changing rapidly. Hence this minimum may signify nothing more than the slow response time of this particular sensor. It is significant that the large temperature variation during discharge occurs at UF = 0.757, the minimum point on the rate against UF curve. It is therefore thought that the subcooling phenomenon was responsible, a hypothesis further supported by evidence that it only occured at the inlet.

4.5.2.5. Variation of the charge/discharge rate with UF

At the extremely low Reynolds numbers used in the store there appears to be significant natural convection effects. These were observed in figure 4.11, where the charge rate is dramatically improved by operating the store in top-down mode. A crucial characteristic in this plot is the decrease in rate at high UF. The steep gradient implies that it is possible to charge the store at a high rate even as it approaches a completely charged condition. Hence the ideal shape of this charge rate-UF curve would be a constant rate (horizontal line) at the maximum heat pump output (7.5 kW) until fully charged (UF=1).

Increasing the charge temperature from 60°C to 66°C is shown to improve the charge rate. However the heat pump COP has been shown to decrease significantly as the circulating temperature increases (see figure 1.2) and a compromise of 63°C was selected.

For similar condensing temperatures (and thus similar COP) it is possible

to increase the circulating water temperature by decreasing the flow rate, as this allows heat removal from the superheated refrigerant. However, since the store outlet temperature is limited by the store condition, an improved charge rate is attained by increasing the flow rate.

The discharge profiles in general have larger variations from the ideal (constant discharge rate) curves. They all exhibit a minimum at a UF of 0.75 ±0.03 (see figure 4.13). This was due to a partial subcooling effect whereby a significant proportion of the sensible heat was transferred before phase change was initiated (see section 4.4.2).

Again it is shown that natural convection effects are significant; and discharging top-down (against the natural buoyancy) results in a very much poorer performance. A discharge temperature of 50°C is not low enough to discharge the store completely at the standard flow rate of 11.5 lit/min. However, although the actual circulating water return (discharge) temperature affects the heating system performance, it was not so critical as the charge temperature, and 44°C was selected for normal operation.

The standard discharge rate is higher than the standard charge rate because of the difference in temperature driving forces, 12 degC in the former case and only 8 degC in the latter.

4.5.2.6. Variation of charge/discharge rate with time

Analysis of the charge rate against time shows that if the store has to be charged fully with off-peak electricity which is available for 7.5 hours, then the flow rate must not be less than 11.5 lit/min, the charge temperature not less than 64°C and the store must be operated in top-down mode.

4.5.2.7. Approximate heat transfer coefficient

The experimental UF values presented in figures 4.17 and 4.18 were scaled by a factor of 1/0.93 (so that a charge/discharge rate of zero corresponded to a UF of 1 and 0 respectively) to allow comparison with model data. Figure 4.17 shows that during charge the approximate heat transfer coefficient drops rapidly for all runs as the UF approaches unity. However a significant variation in the rate of this linear decrease (-70 to -150 W/m^2K) would prevent this being employed as a reliable method for determining the exact store condition

from performance data.

During discharge the approximate heat transfer coefficient exhibits a minimum for UF of 0.7 and then decreases slowly for $0.1<UF<0.6$ before decreasing more rapidly (50 to 100 W/m^2K) to zero for $0<UF<0.1$.

It was shown dramatically in the pilot storage device that the centre-line temperature does not remain constant at the melting point temperature and this assumption may be more or less valid for different operating flow rates and charge/discharge inlet temperatures. Hence the limitations of the above assumption and the practical difficulties of installing thermocouples in the PCM tubes do not recommend the approximate heat transfer coefficient as a method of determining the store condition.

4.6. Conclusions

1. Neither ASHRAE Standard 94-77 or 94.2-81 provided completely suitable test procedures for evaluating the performance of the Edinburgh store. Since the former was widely recognised as a standard test procedure it was adopted into the experimental program with the following modifications:

   1. Heat loss test should be performed at typical operating temperatures and flow rates
   2. Mass flow rate and test time should be typical of those employed in actual system operation i.e. 7-12 lit/min and 7-17 hours
   3. Equation (4.11) which includes the effect of heat loss should be used to calculate the discharge capacity instead of (4.6)
   4. Inlet step temperature change should be achieved with a maximum heat transfer rate determined from intended application

2. Phase change temperature was found to be 56°C.

3. Partial and complete subcooling was experienced in the 25 and 38 mm tubes respectively.

4. From pilot store data it was predicted that a prototype store utilising 25 mm tubes could be charged at 5 kW with a charge temperature of 60°C even as UF approached one, whilst utilising 38 mm tubes limited the maximum UF

to less than 0.925.

5. Operating heat loss coefficient for prototype store was found to be 1.153 W/m^2K, almost four times the theoretically predicted value.

6. Test facility produced reproducible experimental conditions and results.

7. Store cannot be fully utilised if charge temperature less than 62°C or discharge temperature greater than 46°C.

8. Thermal effectiveness of storage device was improved by charging with flow top-down and discharging bottom-up, and by employing low flow rates (8 lit/min).

9. No evidence of flow channeling was detected in prototype store.

10. Maximum charge rates were achieved with flow top-down, high charge temperatures and large flow rates (15 lit/min).

11. Maximum discharge rates were achieved with flow bottom-up, low discharge temperatures and large flow rates (11.5 lit/min)

12. Experimental storage capacities were found to be lower than TSC; it was thought most probable that this error was caused by using too large a value for the phase-stabilised PCM's latent and specific heats.

13. Attempts to determine a relationship between an approximate heat transfer coefficient and store condition were thwarted by experimental errors and assumptions about the temperature of the PCM during the test.

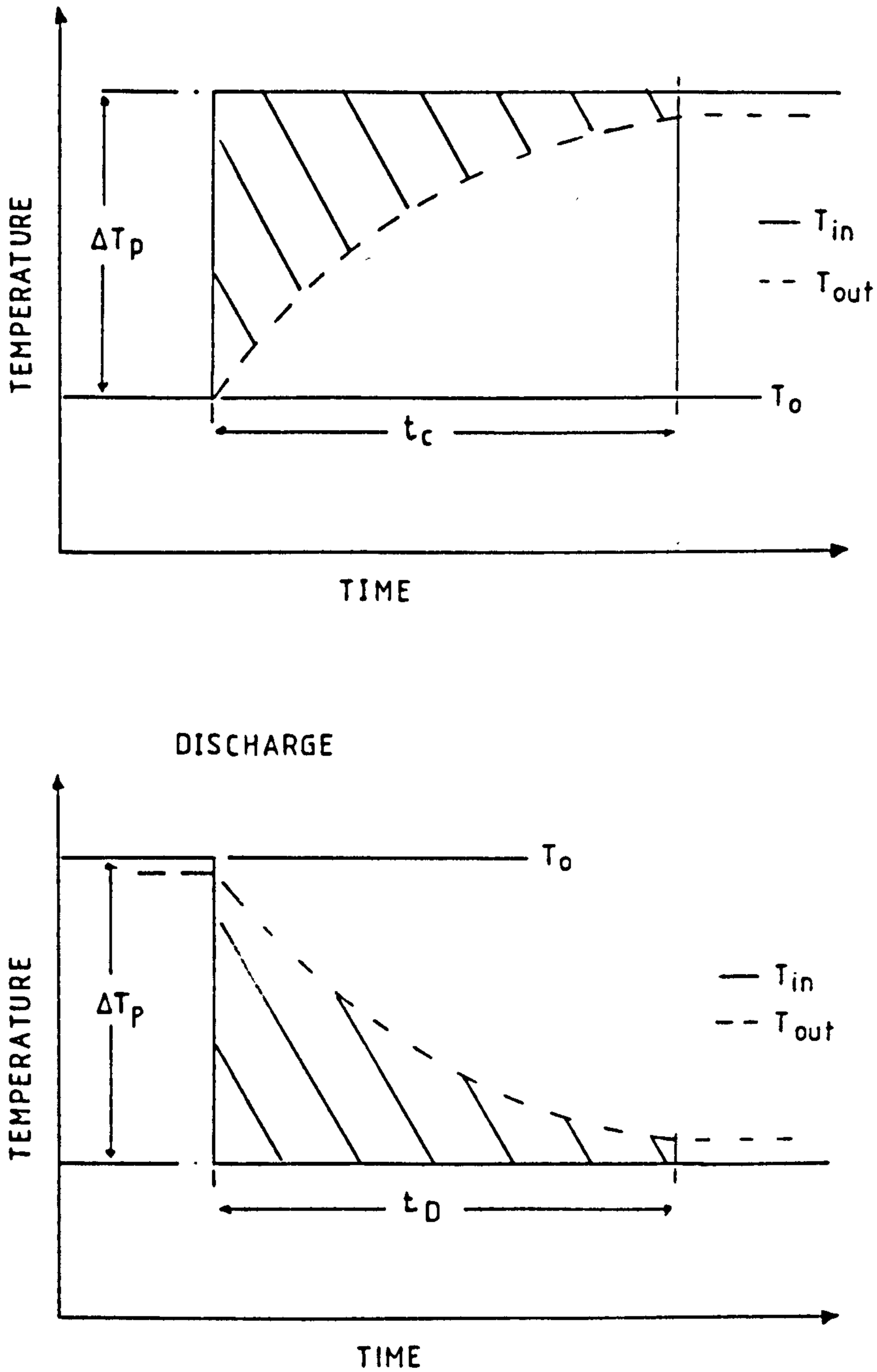

Figure 4.1 Predicted temperature time variation of transfer fluid in sensible heat storage device

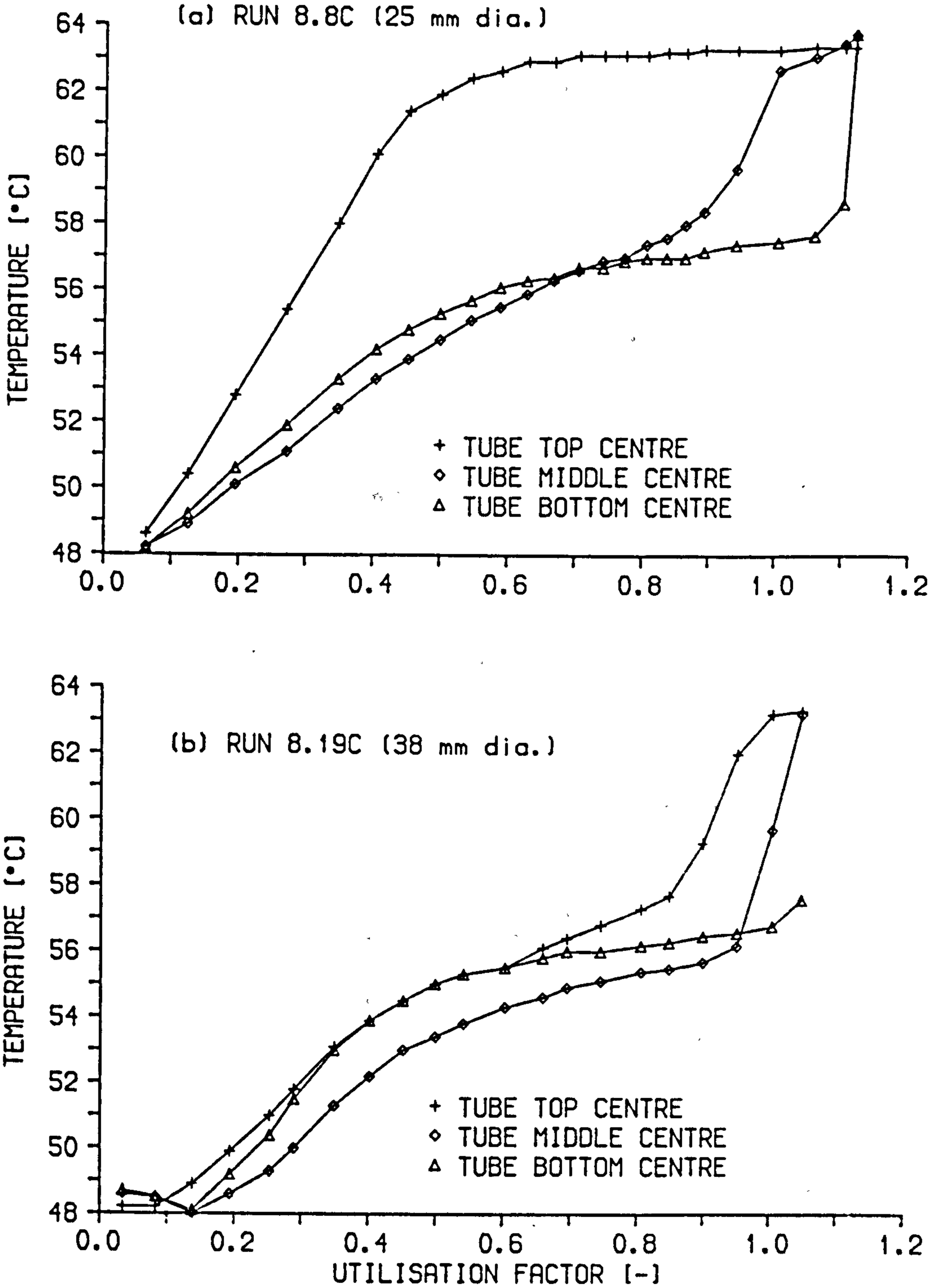

Figure 4.2 Internal temperature profiles of PCM during charge in pilot store

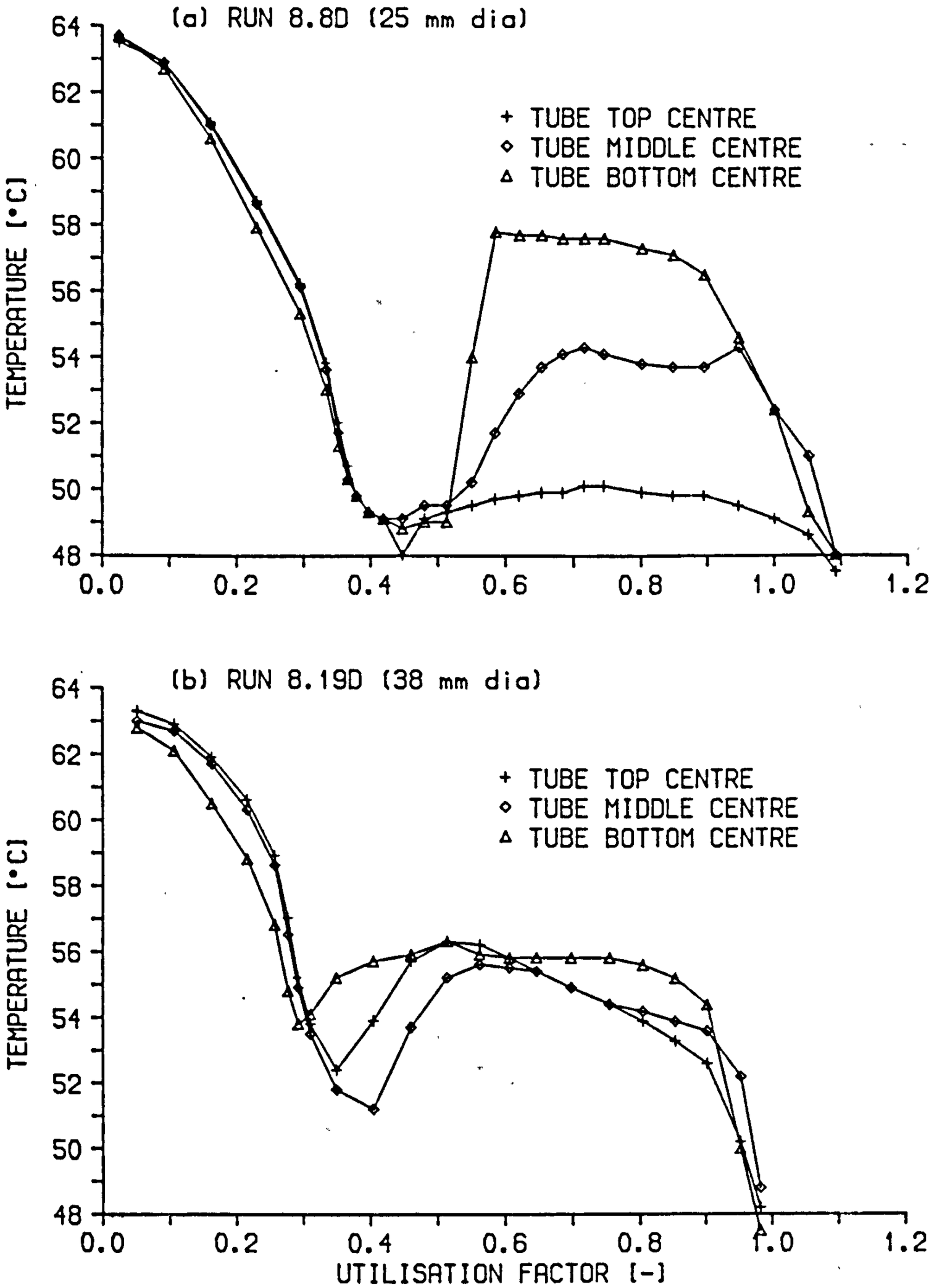

Figure 4.3 Internal temperature profiles of PCM during discharge in pilot store

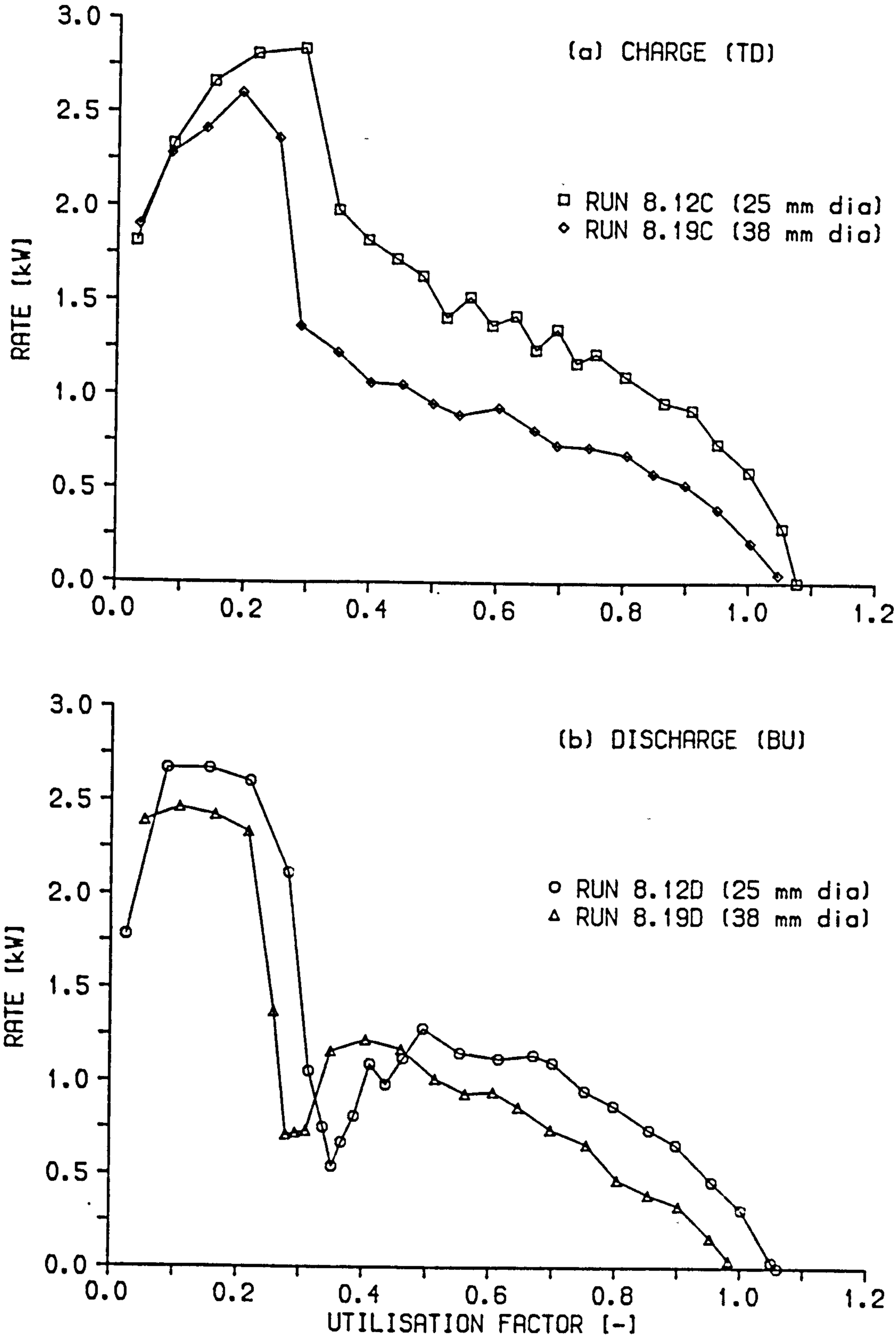

Figure 4.4 Charge/discharge rate against UF for pilot store

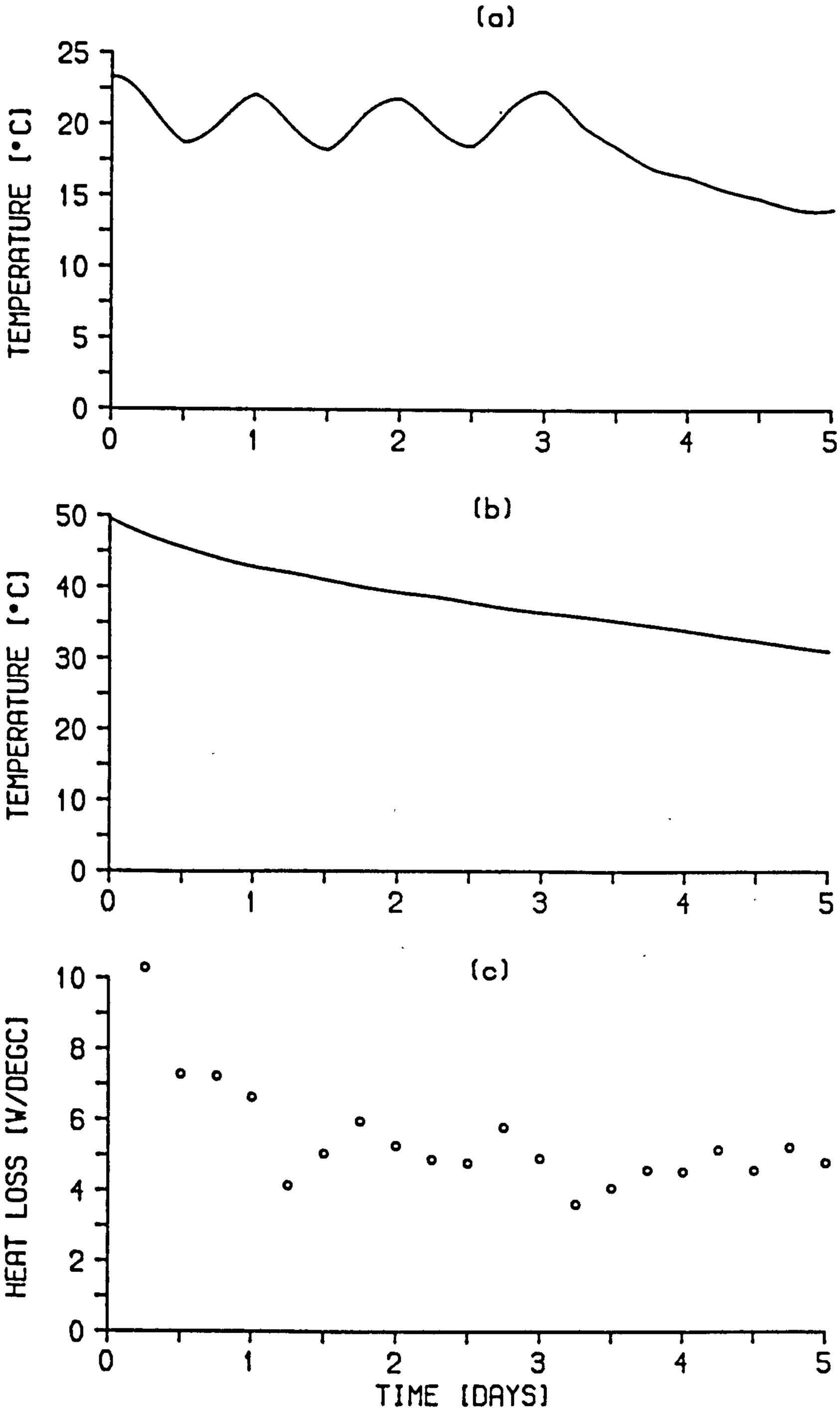

Figure 4.5 Heat loss characteristics of prototype store; (a) ambient temperature, (b) average store temperature and (c) heat loss factor

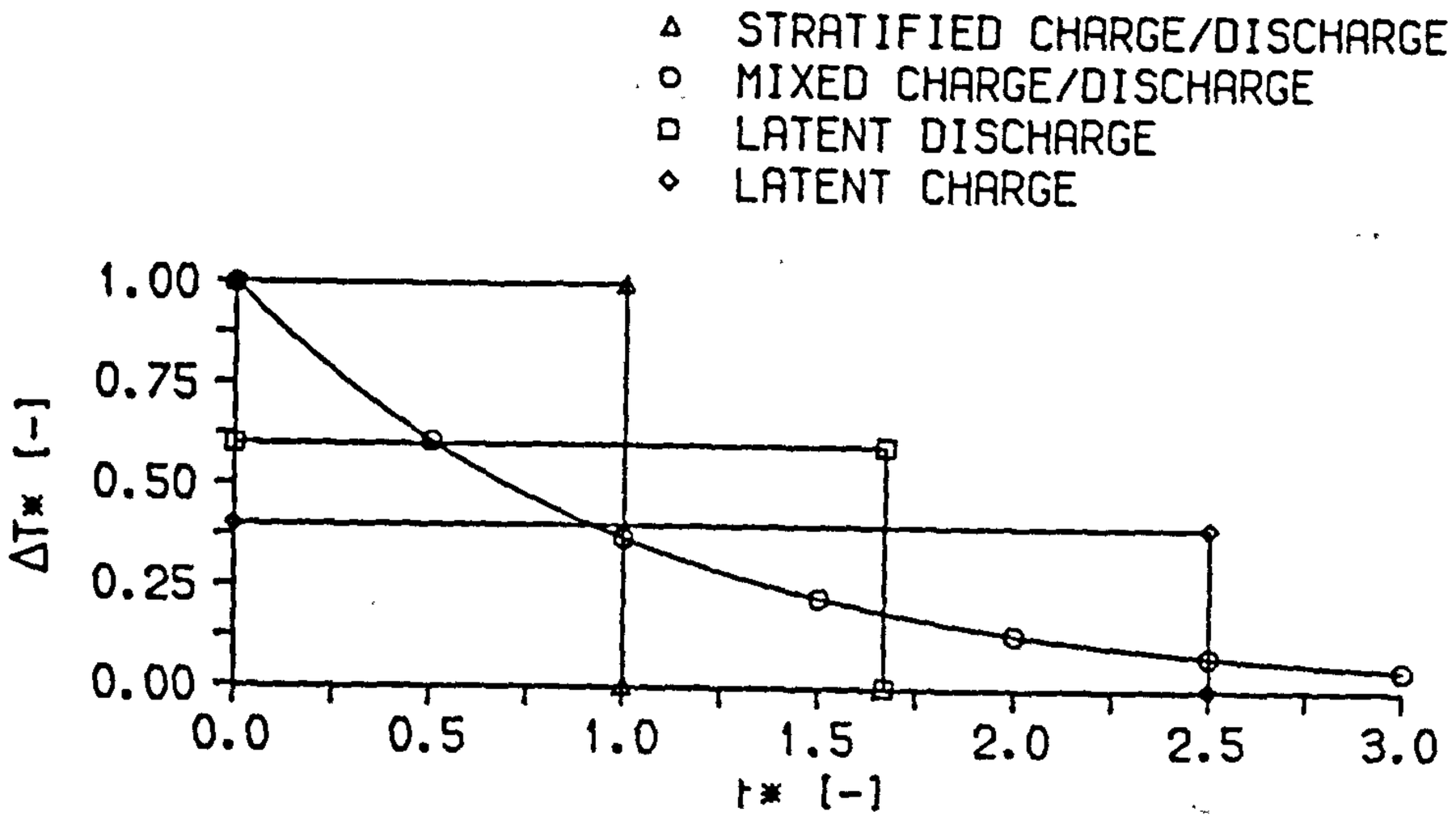

Figure 4.6 Dimensionless temperature difference against dimensionless time for ideal storage devices

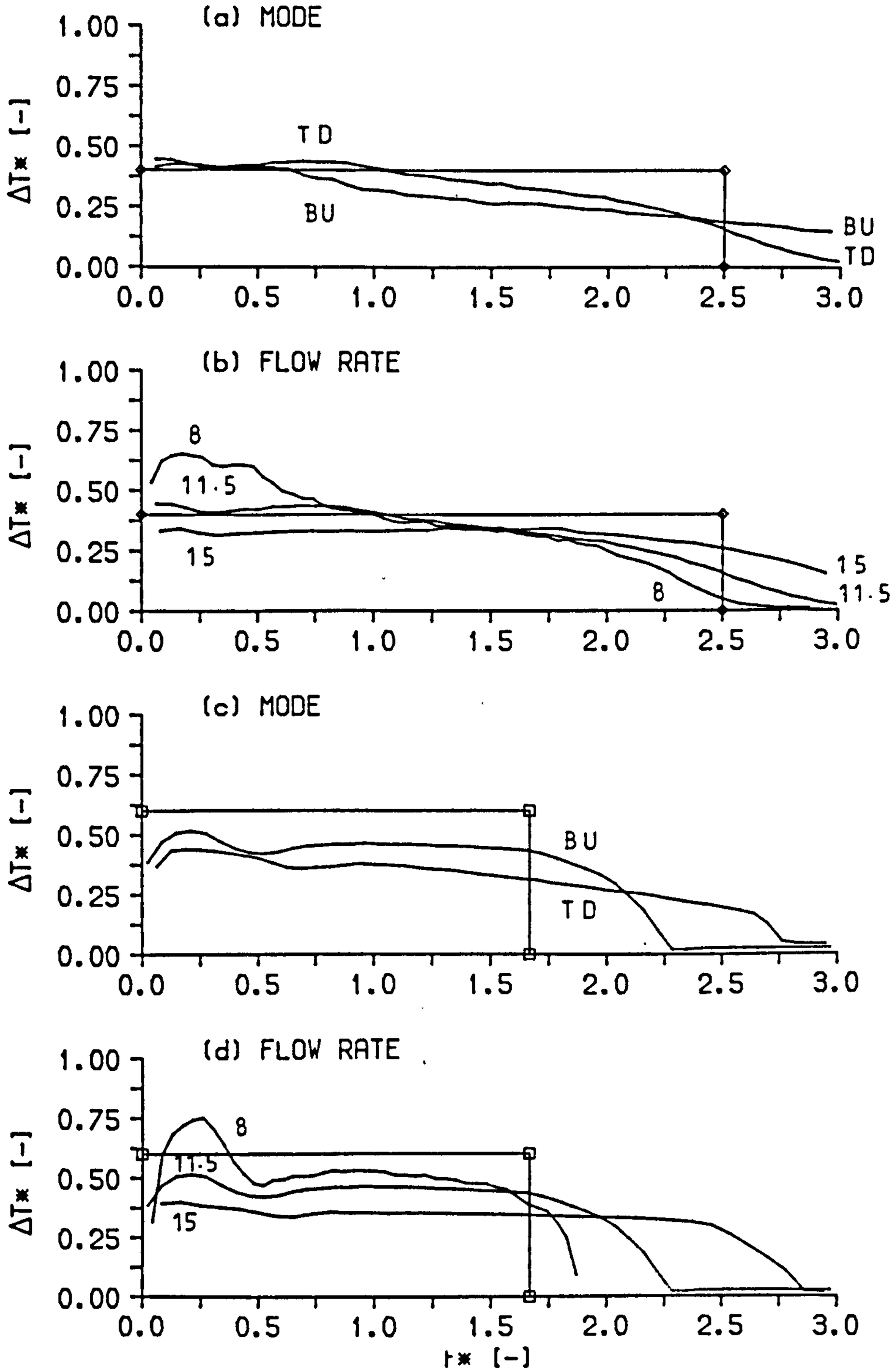

Figure 4.7 ΔT^* against t^* in prototype store during charge (a,b) and discharge (c,d)

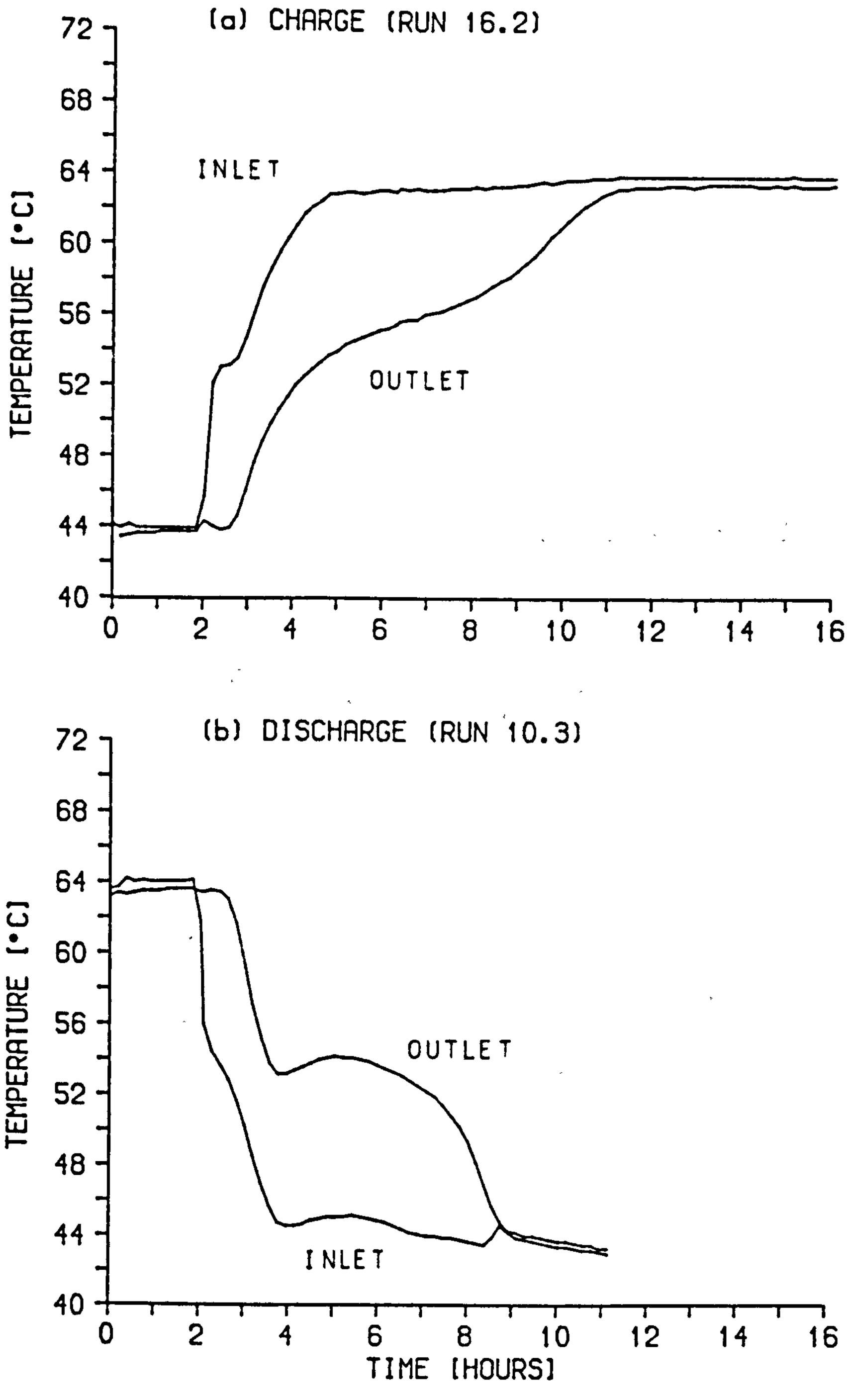

Figure 4.8 Temperature time variation of transfer fluid during charge and discharge of prototype store

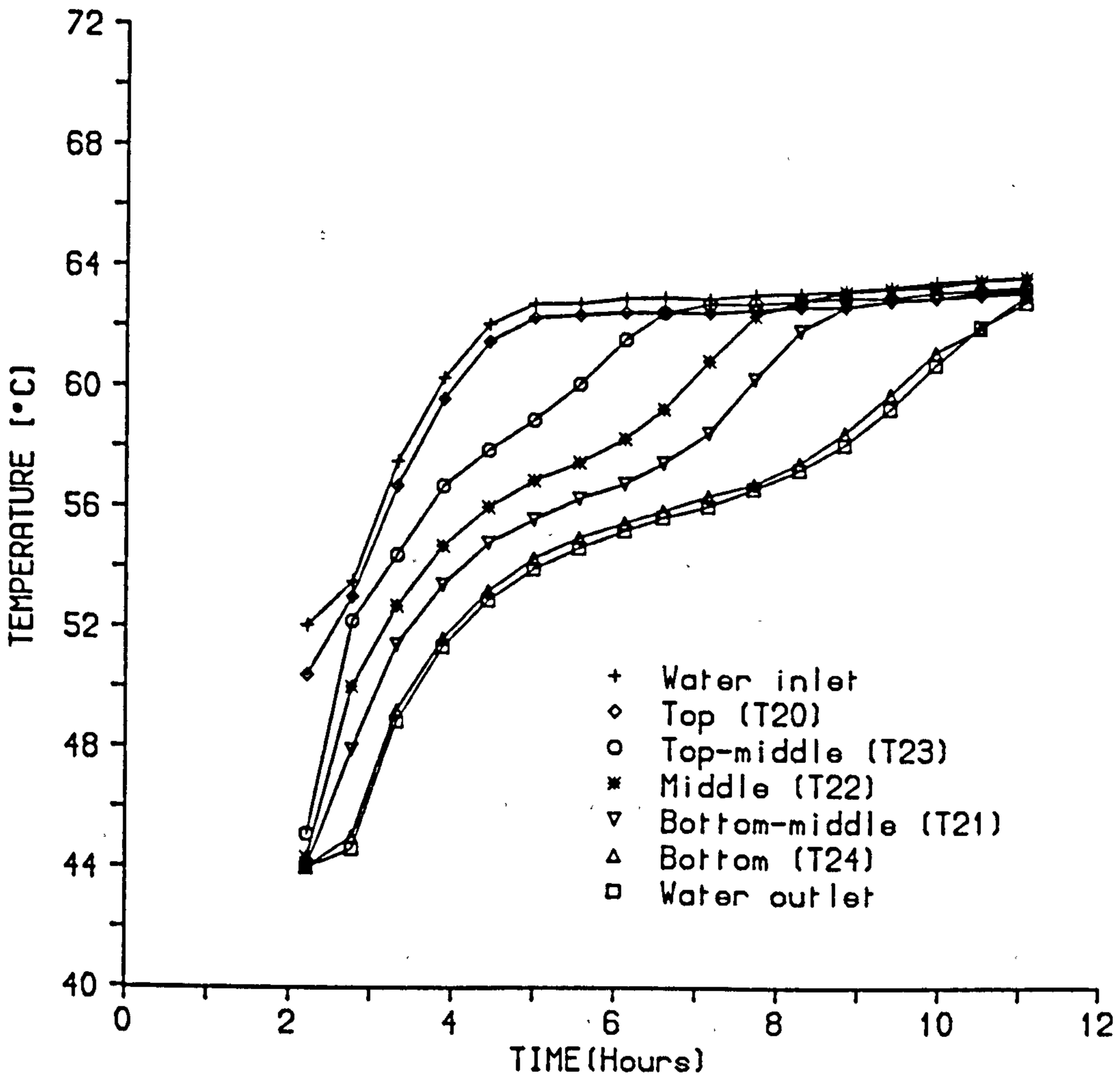

Figure 4.9 Temperature profiles of transfer fluid during charge in prototype store

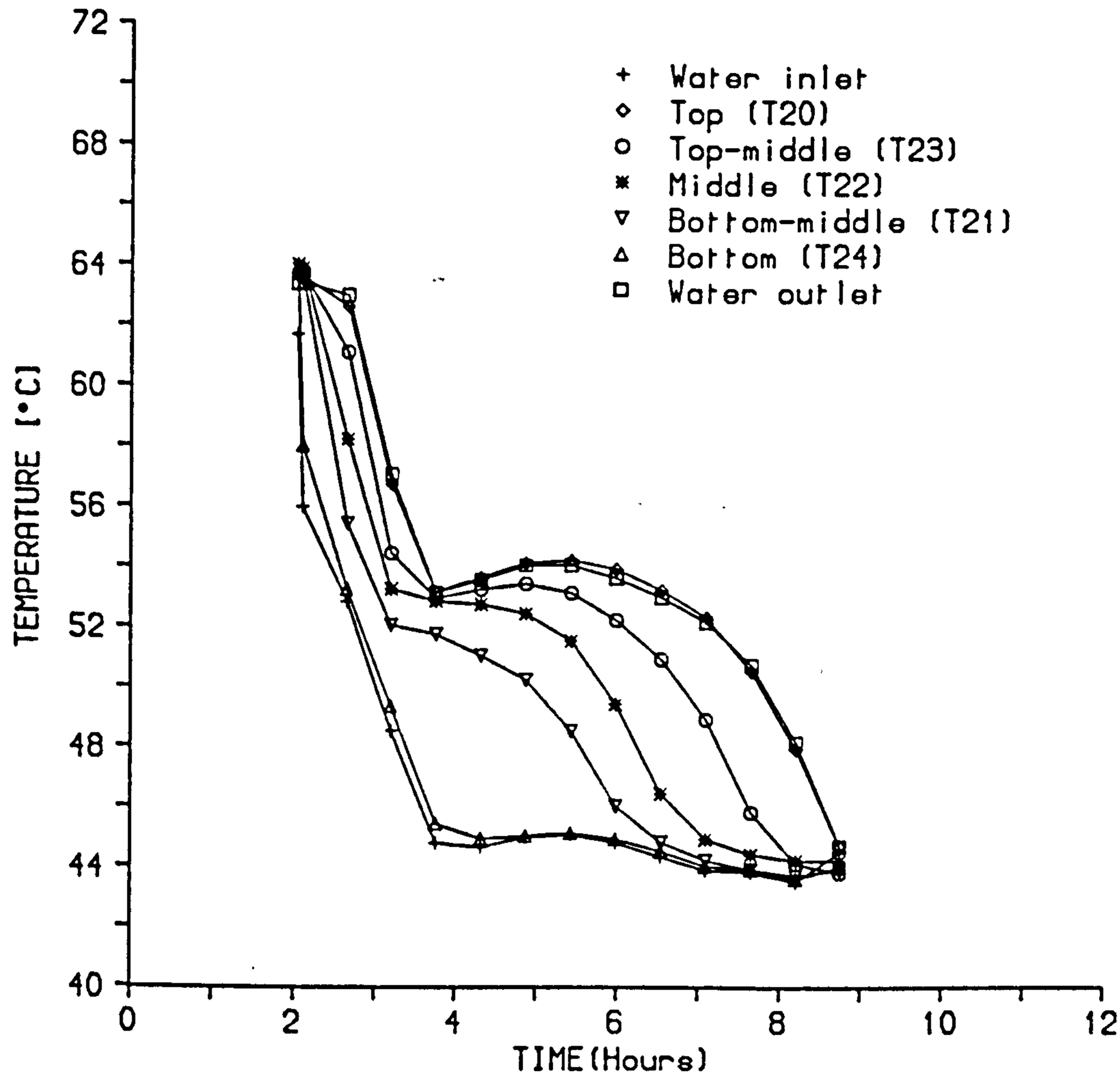

Figure 4.10 Temperature profiles of transfer fluid during discharge in prototype store

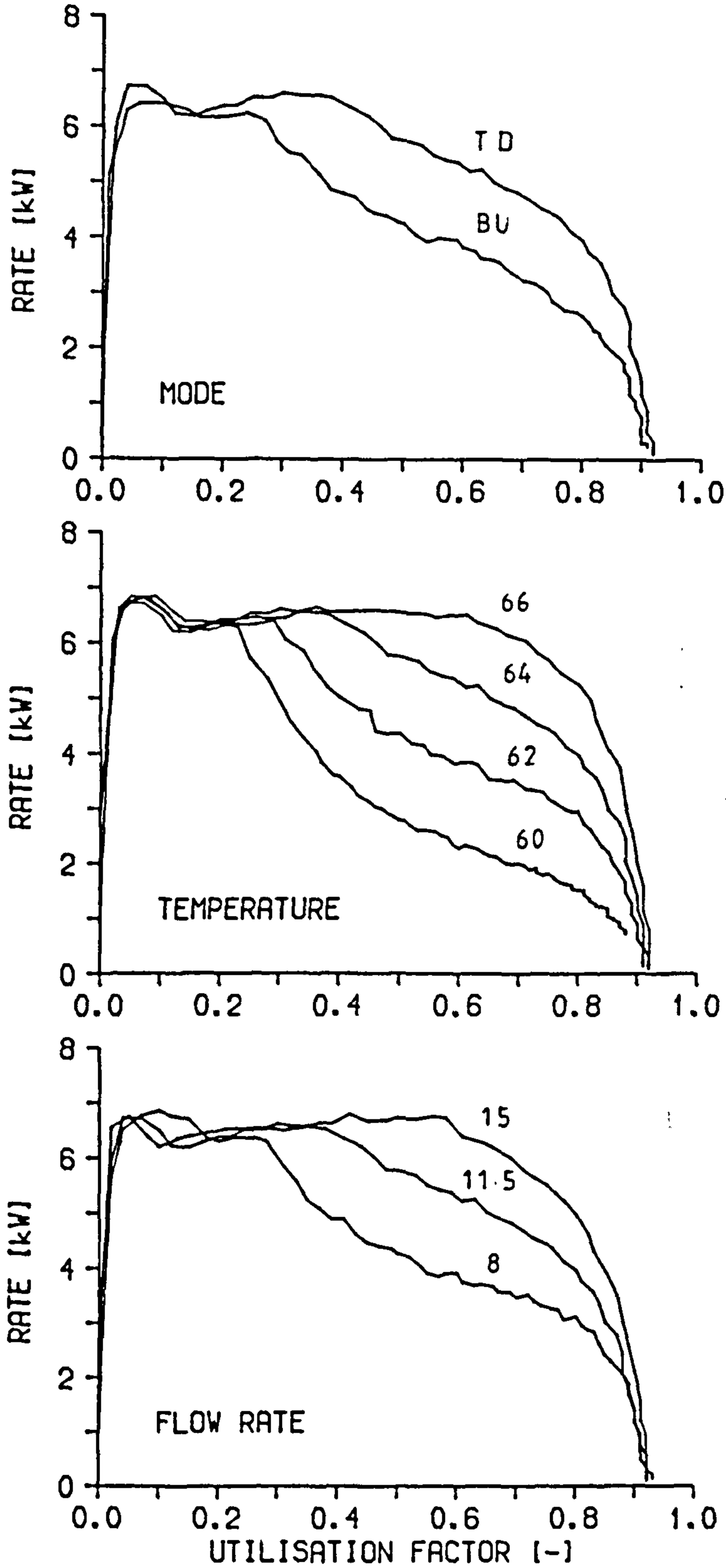

Figure 4.11 Charge rate against UF for prototype store

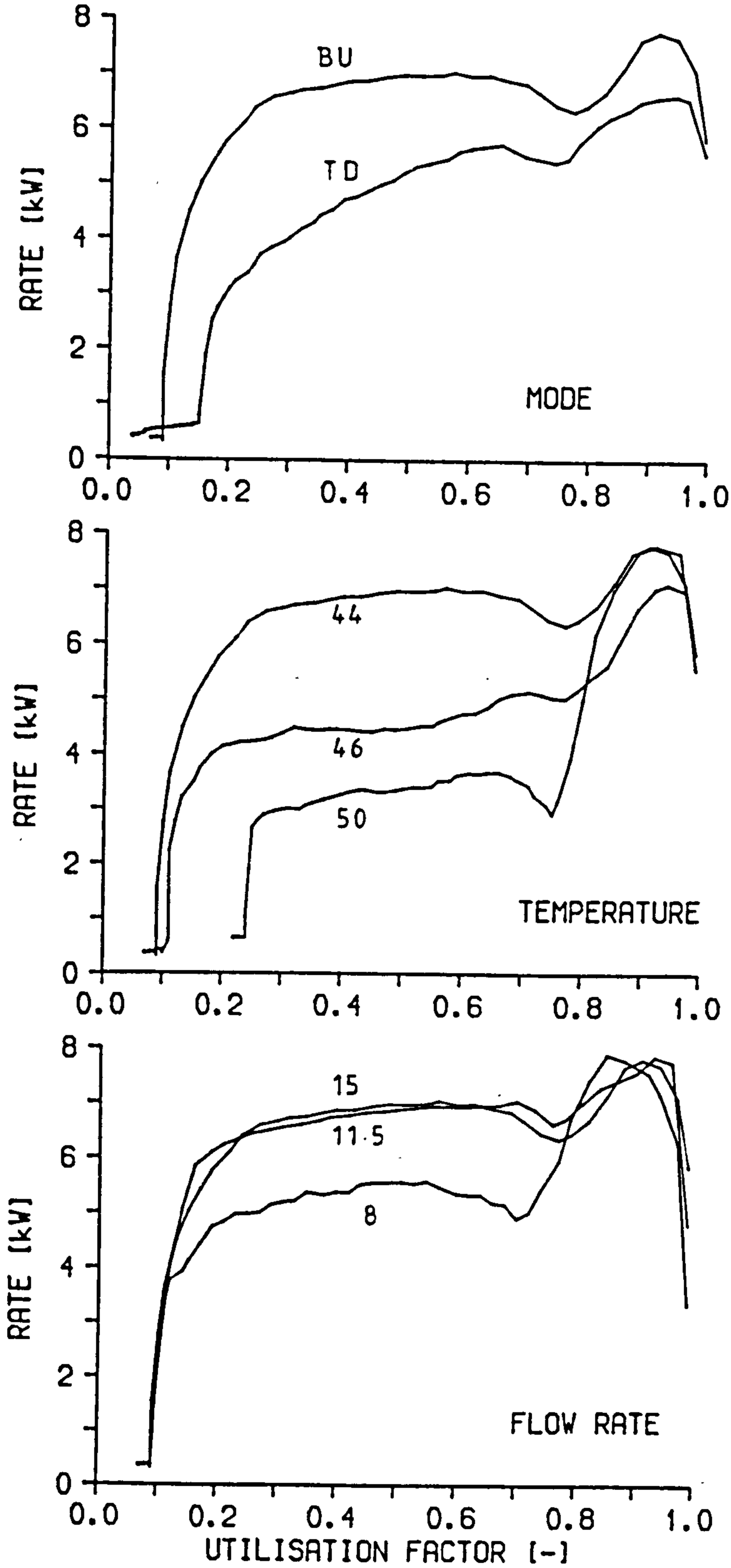

Figure 4.12 Discharge rate against UF for prototype store

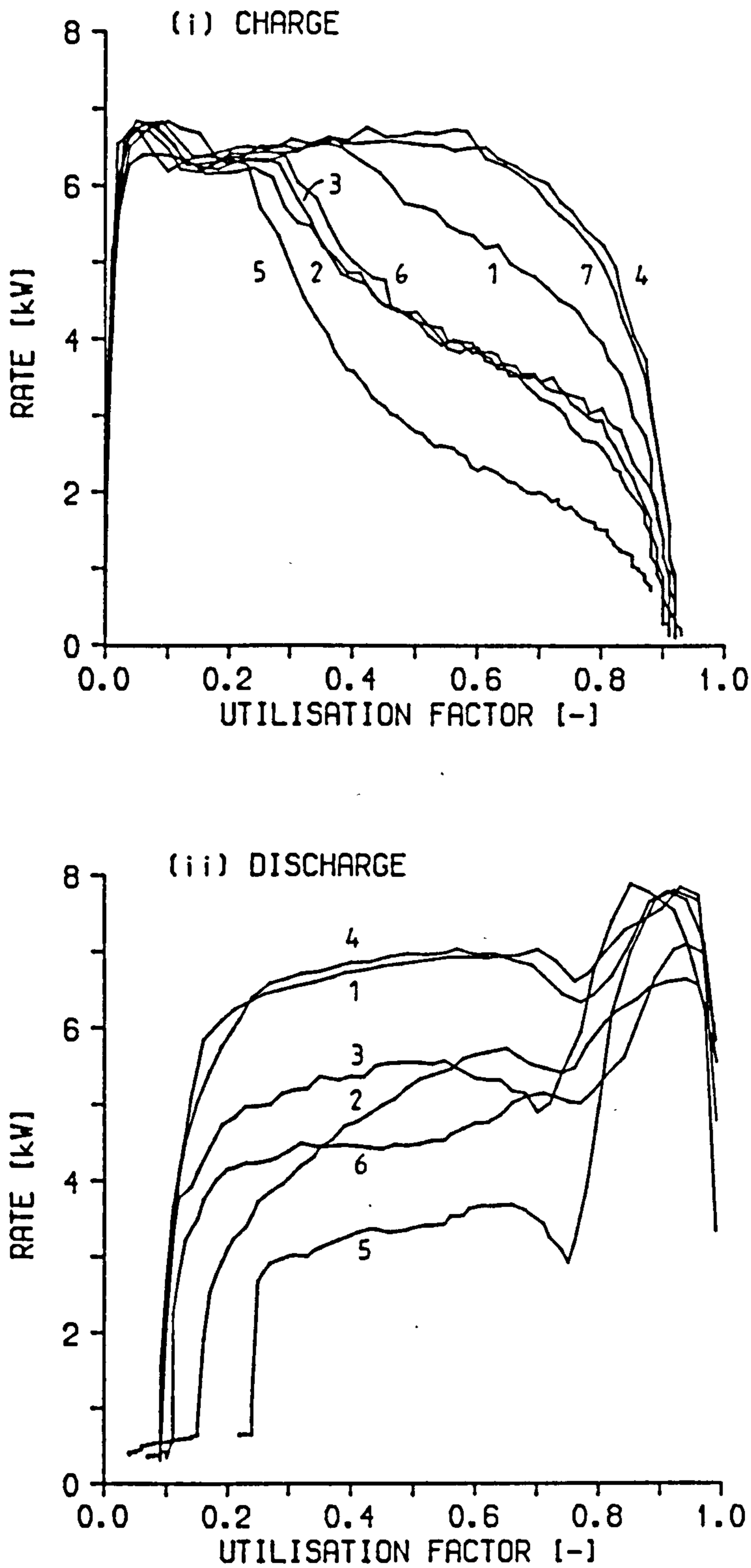

Figure 4.13 Charge/discharge rate against UF for prototype store

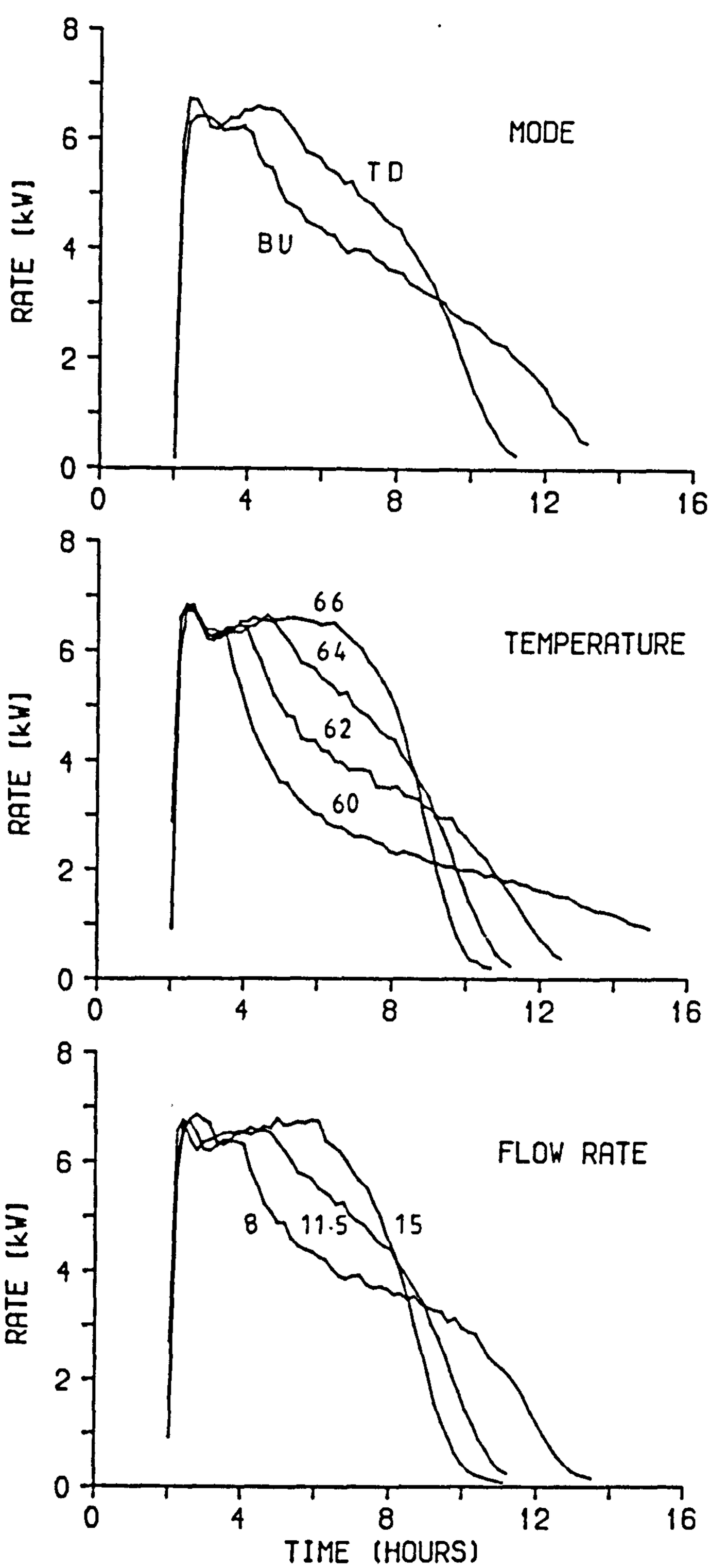

Figure 4.14 Charge rate against time for prototype store

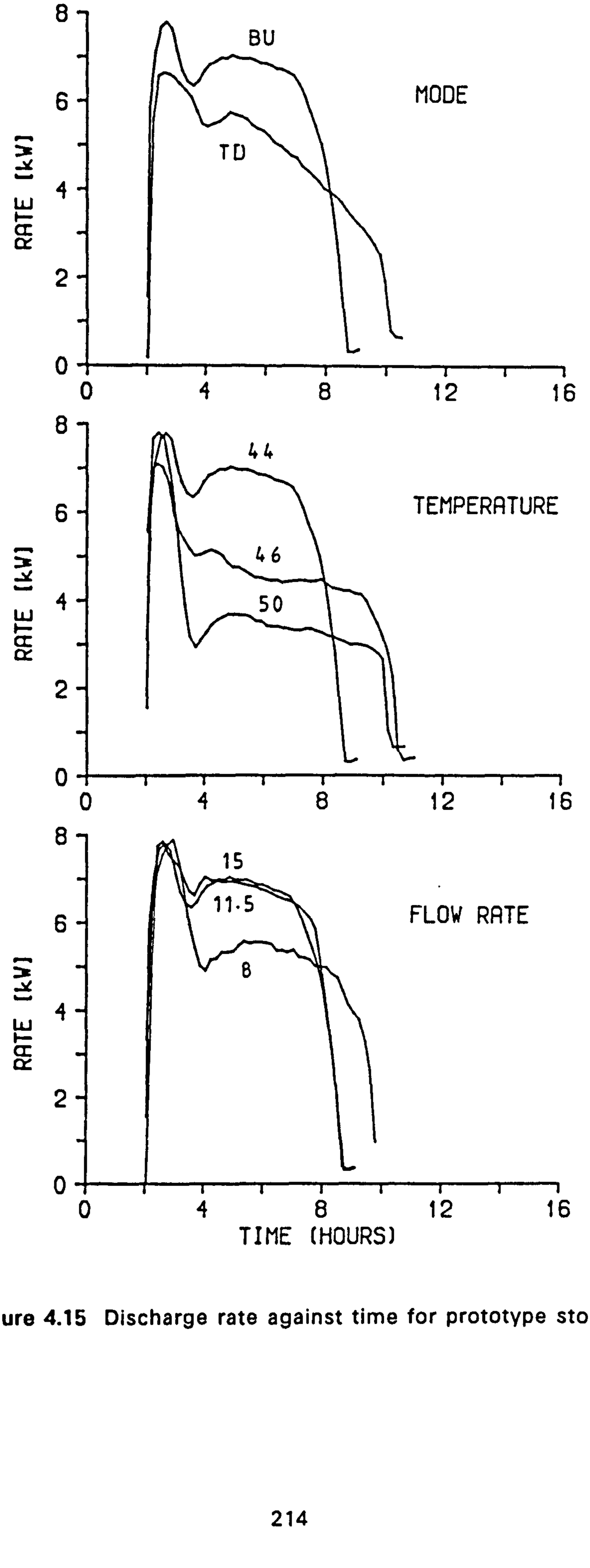

Figure 4.15 Discharge rate against time for prototype store

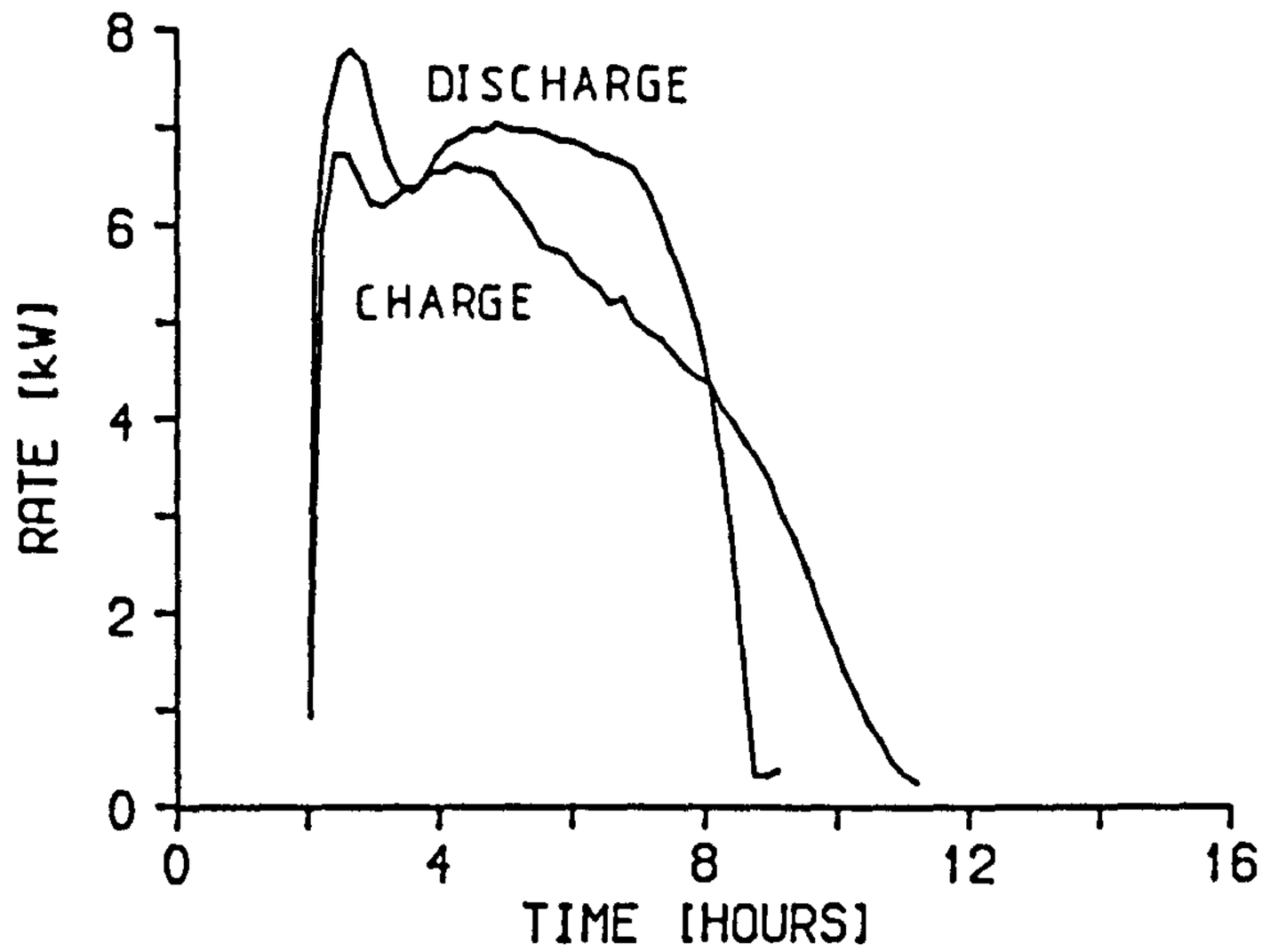

Figure 4.16 Charge/discharge rate against time for prototype store

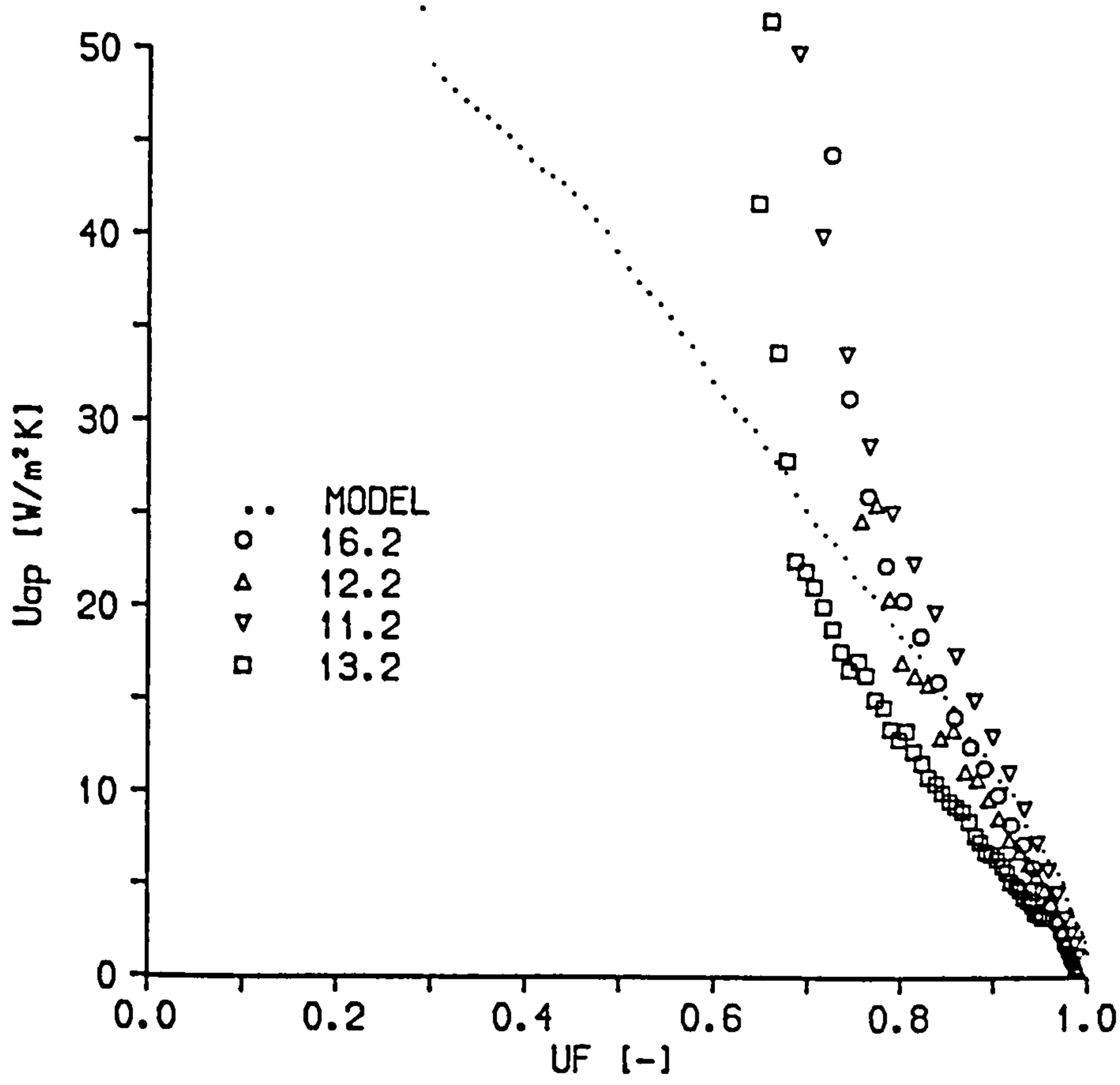

Figure 4.17 Plot of approximate heat transfer coefficient against UF for experimental and model data during charge

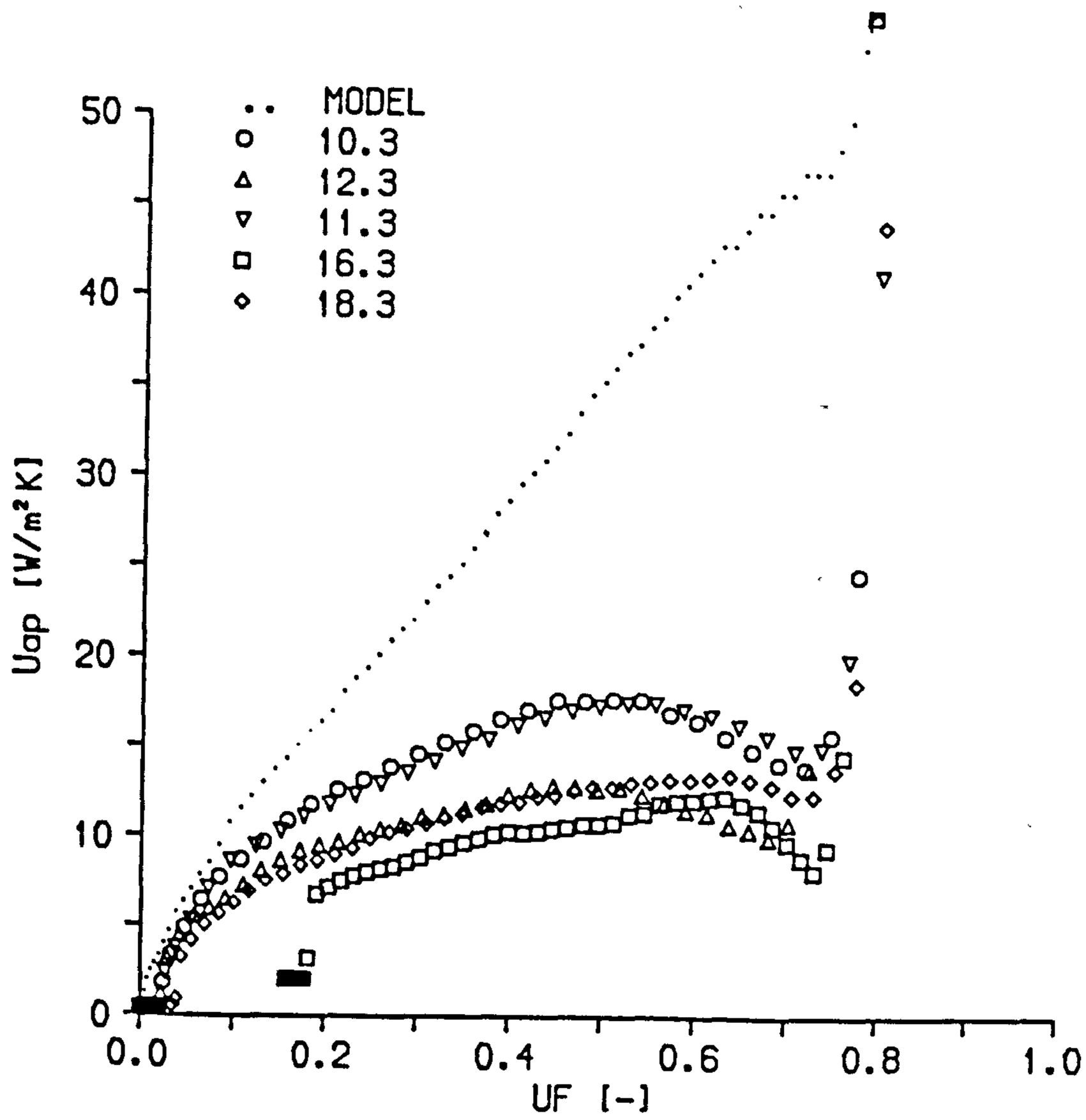

Figure 4.18 Plot of approximate heat transfer coefficient against UF for experimental and model data during discharge

Table 4.1 Experimental results from pilot store

RUN	TUBE [mm]	$\dot{m}$ [kg/s]	T_o [°C]	T_{in} [°]	MODE	UF [-]
8.8C	25	0.192	48	64	TD	1.117
8.19C	38	0.117	48	64	TD	1.047
8.12C	25	0.117	48	64	TD	1.077
8.25C	38	0.117	48	64	BU	1.013
8.16C	25	0.117	48	64	BU	1.080
8.23C	38	0.117	48	66	TD	1.065
8.26C	38	0.192	48	64	TD	1.086
8.8D	25	0.192	64	48	BU	1.093
8.19D	38	0.117	64	48	BU	0.982
8.12D	25	0.117	64	48	BU	1.053
8.24D	38	0.117	64	48	TD	0.982
8.15D	25	0.117	64	48	TD	1.025

Note

In pilot store data the initial UF in any run is zero

Table 4.2 Heat Loss from Prototype Store

Time [hour]	Top-down [W]	Bottom-up [W]
0.0	200	150
0.1	210	220
0.2	210	170
0.3	210	200
0.4	140	120
0.5	180	170
0.6	150	180
0.7	200	150
0.8	140	160
0.9	200	80
1.0	170	120
1.1	160	190
1.2	170	160
1.3	260	180
1.4	180	130
1.5	190	220
1.6	160	160
1.7	220	180
1.8	210	180
1.9	180	170
2.0	260	120
mean	190.5	162.4
average	175	

Table 4.3 Static Heat Loss from Prototype Store

Time [hour]	T_{ave} [°C]	T_a [°C]	L [W/degC]
0	49.6	23.3	-
6	47.3	21.5	10.30
12	45.6	18.7	7.30
18	44.1	20.2	7.25
24	42.9	22.1	6.65
30	42.1	19.8	4.15
36	41.1	18.2	5.05
42	40.1	20.7	5.96
48	39.3	21.8	5.26
54	38.7	19.7	4.87
60	37.9	18.5	4.77
66	37.1	21.1	5.78
72	36.5	22.4	4.91
78	36.0	20.0	3.61
84	35.4	18.4	4.07
90	34.7	16.9	4.55
96	34.0	16.3	4.59
102	33.2	15.4	5.18
108	32.5	14.8	4.59
114	31.7	14.1	5.24
120	31.0	14.1	4.79

Note

$L = (2.495\Delta T_{ave})/(6*3600) = 115.5\ \Delta T_{ave}$

Table 4.4 Experimental Results from Prototype Store

No	RUN	$\dot{m}$ [kg/s]	T_o [°C]	T_{in} [°C]	MODE [-]	UF [-]	η_s [-]	η_l [-]
1*	16.2	0.192	44	64	TD	0.925	0.429	0.883
2	21.2	0.192	44	64	BU	0.911	0.394	0.766
3	12.2	0.133	44	64	TD	0.924	0.534	0.935
4	11.2	0.250	44	64	TD	0.929	0.350	0.817
5	13.2	0.192	44	60	TD	0.885	0.438	0.894
6	14.2	0.192	44	62	TD	0.921	0.455	0.892
7	15.2	0.192	44	66	TD	0.929	0.394	0.852
8	26.2	0.250	44	62	TD	0.900	0.385	0.847
9*	7.2	0.192	44	64	TD	0.934	0.422	0.892
10*	9.2	0.192	44	64	TD	0.928	0.434	0.894
11*	22.2	0.192	44	64	TD	0.918	0.435	0.896
12*	23.2	0.192	44	64	TD	0.922	0.423	0.887
1*	10.3	0.192	64	44	BU	0.092	0.473	0.782
2	19.3	0.192	64	44	TD	0.152	0.396	0.633
3	12.3	0.133	64	44	BU	0.097	0.561	0.890
4	11.3	0.250	64	44	BU	0.095	0.387	0.614
5	16.3	0.192	64	50	BU	0.239	0.439	0.790
6	18.3	0.192	64	46	BU	0.111	0.424	0.672
7*	7.3	0.192	64	44	BU	0.102	0.437	0.774
8*	22.3	0.192	64	44	BU	0.104	0.419	0.725
9*	23.3	0.192	64	44	BU	0.103	0.417	0.727

Table 4.5 Transverse Temperature Profiles during Standard Charge in Prototype Store

(a) Top Plate (Run 22.2)

UF [-]	T25 [°C]	T26 [°C]	T27 [°C]	T31 [°C]	T32 [°C]
0.000	43.8	44.1	44.4	44.0	44.1
0.001	44.6	44.9	45.1	44.5	44.7
0.073	53.0	53.3	53.6	53.2	53.4
0.152	55.6	55.6	56.1	55.6	55.8
0.229	58.7	59.0	59.3	58.8	59.0
0.289	60.4	60.6	60.9	60.3	60.6
0.367	61.8	62.1	62.3	61.8	62.1
0.444	62.3	62.6	62.9	62.4	62.6
0.515	62.4	62.7	62.9	62.5	62.7
0.583	62.5	62.8	63.1	62.7	62.9
0.647	62.5	62.8	63.1	62.7	62.9
0.706	62.6	62.9	63.1	62.8	62.9
0.762	62.7	63.0	63.2	62.9	63.0
0.812	62.7	63.0	63.2	62.9	63.0
0.853	62.8	63.1	63.3	63.0	63.1
0.884	63.0	63.3	63.5	63.2	63.3
0.901	63.1	63.4	63.7	63.3	63.4
0.908	63.2	63.5	63.7	63.4	63.6

(b) Bottom Plate (Run 23.2)

UF [-]	T28 [°C]	T29 [°C]	T30 [°C]	T33 [°C]	T34 [°C]
0.000	43.5	43.8	43.9	43.6	43.4
0.005	43.6	43.8	44.0	43.7	43.4
0.080	44.0	44.0	44.3	44.4	43.7
0.156	48.0	47.5	48.2	48.6	47.5
0.232	50.7	50.5	51.0	51.2	50.3
0.310	52.4	52.4	52.7	52.9	52.0
0.387	53.6	53.6	53.8	54.0	53.2
0.440	54.2	54.2	54.4	54.5	53.8
0.511	54.8	54.8	55.0	55.2	54.4
0.578	55.2	55.3	55.5	55.6	54.9
0.642	55.7	55.8	56.0	56.1	55.3
0.702	56.2	56.2	56.4	56.6	55.8
0.757	56.7	56.7	56.9	57.2	56.3
0.808	57.4	57.4	57.7	58.0	57.0
0.851	58.6	58.4	59.0	59.4	58.0
0.884	60.2	59.9	60.7	61.1	59.3
0.903	61.7	61.5	62.2	62.5	60.9
0.912	62.7	62.7	63.2	62.9	62.0
0.922	63.2	63.3	63.5	63.2	63.0

Table 4.6 Transverse Temperature Profiles during Standard Discharge in Prototype Store

(a) Top Plate (Run 22.3)

UF	T25	T26	T27	T31	T32
[-]	[°C]	[°C]	[°C]	[°C]	[°C]
1.000	63.4	63.7	64.0	63.5	63.8
0.985	63.5	63.8	64.0	63.6	63.8
0.900	62.3	62.9	62.8	62.6	62.6
0.824	56.2	56.8	56.7	56.6	56.6
0.758	52.8	53.1	53.1	53.0	53.1
0.685	52.8	53.2	53.4	53.0	53.2
0.603	53.4	53.6	53.7	53.3	53.5
0.520	53.5	53.7	53.7	53.4	53.6
0.437	53.1	53.3	53.4	53.1	53.2
0.357	52.5	52.7	52.9	52.6	52.7
0.279	51.9	52.3	52.4	52.0	52.2
0.205	50.8	51.3	51.4	51.0	51.3
0.143	49.0	49.5	49.7	49.8	49.1
0.104	45.6	46.2	46.4	46.2	45.7
0.097	44.2	44.5	44.6	44.2	44.5
0.084	43.5	43.9	44.1	43.7	43.9

(b) Bottom Plate (Run 23.3)

UF	T28	T29	T30	T33	T34
[-]	[°C]	[°C]	[°C]	[°C]	[°C]
1.000	63.6	63.9	63.7	63.3	63.8
0.992	59.7	61.7	61.0	59.8	60.1
0.906	53.2	53.6	53.7	53.2	53.4
0.827	49.7	50.6	50.5	49.9	50.0
0.757	46.0	47.0	48.0	46.2	46.9
0.686	44.9	45.7	46.2	45.1	45.5
0.604	44.9	45.3	45.4	45.0	45.1
0.522	44.8	45.1	45.4	44.9	45.0
0.439	44.5	44.9	45.1	44.6	44.7
0.357	44.2	44.6	44.7	44.3	44.4
0.276	43.9	44.3	44.4	44.0	44.1
0.203	43.8	44.2	44.3	43.9	44.0
0.142	43.6	44.0	44.2	43.7	43.8
0.103	43.3	43.7	43.8	43.4	43.6
0.082	43.0	43.4	43.6	43.1	43.2

CHAPTER 5

PERFORMANCE OF HEAT PUMP

Performance data for the heat pump was available from the manufacturer's installation instruction booklet. However, Foxley and Weaver (1981) note that the data quoted by manufacturers represents operation of the heat pump under steady conditions, which gives the best possible results. Consequently it was decided to test the heat pump for operation with a variety of real source conditions and selected artificial loads in the laboratory. In the course of these tests some extremely useful operating experience was gained and many of the control functions experimentally verified.

5.1. Test Procedures

The ASHRAE Standard 116-1983 presents methods of testing for seasonal efficiency of unitary air conditioners and heat pumps. Unfortunately since ASHRAE is an American organisation the standard deals exclusively with air-to-air heat pumps which as discussed in chapter two are preferred in the US since they also may be employed as air conditioners in the summer season. This guide however, does provide some useful guidelines for devising a test procedure for an air-to-water heat pump, including the need to distinguish between:

1. Steady state operation
2. Cyclic operation at low ambient temperature due to defrost
3. Cyclic operation at high ambient temperature due to part load

In addition, a method for determining a seasonal COP based on the ASHRAE temperature bin analysis was presented. This standard requires that the heat pump be tested for a variety of source conditions which necessitates construction of a controlled environment facility (CEF) of some description. Other research establishments in the UK have developed excellent CEFs (see Buick et al. 1977) and it was thought unnecessary to replicate their work at Edinburgh. Instead the test facility was designed to be capable of accurately monitoring and datalogging the real source air temperature and condition (see section 3.2).

Leakage of refrigerant from prototype heat pump facilities is a very real hazard due to the temporary nature of some of the connections in the refrigerant piping circuit. Refrigerant loss causes a significant reduction in

heat pump performance and checking that the heat pump is fully charged must become an essential part of any test procedure. Hence section 5.1.1 includes details on (a) detecting a loss of refrigerant and (b) replacing lost refrigerant. Section 5.1.2 specifies the experimental procedure employed to obtain the performance curves, and demonstrate operation of the heat pump controls. Verification of these controls was important as the integrated system had to be left running unattended overnight to gain access to off-peak electricity tariffs.

5.1.1. Refrigerant charging procedure

Most heat pumps are designed with a sight glass in the refrigerant circuit between the liquid receiver and the filter dryer (see figure 3.10). A shortage of refrigerant in the circuit causes gassing in the flow through the sight glass which results in an opaque mixture. For a heat pump operating with a complete charge of refrigerant there is no vapour present and the fluid in the sight glass is transparent. It should be noted that a little gassing will always occur on start-up and following a sudden change in condenser pressure. Since a refrigerant leak reduces the heat pump performance the first indication may be a reduced COP and a low evaporator temperature (i.e. more than 10°C cooler than ambient temperature).

Once the need for charging the heat pump has been identified it is relatively straightforward to add the necessary refrigerant. A Ritchie Yellow Jacket charging connector is permanently mounted, as part of the test facility, since the pressure gauges give a useful indication of heat pump operating performance. The charging procedure noted below is then followed.

1. Connect a weighed R502 cylinder (correct way up) to middle connection via a pressure hose.
2. Empty hose of air by slightly unscrewing hose connection to cylinder and allowing refrigerant to escape from heat pump, via valve under evaporator pressure gauge, through hose for a short period (10 seconds), and then re-close valve.
3. Thoroughly tighten all connections and open cylinder valve.
4. Start-up heat pump (see section 5.1.2.1).
5. Open valve under evaporator pressure gauge for up to a minute at

a time.

6. After five minutes if gassing has still not disappeared then repeat previous step. If this step has already been repeated five times then either there is a large leak in the circuit or the refrigerant has frozen in the cylinder. In the former case the circuit should be leak tested and for the latter the cylinder should be placed in a bath of warm water for 15 minutes and the previous two steps repeated.
7. Record final weight of R502 cylinder and note how much refrigerant has been transferred to heat pump.

5.1.2. Experimental Heat Pump Procedure

5.1.2.1. Start-up Procedure

To avoid unnecessary trip-outs of the heat pump it is essential to ensure that both primary and secondary flows are established either before or at the same time as the heat pump is switched on. In the later stages of the development work care had to be taken to ensure that the control program could not switch the heat pump on inadvertently and that the primary fluid flow direction was set in the correct mode. Before the control program was fully operational the heat pump was switched on/off manually by an ordinary 13 amp power point on the control board and this facility was maintained to allow immediate manual isolation of the heat pump if necessary.

5.1.2.2. Shut-down procedure

The heat pump must be isolated before either the primary or secondary fluid flows are stopped to prevent unnecessary trip-outs from high refrigerant temperatures.

5.1.2.3. Experimental test procedure

Once the heat pump had been started, the selected load, flow rate and/or outlet temperature were achieved by suitable adjustment of primary and secondary flow rates. When steady state (defined as a variation of less than ± 0.5°C in outlet primary fluid temperature for a variation of ambient temperature of less than 0.5°C, over a minimum period of 30 minutes) had been achieved, data could be recorded. If the test was intended to

demonstrate the operation of a control device the time step was reduced to record the performance at one minute intervals.

5.2. Results

A series of tests were performed on the heat pump during development of the experimental facility. The tests were not intended to provide comprehesive performance data but rather to allow observation of the actual performance under various operating conditions.

5.2.1. Steady State Performance

Table 5.1 summarises the important data recorded for runs performed with transfer fluid temperatures in the region of interest for integrated system operation (i.e. 55-65°C). All runs were performed with a transfer fluid flow rate of 0.117 kg/s except 4.5d which was performed at half the normal flow rate.

5.2.1.1. Typical performance curves

Heat pump performance is dependent on the components selected and the evaporating and condensing temperatures of the cycle. The former is decreased by lowering the ambient temperature and the latter increased by raising the transfer fluid temperature; while the effect of either of these changes is to increase the temperture lift which lowers the COP. In figures 5.1 and 5.2 the heat output, power input and hence COP are plotted against both transfer fluid and ambient temperature respectively.

Since the input air condition could not be controlled it was not possible to produce experimental data for direct comparison with that quoted by the manufacturer. However a correlation based on the theoretical Rankine cycle COP and a few simplifying assumptions was developed and is presented in section 7.1.1.2. This correlation formed the basis of a program HPMODEL_RANKCOP which calculated the expected COP (extrapolated from manufacturer's data) of the heat pump for specified ambient and transfer fluid temperatures. The COP values determined by this method are shown in figures 5.1 and 5.2 to be significantly greater than the experimental values.

In section 7.1.1.4 a method for predicting the total power input to the heat

pump is described. A program HPMODEL_POWERIN utilised this technique to calculate the expected power input and figures 5.1 and 5.2 show these to compare very well with those found experimentally. Multiplication of this power input by the COP predicted by the model gives the expected thermal output which is also presented in figures 5.1 and 5.2.

As expected the total power input was found to increase slightly with both ambient and transfer fluid temperature. Thermal output was observed to increase with the ambient temperature and decrease with the transfer fluid temperature. Since the thermal output effect is more significant the COP follows its trend.

5.2.1.2. Performance parameters

In section 7.1.1.2 a program HPMODEL_EXPCOP is described which was written to analyse the experimental data obtained from the heat pump. The program calculates six performance parameters for each run and the results are presented in table 5.2. In section 5.2.2 each individual heat pump component is considered and its performance analysed with recourse to these values.

5.2.1.3. Performance of heat pump as DHW heater

High flow rates were shown in chapter 4 to improve the thermal performance of the prototype storage device; hence some tests were performed to establish the effect of flow rate on heat pump performance. It was extremely difficult to obtain steady state data with both ambient temperature and load approximately constant. Consequently only data for two flow rates was presented in table 5.4 since it proved impossible to achieve steady state at a third lower flow rate. Steady state in this analysis was achieved at an ambient temperature of 5.3°C ± 0.2°C and a DHW flow temperature of 61.5°C ± 0.2°C for ten readings over a 12 minute period at each flow rate.

During both these tests the specified DHW load was 4.5 kW. At the normal flow rate of 11.5 lit/min the heat pump supplied 4.35 kW while a higher flow rate of 14.3 lit/min could only deliver 4.21 kW (decrease of 3.2%) at the same DHW flow temperature. For the higher flow rate the condensing temperature

is increased which lowers the COP.

From this analysis it would appear that there is almost no significant decrease in heat pump performance as a hot water heater when the transfer fluid flow rate is increased. Calculation of the Reynolds number for water flow through the condenser shows that the flow is highly turbulent (>10000) over the range of water flow rates (8 - 15 lit/min). Hence since the resistance to heat transfer is large on the refrigerant side an increase in the water side velocity would not be expected to cause a significant improvement in the overall heat transfer coefficient to counter-act the decrease in the log mean temperature difference.

5.2.2. Performance of Individual Components

5.2.2.1. Condens :r

A co-axial tube-in-tube heat exchanger is employed as the condenser in the heat pump prototype. This consists of a continuous length of longitudinally finned (solder-bonded) inner tube with an outer tube serving as a shell. The copper inner tube serves as the cooling water circuit while the refrigerant flows through the annular space, where the surface area is increased by the fins since the refrigerant side heat transfer coefficients are generally much lower than those for water.

A simple heat balance across the condenser can be employed to determine the refrigerant mass flow rate.

$$(\dot{m}\, Cp)_{tf}\, [T_9 - T_{10}] = \dot{m}_{ref}\, [h_2 - h_3] \qquad (5.1)$$

From the data presented in table 5.3 the refrigerant mass flow rate was found to be 0.0446 kg/s.

The heat transfer taking place in the condenser may be divided into three distinct regions:

1. Vapour superheat removal
2. Condensation
3. Liquid subcooling

By reference to figure 5.3 and table 5.3 we see that only $(h_{2sat}-h_{3sat})/(h_2-h_3)$ = 56% of the heat is transferred during condensation of the vapour. A very significant amount of the heat is transferred as the vapour is de-superheated (29.7%) and the remainder during subcooling (14.3%). Since it is known that the film coefficient for vapour-liquid heat transfer is much lower than that for condensation or liquid-liquid (subcooling) heat transfer, then a large proportion (>29.7%) of the condenser heat transfer area will be required for the de-superheating duty. As the amount of de-superheating increases, the condenser temperature approach (i.e. the difference between the condenser saturation temperature and transfer fluid temperature) tends to zero, thus maintaining a constant COP for a higher circulating fluid temperature.

5.2.2.2. Evaporator

A standard finned tube heat exchanger was employed as the evaporator in the prototype heat pump. Little information was available on the evaporator, hence an analysis of its performance was limited to considering a heat balance. It was difficult to determine the heat input to the evaporator accurately since it required:

1. Measurement of volumetric flow rate through a large duct
2. Calculation of a temperature difference which must be kept to a minimum (usually 3-4 degC) and therefore introduces large errors using standard thermocouples
3. Determination of inlet and outlet humidity which may vary significantly over the cross section

The heat balance across the evaporator has to include the sensible heat transferred from the air in addition to the latent heat gained as a consequence of condensation of water vapour

$$q_{ev} = (\dot{V}\rho Cp)_{air}\,[T_5-T_7] + (\dot{V}\rho)_{air}\lambda_{wv}[H_{in}-H_{out}] = \dot{m}_{ref}(h_1-h_4) \qquad (5.2)$$

In table 5.3 the recorded output from the data-logging program presents the wet and dry bulb temperatures for the inlet and outlet air. These were converted to humidity values (i.e. mass of water vapour per unit mass of dry

air) for use in the equation above (see section 9.1.1). The properties of air and water vapour used in this equation are presented in section 9.1.2. A vane anemometer was used to determine the average volumetric air flow rate out of the sides of the heat pump. The flow rate was found to be 1 m^3/s by this method, which is significantly less than the nominal flow rate of 1.18 m^3/s. The total heat input to the evaporator was calculated to be 5.733 kW with the latent heat contribution amounting to 1.819 kW. A much smaller (more reasonable) latent heat contribution of 0.2 kW may be determined from equation (5.2) employing the refrigerant flow rate calculated in section 5.2.2.1.

The temperature of the refrigerant entering the evaporator (T_4) is greater than the ambient temperature. While it was expected that T_4 would be greater than T_1 due to the pressure drop across the evaporator, it is still difficult to understand how it could be repeatably greater than the ambient. The sensor itself had been removed and its satisfactory operation confirmed in a water bath, before being carefully re-mounted with heat sink compound to improve thermal contact, and insulation to protect it from the surrounding air temperature.

5.2.2.3. Compressor

In table 5.2 the average adiabatic efficiency was found to be 56.8%, which is significantly lower than the figure of 75% reported by Bartlett and Chabra (1983). The electric motor efficiency is defined as the proportion of the power input actually delivered to the refrigerant. Characteristic curves for compressor performance were used to calculate the electric motor efficiency for the following set of operating conditions: T_{co} = 58.8°C, T_{ev} = 0°C, T_{sup} = 32°C and T_{sub} = 26.8°C. These values were then input to HPMODEL_REALCOP1 to determine the following state point enthalpies (assuming an adiabatic efficiency of 75%): h_1 = 212.3 kJ/kg, h_2 = 252.1 kJ/kg and h_3 = 80.6 kJ/kg.

A chart was then used to determine the refrigerant mass flow rate for a specified evaporator temperature at one of four condenser temperatures. The refrigerating capacity was then calculated as the product of the refrigerant mass flow rate (0.0486 kg/s) and the difference in the enthalpies. This value could be checked on a second chart which was a plot of refrigerating capacity against evaporating temperature for one of four specified condenser temperatures. The required power input to the compressor was calculated

from the refrigerant flow rate and state point enthalpies 1 and 2 to be 1.93 kW. Motor input power was determined from a third chart to be 2.9 kW and the electric motor efficiency therefore found to be 66.6%. If the average adiabatic efficiency of 56.8% determined from table 5.2 is employed to determine the enthalpies, the heat losses are smaller and the electric motor efficiency would be calculated as 88%

5.2.2.4. Expansion valve

An externally equalised TEV is employed to regulate flow of refrigerant in the heat pump (see figure 3.10). This was found to work extremely well, maintaining 5.8 ± 0.8 degC of superheat over the complete range of operating conditions. The actual degree of superheat during any run was found to vary by ± 0.5°C as recorded in the data-logger print-out. However if a Comark was attached to the temperature sensor T_1 it was found that the temperature varied by ± 2°C in a regular fashion. The temperature would drop instantaneously and then increase rapidly to to a pseudo steady value (that recorded by data-logger) before decreasing again. This cycle which had a period of approximately 15 seconds was caused by the lag time in the control circuit as the refrigerant flowed through the evaporator.

5.2.2.5. Overall heat balance

It is difficult to perform an overall energy balance for the heat pump due to the lack of confidence in the heat input determined for the evaporator.

5.2.3. Verification of Controls

5.2.3.1. Safety controls

The high pressure trip was demonstrated to be working satisfactorily at a setting of 20 barg. Initially the differential between the trip-out and reset pressure was very small (approximately 4 barg) and the heat pump was re-started almost instantaneously (approx. 10 seconds). A higher differential of 7.5 barg increased the time before re-start to two minutes, which was considered satisfactory for development work. The data-logger recorded a trip pressure of approx. 18 barg on both occasions, which implied that the controller read high by 2 barg. Since the condenser was designed for

operating pressures up to 30 barg the controller was set for 32 barg.

The low pressure trip was demonstrated dramatically in the laboratory during early developmental work. A pressure hose rated at 35 barg, which connected the pressure gauge to the liquid receiver, burst. The subsequent loss of refrigerant caused the evaporator pressure to drop and the heat pump tripped out while the refrigerant pressure was still 1 bar greater than the atmospheric pressure. Consequently no attempt was made to adjust this control as it had performed exactly as intended in this accident.

5.2.3.2. Motor starting controls

The soft start technique employed to lower the starting current drawn by the compressor worked well. Ordinary domestic 13 Amp fuses were found adequate except when the heat pump was operated with high transfer fluid temperatures during periods of high ambient temperature which increased the required power input to 3.3 kW (see figures 5.1 and 5.2). The number of starts per hour was limited by adjustment of the water flow temperature controller (see section 5.2.3.4).

5.2.3.3. Defrost control

In figure 5.4 the cyclic operation of the heat pump during defrost is shown. The primary transfer fluid temperature is shown to decrease and then asymtotically approach its previous value. During reverse cycle operation the air inlet temperature sensor records a significant increase. Power input to the compressor increases with the increased evaporator temperature (see section 5.2.1.1). As expected the COP decreases and slowly builds up to a pseudo steady state value again. At this particular temperature and load condition the cycle period was approximately 34 minutes and resulted in an average COP (calculated roughly by summed squares) 3.5% less than the pseudo steady state value of 1.8.

5.2.3.4. Optimum operation control

The temperature scale on the thermostat controller was only intended as an approximate guide. Hence the transfer fluid temperature was allowed to increase gradually until the heat pump tripped out, with the controller being adjusted in small increments until the desired trip-out temperature of 63.5°C

was achieved. The reset was set at 10 degC which allows the transfer fluid temperature in the circuit and buffer tank (approx. 70 litres total) to fall 4 degC, since for an output of 5 kW at a typical flow rate of 0.192 kg/s the transfer fluid temperature will instantaneously drop by 6 degC. For a required load of 3 kW the time for the transfer fluid temperature to fall 4 degC can be calculated to be 6.5 minutes. After this period the heat pump would be switched on again and the surplus output (2 kW) would cause the circulating transfer fluid temperature to rise 4 degC in 9.75 minutes and result in the heat pump being tripped out again. This gives a total cycle time of over 15 minutes or a switching frequency of less than 4 per hour. Figure 5.5 presents the performance of the heat pump while operating in a thermal cycle mode. The cycle periods were not identical to that noted above due to the variation in domestic hot water load and effect of heat losses.

5.3. Discussion of Results

5.3.1. Steady State Performance

The significant discrepancy between the expected and actual performance shown in figures 5.1 and 5.2 may be caused by:

1. Limited accuracy of the correlation employed to calculate the expected performance. In table 7.3 it is shown that the correlation tends to over-estimate the COP for the range of operating conditions shown.
2. Extrapolation of this correlation for use with transfer fluid temperatures 10°C higher than those used to derive the correlation.
3. Uncertainty about the refrigerant charge; El Meniawy (1981) reported that this has very significant effect on performance.
4. The measurement errors in temperatures, flow rates etc., are unlikely to result in a performance consistently low but still cannot be neglected.

5.3.2. Performance of Individual Components

A greater understanding of the performance of the heat pump would have been achieved if a refrigerant flowmeter had been placed in the cycle. It would have to operate with a low pressure drop to permit normal operation and should be placed just before the expansion valve where liquid refrigerant flow is guaranteed. Pressure sensors, especially at the inlet to the evaporator and the outlet of the compressor, would have produced useful data on flow through the cycle.

Improvement of the instrumentation employed to determine the thermal input to the evaporator and inclusion of a reliable method of measuring the volumetric air flow rate would permit determination of an accurate energy balance on the system. It would then be possible to investigate more thoroughly the effect of inlet air condition on evaporator performance. Condensation of 2.5 litres of water per hour (as determined by the existing instrumentation) seems larger than the actual volume of water observed to condense. A much smaller figure of 0.28 litres per hour, calculated from equation (5.2) using the refrigerant flow rate found in section 5.2.2.1, is more believable. The saturation temperature at various points along the refrigerant flow through the evaporator should also be checked in an attempt to verify T_4 and offer an explanation.

The experimentally determined adiabatic efficiency compares very poorly with the figure of 75% reported by Bartlett and Chabra (1983) and reasonably well with that of 65% suggested by McMullan et al. (1981). Heap (1983) assumed a typical adiabatic efficiency of 60% and an electric motor efficiency of 80% in his analysis of heat pump cycles. The former compares extremely well with that found in this work while the discrepancy of 10% in the latter gives rise to concern. No evidence was available but it was thought possible that there may be a limited inefficiency due to the soft-start technique utilised in this heat pump.

5.3.3. Verification of Controls

The net decrease in COP of 3% experienced for operation during a defrost cycle represents a significant loss in performance. This may be even more significant for conditions of increased humidity and lower ambient

temperature. Note however that the COP does remain greater than 1 for the complete cycle and is therefore to be favoured over direct electric methods of defrosting. Detailed investigation of the heat pump performance during thermal cycling would require significantly improved instrumentation and control in the experimental facility.

5.4. Conclusions

1. Refrigerant leaked from the prototype heat pump, and caused substantial variation in its performance.

2. COP was improved for lower transfer fluid temperature and higher ambient temperatures.

3. A model based on an extrapolated correlation of the manufacturer's quoted data to the Rankine cycle COP was found to predict a COP significantly greater than that determined experimentally.

4. The adiabatic and electric motor efficiencies of the compressor were found to be 56.8 and 70.3% respectively.

5. The safety and hot water temperature controls were experimentally verified.

6. A reversing valve was utilised for defrost which minimised the reduction in overall COP to less than 5% for typical operating conditions.

7. Further research could include detailed investigation

- of heat pump as domestic hot water heater, since this could be achieved with no modifications to existing test facility
- into the effect of transfer fluid flow rate on heat pump performace
- of heat balances around heat pump, including refrigerant mass flow rate, air flow rate and humidity over evaporator
- of performance during part-load operation

and should include the installation of a refrigerant flowmeter on the prototype heat pump.

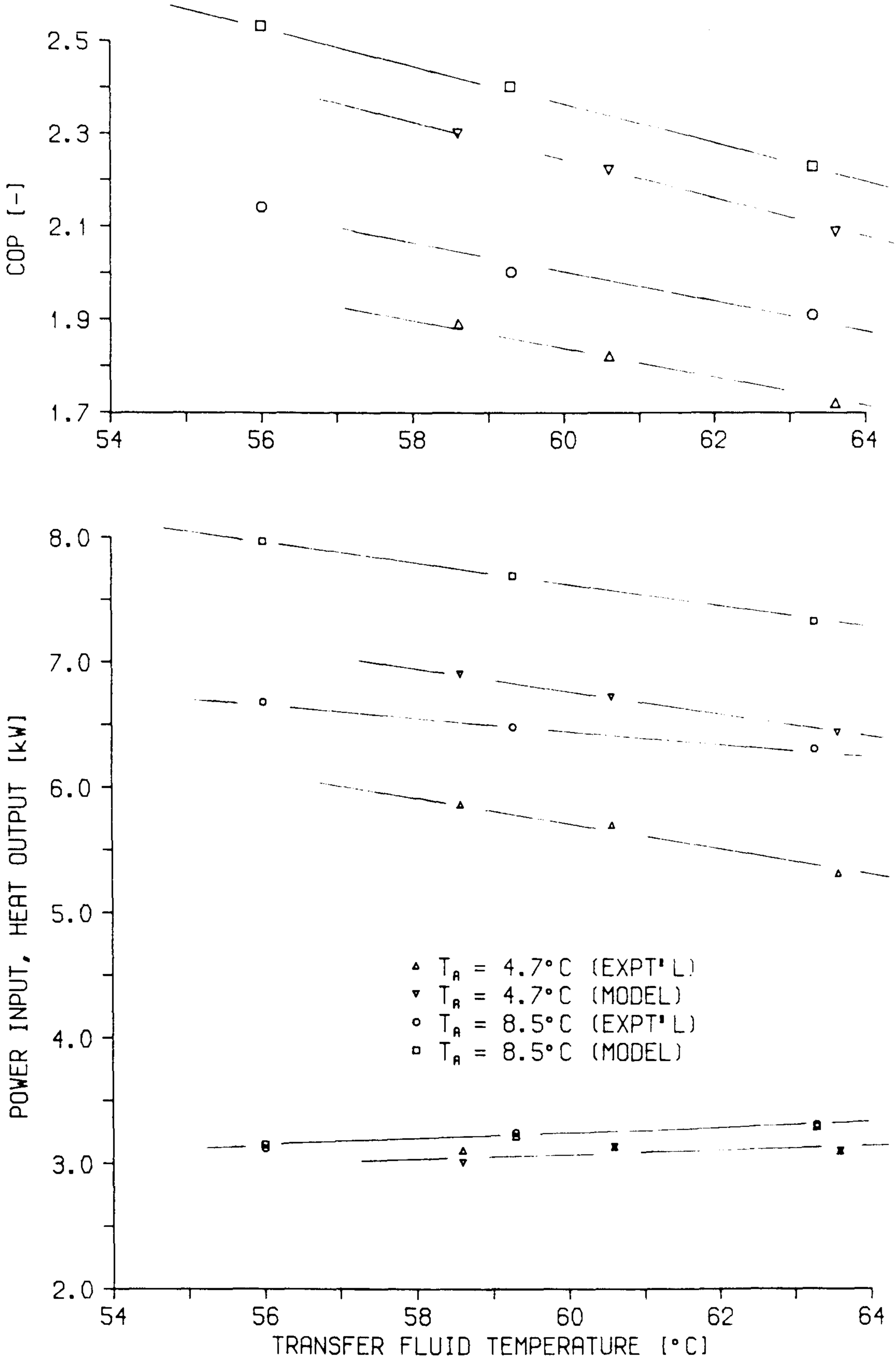

Figure 5.1 Performance of heat pump (1)

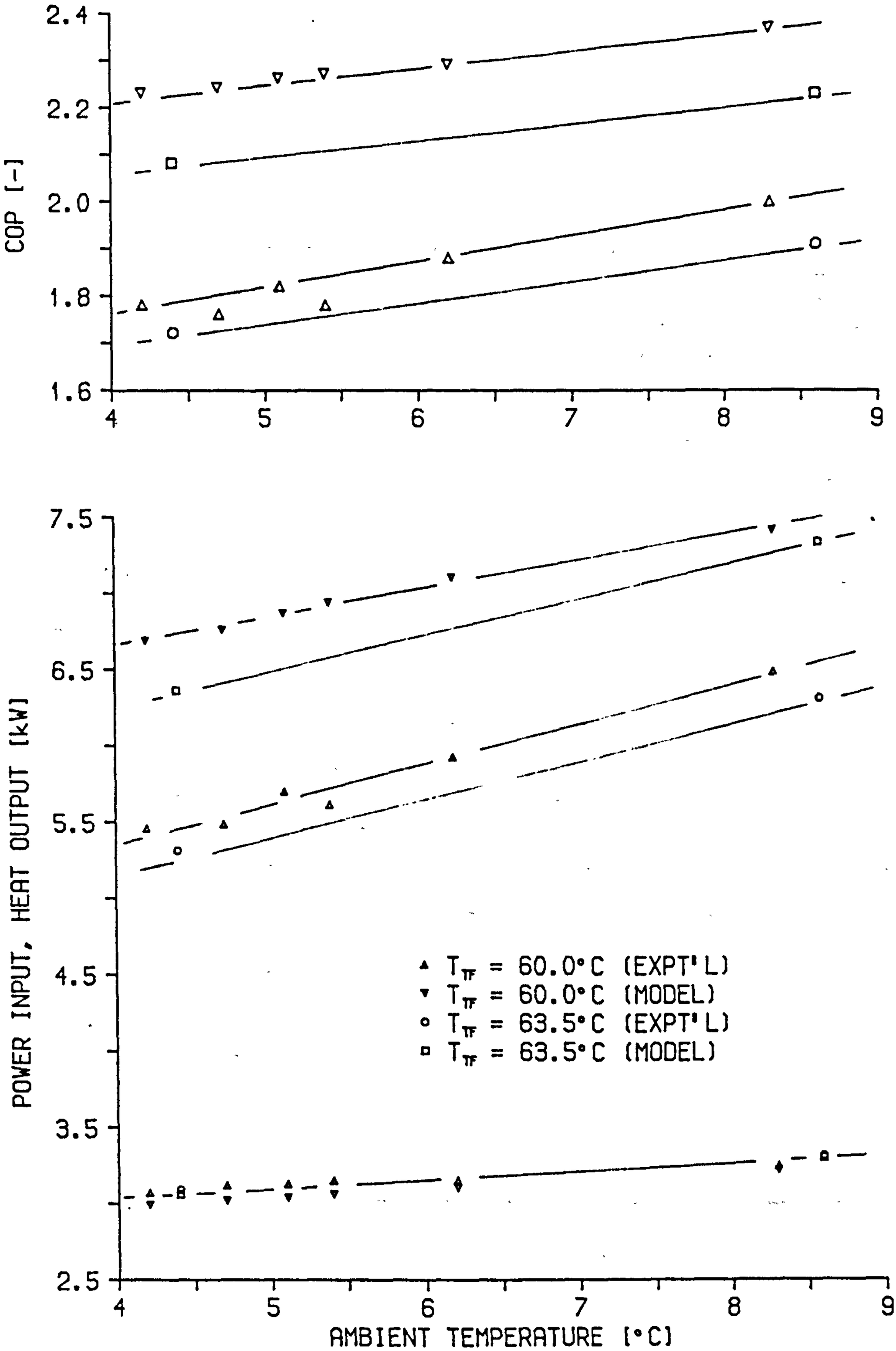

Figure 5.2 Performance of heat pump (2)

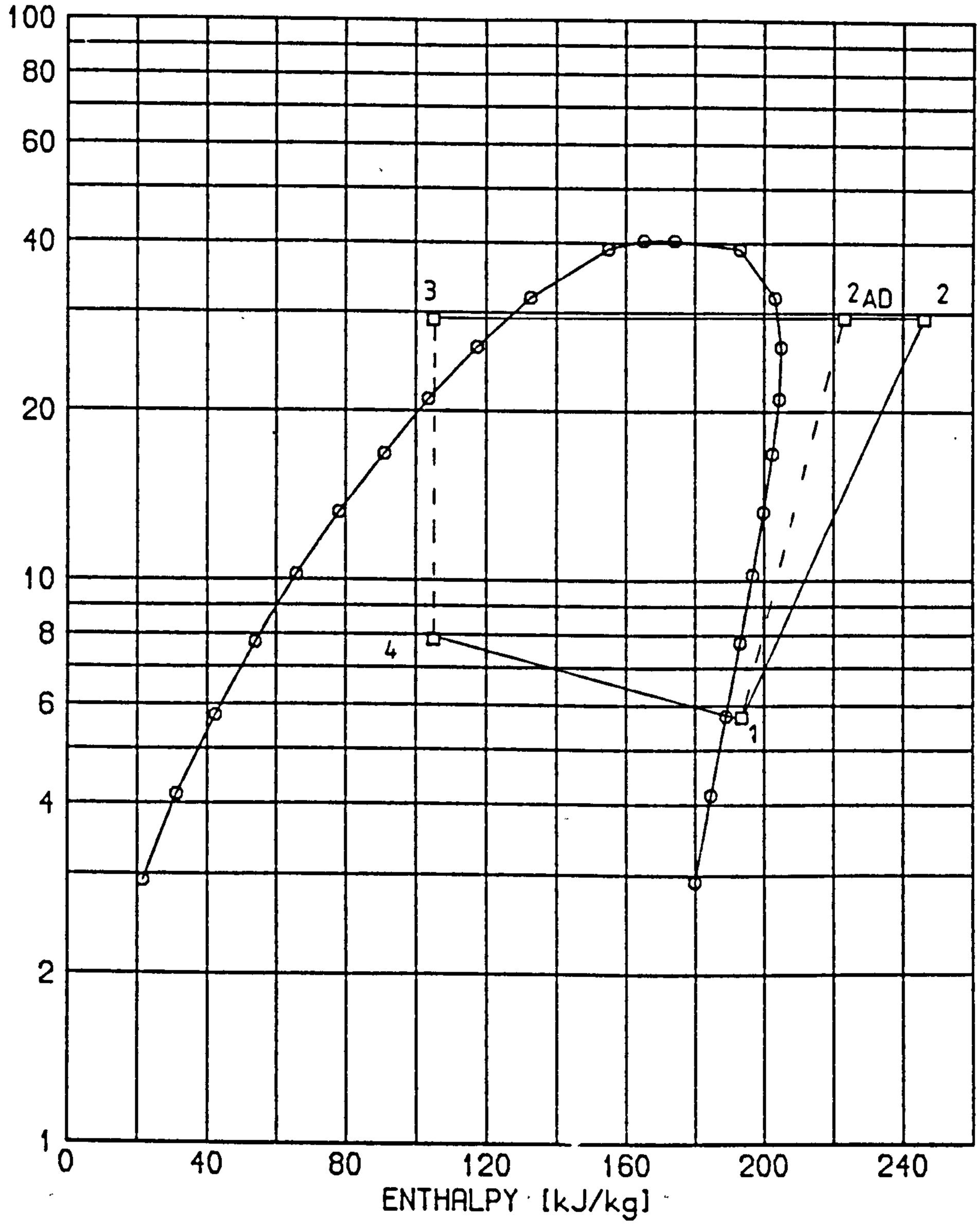

Figure 5.3 Pressure-enthalpy diagram for prototype heat pump

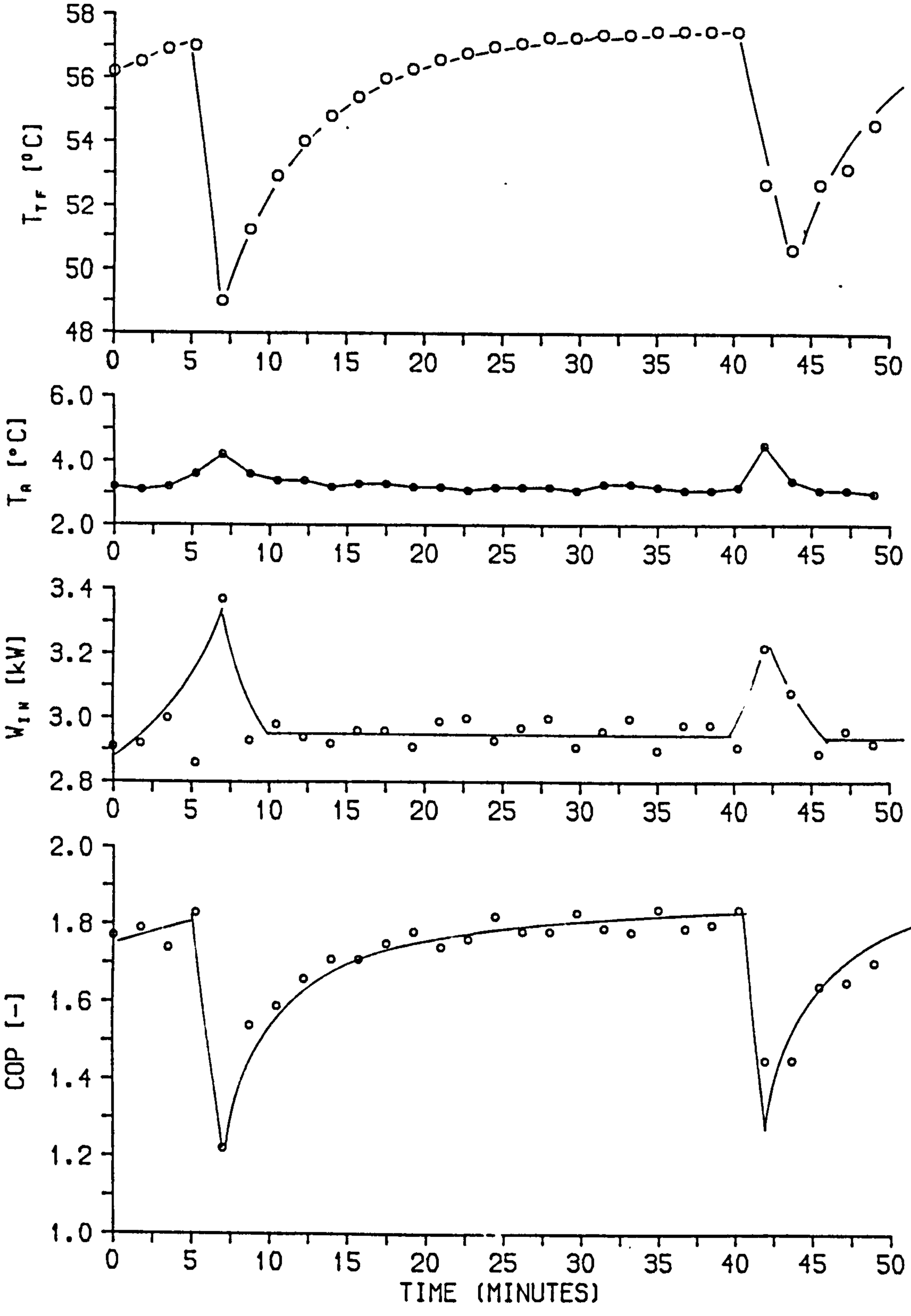

Figure 5.4 Operation of heat pump during defrost cycle

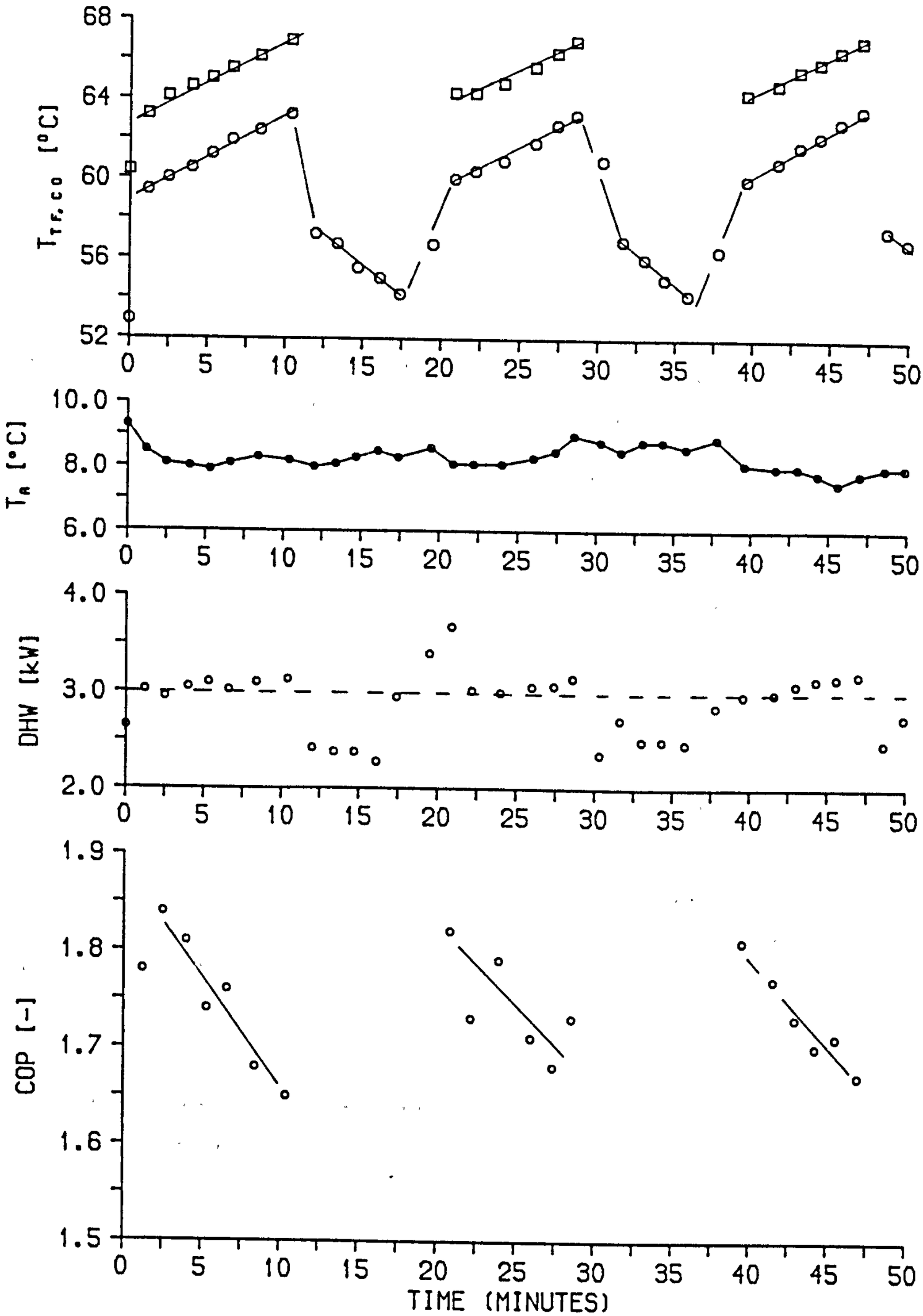

Figure 5.5 Operation of heat pump during thermal cycling

Table 5.1 Steady State Performance of Heat Pump

RUN	T_1 [°C]	T_2 [°C]	T_3 [°C]	T_{ev} [°C]	T_{co} [°C]	q_{co} [kW]	W_{in} [kW]	T_a [°C]	T_{tf} [°C]
4.2a	4.2	95.1	43.6	-2.2	58.6	6.69	3.14	7.9	56.0
4.2b	6.2	101.9	50.9	-0.1	65.4	6.30	3.30	8.5	63.3
4.2c	5.1	98.5	46.9	-1.2	61.8	6.48	3.24	8.3	59.3
4.3a	3.3	99.4	46.4	-2.5	61.5	5.92	3.15	6.2	58.9
4.3b	3.2	101.0	47.7	-2.8	63.0	5.61	3.15	5.4	60.5
4.3c	2.0	100.7	47.1	-3.2	62.3	5.49	3.12	4.7	59.7
4.4a	0.0	98.8	43.2	-5.8	61.1	5.52	2.89	1.2	57.0
4.5a	1.7	97.0	45.9	-3.5	61.9	5.82	3.08	4.5	58.6
4.5b	2.4	100.3	48.0	-2.7	64.0	5.70	3.13	5.1	60.6
4.5c	2.1	103.5	50.3	-3.2	66.9	5.31	3.09	4.4	63.6
4.5d[1]	0.3	101.5	43.0	-4.9	64.8	5.44	2.97	2.9	62.5
4.6a	1.8	97.3	47.0	-3.8	62.7	5.46	3.07	4.2	59.4
4.6b	1.4	97.2	44.5	-5.2	61.0	5.35	2.91	3.2	57.5

Notes:

1. At half the normal transfer fluid flow rate
2. Parameters defined in table 5.3

Table 5.2 Analysis of Experimental Heat Pump Performance

RUN	θ_{co} [degC]	θ_{ev} [degC]	T_{sup} [degC]	T_{sub} [degC]	η_{ad} [%]	η_{em} [%]
4.2a	2.6	10.1	6.4	15.0	55.8	75.4
4.2b	2.1	8.6	6.3	14.5	56.3	73.2
4.2c	2.5	9.5	6.3	14.9	55.8	73.5
4.3a	2.6	8.7	5.8	15.1	54.9	70.9
4.3b	2.5	8.2	6.0	15.3	55.5	68.9
4.3c	2.6	7.9	5.2	15.2	54.5	68.4
4.4a	4.1	7.0	5.8	17.9	57.2	71.9
4.5a	3.3	8.0	5.2	16.0	57.9	70.1
4.5b	3.4	7.8	5.1	16.0	56.6	70.1
4.5c	3.3	7.6	5.3	16.6	57.5	68.7
4.5d[1]	2.3	7.8	5.2	21.8	58.0	69.2
4.6a	3.3	8.0	5.6	15.7	59.2	66.3
4.6b	3.5	8.4	6.6	16.5	59.2	67.7
Average	2.9	8.3	5.8	16.2	56.8	70.3
Max. error	1.2	1.8	0.8	1.7	2.4	5.1

Notes:

1. At half the normal transfer fluid flow rate

Table 5.3 Heat Pump Performance Data for Typical Run (4.2b)

(i) Recorded data			
Mass flow rate of transfer fluid	$\dot{m}_{tf}$	[kg/s]	0.117
Condenser inlet flow temperature	T10	[°C]	50.4
Condenser outlet flow temperature	T9	[°C]	63.3
Inlet air dry bulb temperature	T5	[°C]	8.5
Inlet air wet bulb temperature	T6	[°C]	5.5
Inlet air relative humidity	RI	[%]	63.2
Outlet air dry bulb temperature	T7	[°C]	5.4
Outlet air wet bulb temperature	T8	[°C]	3.1
Outlet air relative humidity	RE	[%]	68.5
Compressor inlet refigerant temperature	T_1	[°C]	6.2
Compressor outlet refrigerant temperature	T_2	[°C]	101.9
Condenser outlet refrigerant temperature	T_3	[°C]	50.9
Evaporator inlet refrigerant temperature	T_4	[°C]	10.4
Condenser saturation temperature	T_{co}	[°C]	65.4
Evaporator saturation temperature	T_{ev}	[°C]	-0.1
Condenser saturation pressure	P_{co}	[bar]	27.73
Evaporator saturation pressure	P_{ev}	[bar]	4.63
Compression ratio		[-]	5.08
Power input to heat pump	W_{IN}	[kW]	3.30
Heat output from condenser	q_{co}	[kW]	6.30
(ii) Derived data			
Enthalpy at compressor inlet	h_1	[kJ/kg]	193.5
Enthalpy at compressor outlet	h_2	[kJ/kg]	246.1
Ditto for adiabatic compression	h_{2ad}	[kJ/kg]	223.1
Enthalpy at condenser outlet	h_3	[kJ/kg]	105.0
Condenser saturated vapour enthalpy	h_{2sat}	[kJ/kg]	204.2
Condenser saturated liquid enthalpy	h_{3sat}	[kJ/kg]	125.2
Evaporator saturated vapour enthalpy	h_{1sat}	[kJ/kg]	188.8
Inlet air humidity ratio	H_1	[kg/kg]	0.00434
Outlet air humidity ratio	H_2	[kg/kg]	0.00376

Table 5.4 Comparison of Heat Pump Performance as DHW Heater at Medium and High Flow Rates

(i) Recorded Data

Transfer fluid flow rate	$\dot{m}_{tf}$	[kg/s]	0.1933	0.2383
Ambient air temperature	T5	[°C]	5.4	5.3
DHW outlet temperature	T18	[°C]	61.5	61.5
Transfer fluid inlet temperature	T9	[°C]	63.3	63.0
Transfer fluid outlet temperature	T10	[°C]	57.5	58.5
DHW inlet temperature	T17	[°C]	18.3	18.5
Condenser saturation temperature	CT	[°C]	67.5	67.8
DHW flow rate	$\dot{m}_{cw}$	[kg/s]	0.02583	0.02583
Condenser thermal output	q_{co}	[kW]	4.74	4.60
Work input	W	[kW]	2.97	2.96
Coefficient of performance	COP	[-]	1.59	1.55
DHW load	DHW	[kW]	4.35	4.21

(ii) Derived data

Log mean ΔT	ΔT_{LM}	[degC]	12.14	11.73
Overall h.t.c.	U	[W/m^2K]	640	641
Transfer fluid h.t. rate	q_h	[kW]	4.41	4.22
DHW h.t. rate	q_c	[kW]	4.67	4.65

CHAPTER 6

PERFORMANCE OF INTEGRATED SYSTEM

6.1. Procedure

6.1.1. Introduction

No recommended procedure for evaluating the performance of integrated systems was available in the literature, hence the experimental facility was designed to simulate operation of the system in an actual dwelling. The heat pump was therefore located to utilise "actual" ambient air rather than that pre-conditioned in a controlled environment laboratory.

Since there is no such thing as a standard heat demand, a "typical" space heating design load was simulated using a plate heat exchanger. This exchanger was capable of simulating a design load of 6.5 kW and its full specification was presented in section 3.2.2.2. An additional advantage of using such an arrangement is that the performance of the system for meeting a domestic hot water requirement may be evaluated from the same set of results. The load was determined from

$$q = (UA)_L(T_{set}-T_a), \tag{6.1}$$

where $(UA)_L$ was a typical load factor and T_{set} was the internal temperature setpoint of the dwelling, corrected for casual gains (see section 2.1.4.1). The ambient temperature T_a was monitored every half hour and the load for the next 30 minutes then calculated. It may be desired to keep the load constant for performance evaluation and an option to specify the load in kW was included.

In a real system it is unlikely that the heating system would run continuously from 7 a.m. until midnight, an assumption often made to simplify performance analysis. Hence an option to specify two other more realistic operating periods was included:

1. 7 a.m. to 9 a.m., 1 p.m. to 2 p.m. and 5 p.m. to midnight
2. 7 a.m. to 9 a.m. and 5 p.m. to 10 p.m.

6.1.2. Experimental Test Procedure

The store was initially brought to steady state at a known temperature, a procedure normally achieved by performing a charge test (see section 4.1) with the initial temperature set to 44°C and the steady state period to 12 hours. If the absolute heat transfer rate at the end of this period was greater than 200 W then this procedure was repeated. For a value less than 200 W it was assumed that the store was at steady state with a UF of zero. The integrated system control program was then loaded and its start up instructions followed (see section 3.2.6).

A starting time of midnight with the store completely discharged was normally used, although specifying any other time would be acceptable as long as the UF was known. The only restriction on starting time is that it should be a multiple of 30 minutes to prevent conflict between the load prediction and the operating periods specified in section 6.1.1.

6.2. Runs Performed in Autumn 1985

6.2.1. Results

Figures 6.1 to 6.4 present the first set of results obtained from the integrated system while operated in real time from 29th October to 1st November 1985. On the 28th October steady state at 44°C was established by 5 p.m. using the standard charge/discharge test procedure. The run was initiated at 5.30 p.m. but since the initial UF was specified to be 0, the actual run did not commence until midnight when the store (still with a UF of 0) was charged by the heat pump using off-peak electricity.

It was decided to test the system with a fixed load of 3 kW, which is approximately equal to the heat loss from a dwelling with $(UA)_L$=329 W/degC and T_{set}=15.5°C, and a mean ambient temperature of 7°C.

The following observations about integrated system operation may be noted from figures 6.1 to 6.4:

1. During the off-peak period the ambient temperature is always lower than the mean daily temperature, by as much as 3°C on some days
2. A maximum in the ambient temperature occurs between 1200-1400

hours on each day

3. Defrost cycling which occurs due to low ambient temperature on 1.11.85 results in a jagged temperature-time profile for the inlet temperature of the transfer fluid and a much smaller off-peak charge
4. The charge rate (5 kW) delivered by the heat pump was lower than that found for the heat pump alone, see figure 5.1, and was hence incapable of completely charging the store overnight
5. In the first 30 minutes of any discharge period the load supplied by the store is significantly greater than that required
6. As the run proceeds the apparent minimum UF at which the store may still be usefully employed to supply the required load increases, rising to 0.18 after 4 days

6.2.2. Discussion of Results

Due to the relationship between heat pump performance and ambient temperature the performance of a heat pump operated solely on off-peak electricity will be adversely affected by the diurnal variation of ambient temperature. If it was decided to charge the store for a short period during the day, the best time would be between 1200-1400 hours, since the ambient temperature is generally highest during this period.

The COP is also a function of the transfer fluid temperature and consequently was found to decrease from 2.10 to 1.70 during the off-peak period.

The initial peak in discharge rate is caused by the method originally used to control the flow rate of cold water. This control technique which required decreasing the flow rate slowly from its maximum to the setpoint value was discussed in detail in section 3.2.5.4.

The method of tracking the store condition is considered inaccurate, since the UF at which the store can no longer supply the specified load increases during the test period. One possible reason for this is that there was no allowance for heat loss from the store during conditions of no flow. It should be noted that even a very small error in the determination of the UF, would become significant after a few weeks of continuous operation, which suggests

that an alternative method of inferring the store condition is required.

6.3. Runs Performed in June 1986

6.3.1. Results

In figure 6.5, typical output for a 24-hour period in the middle of a two week run from 23rd May to 6th June 1986 is presented. The experimental facility had been improved by the inclusion of a control valve on the cold water mains to give more accurate control of cold water flow rate, hence allowing a much greater control and range of load conditions. The control program had been modified so that the user could specify $(UA)_L$ and T_{set} from which the program would calculate the design load using the actual ambient temperature. This facility was not employed in this run as the high ambient temperatures would result in a low load for a typical dwelling heat loss factor. These small loads would produce only a limited range of performance data, hence the fixed rate of 3 kW employed in the previous run was investigated again.

In an attempt to stop the UF drifting, the heat loss occuring during periods of non-flow was calculated and can be observed as a small negative rate between 0900-1300 and 1400-1700 and a slope of just less than zero in the UF-time profile during the same periods. Since the ambient temperature in June is greater than that in November the store charge rate is greater. Consequently as the store inlet temperature becomes greater than 63°C, a proportion (2 kW) of the heat pump output is diverted to the heat exchanger to simulate pre-heating of the dwelling or heating of the domestic hot water utilising off-peak electricity. The omission of a 3 kW load from 1300-1400 in this run was due to difficulties experienced with the load control software.

6.3.2. Discussion of results

For the run on 1.6.86 the heat pump output was recorded and was found to be greater than the store charge rate by 0.6 kW. The source of this discrepancy was later confirmed to be a combination of heat loss from the transfer fluid circuit and large experimental error in the measurement of temperature drop using a pair of thermocouples.

6.4. Runs Performed in March 1987

6.4.1. Results

Figures 6.6 to 6.9 present performance data obtained for the integrated system over the period 12/3/87 to 15/3/87. Tables 9.1 to 9.4 in the appendices present the store experimental data in tabular form.

Prior to the start of the run on 12/3 the store was carefully brought to steady state by the technique described in section 6.1.2. A charge/discharge cycle was commenced at midnight with a flow rate of 11.5 lit/min, and the store was completely discharged by 1315 hours. The run was completed at 1700 hours and the store again brought to steady state in preparation for a charge/discharge cycle at 8 lit/min on 13/3. Unfortunately the paper in the printer jammed at 0400 hours, so the work input, thermal output, COP and domestic heating load (data which are not transferred to the disk) have been presented as approximate values until the problem was rectified at 1015 hours. At 1600 hours the flow rate was changed back to 11.5 lit/min and the run continued without human interuption until the store was completely discharged at 1515 hours on 15/3.

In section 5.2.3.4 it was noted that the trip-out temperature on the transfer fluid thermostat was set to 63.5°C. To avoid thermal cycling during heat pump charge the program controller was set to enter part-load heat pump charge if the transfer fluid temperature became greater than 63°C. The program controller entered heat pump only mode once the store was determined to be completely discharged, i.e. if

1. UF was less than zero
2. Store top temperature (T20) < 44°C
3. Discharge rate 0.5 kW less than specified load for more than ten minutes.

During these tests the load was set to a constant 3 kW, rather than a load calculated from a dwelling loss coefficient and real ambient temperature, in order to simplify analysis of the performance data.

The following observations may be noted from figures 6.6 to 6.9, table 6.1

and tables 9.1 to 9.4:

1. A significant variation in ambient air temperature was again noticed during the daily cycle.
2. Defrost was observed as a slight increase in work input and significant decrease in condenser output rates. The accompanying condenser outlet temperature drop decreases as the ambient temperature rises.
3. Thermal cycling was observed as a significant decrease in work input (often to zero) and decrease in condenser output rate during the heat pump only periods. The condenser inlet and outlet temperature both exhibit a rapid decrease followed by a slower increase during a thermal cycle. This increase in condenser inlet temperature causes the condenser output rate to decrease over the thermal cycling period. For low ambient temperatures in heat pump only mode the effect of defrost was observed to be superimposed on the thermal cycling characteristic due to excess heat pump thermal output.
4. A sharp maximum of about 6 kW was observed in the domestic heating load as the flow through the store was reversed, and the store discharge rate against time also describes a peak. This peak has a period of approximately ten minutes while the load control system brings the cold water flow rate to its specified value. In order to prevent premature termination of the discharge cycle being caused by occasional low discharge rates due to experimental error, the program attempts to maintain the load at a value 10% greater than that specified. In all the figures noted above the heating load was shown to remain approximately constant and in table 6.1 the average domestic heating load was reported to be 3.3 ±0.07 kW for all runs.
5. The store charge rate decreases slightly over the charge period (as the transfer fluid temperature increases causing the heat pump output to decrease) with periodic decreases due to defrost superimposed on this profile. In the tables which present the detailed experimental data a constant discrepancy of approximately 500 W betweeen condenser output and store charge rate (see table

9.1 at 0200 hours) was noted and determined to be due to heat losses from the pipework and the storage device.

6. A variable discrepancy of 350 W to 0 W between store discharge rate and domestic heating load was determined to be primarily due to experimental error in measurement of the latter (see section 9.3.2.2).
7. As the ambient temperature increases the heat pump thermal output increases and the UF achieved at the end of the charge period increases accordingly. The UF was known to be exactly zero at the beginning of the charge on 12/3 and 13/3. However the exact UF at the beginning of the charge cycle on 14/3 is uncertain since the store would lose heat to the surroundings during the period 1430 to 2400 hours on 13/3. In the experimental control program UF was only corrected for heat loss if greater than zero, since it was incorrectly assumed that an error would have occured if UF became less than zero.
8. The average COP decreases during the store charge and is lower than expected due to heat losses from the pipework and store. Defrost also lowers COP periodically as shown in figure 5.4.
9. The average ambient temperature for heat pump charge on 12/3 and 14/3 remained approximately constant which allowed the performance of the integrated system at low (8 lit/min) and high (11.5 lit/min) flow rates to be compared. The average COP was found to be almost identical, hence operation at high flow rates is recommended since it lowers condenser outlet temperature thus increasing maximum charge rate as UF approaches unity.

6.4.2. Discussion of Results

Heat losses from the thermal storage device at 0200 hours on 12/3 were calculated to be 221 W by multiplying the difference between the average store temperature (51.6°C) and laboratory temperature (20°C) by the heat loss factor (7 W/degC). Hence losses from the pipework and buffer tank were assumed to be 279 W, a value which seemed reasonable.

6.5. Conclusions and Recommendations

A significant decrease (25%) in the performance of the heat pump during the off-peak charge period, caused by the increasing transfer fluid temperature, was observed.

The store discharge rate could be controlled to ±0.5 kW but due to flow reversal at the beginning of the discharge period it proved impossible to eliminate an initial peak as the rate approached its setpoint. However replacement of the original cold water pump with a pneumatic control valve on the mains water supply significantly reduced the period of the peak.

Despite inclusion of a heat loss term during non charge/discharge periods it was impossible to track the UF accurately for longer than a couple of days. This was thought to be due to accumulation of the experimental errors incurred in calculating the UF. Once the UF became inaccurate the experimental data was of limited use and therefore the runs had to be completed one day at a time which required careful and time consuming preparation to bring the store to steady state. Hence improved instrumentation or some alternative method of inferring the store condition is required.

Off-peak DHW heating was simulated during periods of high ambient by diverting excess heat pump output (>2 kW) to the plate heat exchanger when the transfer fluid temperature reached 63°C.

The experimental facility was capable of simulating a variable load determined from a dwelling loss coefficient, internal temperature setpoint and outside air temperature. This option was not employed in the test runs to simplify analysis of the performance data.

Heat losses of 500 W from the pipework and storage device were found to significantly reduce the COP of the integrated system.

Higher flow rates result in greater charge rates with identical COPs and a facility to increase flow rate as store becomes fully charged would prevent inefficient thermal cycling.

It had been hoped to evaluate various use strategies for the experimental

system but the random variation of ambient conditions and experimental error in controlling the load made this impossible to achieve. Effort was diverted instead towards developing computer models of the experimental system which could accurately simulate its performance for the actual recorded conditions. Once such a model was experimentally verified a researcher would have a very powerful tool with which to investigate potential integrated systems operated with a selected use strategy in a given type of dwelling.

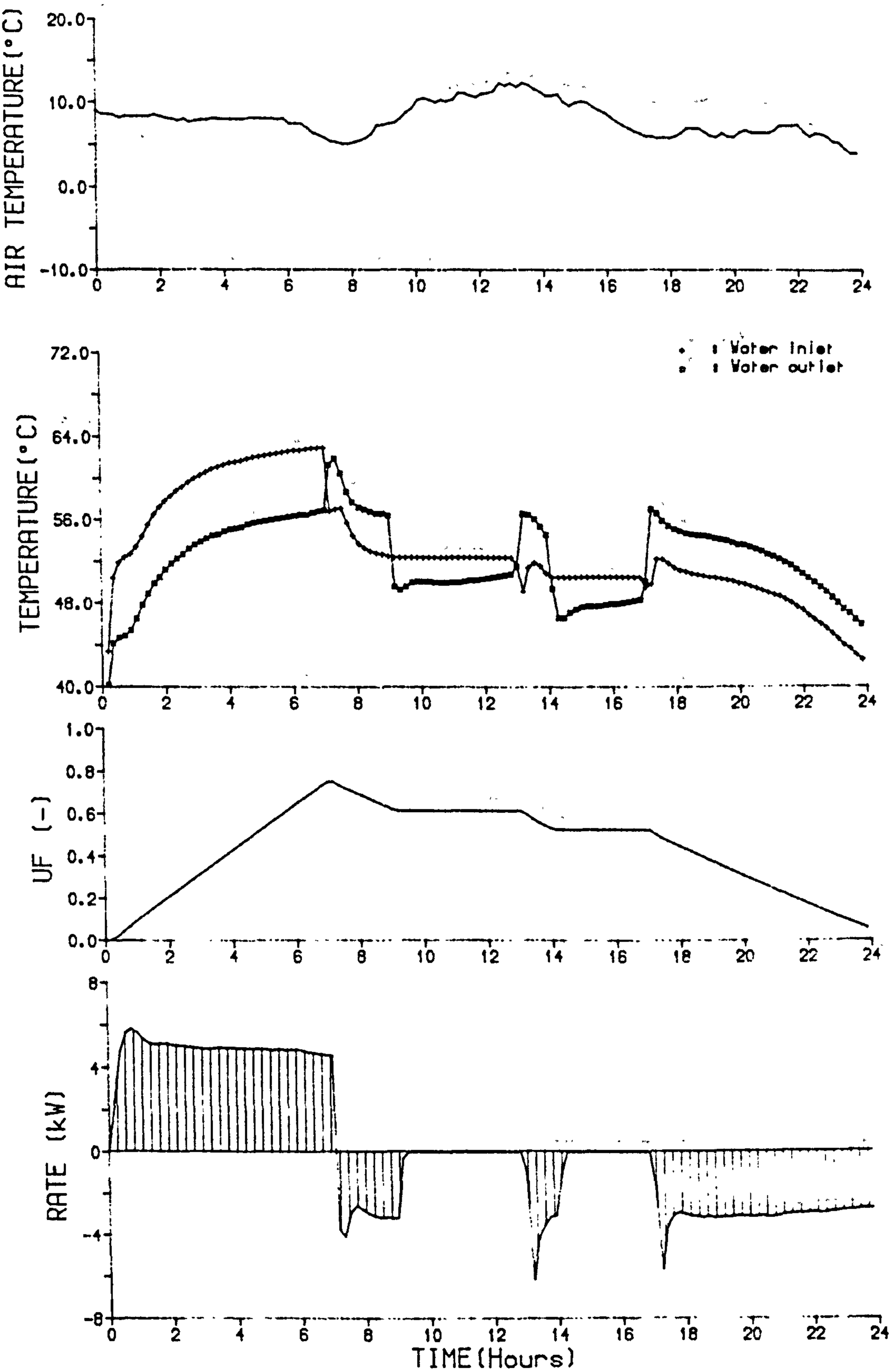

Figure 6.1 Performance of integrated system on 29/10/85

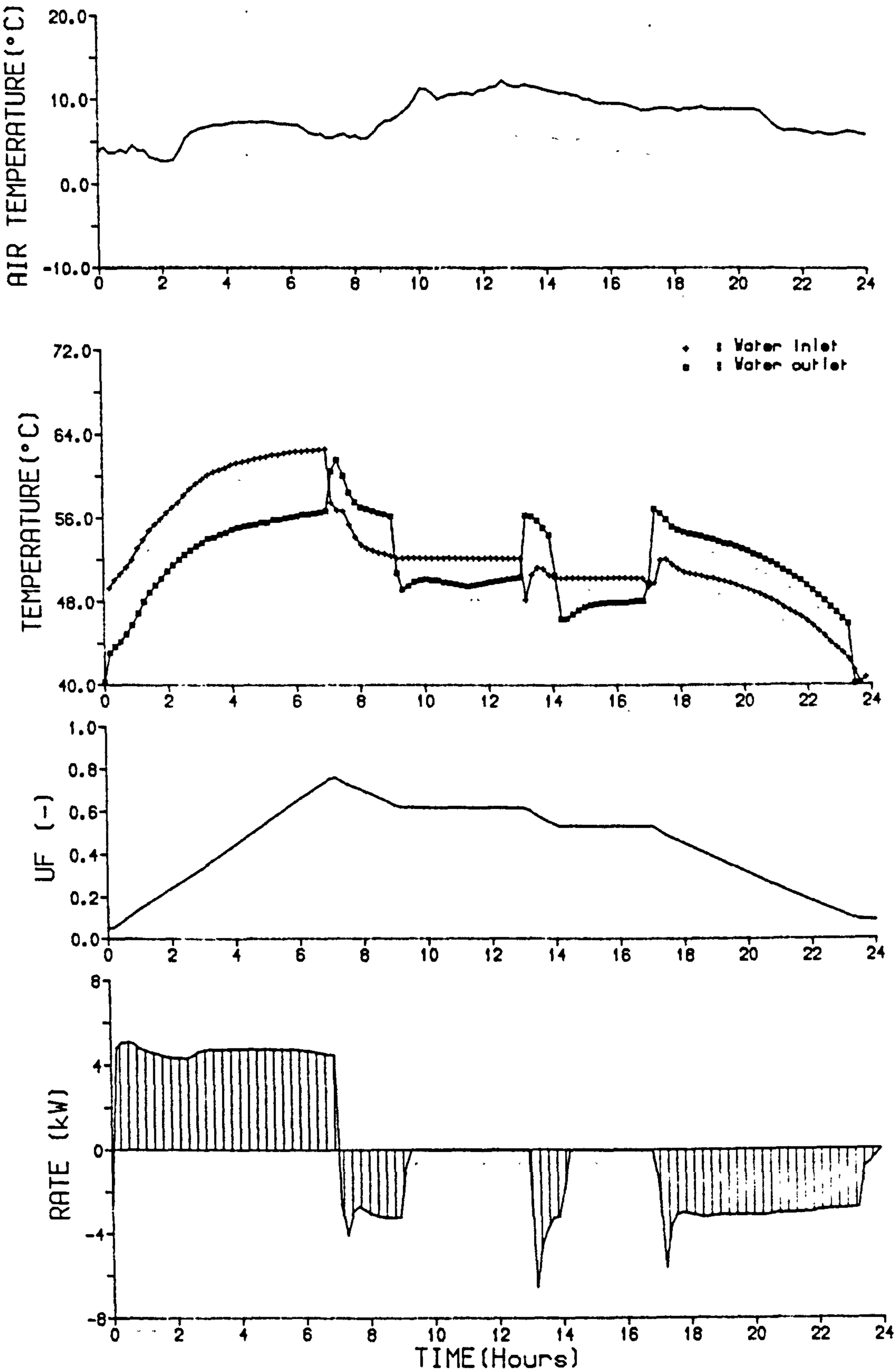

Figure 6.2 Performance of integrated system on 30/10/85

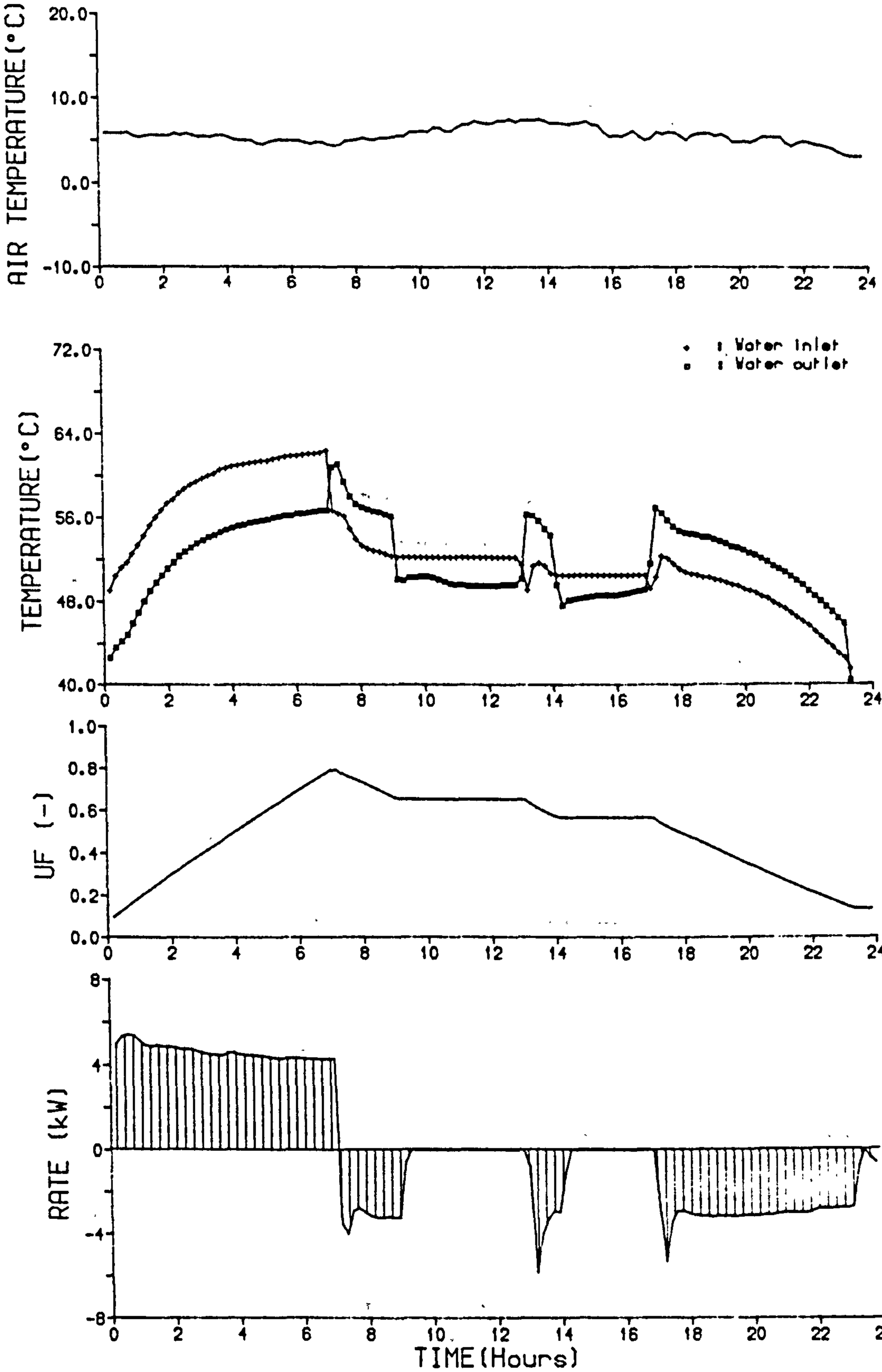

Figure 6.3 Performance of integrated system on 31/10/85

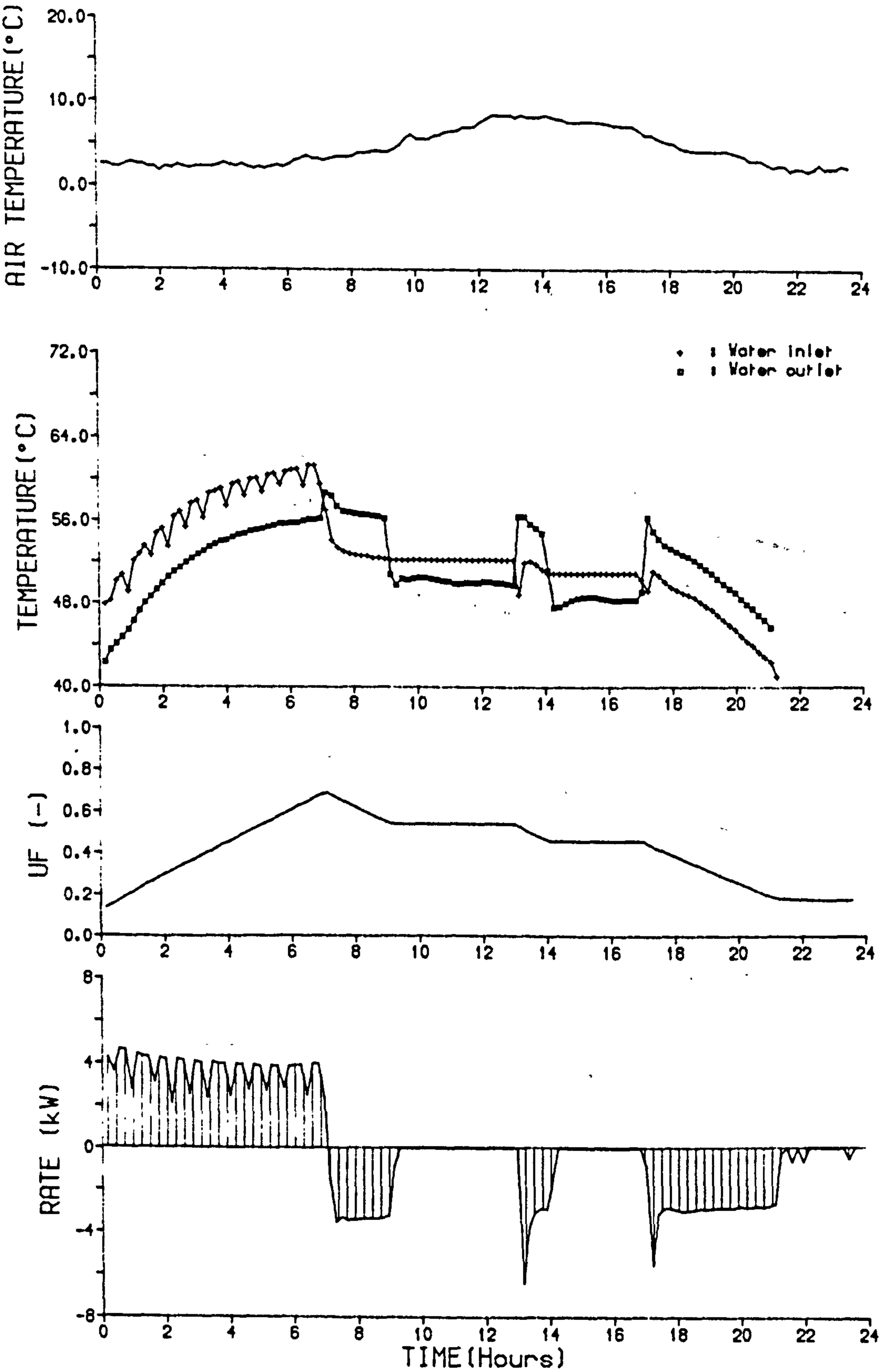

Figure 6.4 Performance of integrated system on 1/11/85

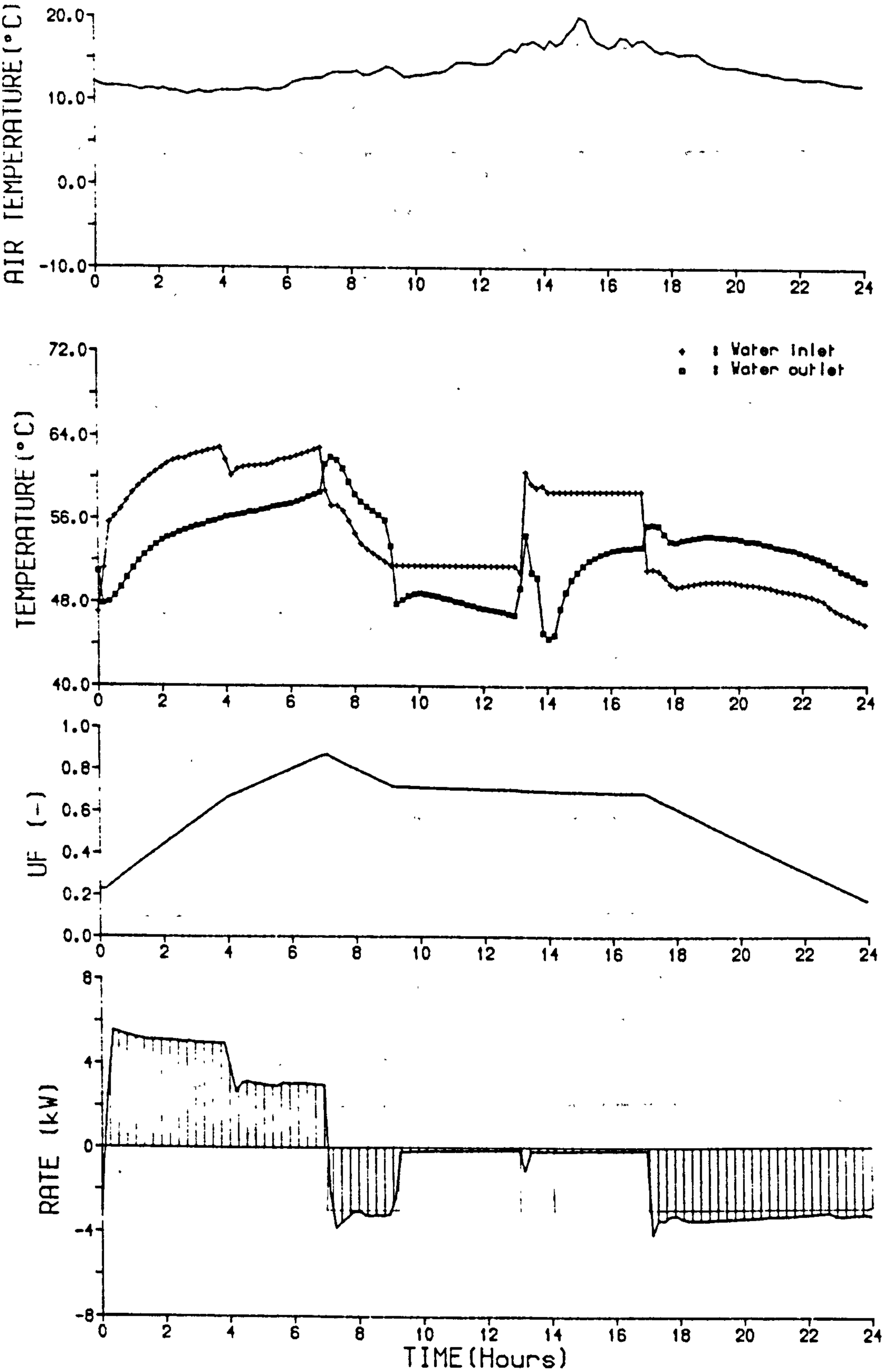

Figure 6.5 Performance of integrated system on 1/6/86

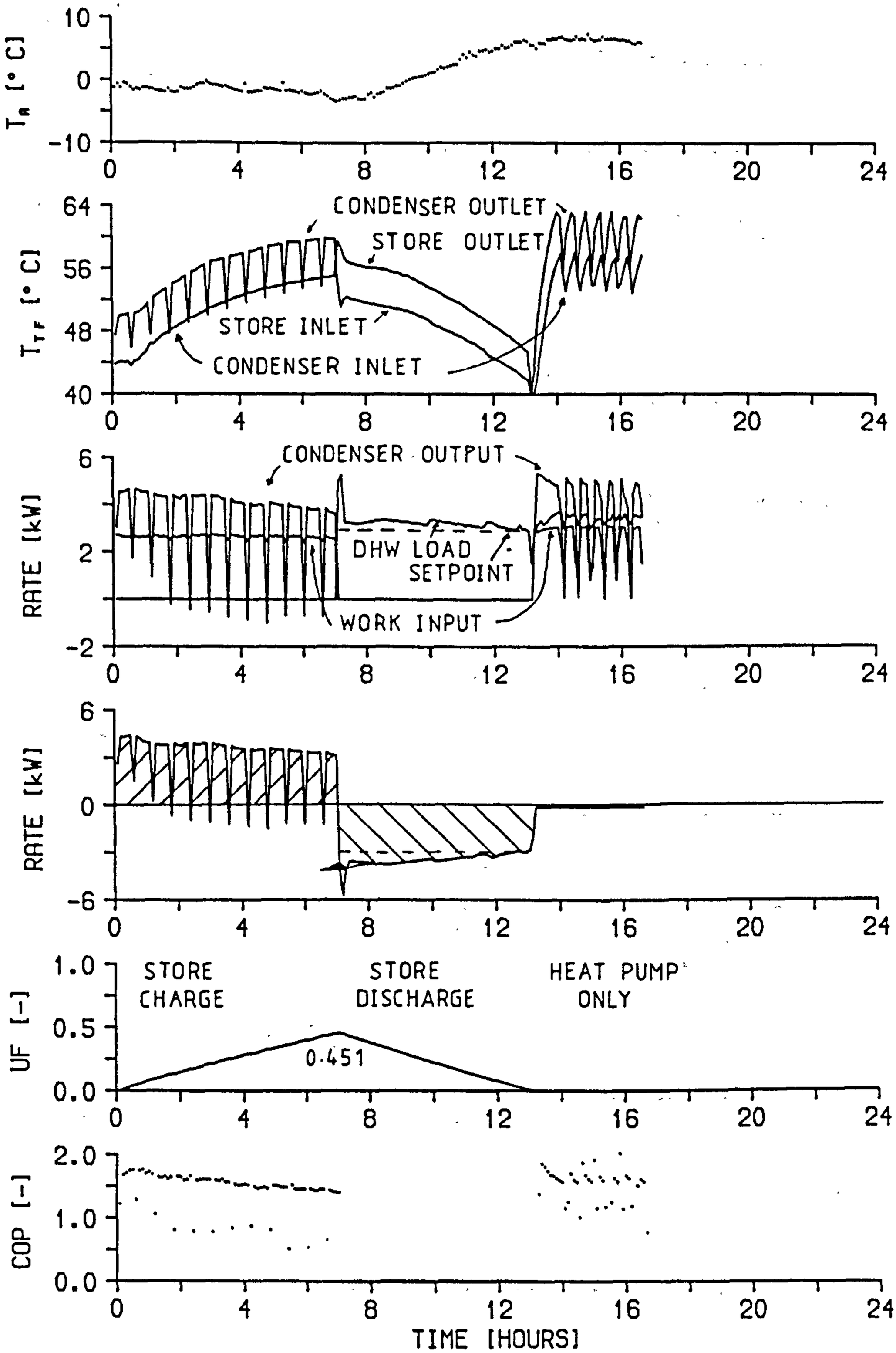

Figure 6.6 Performance of integrated system on 12/3/87

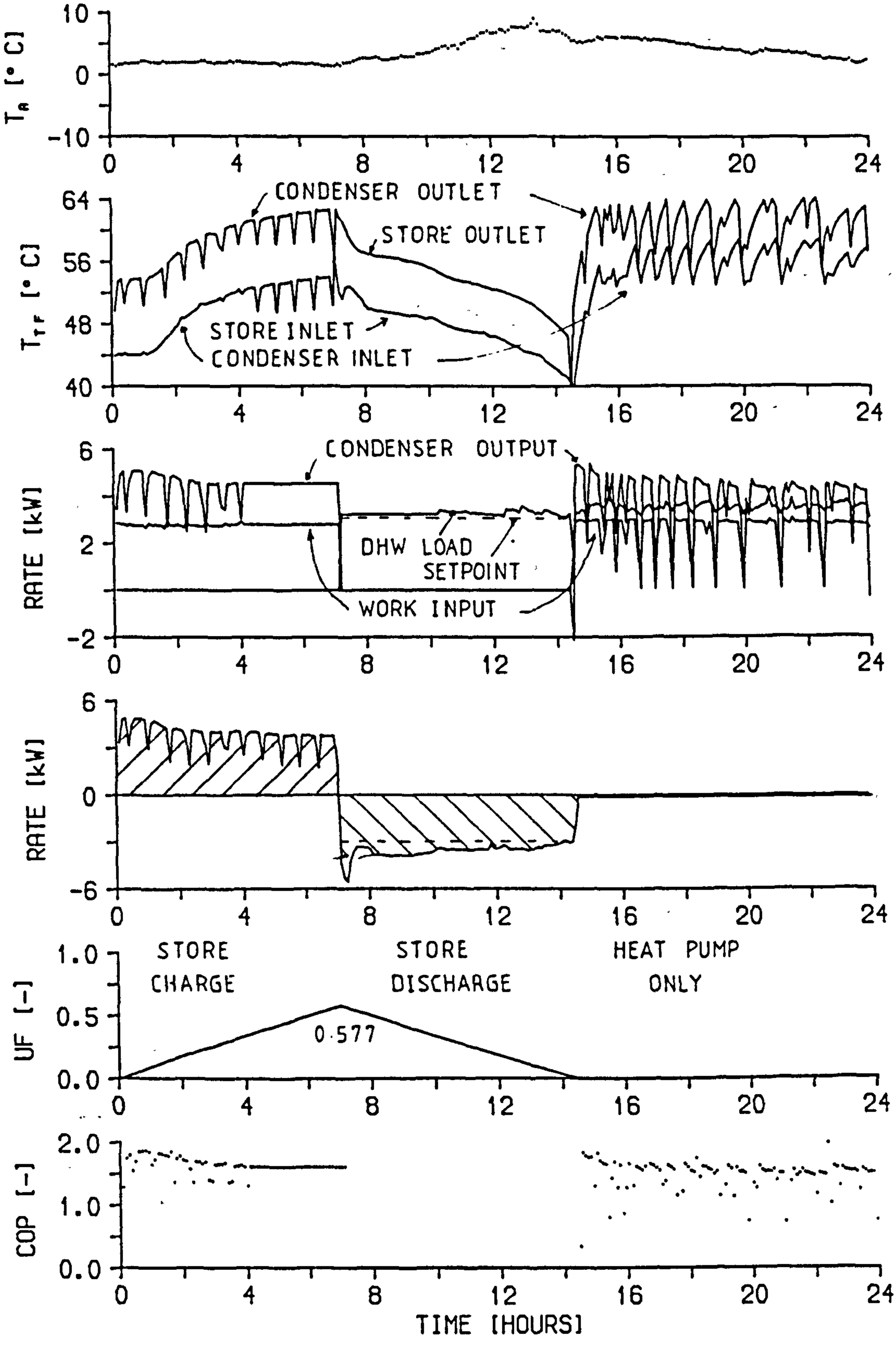

Figure 6.7 Performance of integrated system on 13/3/87

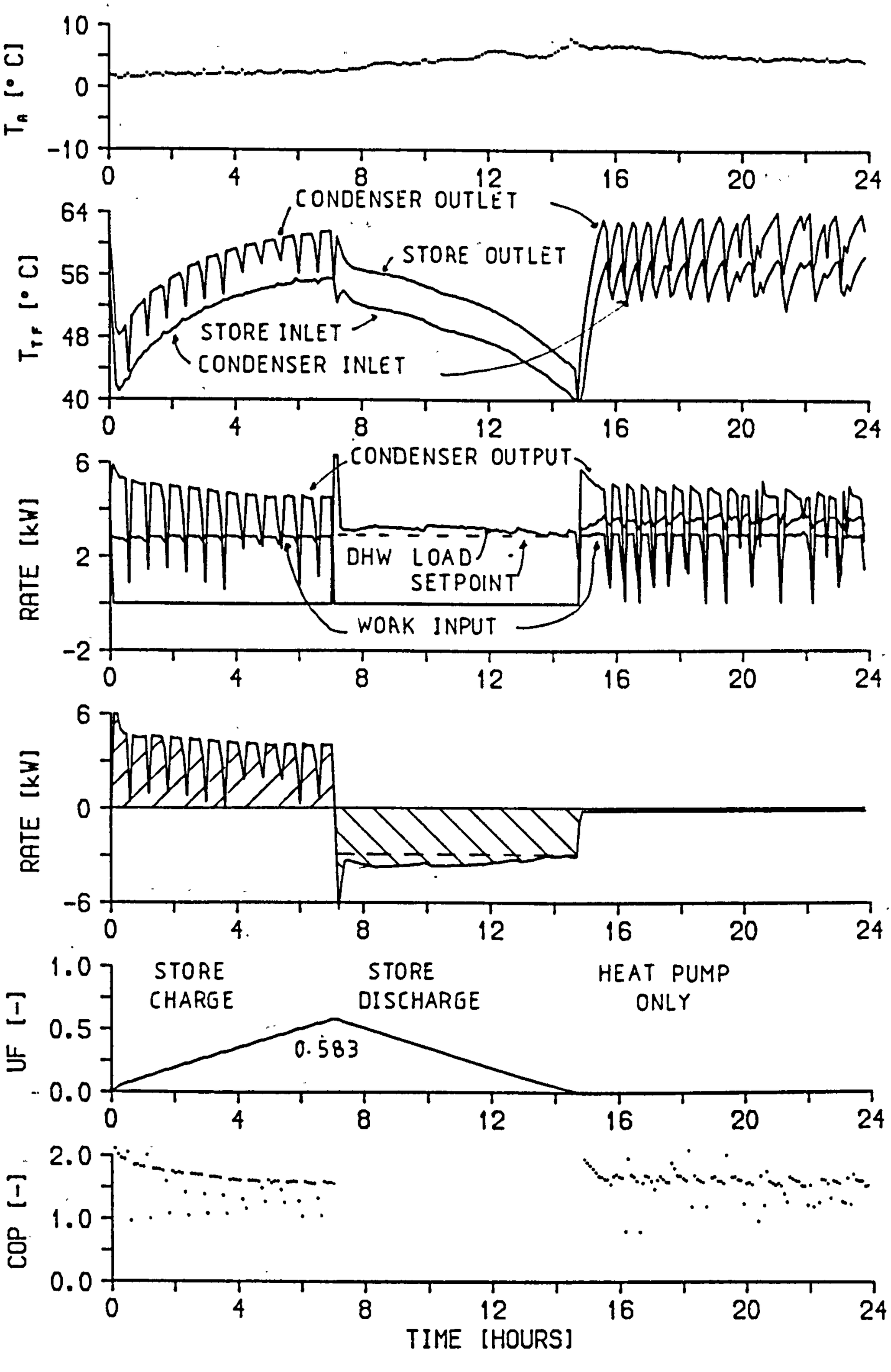

Figure 6.8 Performance of integrated system on 14/3/87

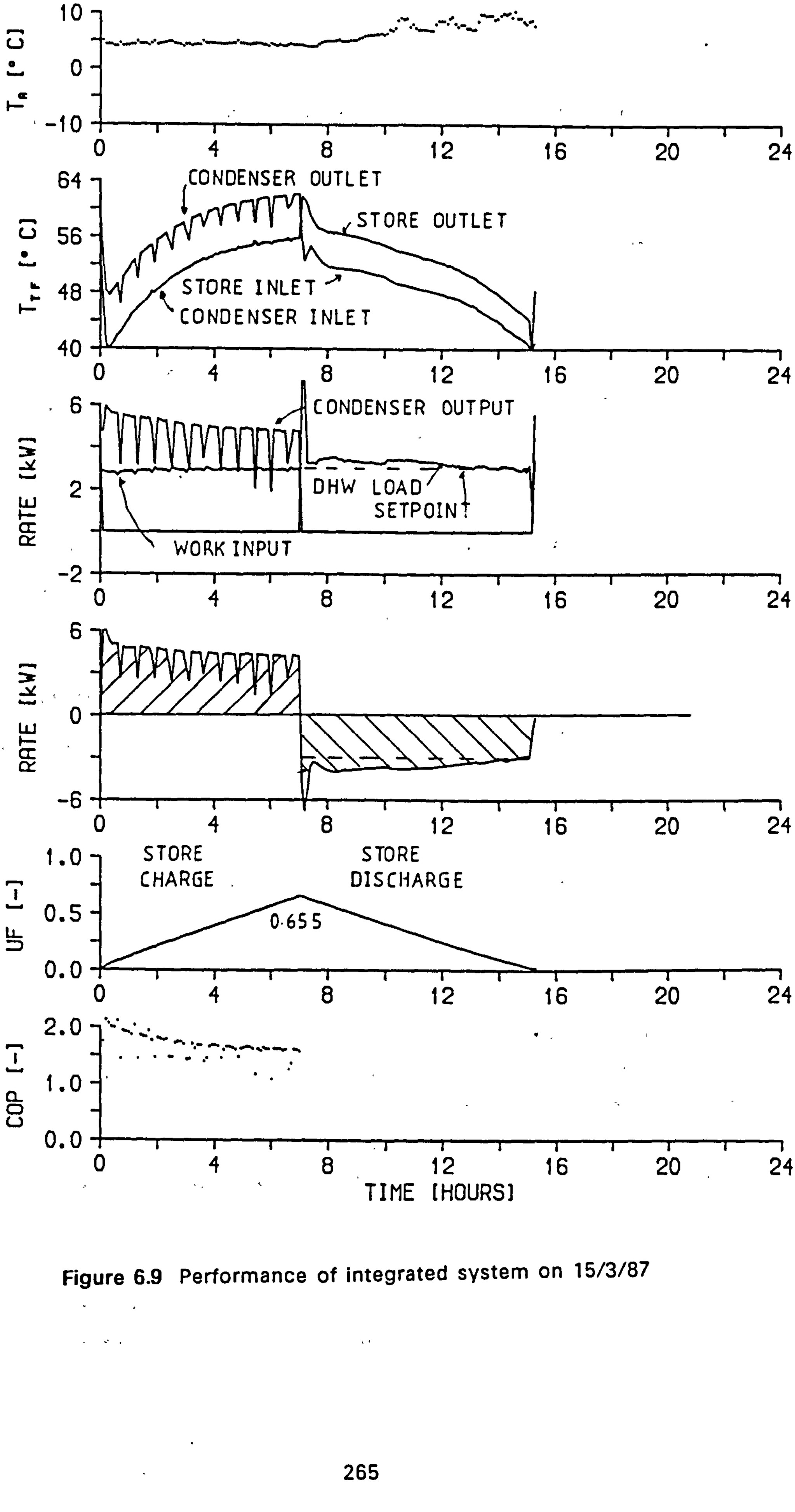

Figure 6.9 Performance of integrated system on 15/3/87

Table 6.1 Analysis of Experimental Integrated System Performance

		12/3	13/3	14/3	15/3
Charging store					
Charge period	[hours]	7.05	7.15	7.05	7.05
Average ambient temperature	[°C]	-1.6	1.7	2.1	4.4
Total power input	[kWh]	18.48	19.79	19.68	20.46
Final UF	[-]	0.457	0.577	0.583	0.655
Total charge[1]	[kWh]	20.29	25.62	25.89	29.08
Average COP	[-]	1.10	1.29	1.32	1.42
Initial COP (0030-0045)	[-]	1.76	1.86	1.86	2.00
Final COP (0645-0700)	[-]	1.40	1.61	1.56	1.61
Maximum condenser outlet	[°C]	59.8	62.6	61.6	62.1
Discharging store					
Discharge period	[hours]	6.15	7.25	7.75	8.15
Final UF	[-]	0.000	0.000	0.00	0.024
Total discharge	[kWh]	20.29	25.62	25.89	28.02
Total domestic heating load	[kWh]	19.89	23.80	25.31	27.11
Average domestic heating load	[kW]	3.23	3.28	3.27	3.33
Minimum store outlet[2]	[°C]	45.4	46.4	44.1	44.1
Heat pump only					
Heat pump only period	[hours]	3.5	9.55	9.05	0.10
Total domestic heating load	[kWh]	11.81	33.37	32.37	0.35
Total power input	[kWh]	8.48	24.24	22.81	0.32
Average COP	[-]	1.39	1.38	1.42	1.09
Average domestic heating load	[kW]	3.37	3.49	3.58	3.50

Notes:

1. For total TSC of 44.4 kWh (159.9 MJ)
2. For discharge rate greater than 2.5 kW

CHAPTER 7

MODELS FOR SIMULATING INTEGRATED SYSTEM

7.1. MODELLING HEAT PUMP SYSTEMS

Downing (1974) presented the equations necessary to calculate the thermodynamic properties of most refrigerants. Kartsounes and Erth (1971) developed a suite of programs to calculate the properties of refrigerants R12, R22, and R502. More recently, McMullan et al. (1985) produced a suite of computer programs suitable for calculating the properties of most refrigerants including R13B1. Unfortunately both programs were written in Fortran rather than the author's preferred language, IMP80. While it would have been possible to run these programs on the Edinburgh system, further development would have become unnecessarily complicated. Hence the constants and equations presented by Downing were employed as the basis for developing a package written in IMP80 to model the performance of a heat pump.

7.1.1. Development of Package

The first stage in developing the package was to write a program which would predict the saturation properties of a refrigerant. This allowed the individual routines to be checked and resulted in a program which was useful to other researchers in the department as a method of plotting pressure-enthalpy diagrams of common refrigerants.

The next stage was to further develop the program to calculate Rankine cycle COPs at specified condenser and evaporator temperatures. A simple correlation was then employed to relate the actual COP (quoted by the manufacturer) to the Rankine cycle COP.

To analyse the performance of the heat pump on a pressure-enthalpy diagram the program was developed to calculate the state point enthalpies and hence diagram COP from performance data obtained during test runs. This analysis yielded parameter values such as the adiabatic efficiency which characterised the actual heat pump performance.

The final stage of development was a program which predicted the heat pump performance for specified operating conditions. In addition to averaged values of the performance parameters, the only input required was the circulating transfer fluid temperature and the ambient air temperature. Copies of the programs included in the package are listed in section 9.2.3.

7.1.1.1. Prediction of thermodynamic properties

Downing (1974) presents equations to calculate the following basic properties of refrigerants:

1. Liquid density
2. Vapour pressure
3. Equation of state of the vapour
4. Heat capacity of the vapour

These four basic equations can be combined by exact thermodynamic relationships to calculate the properties employed in heat pump research:

1. Latent heat
2. Enthalpy of vapour
3. Entropy of vapour

Developing a program to determine the refrigerant properties is therefore a straightforward matter of writing routines to solve equations for each of the above properties. Since it was intended to use the equation of state primarily to determine the specific volume of the vapour, and the equation was explicit in pressure, a Newton Raphson technique (see Lennox and Chadwick, 1977) was developed as shown below

$$v^1 = v^0 - f(v^0)/f'(v^0) \qquad (7.1)$$

In the above, v^0 is the initial guess of the specific vapour volume. A first approximation was made using a re-arranged version of the equation of state including only the first term

$$v^0 = RT/P + b. \qquad (7.2)$$

This normally converged to the root very rapidly. However within 20°C of the critical temperature the method did not converge for all refrigerants. If a better approximation (obtained from tables) was used the method still performed satisfactorily even at the critical temperature. Hence a simple technique of evaluating f(v) for a maximum expected specific volume (at

-20°C) and decreasing in small steps until the function value changed sign was used to obtain a better initial guess. This method worked very satisfactorily and was incorporated into the routine and employed for temperatures within 20°C of the critical.

This first version of the program HPMODEL_CREFPROP prompts for temperature and refrigerant data file. The data base is a partitioned file with the specified refrigerant as member name, e.g. REFDATA_R502 contains values for all the constants used in the equations for refrigerant R502. All the equations are in Imperial units so the first step in the program is to convert the input temperature. The routines are then called in the same order as they are introduced above. In the section converting the output data into SI units the liquid enthalpies and entropies are calculated using the vapour properties, temperature and latent heat. The final step in the program is to produce a hard copy print-out of the data.

This version was further developed into HPMODEL_PHDATA which evaluates the pressure-enthalpy data for -20°C to the critical temperature at 10°C intervals. The output is a set of h,P data in a file PHDATA which can be used as input to a program HPMODEL_PHDIA to plot a pressure-enthalpy saturation curve on log-linear scales for any refrigerant.

7.1.1.2. Prediction of Rankine cycle COP

Tai et al. (1982) presented theoretical Rankine cycle COP data for heat pump systems operating with refrigerant R502. These values were listed in tabular form for a range of temperature lifts and associated condensing temperatures.

Figure 2.3 shows the operation of a vapour compression heat pump on both pressure-enthalpy and temperature-entropy diagrams. This ideal vapour compression cycle is often referred to as a Rankine cycle, and the COP defined as in equation (2.2). Since the compression in the cycle is assumed to be isentropic the enthalpy at state point 2 may be related to the saturated vapour enthalpy (h_{2sat}) at the condensing temperature

$$h_2 = h_{2sat} + (s_1 - s_{2sat})\, T_{co}. \qquad (7.3)$$

The program HPMODEL_RANKCOP prompts for selected evaporator and condenser temperature, and refrigerant. Saturation vapour and liquid properties are determined at both temperatures and the enthalpy of the superheated vapour discharged from the compressor is calculated according to equation (7.3). The Rankine cycle COP is then calculated using equation (2.2) and printed out with the refrigerant properties at the state points.

An actual COP is determined from a correlation relating the Rankine COP to that quoted by the manufacturer of the heat pump. For the purpose of this simple correlation the evaporating temperature was assumed to be 5 degC less than ambient and the condenser temperature equal to the water flow temperature. A third order polynomial was fitted to the data as reported below, and was employed to extrapolate the manufacturer's data to the experimental operating conditions

$$COP_A = 0.0107\ (COP_R)^3 - 0.2196\ (COP_R)^2 + 1.6488\ (COP_R) - 1.3740. \quad (7.4)$$

This actual COP, the pressure ratio and the Carnot COP (calculated from equation (2.1)) also form part of the output data from the program.

7.1.1.3. Analysis of heat pump performance

The primary aim in developing this package which could calculate refrigerant properties was to predict the actual heat pump performance accurately. By analysis of the actual cycle on a pressure-enthalpy diagram it is possible to determine parameters which characterise the performance of the heat pump. A program HPMODEL_EXPCOP was written which so analysed the experimental performance of the heat pump for any set of operating conditions.

The experimental values required as input to this program were:

1. State point temperatures T_1, T_2 and T_3 (see figure 3.10)
2. Condenser and evaporator saturation temperatures
3. Heat output from condenser
4. Power input to the heat pump (i.e. compressor and fan)
5. Ambient temperature
6. Mass flow rate and temperature of transfer fluid

Vapour entering the compressor in a real heat pump cycle is normally superheated by between 5 and 10 degC. Hence the enthalpy and entropy at state point 1 (see figure 5.3) are found by calculating the evaporator saturation pressure, the specific volume at point 1 and inputing these values to the enthalpy and entropy routines. The saturation properties of the vapour at the condensing temperature are calculated by the method outlined in section 7.1.1.1. The enthalpy at state point 2 for isentropic compression is found using equation (7.3). Actual enthalpy at the compressor outlet is determined by calculating the specific volume for T_2 and condenser saturation pressure and then employing these values in the enthalpy equation.

Prediction of the properties of liquid refrigerant is complex but may be simplified by the approach adopted by McMullan et al. (1985). They noted that the correlation expression for density does not change along an isothermal line. Hence it can be argued that Cv and h do not change along an isothermal line and that the isothermal lines will be vertical in the liquid region. This is not strictly correct but allows approximation of the liquid enthalpy and entropy at a given temperature to that determined for the saturation temperature. The enthalpy at state point 3 was then calculated as the saturation liquid enthalpy for a saturation temperature equal to T_3. A diagram COP could then be calculated by equation (2.2)

Adiabatic efficiency of the compressor is calculated from the following ratio

$$\eta_{ad} = (h_{2ad} - h_1)/(h_2 - h_1). \qquad (7.5)$$

Power input to the heat pump includes that delivered to the compressor and the fan. Since the fan power is constant at 90 W the work input solely to the compressor can easily be determined. An actual COP of the heat pump for comparison with diagram COP (defined as the heat output from the condenser divided by the work input to the compressor) can be calculated. The ratio of this actual COP to the diagram COP was used to determine the efficiency of the compressor's electric motor. Other straightforward parameter values which characterised the heat pump performance were calculated:

1. Condenser approach - difference between condenser saturation

temperature and transfer fluid temperature

2. Evaporator approach - difference between ambient temperature and evaporator saturation temperature
3. Degrees of superheat - difference between T_1 and evaporator saturation temperature
4. Degrees of subcooling - difference between condenser saturation temperature and T_3

The output from this program was output to a file EXHPDATA and then copied into a partitioned file HPDATA where the member name specified the test run number.

7.1.1.4. Prediction of real cycle performance

A program HPMODEL_REALCOP1 was developed which predicted the real cycle COP for a specified set of operating conditions. The required input to this program was:

1. Ambient temperature
2. Transfer fluid temperature and flow rate
3. Averaged performance data output from the experimental analysis discussed in section 7.1.1.3 (i.e. condenser and evaporator approach, degrees of superheat and subcooling, and the adiabatic and electric motor efficiencies)

The program firstly determines the evaporator and condenser temperatures and then T_1 and T_3. Next the saturation pressures at the condenser and evaporator are determined. The enthalpy and entropy at the state points and for saturation are determined by the method outlined in section 7.1.1.3. The predicted enthalpy of the vapour discharged from the compressor is found from a re-arranged form of equation (7.5)

$$h_2 = h_1 + (h_{2ad} - h_1)/(\eta_{ad}/100). \qquad (7.6)$$

Using these enthalpies the diagram COP can be determined from equation (2.2)

and the electric motor efficiency

$$COP = (h_2 - h_3)/(h_2 - h_1)\ (\eta_{em}/100). \qquad (7.7)$$

In order to calculate the actual heat output from the condenser the total power input to the heat pump has to be determined. It is known that the power input is a function of both the ambient and transfer fluid temperatures. Figure 7.1 shows the relationship between power input and flow temperature for data quoted by the manufacturer. Despite the limited data available it is permissable to derive a linear relationship between power input and flow temperature for each of the four ambient temperatures. The manufacturer's quoted data had a maximum flow temperature of 55°C and the linear nature of the relationship was utilised to graphically determine the power input at flow temperatures of 60 and 65 °C for each of the ambient temperatures. In figure 7.1(b) the relationship between power input and ambient temperature for a given flow temperature is clearly not linear but in each case was found to be well approximated by a second order polynomial.

A routine was written which calculated the power input for a given ambient temperature at flow temperatures of 50, 55, 60 and 65 °C. For a specified flow temperature the two curves either side of the specified value were used and the actual power input interpolated from these values.

Subtraction of the fixed fan power input from the total determined by the routine above yielded the compressor power input. This, multiplied by the diagram COP, gives the heat output from the condenser; and the actual COP may be calculated as the ratio of the heat out of the condenser to the total power input to the heat pump.

7.1.2. Results Obtained from Model

7.1.2.1. Prediction of thermodynamic properties

HPMODEL_CREFPROP was used to predict the thermodynamic properties of R12 over the range of possible operating temperatures. These values were then compared with data presented by Haywood (1978) in the form of a large pressure-enthalpy diagram. In table 7.1 the output from the program is

compared with that tabulated by Haywood for the lowest expected evaporating temperature (-20°C) and the highest tabulated saturation temperature (50°C). This table inspires confidence in the individual routines for prediction of refrigerant properties.

It wasn't as simple to perform such a thorough check with the R502 data since the available charts and tables were in Imperial units and used a different datum state for zero enthalpy and entropy.

The extended version of this program HPMODEL_PHDATA which calculates enthalpy-pressure data for saturation temperatures in the range -20°C to critical temperature in 10°C steps was used to plot figure 5.3.

7.1.2.2. Prediction of Rankine cycle COP

The Rankine cycle COP, tabulated in table 7.2, predicted by the model is almost identical to that presented by Tai et al. (1982). Also included in the table is the Carnot cycle COP defined in equation (2.1). Both COP_C and COP_R values for a condensing temperature of 65°C are presented since a high transfer fluid temperature is required to charge the store in an integrated system. Operation at high condensing temperature is seen to significantly lower performance i.e. a 12% decrease in COP_R is suffered by increasing condenser temperature from 60 to 65 °C at an evaporating temperature of 0°C.

A correlation relating COP_R to the actual COP (quoted by the manufacturer) was presented in section 7.1.1.1. This correlation is employed to predict the COP_A for a range of operating conditions and the results obtained are tabulated in table 7.3. The actual data employed to derive the correlation are included to allow the accuracy of the correlation to be approximated. From this data it is expected that the COP for a flow temperature of 65°C will fall below 2 at an ambient temperature of approximately 4°C.

7.1.2.3. Analysis of heat pump performance

Table 5.1 specifies the experimental conditions which were employed for the analysis. Table 5.2 presents performance parameter values for each run, along with an average value and maximum error bounds.

The difference between the maxima and minima are relatively large but since the mean lies in the middle of the range the maximum error is minimised.

7.1.2.4. Prediction of real cycle performance

In table 7.4 the thermal output and power input of the heat pump are tabulated for the experimental runs noted in table 5.1. This shows that, for a specified ambient and transfer fluid temperature, the maximum error incurred by employing the averaged experimental performance parameter values is ± 3.7%. Runs 4.4a and 4.5d have larger error bounds due to the effect of defrost cycling on heat pump performance.

A standard run was employed to investigate the sensitivity of heat pump performance to variations in the experimental performance parameter values. The mean British winter temperature is generally accepted to be 7°C and the maximum store charge rate is obtained with a limiting charge temperature of 63°C; hence these two values were employed in the standard run. This standard run used the averaged experimental performance parameter values (run 0). The best theoretical performance is found by letting each of the performance parameters equal the value necessary for the cycle to approximate the Rankine cycle (run 0a). The following runs consider the effect of varying each performance parameter individually according to the code nN where n is the parameter being investigated (θ_{cs} = 1 etc.) and N is defined:

- a, ideal value assumed
- b, existing value improved by 25% (relative to ideal value)
- c, existing value relaxed by 25% (relative to ideal value)

From table 7.5 it is obvious that the two efficiencies have the greatest impact on performance. Increasing the degrees of subcooling by 25% and decreasing the evaporator approach by the same amount both improve thermal output by approximately 4%. Decreasing the condenser temperature approach is much less significant, while changing the degree of superheat has no significant effect at all.

7.1.3. Discussion of Results

7.1.3.1. Prediction of thermodynamic properties

A derivation described by McMullan et al. (1985) yielded the following equation to predict the vapour specific heat at constant pressure.

$$Cp = Cv - T\,(\delta P/\delta T)_v^2/(\delta P/\delta v)_T \qquad (7.8)$$

This equation was evaluated in a routine included in the program HPMODEL_GAMMA. When the output data was compared with that derived for superheated vapour by Haywood (1978) it was found to be satisfactory (± 1%) for low pressures in the range 1.5 to 6.5 bara. However for a higher pressure of 12.5 bara it was found to over-predict the vapour specific heat by 5%. Some time spent finding the error in this program would extend the utility of the thermodynamic properties package.

It would also have been useful to further develop HPMODEL_PHDIA to plot and annotate the constant temperature lines in the saturated region of the pressure-enthalpy diagram. An interesting additional development to the package would be a program capable of determining and plotting the isentropic, isothermal and constant volume lines in the superheated region.

7.1.3.2. Prediction of Rankine cycle COP

Rankine cycle COP data can be employed as an aid in selecting a refrigerant for a particular application. Other design considerations (see section 2.1.2) must also be considered and saturation pressures, vapour density at compressor inlet and slope of saturated liquid line may all be found using HPMODEL_CREFPROP and HPMODEL_PHDIA.

A simulation of the heat pump performance may be achieved using the COP predicted by the simple correlation in equation (7.4). An expression like this is useful in the development of a model to simulate the performance of an integrated heat pump/ heat storage system.

7.1.3.3. Analysis of heat pump performance

The program HPMODEL_EXPCOP despite its simplicity is an extremly useful tool in comparing the performance of an experimental heat pump with a theoretically ideal cycle. However, further development would aid our understanding of the factors affecting heat pump performance and permit identification of areas for further improvement. The logical extension of the program would be to model each component of the cycle individually. For example the condenser could be modelled from correlations for heat transfer in tube-in-tube heat exchangers. If the experimental data verified this condenser model it could then be incorporated into HPMODEL_REALCOP1 to predict the heat pump performance over the complete range of possible transfer fluid flow rates and inlet temperatures.

It was hoped to examine the compressor performance in greater detail by calculating the individual compressor efficiencies. However this was thwarted by an inability to determine the specific heats at constant volume and pressure correctly.

7.1.4. Conclusions and Recommendations

A thermodynamics properties package (IMP80) was written which allowed the user to determine saturation properties of refrigerants R12, R22 and R502 at a specified temperature. This package was developed in a form suitable for expansion to include most refrigerants.

A program was developed which allowed the calculation of the Rankine cycle COP for a heat pump operating between two specified temperatures using refrigerants R12, R22 and R502.

Two programs were developed to analyse and compare the performance of real heat pumps relative to that predicted for a Rankine cycle. The first calculates parameter values which summarise the discrepancies between the cycles and the second predicts the performance of a heat pump for specified values of these parameters.

7.2. ANALYTICAL MODELS FOR SIMULATING STORAGE DEVICES

The first two subsections deal with analytical models of sensible and latent heat storage in a slab. These models were developed primarily to determine data which could confirm the accuracy of the finite difference techniques employed in the real time simulation of the Edinburgh store. The final subsection presents an approximate model which determines the rate at which the interface moves through the PCM and hence may be employed to predict charge/discharge rate against time or UF data.

7.2.1. Sensible Heat Storage in a Slab

7.2.1.1. Development of model

The theory employed in this model (see HSMODEL_ANXASESL in section 9.2.3) was presented in section 2.4.1.1. Equation (2.16) was used to calculate the unaccomplished temperature change (T*) as a function of time (Fo) and position within the slab (x*). The user can choose to present the temperature-time-position relationship in the general dimensionless form or dimensionally for a particular situation. If the latter is selected the slab material (ice, C58 or general metal), slab half thickness, total time of simulation, initial temperature and surface temperature must be specified. In both cases the program prompts for the number of nodes to be considered.

7.2.1.2. Results

The dimensionless output of the program is presented in table 7.6 for Fo in the range 0-2.

7.2.1.3. Discussion of results

The dimensionless data reported in table 7.6 was verified by comparison with a plot presented by McAdams (1954) to the limited accuracy achievable by such a plot.

7.2.2. Latent Heat Storage in a Semi-infinite Slab

7.2.2.1. Development of model

This model (see HSMODEL_ANXALASL in section 9.2.3) was based on the theory presented in section 2.4.1.2, assuming that the semi-infinite region was initially at its fusion point, which permits use of equation (2.32) to determine the root Λ. This region was considered to be a semi-infinite slab of thickness x_n where the right hand surface of the slab remained at its melting point over the freezing period considered. The slab thickness, material (again ice, C58 or general metal), number of nodes, Fourier number (determines time step size), surface temperature and total time are prompted for by the program. The metal properties correspond to those utilised by Murray and Landis (1959) and the program advises on the required input to allow comparison of the output data with that presented by Murray and Landis.

The root Λ of equation (2.32) was found using the routine BISEARCH which utilises a sectioning algorithm. Initial limits of the search were set to 0 and 1 and the accuracy was specified to be a difference of less than 0.01% on the value calculated by the previous sectioning.

7.2.2.2. Results

The output can be presented in Imperial units, SI units or in a dimensionless format. The first of these presents the interface position (feet) and the temperature excess (degF) over the melting point for each node position against time. In the Stefan problem considered by Murray and Landis (1959) the temperature excess was initially zero since the region was assumed to be at its melting point. A step decrease of 1000 degF in the boundary temperature occured at t=0 and the temperature excess above the melting point was recorded at 0.1 foot intervals until the interface penetrated the region to a depth of 0.8 feet. The thermal properties of the metal slab analysed by Murray and Landis are presented in section 9.1.2. Table 7.7 shows a sample output for comparison with the Murray and Landis data. The dimensionless form of the same data is presented in table 7.8 to allow comparison of this analytical solution with various finite difference approximations.

7.2.2.3. Discussion of results

The prediction of the interface position showed excellent agreement with the analytical solution plotted by Murray and Landis (1959). The temperature histories were much more difficult to confirm (due to the 1000 degF to 4 cm scale) but appear to be in good agreement.

7.2.3. Approximation for Latent Heat Storage in Various Geometries

7.2.3.1. Development of model

The theory on which this model is based is presented in section 2.4.1.3. In the program (see HSMODEL_ANAPSESL in section 9.2.3) the dimensionless time t* required for the interface to move radially inward is calculated from equation (2.47) and the time required for complete phase change from (2.48). The equivalent expressions for a slab

$$t^* = (1/Bi)(1-X^*) + 0.5(1-X^*)^2, \tag{7.9}$$

$$t^*_{X^*=0} = (1/Bi) + 0.5, \tag{7.10}$$

were taken from Seban and London (1945).

The user can select from three PCMs (ice, C58 or metal), two geometries (cylinder or slab) and can specify the cylinder radius (slab half thickness), number of nodes, ambient temperature and th heat transfer coefficient for the fluid film plus tube wall. A table of the dimensionless and dimensional interface position against time is output from the program.

The model was further developed to calculate the total rate of heat transfer per unit length for a cylindrical geometry (see HSMODEL_ANLAPPROX in section 9.2.3). This was found by summing the conduction and convection resistances of the solid or liquid PCM, the tube wall and the transfer fluid film, which gave an expression identical to equation (2.35) with an additional term to allow for the thermal resistance of the tube wall

$$\hat{q} = (T_{mp}-T_a)/[\ln(r_{wi}/r_i)/2\pi k_{PCM} + \ln(r_{wo}/r_{wi})/2\pi k_w + 1/2\pi r_{wo}h_{wo}]. \tag{7.11}$$

It is often useful to express the above as

$$\hat{q} = U_{wo}A_{wo}(T_{mp}-T_a), \qquad (7.12)$$

where U_{wo} is the overall h.t.c. based on the outside area of the tube and A_{wo} is the outside area per unit length of tube. Comparison of equations (7.11) and (7.12) yields the following expression for the overall h.t.c.

$$U_{wo} = 1/[(r_{wo}/k_{PCM})\ln(r_{wi}/r_i) + (r_{wo}/k_w)\ln(r_{wo}/r_{wi}) + 1/h_{wo}]. \qquad (7.13)$$

Several methods of determing the outside film h.t.c. h_{wo} were reviewed in section 2.4.3.

In this simple model it was assumed that each tube is represented as a solid block of PCM, i.e. the liquid phase behaves as a solid phase, but with different thermal properties. Since approximately 70% of the TSC is latent heat (see chapter 3), the driving force for heat transfer was approximated to the difference between the charge/discharge temperature and the phase change temperature. It was assumed that during charge the phase change interface moved radially inward and could therefore be related to the UF. Hence a UF of 0.5 implied that half the PCM had undergone phase change and the phase change interface diameter could be calculated from the square root of the area ratio

$$D_i/D_{wi} = \surd(A_i/A_{wi}) = \surd(1-UF). \qquad (7.14)$$

During charge, the maximum rate will occur for a UF of 0. As the UF tends to 1 the charge rate will approach 0.

7.2.3.2. Results

The output from the approximate model, for simulation of the experimental runs 8.12C and 8.16C (see table 4.1) in the pilot store, is presented in table 7.9. In this simulation the film heat transfer coefficient was calculated by the method presented by Dwyer and Berry (1970) for fully developed in-line flow over a rod bundle (see section 2.4.3.2). An alternative method of determining the heat transfer coefficient (described in section 2.4.3.3) where the channel formed between the tubes was approximated to a pipe was also employed in the simulation runs. In figures 7.2 to 7.5 the output determined by both

methods is shown and the following observations noted on the agreement between the model and experimental results:

1. The pipe model most closely approximates experimental results for a store comprised of 38 mm tubes
2. A much smaller difference exists between the two models for a store comprised of 25 mm tubes
3. The discrepancy between experimental charge and discharge; top-down and bottom-up performance is more significant with 25 mm tubes
4. Neither model simulates the initial maximum in both charge and discharge profiles or the minimum in the discharge performance described by the experimental results

Charge rate against time and UF curves predicted by the approximate model for a prototype store based on 25 and 38 mm tubes are presented in figures 7.6 and 7.7. For an inlet temperature of 60°C and a mass flow rate of 0.192 kg/s it was found that the charge rate fell below 5 kW at a UF of only 0.775 for the 38 mm tubes, while utilisation of 25 mm tubes guaranteed a minimum charge rate of 5 kW up to a UF of 0.983.

7.2.3.3. Discussion of Results

(a) General

During both charge and discharge the experimental rate profiles describe a maximum immediately after the start of the test period. This peak is due to the sensible heat of the transfer fluid initially in the store and was discussed in section 4.5.2.1. During discharge this maximum is followed by a minimum at a UF of 0.27-0.4. This is caused by subcooling of the PCM and was discussed in section 4.4.2. No attempt was made to simulate either of these characteristics in the approximate model.

It is interesting to calculate the maximum theoretical overall heat transfer coefficient for a negligible thermal resistance in the fluid film. This is found by assuming that h_{wo} is infinite which causes the last term in equation (7.13) to tend to zero. Substituting the other values for a UF of 0.91 (see table 7.9)

into the equation yields an overall h.t.c. of 30.2 W/m^2K giving a maximum possible improvement on the value predicted by Dwyer and Berry (1970), and confirmed experimentally in figure 7.3, of 15.8%.

There is therefore little scope for improving the limiting heat transfer rate by modifying the flow channels in the store. In comparison, increasing the thermal conductivities of the tube wall and PCM by 50% would improve the heat transfer coefficient by 8.1% and 26.8% respectively. Consequently research effort should be directed at improving the effective thermal conductivity of the PCM, perhaps by the use of a copper wire mesh, a technique successfully employed by Kopecky (1984) at Cranfield.

(b) Calculation of film h.t.c.

Although the overall performance (at the end of a charge or discharge period) is relatively insensitive to small changes in the value of the fluid film coefficient it is important to note the following limitations of the approximations made in this simulation.

(i) Calculation of equivalent diameter

Consideration of figure 3.2 shows that the tubes in the pilot store were not arranged in a regular equilateral triangular array. In many cases the channels formed were bounded by four or even five tubes. This would have the effect of increasing the equivalent diameter, and hence decrease the heat transfer coefficient for constant Nu. The heat transfer coefficient would also decrease using the pipe approximation, since in the Sieder and Tate correlation (see equation (2.105)) $Nu \propto De^{0.667}$.

(ii) Effect of natural convection

The experimental charge rate against UF profiles for the pilot store comprised of 25 mm tubes distinctly show the expected characteristics of mixed convection heat transfer, described in section 2.2.7.4. When the buoyancy forces are in the same direction as the external flow (i.e. fluid being cooled in top-down flow), heat transfer is enhanced and is greater than that predicted by either model. However when the buoyancy and external forces act in opposite directions (i.e. fluid being cooled in bottom-up flow), heat transfer is reduced and is less than that predicited by either model.

The dimensionless group $Gr_{De}Pr(De/L)$ will be a linear function of the temperature difference (ΔT) between the bulk of the fluid and the wall for any channel (fixed equivalent diameter) and specified operating temperature range (defines fixed thermal properties). For example, operating a thermal storage device between 48 and 64°C (properties evaluated at 56°C) with channels having an equivalent diameter of 7.154 and 8.428 mm yields

$$Gr_{De}\ Pr\ (De/L) = 158.8\Delta T, \qquad (7.15)$$

$$Gr_{De}\ Pr\ (De/L) = 306.0\Delta T, \qquad (7.16)$$

for 25 and 38 mm tubes arranged in a regular equilateral triangular array with a pitch of 27 and 40 mm respectively. Since the thermal conductivities of the transfer fluid and the PCM are similar then even considering conductive heat transfer alone, the temperature drop between the bulk fluid and the tube wall will only be a small proportion of the temperature difference driving force ($T_{in}-T_{mp}$). For the experimental conditions reported in figure 7.3 the Reynolds number was found to be 129. In figure 2.26 it can be seen that a $Gr_{De}Pr(De/L)$ of at least 500 would therefore be required before mixed convection effects would be expected to become significant. This would correspond to a temperature difference between the fluid bulk and the tube wall of approximately 3 degC for the 25 mm tubes. A slightly lower value of 2 degC was deduced in the same fashion for the 38 mm tubes.

Since the difference between bottom-up and top-down operation is more pronounced in the store comprised of 25 mm tubes (indicating more significant natural convection effects), it was thought that the required temperature difference to initiate mixed convection would be lower. However from the above analysis this is obviously not the case and the exact effect of natural convection in the pilot store therefore remains a mystery.

(iii) Assumption of uniform surface temperature

In electrically heated rods it is reasonable to assume that the heat flux will be axially uniform, and that for a high thermal conductivity cladding the circumferential temperature will be constant. For the flow of a condensing fluid such as steam through a pipe the surface temperature is generally assumed to be constant. For the PCM filled tubes, the approximate model

assumed that both the circumferential and axial surface temperature of the tube was uniform.

Since the temperature drop across the store is approximately 2 degC (for a heat transfer rate of 1 kW at a flow rate of 0.117 kg/s) the assumption of uniform axial wall temperature is of questionable validity. Despite attempts to guarantee a minimum gap of 2 mm between tubes (see chapter 3) numerous tubes were not straight and were therefore in contact with their immediate neighbours. The temperature of the tube surface in contact with a neighbouring tube will not respond to an increase in transfer fluid temperature at the same rate as the free surface. Hence it is dubious whether it can be assumed that a uniform circumferential surface temperature exists.

(iv) Selection of most appropriate film h.t.c.

For a Reynolds number of 129, in the store comprised of 25 mm tubes, and with a Prandtl number of 3.23, fully-developed velocity and temperature profiles are established 4.6 and 15.0 cm from the duct inlet. Since the duct length is 1 m the Nusselt number determined by Dwyer and Berry (1970) for fully developed flow over rod bundles should be used to calculate the film h.t.c.

(c) Application of results to design of prototype store

The approximate model was developed primarily as an aid for designing the prototype storage device. At that time the finite difference model was not available and the selection of 25 mm tubes was based on the results of the approximate model. The prototype storage device required:

1. A minimum charge rate of 5 kW
2. A maximum charging period of 6 hours (to allow house pre-heat or production of DHW for 1 hour during off-peak period)
3. As low a charging temperature as possible, preferably less than or equal to 60°C (to improve COP and prevent refrigerant/oil breakdown)

For stores comprised of both 38 and 25 mm tubes the agreement between predicted and experimental charge rates was poor but acceptable (± 30% for

0.4 < UF < 0.95) given the experimental errors and previously discussed limitations of the model.

Since the predicted performance presented in figures 7.6 and 7.7 was considered to represent the maximum possible charge rate, a prototype store based on 25 mm tubes was selected to ensure that a minimum charge rate of 5 kW could be maintained for the entire off-peak period. If the same performance had been predicted by a more detailed model it is possible that the decision would be reversed. This is because the 38 mm tubes have an additional 33% heat storage capacity per unit volume which means that even utilisation of only 77.5% of its heat content represents an effective TSC 3% greater than that of the 25 mm tubes. The final choice would require evaluation of economic considerations such as the relative costs of the raw materials and encapsulation.

7.2.4. Conclusions and Recommendations

An exact analytical solution was found for a sample problem of latent heat storage in a slab and verified with data presented by previous workers.

An approximate model satisfactorily simulated (± 30%) the performance of the pilot storage device and was then employed to select 25 mm tubes for the prototype storage device. This model made no attempt to include sensible heat effects or subcooling of the PCM. It was shown that mixed convection flow could not account for the experimentally observed difference between top-down and bottom-up flow.

7.3. FINITE DIFFERENCE MODELS FOR SIMULATING THERMAL STORAGE DEVICES

The first subsection presents two solution methods, the explicit and Crank Nicolson semi-implicit techniques, for modelling the sensible heat storage in a slab. These models are then developed in the following subsection to include latent heat storage. In the final subsection an explicit solution technique with derivative boundary conditions was developed to model the actual store in cylindrical coordinates. This was then further refined to include the longitudinal temperature gradient in the flow channels formed between the tubes in the prototype store.

7.3.1. Sensible Heat Storage in a Slab

7.3.1.1. Development of model

The FDEs used in the explicit model HSMODEL_FDEXSESL (see section 9.2.3) were derived in section 2.4.2.2. Two initial conditions were included in the program

$$T^*=x^* \quad \text{for} \quad 0<x^*<=1, \tag{7.17}$$

$$\text{or} \quad T^*=1 \quad \text{for} \quad 0<x^*<=1, \tag{7.18}$$

where the former allows comparison of the output data with examples presented by Smith (1978) and the latter with the output from the analytical solution presented in section 7.2.1. The boundary conditions are specified as $T^*=0$ at the surface $x^*=0$ and by symmetry, see equation (2.68), at $x^*=1$. The routine EXFDSOL calculates the new temperature at node $1<i<N$ using equation (2.67), and at the central node N using equation (2.68).

The user is firstly prompted for the Fourier number and the number of nodes. There is no exit condition on the value of Fo so that the user can obtain an unstable solution for $Fo>0.5$ for demonstration purposes if desired. Since the solution is in a dimensionless form (slab half thickness $x=x_n$, $x^*=1$) the number of nodes specifies δx^* and hence δt^* is fixed by Fo and δx^*. The user is then prompted for the total run time (t^*) and print-out details.

The FDE used in the Crank Nicolson solution technique is also derived in section 2.4.2.2. In this program HSMODEL_FDCNSESL (see section 9.2.3) the

Fourier number is specified as 1 which was reported to combine good accuracy with reasonable computer time. If a Fo of 1 is substituted into equation (2.69) then the coefficients a,b and d in the set of equations (2.70) may be determined. In the model these coefficients are specified in the routine INPUTDATA, as -1,-1,4 for the general node $1<i<N$. At node N on the axis of symmetry $T^*_{N+1,j+1}=T^*_{N-1,j+1}$ and hence the coefficients are specified as 0,-2,4. For the node next to the slab surface $T^*_{0,j+1}=T^*_{0,j}$ which allows this term to be included on the r.h.s. of the expression and the coefficients specified as -1,0,4. A tridiagonal matrix algorithm, described in section 2.4.2.2, is employed in routine TDMA to solve the algebraic set of equations formed at each time step. The r.h.s. of equation (2.69) for a Fo of 1 reduces to the simple expression $T^*_{i-1,j}+T^*_{i+1,j}$ for nodes $1<i<N$. At the central node $T^*_{N+1,j}=T^*_{N-1,j}$ which for a Fo of 1 reduces the r.h.s. to $2T^*_{N-1,j}$ while at node 1, adjacent to the surface the r.h.s. will become $2T^*_{0,j}+T^*_{2,j}$. The user has the same options as those described for the explicit method with the exception of selecting a Fourier number.

7.3.1.2. Results

Table 7.10 shows the output of the explicit method for the second initial condition with a Fo of 0.5, 1 and 0.2. The effect of doubling the number of nodes on accuracy is shown by using 10 nodes in the second run with a Fo of 0.2. Table 7.11 presents the output of the Crank Nicolson method for a Fo of 1 with both 5 and 10 nodes.

7.3.1.3. Discussion of results

Table 7.10(a) shows the explicit solution for the limiting value (0.5) of Fo. This solution oscillates (see exact analytical solution in table 7.6) about the true solution without becoming unstable. The solution required 50 cycles and produced a maximum error of 7.3% at $t^*=1$. A Fo of 1 was shown in part (b) of the table to result in an oscillating solution which became unstable. Reducing the Fo to 0.2 produced a non-oscillating solution shown in part (c) of the table which had a significantly lower error of 1.2% but required a much larger (125) number of cycles. Table 7.10(d) shows that the error can be further reduced to 0.3% by doubling the number of nodes at the expense of quadrupling the number of cycles.

The Crank Nicolson solution technique offers much greater accuracy for considerably less computer effort. Table 7.11(a) shows that there is a maximum error of <1% for only 25 cycles at t*=1. Doubling the number of nodes further reduces this error to 0.3% but again quadruples the computer effort.

7.3.2. Latent Heat Storage in a Semi-infinite Slab

7.3.2.1. Development of model

The explicit and semi-implicit models developed in section 7.3.1 were modified to include latent heat storage. Since it was intended to compare the output with that produced by the analytical solution in section 7.2.2 the boundary condition at the centre node had to be modified. The PCM was initially at its melting point T*=1, and since the phase change front moves into the liquid the right hand boundary must always be maintained at its fusion point. This was achieved by specifying a slab thickness $x=x_n$, $x^*=1$ greater than the maximum expected movement of the phase change front in the time interval being considered. This boundary condition was easily incorporated into the explicit solution technique by using equation (2.67) for nodes $1<i<N$ and $T^*=0$ and $T^*=1$ for nodes 0 and N respectively.

In the semi-implicit technique, the value of the coefficients a,b and d at node N-1 were specified as 0,-1,4, while the r.h.s. of equation (2.69) for a Fo of 1 reduced to $T^*_{N-2,j}+2T^*_{N,j}$ since $T^*_{N,j+1}=T^*_{N,j}$. Hence routine TDMA was modified to solve N-1 simultaneous equations with N-1 unknown values at each time step.

In both solution methods the temperature arrest technique described in section 2.4.2.3 was utilised to model the phase change effect. After the new temperature for each node had been calculated, any node whose predicted temperature was greater than the melting point was reset to the fusion temperature until its latent heat capacity had been removed. This equivalent phase change temperature defined in equation (2.71) was specified as 0.5 units for the sample problem presented by Murray and Landis (1959).

7.3.2.2. Results

The dimensionless output predicted by the explicit solution technique for a Fourier number of 0.2 utilising 16 nodes is presented in table 7.12(a). Selected output is also presented for the same Fo with 8, 40 and 80 nodes in parts (b), (c) and (d) of the table respectively. The predicted output for the Crank Nicolson technique utilising a Fo of 1 with 40 nodes is shown in table 7.13(a). Sample output for a solution with only 8 nodes is presented in part (b) of the table.

7.3.2.3. Discussion of results

The predicted dimensionless temperature shown in table 7.13 for the four solutions with different numbers of nodes were compared with the exact solution presented in table 7.8. At t*=0.125 the maximum error for a Fo of 0.2 with 16 nodes was found to be less than 1.2%. Halving the number of nodes (reducing the number of required cycles by a quarter) significantly increases the error, especially in the region undergoing phase change, and particularly for short times (see t* = 0.015625). From parts (c) and (d) it can be seen that the error can be effectively reduced to zero as the number of nodes is increased. It should be noted that doubling the number of nodes quadruples the number of cycles required by the solution. If 160 nodes are used the solution is slower than real time!

The Crank Nicolson solution for a Fo of 1 with 40 nodes required 25% more cycles than the explicit solution for a Fo of 0.2 with 16 nodes, but yielded no improvement in accuracy. Reducing the number of nodes to 16 produces a solution requiring 25% fewer cycles than an explicit solution with a Fo of 0.2 and 8 nodes, which had a lower overall error (approx. 3% at t*=0.125) but was consistent in the region close to that undergoing phase change.

From the above results for latent heat storage it appears that the semi-implicit approach does not offer a saving in computation time to achieve a specified accuracy as it did for sensible heat storage. The explicit method involves prediction of a nodal temperature in a forward stepping process. When a node begins to change phase, its temperature can be adjusted to the fusion value before proceeding to temperature predictions of neighbouring nodes. In the semi-implicit method however, the nodal temperatures are

predicted simultaneously. Consequently those nodes experiencing phase change are in reality overpredicted, and these values in turn affect the accuracy of the predicted temperatures of neighbouring nodes.

7.3.3. Simulation of Edinburgh Prototype Storage Device

7.3.3.1. Development of model

The theory on which this model (HSMODEL_FDEXLACY2) is based was presented in section 2.4.2.4

(a) Data input and output

The user is prompted:

1. To select the PCM, for thermal property data
2. For encapsulation and storage device details; viz. radius of PCM cylinder, thickness and thermal conductivity of tube wall, cross sectional area and height of storage device, number and length of tubes, and voidage in each tube
3. For run parameters; viz. initial UF, flow direction, transfer fluid maximum or minimum inlet temperature and mass flow rate, initial temperature of PCM, film heat transfer coefficient and total run time
4. For model parameters; viz. number of radial and axial nodes, and Fourier number
5. For print-out specifications; viz. number of radial and axial nodes, and desired time interval between print-outs
6. For initial conditions in store

Property data available to the model includes C58, ice and the metal investigated by Murray and Landis (1959). A facility is provided to allow the data requested in sections (2) to (5) above to be entered from a user specified data file so that variations in performance due to a single parameter might be easily investigated.

For comparison with the experimental data (presented in section 4.3) the desired initial conditions will normally correspond to all temperatures in the store being set equal to the initial steady state temperature requested by (3).

However during integrated system operation the initial conditions are unlikely to correspond to a steady state condition, e.g. charge after an incomplete discharge. Hence a facility to allow the user to specify a data file containing the initial conditions was provided. This file must contain the number of radial and axial nodes (which replace those specified by (5) if necessary), the transfer fluid temperature, and the PCM temperature and condition radially inward at each axial node. The condition of each node is recorded as a value between 0 and PCT (see definition of PCT in section 2.2.6.3), where 0 corresponds to a pure solid phase and PCT to a pure liquid phase.

The output from the program can be printed to the screen or to a user specified file. A similar choice is offered for the final temperature and condition of the nodes, so that the output from one run may be used as the input to the next, an essential facility for modelling the integrated system.

(b) Calculation of derived data and stability check

Once the Biot number has been calculated the user specified Fourier number is compared with the r.h.s. of equations (2.80) and (2.81) and the simulation stopped with a warning message if the Fo was found to be too large. The TSC of the device was found from the total weight of PCM and transfer fluid in the store and the appropriate latent and specific heats. Since the former was determined from the internal volume of the tube and the density of the PCM, an average voidage had to be determined from the quoted weight of PCM in each tube.

The transfer fluid capacity rate, conductance and heat capacity were calculated from equations (2.83), (2.84) and (2.85). The conductance was determined assuming that all the voidage occured at the top of the tube. Hence the effective length of tube available for heat transfer in EQ2PC was found from (1-void) times the actual tube length. Since it was desired to predict the store outlet temperature accurately, the volume of fluid in each element ($A_f \delta z$ in EQ2PD) was approximated to the total volume of transfer fluid in the storage device divided by the number of axial nodes. These values were then substituted into equations (2.87) and (2.88), and if the time step and axial step size were too large (therefore causing instability in the solution) a warning message was printed out and the simulation stopped.

(c) Actual program procedure

The inlet temperature is calculated from its value at the previous time step plus the heat input rate (either from heating elements or heat pump) divided by the transfer fluid heat capacity. If this value exceeds the maximum or minimum inlet temperature specified by the run conditions it is modified appropriately.

Since the transfer fluid nodes are located equidistant on each side of the PCM surface node (see figure 2.24) the fluid temperature T_a required in equation (2.76) was calculated from the average of the two adjacent nodes. The new temperature of the transfer fluid is known at the node upstream of the PCM surface node but the temperature at the previous time step has to be used for the node downstream in calculation of the average value. The simulation then moves radially inwards through the PCM employing the appropriate FDE. (2.74) or (2.78) for boundary or central nodes respectively. The new transfer fluid temperature at the node immediately downstream of the PCM surface node is then calculated from equation EQ2PC and the procedure with the radial nodes repeated. The cycle is continued until the store outlet is reached at which point the heat transfer rate between fluid and PCM is determined from the transfer fluid temperature drop across the store and its capacity rate. This is multiplied by the time interval and added to the total energy content of the tubes, so that the overall condition (i.e. UF) can be monitored.

7.3.3.2. Results

The predicted charge and discharge rate against UF and time for the standard run (see * in table 4.4) was plotted against the experimental results in figures 7.8 and 7.9. Note that in figures 7.8 to 7.13 the experimentally determined utilisation factor has been scaled to ensure that a fully charged condition has a UF of 1 rather than 0.93, and similarly a complete discharge a UF of 0 rather than 0.07. In figures 7.10 and 7.11 the response of the model to a change in the inlet temperature was compared with the experimental data of runs 16.2, 13.2, 10.3, 18.3 and 16.3. Figures 7.12 and 7.13 show the predicted output of the model over a range of flow rates and compare the data with experimental results from runs 12.2, 16.2, 11.2, 12.3, 10.3 and 11.3.

The predicted charge and discharge rate of stores comprising 25 and 38

mm tubes is presented in figures 7.14 and 7.15. The data was determined for standard run conditions.

Finally the predicted inlet and outlet temperature for both charge and discharge is compared with experimental data for the standard run in figure 7.16.

7.3.3.3. Discussion of results

(a) General

It was essential to scale the experimentally determined UF to allow the accuracy of the simulated output to be assessed. In chapter 4 it was noted that the final UF corresponded to a negligible heat transfer rate and indicated that the calculation of the TSC was the probable source of error. If this is assumed to be the case then scaling of the UF for comparison with the model data is an acceptable procedure.

All the predicted performance data is extremely sensitive to the thermal properties employed by the model for the PCM, transfer fluid and encapsulation materials. For example, the 2°C difference between the melting point of the pure sodium acetate trihydrate and that deduced for the phase stabilised mixture would have a dramatic effect on charge and discharge rates.

The sensible heat capacity effects of the tube walls and store cabinet are not included in the model since their total contribution is only 3% of the TSC. It would be possible to include the sensible heat of the tube wall by employing an effective thermal conductivity and specific heat for a boundary node comprised of both polypropylene and PCM. An effective specific heat for the transfer fluid could be defined to include the sensible heat capacity of the storage device walls.

An explicit finite difference technique was employed by the model since the semi-implicit method was shown to be unsatisfactory for latent heat storage in section 7.3.2. The solution was kept stable by employing a Fourier number of 0.2. The results presented in figures 7.8 to 7.13 were all achieved using 10 radial and 8 axial nodes. Decreasing the step sizes by employing 20 radial and 20 axial nodes resulted in negligible difference to the predicted output but caused a dramatic increase in required CPU time. A 10-hour

simulation utilised approx. 500 CPU seconds and took approximately two and a half times that period to run in background mode. Hence simulation of the storage device over a 24-hour period would require 1200 CPU seconds and take 50 minutes to run in background mode, which seems reasonable for detailed simulation work.

The method of including the voidage in the tubes was clumsy and inconsistent. Although it was assumed that no PCM was contained in the top of the tube, the results were presented with the total height of the store approximated to the level of PCM contained in the tubes. Hence the transfer fluid temperature does not show the expected (for voidage only at top) constant temperature region at the top of the store.

During the experimental testing of the prototype storage device the maximum heat input from the heating elements varied between 6 and 7 kW. Hence a value of 6.5 kW was specified for the simulation runs. The heat removal rate during an experimental run was not a constant but dependent on the store outlet temperature, cold water inlet temperature and flow rate. A maximum cooling rate of 8.2 kW could be achieved for a store outlet temperature of 64°C (approach of 0.5 degC, cold water flow rate of 3.5 lit/min and inlet temperature of 20°C). For an outlet temperature equal to the phase change temperature, the rate of heat removal decreases to 6.22 kW. Hence the value of 6.5 kW employed in the simulation approximated the experimental conditions well once the initial sensible heat period (1.5 hours) had passed. This variation in the maximum rate of heat removal by the test facility was thought to account for the poorer agreement between experimental and predicted output for discharge than that achieved during charge. The actual rate of heat removal during the run could have been predicted from the store outlet temperature employing an assumed cold water flow rate and inlet temperature, but was considered an unnecessary complication.

(b) Mode

During both charge and discharge the predicted output was mostly found to be greater than that for either top-down or bottom-up mode (see figures 7.8 and 7.9). It was expected that, because of free convection effects, use of the heat transfer coefficient for fully developed flow in a rod bundle (153.1 W/m^2K) would result in the predicted rate falling between that found

experimentally for the two modes. Therefore the experimental results indicate that when free convection opposes forced flow the heat transfer coefficient is reduced more than it is increased for both forces acting in the same direction.

To assess the significance of the heat transfer coefficient on overall performance, the simulations were repeated with values ± 25% of the actual value. The predicted output was found to remain almost identical to the original data. Hence the reduction in heat transfer coefficient must be extremely large to cause the discrepancy observed experimentally between the two modes.

(c) Inlet temperature

Lowering the charge inlet temperature results in a decrease in the predicted charge rate after the initial sensible heat period (UF>0.2). For an outlet temperature remaining approximately equal to the phase change temperature this charge rate should be approximately constant at 3 kW. The experimental profile does not describe the predicted rapid decrease at UF=0.2 to a constant rate region, although the slope does become less steep as it passes through the predicted profile at UF=0.5.

If the discharge inlet temperature is increased to 50°C both the experimental and predicted output describe a constant rate region (0.2 < UF < 0.7), although the predicted rate (4 kW) is significantly greater than that found experimentally (3 kW). A complete discharge is achieved in the simulation, while in the experimental run a significant amount (20%) of the stored heat is still unreleased at the end of the discharge period. The model predicts virtually no difference in performance for inlet temperatures lower than 46°C, since the maximum rate of heat removal (6.5 kW) is possible down to a UF of 0.15.

(d) Flow rate

As has been discussed previously in (c) above, the experimental charge rate profiles do not describe the constant rate region expected for a latent heat storage device. Consequently as is shown in figure 7.12, the model underpredicts the rate for UF < 0.5 and overpredicts the rate for UF > 0.5. Despite this error the effect of flow rate on the performance of the store

predicted by the model is in good agreement with the experimentally determined trend.

For low flow rates (0.133 kg/s) the model overpredicted the discharge rate for 0.05 < UF < 0.75 by approximately 20%. For higher flow rates (>= 0.192 kg/s) both experimental and model results showed that the design maximum rate of heat removal (6.5 kW) from the store was possible down to a UF of 0.15.

(e) Tube diameter

The maximum charge rate achievable by stores comprised of 25 and 38 mm tubes is very similar for a period of 5.5 hours with the 25 mm tubes giving a slightly better performance. However after 7 hours the 38 mm tubes have a charge rate of 4.8 kW, a performance significantly better (by 33%) than the smaller diameter tubes. Maximum discharge rates are achieved by both tube sizes for the first six hours. The extra storage capacity of the 38 mm tubes allows continuation of this performance for another hour while the discharge rate of the 25 mm tubes rapidly drops to zero.

(f) Temperature profiles

During charge the predicted outlet temperature rapidly rises and remains constant (for approx. 3 hours) at the phase change temperature. The experimentally recorded outlet temperature however, initially rises rapidly but its rate of increase falls off before reaching the phase change temperature. This suggests a greater sensible heat storage effect than that predicted by the model. After four hours the agreement between the model and experimental data was extremely good.

The discharge inlet and outlet temperatures predicted by the model were significantly greater (2°C) than those found experimentally although the actual profiles were very similar in character. No allowance however was made in the model to account for subcooling, known to be significant in the 25 mm tubes, which causes a trough in the experimental profiles.

7.3.4. Conclusions and Recommendations

The Crank Nicolson solution method for solving FDEs offered much greater accurac/ for similar computer effort than the explicit technique of modelling sensible heat storage in a slab.

For latent heat storage in a semi-infinite slab the Crank Nicolson solution method was found to be less accurate than an axplicit technique for similar computer effort. This is because the former method predicts all the nodal temperatures simultaneously, therefore overpredicting the temperature of nodes experiencing phase change which in turn affects the accuracy of the predicted temperatures of neighbouring nodes. Consequently an explicit FDE solution technique was employed to simulate the prototype storage device.

No significant improvement was recorded by increasing the number of radial and axial nodes from 10 and 8 respectively. A ten hour simulation required 1200 CPU seconds and typically took 50 minutes to run in background mode.

Inclusion of mixed convection heat transfer effects in the model failed predict the experimentally determined difference between top-down and bottom-up flow.

The constant rate regions expected from a latent heat storage device are much less pronounced in the experimental results than in the simulted data, however the agreement for the standard run is reasonably good. This agreement remains reasonable for a range of operating flow rates and inlet temperatures.

7.4. ELEMENTARY MODELS OF INTEGRATED HEAT PUMP/LATENT HEAT STORE

A simple model was developed to predict the overall performance of an integrated heat pump latent heat store. This model was constructed as an aid to optimising the design of a system for a particular application, and to demonstrate the potential savings achievable over a conventional heat pump. An improved version of this model was developed to simulate more closely the Edinburgh integrated system and details of modifications made and results obtained are presented in section 7.4.5.

7.4.1. Development of Program

7.4.1.1. Ambient temperature input

In this model (HPHSMODEL_ELVERS1) the ambient temperature can be:

1. Set equal to the average monthly temperature
2. Cycled through the same diurnal temperature cycle for each day in a month (the first day is normally selected)
3. Cycled through an experimentally recorded temperature for every hour of the heating season

The simplest method of analysing the performance of any heat pump system is to assume an average monthly temperature. Tassou et al. (1981) presented a typical set of temperature data and this was utilised in method (1). This technique will produce the desired variation in seasonal performance but will lack the data necessary on the diurnal cycle which is considered to be significant. Evans (1985), a research student at Cranfield Institute of Technology, utilised experimental weather data recorded for each hour in a 250 day heating season for a model developed in his M.Sc. thesis. This ambient temperature data for days 1-134 and 250-365 (where January first equals day 1) was employed in methods (2) and (3) noted above. In (2) the missing data was assumed to be identical to that recorded at the start and finish of the heating season, i.e. if day$<$192 then data for day 134 was used while if day$>$192 then data for day 250 was employed. Since it was hoped to compare the output data from this work with that produced at Cranfield, method (3) set the ambient temperature for days outwith the heating season equal to the inside set point temperature.

7.4.1.2. Other input

To permit detailed analysis without excessive computer print-out, the output from the model can be presented in three different formats. The first presents the hourly performance of the system for one day in each month (usually the first). A summary of the daily performance is achieved using the second while the third presents the monthly performance with annual totals and averages.

Armor (1981) reports that off-peak tariff electricity is normally available from midnight to 7am. Since the local electricity board advised that it is actually available from 11pm to 7.30am, a facility to select either off-peak period was included.

In developing this model it was simplest to assume that the heat demand period corresponded to the period during which off-peak electricity was unavailable. However personal experience suggests that in a large number of dwellings the demand actually closely follows the movements of the occupants. Hence, in the model, heating periods corresponding to either of the on-peak electricity tariff periods or to an occupancy between 7am-9am, 1pm-2pm and 5pm-midnight could be selected.

The model was developed so that the seasonal performance of a heat pump alone could also be investigated. This allowed a comparison to be made with the integrated system and the potential benefits evaluated. It was considered to be beyond the scope of this project to make detailed comparisons with other conventional forms of heating. Several researchers including Kernan and Brady (1977) have already completed detailed comparisons between heating systems utilising heat pumps and those based on conventional fuels.

Six parameters were identified which characterised the performance of an integrated system and were thus prompted for as input to the model. The heat loss from the building

$$q_L = (UA)_L\ (T_{set}-T_a), \tag{7.19}$$

was determined from the first two; heat loss coefficient and the inside set

point temperature. The former is dependent on the construction of the building (see section 2.1.4.1) and the latter is dependent on the individual occupant and also to a certain extent on the construction. The third and fourth parameters are the sizes of the two primary components; the store and heat pump. Storage capacity is specified in kWh while the heat pump size is defined as its thermal output at -1°C. The final parameter is the cost per unit kWh of on and off peak electricity, which are only subject to slight variation between generating boards. However, including these parameters allows evaluation of the potential benefits for different tariff structures.

7.4.1.3. Operating modes

Three operating modes were utilised to simulate the integrated system operation:

1. MODEA where the heat pump alone supplied the required load
2. MODEB which represented the store being fully charged by the heat pump
3. MODED where the load was supplied solely by discharging the store

In MODEA and MODEB the thermal output from the heat pump was determined using a correlation for the COP, power input and a scaling factor for the design output of the heat pump at -1°C. MODEA then calculates the building heat loss using equation (7.19) and determines the dwelling load in kWh. If the heat pump can supply the load, then the required heat pump output and power input in kWh are determined. It was assumed that the heat pump could be cycled on/off up to 8 times an hour to allow it to supply loads less than its steady state output. If the heat pump is incapable of meeting the load then the required auxiliary power input (to an electric resistance heater) is calculated. The cost for a time interval was determined from the total power input to the heat pump and auxiliary heater using the appropriate electricity tariff.

After calculating the heat pump thermal output MODEB calculates the maximum attainable charge rate, from a simple function of the UF. If this charge rate is less than the thermal output of the heat pump then it is assumed that the required heat pump output is achieved by cycling. To

prevent overcharging of the store the routine predicts the store condition if it was charged at the rate calculated above. If the predicted UF>1 then the rate is adjusted until it would just totally charge the store (i.e. to UF=1). The necessary heat pump output and power input in kWh are then determined and the latter is used with the appropriate electricity tariff to calculate the cost. A record is made of the thermal input to the store and the store condition updated. Since any charging of the store increases the UF a flag (set at 1 for a store incapable of supplying the design load) is reset to zero.

MODED checks the store condition and if UF<=0 a flag is set to 1, indicating that the store cannot meet the required load. When the flag is set to 1 the system exits MODED and returns to the control section of the program which will then call MODEA (i.e. use the heat pump alone to supply the required load). A theoretical discharge rate was again determined from a simple function of the UF. The building heat loss was calculated from equation (7.19) and if the discharge rate is lower than this then the flag is again set to 1. A third check is made to ensure that the store could sustain the required discharge rate for the duration of the time interval. Failure for this condition again results in the flag being set to one. The dwelling load in kWh is then determined, a record made of the store thermal output, and the store condition updated.

7.4.1.4. Control philosophy

This is best represented on a flow diagram as shown in figure 7.17. The interaction of the three operating modes can be observed.

7.4.1.5. Output data

The output data is presented in the form of a table with the hourly, daily or monthly averaged COP and ambient temperature; final UF (at end of period); and the required load, auxiliary heating, store input and output and heat pump output and input.

7.4.2. Results from Integrated System Simulation

The following set of conditions and assumptions were employed in the first attempt to simulate an integrated system. These results were included in a paper (Cooke and Pritchard, 1986) presented at the World Congress III of

Chemical Engineering in Japan.

Heat loss factor = 380 W/degC (7.20)

Inside temperature setpoint = 20°C

Store size = 44 kWh

Heat pump output (at -1°C) = 6kW

Cost of peak period electricity = 4.4 p/kWh

Fractional cost of off-peak electricity = 0.40

Ambient temperature = monthly average reported by Tassou et al. (1981)

Off-peak period = 0000 - 0700 hours

Heating period = 0700 - 2400 hours

COP = 2.28 + 0.04625 T_a

Power input = 3 kW

Store charge rate = 25 - 20*UF (UF >= 0.75), = 10 (UF < 0.75)

Store discharge rate = 5 + 20*UF (UF <= 0.25, = 10 (UF > 0.25)

The effect of store size, heat pump size, heating requirements and cost of electricity on the predicted annual running cost for integrated and heat pump only systems was investigated and the results are presented in table 7.14.

7.4.3. Discussion of Results from Integrated System Simulation

7.4.3.1. Discussion of simulation employing simple assumptions

In the analysis of these results note that run A1 approximates the integrated system developed at Edinburgh, while run A3 was performed utilising the heat pump alone. From these predicted costs it is apparent that the integrated system offers cost savings of £140.80 (or 36.1%) over a straightforward heat pump. However the actual cost savings after accounting for the additional capital cost of the storage device are significantly lower and are considered in greater detail in section 7.4.4.

Increasing the size of the store from 5-55 kWh (runs A15, A10, A9, A6, A1

and A5) results in the expected increase in the potential cost savings. However during the coldest months, December to February, where the ambient temperature is <5°C, the maximum output of the heat pump during the off-peak period will be 7.5 kW for 7 hours or approx. 53 kWh. As the ambient temperature increases, the heat pump output will also increase but the load will decrease; hence for an ambient temperature of 12°C the heat pump output during the offpeak period would be approx. 60 kWh but the load only approx. 52 kWh. Therefore the maximum useful size of store for this particular size of heat pump with this load requirement is approximately 55 kWh.

Decreasing the size of the heat pump from 6 kW to 4.5 kW (run A8) reduces the cost savings. This is mainly because the heat pump can no longer meet the load for the lowest ambient temperatures in January and February and auxiliary heating is required. The remainder of the additional cost is due to incomplete charging of the store in the months with low ambient temperatures. Increasing the size of the heat pump to 7.5 kW (run A7) yields no further cost savings; since the 6 kW heat pump can fully charge the store even during the coldest month. However utilising a 66 kWh store with the 7.5 kW heat pump does result in an increased proportion of the load being supplied from the store, thereby increasing the cost savings.

The heating requirement of the dwelling was reduced by decreasing the temperature setpoint from 20°C to 15°C (runs A14 and A4) and the percentage cost savings of the integrated system as compared to the heat pump alone increased from 36.1% to 47.4%. It should be noted that this lower load requirement would not require a 6 kW heat pump; hence varying the load without re-specifying the heat pump size is not realistic. However, further cost calculations may indicate that it is economically attractive to invest in a larger (higher capital cost) heat pump in order to supply more of the load with off-peak electicity.

Two final runs were performed (A17 and A18) to investigate the effect of using the third type of load profile. Since the heating requirement was lowered the percentage cost savings were increased from 36.1% to 52.9% These savings are realistic as the heat pump would still have to have an output of 6 kW to cope with the load. Note that the maximum cost savings would be 62% and would correspond to the total demand being supplied from

the heat pump operating with off-peak electricity.

7.4.3.2. Criticism of simulation employing simple assumptions

Employing average monthly ambient temperatures doesn't test the performance of the system under the most demanding real conditions. The lowest temperature used was 3.9°C for January while Heap (1977), see figure 1.3, reports that the ambient temperature at Turnhouse was recorded below 0°C for 720 hours in a year (8.2%).

The daily variation in ambient temperature will result in the heat pump having a lower performance during the off-peak period and the heat load being lower during the day than that determined utilising the average temperature. Consequently the runs performed with the improved elementary model use real hourly temperature data.

7.4.4. Economics of Integrated Systems using Model Results

In order to assess the cost effectiveness of the integrated system as compared with a heat pump, the capital recovery factor (crf) method of allocating the additional capital cost of the store over its working life was employed. Kernan and Brady (1977) utilised this technique for comparing heat pump systems with other conventional heating systems.

7.4.4.1. Definition of capital recovery factor

This paragraph is included to derive an expression for the capital recovery factor and a more detailed derivation may be found in Peters and Timmerhaus (1980). An amount of capital invested in a scheme bearing a rate of interest i, over a period of n years would yield a total sum S, calculated from the equation given below

$$S = P(1+i)^n \qquad (7.21)$$

An annuity scheme where n annual repayments R, each accumulating interest could also be used to yield the same sum. If the first payment is made at the end of the first year then it will bear interest for n-1 years. Thus at the end of the annuity period the first payment would have accumulated to an amount $R(1+i)^{n-1}$, and the second to $R(1+i)^{n-2}$ etc. Hence the accumulated total of the

repayments will be

$$S = R(1+i)^{n-1} + R(1+i)^{n-2} + \ldots + R(1+i) + R. \quad (7.22)$$

The above may be simplified by muliplying each side by (1+i) and subtracting the original to yield

$$S = R[(1+i)^n - 1]/i. \quad (7.23)$$

Substitution of equation (7.21) into the above gives the following definition of the crf

$$R = P[i(1+i)^{n-1}]/[(1+i)^n - 1] = P*crf. \quad (7.24)$$

Hence the additional capital cost (P) incurred by incorporating a store into a heat pump system may be broken down into annual payments (R) over the life time of the store.

7.4.4.2. Results of economic analysis on integrated system

Two methods of presenting the results were used. The first involved determining the absolute maximum permissable cost of the store per kWh, and the second calculated the potential cost savings for a given store cost. The latter was assumed to be the sum of a fixed cost of the tank and ancillary equipment (valves, relays etc.) plus the cost of the PCM and encapsulation which would vary linearly with the storage capacity. A program was written to analyse the data which required the following input:

1. Integrated system running cost per annum
2. Heat pump running cost per annum
3. Interest rate
4. Working life of store .
5. Cost of tank and ancillary equipment
6. Cost of PCM and encapsulation

The running costs were obtained from the simulation results presented in section 7.5.2, for the six runs comparing different size of store from 11-66

kWh for the same load and heat pump size. A working life of 10-15 years was used to calculate the crf defined in equation (7.24). Fixed costs of £150-450 were used for the storage device while PCM and encapsulation costs in the range 7.5-12.5 £/kWh were considered. Interest charges on the capital cost of the store were chosen from the range 5-15%.

Potential savings were evaluated as the difference between the annual heat pump running costs and the capital (allocated by crf) plus running costs of the integrated system.

$$SAVING = HPRCOST - (ISRCOST + STCOST*CRF) \quad (7.25)$$

where the store cost was calculated from

$$STCOST = TKCOST + PCMCOST \quad (7.26)$$

The maximum possible cost for the store was found by letting the tank cost equal zero and calculating the store cost to yield zero savings. The results achieved from this analysis are presented in table 7.15.

7.4.4.3. Discussion of Economic Analysis on Integrated systems

The store developed at Edinburgh had a storage capacity of approximately 44 kWh, a PCM cost of £10/kWh and a target cost of less than £300 for the tank and ancillary equipment. A working life of 10 years and an interest rate of 10% were considered reasonable; hence the cost data for these parameter values was used as a standard for comparison.

Tha annual cost saving for this standard was found to be £20.37 which amounts to a reduction of approximately 5.2% in the heating bill which, although significant, was not as attractive as had been hoped. One of the attractions in utilising heat pumps in domestic heating systems is that if the electricity is generated from renewable energy sources such as hydro-electric or wave power then it decreases the rate at which finite energy resources (also essential as chemical feedstocks) such as oil, gas and coal are depleted. Obviously a heat pump is a much more energy-efficient method of utilising electricity for space heating than direct use of resistive elements. If government policy therefore was to encourage the use of heat pump systems

then it would be expected that lower interest rates (say 5%) would be acceptable, which would allow cost savings of 11.5% to be achieved. A high interest rate of 15% was shown to result in no net savings.

Kernan and Brady (1977) defined the working life of a heat pump to be 15 years in their economic analysis. If the PCM could be relied on to maintain its storage capacity it would be reasonable to assume that since the store is less complex than a heat pump that it should have at least the same working life. Increasing the working life by 50% to 15 years more than doubles the cost savings (11.2%)

Increasing the cost of the tank and ancillary equipment in multiples of £150 reduces the potential cost savings by 6.3%. Hence a tank cost of £450 results in no net cost savings at all. For a higher interest rate (15%) the effect on cost savings is more significant (7.7%). Reducing the PCM and encapsulation costs by 25% to 7.5 £/kWh almost doubles the cost savings to 9.8%.

It was noted earlier that most of the runs were performed at a peak tariff cost of 4.4 p/kWh to allow comparison with previously determined data. The actual cost per unit in the SSEB area has increased to 5.34 p/kWh which gives much larger cost savings for the integrated system of 10.7%.

7.4.5. Improved Elementary Model

7.4.5.1. Modifications to original program

The existing elementary model (HPHSMODEL_ELVERS2A) was modified in an attempt to approximate more closely the performance of the prototype integrated system. This was achieved by writing new routines to simulate heat pump and heat store performance. The heat pump thermal output and work input were determined from multiple regression equations (fitted to typical experimental data, see section 7.5.1.1) using real ambient air temperature and user specified condenser inlet temperature.

Limiting charge and discharge rates for the prototype store were calculated from an approximate heat transfer coefficient found from a simple function of the UF, shown as dotted lines in figures 4.17 and 4.18. The temperature

differences at the store inlet and outlet were found by assuming that the centre-line temperature of the PCM remained at the PCM melting point throughout the charge/discharge cycle. Hence the heat transfer rate to/from the store could be found from

$$q_{C,D} = \dot{m}\, Cp(\Delta T_{in} - \Delta T_{out}). \qquad (7.27)$$

Since this was equal to

$$q_{C,D} = U_{ap} A \Delta T_{LM}, \qquad (7.28)$$

where ΔT_{LM} is defined in equation (3.12), re-arrangement allowed the outlet temperature to be predicted from

$$\Delta T_{out} = \Delta T_{in} / e^{(U_{ap}A/\dot{m}Cp)} \qquad (7.29)$$

7.4.5.2. Results

For a balance point temperature of -1°C and condenser inlet temperature of 56°C the maximum dwelling load coefficient which could be supplied by this heat pump was found to be 212 W/degC for an internal temperature setpoint of 15.5°C. No attempt was made to analyse the effect of shifting the balance point as the primary reason for performing these simulations was to develop a technique to determine the optimal heat storage device to be combined with a heat pump in a particular dwelling.

In this set of runs the store size was varied from 5-44 kWh and the total load changed from 6048 kWh/pa to 3781 kWh/pa. The remaining assumptions and conditions were kept constant and are summarised below:

Heat loss factor = 212 W/degC (7.30)

Inside temperature setpoint = 15.5°C

Cost of peak period electricity = 5.34 p/kWh

Fractional cost of off-peak electricity = 0.38

Ambient temperature = hourly each day as reported by Evans (1985)

Off-peak period = 0000 - 0700 hours

Heating period (runs A to E) = 0700-2400 hours

Heating period (runs F,G) = 0700 - 0900, 1300-1400, 1700-2300 hours

Heat pump performance:

(a) $q_{co} = 7.65 + 0.159T_a - 0.0633T_{co,in}$

(b) $W = 2.36 + 0.0465T_a + 0.00730T_{co,in}$

(c) Inlet temperature ($T_{co,in}$) = 56

Store size (runs B to E) = 5 to 44 kWh

Store size (run G) = 22 to 44 kWh

Heat store charge performance:

(a) Maximum UF for constant U_{ap} = 0.7

(b) Slope of U_{ap} vs UF as UF->1 = -100 W/m^2K

(c) Inlet temperature to store = 63°C

Heat store discharge performance:

(a) Minimum UF for constant U_{ap} = 0.18

(b) Slope of U_{ap} vs UF as UF->0 = 66.7 W/m^2K

(c) Inlet temperature to store = 44°C

Mass flow rate of transfer fluid = 0.192 kg/s

Melting point of PCM = 56°C

The minimum running cost (see section 7.4.4) for each of the runs was determined for typical interest rates, store working life, tank and ancillaries cost, PCM and encapsulation costs, and these are presented in table 7.16 and shown graphically in figure 7.18. It was noted that the store size for minimum cost decreases as the capital recovery factor decreases, i.e. for increased working life or reduced interest rates. Decreasing the heating period also reduces the size of store for minimum cost.

The running cost of an integrated system could potentially be very low but considerable effort will have to be devoted to reducing capital cost of storage device and increasing its working life. Further reductions in running cost

could be made if government policy was designed to encourage the use of heat pumps for domestic heating systems by reducing the interest rate for any such system.

7.4.5.3. Discussion of results

The simulation of the integrated system in this series of runs is much closer to the experimental performance but is still of limited appliciation due to the following assumptions:

1. Extrapolated output from multiple regression expression determined for $-2 < T_a < 4°C$ for use in the range $-2 < T_a < 15.5$ °C
2. No variation of transfer fluid temperature will significantly effect heat pump performance, especially during heat pump charge. In addition the effect of thermal cycling on performance of integrated system and heat pump only operation cannot be compared. One of the advantages of integrated system operation was considered to be reduced thermal cycling, which increases the life of many components, and it would have been useful to be able to assess the effect of store size on thermal cycling characteristics.
3. Constant PCM centre-line temperature and constant inlet temperature over-simplify the experimental results (see chapter 4) and introduce errors into the calculation of limiting charge/discharge rates.
4. The approximate heat transfer coefficient was found from the mean of experimentally determined values. It would have been possible to fit a curve to the data predicted by the finite difference model but this method was not employed due to the discrepancy between the model and experimental values determined during discharge.
5. The limiting charge and discharge rates for the smaller storage devices were determined by assuming that the heat transfer area was directly proportional to the store size. This method results in discharge rates incapable of meeting the design load at -1°C if the store size is reduced below 22 kWh. Since a store would normally be designed to be capable of supplying the full domestic heating load at -1°C (certainly for UF>0.25), the running costs determined for storage devices of less than 22 KWh capacity are artificially high

due to poor design.

6. The effect of defrost which lowers total charge has not been included. Defrost would occur during heat pump only operation as well but the effect on performance may be less significant due to higher ambient temperatures during on-peak periods.
7. Heat losses from the store will reduce both the COP during heat pump charge and the total amount of heat that can be recovered from the store during discharge.

Use of the real ambient temperature reported by Evans resulted in a small amount of auxiliary heating (8-16 kWh) being required in all runs, with the lowest amount required for the largest store size. Only a very small amount of auxiliary heating was required as the temperature was less than -1°C for only 101 hours (34 off-peak) during the whole year. This proportion (1.15%) is significantly smaller than that reported (approx. 6%) by Heap (1977) and presented in figure 1.3.

7.4.6. Conclusions and Recommendations

The annual cost saving was found to be a function of many variables such as interest rate, cost of tank and ancillaries, cost of PCM and cost of electricity in addition to the size and performance of the major components. With the assumptions for the simple model specified in section 7.4.2, an interest rate of 10%, working life of ten years, capital cost of £300 for the tank and ancillaries and a target cost of £/kWh for the PCM and encapsulation, a reduction of 5.2% on the annual heating bill was predicted. An increase in the working life or a reduction in the value of any of the other parameters would increase the expected savings.

The improved model which only requires a few minutes of computer time has been used to simulate the performance of an integrated system 24 hours a day during the year. Hence despite its necessary simplifications it is a useful tool for investigating the suitability of an integrated system for a potential application.

7.5. DETAILED MODEL OF INTEGRATED HEAT PUMP/LATENT HEAT STORE

7.5.1. Development of Model

It was originally intended to simply combine the diagram heat pump model reported in section 7.1 with the finite difference heat store model developed in section 7.3. However the heat pump model when suitably modified into routine form was found to require an immense amount of computer run-time, and hence combination with the finite difference model, itself requiring a large amount of computer run-time, was found to be impractical.

Multiple regression equations, expressing the heat pump thermal output and work input as functions of the ambient temperature and condenser inlet temperature, were utilised instead and their determination is reported in section 7.5.1.1. The modifications required to the finite difference model for heat pump charge and discharge are described in sections 7.5.1.2 and 7.5.1.3. Finally a model developed to simulate the performance of the heat pump when supplying the load once the store has been completely discharged is described in section 7.5.1.4.

7.5.1.1. Use of multiple regression technique to model heat pump

Since it was desired to compare the detailed model simulation with the experimental data determined over the period 12/3 to 15/3, the heat pump performance data over this period was employed to determine the coefficients for the multiple regression expressions. A statistical programming package called MINITAB available on the EMAS system and fully described by Ryan et al. (1985) was employed to determine the coefficients and analyse their statistical significance. The following procedure was followed:

1. The experimentally determined heat pump thermal output, work input, ambient air temperature and tranfer fluid condenser inlet temperature obtained during each heat pump charge with flow rate of 11.5 lit/min (12/3, 14/3 and 15/3) were inserted into columns (C1-C4) in a data file
2. The MINITAB package was then entered and each of the columns in the data file read, "MTB > READ 'DATAFILE' C1-C4"
3. The regression equation for thermal output was then found from

the two predictor variables, ambient air temperature and condenser inlet temperature, "MTB > REGRESS C1 2 C3 C4"

4. The package then calculated and printed out the regression equation on the screen, along with the standard deviation and t-ratio for the constant and each coefficient. The latter was employed to test whether the relationship between predictor and thermal output was significant at the 95% confidence interval by checking for a value greater than 2 (note sample size greater than 50). The standard deviation of thermal output about the regression equation and R-sq, the fraction of the variation in thermal output that is explained by the fitted equation, were calculated and also presented
5. The total sum of squared deviations (total SS) and regression SS were presented in an analysis of variance table.
6. Finally a table of unusual observations, viz. those with large discrepancy between experimental and fitted value for thermal output, was presented to identify suspect experimental data or faulty typing.
7. The procedure was repeated for work input and a summary of the coefficients and statistical analysis is presented in table 7.17.

It was possible to determine expressions with squared terms simply by creating two extra columns with the predictor values squared, "MTB > LET C5 = C3*C3" etc., and then regressing on all four columns. The standard deviation and R-sq could be reduced to 0.04985 and increased to 99% respectively by the addition of two squared and a cross product term. However this improvement was not considered sufficient to justify the additional complexity of the correlation.

7.5.1.2. Simulation of heat pump charge

The program used to simulate heat pump charge (HPHSMODEL_DETVERS2A) was essentially the same as that developed and described in section 7.3.3.1 to model the Edinburgh prototype store for general charge/discharge cycling. A routine to simulate the heat pump performance was included to determine the new transfer fluid temperature at the store inlet at each time step. The

multiple regression expressions employed to simulate heat pump performance (see section 7.5.1.1) required only condenser inlet temperature and ambient air temperature data. An additional selection prompt allowed the user to specify the hourly temperature to be used in each run. Print-out from the program was modified to include the COP and summed work input [kWh].

Since it was desired to simulate heat pump performance over the period 12/3 to 15/3 where the ambient temperature was low, a method of simulating defrost had to be developed. This was achieved by specifying the heat pump thermal output to be -6 kW, COP to be unity and calculating the work input as normal, for a period of 100 seconds in every 30 minutes that the ambint temperature remained below 5°C.

Preliminary comparison of simulated and experimental data demonstrated the need to calculate heat losses from the store and pipework. The former was calculated by averaging the store inlet and outlet temperatures and calculating the loss into a dwelling at 20°C with a coefficient of 7 W/degC. This loss was then employed to calculate the condenser inlet temperature from the predicted store outlet temperature. Pipework losses were assumed fixed at 250 W and the store inlet temperature was calculated from the condenser outlet temperature minus this heat loss.

During periods of high ambient temperature the store would become completely charged at the end of a charge period and cause the condenser outlet temperature to rise above 63.5°C as UF -> 1. In the experimental facility part of the heat pump thermal output (2 kW) is diverted to the plate heat exchanger (to simulate DHW load) when the temperature becomes too high and a similar procedure was included in the model.

7.5.1.3. Simulation of store discharge

The program used to simulate store discharge (HPHSMODEL_FDEXLACY2) was identical to that developed and described in section 7.3.3.1 to model the Edinburgh prototype store for general charge/discharge cycling. However when utilised to simulate the integrated system it was important to specify the data file with the final conditions from the previous charge as initial conditions for the discharge cycle. Since the runs were completed sequentially overnight the correct initial UF could not be predicted; hence the

starting UF in each discharge was taken to be unity. However it was quite a straightforward matter to correct the UFs retrospectively.

7.5.1.4. Simulation of heat pump only

An almost identical procedure to that employed in the simulation of heat pump charge formed the basis for the program (HPHSMODEL_HPONLY) developed to simulate heat pump performance once the store had been completely discharged. The only major modification was to develop a method of simulating the thermal cycling behaviour of a heat pump capable of supplying more heat than that required by the load. This was achieved by setting the COP to zero, heat pump thermal output to zero and condenser outlet equal to condenser inlet temperature if the condenser inlet temperature rose above 63.5°C.

The cycling nature of the transfer fluid temperature was simulated by predicting the outlet temperature from the buffer tank into the condenser from the sum of the heat pump thermal output, domestic heating load and pipe loss multiplied by the simulation time step, and then divided by the thermal capacity (mass times specific heat) of the transfer fluid in the buffer tank.

7.5.2. Results

A summary of the results is presented in table 7.18. Full details of the simulation output for one day only (12/3) are presented in table 9.5 and shown graphically in figure 7.19.

7.5.3. Discussion of Results

Comparison of the simulated data (figure 7.19) with the experimental data (figure 6.6) demonstrates overall good agreement. Defrost is not always shown on the simulated output since the defrost cycle may be out of phase with the print-out frequency. The other major difference is that the simulated load and store discharge rate unlike the experimental values are absolutely constant.

Careful comparison of tables 6.1 and 7.18 show that the agreement while good could still be improved as the error in predicting the store condition at the end of the charge period can be as large as 5% which is greater than the

experimental error.

7.5.4. Conclusions and Recommendations

A detailed model of an integrated heat pump/latent heat store has been developed which goes some way towards providing the researcher with an accurate tool with which to simulate integrated systems in various potential applications.

The major problem with this model is that it requires a large amount of computer time to obtain useful simulation data. One potential method of reducing the required time would be to simulate yearly performance by simulating operation during typical portions of a year, perhaps identifying six one-week periods which include the extremes of the heating season.

Improved instrumentation and control of the test facility would result in data with smaller confidence intervals which would greatly help in the identification of areas requiring further model development. The effect of thermal cycling and defrost on heat pump performance are two areas that should certainly be further investigated both experimentally and theoretically.

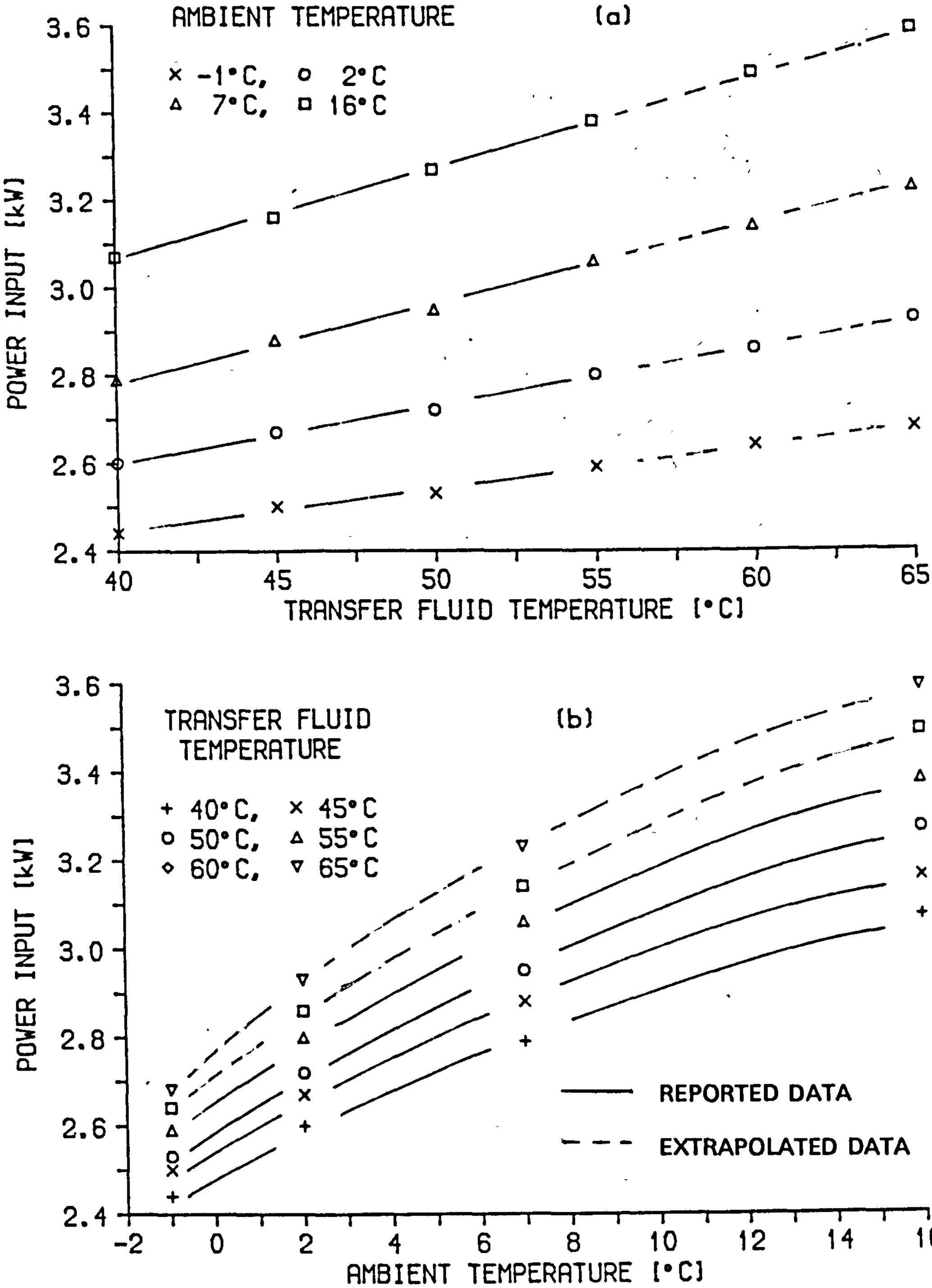

Figure 7.1 Power input against (a) transfer fluid and (b) ambient air temperature

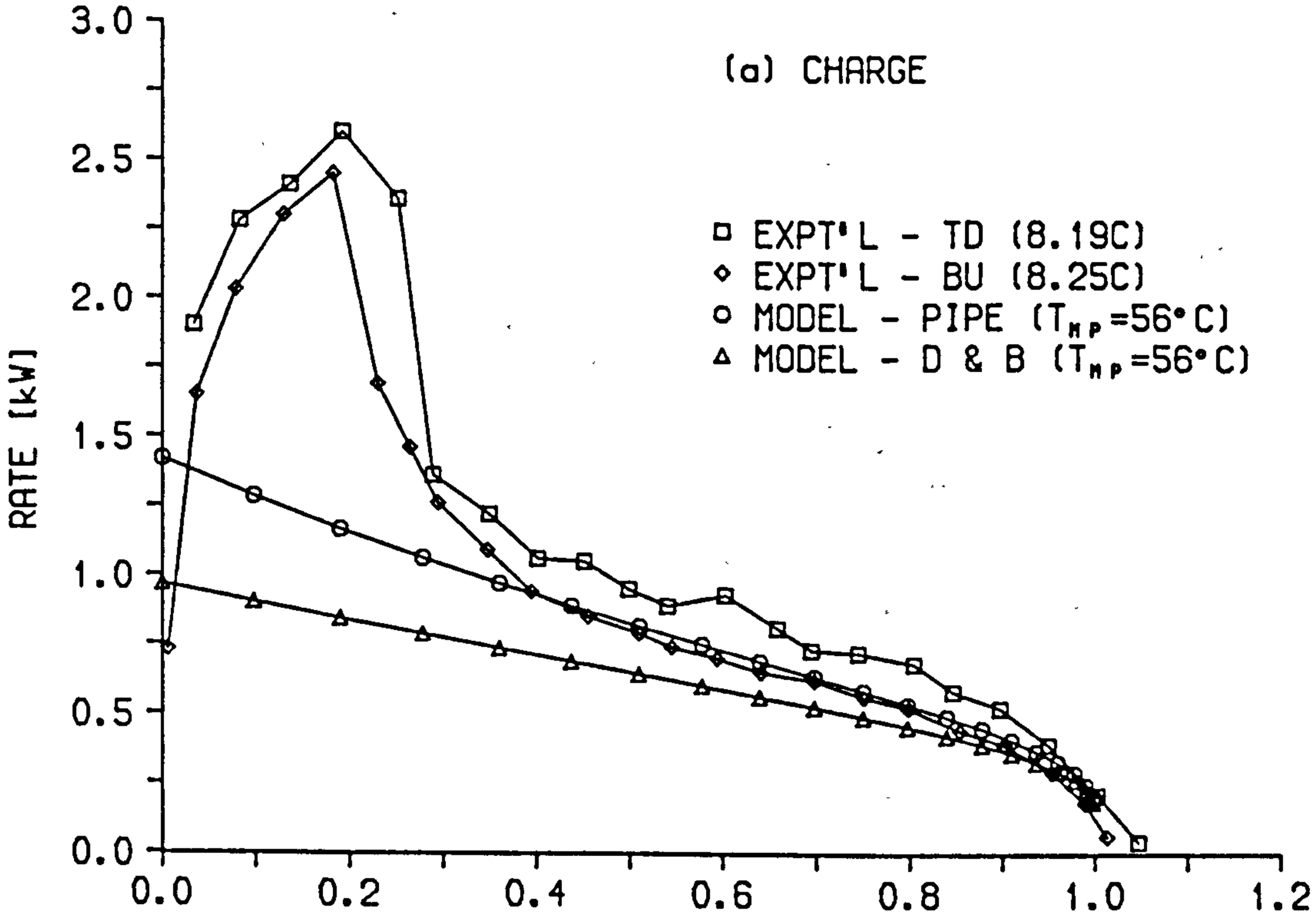

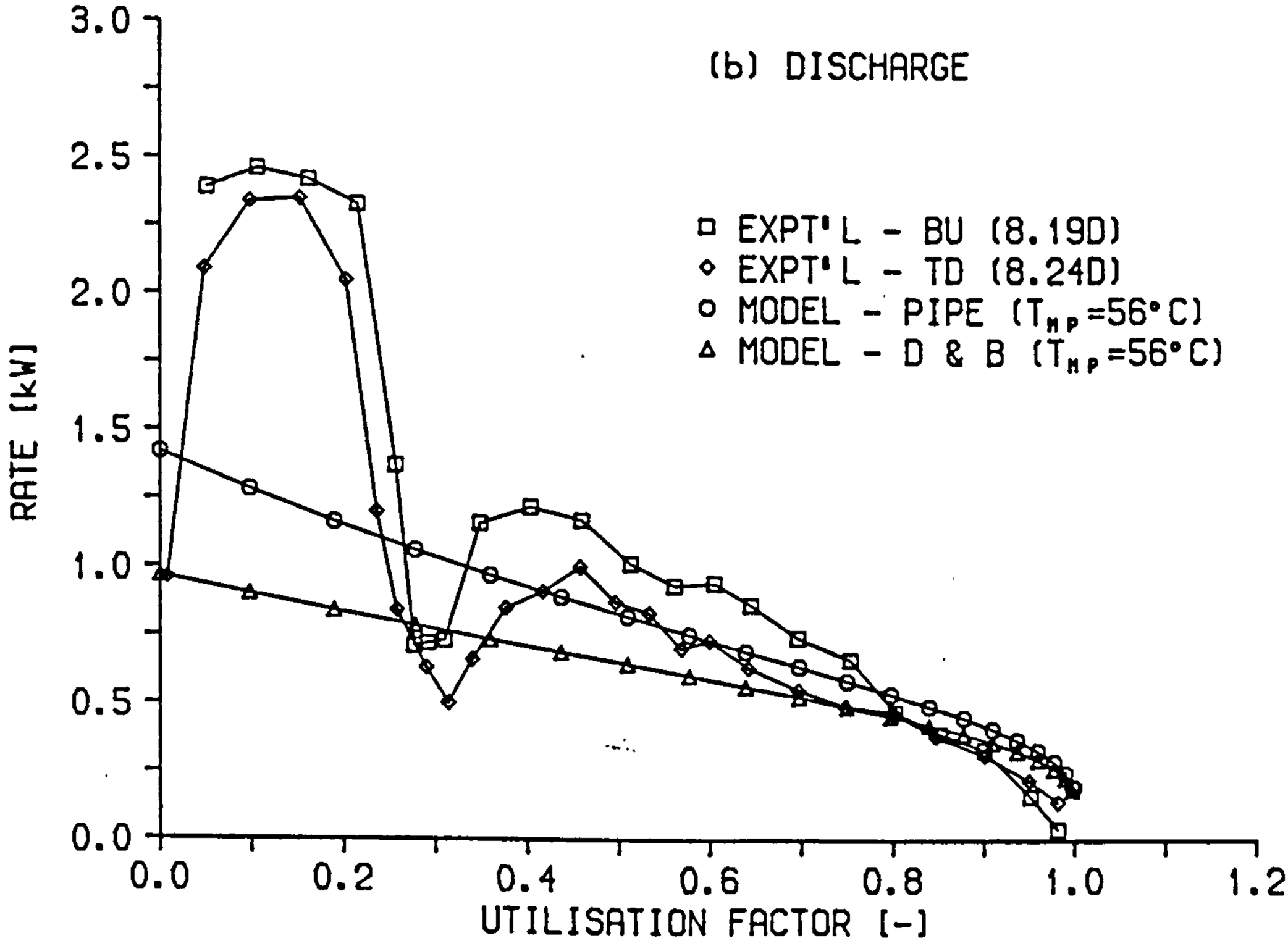

Figure 7.2 Rate against UF for 38 mm tubes in pilot store

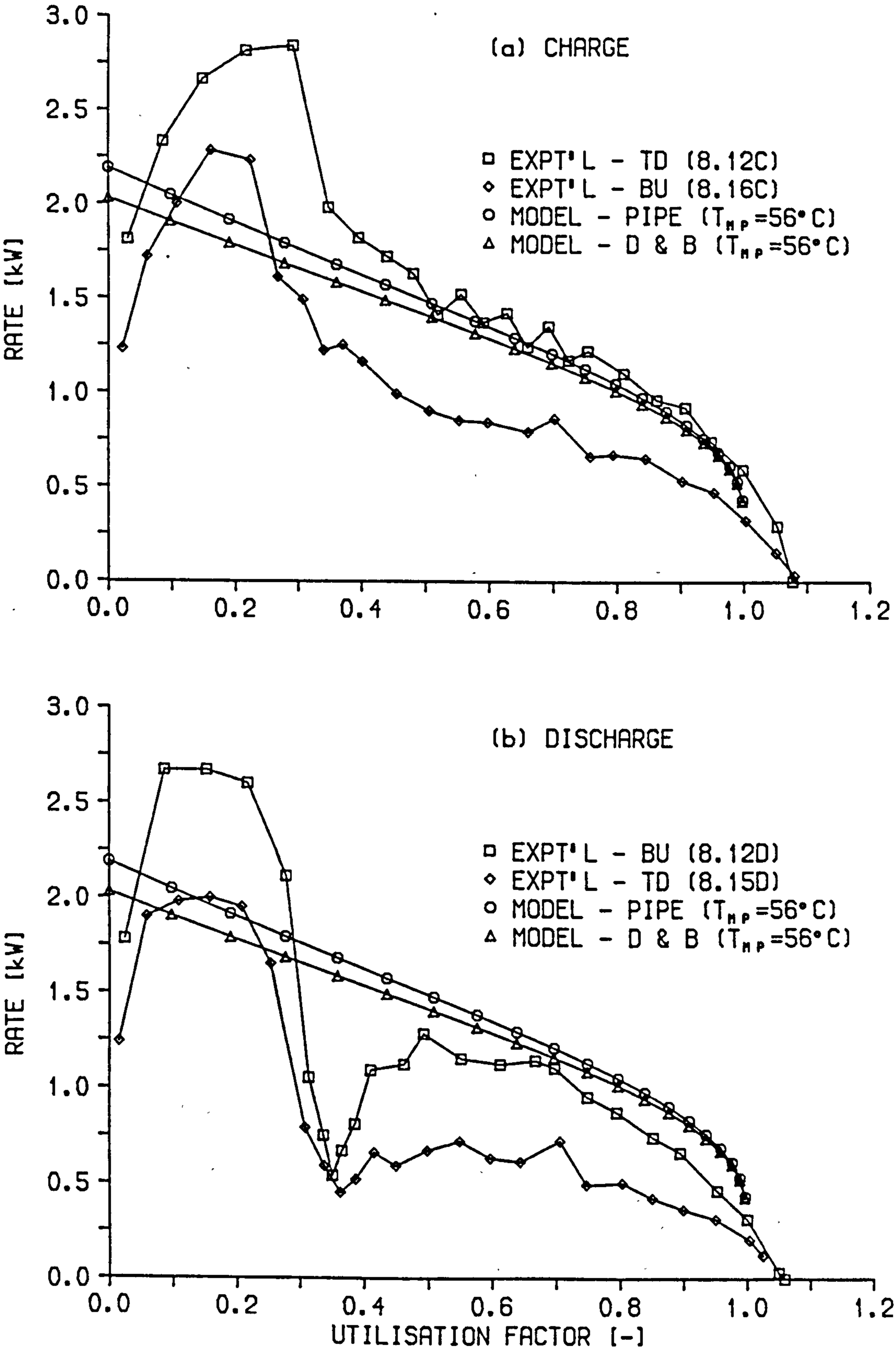

Figure 7.3 Rate against UF for 25 mm tubes in pilot store

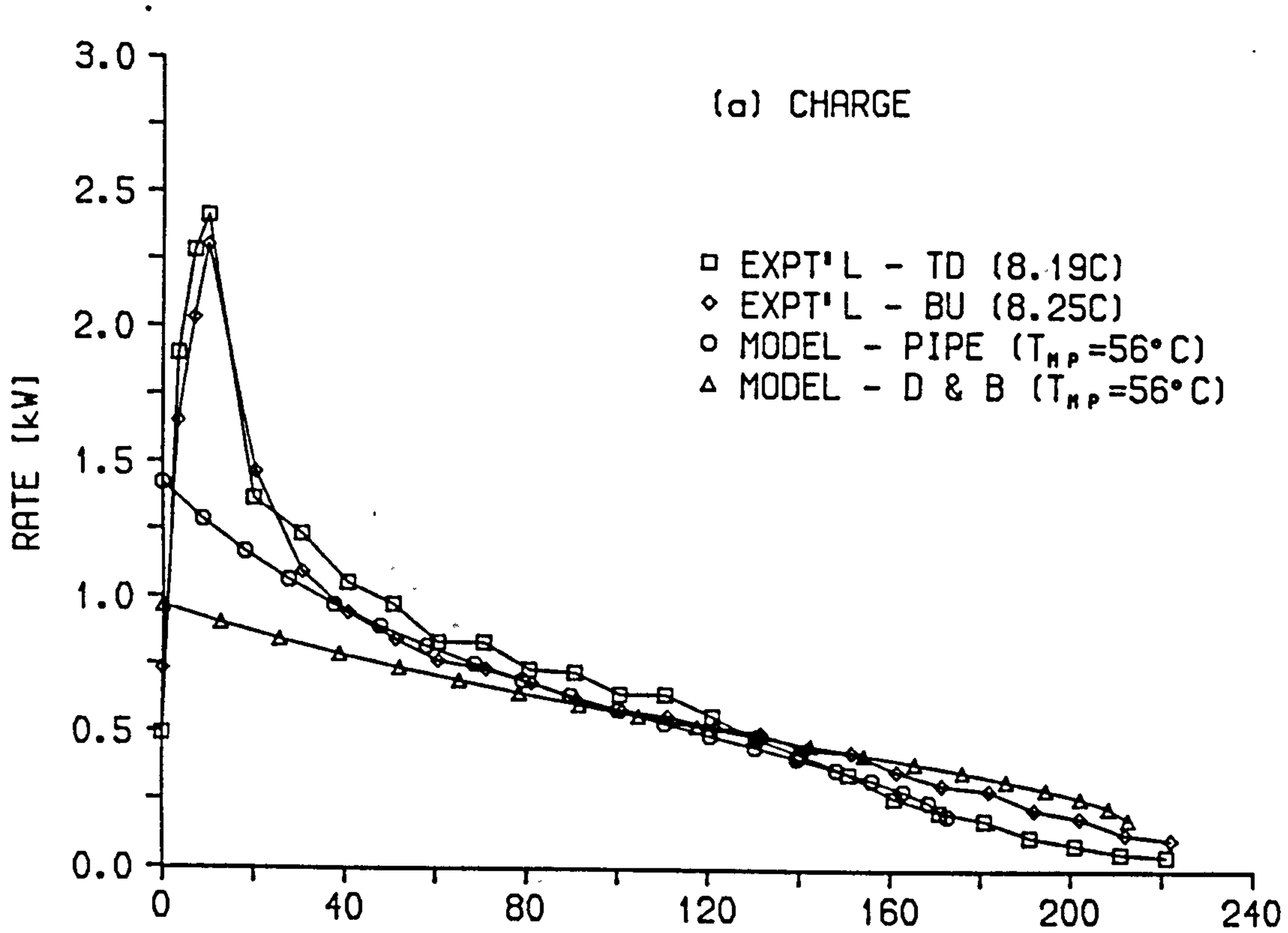

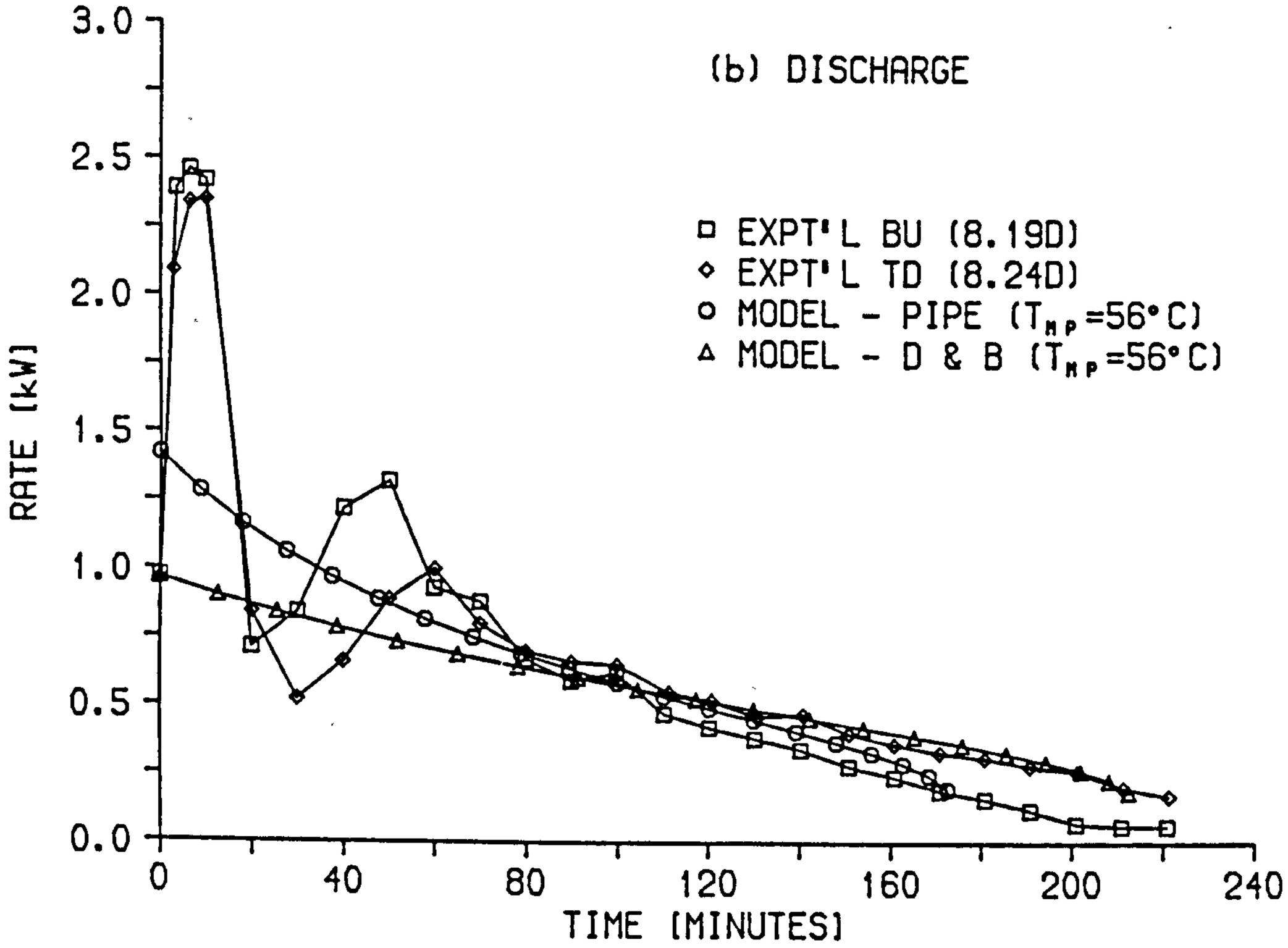

Figure 7.4 Rate against time for 38 mm tubes in pilot store

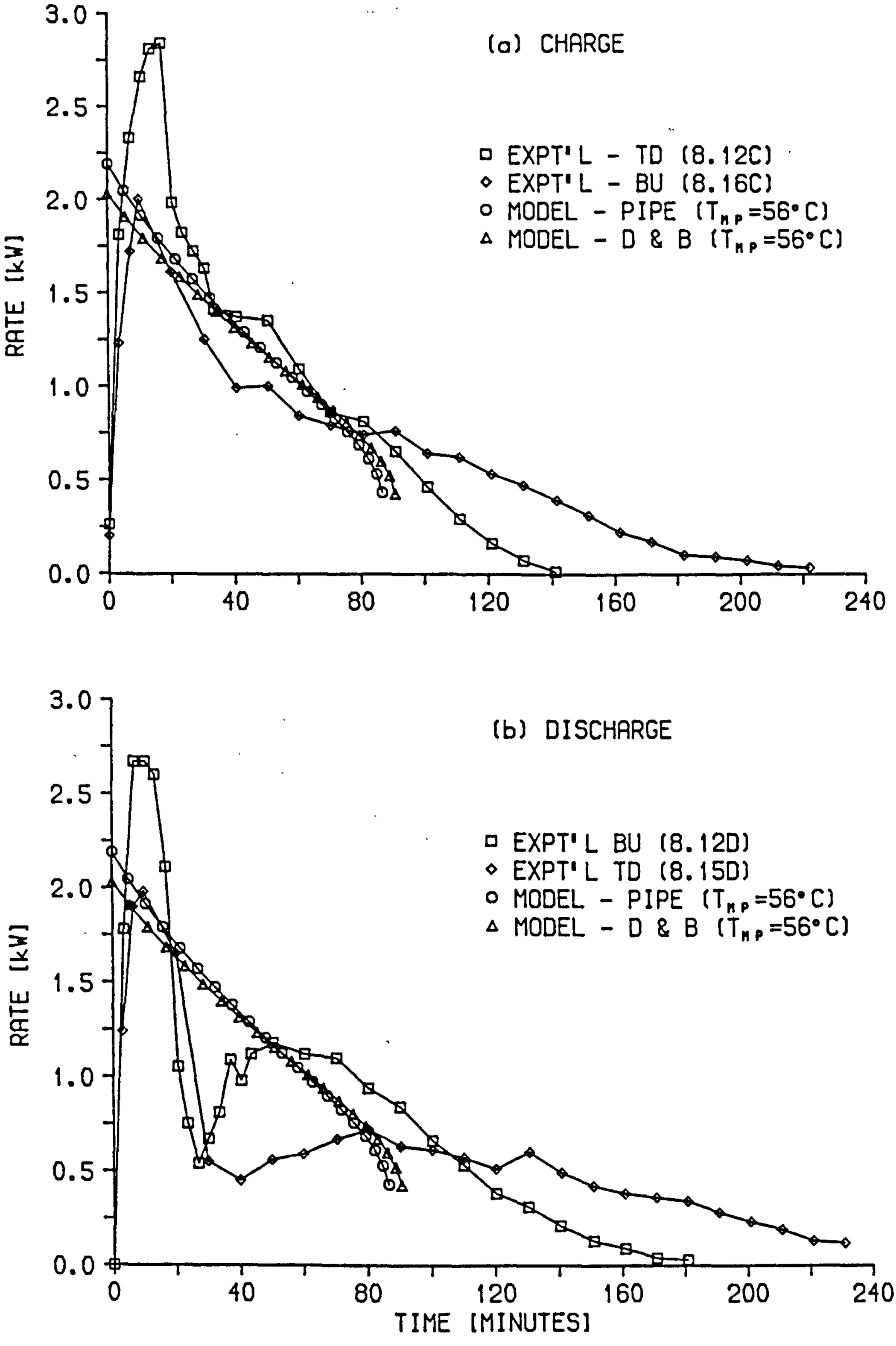

Figure 7.5 Rate against time for 25 mm tubes in pilot store

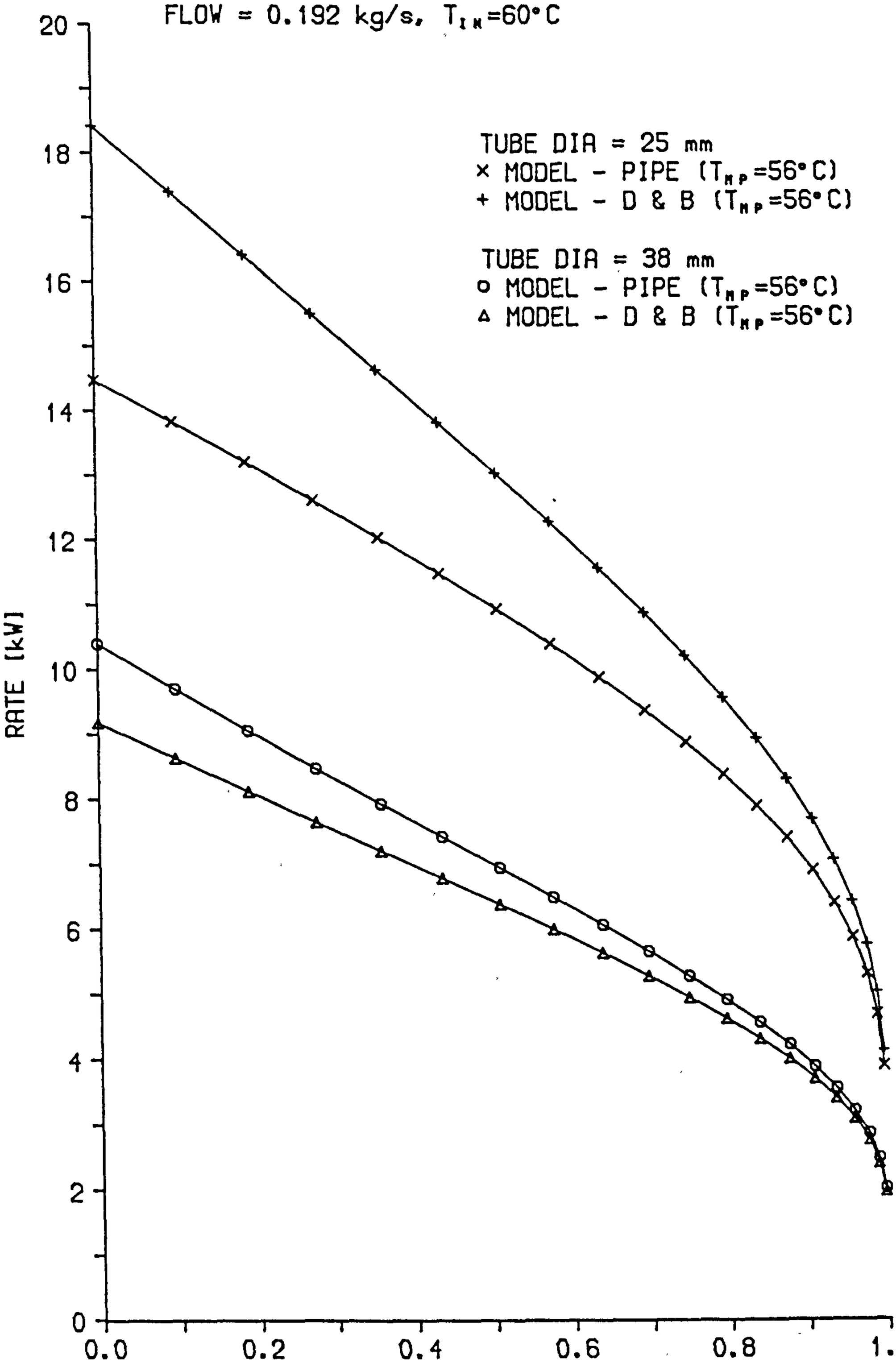

Figure 7.6 Predicted charge rate against UF in prototype store

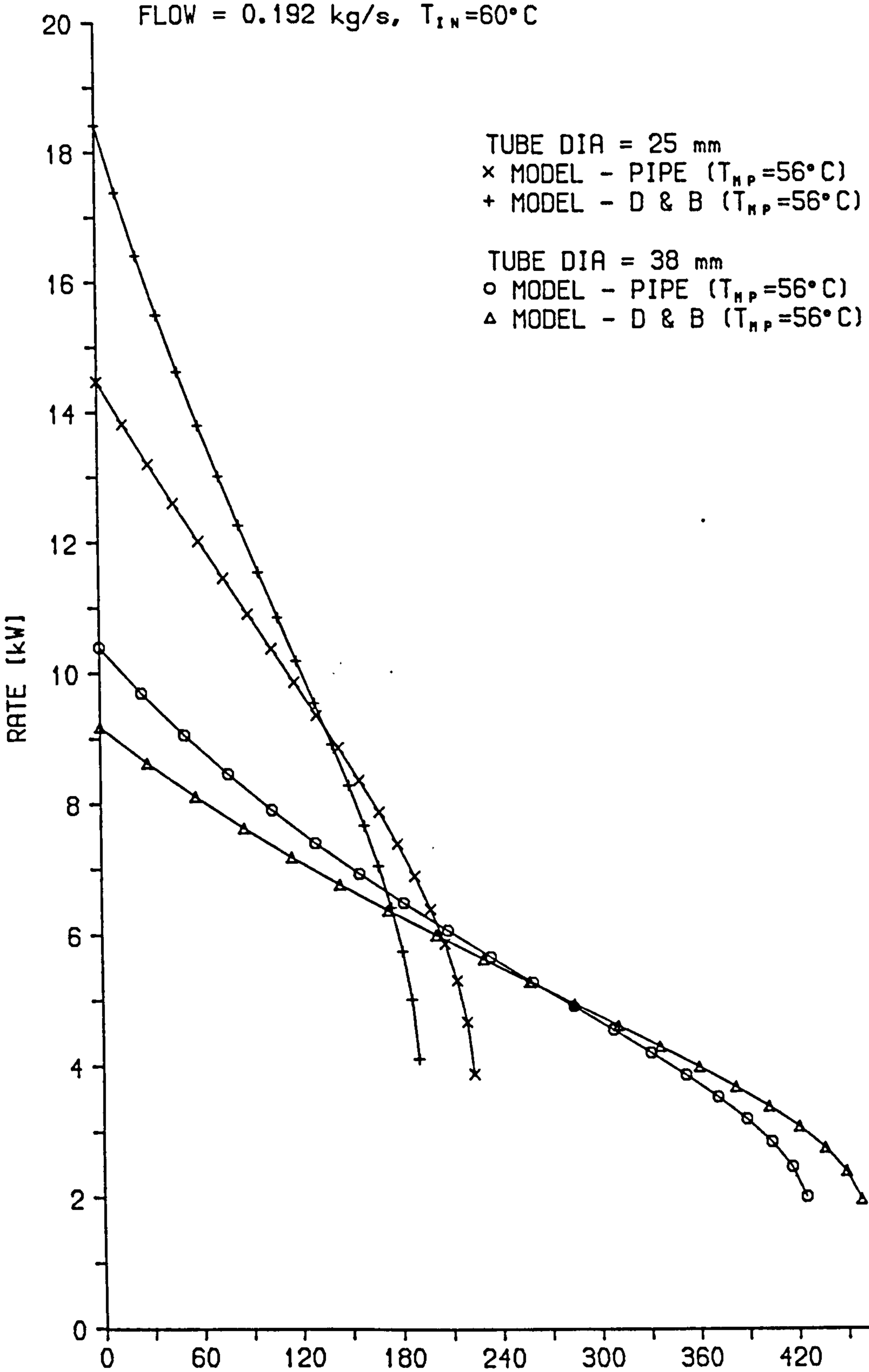

Figure 7.7 Predicted charge rate against time in prototype store

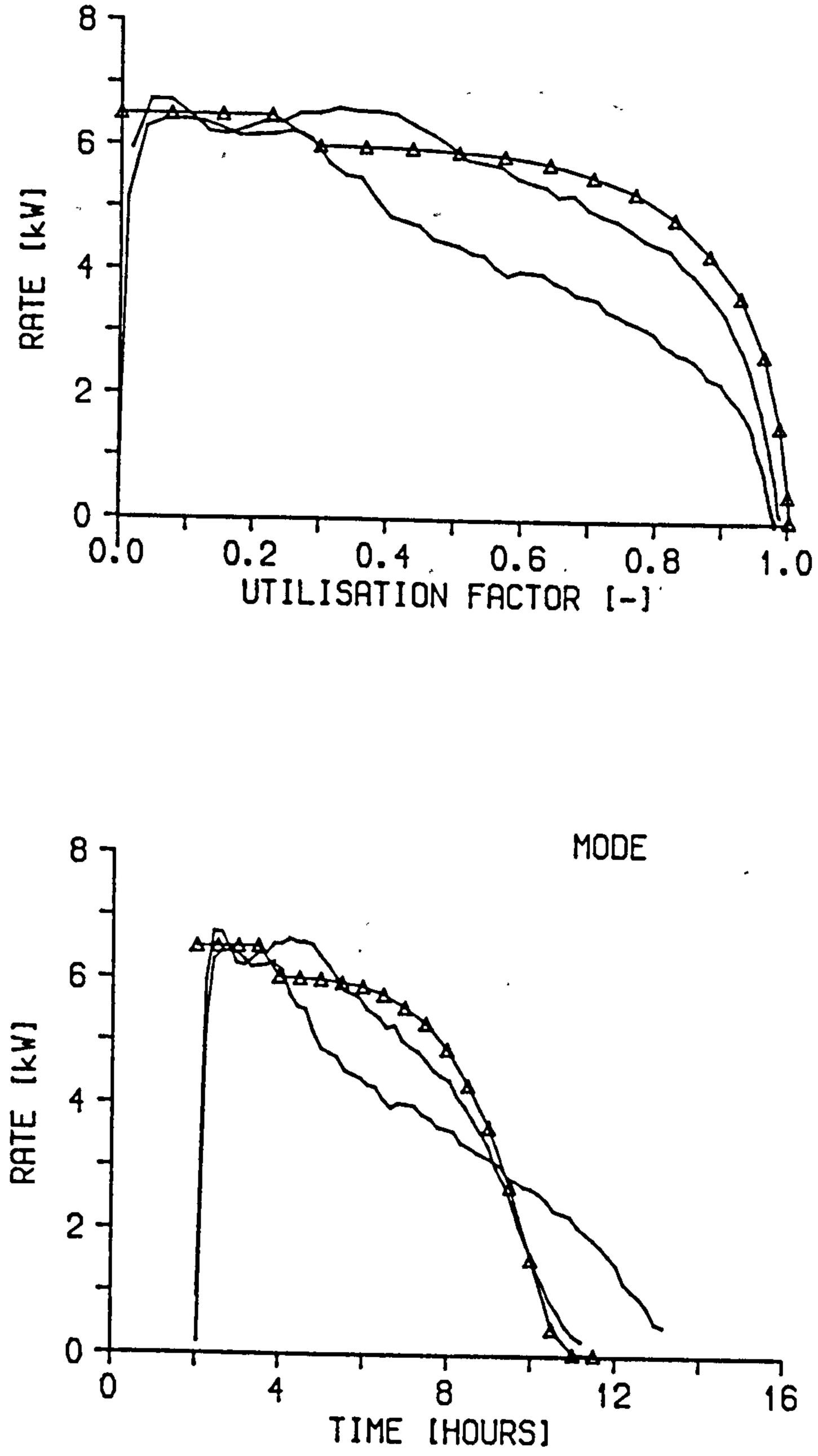

Figure 7.8 Predicted and experimental charge rate against UF and time for prototype store (1)

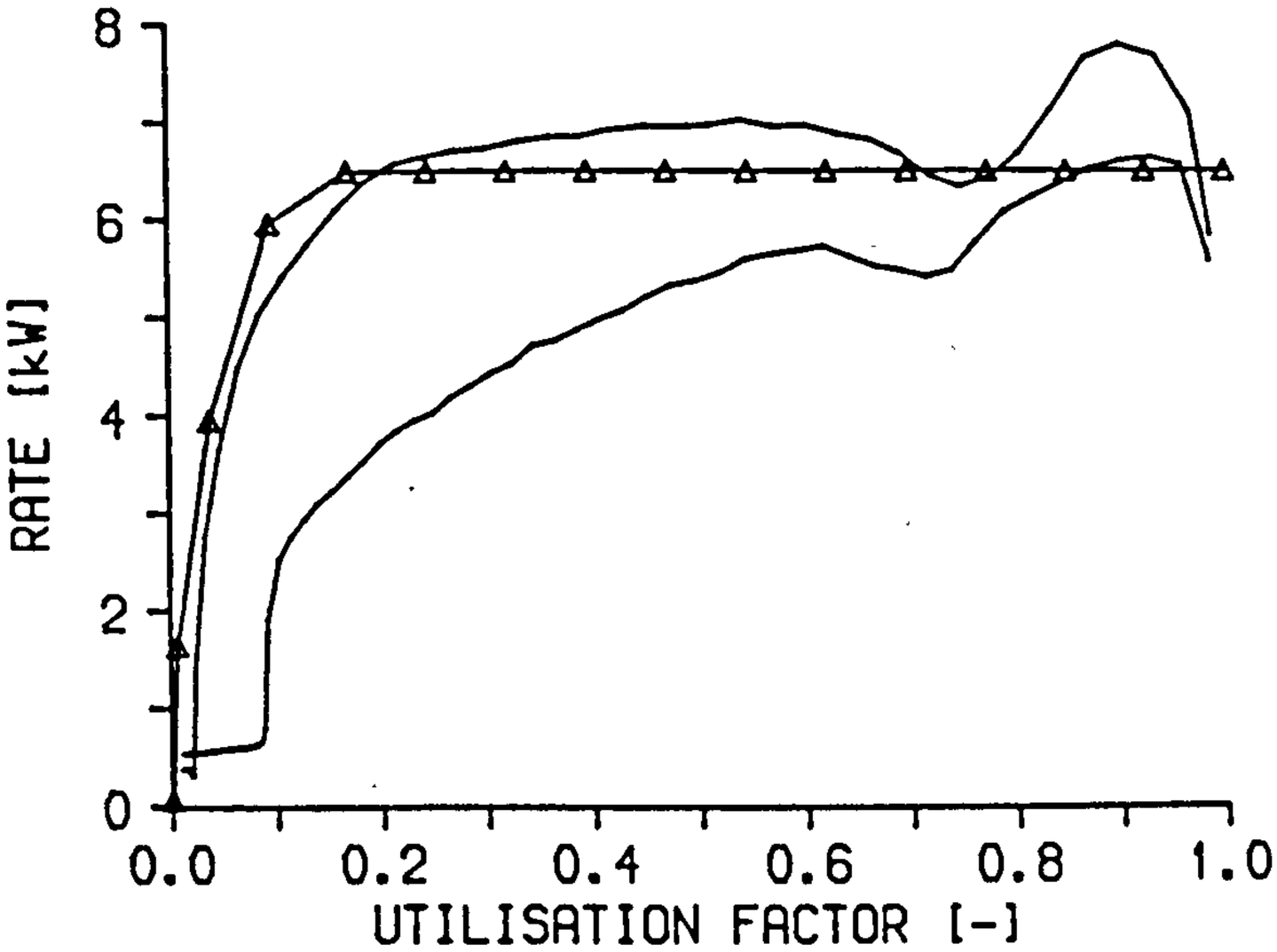

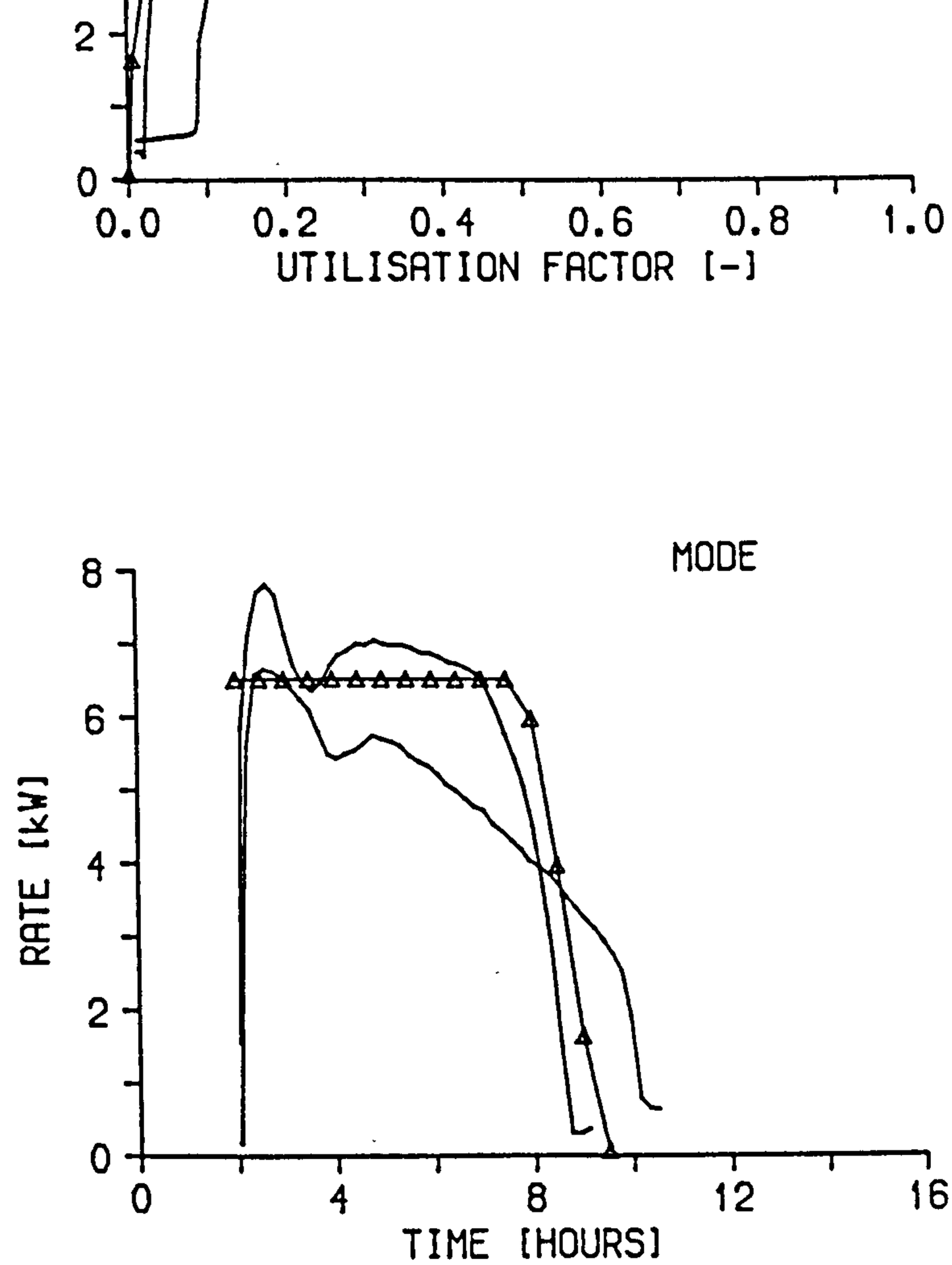

Figure 7.9 Predicted and experimental discharge rate against UF and time for prototype store (1)

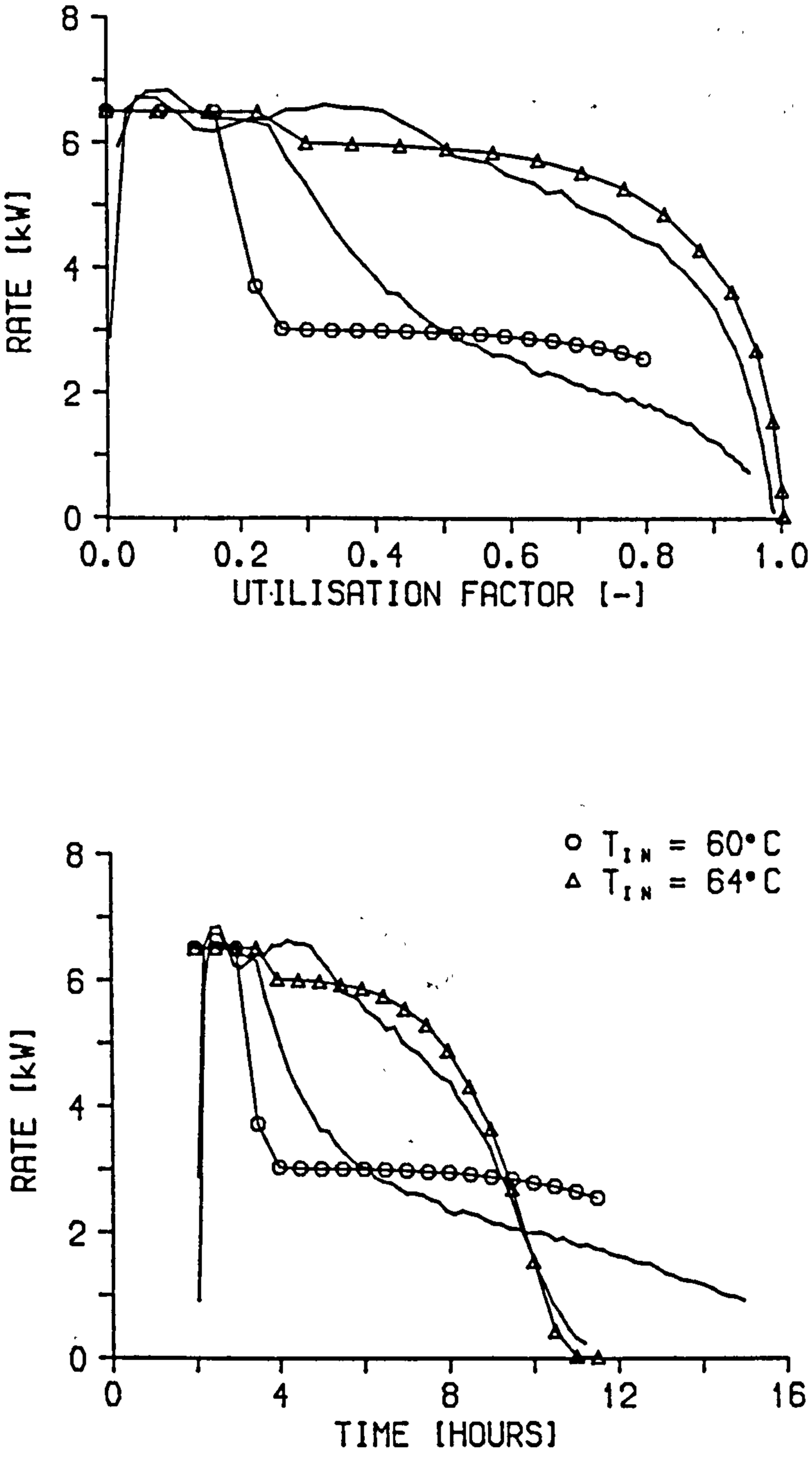

Figure 7.10 Predicted and experimental charge rate against UF and time for prototype store (2)

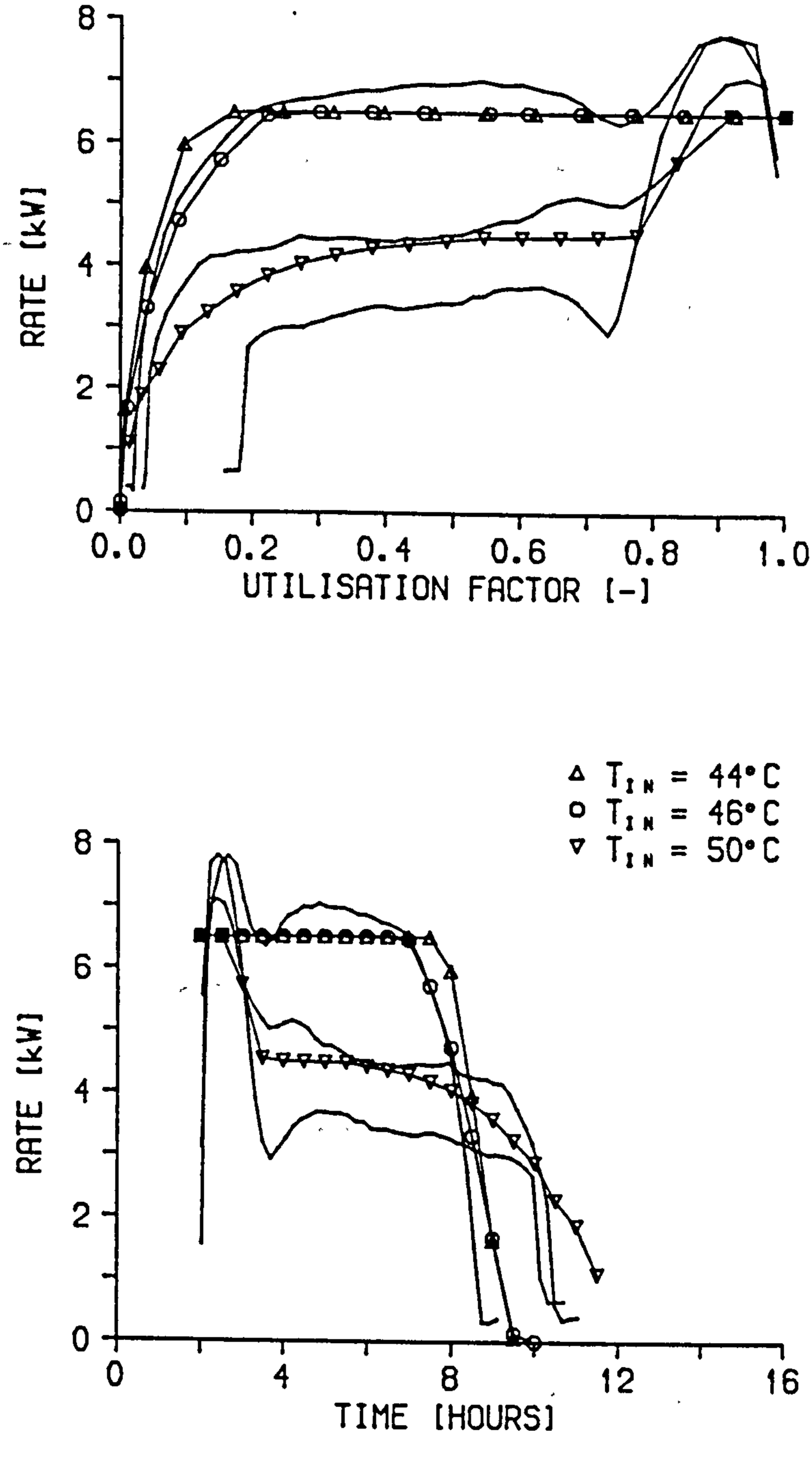

Figure 7.11 Predicted and experimental discharge rate against UF and time for prototype store (2)

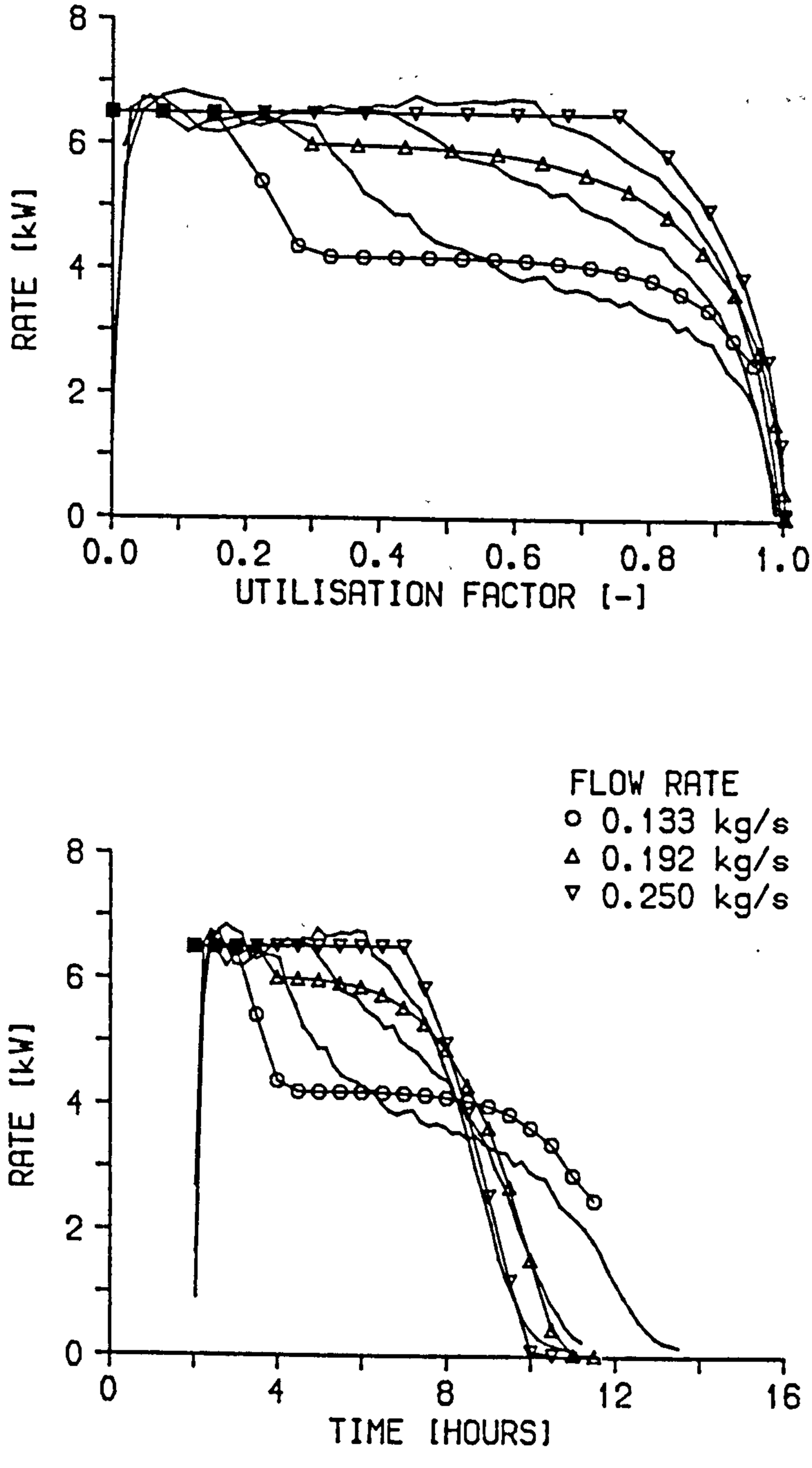

Figure 7.12 Predicted and experimental charge rate against UF and time for prototype store (3)

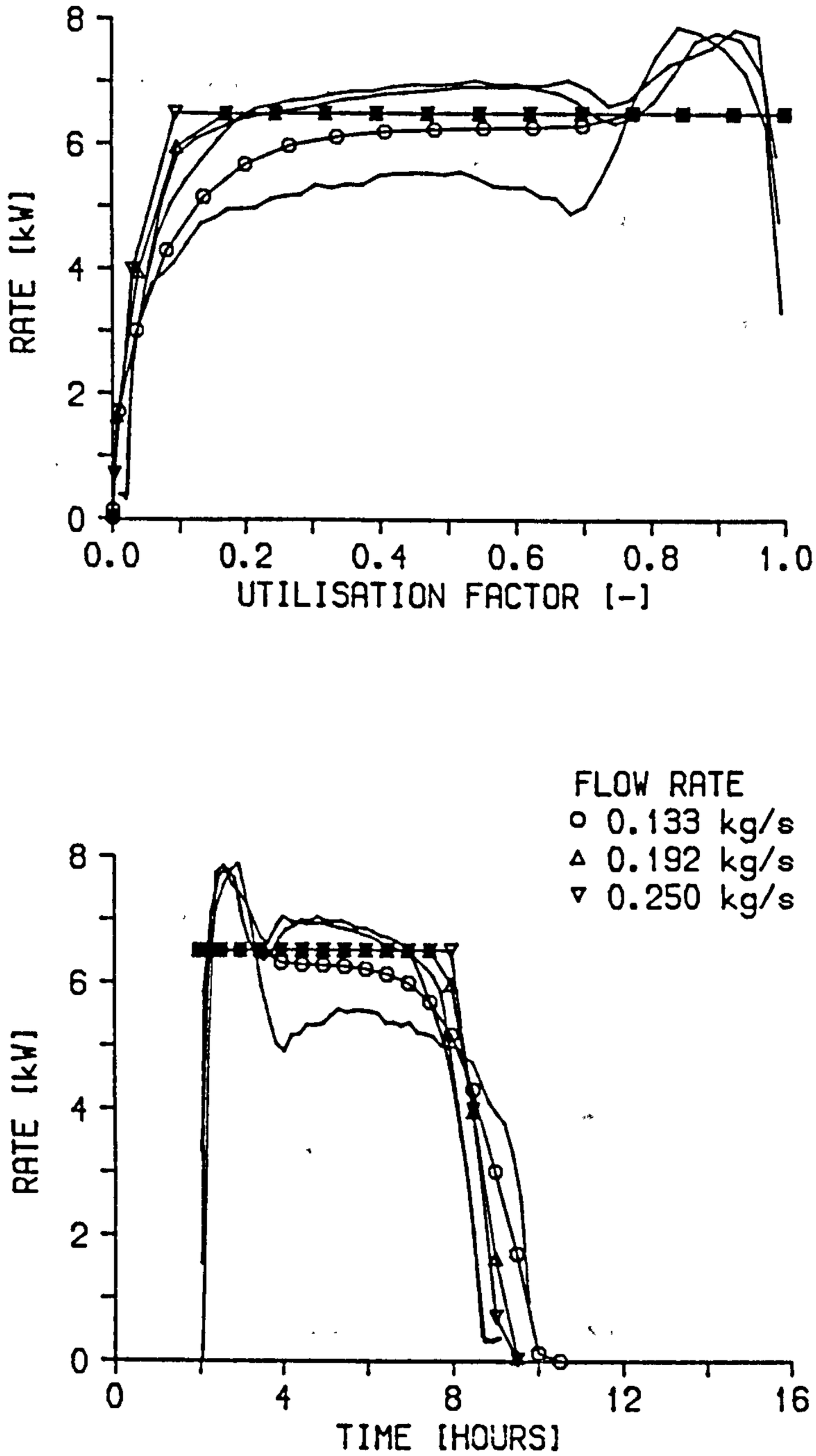

Figure 7.13 Predicted and experimental discharge rate against UF and time for prototype store (3)

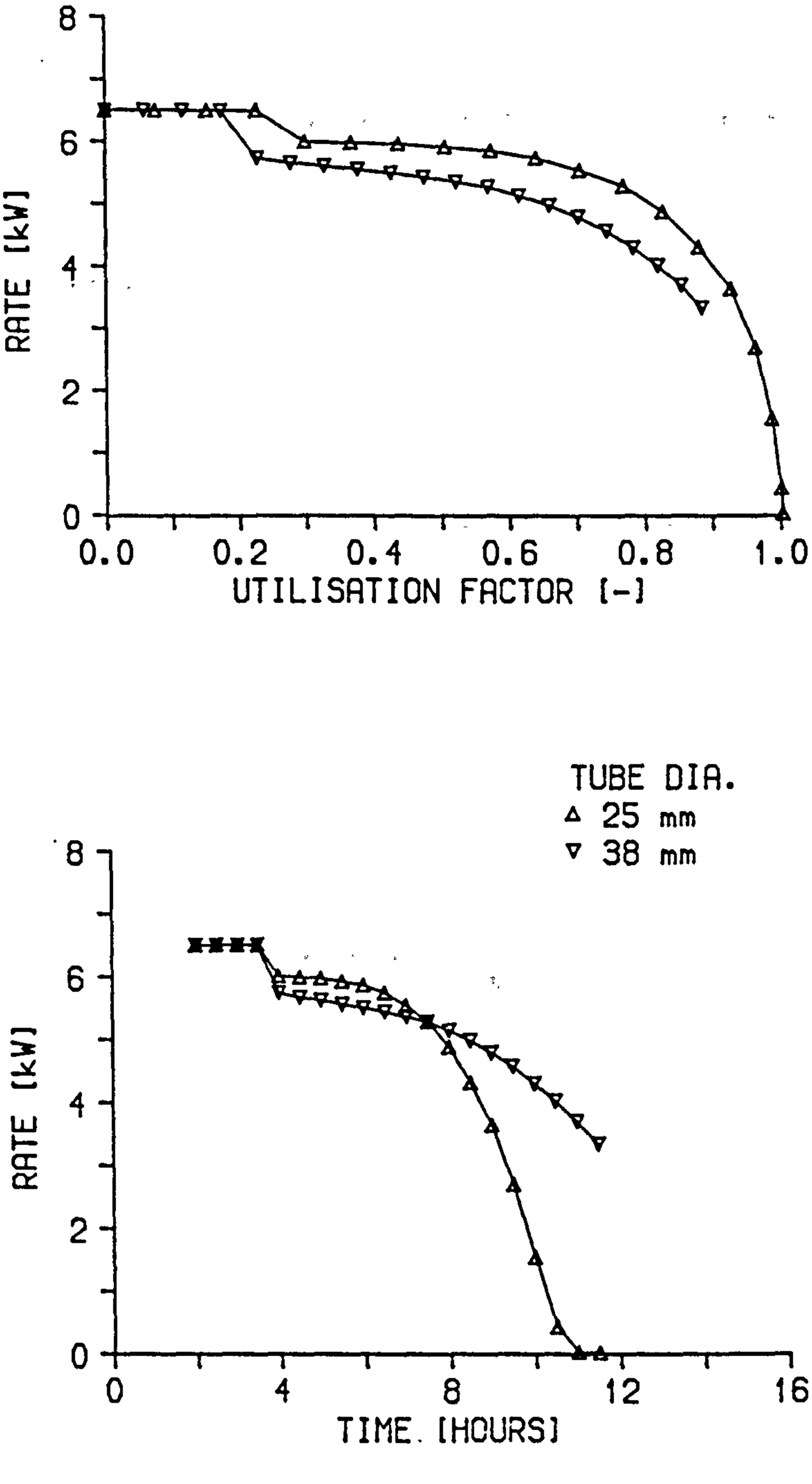

Figure 7.14 Predicted charge rate against UF and time for 25 and 38 mm tubes in prototype store

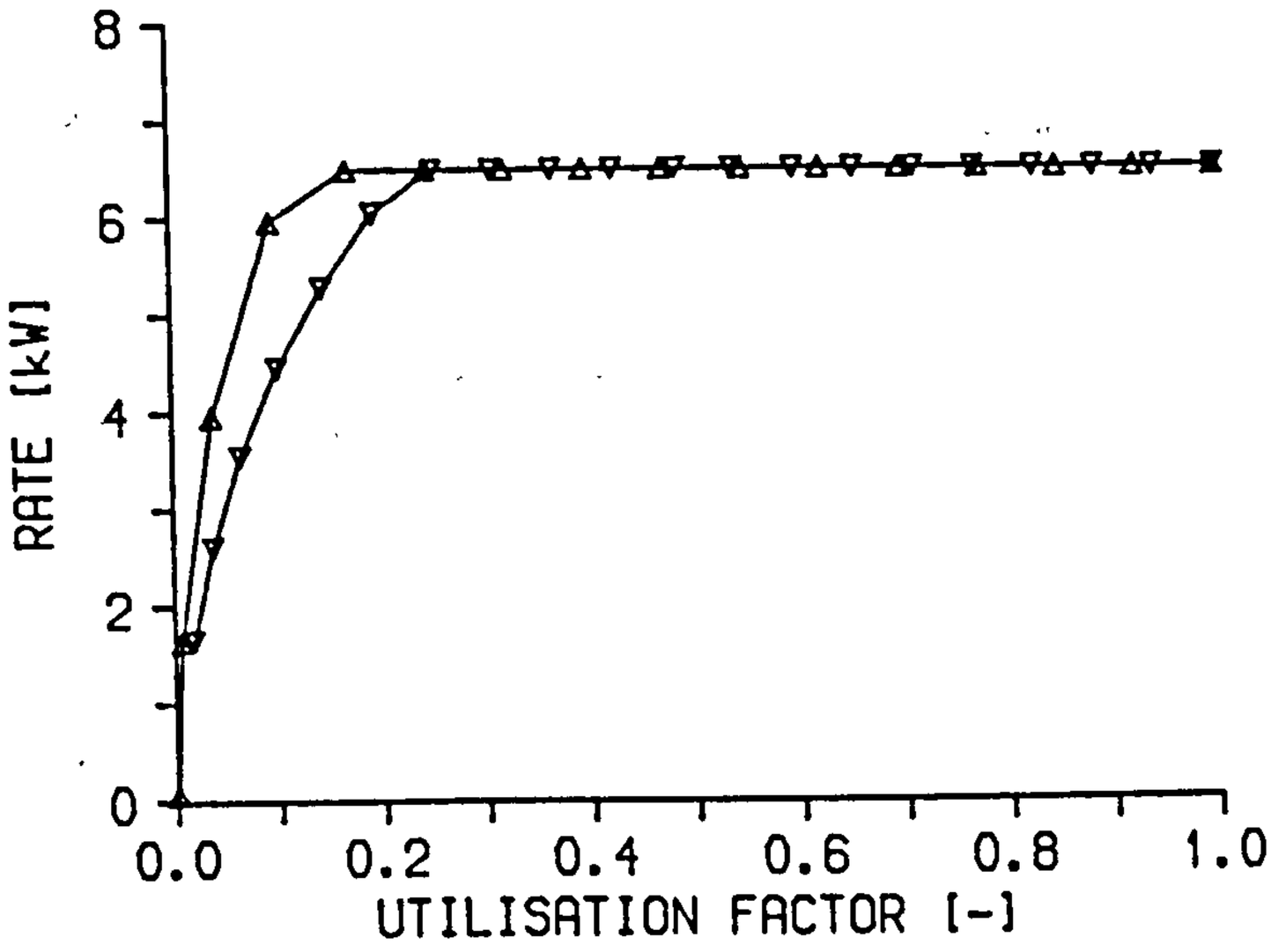

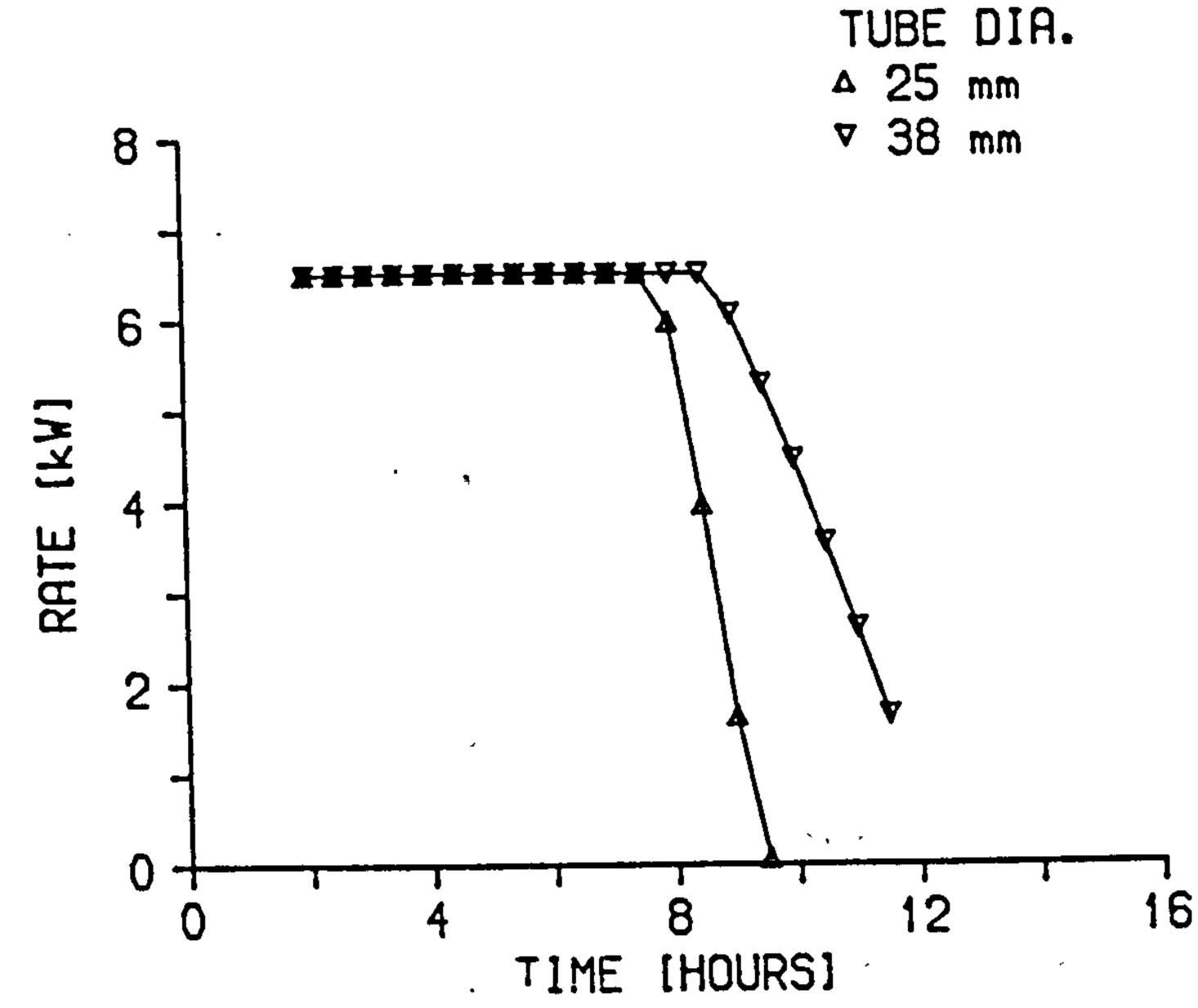

Figure 7.15 Predicted discharge rate against UF and time for 25 and 38 mm tubes in prototype store

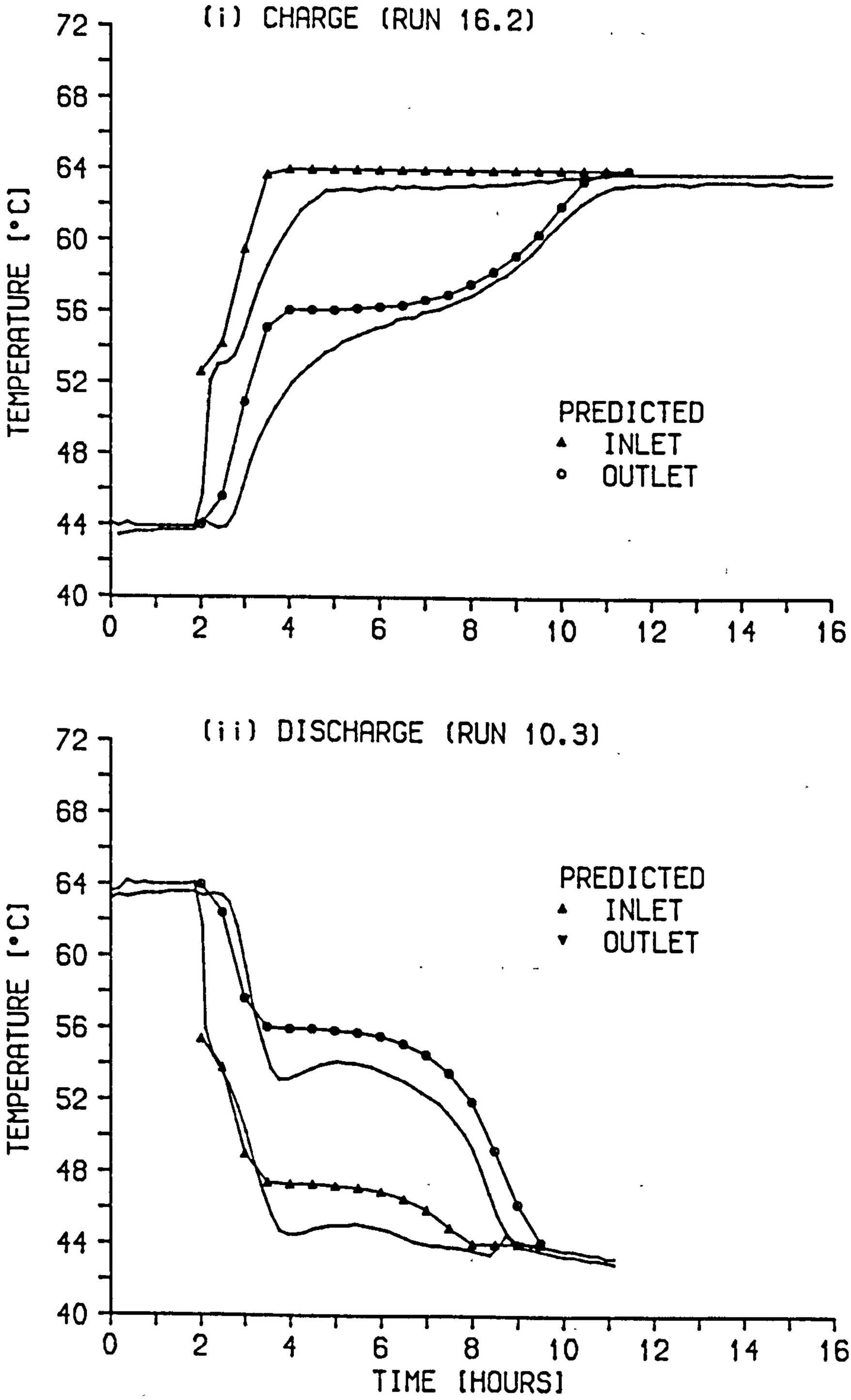

Figure 7.16 Predicted and experimental temperature-time variation of transfer fluid temperature during standard charge and discharge of prototype store

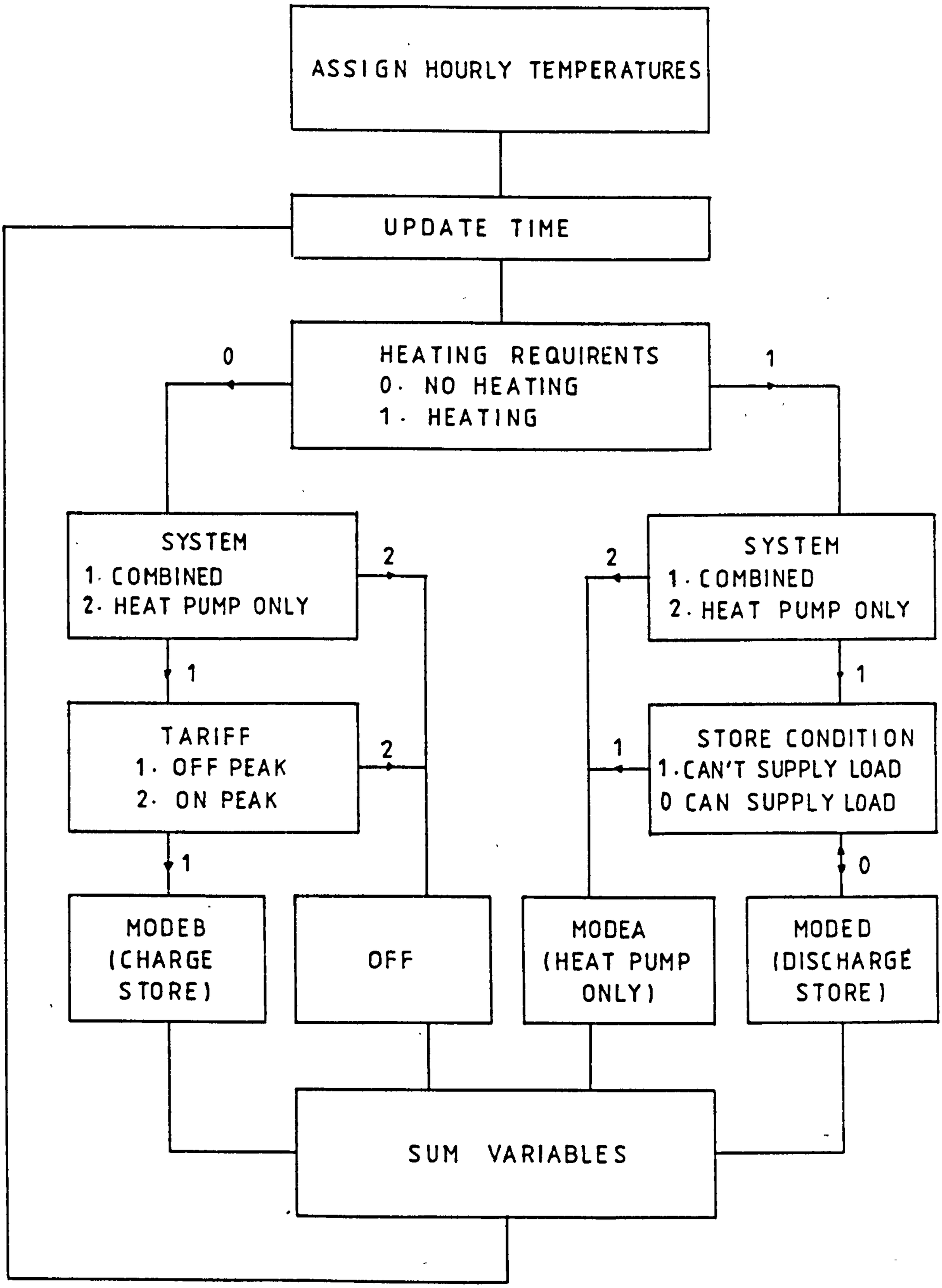

Figure 7.17 Block flow diagram showing control philosophy in elementary integrated system model

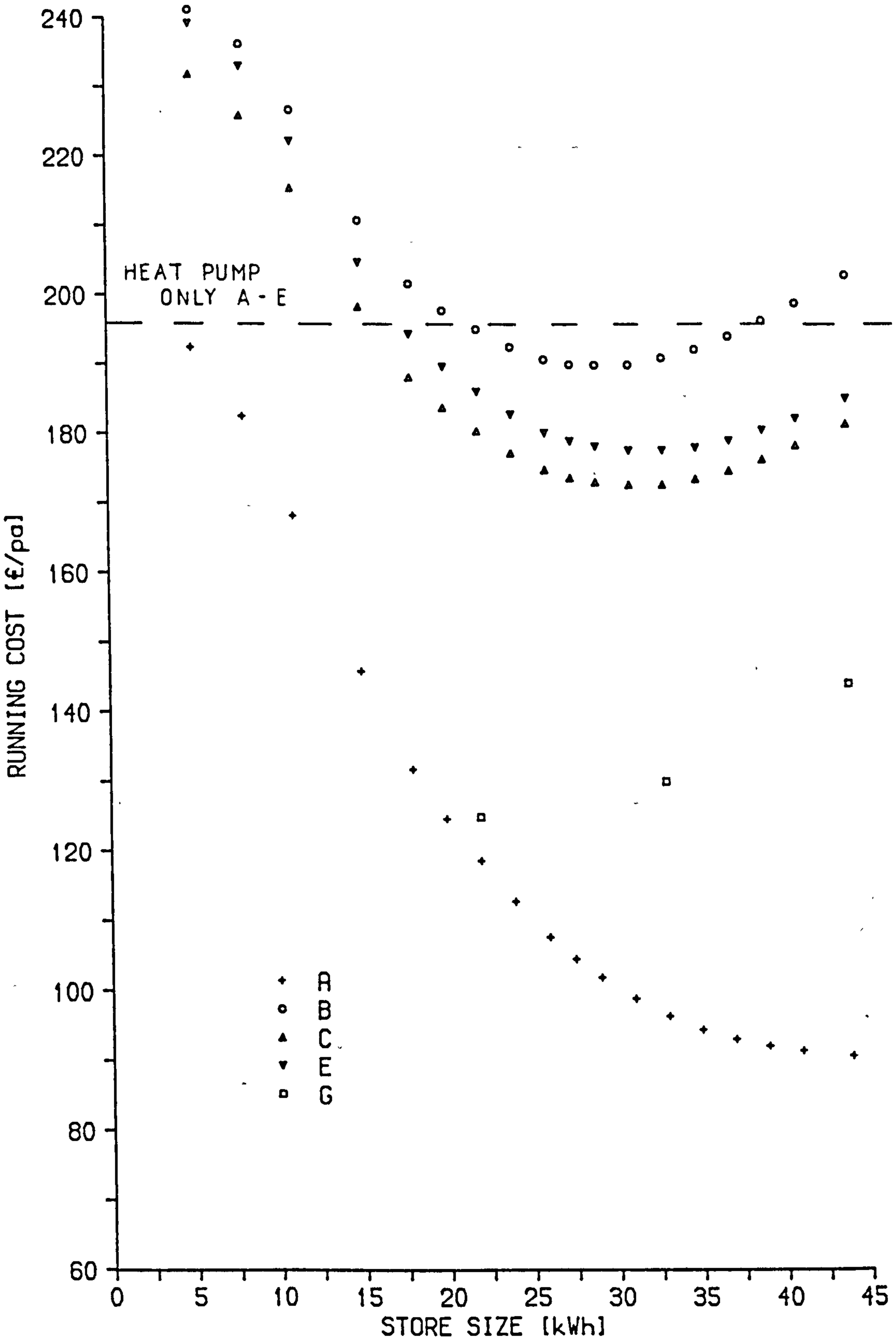

Figure 7.18 Running costs for integrated systems utilising a range of store sizes

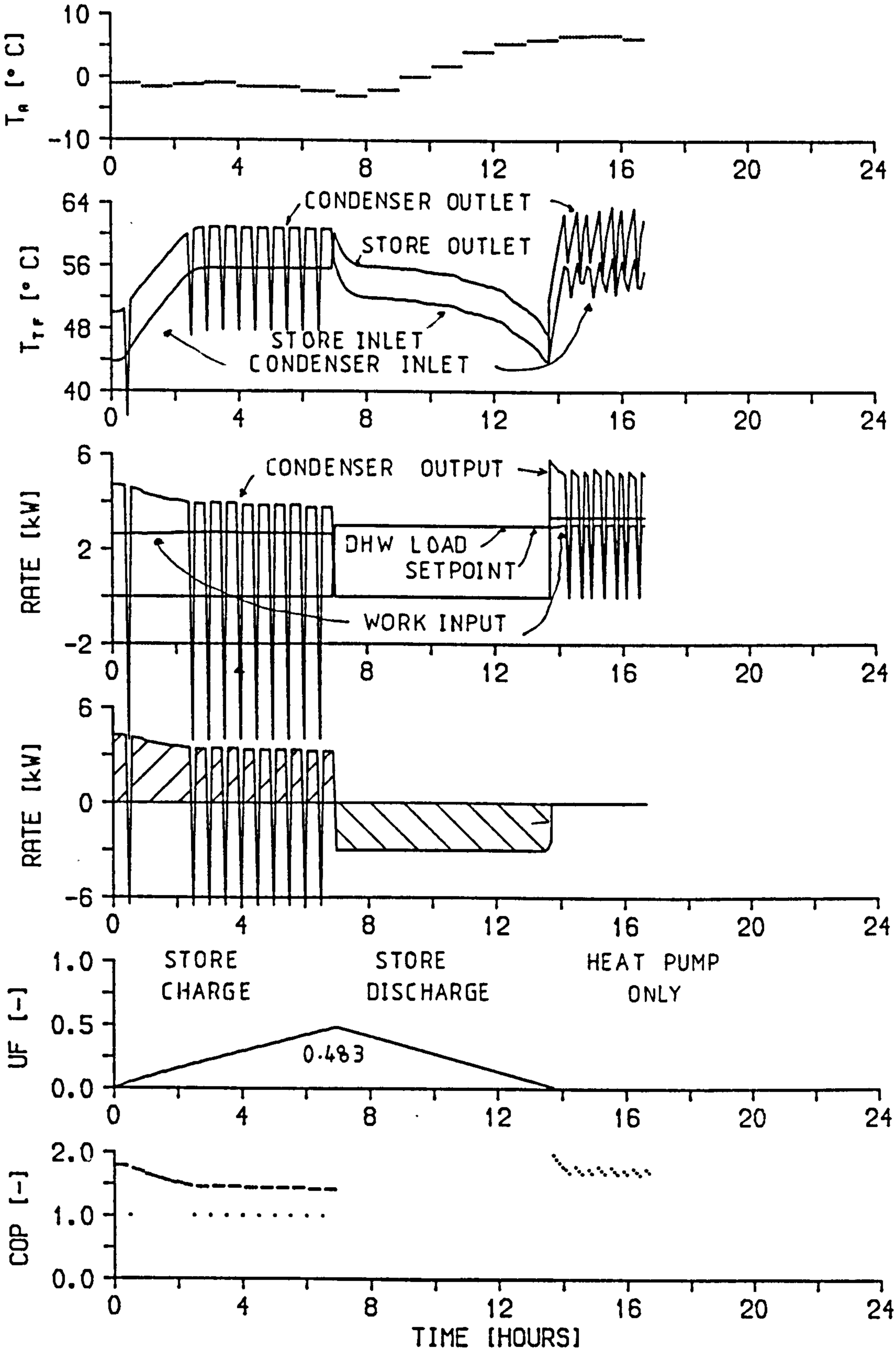

Figure 7.19 Simulated performance of integrated system on 12/3/87

Table 7.1 Thermodynamic Properties of Refrigerant R12

		Haywood (1978)		Model	
Saturation temperature	[°C]	-20	50	-20	50
Pressure	[Bar]	1.508	12.19	1.51	12.19
Specific volume					
liquid	[m^3/kg]	0.00069	0.00083	0.000685	0.000825
vapour	[m^3/kg]	0.1089	0.0142	0.1083	0.0141
Specific enthalpy					
liquid	[kJ/kg]	17.8	84.9	18.4	85.3
vapour	[kJ/kg]	178.7	206.5	178.6	206.3
Specific entropy					
liquid	[kJ/kgK]	0.0731	0.3037	0.0751	0.3047
vapour	[kJ/kgK]	0.7088	0.6797	0.7083	0.6791

Note:

In the above table the arbitrary datum state for zero enthalpy and entropy is that of saturated liquid at -40°C

Table 7.2 Theoretical Rankine and Carnot Cycle COP for R502

T_{ev} [°C]	T_{co} [°C]	ΔT [degC]	COP_R [1] [-]	COP_R [2] [-]	COP_C [2] [-]
15	55	40	6.07	6.02	8.20
10	55	45	5.31	5.26	7.29
5	55	50	4.69	4.65	6.56
0	55	55	4.20	4.15	5.96
-5	55	60	3.78	3.74	5.47
-10	55	65	3.44	3.40	5.05
-15	55	70	3.15	3.10	4.69
-20	55	75	2.89	2.85	4.37
15	60	45	5.22	5.17	7.40
10	60	50	4.62	4.57	6.66
5	60	55	4.13	4.08	6.05
0	60	60	3.72	3.68	5.55
-5	60	65	3.38	3.34	5.12
-10	60	70	3.09	3.05	4.76
-15	60	75	2.84	2.80	4.44
-20	60	80	-	2.59	4.16
15	65	50	-	4.44	6.76
10	65	55	-	3.96	6.15
5	65	60	-	3.57	5.63
0	65	65	-	3.24	5.20
-5	65	70	-	2.96	4.83
-10	65	75	-	2.72	4.51
-15	65	80	-	2.51	4.22
-20	65	85	-	2.33	3.98

Notes:

1. As published by Tai et al. (1982)
2. Output from HPMODEL_RANKCOP

Table 7.3 Prediction of COP_A from COP_R

T_a [°C]	T_{tf} [°C]	T_{ev} [°C]	T_{co} [°C]	COP_A[1] [-]	COP_A[2] [-]
-1	50	-6	50	2.41	2.44
-1	55	-6	55	2.23	2.25
-1	60	-6	60	-	2.05
-1	65	-6	65	-	1.83
7	50	2	50	2.65	2.70
7	55	2	55	2.45	2.52
7	60	2	60	-	2.32
7	65	2	65	-	2.10
16	50	11	50	2.88	2.97
16	55	11	55	2.69	2.81
16	60	11	60	-	2.63
16	65	11	65	-	2.41
-10	60	-15	60	-	1.76
-10	65	-15	65	-	1.55
-15	60	-20	60	-	1.61
-15	65	-20	65	-	1.41

Notes:

1. Data published by manufacturer
2. Output from model

Table 7.4 Comparison of Experimental and Predicted Performance

RUN	T_a [°C]	T_{tf} [°C]	Q_{co}[1] [kW]	W_{in}[1] [kW]	Q_{co}[2] [kW]	W_{in}[2] [kW]
4.2a	7.9	56.0	6.69	3.14	6.50	3.12
4.2b	8.5	63.3	6.30	3.30	6.10	3.28
4.2c	8.3	59.3	6.48	3.24	6.33	3.20
4.3a	6.2	58.9	5.92	3.15	5.93	3.09
4.3b	5.4	60.5	5.61	3.15	5.67	3.07
4.3c	4.7	59.7	5.49	3.12	5.58	3.01
4.4a	1.2	57.0	5.52	2.89	5.05	2.76
4.5a	4.5	58.6	5.82	3.08	5.61	2.99
4.5b	5.1	60.6	5.70	3.13	5.61	3.05
4.5c	4.4	63.6	5.31	3.09	5.30	3.06
4.5d	2.9	62.5	5.44	2.97	5.08	2.95
4.6a	4.2	59.4	5.46	3.07	5.50	2.98
4.6b	3.2	57.5	5.35	2.91	5.42	2.90

Notes

1. Experimental values
2. Output from HPMODEL_RANKCOP

Table 7.5 Simulated Heat Pump Performance

RUN	θ_{co} [degC]	θ_{ev} [degC]	T_{sup} [degC]	T_{sub} [degC]	η_{ad} [%]	η_{em} [%]	Q_{co} [kW]	COP [-]
0	2.9	8.3	5.8	16.5	56.8	70.3	5.85	1.827
0a	0	0	0	0	100	100	12.28	3.836
1a	0	8.3	5.8	16.5	56.8	70.3	6.13	1.917
1b	2.2	8.3	5.8	16.5	56.8	70.3	5.91	1.848
1c	3.6	8.3	5.8	16.5	56.8	70.3	5.78	1.807
2a	2.9	0	5.8	16.5	56.8	70.3	6.71	2.097
2b	2.9	6.2	5.8	16.5	56.8	70.3	6.04	1.889
2c	2.9	10.4	5.8	16.5	56.8	70.3	5.66	1.770
3a	2.9	8.3	0	16.5	56.8	70.3	5.79	1.810
3b	2.9	8.3	4.3	16.5	56.8	70.3	5.83	1.822
3c	2.9	8.3	7.1	16.5	56.8	70.3	5.86	1.831
4a	2.9	8.3	5.8	0	56.8	70.3	4.91	1.536
4b	2.9	8.3	5.8	12.4	56.8	70.3	5.62	1.757
4c	2.9	8.3	5.8	20.6	56.8	70.3	6.06	1.895
5a	2.9	8.3	5.8	16.5	100	70.3	8.63	2.697
5b	2.9	8.3	5.8	16.5	67.6	70.3	6.54	2.045
5c	2.9	8.3	5.8	16.5	46.0	70.3	5.15	1.610
6a	2.9	8.3	5.8	16.5	56.8	100	8.32	2.599
6b	2.9	8.3	5.8	16.5	56.8	77.7	6.46	2.020
6c	2.9	8.3	5.8	16.5	56.8	62.9	5.23	1.635

Notes

T_a=7°C, T_{tf}=63°C

Table 7.6 Dimensionless Temperature Time Position Relationship for Sensible Heat Storage in a Slab (Exact Analytical Solution)

Fo	T* for position x*=				
	0.2	0.4	0.6	0.8	1.0
0.20	0.2442	0.4616	0.6304	0.7363	0.7723
0.40	0.1467	0.2790	0.3839	0.4513	0.4745
0.60	0.0895	0.1703	0.2344	0.2755	0.2897
0.80	0.0547	0.1040	0.1431	0.1682	0.1769
1.00	0.0334	0.0635	0.0874	0.1027	0.1080
1.20	0.0204	0.0387	0.0533	0.0627	0.0659
1.40	0.0124	0.0237	0.0326	0.0383	0.0402
1.60	0.0076	0.0144	0.0199	0.0234	0.0246
1.80	0.0046	0.0088	0.0121	0.0143	0.0150
2.00	0.0028	0.0054	0.0074	0.0087	0.0092

Table 7.7 Interface Position and Temperature Histories for the Stefan Problem (Exact Analytical Solution)

Time	X	Temperature [degF] at postion x =							
[sec]	[ft]	0.1	0.2	0.3	0.4	0.5	0.6	0.7	0.8
36.0	0.160	-299	0	0	0	0	0	0	0
71.9	0.226	-484	-81	0	0	0	0	0	0
107.9	0.277	-573	-211	0	0	0	0	0	0
143.9	0.320	-628	-299	-42	0	0	0	0	0
179.8	0.358	-666	-363	-115	0	0	0	0	0
215.8	0.392	-694	-412	-174	0	0	0	0	0
251.7	0.424	-716	-452	-222	-37	0	0	0	0
287.7	0.453	-734	-484	-264	-81	0	0	0	0
323.7	0.480	-749	-512	-299	-119	0	0	0	0
359.6	0.506	-762	-535	-330	-153	-8	0	0	0
395.6	0.531	-773	-555	-357	-183	-39	0	0	0
431.6	0.555	-782	-573	-381	-211	-67	0	0	0
467.5	0.577	-791	-589	-402	-236	-93	0	0	0
503.5	0.599	-798	-603	-422	-259	-117	0	0	0
539.4	0.620	-805	-616	-440	-280	-140	-21	0	0
575.4	0.640	-811	-628	-456	-299	-161	-42	0	0
611.4	0.660	-817	-639	-471	-317	-180	-62	0	0
647.3	0.679	-822	-648	-484	-333	-198	-81	0	0
683.3	0.698	-826	-657	-497	-349	-215	-98	0	0
719.3	0.716	-831	-666	-509	-363	-231	-115	-15	0
755.2	0.734	-835	-674	-520	-377	-246	-131	-30	0
791.2	0.751	-839	-681	-530	-389	-261	-146	-45	0
827.1	0.768	-842	-688	-540	-401	-274	-160	-60	0

Table 7.8 Dimensionless Interface Position and Temperature Histories for the Stefan Problem (Exact Analytical Solution)

t*	X*	T* at postion x* =						
		0.125	0.250	0.375	0.500	0.625	0.750	0.875
0.015625	0.200	0.7011	1.0000	1.0000	1.0000	1.0000	1.0000	1.0000
0.031250	0.283	0.5158	0.9195	1.0000	1.0000	1.0000	1.0000	1.0000
0.046875	0.347	0.4268	0.7890	1.0000	1.0000	1.0000	1.0000	1.0000
0.062500	0.400	0.3722	0.7011	0.9578	1.0000	1.0000	1.0000	1.0000
0.078125	0.448	0.3343	0.6370	0.8852	1.0000	1.0000	1.0000	1.0000
0.093750	0.490	0.3060	0.5876	0.8263	1.0000	1.0000	1.0000	1.0000
0.109375	0.530	0.2838	0.5482	0.7776	0.9630	1.0000	1.0000	1.0000
0.125000	0.566	0.2659	0.5158	0.7364	0.9195	1.0000	1.0000	1.0000
0.140625	0.600	0.2510	0.4884	0.7011	0.8812	1.0000	1.0000	1.0000
0.156250	0.633	0.2383	0.4650	0.6703	0.8471	0.9919	1.0000	1.0000
0.171875	0.664	0.2274	0.4447	0.6432	0.8165	0.9611	1.0000	1.0000
0.187500	0.693	0.2178	0.4268	0.6192	0.7890	0.9328	1.0000	1.0000
0.203125	0.722	0.2094	0.4110	0.5976	0.7640	0.9067	1.0000	1.0000
0.218750	0.749	0.2019	0.3967	0.5781	0.7412	0.8826	1.0000	1.0000
0.234375	0.775	0.1951	0.3839	0.5605	0.7203	0.8602	0.9787	1.0000
0.250000	0.801	0.1890	0.3722	0.5443	0.7011	0.8394	0.9578	1.0000

Table 7.9 Predicted Interface Position and Charge/Discharge Rate against Time for 25 mm Tubes in Pilot Store

X* [-]	t* [-]	X [mm]	Time [min]	UF [-]	Rate [kW]	U_b [W/m^{2}K]
1.000	0.0000	11.20	0.0	0.000	2.030	66.0
0.950	0.0397	10.64	5.6	0.098	1.906	61.9
0.900	0.0797	10.08	11.3	0.190	1.791	58.2
0.850	0.1201	9.52	17.1	0.278	1.683	54.7
0.800	0.1605	8.96	22.8	0.360	1.583	51.4
0.750	0.2009	8.40	28.5	0.437	1,488	48.3
0.700	0.2412	7.84	34.3	0.510	1.398	45.4
0.650	0.2810	7.28	39.9	0.578	1.313	42.6
0.600	0.3204	6.72	45.5	0.640	1.232	40.0
0.550	0.3589	6.16	51.0	0.698	1.155	37.5
0.500	0.3965	5.60	56.3	0.750	1.081	35.1
0.450	0.4329	5.04	61.5	0.798	1.009	32.8
0.400	0.4679	4.48	66.5	0.840	0.939	30.5
0.350	0.5010	3.92	71.2	0.878	0.871	28.3
0.300	0.5321	3.36	75.6	0.910	0.804	26.1
0.250	0.5606	2.80	79.6	0.937	0.736	23.9
0.200	0.5863	2.24	83.3	0.960	0.668	21.7
0.150	0.6084	1.68	86.4	0.978	0.596	19.4
0.100	0.6263	1.12	89.0	0.990	0.518	16.8
0.050	0.6389	0.56	90.8	0.998	0.423	13.7
0.000	0.6442	0.00	91.5	1.000	0.423	13.7

Notes

Reynolds number 128.8

Fluid film h.t.c. 191.7 W/m^{2}K

Table 7.10 Dimensionless Temperature Time Position Relationship for Sensible Heat Storage in a Slab (Explicit Finite Difference Solution)

t*	T* at position x*=				
	0.2	0.4	0.6	0.8	1.0
(a) Fo = 0.5 , 5 nodes					
0.000	1.0000	1.0000	1.0000	1.0000	1.0000
0.200	0.2441	0.4395	0.6348	0.7080	0.7812
0.400	0.1466	0.2652	0.3839	0.4292	0.4745
0.600	0.0888	0.1606	0.2324	0.2598	0.2873
0.800	0.0537	0.0972	0.1407	0.1573	0.1739
1.000	0.0325	0.0589	0.0852	0.0952	0.1053
(b) Fo = 1 , 5 nodes					
0.000	1.0000	1.0000	1.0000	1.0000	1.0000
0.200	-6.0000	9.0000	-6.0000	4.0000	-1.0000
(c) Fo = 0.2 , 5 nodes					
0.000	1.0000	1.0000	1.0000	1.0000	1.0000
0.200	0.2415	0.4569	0.6245	0.7300	0.7659
0.400	0.1452	0.2762	0.3802	0.4468	0.4698
0.600	0.0886	0.1685	0.2319	0.2726	0.2866
0.800	0.0540	0.1028	0.1415	0.1663	0.1748
1.000	0.0330	0.0627	0.0863	0.1014	0.1067
(d) Fo = 0.2 , 10 nodes					
0.200	0.2436	0.4604	0.6289	0.7348	0.7707
0.400	0.1463	0.2783	0.3830	0.4502	0.4733
0.600	0.0893	0.1698	0.2338	0.2748	0.2889
0.800	0.0545	0.1037	0.1427	0.1677	0.1764
1.000	0.0333	0.0633	0.0871	0.1024	0.1076

Table 7.11 Dimensionless Temperature Time Position Relationship for Sensible Heat Storage in a Slab (Semi-implicit Finite Difference Solution)

t*	T* at position x*=				
	0.200	0.400	0.600	0.800	1.000
(a) Fo =1 , 5 nodes					
0.000	1.0000	1.0000	1.0000	1.0000	1.0000
0.200	0.2430	0.4596	0.6274	0.7330	0.7688
0.400	0.1466	0.2787	0.3836	0.4508	0.4740
0.600	0.0898	0.1707	0.2350	0.2763	0.2905
0.800	0.0550	0.1046	0.1440	0.1693	0.1780
1.000	0.0337	0.0641	0.0882	0.1037	0.1091
(b) Fo = 1 , 10 nodes					
0.000	1.0000	1.0000	1.0000	1.0000	1.0000
0.200	0.2442	0.4614	0.6298	0.7354	0.7712
0.400	0.1467	0.2790	0.3839	0.4512	0.4744
0.600	0.0896	0.1704	0.2346	0.2758	0.2900
0.800	0.0548	0.1042	0.1434	0.1685	0.1772
1.000	0.0335	0.0636	0.0876	0.1030	0.1083

Table 7.12 Dimensionless Temperature Histories for the Stefan Problem (Explicit Finite Difference Solution)

t*	T* at position x*=							
	0.125	0.250	0.375	0.500	0.625	0.750	0.875	1.000
(a) Fo = 0.2 , 16 nodes								
0.000000	1.0000	1.0000	1.0000	1.0000	1.0000	1.0000	1.0000	1.0000
0.015625	0.6887	1.0000	1.0000	1.0000	1.0000	1.0000	1.0000	1.0000
0.031250	0.5089	0.8833	1.0000	1.0000	1.0000	1.0000	1.0000	1.0000
0.046875	0.4216	0.7761	1.0000	1.0000	1.0000	1.0000	1.0000	1.0000
0.062500	0.3661	0.6985	0.9417	1.0000	1.0000	1.0000	1.0000	1.0000
0.078125	0.3293	0.6273	0.8825	1.0000	1.0000	1.0000	1.0000	1.0000
0.093750	0.3032	0.5813	0.8124	1.0000	1.0000	1.0000	1.0000	1.0000
0.109375	0.2807	0.5439	0.7771	0.9465	1.0000	1.0000	1.0000	1.0000
0.125000	0.2637	0.5109	0.7281	0.9140	1.0000	1.0000	1.0000	1.0000
0.140625	0.2488	0.4852	0.6977	0.8704	1.0000	1.0000	1.0000	1.0000
0.156250	0.2365	0.4612	0.6638	0.8409	1.0000	1.0000	1.0000	1.0000
0.171875	0.2256	0.4416	0.6399	0.8101	0.9434	1.0000	1.0000	1.0000
0.187500	0.2163	0.4236	0.6137	0.7817	0.9299	1.0000	1.0000	1.0000
0.203125	0.2078	0.4079	0.5941	0.7607	0.8970	1.0000	1.0000	1.0000
0.218750	0.2005	0.3940	0.5738	0.7343	0.8742	1.0000	1.0000	1.0000
0.234375	0.1937	0.3809	0.5563	0.7166	0.8599	0.9661	1.0000	1.0000
0.250000	0.1876	0.3697	0.5409	0.6961	0.8309	0.9464	1.0000	1.0000
(b) Fo = 0.2 , 8 nodes								
0.015625	0.6080	1.0000	1.0000	1.0000	1.0000	1.0000	1.0000	1.0000
0.125000	0.2616	0.5089	0.7223	0.8833	1.0000	1.0000	1.0000	1.0000
0.250000	0.1855	0.3661	0.5379	0.6985	0.8397	0.9417	1.0000	1.0000
(c) Fo = 0.2 , 40 nodes								
0.015625	0.6912	1.0000	1.0000	1.0000	1.0000	1.0000	1.0000	1.0000
0.125000	0.2648	0.5137	0.7341	0.9141	1.0000	1.0000	1.0000	1.0000
0.250000	0.1884	0.3711	0.5428	0.6992	0.8368	0.9556	1.0000	1.0000
(d) Fo = 0.2 , 80 nodes								
0.015625	0.6965	1.0000	1.0000	1.0000	1.0000	1.0000	1.0000	1.0000
0.125000	0.2653	0.5147	0.7349	0.9186	1.0000	1.0000	1.0000	1.0000
0.250000	0.1887	0.3716	0.5435	0.7000	0.8382	0.9565	1.0000	1.0000

Table 7.13 Dimensionless Temperature Histories for the Stefan Problem (Semi-implicit Finite Difference Solution)

t*	T* at position x*=							
	0.125	0.250	0.375	0.500	0.625	0.750	0.875	1.000
(a) Fo = 1 , 40 nodes								
0.000000	1.0000	1.0000	1.0000	1.0000	1.0000	1.0000	1.0000	1.0000
0.015625	0.6774	1.0000	1.0000	1.0000	1.0000	1.0000	1.0000	1.0000
0.031250	0.5028	0.9051	1.0000	1.0000	1.0000	1.0000	1.0000	1.0000
0.046875	0.4182	0.7740	1.0000	1.0000	1.0000	1.0000	1.0000	1.0000
0.062500	0.3658	0.6901	0.9414	1.0000	1.0000	1.0000	1.0000	1.0000
0.078125	0.3292	0.6279	0.8706	1.0000	1.0000	1.0000	1.0000	1.0000
0.093750	0.3016	0.5794	0.8171	1.0000	1.0000	1.0000	1.0000	1.0000
0.109375	0.2800	0.5412	0.7678	0.9536	1.0000	1.0000	1.0000	1.0000
0.125000	0.2626	0.5095	0.7283	0.9095	1.0000	1.0000	1.0000	1.0000
0.140625	0.2480	0.4829	0.6934	0.8707	1.0000	1.0000	1.0000	1.0000
0.156250	0.2357	0.4600	0.6632	0.8385	1.0000	1.0000	1.0000	1.0000
0.171875	0.2250	0.4401	0.6367	0.8091	0.9515	1.0000	1.0000	1.0000
0.187500	0.2156	0.4225	0.6130	0.7818	0.9226	1.0000	1.0000	1.0000
0.203125	0.2073	0.4069	0.5919	0.7571	0.8975	1.0000	1.0000	1.0000
0.218750	0.1999	0.3929	0.5728	0.7347	0.8744	1.0000	1.0000	1.0000
0.234375	0.1933	0.3803	0.5554	0.7141	0.8525	0.9700	1.0000	1.0000
0.250000	0.1873	0.3688	0.5395	0.6951	0.8322	0.9492	1.0000	1.0000
(b) Fo =1 , 16 nodes								
0.015625	0.6448	1.0000	1.0000	1.0000	1.0000	1.0000	1.0000	1.0000
0.125000	0.2581	0.5002	0.7124	0.8904	1.0000	1.0000	1.0000	1.0000
0.250000	0.1846	0.3637	0.5326	0.6871	0.8217	0.9328	1.0000	1.0000

Table 7.14 Predicted Annual Running Cost Data for Integrated System

Run	Load	T_{set}	TSC	HPsize	Unit	Cost
[-]	[W/degC]	[°C]	[kWh]	[kW]	**£/kWh**	**£/p.a.**
A1	380	20	44	6	0.044	249.1
A3[1]	380	20	-	6	0.044	389.9
A4	380	15	44	6	0.044	110.2
A5	380	20	55	6	0.044	224.2
A6	380	20	33	6	0.044	277.7
A7	380	20	44	7.5	0.044	249.1
A8	380	20	44	4.5	0.044	311.1
A9	380	20	22	6	0.044	311.1
A10	380	20	11	6	0.044	350.7
A11	380	20	44	6	0.0534	302.3
A12[1]	380	20	-	6	0.0534	473.2
A13	380	20	66	6	0.044	221.4
A14[1]	380	15	-	6	0.044	209.4
A15	380	20	5	6	0.044	372.4
A16	380	20	66	7.5	0.044	202.6
A17[2]	380	20	44	6	0.044	108.1
A18[2]	380	20	44	6	0.044	229.3

Notes

1. Performed with heat pump only
2. All runs assumed a heating period from 0700-2400 apart from these two which assumed an occupancy (and hence demand) during the periods 0700-0900, 1300-1400 and 1700-2400

Table 7.15 Predicted Savings in Annual Running Costs of Integrated Systems over Conventional Heat Pumps

Cost		Store size [kWh]					
Tank [£]	PCM [£]	11 [£/pa]	22 [£/pa]	33 [£/pa]	44 [£/pa]	55 [£/pa]	66 [£/pa]
(a) Interest rate 10%, working life 10 years							
0	10	21.30	43.00	58.49	69.19	75.99	61.09
150	10	-3.11	18.58	34.08	44.78	51.58	36.68
300	10	-27.53	-5.83	9.67	20.37[1]	27.17	12.26
450	10	-51.94	-30.24	-14.74	-4.04	2.75	-12.15
150	12.5	-7.59	9.63	20.66	26.88	29.20	9.82
300	12.5	-32.00	-14.78	-3.76	2.47	4.79	-14.59
150	7.5	1.36	27.54	47.51	62.68	73.96	63.53
300	7.5	-23.05	3.12	23.10	38.27	49.54	39.12
(b) Interest rate 15%, working life 10 years							
15.0	10	-12.61	5.08	16.56	23.24	26.02	7.11
300	10	-42.49	-24.81	-13.33	-6.65	-3.86	-22.78
(c) Interest rate 5%, working life 10 years							
150	10	5.53	30.88	50.04	64.39	74.85	63.60
300	10	-13.90	11.46	30.61	44.97	55.42	44.18
(d) Interest rate 10%, working life 15 years							
150	10	5.02	30.15	49.09	62.23	73.47	62.01
300	10	-14.70	10.43	29.37	43.51	53.75	43.29

Notes

1. Assumed standard for comparison
2. Heat pump alone running cost was £389.90 pa

Table 7.16 Economic Analysis of Integrated System Running Costs

RUN		B	C	D	E	G
Interest rate	[%]	10	10	5	10	10
Working life	[years]	10	15	10	10	10
Tank and ancillaries	[£]	250	250	250	250	250
PCM and encapsulation	[£/kWh]	10	10	10	7.5	10
Crf	[-]	0.1627	0.1315	0.1295	0.1627	0.1627
Total load	[kWh]	6048	6048	6048	6048	3781
Heat pump only	[£/pa]	196.4	196.4	196.4	196.4	123.1
	[p/kWh]	3.25	3.25	3.25	3.25	3.25
Minimum running	[£/pa]	189.6	172.3	171.2	177.2	124.6
	[p/kWh]	3.13	2.85	2.83	2.93	3.29
For store size	[kWh]	29	31	31	31-33	22

Notes:

1. Running costs for Run A do not include capital cost of storage device

Table 7.17 Multiple Regression Expressions for Heat Pump Performance

	Thermal Output[kW]	Work Input
Coefficients		
Constant	7.65	2.36
Ambient temperature	0.159	0.0465
Condenser inlet temperature	−0.0633	0.00730
t−ratio		
Constant	91.76	56.90
Ambient temperature	55.87	32.32
Condenser inlet temperature	−38.46	8.76
Standard deviation	0.06178	0.03128
R−sq, coefficient of determination	98.3%	93.9%
Sum of squares		
Regression	16.9113	1.12172
Error	0.2863	0.07337
Total	17.1976	1.19509

Table 7.18 Analysis of Simulated Integrated System Performance

		12/3	13/3	14/3	15/3
Charging store					
Charge period	[hours]	6.9	-	6.9	6.9
Average ambient temperature	[°C]	-1.6	1.7	2.1	4.4
Total power input	[kWh]	18.48	-	19.62	20.40
Final UF	[-]	0.483	-	0.568	0.621
Total charge[1]	[kWh]	20.82	-	24.48	26.77
Average COP	[-]	1.13	-	1.25	1.31
Initial COP (0030-0045)	[-]	1.74	-	1.81	1.88
Final COP (0645-0700)	[-]	1.42	-	1.56	1.61
Maximum condenser outlet	[°C]	60.4	-	61.4	61.9
Discharging store					
Discharge period	[hours]	6.7	-	8.0	8.7
Final UF	[-]	0.017	-	0.013	0.016
Total discharge	[kWh]	20.08	-	23.92	26.08
Total domestic heating load	[kWh]	20.10	-	24.00	26.10
Average domestic heating load	[kW]	3.00	-	3.00	3.00
Minimum store outlet[2]	[°C]	47.2	-	46.9	47.3
Heat pump only					
Heat pump only period	[hours]	3.5	9.55	9.05	0.10
Load set to	[kW]	3.37[D	3.49	3.58	-
Total domestic heating load	[kWh]	11.81	33.37	32.37	0.35
Total power input	[kWh]	7.91	23.58	21.57	-
Average COP	[-]	1.49	1.41	1.50	-

Notes:

1. For total TSC of 44.4 kWh (159.9 MJ)
2. For discharge rate greater than 2.5kW

CHAPTER 8

CONCLUSIONS AND RECOMMENDATIONS

A detailed list of conclusions and recommendations is presented at the end of each experimental chapter and at the end of each section in the modelling chapter; hence only a brief overview of the general conclusions and recommendations that can be drawn from this work will be presented here.

An experimental facility was constructed which permitted the performance of prototype heat pumps and thermal storage devices to be evaluated. The experimental error in determining heat transfer rates was small but could be significantly improved by employing a flowmeter with greater accuracy or one of similar design with a lower maximum design flow rate. Thermopiles were found to dramatically reduce the error in determining temperature differences of less than ten degrees Celsius. A control and datalogging program was written which supervised the experimental procedure for obtaining thermal storage device performance data. A modified version was successfully employed to operate and log data from an integrated heat pump/latent heat store system over periods up to ten days.

Pilot and prototype stores were subjected to ASHRAE type charge/discharge tests with a range of operating flow rates, inlet temperatures and flow direction (top-down or bottom-up). Maximum charge rates were achieved with high flow rates, high inlet temperatures and flow top-down, while maximum discharge rates were achieved for high flow rates, low inlet temperatures and flow bottom-up.

A finite difference model for simulating the performance of the prototype store was developed. An explicit solution technique was found to combine good accuracy with reasonable computer run-time. The finite difference technique was verified by comparison with an analytical solution for latent heat storage in a semi-infinite slab. Predicted temperature profiles and heat transfer rates were in reasonable agreement with experimental data and showed a dramatic improvement on results obtained with the conventional approximate analytical model.

Heat pump performance was shown to improve with increasing ambient air temperature and decreasing transfer fluid temperature. Defrosting was shown to reduce the average COP by approximately 3.5% and thermal cycling found to result in a COP which was dependent on the load being supplied and thermal capacity of the fluid in the buffer tank.

Parameters which described the deviation of the experimental heat pump performance from that of the ideal Rankine cycle were determined and successfully employed by a diagram heat pump model to predict heat pump performance.

Experimental performance of the integrated system was reported over a range of real ambient conditions. Tracking the store condition over a period of more than a few days proved to be the major obstacle to overcome in future research work.

A detailed integrated system model which combined the finite difference model with multiple regression expressions for heat pump performance, very successfully simulated the daily performance of the system. Unfortunately the amount of computer time prevented detailed simulation for any significant period but methods of reducing the computer run-time to allow the economic evaluation of potential systems have been recommended.

An elementary model of the prototype integrated system, which included many simplifications was employed to determine the yearly running costs of the prototype heat pump combined with various thermal storage devices (from 0 to 44 kWh) for a typical dwelling. For an interest rate of 5%, working life of 10 years, costs of £250 for tank and ancillaries, and £10 per kWh for the PCM and encapsulation, a storage device with a thermal capacity of 31 kWh was found to offer the maximum savings and reduce the annual running costs by 12.8%.

In addition to the recommendations given above future research effort should be directed at:

1. reducing heat loss from the experimental facility

2. determining the sensible and latent heats of the PCM experimentally by calorimetry

3. developing a method of simulating the heat pump utilising the water bath heaters, thereby reducing the dependence on the unreliable prototype heat pump and increasing the flexibility of the test facility

4. gaining a better understanding of the phase change mechanism by comparison of the theoretical and experimental transfer fluid temperature profiles

5. evaluation of potential use strategies (including commercial applications where there also may be a demand for cooling) with integrated system model

CHAPTER 9

APPENDICES

9.1. Pertinent Data

9.1.1. Calibration Data

9.1.1.1. Measurement

(a) Thermocouples

For type K (NiCr-NiAl), range 0-100°C

$$T = 2.534\times10^{-2}\,V - 3.85\times10^{-7}\,V^2 + 4\times10^{-11}\,V^3 - 2.5\times10^{-16}\,V^4 \qquad (9.1)$$

where V is voltage [μV]

Accuracy: ± 0.02°C (CIL data)

± 0.1°C (experimental)

Sensitivity: 0.0625°C

(b) Thermopile

$$\Delta T = V/41 \qquad (9.2)$$

where V is voltage [μV]

Accuracy: ± 0.02 degC (experimental)

Sensitivity: 0.012 degC

(c) Hot water flow rate

$$F = 2.323\times10^{-2}\,B + 5.558 \text{ (antifreeze)} \qquad (9.3)$$

$$F = 2.548\times10^{-2}\,B + 5.029 \text{ (water)} \qquad (9.4)$$

Accuracy: ± 1% FSD (Rhodes)

± 2% FSD (experimental) ± 0.2 lit/min at 11.5 lit/min

Sensitivity: 0.025 lit/min

(d) Cold water flow rate

$$F = -6.055\times10^{-6}\ B^2 + 1.155\times10^{-2}\ B + 6.003 \qquad (9.5)$$

Accuracy: ± 0.1 lit/min (experimental)

Sensitivity: 0.0085 lit/min

(e) Pressure

$$P = 3.9868\times10^{-3}\ B \quad \text{(for 15 barg max.)} \qquad (9.6)$$

$$P = 9.2801\times10^{-3}\ B \quad \text{(for 35 barg max.)} \qquad (9.7)$$

Accuacy: ± 2% (experimental)

(f) Power

$$W = \omega/3 \qquad (9.8)$$

where ω is rotation speed of disk [rpm]

Accuracy: ± 2% (experimental)

(g) Humidity

$$\log_{10} P = 28.5907 - 8.2 \log_{10} T + 0.0024804\ T - 3142.31\ T^{-1} \qquad (9.9)$$

where T is temperature [K] and P is vapour pressure of water [bar] (see Rosell et al. 1983b).

$$W = 0.622\ P_T/(P_T - p) \qquad (9.10)$$

where p is partial pressure of vapour [bar], P_T is total pressure [bar] and W is humidity of moist air [kg/kg]

$$W = W^*_s - Cp_a/\lambda_w(T_{DB}-T_{WB}). \quad (9.11)$$

where W^*_s is the saturation humidity, Cp_a is specific heat of dry air and λ_w is the latent heat of evaporation of water. Note that Cp_a/λ_w is the slope of the adiabatic saturation line.

9.1.1.2. Control

(a) Temperature – heat input

Heat Demand (kW)	R1 (3 kW)	R2 (2x3 kW)
$0 < q < 3$	1,0	0
$3 < q < 6$	1	0
$6 < q < 9$	0	1
$q > 9$	1	1

Note: R1 connected to single 3 kW heating element while R2 controlled the operation of two 3 kW elements (see figure 3.8).

(b) Hot water flow rate

$$B = -4.074\ F^3 + 116.5\ F^2 - 1152\ F + 5290 \quad (9.12)$$

(c) Cold water flow rate

$$B = -32.29\ F^3 + 151.4\ F^2 - 289.1\ F + 1759 \quad (9.13)$$

9.1.2. Property Data

9.1.2.1. Properties of PCMs

(a) Calortherm 58

T_{mp}	(Experimental)	[°C]	56
ρ	(Calor)	[kg/m^3]	1460

	λ	(Calor)	[kWh/litre]	0.098
			[kJ/kg]	242
	Cp	(Calor)	[kWh/litre]	0.001
			[J/kgK]	2470
	k	(Calor)	[W/mK]	0.65

(b) Metal, all data taken from Murray and Landis (1959)

T_{mp}		[°C]	555.6
ρ		[kg/m^3]	8000
λ		[kJ/kg]	116.3
Cp		[kJ/kgK]	418.7
k		[W/mK]	86.5

9.1.2.2. Properties of encapsulation and storage device materials

(a) Encapsulation

Polypropylene	Cp	(Perry p23-63)	[J/kgK]	1926
	k	(Calor)	[W/mK]	0.138
		(Perry p23-63)	[W/mK]	0.14

(b) Storage Devices

Glass	Cp	(Perry p23-60)	[J/kgK]	778
	k	(Foust p60)	[W/mK]	0.5
Brass	Cp	(Perry p23-49)	[J/kgK]	377
Dural	Cp	(Perry p23-48)	[J/kgK]	962
Mild steel	Cp	(Perry p23-38)	[J/kgK]	460
Stainless steel	k	(McC & S p999)	[W/mK]	16.3

(c) Insulation

Fibre glass	k		[W/mK]	0.035
Polystyrene	k	(Perry p11-51)	[W/mK]	0.026

9.1.2.3. Properties of transfer fluid

(a) Water

All data was interpolated from table presented in McCabe and Smith (1980) p1002.

At 35.5°C	μ		[kg/ms]	0.723 x10^{-3}
	k		[W/mK]	0.623
	ρ		[kg/m^3]	992.7
At 44°C	μ		[kg/ms]	0.613 x10^{-3}
	k		[W/mK]	0.635
	ρ		[kg/m^3]	989.4
At 56°C	μ		[kg/ms]	0.502 x10^{-3}
	k		[W/mK]	0.65
	ρ		[kg/m^3]	984
	Cp		[J/kgK]	4185
	β	(CRC F-5)	[K^{-1}]	4.98 x10^{-4}

(b) Antifreeze

For 25% commercial antifreeze mixture

At 56°C	ρ	(experimental)	[kg/m^3]	995.7
	μ	(experimental)	[kg/ms]	0.88 x10^{-3}

For 25% ethylene glycol solution

At 56°C	ρ	(Perry p12-48)	[kg/m^3]	1015
	μ	(Perry p12-47)	[kg/ms]	0.80 x10^{-3}
	Cp	(Perry p12-47)	[J/kgK]	3936
	k	(Perry p12-48)	[W/mK]	0.519

9.1.2.4. Properties of moist air

(a) Water vapour

-10<T<20°C	λ	(Rosell 1983b)	[kJ/kg]	2501

(b) Dry air

-10<T<20°C	Cp	(Rosell 1983b)	[J/kgK]	1002.5

At 5°C ρ (CRC F-11*) [kg/m^3] 1.27

* $\rho = 0.001293/(1+0.00367T)(P/76)$ (9.14)

where ρ is density [g/ml] and P is pressure [cm Hg].

9.2. Computer Software

9.2.1. Experimental Facility Programs

These are not actually contained in the thesis but are reproduced in a separate appendix held in the department.

9.2.2. Simulation Programs

These are not actually contained in the thesis but are reproduced in a separate appendix held in the department.

9.2.2.1. Heat pump models

1. HPMODEL_PHDATA
2. HPMODEL_RANKCOP
3. HPMODEL_EXPCOP
4. HPMODEL_REALCOP1

9.2.2.2. Heat store models

1. HSMODEL_ANXASESL
2. HSMODEL_ANXALASL
3. HSMODEL_ANLAPPROX
4. HSMODEL_FDEXSESL
5. HSMODEL FDCNSESL
6. HSMODEL_FDEXLASL
7. HSMODEL_FDCNLASL
8. HSMODEL_FDEXLACY2

9.2.2.3. Integrated heat pump – heat store models

1. HPHSMODEL_ELVERS1
2. HPHSMODEL_ELVERS2A
3. HPHSMODEL_DETVERS2A
4. HPHSMODEL_HPONLY1

9.3. Error Analysis

Thermal properties were assumed to introduce negligible error in this analysis and justification for this assumption is discussed in the appropriate section of text. The accuracy of instrumentation employed in determining the following derived quantity errors were taken from section 9.1.1.1.

9.3.1. Heat Storage Device Results

9.3.1.1. Rate of heat transfer to/from pilot store

The rate of heat transfer to/from the pilot store was calculated using equation (4.17). The experimental errors in this calculation were:

1. Mass flow rate, ± 2.85% (at 7 lit/min)
2. Temperature drop measured by thermopile, ± 1.6% (1 kW at 7 lit/min)

Hence the total error in determination of heat transfer rate to/from the pilot store for typical conditions was found to be ± 4.5%.

9.3.1.2. Rate of heat transfer to/from prototype storage device

The rate of heat transfer to/from the prototype store was calculated using equation (4.17). The experimental errors in this calculation were:

1. Mass flow rate, ± 1.75% (at 11.5 lit/min)
2. Temperature drop measured by thermopile, ± 0.25% (6 kW at 11.5 lit/min)

Hence the total error in determination of the heat transfer rate to/from the

prototype storage device for typical operating conditions was found to be ± 2%.

9.3.1.3. Loss coefficient from prototype storage device

The rate of heat loss from the store was calculated from equation (4.17) with the following experimental errors:

1. Mass flow rate, ± 1.75% (at 11.5 lit/min)
2. Temperature drop measured by thermopile, ± 8.65% (175 W at 11.5 lit/min)

For a difference of 25 degC between the store and ambient measured by two individual thermocouples a further error of ± 0.8% is introduced, Hence the total error in calculating the heat loss coefficient was found to be ± 11.2%.

9.3.1.4. Approximate heat transfer coefficient in prototype store

The approximate heat transfer coefficient was calculated from equation (4.16) with the following experimental errors:

1. Heat transfer rate, ± 2.25% (see 9.3.1.2 above)
2. Log mean temperature difference, ± 3.75% (3 kW at 11.5 lit/min, with inlet temperature of 64°C), note that since the tube centre-line temperature was specified the error in ΔT_1 and ΔT_2 was assumed to ± 0.1 degC

Hence the total error in calculating the approximate heat transfer coefficient at limiting charge/discharge rates (less than 3 kW) was found to be ± 6%.

9.3.1.5. Amount of heat transferred to/from prototype store

The PET internal clock measures time in jiffies (1/60th of a second) and since the average time step was one minute, the error in measuring the time interval was negligible (less than 0.03%). Hence the experimental error in determining the store condition for typical operating conditions was found to be ± 2% (see section 9.3.1.2).

9.3.2. Heat Pump Results

9.3.2.1. Rate of heat transfer at condenser

The rate of heat transfer from the condenser was determined from equation (4.17), which had the same error (± 2%) as that determined in 9.3.1.2 when utilising a thermopile to measure the temperature drop. Earlier data was determined using two individual thermocouples which increased the temperature drop measurement error by an order of magnitude and resulted in an overall error of ± 4.25%.

9.3.2.2. Rate of heat transfer to load

The rate of heat transfer to load was determined from equation (4.17) with the following experimental errors:

1. Mass flow rate, ± 1.75% (at 11.5 lit/min)
2. Temperature drop measured by two thermocouples, ± 5% (3 kW at 11.5 lit/min)

Hence the total error was found to be ± 6.75% for normal operating conditions.

9.3.2.3. Coefficient of Performance

The COP was determined from equation (2.1) and was subject to the following experimental errors:

1. Rate of heat transfer at condenser, ± 2% or ± 4.25% (see 9.3.2.1)
2. Rate of work input, ± 2%

Hence the experimental error in calculating the COP was found to be ± 4% using a thermopile or ± 6.3% if two independent thermocouples were used to measure the temperature drop across the condenser.

Table 9.1 Results from Run Performed on 12/3/87

	HEAT PUMP							HEAT STORE			
t	T_{out}	T_{in}	T_a	W	q_{co}	COP	q_{DHW}	T_{in}	T_{out}	$q_{C,D}$	UF
[hr]	[°C]	[°C]	[°C]	[kW]	[kW]	[-]	[kW]	[°C]	[°C]	[kW]	[-]
0.11	47.5	43.8	-1.3	2.71	3.06	1.22	0.00	47.5	44.1	2.63	0.002
0.21	49.8	44.0	-0.7	2.69	4.53	1.68	0.00	49.8	44.0	4.31	0.011
0.31	50.0	44.1	-1.3	2.63	4.52	1.71	0.00	50.0	44.1	4.30	0.020
0.41	50.0	44.0	-0.5	2.61	4.58	1.75	0.00	50.0	44.0	4.36	0.030
0.51	50.2	44.1	-0.7	2.63	4.64	1.76	0.00	50.2	44.1	4.42	0.040
0.61	45.9	43.6	-1.2	2.56	1.73	1.29	0.00	45.9	43.6	1.56	0.044
0.71	50.3	44.2	-1.7	2.66	4.65	1.75	0.00	50.3	44.3	4.36	0.052
0.81	50.4	44.3	-1.4	2.60	4.62	1.77	0.00	50.4	44.6	4.23	0.061
0.91	50.6	44.7	-1.7	2.63	4.52	1.71	0.00	50.6	45.0	4.03	0.071
1.01	51.0	45.1	-1.4	2.59	4.52	1.74	0.00	51.0	45.5	3.97	0.080
1.11	51.5	45.6	-1.3	2.66	4.52	1.70	0.00	51.5	46.0	3.96	0.088
1.21	47.6	46.4	-1.5	2.55	0.93	1.06	0.00	47.6	47.0	0.29	0.092
1.31	52.3	46.4	-1.5	2.69	4.43	1.65	0.00	52.3	46.9	3.87	0.098
1.41	52.6	46.8	-1.8	2.66	4.38	1.64	0.00	52.6	47.4	3.83	0.106
1.51	52.9	47.2	-1.9	2.60	4.34	1.66	0.00	52.9	47.6	3.81	0.114
1.59	53.2	47.5	-1.9	2.66	4.32	1.62	0.00	53.2	47.9	3.81	0.122
1.69	53.4	47.7	-2.0	2.60	4.31	1.65	0.00	53.4	48.1	3.82	0.130
1.79	47.7	48.0	-1.5	2.52	-0.20	0.81	0.00	47.7	48.4	-0.66	0.133
1.90	54.1	48.3	-2.0	2.65	4.40	1.66	0.00	54.1	48.6	3.92	0.137
1.99	54.2	48.5	-2.1	2.60	4.30	1.65	0.00	54.2	48.9	3.80	0.146
2.10	54.4	48.8	-2.0	2.63	4.24	1.60	0.00	54.4	49.1	3.75	0.154
2.19	54.8	49.0	-1.3	2.70	4.37	1.61	0.00	54.8	49.4	3.88	0.163
2.30	55.0	49.3	-1.5	2.64	4.41	1.67	0.00	55.0	49.6	3.92	0.172
2.40	49.1	49.7	-1.5	2.59	-0.43	0.79	0.00	49.1	50.1	-0.92	0.173
2.50	55.6	49.7	-1.5	2.74	4.40	1.60	0.00	55.6	50.1	3.90	0.179
2.60	55.7	49.9	-1.2	2.69	4.36	1.61	0.00	55.7	50.2	3.85	0.187
2.70	56.0	50.1	-0.9	2.69	4.36	1.62	0.00	56.0	50.5	3.86	0.195
2.80	56.2	50.3	-0.7	2.70	4.39	1.62	0.00	56.2	50.7	3.89	0.204
2.90	56.4	50.5	-0.7	2.70	4.39	1.62	0.00	56.4	50.8	3.89	0.212
3.00	50.0	50.8	-0.3	2.63	-0.55	0.78	0.00	50.0	51.2	-1.04	0.215
3.10	56.9	51.0	-0.7	2.74	4.40	1.60	0.00	56.9	51.3	3.89	0.218
3.20	56.9	51.1	-0.9	2.72	4.34	1.59	0.00	56.9	51.5	3.83	0.227
3.30	57.0	51.3	-0.9	2.69	4.35	1.62	0.00	57.0	51.6	3.84	0.236
3.40	57.1	51.5	-1.0	2.70	4.25	1.57	0.00	57.1	51.8	3.74	0.244
3.50	57.2	51.6	-1.2	2.69	4.23	1.57	0.00	57.2	52.0	3.72	0.252
3.60	50.9	51.9	-1.0	2.50	-0.73	0.84	0.00	50.9	52.2	-1.21	0.253
3.70	57.5	51.9	-1.3	2.74	4.24	1.54	0.00	57.5	52.3	3.73	0.258
3.80	57.6	52.2	-1.5	2.70	4.11	1.52	0.00	57.6	52.5	3.60	0.266
3.90	57.7	52.3	-1.7	2.68	4.10	1.53	0.00	57.7	52.7	3.60	0.275
4.00	57.8	52.4	-1.8	2.64	4.07	1.54	0.00	57.8	52.8	3.56	0.283
4.10	57.9	52.6	-1.9	2.63	4.04	1.53	0.00	57.9	52.9	3.54	0.290
4.20	51.7	52.9	-0.7	2.45	-0.84	0.87	0.00	51.7	53.2	-1.33	0.292
4.30	58.2	52.9	-2.0	2.68	4.05	1.50	0.00	58.2	53.2	3.54	0.295
4.40	58.2	53.0	-2.0	2.68	3.95	1.47	0.00	58.2	53.3	3.44	0.302
4.50	58.3	53.1	-1.9	2.67	3.99	1.49	0.00	58.3	53.4	3.49	0.310
4.60	58.5	53.2	-1.8	2.67	4.02	1.50	0.00	58.5	53.6	3.52	0.318

4.70	58.6	53.4	-1.8	2.67	3.96	1.48	0.00	58.6	53.7	3.47	0.326
4.81	52.3	53.6	-1.3	2.45	-0.98	0.81	0.00	52.3	53.9	-1.48	0.327
4.90	58.9	53.5	-1.5	2.69	4.10	1.52	0.00	58.9	53.8	3.60	0.331
5.01	58.9	53.6	-1.4	2.66	4.06	1.52	0.00	58.9	53.9	3.56	0.339
5.11	59.0	53.7	-1.5	2.69	4.04	1.50	0.00	59.0	54.0	3.54	0.347
5.21	59.1	53.8	-1.7	2.67	3.99	1.49	0.00	59.1	54.1	3.49	0.354
5.31	59.1	53.9	-1.8	2.68	4.00	1.49	0.00	59.1	54.2	3.50	0.361
5.41	52.9	53.8	-0.5	2.44	-0.68	0.51	0.00	52.9	54.1	-1.14	0.361
5.51	59.4	54.1	-1.8	2.63	4.05	1.53	0.00	59.4	54.4	3.54	0.368
5.61	59.4	54.2	-1.7	2.67	3.93	1.46	0.00	59.4	54.4	3.43	0.375
5.71	59.4	54.2	-1.8	2.68	3.91	1.45	0.00	59.4	54.5	3.42	0.383
5.81	59.4	54.3	-1.9	2.67	3.91	1.46	0.00	59.4	54.6	3.42	0.390
5.91	59.4	54.3	-2.1	2.67	3.90	1.46	0.00	59.4	54.6	3.40	0.397
6.01	53.5	54.5	-1.8	2.42	-0.68	0.54	0.00	53.5	54.8	-1.16	0.397
6.11	59.6	54.5	-2.1	2.68	3.91	1.46	0.00	59.6	54.8	3.40	0.402
6.21	59.6	54.6	-2.3	2.64	3.81	1.44	0.00	59.6	54.9	3.31	0.409
6.31	59.7	54.7	-2.3	2.65	3.81	1.43	0.00	59.7	55.0	3.31	0.417
6.41	59.7	54.7	-2.3	2.60	3.80	1.46	0.00	59.7	55.0	3.30	0.425
6.51	59.7	54.7	-2.1	2.59	3.80	1.46	0.00	59.7	55.0	3.30	0.432
6.61	53.8	54.9	-1.8	2.45	-0.73	0.66	0.00	53.8	55.2	-1.22	0.432
6.71	59.9	54.9	-2.3	2.67	3.84	1.44	0.00	59.9	55.2	3.35	0.437
6.81	59.8	54.9	-2.6	2.60	3.70	1.42	0.00	59.8	55.2	3.23	0.444
6.91	59.8	55.0	-3.0	2.58	3.66	1.41	0.00	59.8	55.2	3.19	0.451
7.01	59.8	55.0	-3.3	2.56	3.60	1.40	0.00	59.8	55.2	3.14	0.457
7.11	54.4	54.4	-3.5	0.00	0.00	0.00	5.00	54.4	59.5	-4.04	0.455
7.21	51.2	51.2	-3.3	0.00	0.00	0.00	5.27	51.2	58.7	-5.73	0.447
7.31	52.1	52.1	-3.0	0.00	0.00	0.00	3.26	52.1	57.4	-4.12	0.435
7.41	52.4	52.4	-3.0	0.00	0.00	0.00	3.23	52.4	56.9	-3.61	0.427
7.51	52.2	52.2	-2.8	0.00	0.00	0.00	3.22	52.2	56.7	-3.54	0.419
7.60	52.1	52.1	-2.8	0.00	0.00	0.00	3.20	52.1	56.6	-3.58	0.412
7.69	52.0	52.0	-2.6	0.00	0.00	0.00	3.18	52.0	56.5	-3.60	0.405
7.79	51.9	51.9	-3.0	0.00	0.00	0.00	3.19	51.9	56.4	-3.59	0.397
7.89	51.8	51.8	-3.1	0.00	0.00	0.00	3.22	51.8	56.3	-3.61	0.390
7.99	51.7	51.7	-3.0	0.00	0.00	0.00	3.25	51.7	56.2	-3.63	0.381
8.09	51.6	51.6	-2.3	0.00	0.00	0.00	3.29	51.6	56.2	-3.65	0.374
8.19	51.5	51.5	-2.0	0.00	0.00	0.00	3.30	51.5	56.1	-3.70	0.365
8.29	51.4	51.4	-2.8	0.00	0.00	0.00	3.34	51.4	56.1	-3.74	0.357
8.39	51.3	51.3	-2.3	0.00	0.00	0.00	3.33	51.3	56.0	-3.71	0.349
8.49	51.2	51.2	-2.1	0.00	0.00	0.00	3.36	51.2	55.9	-3.74	0.340
8.60	51.1	51.1	-1.9	0.00	0.00	0.00	3.36	51.1	55.9	-3.74	0.332
8.69	51.1	51.1	-1.3	0.00	0.00	0.00	3.35	51.1	55.8	-3.74	0.324
8.80	51.0	51.0	-1.3	0.00	0.00	0.00	3.32	51.0	55.6	-3.70	0.315
8.90	50.9	50.9	-1.2	0.00	0.00	0.00	3.31	50.9	55.5	-3.68	0.307
9.00	50.9	50.9	-0.9	0.00	0.00	0.00	3.32	50.9	55.5	-3.67	0.300
9.10	50.8	50.8	-0.9	0.00	0.00	0.00	3.28	50.8	55.3	-3.62	0.292
9.20	50.6	50.6	-0.5	0.00	0.00	0.00	3.27	50.6	55.1	-3.60	0.283
9.30	50.6	50.6	-0.2	0.00	0.00	0.00	3.29	50.6	55.1	-3.59	0.275
9.40	50.4	50.4	0.1	0.00	0.00	0.00	3.22	50.4	54.9	-3.55	0.267
9.50	50.3	50.3	0.3	0.00	0.00	0.00	3.22	50.3	54.7	-3.53	0.260
9.60	50.1	50.1	0.4	0.00	0.00	0.00	3.21	50.1	54.5	-3.48	0.252
9.70	49.9	49.9	0.5	0.00	0.00	0.00	3.20	49.9	54.2	-3.45	0.244
9.80	49.8	49.8	0.6	0.00	0.00	0.00	3.16	49.8	54.1	-3.44	0.237
9.90	49.6	49.6	0.8	0.00	0.00	0.00	3.15	49.6	53.8	-3.39	0.229
10.00	49.3	49.3	1.0	0.00	0.00	0.00	3.36	49.3	53.6	-3.42	0.222

10.10	48.9	48.9	1.1	0.00	0.00	0.00	3.37	48.9	53.4	-3.53	0.215
10.20	48.7	48.7	1.2	0.00	0.00	0.00	3.31	48.7	53.2	-3.54	0.207
10.28	48.6	48.6	1.6	0.00	0.00	0.00	3.33	48.6	53.0	-3.53	0.200
10.38	48.4	48.4	2.0	0.00	0.00	0.00	3.28	48.4	52.8	-3.48	0.192
10.48	48.2	48.2	1.8	0.00	0.00	0.00	3.26	48.2	52.5	-3.47	0.184
10.59	48.0	48.0	2.0	0.00	0.00	0.00	3.26	48.0	52.3	-3.44	0.177
10.69	47.9	47.9	2.2	0.00	0.00	0.00	3.21	47.9	52.1	-3.40	0.170
10.79	47.6	47.6	2.4	0.00	0.00	0.00	3.18	47.6	51.9	-3.37	0.162
10.89	47.5	47.5	2.4	0.00	0.00	0.00	3.20	47.5	51.7	-3.33	0.154
10.99	47.3	47.3	3.2	0.00	0.00	0.00	3.18	47.3	51.5	-3.30	0.146
11.09	47.1	47.1	4.0	0.00	0.00	0.00	3.10	47.1	51.2	-3.27	0.140
11.19	46.8	46.8	3.5	0.00	0.00	0.00	3.15	46.8	50.9	-3.25	0.133
11.29	46.6	46.6	4.4	0.00	0.00	0.00	3.12	46.6	50.6	-3.26	0.126
11.39	46.5	46.5	3.9	0.00	0.00	0.00	3.09	46.5	50.4	-3.16	0.119
11.49	46.2	46.2	3.7	0.00	0.00	0.00	3.08	46.2	50.1	-3.12	0.112
11.59	45.9	45.9	4.5	0.00	0.00	0.00	3.04	45.9	49.9	-3.09	0.104
11.69	45.7	45.7	4.6	0.00	0.00	0.00	3.11	45.7	49.6	-3.10	0.097
11.79	45.2	45.2	4.8	0.00	0.00	0.00	3.31	45.2	49.3	-3.20	0.091
11.89	44.8	44.8	4.3	0.00	0.00	0.00	3.26	44.8	49.0	-3.31	0.083
11.99	44.6	44.6	4.5	0.00	0.00	0.00	3.19	44.6	48.7	-3.28	0.076
12.09	44.4	44.4	4.9	0.00	0.00	0.00	3.11	44.4	48.5	-3.18	0.070
12.19	44.2	44.2	4.9	0.00	0.00	0.00	3.05	44.2	48.2	-3.12	0.063
12.29	44.0	44.0	5.4	0.00	0.00	0.00	3.05	44.0	47.9	-3.09	0.056
12.39	43.7	43.7	5.0	0.00	0.00	0.00	3.01	43.7	47.6	-3.03	0.048
12.49	43.5	43.5	5.1	0.00	0.00	0.00	3.00	43.5	47.4	-3.00	0.041
12.59	43.2	43.2	5.5	0.00	0.00	0.00	2.95	43.2	47.0	-2.95	0.035
12.69	43.0	43.0	6.0	0.00	0.00	0.00	2.93	43.0	46.7	-2.89	0.029
12.79	42.6	42.6	6.0	0.00	0.00	0.00	3.13	42.6	46.4	-2.94	0.023
12.88	42.3	42.3	6.0	0.00	0.00	0.00	2.98	42.3	46.1	-2.97	0.017
12.98	42.0	42.0	6.3	0.00	0.00	0.00	2.95	42.0	45.7	-2.91	0.011
13.08	41.8	41.8	6.1	0.00	0.00	0.00	2.89	41.8	45.4	-2.82	0.005
13.18	36.1	36.1	5.5	0.00	0.00	0.00	1.49	36.1	37.2	-1.77	0.000
13.27	42.9	38.6	5.5	2.99	3.16	1.38	2.85	42.9	42.8	-0.15	-0.002
13.36	49.0	41.9	5.0	2.86	5.33	1.86	3.16	49.0	47.9	-0.14	-0.002
13.45	51.9	44.8	5.9	2.92	5.30	1.81	3.34	51.9	50.2	-0.14	-0.002
13.54	54.4	47.5	5.8	2.98	5.20	1.74	3.15	54.4	51.9	-0.14	-0.002
13.63	56.8	50.1	5.8	3.01	5.08	1.68	3.26	56.8	53.1	-0.13	-0.002
13.72	58.9	52.2	6.4	3.02	5.06	1.67	3.41	58.9	54.8	-0.13	-0.002
13.81	60.6	54.1	6.3	3.01	4.93	1.63	3.52	60.6	55.5	-0.13	-0.002
13.90	62.0	55.6	6.6	3.03	4.86	1.60	3.60	62.0	55.9	-0.13	-0.002
13.99	63.2	56.8	6.5	3.05	4.81	1.57	3.67	63.2	56.9	-0.13	-0.002
14.09	62.6	57.9	6.8	2.32	3.54	1.15	3.65	62.6	55.6	-0.13	-0.002
14.18	55.4	55.3	6.9	0.81	0.07	1.25	3.02	55.4	45.4	-0.13	-0.002
14.27	60.0	53.2	6.5	3.05	5.18	1.70	3.59	60.0	51.3	-0.13	-0.002
14.36	61.6	55.1	6.4	3.08	4.95	1.60	3.50	61.6	53.9	-0.13	-0.002
14.45	63.1	56.7	6.3	3.11	4.86	1.56	3.60	63.1	55.9	-0.13	-0.002
14.55	62.6	58.1	6.5	1.54	3.47	1.01	3.59	62.6	55.2	-0.13	-0.002
14.64	55.3	55.2	7.0	0.79	0.10	1.87	3.16	55.3	45.0	-0.13	-0.002
14.73	60.0	53.3	6.5	3.06	5.12	1.67	3.47	60.0	52.5	-0.13	-0.002
14.82	61.8	55.3	6.6	3.06	4.93	1.61	3.62	61.8	55.2	-0.13	-0.002
14.91	63.3	56.9	6.5	3.10	4.89	1.57	3.61	63.3	56.4	-0.13	-0.002
15.01	59.6	57.7	7.4	0.83	1.47	1.92	3.00	59.6	50.6	-0.13	-0.002
15.09	55.7	54.0	6.6	1.55	1.35	1.15	3.17	55.7	45.8	-0.13	-0.002
15.18	60.7	54.0	6.3	3.05	5.06	1.65	3.33	60.7	52.5	-0.13	-0.002

15.27	62.4	55.9	6.4	3.08	4.91	1.59	3.43	62.4	54.9	-0.13	-0.002
15.37	63.2	57.7	6.5	2.31	4.15	1.17	3.40	63.2	55.7	-0.13	-0.002
15.46	56.2	56.1	7.0	0.05	0.09	0.00	3.19	56.2	46.9	-0.13	-0.002
15.55	58.3	53.2	6.5	3.08	3.83	1.25	3.33	58.3	50.1	-0.13	-0.002
15.64	61.6	55.0	6.5	3.08	5.01	1.62	3.36	61.6	54.6	-0.13	-0.002
15.73	63.2	56.7	6.6	3.06	4.85	1.57	3.60	63.2	55.9	-0.13	-0.002
15.83	59.1	57.3	6.6	0.81	1.41	2.02	3.35	59.1	51.5	-0.13	-0.002
15.92	57.0	53.6	6.5	2.29	2.61	1.14	3.54	57.0	48.3	-0.13	-0.002
16.01	60.9	54.1	6.4	3.05	5.09	1.66	3.40	60.9	53.9	-0.13	-0.002
16.10	62.5	55.9	6.5	3.05	4.35	1.62	3.61	62.5	55.6	-0.13	-0.002
16.20	62.6	57.5	6.3	2.30	3.86	1.18	3.27	62.6	55.1	-0.13	-0.002
16.29	56.0	55.9	6.3	0.05	0.09	0.00	3.20	56.0	46.8	-0.13	-0.002
16.38	59.0	52.9	5.9	2.95	4.48	1.51	3.54	59.0	50.2	-0.13	-0.002
16.47	61.4	54.8	5.8	3.05	4.93	1.61	3.54	61.4	53.7	-0.13	-0.002
16.56	62.8	56.3	6.1	3.06	4.83	1.57	3.48	62.8	55.1	-0.13	-0.002
16.65	62.5	57.7	6.0	1.57	3.58	0.77	3.51	62.5	54.4	-0.13	-0.002

Table 9.2 Results from Run Performed on 13/3/87

	HEAT PUMP							HEAT STORE			
t	T_{out}	T_{in}	T_a	W	q_{co}	COP	q_{DHW}	T_{in}	T_{out}	$q_{C,D}$	UF
[hr]	[°C]	[°C]	[°C]	[kW]	[kW]	[-]	[kW]	[°C]	[°C]	[kW]	[-]
0.10	49.6	43.9	1.5	2.85	3.45	1.28	0.00	49.6	43.7	3.33	0.003
0.20	53.4	44.1	1.2	2.81	4.91	1.74	0.00	53.4	43.9	4.78	0.012
0.30	53.7	44.0	1.5	2.81	5.06	1.79	0.00	53.7	44.0	4.88	0.024
0.40	50.6	44.2	1.5	2.74	3.34	1.54	0.00	50.6	44.1	3.16	0.034
0.50	52.9	44.0	1.7	2.80	4.72	1.69	0.00	52.9	44.0	4.51	0.040
0.60	53.6	44.0	1.6	2.74	5.06	1.84	0.00	53.6	44.0	4.83	0.051
0.70	53.7	44.0	1.7	2.74	5.08	1.85	0.00	53.7	44.1	4.85	0.061
0.81	53.7	44.0	1.7	2.73	5.08	1.86	0.00	53.7	44.0	4.85	0.073
0.91	53.8	44.0	1.7	2.74	5.04	1.83	0.00	53.8	44.1	4.81	0.083
1.01	50.3	44.3	2.0	2.65	3.17	1.64	0.00	50.3	44.3	2.95	0.093
1.11	53.5	44.1	2.0	2.83	4.84	1.72	0.00	53.5	44.3	4.55	0.100
1.21	54.0	44.3	2.0	2.76	5.05	1.82	0.00	54.0	44.6	4.70	0.111
1.31	54.1	44.5	1.8	2.77	5.02	1.81	0.00	54.1	44.9	4.58	0.120
1.41	54.4	44.8	1.8	2.75	4.94	1.79	0.00	54.4	45.3	4.45	0.130
1.51	54.7	45.2	1.7	2.75	4.91	1.78	0.00	54.7	45.8	4.35	0.141
1.59	55.1	45.6	1.7	2.64	4.86	1.85	0.00	55.1	46.3	4.26	0.148
1.69	51.4	46.1	2.0	2.93	2.71	1.36	0.00	51.4	46.9	2.12	0.153
1.79	55.7	46.5	1.8	2.75	4.81	1.74	0.00	55.7	47.4	4.15	0.163
1.89	56.2	47.0	1.7	2.72	4.85	1.78	0.00	56.2	47.8	4.21	0.172
1.99	56.6	47.5	1.7	2.77	4.77	1.72	0.00	56.6	48.2	4.15	0.180
2.09	57.0	47.9	1.7	2.75	4.69	1.70	0.00	57.0	48.7	4.08	0.190
2.19	56.9	48.7	1.7	2.66	4.23	1.57	0.00	56.9	49.4	3.66	0.198
2.29	53.6	48.7	1.8	2.87	2.50	1.36	0.00	53.6	49.3	1.94	0.202
2.40	58.0	49.0	1.8	2.75	4.65	1.69	0.00	58.0	49.7	4.07	0.211
2.49	58.3	49.3	1.7	2.74	4.65	1.69	0.00	58.3	49.9	4.09	0.221
2.60	58.4	49.6	1.7	2.74	4.54	1.65	0.00	58.4	50.1	4.01	0.229
2.69	58.7	49.9	1.7	2.71	4.57	1.68	0.00	58.7	50.4	4.03	0.238
2.80	57.8	50.5	1.8	2.68	3.81	1.40	0.00	57.8	51.0	3.31	0.247
2.90	55.1	50.5	2.0	2.85	2.48	1.38	0.00	55.1	50.8	1.98	0.250
3.00	59.3	50.5	2.0	2.75	4.52	1.64	0.00	59.3	51.0	4.01	0.258
3.10	59.5	50.7	1.7	2.73	4.52	1.65	0.00	59.5	51.2	4.01	0.267
3.20	59.5	50.9	1.7	2.74	4.49	1.65	0.00	59.5	51.4	3.98	0.277
3.30	59.5	51.0	1.6	2.73	4.56	1.67	0.00	59.5	51.5	4.05	0.286
3.40	57.9	51.3	1.8	2.73	3.52	1.36	0.00	57.9	51.7	3.04	0.295
3.50	57.4	51.0	1.8	2.84	3.43	1.38	0.00	57.4	51.4	2.94	0.298
3.60	60.2	51.6	1.7	2.78	4.52	1.62	0.00	60.2	52.0	4.01	0.307
3.70	60.4	51.8	1.8	2.77	4.51	1.62	0.00	60.4	52.2	4.01	0.317
3.80	60.4	51.9	2.0	2.77	4.55	1.64	0.00	60.4	52.4	4.06	0.326
3.90	60.6	52.0	1.7	2.80	4.54	1.61	0.00	60.6	52.5	4.03	0.334
4.00	58.2	52.4	2.0	2.93	3.05	1.31	0.00	58.2	52.8	2.57	0.342
4.10	60.4	51.8	2.0	2.80	4.54	1.61	0.00	60.4	52.8	3.75	0.349
4.20	60.9	52.3	1.8	2.80	4.54	1.61	0.00	60.9	52.9	3.96	0.358
4.30	61.1	52.5	1.8	2.80	4.54	1.61	0.00	61.1	53.1	3.99	0.366
4.40	61.2	52.6	1.8	2.80	4.54	1.61	0.00	61.2	53.2	3.99	0.375
4.50	61.2	52.6	1.7	2.80	4.54	1.61	0.00	61.2	53.2	3.95	0.384
4.60	58.2	49.6	1.8	2.80	4.54	1.61	0.00	58.2	53.5	2.26	0.391

4.70	61.1	52.5	1.6	2.80	4.54	1.61	0.00	61.1	53.4	3.79	0.397
4.80	61.4	52.8	1.6	2.80	4.54	1.61	0.00	61.4	53.5	3.90	0.405
4.90	61.5	52.9	1.6	2.80	4.54	1.61	0.00	61.5	53.6	3.87	0.415
5.00	61.6	53.0	1.6	2.80	4.54	1.61	0.00	61.6	53.9	3.86	0.423
5.10	61.7	53.1	1.6	2.80	4.54	1.61	0.00	61.7	53.9	3.86	0.432
5.20	58.1	49.5	1.7	2.80	4.54	1.61	0.00	58.1	54.0	1.89	0.440
5.31	61.7	53.1	1.6	2.80	4.54	1.61	0.00	61.7	54.1	3.77	0.444
5.40	61.8	53.2	1.3	2.80	4.54	1.61	0.00	61.8	54.2	3.76	0.452
5.51	61.8	53.2	1.6	2.80	4.54	1.61	0.00	61.8	54.2	3.77	0.460
5.60	61.9	53.3	1.6	2.80	4.54	1.61	0.00	61.9	54.3	3.80	0.469
5.70	62.0	53.4	1.7	2.80	4.54	1.61	0.00	62.0	54.3	3.77	0.477
5.81	58.2	49.6	1.8	2.80	4.54	1.61	0.00	58.2	54.3	1.80	0.485
5.91	62.2	53.6	1.7	2.80	4.54	1.61	0.00	62.2	54.5	3.81	0.491
6.01	62.1	53.5	1.7	2.80	4.54	1.61	0.00	62.1	54.6	3.77	0.499
6.11	62.2	53.6	1.6	2.80	4.54	1.61	0.00	62.2	54.6	3.82	0.506
6.21	62.2	53.6	1.5	2.80	4.54	1.61	0.00	62.2	54.7	3.75	0.516
6.31	62.3	53.7	1.6	2.80	4.54	1.61	0.00	62.3	54.7	3.71	0.523
6.41	58.4	49.8	1.7	2.80	4.54	1.61	0.00	58.4	54.7	1.72	0.530
6.51	62.6	54.0	1.5	2.80	4.54	1.61	0.00	62.6	54.9	3.80	0.535
6.61	62.4	53.8	1.5	2.80	4.54	1.61	0.00	62.4	54.9	3.72	0.544
6.71	62.5	53.9	1.3	2.80	4.54	1.61	0.00	62.5	55.0	3.74	0.552
6.81	62.5	53.9	1.2	2.80	4.54	1.61	0.00	62.5	55.0	3.74	0.560
6.91	62.6	54.0	1.3	2.80	4.54	1.61	0.00	62.6	55.1	3.74	0.569
7.01	59.0	50.4	1.2	2.80	4.54	1.61	0.00	59.0	54.8	1.98	0.577
7.12	54.6	46.0	1.2	2.80	4.54	1.61	0.00	54.6	62.6	-4.48	0.574
7.21	51.9	51.9	1.5	0.00	0.00	0.00	3.23	51.9	61.6	-5.29	0.569
7.31	51.2	51.2	1.2	0.00	0.00	0.00	3.23	51.2	61.1	-5.53	0.557
7.41	52.6	52.6	1.7	0.00	0.00	0.00	3.23	52.6	60.3	-4.32	0.547
7.51	52.8	52.8	1.8	0.00	0.00	0.00	3.23	52.8	59.2	-3.62	0.539
7.61	52.5	52.5	1.7	0.00	0.00	0.00	3.23	52.5	58.4	-3.35	0.530
7.71	52.0	52.0	2.0	0.00	0.00	0.00	3.23	52.0	57.8	-3.32	0.523
7.81	51.5	51.5	2.2	0.00	0.00	0.00	3.23	51.5	57.4	-3.36	0.516
7.91	51.1	51.1	2.4	0.00	0.00	0.00	3.23	51.1	57.2	-3.35	0.509
8.01	50.3	50.3	2.5	0.00	0.00	0.00	3.23	50.3	57.1	-3.49	0.500
8.11	49.9	49.9	2.5	0.00	0.00	0.00	3.23	49.9	56.9	-3.81	0.493
8.21	49.9	49.9	2.4	0.00	0.00	0.00	3.23	49.9	56.9	-3.85	0.484
8.31	49.7	49.7	2.5	0.00	0.00	0.00	3.23	49.7	56.7	-3.86	0.476
8.41	49.6	49.6	2.7	0.00	0.00	0.00	3.23	49.6	56.6	-3.85	0.467
8.51	49.6	49.6	2.5	0.00	0.00	0.00	3.23	49.6	56.6	-3.89	0.459
8.61	49.5	49.5	2.2	0.00	0.00	0.00	3.23	49.5	56.6	-3.91	0.449
8.71	49.4	49.4	2.2	0.00	0.00	0.00	3.23	49.4	56.5	-3.92	0.442
8.81	49.4	49.4	2.2	0.00	0.00	0.00	3.23	49.4	56.5	-3.89	0.432
8.91	49.3	49.3	2.4	0.00	0.00	0.00	3.23	49.3	56.4	-3.90	0.425
9.01	49.3	49.3	2.4	0.00	0.00	0.00	3.23	49.3	56.4	-3.88	0.415
9.11	49.2	49.2	2.5	0.00	0.00	0.00	3.23	49.2	56.3	-3.88	0.407
9.21	49.1	49.1	2.9	0.00	0.00	0.00	3.23	49.1	56.1	-3.86	0.398
9.31	49.1	49.1	2.7	0.00	0.00	0.00	3.23	49.1	56.1	-3.87	0.390
9.41	49.0	49.0	2.7	0.00	0.00	0.00	3.23	49.0	56.0	-3.86	0.381
9.51	49.0	49.0	2.7	0.00	0.00	0.00	3.23	49.0	55.9	-3.80	0.372
9.61	49.0	49.0	2.7	0.00	0.00	0.00	3.23	49.0	55.8	-3.79	0.364
9.71	48.9	48.9	3.2	0.00	0.00	0.00	3.23	48.9	55.7	-3.75	0.357
9.80	48.8	48.8	3.2	0.00	0.00	0.00	3.23	48.8	55.6	-3.72	0.349
9.90	48.6	48.6	3.2	0.00	0.00	0.00	3.23	48.6	55.4	-3.70	0.340
10.00	48.7	48.7	3.4	0.00	0.00	0.00	3.23	48.7	55.2	-3.61	0.332

10.10	48.8	48.8	3.4	0.00	0.00	0.00	3.23	48.8	55.1	-3.47	0.326
10.20	48.6	48.6	3.7	0.00	0.00	0.00	3.23	48.6	54.9	-3.41	0.317
10.30	48.4	48.4	4.0	0.00	0.00	0.00	3.40	48.4	54.6	-3.44	0.309
10.40	48.1	48.1	4.1	0.00	0.00	0.00	3.37	48.1	54.4	-3.54	0.302
10.50	47.9	47.9	4.4	0.00	0.00	0.00	3.35	47.9	54.2	-3.50	0.295
10.60	47.7	47.7	4.5	0.00	0.00	0.00	3.31	47.7	54.0	-3.49	0.287
10.70	47.6	47.6	4.1	0.00	0.00	0.00	3.37	47.6	53.9	-3.53	0.278
10.80	47.4	47.4	4.5	0.00	0.00	0.00	3.32	47.4	53.7	-3.52	0.272
10.90	47.3	47.3	4.6	0.00	0.00	0.00	3.31	47.3	53.6	-3.53	0.263
11.00	47.2	47.2	4.0	0.00	0.00	0.00	3.31	47.2	53.5	-3.52	0.256
11.10	47.1	47.1	4.8	0.00	0.00	0.00	3.35	47.1	53.4	-3.54	0.247
11.20	47.1	47.1	5.0	0.00	0.00	0.00	3.30	47.1	53.4	-3.53	0.241
11.30	47.0	47.0	5.5	0.00	0.00	0.00	3.28	47.0	53.3	-3.52	0.233
11.40	46.9	46.9	5.6	0.00	0.00	0.00	3.27	46.9	53.1	-3.50	0.224
11.50	46.9	46.9	5.6	0.00	0.00	0.00	3.25	46.9	53.1	-3.48	0.217
11.60	46.8	46.8	6.0	0.00	0.00	0.00	3.25	46.8	53.0	-3.51	0.209
11.70	46.9	46.9	6.5	0.00	0.00	0.00	3.24	46.9	52.8	-3.53	0.202
11.81	46.7	46.7	6.6	0.00	0.00	0.00	3.21	46.7	52.7	-3.17	0.194
11.90	46.4	46.4	6.9	0.00	0.00	0.00	3.23	46.4	52.6	-3.42	0.187
12.01	46.4	46.4	6.5	0.00	0.00	0.00	3.19	46.4	52.4	-3.45	0.179
12.11	46.4	46.4	6.5	0.00	0.00	0.00	3.20	46.4	52.4	-3.36	0.172
12.21	46.2	46.2	6.6	0.00	0.00	0.00	3.20	46.2	52.3	-3.24	0.164
12.30	46.0	46.0	7.1	0.00	0.00	0.00	3.14	46.0	52.2	-3.31	0.157
12.39	45.9	45.9	7.0	0.00	0.00	0.00	3.45	45.9	52.1	-3.49	0.151
12.49	45.6	45.6	6.6	0.00	0.00	0.00	3.39	45.6	51.9	-3.50	0.143
12.59	45.4	45.4	7.0	0.00	0.00	0.00	3.43	45.4	51.8	-3.47	0.136
12.69	45.2	45.2	7.5	0.00	0.00	0.00	3.40	45.2	51.6	-3.49	0.128
12.79	45.1	45.1	7.5	0.00	0.00	0.00	3.30	45.1	51.5	-3.45	0.120
12.89	44.8	44.8	7.4	0.00	0.00	0.00	3.58	44.8	51.3	-3.51	0.112
12.99	44.5	44.5	7.5	0.00	0.00	0.00	3.50	44.5	51.1	-3.57	0.104
13.09	44.4	44.4	7.3	0.00	0.00	0.00	3.39	44.4	50.9	-3.49	0.097
13.19	44.3	44.3	7.6	0.00	0.00	0.00	3.35	44.3	50.7	-3.44	0.088
13.29	44.1	44.1	8.0	0.00	0.00	0.00	3.25	44.1	50.4	-3.37	0.081
13.39	44.1	44.1	8.8	0.00	0.00	0.00	3.29	44.1	50.1	-3.40	0.075
13.49	44.0	44.0	7.9	0.00	0.00	0.00	3.23	44.0	49.8	-3.26	0.066
13.59	43.7	43.7	6.9	0.00	0.00	0.00	3.40	43.7	49.5	-3.22	0.060
13.69	43.2	43.2	7.0	0.00	0.00	0.00	3.39	43.2	49.1	-3.25	0.052
13.80	42.9	42.9	6.8	0.00	0.00	0.00	3.31	42.9	48.8	-3.22	0.046
13.90	42.6	42.6	6.8	0.00	0.00	0.00	3.26	42.6	48.4	-3.17	0.039
14.00	42.3	42.3	7.1	0.00	0.00	0.00	3.21	42.3	48.0	-3.11	0.032
14.10	42.0	42.0	6.9	0.00	0.00	0.00	3.13	42.0	47.6	-2.96	0.025
14.20	41.6	41.6	7.0	0.00	0.00	0.00	3.09	41.6	47.2	-2.95	0.019
14.30	41.4	41.4	6.6	0.00	0.00	0.00	3.12	41.4	46.8	-3.06	0.012
14.40	41.1	41.1	6.3	0.00	0.00	0.00	3.24	41.1	46.4	-2.97	0.005
14.50	36.5	37.3	5.9	1.14	-2.12	0.34	1.73	36.5	38.1	-1.84	0.000
14.59	50.3	40.2	5.4	2.90	5.32	1.83	3.31	50.3	47.7	-0.15	-0.002
14.68	53.0	42.9	5.5	2.99	5.35	1.78	3.27	53.0	49.6	-0.15	-0.002
14.77	55.3	45.4	5.1	2.99	5.23	1.75	3.43	55.3	51.6	-0.14	-0.002
14.86	57.3	47.6	5.3	2.91	5.13	1.76	3.35	57.3	52.6	-0.14	-0.002
14.95	53.3	49.6	5.1	2.95	1.99	1.30	2.86	53.3	46.7	-0.13	-0.002
15.04	59.5	49.3	5.3	2.95	5.40	1.82	3.63	59.5	52.5	-0.13	-0.002
15.13	60.6	51.1	5.4	2.96	5.08	1.70	3.60	60.6	53.4	-0.13	-0.002
15.23	61.9	52.6	5.3	2.97	4.94	1.66	3.66	61.9	54.0	-0.13	-0.002
15.32	62.9	54.0	5.5	2.97	4.87	1.64	3.65	62.9	50.0	-0.13	-0.002

15.41	61.8	55.4	6.0	1.55	3.43	0.80	3.54	61.8	52.2	-0.13	-0.002
15.50	58.1	53.3	5.8	2.26	2.52	1.42	3.53	58.1	48.7	-0.13	-0.002
15.59	62.7	53.2	5.6	2.97	4.99	1.68	3.71	62.7	55.1	-0.13	-0.002
15.68	61.3	53.9	6.1	2.98	3.84	1.27	4.10	61.3	53.1	-0.13	-0.002
15.77	63.2	53.8	6.0	3.02	4.94	1.63	3.62	63.2	55.3	-0.13	-0.002
15.87	59.7	55.0	6.0	0.77	2.43	0.86	3.35	59.7	51.9	-0.13	-0.002
15.96	60.2	52.8	6.0	2.96	3.81	1.27	3.66	60.2	52.2	-0.13	-0.002
16.05	63.3	53.8	5.8	2.97	4.91	1.65	3.57	63.3	55.7	-0.13	-0.002
16.19	58.8	54.1	6.0	1.97	2.88	1.30	3.42	58.8	42.8	-0.13	-0.002
16.28	60.1	54.1	5.9	3.00	4.85	1.61	3.36	60.1	42.6	-0.13	-0.002
16.37	61.7	55.7	6.0	3.00	4.75	1.58	3.48	61.7	46.1	-0.13	-0.002
16.46	63.1	57.0	5.9	3.00	4.67	1.55	3.39	63.1	49.0	-0.13	-0.002
16.56	61.3	58.1	5.9	1.52	2.50	1.61	3.34	61.3	48.5	-0.13	-0.002
16.65	55.1	55.0	5.9	0.81	0.07	0.00	3.17	55.1	42.0	-0.13	-0.002
16.74	59.7	53.3	5.8	2.93	4.85	1.65	3.35	59.7	47.9	-0.13	-0.002
16.83	61.3	55.0	5.5	2.93	4.78	1.63	3.55	61.3	50.8	-0.13	-0.002
16.92	62.5	56.3	5.9	2.96	4.72	1.59	3.63	62.5	52.2	-0.13	-0.002
17.01	63.5	57.4	5.6	2.99	4.61	1.54	3.46	63.5	52.5	-0.13	-0.002
17.11	58.9	57.4	5.4	0.05	1.18	1.32	3.39	58.9	47.6	-0.13	-0.002
17.20	56.9	53.6	5.6	2.29	2.51	1.38	3.48	56.9	45.8	-0.13	-0.002
17.29	60.4	53.9	5.5	2.96	4.84	1.63	3.50	60.4	51.6	-0.13	-0.002
17.38	61.8	55.4	5.5	2.98	4.77	1.60	3.44	61.8	53.0	-0.13	-0.002
17.47	62.9	56.7	5.4	2.98	4.66	1.56	3.74	62.9	53.9	-0.13	-0.002
17.57	63.3	57.8	5.4	2.25	4.57	1.15	3.54	63.9	54.7	-0.13	-0.002
17.66	56.6	56.6	5.3	0.05	0.05	0.00	3.37	56.6	45.1	-0.13	-0.002
17.74	58.0	53.1	5.3	3.06	3.67	1.21	3.56	58.0	47.2	-0.13	-0.002
17.84	60.7	54.2	5.3	2.94	4.88	1.65	3.60	60.7	51.6	-0.13	-0.002
17.93	61.9	55.6	5.0	2.92	4.70	1.60	3.60	61.9	52.9	-0.13	-0.002
18.02	62.9	56.7	5.0	2.97	4.59	1.54	3.68	62.9	53.9	-0.13	-0.002
18.11	63.7	57.6	5.0	2.98	4.55	1.52	3.70	63.7	54.8	-0.13	-0.002
18.20	61.6	58.2	4.9	1.51	2.59	1.74	3.45	61.6	50.1	-0.13	-0.002
18.29	55.1	55.0	5.0	0.77	0.09	1.44	3.26	55.1	38.7	-0.13	-0.002
18.38	59.3	53.0	4.8	2.95	4.75	1.61	3.47	59.3	45.4	-0.13	-0.002
18.48	60.8	54.6	4.8	2.92	4.73	1.61	3.57	60.8	49.0	-0.13	-0.002
18.57	61.9	55.9	4.5	2.93	4.61	1.57	3.65	61.9	50.5	-0.13	-0.002
18.66	62.6	56.7	4.4	2.88	4.49	1.55	3.70	62.6	51.7	-0.13	-0.002
18.75	63.3	57.4	4.4	2.37	4.45	1.49	3.73	63.3	53.2	-0.13	-0.002
18.84	63.9	58.1	4.3	2.87	4.43	1.53	3.77	63.9	53.6	-0.13	-0.002
18.93	62.9	58.6	4.3	2.19	3.30	1.14	3.60	62.9	52.2	-0.14	-0.002
19.03	56.2	56.1	4.1	0.05	0.10	0.00	3.29	56.2	43.5	-0.14	-0.002
19.11	57.9	52.9	4.1	2.88	3.73	1.31	3.36	57.9	46.3	-0.14	-0.002
19.20	60.4	54.3	4.0	2.87	4.67	1.62	3.41	60.4	50.4	-0.14	-0.002
19.29	61.5	55.6	4.0	2.89	4.55	1.57	3.54	61.5	52.5	-0.13	-0.002
19.39	60.4	56.4	4.3	2.93	3.07	1.13	3.73	60.4	51.2	-0.13	-0.002
19.48	61.3	55.3	4.0	2.88	4.58	1.59	3.36	61.3	52.1	-0.13	-0.002
19.57	62.4	56.6	3.9	2.89	4.41	1.52	3.48	62.4	54.5	-0.13	-0.002
19.66	63.2	57.5	3.9	2.86	4.38	1.53	3.58	63.2	55.1	-0.13	-0.002
19.75	63.9	58.2	3.9	2.87	4.33	1.50	3.59	63.9	55.5	-0.14	-0.002
19.85	63.0	58.8	3.9	1.46	3.18	0.74	3.53	63.0	53.6	-0.14	-0.002
19.94	56.2	56.1	4.0	0.05	0.08	0.00	3.20	56.2	45.4	-0.14	-0.002
20.02	58.1	52.9	3.7	2.88	3.86	1.34	3.46	58.1	48.9	-0.14	-0.002
20.12	57.5	53.4	3.5	2.99	3.14	1.26	3.51	57.5	48.6	-0.14	-0.002
20.21	59.6	53.4	3.5	2.89	4.67	1.61	3.32	59.6	51.0	-0.14	-0.002
20.30	60.7	54.8	3.2	2.86	4.44	1.55	3.44	60.7	52.7	-0.14	-0.002

20.39	61.7	55.9	3.4	2.87	4.38	1.52	3.46	61.7	53.9	-0.13	-0.002
20.48	62.5	56.7	3.5	2.86	4.37	1.53	3.55	62.5	54.3	-0.13	-0.002
20.57	63.2	57.4	3.9	2.85	4.35	1.52	3.60	63.2	54.4	-0.14	-0.002
20.66	63.8	58.1	3.7	2.78	4.34	1.56	3.66	63.8	54.7	-0.14	-0.002
20.75	62.3	56.8	4.1	3.00	4.11	1.38	3.99	62.3	52.5	-0.14	-0.002
20.85	63.3	57.5	3.9	2.89	4.32	1.49	3.50	63.3	54.7	-0.14	-0.002
20.94	63.9	58.2	3.7	2.85	4.28	1.49	3.52	63.9	55.2	-0.14	-0.002
21.03	63.0	58.8	3.7	1.49	3.17	0.72	3.43	63.0	53.4	-0.14	-0.002
21.12	56.2	56.2	3.7	0.05	0.06	0.00	3.21	56.2	45.0	-0.14	-0.002
21.21	58.3	53.0	3.7	2.99	3.95	1.36	3.44	58.3	47.8	-0.14	-0.002
21.30	60.6	54.5	3.5	2.87	4.47	1.55	3.35	60.6	51.6	-0.14	-0.002
21.39	61.6	56.2	3.5	2.79	4.08	1.45	3.48	61.6	52.9	-0.14	-0.002
21.49	60.7	54.6	3.7	3.04	4.53	1.49	3.86	60.7	51.2	-0.14	-0.002
21.58	61.6	55.7	3.4	2.87	4.47	1.55	3.40	61.6	52.9	-0.14	-0.002
21.67	62.5	56.7	3.4	2.90	4.35	1.50	3.47	62.5	53.9	-0.14	-0.002
21.76	63.1	57.4	3.5	2.86	4.28	1.49	3.47	63.1	53.2	-0.14	-0.002
21.85	63.7	58.1	3.4	2.88	4.25	1.47	3.58	63.7	53.3	-0.14	-0.002
21.94	64.1	58.6	3.4	2.87	4.17	1.45	3.56	64.1	53.4	-0.14	-0.002
22.03	60.3	58.2	3.5	3.00	1.57	1.16	3.20	60.3	49.0	-0.14	-0.002
22.12	63.4	57.7	3.2	2.91	4.36	1.49	3.58	63.4	53.4	-0.14	-0.002
22.21	63.8	58.2	3.0	2.86	4.25	1.48	3.57	63.8	54.0	-0.14	-0.002
22.30	64.2	58.7	2.9	2.83	4.16	1.47	3.57	64.2	54.1	-0.14	-0.002
22.40	61.7	58.9	2.9	1.44	2.11	1.97	3.51	61.7	51.0	-0.14	-0.002
22.49	55.4	55.3	2.9	0.75	0.07	1.02	3.34	55.4	43.9	-0.14	-0.002
22.58	59.2	53.1	2.5	2.80	4.51	1.61	3.45	59.2	50.2	-0.14	-0.002
22.67	60.4	54.5	2.5	2.83	4.45	1.57	3.44	60.4	52.3	-0.14	-0.002
22.76	58.6	54.2	2.7	2.77	3.30	1.29	3.64	58.6	49.3	-0.14	-0.002
22.85	60.1	54.1	2.5	2.85	4.51	1.58	3.65	60.1	51.3	-0.14	-0.002
22.94	60.9	55.1	2.5	2.87	4.44	1.54	3.66	60.9	51.8	-0.14	-0.002
23.03	61.5	55.8	2.4	2.84	4.37	1.53	3.73	61.5	51.8	-0.14	-0.002
23.12	61.9	56.2	2.4	2.83	4.33	1.52	3.69	61.9	52.6	-0.14	-0.002
23.21	62.3	56.7	2.2	2.82	4.32	1.53	3.82	62.3	53.0	-0.14	-0.002
23.31	62.6	57.0	2.2	2.81	4.23	1.50	3.65	62.6	53.1	-0.14	-0.002
23.40	57.8	55.3	2.5	2.84	1.91	1.23	3.34	57.8	46.8	-0.14	-0.002
23.49	61.0	55.2	2.0	2.83	4.43	1.56	3.48	61.0	51.6	-0.14	-0.002
23.58	61.8	56.1	1.8	2.79	4.30	1.53	3.54	61.8	52.9	-0.14	-0.002
23.67	62.3	56.7	1.7	2.83	4.24	1.49	3.63	62.3	53.6	-0.14	-0.002
23.76	62.7	57.2	1.8	2.79	4.21	1.50	3.62	62.7	53.5	-0.14	-0.002
23.85	63.1	57.6	2.0	2.80	4.21	1.50	3.61	63.1	53.9	-0.14	-0.002
23.94	57.4	57.9	2.2	2.66	-0.29	0.75	3.08	57.4	46.8	-0.14	-0.002

Table 9.3 Results from Run Performed on 14/3/87

	HEAT PUMP							HEAT STORE			
t	T_{out}	T_{in}	T_a	W	q_{co}	COP	q_{DHW}	T_{in}	T_{out}	$q_{C,D}$	UF
[hr]	[°C]	[°C]	[°C]	[kW]	[kW]	[-]	[kW]	[°C]	[°C]	[kW]	[-]
0.01	60.9	54.4	2.0	2.86	4.93	1.72	3.48	60.9	50.5	-0.14	-0.002
0.11	56.4	48.8	1.8	2.79	5.89	2.11	0.00	56.4	37.2	14.56	0.020
0.21	49.1	41.8	1.7	2.75	5.57	2.02	0.00	49.1	40.1	6.73	0.040
0.31	48.2	41.1	1.3	2.72	5.34	1.96	0.00	48.2	41.3	5.01	0.052
0.41	48.6	41.6	1.3	2.73	5.33	1.94	0.00	48.6	42.2	4.75	0.064
0.51	49.3	42.4	1.6	2.61	5.26	2.05	0.00	49.3	42.9	4.68	0.073
0.61	43.6	42.5	2.0	2.65	0.86	0.96	0.00	43.6	42.9	0.41	0.076
0.71	50.6	43.6	1.5	2.80	5.20	1.85	0.00	50.6	44.2	4.60	0.086
0.81	51.2	44.3	1.5	2.75	5.14	1.86	0.00	51.2	44.9	4.50	0.096
0.91	51.8	45.0	1.5	2.80	5.09	1.82	0.00	51.8	45.5	4.49	0.104
1.01	52.2	45.4	1.5	2.76	5.04	1.82	0.00	52.2	45.9	4.49	0.114
1.11	52.7	46.0	1.6	2.61	5.07	2.01	0.00	52.7	46.4	4.55	0.125
1.21	48.1	46.2	2.2	2.68	1.43	1.00	0.00	48.1	46.6	0.98	0.129
1.31	53.6	46.8	1.7	2.84	5.10	1.79	0.00	53.6	47.0	4.61	0.137
1.41	53.9	47.1	2.0	2.83	5.07	1.79	0.00	53.9	47.4	4.57	0.147
1.52	54.1	47.4	2.0	2.82	5.04	1.78	0.00	54.1	47.7	4.54	0.157
1.61	54.4	47.7	2.0	2.83	5.00	1.76	0.00	54.4	48.1	4.52	0.167
1.72	54.3	48.5	1.7	2.61	4.37	1.59	0.00	54.3	49.0	3.81	0.177
1.81	50.4	48.4	2.2	2.75	1.51	1.08	0.00	50.4	48.8	1.03	0.179
1.92	55.3	48.6	2.0	2.86	5.02	1.75	0.00	55.3	49.0	4.51	0.188
2.02	55.6	49.0	2.0	2.87	4.97	1.72	0.00	55.6	49.3	4.44	0.198
2.12	55.8	49.2	1.8	2.84	4.97	1.74	0.00	55.8	49.6	4.45	0.208
2.22	56.1	49.6	2.0	2.85	4.93	1.72	0.00	56.1	49.9	4.41	0.217
2.32	55.3	50.2	2.0	2.63	3.80	1.42	0.00	55.3	50.6	3.26	0.227
2.42	51.9	50.1	2.0	2.79	1.34	1.05	0.00	51.9	50.5	0.84	0.227
2.52	56.9	50.3	2.2	2.88	4.94	1.71	0.00	56.9	50.7	4.43	0.237
2.62	57.1	50.6	2.0	2.85	4.90	1.71	0.00	57.1	51.0	4.37	0.247
2.72	57.2	50.8	1.7	2.84	4.85	1.70	0.00	57.2	51.1	4.34	0.256
2.82	57.5	51.1	2.0	2.85	4.88	1.70	0.00	57.5	51.4	4.37	0.266
2.92	56.2	51.2	2.0	2.65	3.78	1.39	0.00	56.2	51.6	3.28	0.275
3.02	52.9	51.7	2.7	2.87	0.92	1.08	0.00	52.9	52.0	0.42	0.275
3.12	58.1	51.7	2.0	2.87	4.83	1.67	0.00	58.1	52.0	4.32	0.283
3.22	58.2	51.8	2.0	2.87	4.82	1.67	0.00	58.2	52.2	4.31	0.293
3.32	58.3	52.0	2.0	2.85	4.75	1.66	0.00	58.3	52.3	4.24	0.302
3.42	58.5	52.2	2.0	2.86	4.75	1.65	0.00	58.5	52.6	4.25	0.312
3.52	57.3	52.4	2.2	2.67	3.68	1.37	0.00	57.3	52.8	3.18	0.320
3.62	53.5	52.7	3.0	2.87	0.61	1.08	0.00	53.5	53.0	0.14	0.320
3.72	58.9	52.7	2.2	2.89	4.69	1.62	0.00	58.9	53.1	4.19	0.329
3.82	59.0	52.9	2.2	2.87	4.70	1.63	0.00	59.0	53.2	4.19	0.337
3.92	59.2	53.1	2.2	2.87	4.66	1.62	0.00	59.2	53.4	4.16	0.347
4.02	59.3	53.2	2.0	2.87	4.64	1.61	0.00	59.3	53.5	4.15	0.357
4.12	58.0	53.3	2.2	2.78	3.60	1.31	0.00	58.0	53.6	3.11	0.365
4.22	56.3	53.3	2.7	2.91	2.34	1.16	0.00	56.3	53.6	1.87	0.368
4.32	59.7	53.6	2.0	2.88	4.65	1.61	0.00	59.7	53.9	4.15	0.377
4.42	59.7	53.6	2.2	2.85	4.60	1.61	0.00	59.7	54.0	4.10	0.385
4.52	59.8	53.8	2.0	2.86	4.62	1.61	0.00	59.8	54.1	4.13	0.395

4.62	59.9	53.9	2.2	2.87	4.60	1.59	0.00	59.9	54.2	4.10	0.404
4.73	58.6	54.0	2.5	2.55	3.47	1.49	0.00	58.6	54.3	2.98	0.412
4.83	57.4	54.2	2.5	2.89	2.45	1.27	0.00	57.4	54.5	1.98	0.415
4.93	60.2	54.2	2.2	2.82	4.57	1.62	0.00	60.2	54.5	4.08	0.425
5.03	60.3	54.3	2.2	2.85	4.50	1.57	0.00	60.3	54.6	4.01	0.432
5.13	60.4	54.4	2.2	2.82	4.52	1.60	0.00	60.4	54.7	4.02	0.442
5.23	60.4	54.4	2.2	2.83	4.54	1.60	0.00	60.4	54.7	4.05	0.451
5.33	59.0	54.8	2.4	2.53	3.23	1.46	0.00	59.0	55.1	2.69	0.459
5.43	57.8	54.7	2.7	3.03	2.35	1.26	0.00	57.8	55.0	1.87	0.460
5.53	60.7	54.7	2.2	2.87	4.54	1.58	0.00	60.7	55.0	4.04	0.469
5.63	60.8	54.8	2.4	2.87	4.58	1.59	0.00	60.8	55.1	4.08	0.479
5.73	60.9	54.8	2.4	2.85	4.57	1.60	0.00	60.9	55.1	4.08	0.487
5.83	61.0	55.0	2.4	2.83	4.53	1.59	0.00	61.0	55.3	4.03	0.497
5.91	59.8	55.5	2.4	2.58	3.31	1.28	0.00	59.8	55.8	2.78	0.505
6.01	56.2	55.2	2.5	2.90	0.80	1.04	0.00	56.2	55.5	0.30	0.504
6.11	61.1	55.1	2.4	2.87	4.60	1.59	0.00	61.1	55.4	4.10	0.512
6.21	61.1	55.2	2.4	2.86	4.52	1.57	0.00	61.1	55.5	4.02	0.520
6.31	61.2	55.2	2.2	2.86	4.47	1.56	0.00	61.2	55.5	3.98	0.530
6.41	61.2	55.2	2.2	2.86	4.47	1.56	0.00	61.2	55.5	3.98	0.539
6.52	60.0	55.4	2.4	2.62	3.49	1.33	0.00	60.0	55.7	3.00	0.547
6.61	56.4	54.9	2.7	2.83	1.17	1.05	0.00	56.4	55.0	0.78	0.547
6.72	61.5	55.4	2.4	2.85	4.53	1.59	0.00	61.5	55.7	4.04	0.555
6.82	61.5	55.5	2.4	2.87	4.52	1.57	0.00	61.5	55.8	4.03	0.564
6.92	61.6	55.6	2.5	2.85	4.52	1.58	0.00	61.6	55.8	4.03	0.574
7.02	61.6	55.6	2.5	2.89	4.54	1.56	0.00	61.6	55.9	4.04	0.583
7.11	55.3	55.3	2.7	0.00	0.00	0.00	6.33	55.3	55.5	-0.38	0.581
7.22	52.5	52.5	2.9	0.00	0.00	0.00	6.33	52.5	60.9	-6.41	0.574
7.32	53.6	53.6	2.7	0.00	0.00	0.00	3.26	53.6	59.6	-4.62	0.562
7.42	54.0	54.0	2.7	0.00	0.00	0.00	3.13	54.0	58.3	-3.37	0.554
7.52	53.5	53.5	2.7	0.00	0.00	0.00	3.16	53.5	57.6	-3.26	0.545
7.62	53.0	53.0	3.0	0.00	0.00	0.00	3.14	53.0	57.2	-3.36	0.539
7.72	52.6	52.6	3.0	0.00	0.00	0.00	3.10	52.6	56.9	-3.43	0.530
7.82	52.4	52.4	3.0	0.00	0.00	0.00	3.13	52.4	56.8	-3.47	0.523
7.92	52.3	52.3	3.0	0.00	0.00	0.00	3.17	52.3	56.7	-3.54	0.516
8.02	52.1	52.1	3.2	0.00	0.00	0.00	3.20	52.1	56.6	-3.56	0.507
8.12	52.0	52.0	3.2	0.00	0.00	0.00	3.22	52.0	56.5	-3.60	0.500
8.22	51.8	51.8	3.5	0.00	0.00	0.00	3.28	51.8	56.4	-3.67	0.491
8.32	51.8	51.8	3.7	0.00	0.00	0.00	3.27	51.8	56.4	-3.72	0.483
8.42	51.7	51.7	3.9	0.00	0.00	0.00	3.33	51.7	56.3	-3.76	0.476
8.52	51.6	51.6	3.9	0.00	0.00	0.00	3.27	51.6	56.2	-3.73	0.467
8.62	51.6	51.6	3.9	0.00	0.00	0.00	3.26	51.6	56.1	-3.71	0.459
8.72	51.5	51.5	4.0	0.00	0.00	0.00	3.25	51.5	56.1	-3.70	0.451
8.82	51.5	51.5	4.0	0.00	0.00	0.00	3.25	51.5	56.1	-3.70	0.442
8.92	51.4	51.4	4.0	0.00	0.00	0.00	3.24	51.4	55.9	-3.68	0.434
9.02	51.2	51.2	3.9	0.00	0.00	0.00	3.25	51.2	55.8	-3.66	0.426
9.12	51.2	51.2	3.7	0.00	0.00	0.00	3.22	51.2	55.8	-3.65	0.419
9.22	51.1	51.1	3.7	0.00	0.00	0.00	3.25	51.1	55.7	-3.66	0.410
9.32	51.0	51.0	4.0	0.00	0.00	0.00	3.21	51.0	55.6	-3.63	0.402
9.42	50.9	50.9	3.9	0.00	0.00	0.00	3.21	50.9	55.4	-3.62	0.395
9.52	50.8	50.8	3.7	0.00	0.00	0.00	3.20	50.8	55.3	-3.59	0.386
9.62	50.7	50.7	3.9	0.00	0.00	0.00	3.16	50.7	55.2	-3.56	0.379
9.73	50.5	50.5	3.9	0.00	0.00	0.00	3.24	50.5	55.0	-3.58	0.370
9.83	50.4	50.4	3.9	0.00	0.00	0.00	3.14	50.4	54.8	-3.50	0.363
9.93	50.3	50.3	4.4	0.00	0.00	0.00	3.12	50.3	54.7	-3.46	0.354

10.03	50.0	50.0	4.5	0.00	0.00	0.00	3.33	50.0	54.5	-3.53	0.347
10.13	49.8	49.8	4.1	0.00	0.00	0.00	3.36	49.8	54.4	-3.65	0.340
10.22	49.6	49.6	4.0	0.00	0.00	0.00	3.35	49.6	54.3	-3.67	0.332
10.31	49.5	49.5	4.0	0.00	0.00	0.00	3.33	49.5	54.1	-3.66	0.324
10.41	49.3	49.3	4.3	0.00	0.00	0.00	3.31	49.3	53.9	-3.65	0.317
10.51	49.1	49.1	4.5	0.00	0.00	0.00	3.34	49.1	53.7	-3.65	0.309
10.61	49.0	49.0	4.5	0.00	0.00	0.00	3.30	49.0	53.6	-3.66	0.300
10.71	48.9	48.9	4.5	0.00	0.00	0.00	3.32	48.9	53.5	-3.64	0.292
10.81	48.8	48.8	4.6	0.00	0.00	0.00	3.30	48.8	53.4	-3.61	0.283
10.91	48.8	48.8	4.5	0.00	0.00	0.00	3.30	48.8	53.4	-3.63	0.275
11.01	48.6	48.6	4.5	0.00	0.00	0.00	3.27	48.6	53.2	-3.62	0.267
11.11	48.5	48.5	4.5	0.00	0.00	0.00	3.33	48.5	53.1	-3.61	0.261
11.21	48.4	48.4	4.5	0.00	0.00	0.00	3.26	48.4	53.0	-3.63	0.252
11.31	48.3	48.3	4.5	0.00	0.00	0.00	3.27	48.3	52.9	-3.58	0.244
11.41	48.2	48.2	4.6	0.00	0.00	0.00	3.28	48.2	52.7	-3.59	0.237
11.52	48.1	48.1	4.6	0.00	0.00	0.00	3.29	48.1	52.6	-3.58	0.228
11.61	47.9	47.9	4.9	0.00	0.00	0.00	3.23	47.9	52.4	-3.53	0.221
11.72	47.8	47.8	5.0	0.00	0.00	0.00	3.25	47.8	52.3	-3.54	0.212
11.82	47.7	47.7	5.3	0.00	0.00	0.00	3.28	47.7	52.1	-3.54	0.204
11.92	47.5	47.5	5.6	0.00	0.00	0.00	3.21	47.5	51.9	-3.49	0.197
12.02	47.4	47.4	5.8	0.00	0.00	0.00	3.19	47.4	51.8	-3.46	0.190
12.12	47.2	47.2	5.8	0.00	0.00	0.00	3.14	47.2	51.5	-3.42	0.182
12.22	47.1	47.1	5.9	0.00	0.00	0.00	3.20	47.1	51.4	-3.44	0.174
12.32	46.9	46.9	5.8	0.00	0.00	0.00	3.12	46.9	51.1	-3.39	0.167
12.42	46.7	46.7	5.9	0.00	0.00	0.00	3.15	46.7	50.9	-3.35	0.160
12.52	46.5	46.5	5.9	0.00	0.00	0.00	3.12	46.5	50.7	-3.31	0.152
12.62	46.4	46.4	5.6	0.00	0.00	0.00	3.06	46.4	50.4	-3.26	0.145
12.72	46.1	46.1	5.5	0.00	0.00	0.00	3.05	46.1	50.2	-3.25	0.137
12.82	45.9	45.9	5.5	0.00	0.00	0.00	3.10	45.9	49.9	-3.22	0.130
12.90	45.6	45.6	5.5	0.00	0.00	0.00	3.28	45.6	49.8	-3.32	0.123
13.00	45.3	45.3	5.4	0.00	0.00	0.00	3.20	45.3	49.5	-3.34	0.116
13.10	45.0	45.0	5.3	0.00	0.00	0.00	3.18	45.0	49.2	-3.33	0.110
13.20	44.8	44.8	5.0	0.00	0.00	0.00	3.12	44.8	48.9	-3.26	0.103
13.30	44.5	44.5	5.1	0.00	0.00	0.00	3.12	44.5	48.6	-3.24	0.096
13.40	44.3	44.3	5.1	0.00	0.00	0.00	3.09	44.3	48.3	-3.19	0.088
13.51	44.0	44.0	5.3	0.00	0.00	0.00	3.04	44.0	48.0	-3.13	0.081
13.61	43.8	43.8	5.0	0.00	0.00	0.00	2.97	43.8	47.7	-3.09	0.075
13.71	43.5	43.5	5.1	0.00	0.00	0.00	2.96	43.5	47.3	-3.02	0.068
13.81	43.3	43.3	5.0	0.00	0.00	0.00	2.92	43.3	47.1	-2.99	0.060
13.91	42.9	42.9	5.3	0.00	0.00	0.00	3.07	42.9	46.7	-3.03	0.055
14.01	42.5	42.5	5.4	0.00	0.00	0.00	3.03	42.5	46.4	-3.03	0.048
14.11	42.2	42.2	5.8	0.00	0.00	0.00	3.03	42.2	46.1	-3.01	0.040
14.21	41.9	41.9	6.1	0.00	0.00	0.00	2.95	41.9	45.7	-3.01	0.035
14.31	41.6	41.6	6.6	0.00	0.00	0.00	2.94	41.6	45.4	-2.97	0.028
14.41	41.4	41.4	6.6	0.00	0.00	0.00	2.96	41.4	45.0	-2.94	0.022
14.51	41.0	41.0	6.8	0.00	0.00	0.00	3.17	41.0	44.9	-3.02	0.015
14.61	40.5	40.5	8.0	0.00	0.00	0.00	3.12	40.5	44.4	-3.07	0.008
14.71	40.2	40.2	7.5	0.00	0.00	0.00	3.10	40.2	44.1	-3.05	0.001
14.80	34.3	34.3	7.5	0.00	0.00	0.00	1.98	34.3	32.9	-0.87	-0.002
14.89	46.2	38.6	7.0	2.93	5.73	1.95	3.26	46.2	44.5	-0.16	-0.002
14.98	49.5	41.9	7.0	2.96	5.66	1.90	3.22	49.5	47.4	-0.15	-0.002
15.07	52.4	45.1	6.8	2.95	5.48	1.85	3.28	52.4	50.1	-0.15	-0.002
15.16	54.9	47.8	6.5	2.95	5.33	1.80	3.41	54.9	52.1	-0.14	-0.002
15.25	57.0	50.0	6.5	3.00	5.23	1.74	3.40	57.0	53.6	-0.14	-0.002

15.34	59.0	52.1	6.8	3.02	5.10	1.68	3.45	59.0	54.9	-0.14	-0.002
15.44	60.7	53.9	6.8	3.03	5.07	1.67	3.60	60.7	55.8	-0.14	-0.002
15.53	62.0	55.4	6.6	3.01	4.94	1.63	3.63	62.0	56.1	-0.14	-0.002
15.62	63.1	56.6	6.6	3.00	4.90	1.63	3.80	63.1	56.5	-0.14	-0.002
15.71	61.8	57.8	6.8	1.52	3.03	1.55	3.50	61.8	54.2	-0.14	-0.002
15.80	55.7	54.5	7.0	0.74	0.94	1.68	3.40	55.7	46.1	-0.14	-0.002
15.89	59.9	53.1	6.6	2.99	5.13	1.71	3.59	59.9	50.8	-0.14	-0.002
15.98	61.6	54.9	6.8	3.01	5.06	1.67	3.66	61.6	53.5	-0.14	-0.002
16.08	62.8	56.3	6.8	2.99	4.96	1.65	3.70	62.8	55.0	-0.14	-0.002
16.17	62.3	57.5	6.8	1.53	3.62	0.80	3.40	62.3	54.7	-0.14	-0.002
16.26	55.0	54.8	6.8	0.81	0.15	1.96	3.32	55.0	45.6	-0.14	-0.002
16.35	59.8	53.0	6.6	3.00	5.13	1.70	3.59	59.8	51.8	-0.14	-0.002
16.44	61.5	54.8	6.8	3.00	5.02	1.67	3.57	61.5	54.3	-0.14	-0.002
16.54	62.9	56.4	6.9	3.03	4.87	1.60	3.59	62.9	55.6	-0.14	-0.002
16.63	62.3	57.6	6.6	1.54	3.58	0.79	3.42	62.3	54.5	-0.14	-0.002
16.72	55.2	55.1	6.8	0.80	0.09	1.57	3.22	55.2	45.3	-0.14	-0.002
16.81	59.7	52.9	6.5	3.00	5.10	1.69	3.57	59.7	51.4	-0.14	-0.002
16.90	61.5	54.9	6.5	2.98	4.98	1.67	3.41	61.5	54.2	-0.14	-0.002
16.99	62.9	56.5	6.5	3.01	4.83	1.60	3.52	62.9	55.5	-0.14	-0.002
17.09	62.4	57.9	6.5	1.52	3.44	1.47	3.64	62.4	54.2	-0.14	-0.002
17.18	55.8	54.6	6.3	0.75	0.95	1.62	3.35	55.8	45.7	-0.14	-0.002
17.27	60.0	53.3	6.1	2.96	5.00	1.68	3.48	60.0	51.6	-0.14	-0.002
17.36	61.5	54.9	6.0	3.00	4.91	1.63	3.59	61.5	53.6	-0.14	-0.002
17.45	62.6	56.2	6.0	3.00	4.80	1.59	3.67	62.6	54.2	-0.14	-0.002
17.54	63.6	57.3	6.1	3.02	4.81	1.58	3.79	63.6	54.3	-0.14	-0.002
17.64	58.9	57.3	6.1	0.80	1.22	1.89	3.44	58.9	48.6	-0.14	-0.002
17.72	56.8	53.4	6.1	1.74	2.59	1.80	3.45	56.8	45.8	-0.14	-0.002
17.81	60.5	53.8	6.0	3.00	5.10	1.69	3.66	60.5	51.5	-0.14	-0.002
17.91	61.8	55.3	6.0	2.95	4.97	1.68	3.73	61.8	53.5	-0.14	-0.002
18.00	62.8	56.4	6.0	2.96	4.87	1.64	3.89	62.8	54.7	-0.14	-0.002
18.09	63.5	57.2	5.9	2.99	4.82	1.61	3.91	63.5	55.1	-0.14	-0.002
18.18	60.9	57.7	5.8	1.55	2.43	2.09	3.53	60.9	52.0	-0.14	-0.002
18.27	56.1	54.4	5.9	1.50	1.32	1.19	3.47	56.1	45.7	-0.14	-0.002
18.36	59.8	53.1	5.8	2.99	5.06	1.69	3.60	59.8	50.7	-0.14	-0.002
18.45	61.3	54.8	5.6	3.00	4.91	1.63	3.56	61.3	53.1	-0.14	-0.002
18.54	62.5	56.1	5.5	2.99	4.81	1.60	3.68	62.5	54.6	-0.14	-0.002
18.63	63.3	57.1	5.3	2.96	4.71	1.58	3.67	63.3	55.0	-0.14	-0.002
18.73	63.4	58.1	5.1	2.23	4.02	1.19	3.64	63.4	54.8	-0.14	-0.002
18.83	55.8	55.7	5.3	0.05	0.13	0.00	3.22	55.8	45.2	-0.14	-0.002
18.92	59.3	52.8	5.1	2.94	4.89	1.65	3.67	59.3	49.4	-0.14	-0.002
19.01	60.8	54.3	5.3	2.96	4.97	1.67	3.67	60.8	52.5	-0.14	-0.002
19.10	62.0	55.6	5.1	3.00	4.82	1.60	3.75	62.0	53.9	-0.14	-0.002
19.19	62.9	56.6	5.3	2.97	4.76	1.60	3.78	62.9	54.6	-0.14	-0.002
19.28	63.6	57.4	5.1	2.95	4.69	1.56	3.88	63.6	55.4	-0.14	-0.002
19.38	62.7	58.0	5.3	2.28	3.53	2.01	3.65	62.7	54.0	-0.14	-0.002
19.47	55.8	55.7	5.4	0.05	0.12	0.00	3.22	55.8	45.0	-0.14	-0.002
19.55	59.3	52.9	5.0	2.92	4.86	1.66	3.83	59.3	49.4	-0.14	-0.002
19.65	60.8	54.3	5.0	2.96	4.95	1.67	3.61	60.8	52.3	-0.14	-0.002
19.74	62.0	55.6	5.0	2.98	4.84	1.62	3.75	62.0	53.7	-0.14	-0.002
19.83	62.8	56.6	5.0	2.89	4.67	1.61	3.72	62.8	54.6	-0.14	-0.002
19.92	58.6	55.4	5.1	3.06	2.43	1.23	3.32	58.6	47.8	-0.14	-0.002
20.01	62.7	56.6	4.8	2.97	4.65	1.56	3.69	62.7	53.5	-0.14	-0.002
20.10	63.4	57.3	4.9	2.93	4.64	1.58	3.84	63.4	54.4	-0.14	-0.002
20.19	64.0	57.9	5.0	2.98	4.61	1.54	3.85	64.0	55.4	-0.14	-0.002

20.29	59.0	57.5	5.0	0.76	1.20	0.00	3.44	59.0	48.8	-0.14	-0.002
20.38	56.7	53.5	4.8	2.23	2.44	0.96	3.51	56.7	45.9	-0.14	-0.002
20.47	60.0	53.6	4.5	2.89	4.87	1.68	3.55	60.0	50.9	-0.14	-0.002
20.56	58.5	55.3	5.0	3.05	2.47	1.21	3.37	58.5	49.7	-0.14	-0.002
20.65	60.9	54.0	4.6	2.98	5.25	1.75	3.63	60.9	51.6	-0.14	-0.002
20.74	61.6	55.4	4.5	2.94	4.67	1.59	3.64	61.6	53.2	-0.14	-0.002
20.83	62.3	56.2	4.5	2.95	4.61	1.56	3.69	62.3	54.3	-0.14	-0.002
20.93	63.0	56.9	4.6	2.98	4.58	1.53	3.79	63.0	54.4	-0.14	-0.002
21.02	63.6	57.6	4.8	2.94	4.60	1.56	3.84	63.6	54.9	-0.14	-0.002
21.11	64.1	58.1	4.8	2.98	4.55	1.52	3.86	64.1	55.2	-0.14	-0.002
21.20	59.0	57.5	4.8	0.05	1.19	1.39	3.45	59.0	48.6	-0.14	-0.002
21.29	56.4	53.6	5.0	2.17	2.10	1.26	3.88	56.4	45.0	-0.14	-0.002
21.38	58.2	51.6	4.8	2.96	4.93	1.66	3.32	58.2	48.9	-0.14	-0.002
21.47	60.0	53.6	4.9	2.97	4.87	1.63	3.44	60.0	52.0	-0.14	-0.002
21.56	61.3	55.0	4.9	2.98	4.77	1.60	3.58	61.3	52.8	-0.14	-0.002
21.65	62.4	56.2	4.8	2.92	4.66	1.59	3.62	62.4	54.0	-0.14	-0.002
21.75	63.2	57.1	4.8	2.98	4.54	1.52	3.64	63.2	55.2	-0.14	-0.002
21.84	63.8	57.8	4.6	2.97	4.50	1.51	3.73	63.8	56.3	-0.14	-0.002
21.93	62.1	57.2	5.0	3.09	3.68	1.21	4.03	62.1	52.7	-0.14	-0.002
22.02	63.5	57.5	4.8	2.95	4.54	1.53	3.71	63.5	54.6	-0.14	-0.002
22.11	64.1	58.1	4.8	2.19	4.56	1.18	3.79	64.1	54.7	-0.14	-0.002
22.21	56.7	56.7	4.9	0.05	0.03	0.00	3.27	56.7	45.9	-0.14	-0.002
22.29	57.9	53.0	4.6	2.98	3.72	1.25	3.42	57.9	47.4	-0.14	-0.002
22.38	60.6	54.2	4.5	2.94	4.79	1.62	3.53	60.6	52.1	-0.14	-0.002
22.48	61.8	55.5	4.6	2.91	4.69	1.61	3.57	61.8	53.8	-0.14	-0.002
22.57	62.7	56.5	4.6	2.93	4.63	1.55	3.69	62.7	54.7	-0.14	-0.002
22.66	58.6	56.0	5.0	3.03	2.03	1.32	3.18	58.6	48.1	-0.14	-0.002
22.75	62.6	56.5	4.5	2.89	4.63	1.60	3.70	62.6	53.6	-0.14	-0.002
22.84	63.3	57.3	4.5	2.88	4.55	1.58	3.72	63.3	54.8	-0.14	-0.002
22.93	63.8	57.9	4.5	2.90	4.51	1.55	3.70	63.8	54.9	-0.14	-0.002
23.03	61.0	58.1	4.4	0.74	2.25	1.26	3.60	61.0	51.4	-0.14	-0.002
23.12	55.8	54.2	4.6	1.47	1.26	1.24	3.31	55.8	44.5	-0.14	-0.002
23.21	60.1	53.7	4.6	2.93	4.83	1.64	3.42	60.1	50.8	-0.14	-0.002
23.30	59.2	55.1	4.9	2.84	3.15	1.22	2.98	59.2	50.8	-0.14	-0.002
23.39	61.0	54.3	4.6	2.95	5.03	1.70	3.69	61.0	52.1	-0.14	-0.002
23.48	61.7	55.5	4.5	2.87	4.66	1.61	3.56	61.7	53.4	-0.14	-0.002
23.57	62.7	56.6	4.5	2.90	4.63	1.59	3.63	62.7	54.2	-0.14	-0.002
23.66	63.3	57.3	4.5	2.87	4.57	1.59	3.72	63.3	55.0	-0.14	-0.002
23.75	63.9	58.0	4.4	2.96	4.48	1.51	3.73	63.9	54.5	-0.14	-0.002
23.85	62.0	58.5	4.1	1.49	2.70	1.52	3.42	62.0	52.0	-0.14	-0.002

Table 9.4 Results from Run Performed on 15/3/87

	HEAT PUMP							HEAT STORE			
t	T_{out}	T_{in}	T_a	W	q_{co}	COP	q_{DHW}	T_{in}	T_{out}	$q_{C,D}$	UF
[hr]	[°C]	[°C]	[°C]	[kW]	[kW]	[-]	[kW]	[°C]	[°C]	[kW]	[-]
0.00	59.3	52.9	4.4	2.85	4.80	1.68	3.47	59.3	50.7	-0.14	-0.002
0.10	53.2	46.9	5.0	2.84	4.76	1.75	0.00	53.2	36.3	12.62	0.017
0.20	48.3	40.5	4.3	2.79	5.94	2.13	0.00	48.3	39.1	6.83	0.036
0.31	47.6	40.0	4.3	2.76	5.75	2.07	0.00	47.6	40.4	5.33	0.050
0.40	48.1	40.6	4.3	2.79	5.61	2.01	0.00	48.1	41.2	5.03	0.060
0.50	48.6	41.2	4.0	2.79	5.61	2.00	0.00	48.6	41.7	5.05	0.071
0.61	49.2	41.9	4.0	2.66	5.58	2.11	0.00	49.2	42.3	5.05	0.083
0.71	46.5	42.3	4.5	2.81	3.20	1.44	0.00	46.5	42.6	2.68	0.088
0.81	50.2	42.9	4.0	2.83	5.52	1.94	0.00	50.2	43.5	4.86	0.100
0.91	50.8	43.6	4.1	2.85	5.48	1.92	0.00	50.8	44.2	4.77	0.111
1.01	51.4	44.2	4.1	2.85	5.46	1.91	0.00	51.4	44.9	4.77	0.120
1.11	52.1	44.9	4.3	2.87	5.40	1.87	0.00	52.1	45.4	4.75	0.131
1.21	52.6	45.3	4.3	2.70	5.41	2.04	0.00	52.6	45.9	4.80	0.141
1.31	50.1	45.8	4.9	2.88	3.18	1.44	0.00	50.1	46.3	2.63	0.147
1.41	53.5	46.2	4.4	2.90	5.43	1.86	0.00	53.5	46.7	4.86	0.158
1.51	53.8	46.6	4.4	2.92	5.40	1.84	0.00	53.8	47.0	4.82	0.170
1.61	54.1	46.9	4.4	2.91	5.35	1.83	0.00	54.1	47.4	4.76	0.179
1.71	54.5	47.4	4.1	2.91	5.36	1.94	0.00	54.5	47.8	4.78	0.190
1.81	54.7	48.1	4.5	2.77	4.96	1.77	0.00	54.7	48.6	4.29	0.201
1.91	52.3	48.0	4.9	3.01	3.20	1.47	0.00	52.3	48.5	2.64	0.206
2.01	55.5	48.4	4.3	2.93	5.35	1.82	0.00	55.5	48.9	4.74	0.217
2.11	55.7	48.7	4.5	2.94	5.30	1.80	0.00	55.7	49.2	4.69	0.227
2.21	56.1	49.1	4.5	2.92	5.21	1.78	0.00	56.1	49.6	4.60	0.237
2.31	56.4	49.4	4.6	2.92	5.27	1.80	0.00	56.4	49.9	4.65	0.247
2.41	55.3	49.8	4.8	2.83	4.13	1.47	0.00	55.3	50.3	3.53	0.258
2.51	54.1	50.1	4.8	3.02	3.03	1.47	0.00	54.1	50.5	2.45	0.261
2.61	57.2	50.4	4.5	2.97	5.16	1.73	0.00	57.2	50.8	4.55	0.270
2.71	57.4	50.6	4.4	2.94	5.15	1.75	0.00	57.4	51.1	4.54	0.281
2.81	57.6	50.9	4.3	2.91	5.13	1.75	0.00	57.6	51.4	4.53	0.290
2.91	57.9	51.2	4.0	2.94	5.06	1.71	0.00	57.9	51.7	4.46	0.300
3.01	56.6	51.4	4.4	2.81	3.96	1.43	0.00	56.6	51.7	3.38	0.310
3.11	55.5	51.6	4.4	3.01	3.02	1.44	0.00	55.5	51.9	2.48	0.314
3.22	58.5	51.8	4.1	2.94	5.04	1.71	0.00	58.5	52.3	4.45	0.324
3.31	58.7	52.1	4.3	2.93	5.05	1.63	0.00	58.7	52.5	4.45	0.334
3.41	58.9	52.3	4.4	2.96	5.02	1.69	0.00	58.9	52.7	4.44	0.344
3.52	59.1	52.5	4.3	2.95	4.99	1.69	0.00	59.1	52.8	4.41	0.354
3.62	57.4	52.8	5.0	2.89	3.52	1.40	0.00	57.4	53.2	2.94	0.363
3.72	58.5	52.7	4.6	3.06	4.42	1.46	0.00	58.5	53.0	3.88	0.369
3.82	59.6	53.0	4.5	3.01	5.02	1.66	0.00	59.6	53.4	4.44	0.377
3.92	59.7	53.1	4.5	2.94	4.97	1.69	0.00	59.7	53.5	4.40	0.388
4.02	59.9	53.4	4.5	2.93	4.97	1.69	0.00	59.9	53.8	4.39	0.397
4.12	59.9	53.4	4.4	2.94	4.93	1.67	0.00	59.9	53.9	4.36	0.408
4.22	57.6	53.7	4.4	2.92	2.99	1.46	0.00	57.6	54.1	2.45	0.417
4.32	60.1	53.7	4.3	3.01	4.86	1.61	0.00	60.1	54.1	4.30	0.423
4.42	60.3	53.8	4.4	2.95	4.93	1.67	0.00	60.3	54.2	4.36	0.432
4.52	60.5	54.0	4.5	2.94	4.92	1.67	0.00	60.5	54.4	4.36	0.442

4.62	60.6	54.1	4.5	2.96	4.91	1.65	0.00	60.6	54.5	4.34	0.451
4.72	60.6	54.1	4.5	3.00	4.89	1.62	0.00	60.6	54.6	4.32	0.460
4.82	58.2	54.4	5.0	2.90	2.89	1.48	0.00	58.2	54.8	2.32	0.469
4.92	60.8	54.4	4.5	3.01	4.92	1.63	0.00	60.8	54.7	4.36	0.476
5.02	61.0	54.5	4.5	2.95	4.88	1.65	0.00	61.0	54.9	4.33	0.485
5.12	61.0	54.6	4.4	2.95	4.94	1.67	0.00	61.0	54.9	4.38	0.494
5.22	61.1	54.7	4.3	2.93	4.89	1.66	0.00	61.1	55.0	4.34	0.505
5.32	61.2	54.8	4.4	2.98	4.87	1.63	0.00	61.2	55.1	4.31	0.513
5.42	58.1	55.4	4.5	2.89	2.08	1.17	0.00	58.1	55.8	1.48	0.523
5.52	61.3	54.8	4.5	3.03	4.93	1.62	0.00	61.3	55.2	4.37	0.527
5.62	61.4	55.0	4.5	3.03	4.83	1.59	0.00	61.4	55.3	4.28	0.537
5.72	61.5	55.1	4.3	2.94	4.87	1.65	0.00	61.5	55.5	4.31	0.545
5.82	61.6	55.2	4.3	2.93	4.83	1.62	0.00	61.6	55.5	4.27	0.555
5.92	61.5	55.2	4.0	2.95	4.79	1.62	0.00	61.5	55.5	4.24	0.564
6.02	57.4	55.0	4.5	2.90	1.89	1.09	0.00	57.4	55.2	1.44	0.573
6.12	61.7	55.3	4.3	2.95	4.84	1.63	0.00	61.7	55.7	4.28	0.577
6.23	61.7	55.4	4.1	2.94	4.81	1.63	0.00	61.7	55.7	4.25	0.587
6.32	61.8	55.5	4.3	2.95	4.82	1.63	0.00	61.8	55.8	4.26	0.597
6.43	61.8	55.5	4.1	2.97	4.75	1.60	0.00	61.8	55.9	4.20	0.605
6.52	61.8	55.5	4.0	2.95	4.78	1.62	0.00	61.8	55.9	4.23	0.615
6.61	60.1	55.8	4.3	2.87	3.26	1.26	0.00	60.1	56.2	2.70	0.624
6.71	60.6	55.4	4.5	3.04	3.99	1.37	0.00	60.6	55.6	3.49	0.628
6.81	62.0	55.7	4.3	2.95	4.81	1.62	0.00	62.0	56.0	4.26	0.637
6.91	62.1	55.8	4.3	2.97	4.78	1.61	0.00	62.1	56.1	4.23	0.646
7.01	62.1	55.8	4.3	3.00	4.76	1.58	0.00	62.1	56.2	4.20	0.655
7.11	55.4	55.4	4.3	0.00	0.00	0.00	7.16	55.4	61.8	-5.10	0.654
7.20	52.7	52.7	4.1	0.00	0.00	0.00	7.16	52.7	61.4	-6.73	0.645
7.30	53.7	53.7	4.0	0.00	0.00	0.00	3.27	53.7	60.5	-5.34	0.634
7.40	54.6	54.6	4.0	0.00	0.00	0.00	3.26	54.6	59.1	-3.58	0.625
7.50	54.1	54.1	4.0	0.00	0.00	0.00	3.25	54.1	58.2	-3.28	0.617
7.60	53.4	53.4	4.1	0.00	0.00	0.00	3.22	53.4	57.6	-3.36	0.609
7.70	52.9	52.9	4.5	0.00	0.00	0.00	3.40	52.9	57.2	-3.54	0.601
7.81	52.4	52.4	4.8	0.00	0.00	0.00	3.43	52.4	57.1	-3.68	0.594
7.90	52.1	52.1	5.0	0.00	0.00	0.00	3.48	52.1	56.9	-3.81	0.585
8.01	51.8	51.8	5.0	0.00	0.00	0.00	3.47	51.8	56.7	-3.88	0.577
8.11	51.7	51.7	5.0	0.00	0.00	0.00	3.51	51.7	56.7	-3.94	0.569
8.21	51.6	51.6	5.0	0.00	0.00	0.00	3.55	51.6	56.5	-3.99	0.560
8.31	51.5	51.5	5.1	0.00	0.00	0.00	3.52	51.5	56.6	-4.00	0.550
8.41	51.5	51.5	5.3	0.00	0.00	0.00	3.44	51.5	56.5	-3.98	0.541
8.51	51.5	51.5	5.0	0.00	0.00	0.00	3.43	51.5	56.4	-3.92	0.533
8.61	51.4	51.4	5.0	0.00	0.00	0.00	3.34	51.4	56.3	-3.86	0.524
8.71	51.4	51.4	5.0	0.00	0.00	0.00	3.40	51.4	56.3	-3.89	0.516
8.81	51.4	51.4	5.1	0.00	0.00	0.00	3.40	51.4	56.2	-3.88	0.507
8.91	51.3	51.3	5.1	0.00	0.00	0.00	3.34	51.3	56.1	-3.82	0.499
9.01	51.2	51.2	5.1	0.00	0.00	0.00	3.37	51.2	56.0	-3.83	0.491
9.11	51.2	51.2	5.4	0.00	0.00	0.00	3.31	51.2	55.9	-3.79	0.483
9.21	51.1	51.1	5.6	0.00	0.00	0.00	3.31	51.1	55.8	-3.77	0.474
9.31	51.0	51.0	5.9	0.00	0.00	0.00	3.28	51.0	55.7	-3.75	0.466
9.41	50.9	50.9	6.0	0.00	0.00	0.00	3.28	50.9	55.6	-3.74	0.457
9.51	50.8	50.8	6.1	0.00	0.00	0.00	3.32	50.8	55.4	-3.72	0.449
9.61	50.7	50.7	6.0	0.00	0.00	0.00	3.30	50.7	55.3	-3.71	0.440
9.71	50.6	50.6	6.1	0.00	0.00	0.00	3.26	50.6	55.2	-3.69	0.432
9.80	50.5	50.5	6.1	0.00	0.00	0.00	3.25	50.5	55.1	-3.67	0.425
9.90	50.4	50.4	6.3	0.00	0.00	0.00	3.25	50.4	54.9	-3.64	0.417

9.99	50.3	50.3	6.0	0.00	0.00	0.00	3.25	50.3	54.8	-3.63	0.409
10.10	50.0	50.0	6.3	0.00	0.00	0.00	3.41	50.0	54.6	-3.67	0.402
10.20	49.8	49.8	7.0	0.00	0.00	0.00	3.43	49.8	54.5	-3.75	0.394
10.30	49.6	49.6	6.8	0.00	0.00	0.00	3.40	49.6	54.3	-3.78	0.385
10.40	49.4	49.4	7.3	0.00	0.00	0.00	3.42	49.4	54.1	-3.76	0.377
10.50	49.3	49.3	8.6	0.00	0.00	0.00	3.45	49.3	54.0	-3.78	0.369
10.60	49.2	49.2	9.1	0.00	0.00	0.00	3.43	49.2	53.9	-3.77	0.360
10.70	49.1	49.1	8.8	0.00	0.00	0.00	3.42	49.1	53.8	-3.77	0.352
10.80	49.0	49.0	9.0	0.00	0.00	0.00	3.43	49.0	53.7	-3.75	0.344
10.90	48.9	48.9	7.5	0.00	0.00	0.00	3.42	48.9	53.6	-3.76	0.335
11.00	48.8	48.8	8.0	0.00	0.00	0.00	3.40	48.8	53.5	-3.73	0.327
11.10	48.7	48.7	7.3	0.00	0.00	0.00	3.40	48.7	53.4	-3.74	0.318
11.20	48.6	48.6	7.0	0.00	0.00	0.00	3.34	48.6	53.3	-3.71	0.310
11.30	48.5	48.5	6.9	0.00	0.00	0.00	3.35	48.5	53.1	-3.70	0.302
11.40	48.4	48.4	7.0	0.00	0.00	0.00	3.34	48.4	52.9	-3.68	0.295
11.50	48.3	48.3	6.9	0.00	0.00	0.00	3.33	48.3	52.9	-3.66	0.286
11.60	48.2	48.2	6.8	0.00	0.00	0.00	3.31	48.2	52.8	-3.67	0.277
11.70	48.1	48.1	6.8	0.00	0.00	0.00	3.30	48.1	52.7	-3.65	0.270
11.80	48.0	48.0	8.0	0.00	0.00	0.00	3.32	48.0	52.5	-3.66	0.261
11.90	47.9	47.9	8.6	0.00	0.00	0.00	3.25	47.9	52.4	-3.58	0.253
12.00	47.8	47.8	8.6	0.00	0.00	0.00	3.28	47.8	52.3	-3.59	0.245
12.10	47.7	47.7	8.6	0.00	0.00	0.00	3.21	47.7	52.2	-3.54	0.238
12.20	47.5	47.5	8.1	0.00	0.00	0.00	3.17	47.5	51.9	-3.51	0.231
12.30	47.4	47.4	9.0	0.00	0.00	0.00	3.17	47.4	51.9	-3.50	0.222
12.39	47.3	47.3	9.3	0.00	0.00	0.00	3.18	47.3	51.7	-3.46	0.216
12.49	47.2	47.2	8.1	0.00	0.00	0.00	3.12	47.2	51.5	-3.41	0.208
12.59	47.1	47.1	7.5	0.00	0.00	0.00	3.15	47.1	51.4	-3.43	0.201
12.69	46.9	46.9	7.9	0.00	0.00	0.00	3.11	46.9	51.1	-3.39	0.194
12.79	46.7	46.7	7.9	0.00	0.00	0.00	3.12	46.7	50.9	-3.35	0.186
12.89	46.5	46.5	7.3	0.00	0.00	0.00	3.09	46.5	50.7	-3.32	0.179
12.99	46.3	46.3	7.3	0.00	0.00	0.00	3.07	46.3	50.5	-3.33	0.172
13.09	46.2	46.2	7.0	0.00	0.00	0.00	3.04	46.2	50.3	-3.27	0.163
13.19	46.0	46.0	7.1	0.00	0.00	0.00	3.11	46.0	50.1	-3.23	0.157
13.29	45.6	45.6	8.5	0.00	0.00	0.00	3.14	45.6	49.7	-3.28	0.150
13.39	45.4	45.4	9.8	0.00	0.00	0.00	3.13	45.4	49.5	-3.30	0.143
13.49	45.1	45.1	9.8	0.00	0.00	0.00	3.15	45.1	49.2	-3.28	0.135
13.59	44.9	44.9	9.5	0.00	0.00	0.00	3.09	44.9	49.0	-3.23	0.128
13.69	44.6	44.6	9.6	0.00	0.00	0.00	3.03	44.6	48.6	-3.18	0.120
13.79	44.4	44.4	9.6	0.00	0.00	0.00	3.04	44.4	48.4	-3.14	0.113
13.89	44.2	44.2	8.8	0.00	0.00	0.00	3.05	44.2	48.1	-3.11	0.106
13.99	43.9	43.9	9.0	0.00	0.00	0.00	3.00	43.9	47.8	-3.07	0.101
14.09	43.6	43.6	9.6	0.00	0.00	0.00	3.11	43.6	47.4	-3.02	0.093
14.19	43.1	43.1	10.0	0.00	0.00	0.00	3.10	43.1	47.1	-3.15	0.086
14.29	42.8	42.8	9.8	0.00	0.00	0.00	3.10	42.8	46.8	-3.19	0.080
14.39	42.6	42.6	10.1	0.00	0.00	0.00	3.05	42.6	46.5	-3.07	0.073
14.49	42.3	42.3	9.3	0.00	0.00	0.00	3.07	42.3	46.1	-3.05	0.065
14.59	42.0	42.0	10.3	0.00	0.00	0.00	2.99	42.0	45.8	-3.00	0.060
14.69	41.8	41.8	9.1	0.00	0.00	0.00	2.94	41.8	45.5	-2.95	0.052
14.80	41.5	41.5	9.1	0.00	0.00	0.00	2.90	41.5	45.2	-2.89	0.046
14.89	41.2	41.2	8.5	0.00	0.00	0.00	2.97	41.2	44.8	-2.84	0.040
14.98	40.9	40.9	8.1	0.00	0.00	0.00	2.86	40.9	44.5	-2.81	0.035
15.08	40.4	40.4	8.6	0.00	0.00	0.00	3.15	40.4	44.1	-2.88	0.029
15.17	36.6	36.6	8.8	0.00	0.00	0.00	1.50	36.6	36.0	-1.29	0.024
15.27	48.3	40.9	7.8	3.09	5.56	1.89	3.41	48.3	45.8	-0.16	0.024

Table 9.5 Simulated Results for Run Performed on 12/3/87

	HEAT PUMP							HEAT STORE			
t	T_{out}	T_{in}	T_a	W	q_{co}	COP	q_{DHW}	T_{in}	T_{out}	$q_{C,D}$	UF
[hr]	[°C]	[°C]	[°C]	[kW]	[kW]	[-]	[kW]	[°C]	[°C]	[kW]	[-]
0.00	50.0	43.8	-1.1	2.63	4.72	1.79	0.00	49.7	44.0	4.29	0.000
0.10	50.0	43.8	-1.1	2.63	4.71	1.79	0.00	49.6	44.0	4.27	0.010
0.20	50.0	43.8	-1.1	2.63	4.71	1.79	0.00	49.7	44.0	4.27	0.020
0.30	50.1	43.9	-1.1	2.63	4.69	1.79	0.00	49.8	44.2	4.26	0.030
0.40	50.4	44.2	-1.1	2.63	4.67	1.78	0.00	50.1	44.5	4.23	0.040
0.50	36.8	44.8	-1.1	2.64	-6.05	1.00	0.00	36.5	45.0	-6.45	0.049
0.60	51.5	45.4	-1.1	2.64	4.60	1.74	0.00	51.2	45.7	4.15	0.052
0.70	52.1	46.1	-1.1	2.65	4.56	1.72	0.00	51.8	46.4	4.10	0.062
0.80	52.7	46.7	-1.1	2.65	4.52	1.71	0.00	52.3	47.0	4.06	0.071
0.90	53.2	47.3	-1.1	2.65	4.48	1.69	0.00	52.9	47.5	4.02	0.081
1.00	53.6	47.8	-1.7	2.63	4.35	1.65	0.00	53.2	48.1	3.89	0.090
1.10	54.1	48.4	-1.7	2.63	4.32	1.64	0.00	53.8	48.7	3.85	0.092
1.20	54.6	49.0	-1.7	2.64	4.27	1.62	0.00	54.3	49.3	3.81	0.101
1.30	55.1	49.5	-1.7	2.64	4.25	1.61	0.00	54.8	49.8	3.77	0.110
1.40	55.6	50.0	-1.7	2.65	4.21	1.59	0.00	55.2	50.3	3.73	0.119
1.50	56.0	50.5	-1.7	2.65	4.19	1.58	0.00	55.7	50.8	3.70	0.127
1.60	56.5	51.0	-1.7	2.65	4.14	1.56	0.00	56.2	51.4	3.66	0.129
1.70	57.0	51.6	-1.7	2.66	4.11	1.55	0.00	56.7	51.9	3.62	0.138
1.80	57.5	52.1	-1.7	2.66	4.08	1.53	0.00	57.1	52.4	3.59	0.146
1.90	57.9	52.5	-1.7	2.66	4.06	1.52	0.00	57.6	52.9	3.56	0.154
2.00	58.4	53.0	-1.3	2.69	4.09	1.52	0.00	58.1	53.3	3.59	0.163
2.10	58.9	53.5	-1.3	2.69	4.06	1.51	0.00	58.6	53.9	3.55	0.165
2.20	59.3	54.0	-1.3	2.69	4.03	1.49	0.00	59.0	54.3	3.52	0.173
2.30	59.7	54.4	-1.3	2.70	4.00	1.48	0.00	59.4	54.7	3.49	0.181
2.40	60.0	54.8	-1.3	2.70	3.97	1.47	0.00	59.7	55.1	3.47	0.189
2.50	47.1	55.1	-1.3	2.70	-6.05	1.00	0.00	46.8	55.4	-6.51	0.197
2.60	60.5	55.3	-1.3	2.70	3.95	1.46	0.00	60.2	55.6	3.43	0.199
2.70	60.7	55.5	-1.3	2.70	3.93	1.45	0.00	60.3	55.8	3.42	0.207
2.80	60.8	55.6	-1.3	2.71	3.93	1.45	0.00	60.4	55.9	3.41	0.214
2.90	60.8	55.6	-1.3	2.71	3.92	1.45	0.00	60.5	56.0	3.40	0.222
3.00	47.7	55.7	-1.0	2.72	-6.04	1.00	0.00	47.4	56.0	-6.52	0.230
3.10	60.9	55.7	-1.0	2.72	3.97	1.46	0.00	60.6	56.0	3.45	0.232
3.20	60.9	55.7	-1.0	2.72	3.97	1.46	0.00	60.6	56.0	3.45	0.240
3.30	60.9	55.7	-1.0	2.72	3.96	1.46	0.00	60.6	56.0	3.45	0.248
3.40	60.9	55.7	-1.0	2.72	3.97	1.46	0.00	60.6	56.0	3.45	0.256
3.50	47.8	55.7	-1.0	2.72	-6.00	1.00	0.00	47.5	56.0	-6.47	0.264
3.60	60.9	55.7	-1.0	2.72	3.96	1.46	0.00	60.6	56.0	3.45	0.266
3.70	60.9	55.7	-1.0	2.72	3.96	1.46	0.00	60.6	56.0	3.45	0.274
3.80	60.9	55.7	-1.0	2.72	3.97	1.46	0.00	60.6	56.0	3.45	0.282
3.90	60.9	55.7	-1.0	2.72	3.96	1.46	0.00	60.6	56.0	3.45	0.290
4.00	47.8	55.7	-1.6	2.69	-6.00	1.00	0.00	47.5	56.0	-6.47	0.297
4.10	60.8	55.7	-1.6	2.69	3.87	1.44	0.00	60.5	56.0	3.35	0.299
4.20	60.8	55.7	-1.6	2.69	3.87	1.44	0.00	60.5	56.0	3.35	0.307
4.30	60.8	55.7	-1.6	2.69	3.87	1.44	0.00	60.5	56.0	3.35	0.315
4.40	60.8	55.7	-1.6	2.69	3.87	1.44	0.00	60.5	56.0	3.35	0.322
4.50	47.8	55.7	-1.6	2.69	-6.00	1.00	0.00	47.5	56.0	-6.47	0.330

4.60	60.8	55.7	-1.6	2.69	3.87	1.44	0.00	60.5	56.0	3.35	0.332
4.70	60.8	55.7	-1.6	2.69	3.87	1.44	0.00	60.5	56.0	3.35	0.339
4.80	60.8	55.7	-1.6	2.69	3.87	1.44	0.00	60.5	56.0	3.35	0.347
4.90	60.8	55.7	-1.6	2.69	3.87	1.44	0.00	60.5	56.0	3.35	0.355
5.00	47.8	55.7	-1.6	2.69	-6.00	1.00	0.00	47.5	56.0	-6.47	0.362
5.10	60.8	55.7	-1.6	2.69	3.87	1.44	0.00	60.5	56.1	3.35	0.364
5.20	60.8	55.7	-1.6	2.69	3.87	1.44	0.00	60.5	56.0	3.35	0.372
5.30	60.8	55.7	-1.6	2.69	3.87	1.44	0.00	60.5	56.0	3.35	0.380
5.40	60.8	55.7	-1.6	2.69	3.87	1.44	0.00	60.5	56.0	3.35	0.388
5.50	47.8	55.8	-1.6	2.69	-6.00	1.00	0.00	47.5	56.1	-6.47	0.395
5.60	60.8	55.7	-1.6	2.69	3.87	1.44	0.00	60.5	56.1	3.35	0.397
5.70	60.8	55.7	-1.6	2.69	3.87	1.44	0.00	60.5	56.1	3.35	0.405
5.80	60.8	55.7	-1.6	2.69	3.87	1.44	0.00	60.5	56.0	3.35	0.412
5.90	60.8	55.7	-1.6	2.69	3.87	1.44	0.00	60.5	56.1	3.35	0.420
6.00	47.8	55.8	-2.2	2.66	-6.00	1.00	0.00	47.5	56.1	-6.47	0.428
6.10	60.7	55.7	-2.2	2.66	3.77	1.42	0.00	60.4	56.1	3.26	0.429
6.20	60.7	55.7	-2.2	2.66	3.77	1.42	0.00	60.4	56.1	3.26	0.437
6.30	60.7	55.7	-2.2	2.66	3.77	1.42	0.00	60.4	56.1	3.26	0.444
6.40	60.7	55.7	-2.2	2.66	3.77	1.42	0.00	60.4	56.1	3.26	0.452
6.50	47.8	55.8	-2.2	2.66	-6.00	1.00	0.00	47.5	56.1	-6.47	0.459
6.60	60.7	55.7	-2.2	2.66	3.77	1.42	0.00	60.4	56.1	3.25	0.461
6.70	60.7	55.7	-2.2	2.66	3.77	1.42	0.00	60.4	56.1	3.26	0.468
6.80	60.7	55.7	-2.2	2.66	3.77	1.42	0.00	60.4	56.1	3.26	0.476
6.90	60.7	55.7	-2.2	2.66	3.77	1.42	0.00	60.4	56.1	3.25	0.483
7.00	44.0	44.0	-2.2	0.00	0.00	0.00	3.00	56.3	60.2	-3.00	0.483
7.10	44.0	44.0	-3.0	0.00	0.00	0.00	3.00	55.2	59.1	-3.00	0.476
7.20	44.0	44.0	-3.0	0.00	0.00	0.00	3.00	54.1	58.1	-3.00	0.469
7.30	44.0	44.0	-3.0	0.00	0.00	0.00	3.00	53.4	57.4	-3.00	0.462
7.40	44.0	44.0	-3.0	0.00	0.00	0.00	3.00	52.9	56.9	-3.00	0.455
7.50	44.0	44.0	-3.0	0.00	0.00	0.00	3.00	52.6	56.6	-3.00	0.448
7.60	44.0	44.0	-3.0	0.00	0.00	0.00	3.00	52.4	56.3	-3.00	0.441
7.70	44.0	44.0	-3.0	0.00	0.00	0.00	3.00	52.2	56.1	-3.00	0.434
7.80	44.0	44.0	-3.0	0.00	0.00	0.00	3.00	52.1	56.0	-3.00	0.427
7.90	44.0	44.0	-3.0	0.00	0.00	0.00	3.00	52.0	56.0	-3.00	0.420
8.00	44.0	44.0	-3.0	0.00	0.00	0.00	3.00	52.0	55.9	-3.00	0.413
8.10	44.0	44.0	-2.0	0.00	0.00	0.00	3.00	51.9	55.9	-3.00	0.406
8.20	44.0	44.0	-2.0	0.00	0.00	0.00	3.00	51.9	55.9	-3.00	0.399
8.30	44.0	44.0	-2.0	0.00	0.00	0.00	3.00	51.9	55.9	-3.00	0.393
8.40	44.0	44.0	-2.0	0.00	0.00	0.00	3.00	51.9	55.9	-3.00	0.386
8.50	44.0	44.0	-2.0	0.00	0.00	0.00	3.00	51.9	55.8	-3.00	0.379
8.60	44.0	44.0	-2.0	0.00	0.00	0.00	3.00	51.9	55.8	-3.00	0.372
8.70	44.0	44.0	-2.0	0.00	0.00	0.00	3.00	51.8	55.8	-3.00	0.365
8.80	44.0	44.0	-2.0	0.00	0.00	0.00	3.00	51.8	55.7	-3.00	0.358
8.90	44.0	44.0	-2.0	0.00	0.00	0.00	3.00	51.7	55.7	-3.00	0.351
9.00	44.0	44.0	-2.0	0.00	0.00	0.00	3.00	51.7	55.7	-3.00	0.344
9.10	44.0	44.0	0.1	0.00	0.00	0.00	3.00	51.7	55.6	-3.00	0.337
9.20	44.0	44.0	0.1	0.00	0.00	0.00	3.00	51.7	55.6	-3.00	0.330
9.30	44.0	44.0	0.1	0.00	0.00	0.00	3.00	51.6	55.6	-3.00	0.323
9.40	44.0	44.0	0.1	0.00	0.00	0.00	3.00	51.6	55.6	-3.00	0.316
9.50	44.0	44.0	0.1	0.00	0.00	0.00	3.00	51.6	55.6	-3.00	0.309
9.60	44.0	44.0	0.1	0.00	0.00	0.00	3.00	51.5	55.5	-3.00	0.302
9.70	44.0	44.0	0.1	0.00	0.00	0.00	3.00	51.4	55.4	-3.00	0.295
9.80	44.0	44.0	0.1	0.00	0.00	0.00	3.00	51.3	55.3	-3.00	0.288
9.90	44.0	44.0	0.1	0.00	0.00	0.00	3.00	51.2	55.2	-3.00	0.281

10.00	44.0	44.0	0.1	0.00	0.00	0.00	3.00	51.2	55.2	-3.00	0.274
10.10	44.0	44.0	1.8	0.00	0.00	0.00	3.00	51.2	55.1	-3.00	0.267
10.20	44.0	44.0	1.8	0.00	0.00	0.00	3.00	51.1	55.1	-3.00	0.260
10.30	44.0	44.0	1.8	0.00	0.00	0.00	3.00	51.1	55.0	-3.00	0.253
10.40	44.0	44.0	1.8	0.00	0.00	0.00	3.00	51.0	55.0	-3.00	0.246
10.50	44.0	44.0	1.8	0.00	0.00	0.00	3.00	51.0	55.0	-3.00	0.239
10.60	44.0	44.0	1.8	0.00	0.00	0.00	3.00	51.0	54.9	-3.00	0.232
10.70	44.0	44.0	1.8	0.00	0.00	0.00	3.00	50.9	54.9	-3.00	0.225
10.80	44.0	44.0	1.8	0.00	0.00	0.00	3.00	50.8	54.8	-3.00	0.218
10.90	44.0	44.0	1.8	0.00	0.00	0.00	3.00	50.6	54.6	-3.00	0.211
11.00	44.0	44.0	1.8	0.00	0.00	0.00	3.00	50.4	54.3	-3.00	0.204
11.10	44.0	44.0	4.1	0.00	0.00	0.00	3.00	50.2	54.2	-3.00	0.197
11.20	44.0	44.0	4.1	0.00	0.00	0.00	3.00	50.1	54.1	-3.00	0.191
11.30	44.0	44.0	4.1	0.00	0.00	0.00	3.00	50.1	54.0	-3.00	0.184
11.40	44.0	44.0	4.1	0.00	0.00	0.00	3.00	49.9	53.9	-3.00	0.177
11.50	44.0	44.0	4.1	0.00	0.00	0.00	3.00	49.9	53.8	-3.00	0.170
11.60	44.0	44.0	4.1	0.00	0.00	0.00	3.00	49.8	53.7	-3.00	0.163
11.70	44.0	44.0	4.1	0.00	0.00	0.00	3.00	49.6	53.6	-3.00	0.156
11.80	44.0	44.0	4.1	0.00	0.00	0.00	3.00	49.5	53.4	-3.00	0.149
11.90	44.0	44.0	4.1	0.00	0.00	0.00	3.00	49.4	53.4	-3.00	0.142
12.00	44.0	44.0	4.1	0.00	0.00	0.00	3.00	49.3	53.3	-3.00	0.135
12.10	44.0	44.0	5.4	0.00	0.00	0.00	3.00	49.1	53.1	-3.00	0.128
12.20	44.0	44.0	5.4	0.00	0.00	0.00	3.00	49.0	53.0	-3.00	0.121
12.30	44.0	44.0	5.4	0.00	0.00	0.00	3.00	48.8	52.8	-3.00	0.114
12.40	44.0	44.0	5.4	0.00	0.00	0.00	3.00	48.4	52.4	-3.00	0.107
12.50	44.0	44.0	5.4	0.00	0.00	0.00	3.00	48.0	52.0	-3.00	0.100
12.60	44.0	44.0	5.4	0.00	0.00	0.00	3.00	47.6	51.6	-3.00	0.093
12.70	44.0	44.0	5.4	0.00	0.00	0.00	3.00	47.4	51.4	-3.00	0.086
12.80	44.0	44.0	5.4	0.00	0.00	0.00	3.00	47.1	51.1	-3.00	0.079
12.90	44.0	44.0	5.4	0.00	0.00	0.00	3.00	46.9	50.8	-3.00	0.072
13.00	44.0	44.0	5.4	0.00	0.00	0.00	3.00	46.6	50.6	-3.00	0.065
13.10	44.0	44.0	6.0	0.00	0.00	0.00	3.00	46.3	50.2	-3.00	0.058
13.20	44.0	44.0	6.0	0.00	0.00	0.00	3.00	46.0	49.9	-3.00	0.051
13.30	44.0	44.0	6.0	0.00	0.00	0.00	3.00	45.6	49.6	-3.00	0.044
13.40	44.0	44.0	6.0	0.00	0.00	0.00	3.00	45.2	49.1	-3.00	0.037
13.50	44.0	44.0	6.0	0.00	0.00	0.00	3.00	44.5	48.5	-3.00	0.030
13.60	44.0	44.0	6.0	0.00	0.00	0.00	3.00	44.0	47.7	-2.82	0.023
13.70	44.0	44.0	6.0	0.00	0.00	0.00	3.00	44.0	47.2	-2.39	0.017
13.72	51.7	44.5	6.0	2.96	5.82	1.97	3.37	44.0	44.0	0.00	0.000
13.80	53.8	46.8	6.0	2.98	5.67	1.90	3.37	44.0	44.0	0.00	0.000
13.90	56.2	49.3	6.0	3.00	5.51	1.84	3.37	44.0	44.0	0.00	0.000
14.00	58.4	51.7	6.0	3.01	5.36	1.78	3.37	44.0	44.0	0.00	0.000
14.10	60.6	54.0	6.6	3.06	5.31	1.74	3.37	44.0	44.0	0.00	0.000
14.20	62.6	56.1	6.6	3.07	5.17	1.68	3.37	44.0	44.0	0.00	0.000
14.30	56.6	55.8	6.6	0.00	0.00	0.00	3.37	44.0	44.0	0.00	0.000
14.40	59.0	52.2	6.6	3.05	5.42	1.78	3.37	44.0	44.0	0.00	0.000
14.50	61.1	54.5	6.6	3.06	5.27	1.72	3.37	44.0	44.0	0.00	0.000
14.60	63.0	56.5	6.6	3.08	5.14	1.67	3.37	44.0	44.0	0.00	0.000
14.70	54.8	54.0	6.6	0.00	0.00	0.00	3.37	44.0	44.0	0.00	0.000
14.80	60.6	54.0	6.6	3.06	5.31	1.74	3.37	44.0	44.0	0.00	0.000
14.90	62.6	56.1	6.6	3.07	5.17	1.68	3.37	44.0	44.0	0.00	0.000
15.00	56.6	55.8	6.6	0.00	0.00	0.00	3.37	44.0	44.0	0.00	0.000
15.10	59.0	52.2	6.7	3.05	5.43	1.78	3.37	44.0	44.0	0.00	0.000
15.20	61.1	54.5	6.7	3.07	5.29	1.72	3.37	44.0	44.0	0.00	0.000

15.30	63.1	56.6	6.7	3.08	5.16	1.67	3.37	44.0	44.0	0.00	0.000
15.40	54.9	54.1	6.7	0.00	0.00	0.00	3.37	44.0	44.0	0.00	0.000
15.50	59.6	52.9	6.7	3.05	5.39	1.77	3.37	44.0	44.0	0.00	0.000
15.60	61.7	55.1	6.7	3.07	5.25	1.71	3.37	44.0	44.0	0.00	0.000
15.70	63.6	57.1	6.7	3.09	5.12	1.66	3.37	44.0	44.0	0.00	0.000
15.80	53.2	52.4	6.7	0.00	0.00	0.00	3.37	44.0	44.0	0.00	0.000
15.90	61.3	54.6	6.7	3.07	5.28	1.72	3.37	44.0	44.0	0.00	0.000
16.00	63.2	56.7	6.7	3.08	5.15	1.67	3.37	44.0	44.0	0.00	0.000
16.10	55.0	54.2	6.2	0.00	0.00	0.00	3.37	44.0	44.0	0.00	0.000
16.20	59.6	53.0	6.2	3.03	5.31	1.75	3.37	44.0	44.0	0.00	0.000
16.30	61.6	55.1	6.2	3.05	5.17	1.70	3.37	44.0	44.0	0.00	0.000
16.40	63.4	57.0	6.2	3.06	5.05	1.65	3.37	44.0	44.0	0.00	0.000
16.50	54.1	53.4	6.2	0.00	0.00	0.00	3.37	44.0	44.0	0.00	0.000
16.60	59.9	53.3	6.2	3.03	5.29	1.74	3.37	44.0	44.0	0.00	0.000
16.70	61.8	55.3	6.2	3.05	5.15	1.69	3.37	44.0	44.0	0.00	0.000

NOMENCLATURE

aa	constant $(\pi/2)^2$	[-]
A	area	[m^2]
b	constant (see equation 7.2)	[m^3/kg]
B	pupi input/output signal	[bits]
crf	capital recovery factor (see section 7.4.4.1)	
C	storage capacity of TES	[J]
C	heat capacity (see equation 2.85)	[J/K]
Cp	specific heat capacity (constant pressure)	[J/KgK]
Cv	specific heat capacity (constant volume)	[J/kgK]
COP	coefficient of performance	[-]
D	diameter	[m]
De	equivalent diameter	[m]
E	energy density	[MJ/m^3]
F	volumetric flow rate of transfer fluid	[lit/min]
G	conductance (see equation 2.12)	[W/K]
h	heat transfer coefficient	[W/m^2K]
h	specific enthalpy	[J/kg]
H	humidity	[kg/kg]
H	conductance (see equation 2.84)	[W/K]
i	interest rate	
K	constant	[-]
k	thermal conductivity	[W/m^2K]
L	length	[m]
L	heat loss factor	[W/degC]
M	mass	[kg]
$\dot{m}$	mass flow rate	[kg/s]
n	period of repayment	[years]
P	amount of capital invested	[£]
P	surface area of duct per unit length	[m]
P	pressure	[bar]
PCT	temperature difference (see equation 2.71)	[K]

PER	primary energy ratio (see equation 2.3)	[-]
q	heat transfer rate	[W]
$\hat{q}$	heat transfer rate per unit length of cylinder	[W/m]
Q	heat energy	[J]
r	radius	[m]
R	ideal gas constant	[J/kgK]
r	annual repayment	[£]
S	total sum	[£]
S	interface density (see equation 3.1)	[m^{-1}]
s	distance between tube centres	[m]
s	specific entropy	[J/kg]
t	time	[s]
T	temperature	[°C]
ΔT	temperature difference	[degC]
ΔTp	temperature step change	[degC]
TSC	theoretical storage capacity	[MJ]
u	velocity	[m/s]
U	overall heat transfer coefficient	[W/m^2K]
v	specific volume	[m^3/kg]
V	capacity rate (see equation 2.83)	[W/K]
$\dot{V}$	volumetric flow rate of air	[m^3/s]
W	work transfer rate	[W]
x	spatial variable	[m]
X	surface of separation between solid and liquid	[m]
y	spatial variable	[m]
z	spatial variable	[m]

Greek Symbols

Λ	numerical constant (see equation 2.28)	[-]
∂	prefix, indicates partial derivative	
Δ	difference	[-]
α	thermal diffusivity ($k/\rho Cp$)	[m^2/s]
ϕ	performance parameter (see equation 2.11)	[kW/kWh]
ε	voidage	[-]
λ	latent heat	[J/kg]
λ'	effective latent heat (see equation 2.49)	[J/kg]

η	effectiveness (see section 4.3.2.2)	[-]
η	efficiency (see equation 7.5)	[-]
μ	viscosity	[kg/ms]
ρ	density	[kg/m^3]
θ	temperature approach	[degC]
θ	polar coordinate	[degrees]
τ	time constant	[s]
ξ	storage material density (see equation 3.2)	[-]
δ	prefix, indicates finite increment	

Non-Dimensional Groups

Bi	Biot number (see equation 2.42)
Fo	Fourier number ($\alpha\delta t/\delta x^2$)
Gr	Grashof number
NTU	number of transfer units (see equation 3.13)
Nu	Nusselt number
Pr	Prandtl number(see equation 3.14)
(q/A)*	heat flux (see equation 2.72)
Re	Reynolds number (see equation 3.7)
Ste	Stefan number ($Cp\Delta Tp/\lambda$)
t*	time (see equations 2.41 and 2.63)
T*	temperature (see equation 2.62)
ΔT*	temperature difference (see equation 4.14)
UF	utilisation factor (see definition p181)
X*	interface position (see equation 2.40)
x*	spatial position (see equation 2.61)

Subscripts

a	ambient
ad	adiabatic
ap	approximate
av	average
A	actual
b	bulk
c	cold
co	condenser

C	charge
C	Carnot cycle
D	discharge
DB	dry bulb
DHW	domestic hot water
em	electric motor
ev	evaporator
f	flow
FDT	fully developed temperature profile
FDV	fully developed velocity profile
h	hot
i	interface between solid and liquid phases
in	inlet
l	liquid phase of PCM
L	heat loss
LM	log mean
m	mean
mp	melting point
n	normal to surface
N	number of nodes
o	initial conditions, t=0
on	on
out	outlet
PCM	phase change material
r	residence
ref	refrigerant
R	Rankine cycle
s	solid phase of PCM
sat	saturated
set	setpoint
SS	steady state
t	tube
tf	transfer fluid
T	total
w	wall
WB	wet bulb

wi	inner wall of cylinder
wo	outer wall of cylinder
wv	water vapour
1	inside tube
2	outside tube
1-4	state points of thermodynamic cycle
5-35	locations for temperature sensors

Superscripts

o	initial value
1	predicted value
'	derivative

BIBLIOGRAPHY

Abhat, A., Aboul-Enein, S. and Malatidis, N. A. (1980). Heat of Fusion Systems for Solar Heating Applications. *Thermal Storage of Solar Energy,* Edited by C. den Ouden, Proceedings of an International TNO-Symposium held in Amsterdam, The Netherlands, 5-6 November. Martinus Nijoff, The Hague. 3, 157-177.

Abhat, A. (1984). Thermal Performance of a Finned Heat Pipe Latent Heat Store. *Journal of Ambient Energy,* 5, 4, 193-206.

AEIC-EEI Heat Pump Committee (1952). Chemical Heat Storage for Heat Pumps. *Refrigerating Engineering,* July, 719-721.

Altman, M. (1971). *Conservation and Better Utilization of Electric Power by means of Thermal Energy Storage and Solar Heating.* National Science Foundation, University of Pennsylvannia Report UPTES-71-1.

Anderson, J. A., Bradford, R. A. and Carrington, C. G. (1985). Assessment of Heat Pump Water Heater. *International Journal of Energy Research,* 9, 1, 77-89.

Aram, J. H. (Ed.) (1984). *Heat Pump Research: Proceedings of the Meeting of SERC Research Grant Holders in Heat Pumps held at Cosener's House, Abingdon on 19 and 20 June 1983.* Rutherford Appleton Laboratory Report RAL-84-060.

Armor, M. (1981). *Heat Pumps and Houses. A Consumers Guide to the Machines which can dramatically reduce domestic heating costs.* Prism Press.

ASHRAE Standard 94-77, *Methods of Testing Thermal Storage Devices Based on Thermal Performance.* The American Society of Heating, Refrigerating and Air-Conditioning Engineers, Atlanta.

ASHRAE Standard 94.2-81, *Methods of Testing Thermal Storage Devices with Electrical Input and Thermal Output Based on Thermal Performance.* The

American Society of Heating, Refrigerating and Air-Conditioning Engineers, Atlanta.

ASHRAE Standard 116-83, *Methods of Testing for Seasonal Efficiency of Unitary Air Conditioners and Heat Pumps.* The American Society of Heating, Refrigerating and Air-Conditioning Engineers, Atlanta.

Barrow, H. (1985). A Note on Frosting of Heat Pump Evaporator Surfaces. *Journal of Heat Recovery Systems,* 5, 3, 195-201.

Bartlett, R. J. and Chabra, J. R. (1983). Engineering Development of a Domestic Heat Pump. *Prospects for Domestic Heat Pumps,* One-Day Symposium at The University of Warwick, 26 September.

Bell, M. A. (1981). Low Grade heat storage using sodium acetate solution. *Papers Presented at the International Conference on Energy Storage,* held at the Bedford Hotel, Brighton, U.K., April 29 - May 1. BHRA Fluid Engineering, Cranfield.

Bell, M. A., Cohen, R. R., Manley, B. J. W., O'Callaghan, P. W. and Wood, R.J. (1983). The Developement and Optimisation of Cost Effective Thermal Energy Storage Systems for Solar Space Heating by means of a Microprocessor Controlled Test Facility. Grant Report ESA/S/039/UK.

Berghams, J. (1981). Domestic Heat Pump Applications in Belgium. *New Energy Conservation Technologies and their Commercialisation,* Edited by J. P. Millhone and E.H.Willis, Paris, France, July. Springer-Verlag, Berlin. 583-586.

Blundell, C. J. (1977). Optimising Heat Exchangers for Air to Air Space Heating Heat Pumps in the UK. *International Journal of Energy Research,* 1, 69-94.

Bochenek, W. and Drury, M. D. (1975). A plastic film crystalliser in the chemical industry. *The Chemical Engineer,* July-August, 435-438.

Buick, T. R., McMullan, J. T., Morgan, R. and Murray, R. B. (1977). A Controlled Enviroment Laboratory for the Testing of Domestic Heat Pumps. *International Journal of Energy Research,* 1, 47-54.

Butler, D. J. G. (1985). The cost effectiveness of heat pumps in highly insulated dwellings: an assessment. Building Research Establishment Report.

Carrington, C. G. (1982). Use of Controlled Water Circulation in Tap Water Heat Pumps. *International Journal of Energy Research*, 6, 233-240.

Carslaw, H. S. and Jaeger, J. C. (1959). *Conduction of Heat in Solids.* Second Edition, Oxford University Press.

Chapman, P. (1981). *Fuel's Paradise: Energy Options for Britain.* Pelican Books.

Cooke, B. H. and Pritchard, C. L. (1986). Performance of a Phase Change Heat Store Designed for use with a Heat Pump. *World Congress III of Chemical Engineering,* September 21-25, Tokyo, Japan, 1, 645-648.

Croft, D. R. and Lilley, D. G. (1977). *Heat Transfer Calculations using Finite Difference Equations.* Applied Science, London.

Dicker (1978). Controls for Heat Pumps. *Refrigeration and Air Conditioning,* April, 120-123.

Dietz, D. (1984). Thermal Performance of a Heat Storage Module using Calcium Chloride Hexahydrate. *Trans. ASME - Journal of Solar Energy Engineering,* 106, 1, 106-111.

Downing, R. C. (1974). Refrigerant Equations. *ASHRAE Transactions,* 80, 2, 158-169.

Downing, R. C. and Gray, J. B. (1972). R502 - A Better Heat Pump Refrigerant. *Refrigeration and Air Conditioning,* 75, 45-46.

Duda, J. L., Malone, M. F. and Notter, R. H. (1975). Analysis of 2-D Diffusion Controlled Moving Boundary Problems. *International Journal of Heat and Mass Transfer,* 18, 2, 901-910.

Dusinberre, G. M. (1961). *Heat Transfer Calculations by Finite Differences.* International Textbook, Scranton.

Dwyer, O. E. and Berry, H. C. (1970). Laminar-Flow Heat Transfer for In-Line

Flow Through Unbaffled Rod Bundles. *Nuclear Science and Engineering,* **42**, 81-88.

Eeles, W. T. (1981). Night Storage Heaters. *Papers Presented at the International Conference on Energy Storage,* held at the Bedford Hotel, Brighton, U.K., April 29 - May 1. BHRA Fluid Engineering, Cranfield.

El-Meniawy, S. A. K., Watson, F. A. and Holland, F. A. (1981). A Study of the Operating Characteristics of a Water to Water Heat Pump System using R22. *Journal of Heat Recovery Systems,* **1**, 1, 209-217.

Evans, K. G. (1985). *The Application of Thermal Energy Storage Within a Heat Pumped Domestic Heating System.* M. Sc. Thesis, Cranfield Institute of Technology.

Fischer, R. D. (1980). Opportunities in the Application of Microcomputers to Heat Pumps. *Proceedings of Third Intersoc. Energy Conversion Engin. Conf.,* 2123-2126.

Fleming, H. (1978). *A Variable Speed Heat Pump,* M. Phil. Thesis, Manchester Polytechnic.

Foster, J. H., 1979, *A Review of Heat Pump Research in UK Universities, Polytechnics and Institutes of Technology,* Rutherford Appleton Laboratory Report RL-79-050.

Foster, J .H. (Ed.) (1980). *Proceedings of the Open Meeting on Heat Pumps held at the Rutherford and Appleton Laboratories on November 20th 1979.* Rutherford Appleton Laboratory Report RL-80-011.

Foster, J .H. (Ed.) (1981). *Proceedings of the Grant Holders Meeting on Heat Pumps.* Rutherford Appleton Laboratory Report RL-81-059.

Foust, A. S., Wenzel, L. A., Clump, C. W., Mans, L. and Anderson, L. B. (1960). *Principles of Unit Operations.* First Edition, Revised, Wiley, New York.

Foxley, D. M. and Weaver, D. R. (1981). Relating Laboratory Testing of Heat Pumps to Seasonal COP. *New Energy Conservation Technologies and their Commercialisation,* Edited by J. P. Millhone and E.H.Willis, Paris, France, July. Springer-Verlag, Berlin. 611-615.

Frysinger, G. R. (1979). Storage Assisted Heat Pumps using Phase Change Materials. *Proceedings of Fourteenth IECEC,* Boston, II, 1730-1733.

Furbo, S. (1980). Heat Storage with an Incongruently Melting Salt Hydrate as Storage Medium Based on the Extra Water Principle. *Thermal Storage of Solar Energy,* Edited by C. den Ouden, Proceedings of an International TNO-Symposium held in Amsterdam, The Netherlands, 5-6 November. Martinus Nijoff, The Hague. 3, 135-146.

Haldane, T. G. N. (1930). The Heat Pump - An Economical Method of Producing Low-Grade Heat from Electricity. *Journal of the Institution of Electrical Engineers,* 68, 666-675.

Haywood, R. W. (1978). *Thermodynamic Tables in S.I. (metric) Units.* Second Edition, Cambridge University Press.

Heap, R. D. (1977). Heat Requirements and Energy Use in British Houses. *Energy and Buildings,* 1, 347-366.

Heap, R. D. (1983). *Heat Pumps.* Second Edition. Spon, London.

Heating and Ventilating Contractors' Association (HVCA) (1983). *Heat Pumps for Domestic Applications: guide to good practice and essential information to customers.*

Henderson, W. D (1982). The Simulation of a Heat Pump Heating a Highly Insulated Dwelling. *Building Services Engineering Research and Technology,* 3, 3, 117-126.

Henderson, W. D. (1984). The Use of Floor Panel Energy Storage in a Heat Pump Heated Dwelling. *International Journal of Energy Research,* 8, 2, 163-184.

Hillier, C. C. and Glicksman, L. R. (1976). *Improving Heat Pump Performance via Compressor Capacity Control.* Massachusetts Institute of Technology Energy Laboratory Report MIT-EL-76-001.

Hillier, C. C. and Glicksman, L. R. (1976). *Improving Heat Pump Performance via Compressor Capacity Control.* Massachusetts Institute of Technology Energy Laboratory Report MIT-EL-76-002.

Hirst, E., Carney, J. and O'Neal, D. (1979). Alternative Technologies for US Residential Water Heating - Energy Savings and Economic Benefits. *Energy Policy,* 71, 4, 307-320.

Jacobsen, S. R. (1981). Introduction and Development of Heat Pump Systems in Denmark. *New Energy Conservation Technologies and their Commercialisation,* Edited by J. P. Millhone and E.H.Willis, Paris, France, July. Springer-Verlag, Berlin. 626-631.

Jardine, D. M. and Kuharich, R. F. (1976). Operational Report on an Integrated Solar-assisted Optimised Heat Pump System. *ASHRAE Transactions,* 82, 2, 426-432.

Jonas, P. J. (1981). Heat Pumps in the United Kingdom. *New Energy Conservation Technologies and their Commercialisation,* Edited by J. P. Millhone and E.H.Willis, Paris, France, July. Springer-Verlag, Berlin. 604-610.

Jones, D. E. and Hill, J.E. (1979). *Testing of Pebble-Bed and Phase-Change Thermal Energy Storage Devices According to ASHRAE Standard 94-77.* National Bureau of Standards Report NBSIR-79-1737.

Kartsounes, G. T. and Erth, R. A. (1971). Computer Calculation of the Thermodynamic properties of Refrigerants 12 , 22 & 502. *ASHRAE Transactions,* 77, 88-103.

Katayama, K., Saito, A., Utaka, Y., Maekawa, H. and Saiullahaza (1981). Heat Transfer Characteristics of the Latent Heat TES Capsule. *Solar Energy,* 27, 2, 91-97.

Kelly, G. E. and Hill, J. E. (1975). *Methods of Testing for Rating Thermal Storage Devices based on Thermal Performance.* National Bureau of Standards Report NBSIR-74-634.

Kernan, G. and Brady, J. (1977). Economic Evaluation of Heat Pumps. *International Journal of Energy Research,* 1, 115-125.

Kopecky, Z. (1984). *Design and Testing of a TES for a Domestic Heat Pump.* M.Sc. Thesis, Cranfield Institute of Technology.

Kreith, F. and Bohn, M. S. (1986). *Principles of Heat Transfer.* Harper and Row, New York.

Lane, G. A. (1983). *Solar Heat Storage.* CRC Press.

Lennox, S. C. and Chadwick, M. (1977). *Mathematics for Engineers and Applied Scientists.* Heinemann, London.

London, A. L. and Seban, R. A. (1943). Experimental Confirmation of Predicted Water Freezing Rates. *Transactions of the American Society of Mechanical Engineers,* 65, 771-778.

MacCracken, C. D. (1981). PCM Bulk Storage. *Papers Presented at the International Conference on Energy Storage,* held at the Bedford Hotel, Brighton, U.K., April 29 - May 1. BHRA Fluid Engineering, Cranfield. 1, 159-164.

Mancini, N. A. (1980). Use of Paraffins for Thermal Storage. *Thermal Storage of Solar Energy,* Edited by C. den Ouden, Proceedings of an International TNO-Symposium held in Amsterdam, The Netherlands, 5-6 November. Martinus Nijoff, The Hague. 3, 99-110.

Manley, B. (1983). *Thermal Energy Storage in Encapsulated Phase Change Materials.* Ph. D. Thesis, Cranfield Institute of Technology.

Marks, S. (1980). An Investigation of the Thermal Energy Storage Capacity of Glauber's Salt with Regard to Thermal Cycling. *Solar Energy,* 25, 1, 255-258.

McAdams, W. H. (1954). *Heat Transmission.* Third Edition, McGraw Hill.

McCabe, W. L. and Smith, J. C. (1976). *Unit Operations of Chemical Engineering.* Third Edition, McGraw-Hill.

McMullan, J. T. and Morgan, R. (1981). *Heat Pumps.* Adam Hilger, Bristol.

McMullan, J. T., Morgan, R. and Hughes, D. W. (1981). The Discrepancy between Heat Pump Field Performance and Test Performance: A Simulation Study. *International Journal of Energy Research,* 5, 83-94.

McMullan, J. T., Hughes, D. W. and Morgan, R. (1985). A Suite of Computer Programs for Calculating Refrigerant Properties. *Journal of Heat Recovery Systems,* 5, 2, 143-180.

Menon, A. S., Weber, M. E. and Mujumdar, A. S. (1983). The Dynamics of Energy Storage for Paraffin Wax in Cylindrical Containers. *Canadian Journal of Chemical Engineering,* 61, 547-653.

Metais, B. and Eckert, E. R. G. (1964). Forced, Mixed and Free Convection Regimes. *Trans ASME - Journal of Heat Transfer,* 86, 295-296.

Michaels, A. I. (1980). An Overview of the U.S.A. program for the Development of Thermal Energy Storage for Solar Energy Applications. *Thermal Storage of Solar Energy.* Edited by C. den Ouden, Proceedings of an International TNO-Symposium held in Amsterdam, The Netherlands, 5-6 November. Martinus Nijoff, The Hague. 3, 79-90.

Mountford, D. J. and Freund, P. (1982). The Performance of a Well Insulated House Heated by an Air to Water Heat Pump. *International Journal of Ambient Energy,* 3, 1, 9-18.

Murray, W. D. and Landis, F. (1959). Numerical and Machine Solutions of Transient Heat Conduction Problems Involving Melting or Freezing. *Trans ASME - Journal of Heat Transfer,* 81, 1, 106-112.

Neal, E. (1983). Heat Pumps - Applications for Heating Conservation and Heat Recovery. *Progress in Energy and Combustion Science,* 9, 3, 179-197.

Page, J. K. R. and Swayne, R. E. H. (1981). Phase Change Thermal storage for Solar Applications. *Papers Presented at the International Conference on Energy Storage,* held at the Bedford Hotel, Brighton, U.K., April 29 - May 1. BHRA Fluid Engineering, Cranfield. 1, 165-170.

Perry, R. H. and Chilton, C. H. (1973). *Chemical Engineers' Handbook.* Fifth Edition, McGraw-Hill Kogakusha, Tokyo.

Peters, M. S. and Timmerhaus, K. D. (1980). *Plant Design and Economics for Chemical Engineers.* Third Edition, McGraw-Hill, New York.

Raju, K. S. N. and Chand, J. (1980). Consider the Plate Heat Exchanger.

Chemical Engineering, 11 August, 133-144.

Reichl, A. (1981). The State of the Development and Introduction of the Heat Pump in Austria. *New Energy Conservation Technologies and their Commercialisation,* Edited by J. P. Millhone and E.H.Willis, Paris, France, July. Springer-Verlag, Berlin. 644-647.

Rosell, J., Morgan, R. and McMullan, J. T. (1982). The Performance of Heat Pumps in Service - A Simulation Study. *International Journal of Energy Research,* 6, 83-99.

Rosell, J., Morgan, R. and McMullan, J. T. (1983a). The Performance of Heat Pumps in Service - Comparison of a Computer Model with a Real Installation. *International Journal of Energy Research,* 7, 3, 227-240.

Rosell, J., Morgan, R., Hughes, D. W. and McMullan J. T. (1983b). Improvements in Controlled Environment Facilities for Testing Domestic Air to Water Heat Pumps. *International Journal of Energy Research,* 7, 35-48.

Russel, F. M. (1982). *Heat storage and heat pumps,* Workshop held at Coseners House on 3-4 February. Rutherford Appleton Laboratory Report RL-82-031.

Ryan, B. F., Joiner, B. L. and Ryan, T. A. (1985). *Minitab Handbook* Second Edition. Duxbury Press, Boston.

Saitoh, T. (1978). Numerical Method for Multidimensional Freezing Problems in Arbitrary Domains. *Trans ASME - Journal of Heat Transfer,* 100, 294-299.

Schilf, L. (1981). A Vacuum-Insulated Hybrid Heat Storage System (HWS). *New Energy Conservation Technologies and their Commercialisation,* Edited by J. P. Millhone and E.H.Willis, Paris, France, July. Springer-Verlag, Berlin. 857-869.

Seban, R. A. and London, A. L. (1945). Experimental Confirmation of Predicted Water-Freezing Rates. *Transactions of the American Society of Mechanical Engineers,* 67, 39-44.

Shah, R. K. and London, A. L. (1978). *Laminar Flow Forced Convection in Ducts (A Source Book for Compact Heat Exchanger Data).* Academic Press, New

York.

Shamsundar, N. (1978). Comparison of Numerical Methods for Diffusion Problems with Moving Boundaries. *Moving Boundary Problems,* Edited by D. G. Wilson, A. D. Solomon and P. Bogg, Symposia held at Gatlinburg, Tennessee on September 26-28. 165-185.

Shamsundar, N. and Sparrow, E. M. (1975). Analysis of Multidimensional Conduction Phase Change Via the Enthalpy Model. *Trans ASME - Journal of Heat Transfer,* 97, 333-340.

Shamsundar, N. and Sparrow, E. M. (1974). Storage of Thermal Energy by Solid-Liquid Phase Change Temperature Drop and Heat Flux. *Trans ASME - Journal of Heat Transfer,* 96C, 1, 541-543.

Shih, Y. P. and Isay, S. Y. (1971). Analytical Solutions for Freezing a Saturated Liquid Inside or Outside Cylinders. *Chemical Engineering Science,* 26, 809-816.

Sigmon, T. W., Davidson, J. W., Doster, J. M., Martin, J. F. and Edwards, J. A. (1980). Simulation and Evaluation of Latent Heat Thermal Energy Storage Heat Pump Systems. *Proceedings 15th IECEC,* Seattle. Paper 809426. 2117-2122.

Smith, G. D. (1978). *Numerical Solution of Partial Differntial Equations: Finite Difference Methods.* Clarendon Press, Oxford.

Sparrow, E. M., Loeffler, A. L. and Hubbard, H. A. (1961). Heat Transfer to Longitudinal Laminar Flow Between Cylinders. *Trans ASME - Journal of Heat Transfer,* 83, 415-422.

Stunic, Z., Djurickovic, V. and Stunic, Z. (1978). Thermal Storage: Nucleation of Melts of Inorganic Salt Hydrates. *Journal of Applied Chemistry & Biotechnology,* 28, 761-764.

Sumner, J. A. (1976). *Domestic Heat Pumps.* Prism Press, Dorchester.

Swisher, J. H. and Frier, W. A. (1981). United States Department of Energy Thermal Storage Program. *Thermal Energy Storage,* Edited by G. Beghi, Lectures of a Course held at the Joint Research Centre, Ispra, Italy, June

1-5, 465-500.

Tai, K. W., Zylla, R., Devotta, S., Watson, F. A. and Holland, F. A. (1982). Derived Thermodynamic Design Data for Heat Pump Systems Operating on R502. *Journal of Heat Recovery Systems,* 2, 1, 209-217.

Talwar, R. and Dilpare, A. L. (1977). A Two Dimensional Numerical Solution to Freezing/Melting in Cylindrical Coordinates. American Society of Mechanical Engineers Paper ASME 77-WA/HT-11.

Tassou, S. A., Green, R. K., Wilson, D. R. and Searle, M. (1981). Energy Conservation Through the use of Capacity Control in Heat Pumps. *Journal of the Institute of Energy,* 30, 30-35.

Tassou, S. A., Marquand, C. J. and Wilson, D. R. (1983). Comparison of the Performance of Capacity Controlled and Conventional On\Off Controlled Heat Pumps. *Applied Energy,* 14, 241-256.

Tassou, S. A., Marquand, C. J. and Wilson, D. R. (1984). Part Load Performance Analysis of Air to Water Heat Pump Systems. *Journal of the Institute of Energy,* 57, 364-367.

Telkes, M. (1980). Thermal Storage in Salt Hydrates. *Solar Materials Science,* Edited by L. E. Murr. Academic Press, New York. 377-404.

Ulman, A. and Valentin, B. (1983). Investigations of Sodium Acetate Trihydrate for Solar Latent Heat Storage Controlling the Melting Point. *Solar Energy Materials,* 9, 2, 177-181.

van Galen, E. (1980). Experimental Results of a Latent Heat Storage System based on Sodium Acetate Trihydrate in a Stabilising Colloidal Polymer Matrix. *Thermal Storage of Solar Energy,* Edited by C. den Ouden, Proceedings of an International TNO-Symposium held in Amsterdam, The Netherlands, 5-6 November. Martinus Nijoff, The Hague. 3, 147-156.

van Galen, E. (1981). An Optimisation Method and Experimental Results of a Phase Change Storage System Based on Sodium Acetate Trihydrate. *Solar Energy Applications to Dwellings,* Edited by W. Palz and T. C. Steemers, Proceedings of the EC Contractors' Meeting held in

Athens, 11-13 November, D. Reidel Publishing Company. Series A, 1, 124-129.

von Cube, H. L. and Steimle, F. (1981). *Heat Pump Technology.* Butterworths.

Wada, T. and Yamamoto, R. (1982). Studies on Salt Hydrate for Latent Heat Storage I. Crystal Nucleation of Sodium Acetate Trihydrate Catalysed by Tetrasodium Pyrophosphate Decahydrate. *Bulletin of the Chemical Society of Japan,* 55, 4, 3603-3606.

Wada, T., Yamamoto, R. and Matsuo, Y. (1984). Heat Storage Capacity of Sodium Acetate Trihydrate during Thermal Cycling. *Solar Energy,* 33, 3/4, 373-375.

Weast, R..C. (1981). *CRC Handbook of Chemistry and Physics.* Sixtieth Edition. CRC Press, Boca Raton.

Webster, J. (1983). Market Prospects and Economics. *Prospects for Domestic Heat Pumps,* One-Day Symposium at The University of Warwick, 26 September.

Wettermark, G., Carlsson, B. and Stymme, H. (1979). *Document D2. Storage of Heat. A Survey of Efforts and Possibilities.* Swedish Council for Building Research Report, 67-110.

Whitaker, S. (1972). Forced Convection Heat Transfer Correlations for Flow in Pipes, Past Flat Plates, Single Cylinders, Single Spheres, and for Flow in Packed Beds and Tube Bundles. *AIChemE Journal,* 18, 2, 361-371.

Wood, R. J., Gladwell, S. D., O'Callaghan, P. W. and Probert, S. D. (1981). Low Temperature Thermal Energy Storage using Packed Beds of Encapsulated Phase Change Material. *Papers Presented at the International Conference on Energy Storage,* held at the Bedford Hotel, Brighton, U.K., April 29 - May 1. BHRA Fluid Engineering, Cranfield. 145-158.